

UNCLASSIFIED

AD NUMBER
AD919430
NEW LIMITATION CHANGE
TO Approved for public release, distribution unlimited
FROM Distribution authorized to U.S. Gov't. agencies only; test and evaluation; June 1974. Other requests shall be referred to Commander, Frankford Arsenal, Philadelphia PA .
AUTHORITY
FA, D/A ltr, 2 Oct 1974

THIS PAGE IS UNCLASSIFIED

AD919430

**FINAL REPORT
SUPPLEMENT TO PARAMETRIC STUDY OF
ADVANCED FORWARD AREA AIR
DEFENSE WEAPON SYSTEM
(AFAADS)**

VOLUME I ANALYSIS

31 January 1974

Submitted to:

**U.S. Army, Frankford Arsenal
Bridge and Tacony Streets
Philadelphia, Pennsylvania 19137**

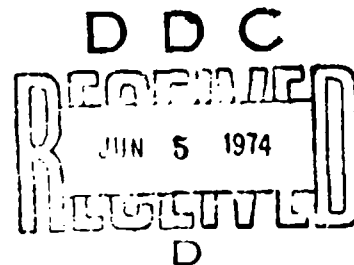
**Prepared Under Contract: DAAA25-73-C0373
(formerly DAAG05-70-C0328) MOD P 00011**

**Distribution limited to U. S. Gov't. agencies only;
Test and evaluation; 5 June 1974. Other requests
for this document must be referred to Commander,
Frankford Arsenal, ATTN: AFSA-FCW-0.**

Prepared by:

**Data Systems Division
Litton Systems, Inc.
8000 Woodley Avenue
Van Nuys, California 91409**

TD 40001



ACKNOWLEDGEMENTS

Litton is happy to acknowledge the excellent guidance and assistance provided on this contract by Mr. Robert Pfeilsticker, Mr. Walter Ryba, Mr. Bernard Kirshtein, Mr. Stanley Goodman, and Mr. Kenneth Heulitt of Frankford Arsenal.

The FACT data reported in Section 4 was obtained as a result of the efforts of Mr. Goodman and Mr. Heulitt, and the support and excellent cooperation of the U. S. Navy. The data analysis was a cooperative effort by Frankford Arsenal and Litton. Mr. Goodman was instrumental in identifying residual program errors in the Litton simulation, and his assistance in the verification tasks was invaluable.

FOREWORD

This report describes the research effort of the Data Systems Division of Litton Systems, Inc., under Modification P00011 to Contract DAAA25-73-C0373, (formerly DAAG05-70-C0328). The objective of this work was to provide additional analytic and simulation effort in support of the parametric analysis of predicted fire air defense systems.

The report is presented in two volumes. Volume I, Analysis, by Herbert K. Weiss reports the analytical effort and the simulation verification procedures. Section 9 on simulation verification was made possible by simulation flowgraphs of the Ginsberg simulation developed by Mr. Barry Seid. Simulation runs were made by Mr. Jacky Onishi. Mr. F. V. Wilson provided analytical support for Section 7.0 on Countermeasures.

Volume II, Data Processing Requirements Analysis, is based on an analyses by Dr. Richard D. Young, Dr. Alfred J. Ess, Mr. Caesar F. Chavez and Mr. Herman A. Fischer.

Earlier effort under this contract at Litton is reported in a previously published series of five volumes, ① ② ③ ④ ⑤

TABLE OF CONTENTS

<u>Section</u>		<u>Page</u>
	ACKNOWLEDGEMENTS	iii
	FOREWORD	iv
1	INTRODUCTION	1-1
2	SUMMARY	2-1
2.1	CONCLUSIONS AND RECOMMENDATIONS	2-1
2.1.1	Frankford Arsenal Aircraft Capabilities Test (FACT) Data	2-1
2.1.2	Closed Loop Predicted Fire Systems	2-2
2.1.3	Rocket and Rocket Assisted Projectile Predicted Fire Systems	2-4
2.1.4	Predicted-Corrected Projectile Systems	2-4
2.1.5	Defense Against Stand-off Munitions	2-6
2.1.6	Countermeasures Resistance	2-6
2.1.7	Data Acquisition and Field Test	2-7
2.2	OVERVIEW OF THE REPORT	2-8
2.2.1	Closed Loop Predicted Fire Systems	2-8
2.2.2	Analysis of Frankford Aircraft Capabilities Test (FACT) Data	2-10
2.2.3	Rocket, Rocket-Assist and Predicted Corrected Projectile Systems	2-11
2.2.4	Defense Against Standoff Munitions	2-13
2.2.5	Countermeasures Resistance	2-13
2.2.6	Cost Considerations	2-14
2.2.7	Simulation Verification	2-15
2.2.8	Program Recommendations	2-15

TABLE OF CONTENTS (Continued)

<u>Section</u>		<u>Page</u>
3	CLOSED LOOP PREDICTED FIRE SYSTEMS	3-1
3.1	RATIONALE	3-1
3.1.1	Historical Perspective	3-2
3.1.2	Miss Vector Components	3-4
3.1.3	Relative Magnitudes of Miss Vector Components	3-5
3.1.4	Is a Closed Loop System Worthwhile?	3-15
3.1.5	General Conclusions with Regard to Bias Reduction	3-26
3.2	SENSORS	3-28
3.2.1	Radar	3-29
3.2.2	3-D Systems with FLIR and Laser	3-30
3.2.3	Unsynchronized FLIR/Laser Systems	3-32
3.2.4	Other FLIR/Laser Hybrids	3-33
3.2.5	Passive 3-D System	3-33
3.2.6	Computer Timed Systems	3-34
3.2.7	The "Spot" Flare	3-36
3.2.8	2-D Systems Using FLIR, TV, Etc.	3-37
3.2.9	Optical Radar	3-37
3.3	PROJECTILE SIGNATURES AND CROSS SECTIONS	3-38
3.3.1	Estimating Relationships for Projectile Radar and Laser Cross Sections	3-38
3.3.2	Estimates of Radar Cross Section of Projectiles	3-47
3.3.3	Estimates for Corner Reflectors	3-50
3.3.4	Comparison of Estimated Radar Cross Sections vs. Measurements	3-57

TABLE OF CONTENTS (Continued)

<u>Section</u>	<u>Page</u>
3.3.5 Callipygean Projectiles (23)	3-64
3.3.6 Infrared Signature of the Projectiles	3-69
3.4 CLOSED LOOP ALGORITHMS	3-84
3.4.1 Introduction	3-84
3.4.2 VISTA Concept	3-86
3.4.3 Development of Closed Loop Algorithms for Elementary Case	3-93
3.4.4 General Solution of Closed Loop Problem in Matrix Form	3-101
3.4.5 Example of 3-D Solution	3-106
3.4.6 Estimate of 3-D System Performance	3-111
3.4.7 Example of 2-D Solution	3-126
3.4.8 Estimates of 2-D System Performance	3-131
3.4.9 General Solution with Expanded Source Vector	3-142
3.4.10 Use of Closed Loop for System Pre-Combat Calibration Firings	3-144
3.5 CONCLUSIONS	3-144
3.5.1 Feasibility	3-144
3.5.2 Advantages and Disadvantages of Closed Loop Systems	3-145
3.5.3 Program Recommendations	3-146
4 FRANKFORD AIRCRAFT CAPABILITIES TEST (FACT)	4-1
4.1 SCOPE OF DATA	4-1
4.2 DIVE/GLIDE BOMBING PASSES	4-2
4.2.1 Aircraft Heading	4-2

TABLE OF CONTENTS (Continued)

<u>Section</u>	<u>Page</u>
4.2.2 Aircraft Dive Angle	4-5
4.2.3 Energy Conservation	4-7
4.2.4 Linear Prediction Errors	4-16
4.3 POP-UP AND DIVE/GLIDE BOMBING PASSES	4-24
4.4 STRAFING PASSES	4-24
4.5 HIGH LEVEL BOMBING	4-27
4.6 LAYDOWN PASSES	4-28
4.7 DEFENSE OF KNOWN POINT ALGORITHMS	4-30
4.8 DATA STATISTICS	4-35
4.8.1 Standard Deviation and Autocorrelation of Radar Noise	4-35
4.8.2 Effect on Prediction Error Statistics	4-44
4.9 CONCLUSIONS	4-48
4.10 RECOMMENDATIONS	4-49
5 COMPARISON OF GUN, ROCKET AND PREDICTED-CORRECTED ROCKET-ASSISTED PROJECTILE SYSTEMS	5-1
5.1 INTRODUCTION	5-1
5.2 COMPARISON OF CHARACTERISTICS	5-3
5.2.1 Muzzle Energy of Guns	5-3
5.2.2 Velocity vs Propellant Weight	5-9
5.2.3 Complete Round Weight vs. Velocity	5-19
5.2.4 Projectile Weight vs. Muzzle Velocity and the Use of Sub-Caliber Projectiles	5-23
5.2.5 Exterior Ballistics	5-25
5.2.6 Tube Life of Guns	5-34

TABLE OF CONTENTS (Continued)

<u>Section</u>	<u>Page</u>
5.2.7 Dispersion	5-37
5.2.8 Rate of Fire of Gun Boosted Rockets	5-39
5.2.9 Installation Weight	5-40
5.3 SUB-OPTIMIZATIONS OF GUN-BOOSTED ROCKETS	5-40
5.3.1 Parameters Trade-offs	5-42
5.3.2 Effectiveness Comparisons	5-47
5.3.3 Controlled Dispersion	5-49
5.4 PREDICTED-CORRECTED PROJECTILE FORWARD AREA AIR DEFENSE SYSTEM	5-52
5.4.1 Concept Objectives	5-53
5.4.2 Functional Options	5-55
5.4.3 Line of Sight Beam Rider Limitations	5-60
5.4.4 Predicted-Corrected Air Defense System Considerations	5-64
5.4.5 Estimated Characteristics and Cost-Effectiveness	5-70
5.5 CONCLUSIONS	5-78
5.6 RECOMMENDATIONS	5-82
6 DEFENSE AGAINST STANDOFF MUNITIONS	6-1
6.1 STANDOFF MUNITIONS CHARACTERISTICS	6-2
6.1.1 Munitions Size and Velocity vs. Standoff Range	6-2
6.1.2 Detectability	6-5
6.1.3 Warhead Characteristics	6-6
6.2 WARHEAD VULNERABILITY	6-8
6.2.1 Penetration Expressions for Projectiles	6-11
6.2.2 Residual Velocity After Plate Perforation	6-17

TABLE OF CONTENTS (Continued)

<u>Section</u>	<u>Page</u>
6.2.3 Detonation of Warhead	6-17
6.2.4 Perforation of Warhead Case versus Angle of Impact	6-19
6.3 DEFENSE EFFECTIVENESS	6-21
6.3.1 Gun/Projectile Characteristics	6-21
6.3.2 Penetration Capability vs. Range and Caliber	6-23
6.3.3 Vulnerability Contours	6-27
6.3.4 Kill Probabilities	6-29
6.4 CONCLUSIONS	6-32
6.5 RECOMMENDATIONS	6-33
7 SYSTEM CONFIGURATIONS TO MINIMIZE THE EFFECT OF ENEMY COUNTERMEASURES	7-1
7.1 STATE OF THE ART IN THE WIZARD WAR AS REPORTED BY AVIATION WEEK	7-1
7.1.1 Initial Actions ²	7-1
7.1.2 Air Defense Weapons Used by the Arabs	7-3
7.1.3 Use of Stand-off Munitions ^{1 5 6 7}	7-6
7.1.4 Use of Dummy SAM Installations ⁷	7-7
7.1.5 Command and Control ^{5 7}	7-8
7.1.6 Golan Heights Action ^{5 13 15}	7-8
7.1.7 Assessment in Terms of U.S. Programs ³	7-9
7.2 IMPLICATIONS FOR AIR DEFENSE SYSTEMS	7-11
7.3 PASSIVE METHODS OF OBTAINING TARGET RANGE	7-12
7.3.1 Short Base Optical Rangefinders	7-12
7.3.2 Extended Base, Multistation Ranging Systems	7-13

TABLE OF CONTENTS (Continued)

<u>Section</u>	<u>Page</u>
7.3.3 Required Range Accuracy	7-17
7.4 THE SIMPLEST "FALL-BACK" MODE	7-19
7.5 CONCLUSIONS	7-19
7.6 RECOMMENDATIONS	7-20
8 COST CONSIDERATIONS	8-1
8.1 "THOSE WERE THE DAYS" (BY GENERAL "BILLY" MITCHELL)	8-1
8.2 COST ELEMENTS OF GUN SYSTEMS FOR AIR DEFENSE	8-2
8.2.1 Complete Fire Units	8-2
8.2.2 Gun Barrels	8-2
8.2.3 Automatic Cannon Costs	8-3
8.2.4 Ammunition Costs	8-7
8.2.5 Vehicle Costs	8-8
8.2.6 Turret Costs	8-8
8.2.7 Sensor and Fire Control Costs	8-9
8.3 COSTS OF UNGUIDED ROCKETS	8-11
8.4 COSTS OF CONVENTIONAL BOMBS	8-11
8.5 PERSONNEL COSTS	8-11
8.6 COSTS OF MISSILE SYSTEMS	8-11
8.6.1 Missile Costs	8-12
8.6.2 System Acquisition and Operating Costs	8-13
8.7 COSTS OF COMMERCIAL AIRCRAFT EQUIPMENT	8-29
8.7.1 Radar	8-29
8.7.2 Autopilots	8-29

TABLE OF CONTENTS (Continued)

<u>Section</u>	<u>Page</u>
8.8 COMMENTS	8-31
9 SIMULATION VERIFICATION PROCEDURE	9-1
9.1 METHOD	9-1
9.2 SIMULATION INPUTS	9-1
9.2.1 Group Content	9-1
9.2.2 Common Inputs in Test Runs	9-3
9.3 PREDICTION MODULE VERIFICATION	9-3
9.3.1 Constant Velocity, Level Straight Line Flight	9-3
9.3.2 Dive and Climb Along Straight Line Under Gravity Acceleration	9-3
9.3.3 Level, Circular Paths at Constant Velocity	9-4
9.3.4 Curved Flight Algorithm	9-4
9.3.5 Defense of Known Point Algorithm	9-7
9.4 COMPUTATION OF FILTER WEIGHTS AND LAG CORRECTIONS	9-9
9.5 EFFECT OF TRACKING BIASES	9-13
9.6 SINGLE SHOT KILL PROBABILITY	9-17
9.7 VERIFICATION OF NOISE MODULES	9-19
9.8 VERIFICATION OF SERVO LAG AND REGENERATION MODULES	9-21
9.9 SIMULATION MODULE FOR MANUAL TRACKING	9-22
9.10 METHOD OF BY-PASSING GLINT COMPUTATION	9-24
9.11 CONCLUSIONS AND RECOMMENDATIONS	9-25
10 ADDITIONAL DATA REQUIREMENTS AND EXPERIMENTAL PROGRAMS	10-1
10.1 FACT TRAJECTORIES	10-1

TABLE OF CONTENTS (Continued)

<u>Section</u>	<u>Page</u>
10.1.1 Accelerometer Records on Aircraft Munition Delivery Paths	10-1
10.1.2 FACT Path Data on Attack Helicopters	10-1
10.1.3 FACT Trajectory Data in Standoff Missiles and their Launch Aircraft	10-2
10.2 PROJECTILE SIGNATURES FOR CLOSED LOOP SYSTEMS	10-2
10.2.1 Signature Measurement	10-2
10.2.2 Projectile Experimental Design Program	10-2
10.3 OPERATIONAL DEGRADATION OF SYSTEM PERFORMANCE	10-2
10.4 TRACKING SENSOR ACCURACIES AND POWER SPECTRAL DENSITIES VS. TARGETS OF AIR DEFENSE SYSTEMS	10-3
10.5 FIELD TEST PROGRAMS OF THE PERFORMANCE OF PREDICTED FIRE SYSTEMS AND COMPONENTS	10-4
11 PROGRAM RECOMMENDATIONS	11-1
11.1 GENERAL	11-1
11.2 CLOSED LOOP PREDICTED FIRE SYSTEMS	11-2
11.3 GUN-BOOSTED PREDICTED FIRE ROCKET SYSTEMS	11-3
11.4 PROJECTILE PREDICTED-CORRECTED SYSTEMS	11-4
11.5 DEFENSE AGAINST STANDOFF WEAPONS	11-5
11.6 PASSIVE RANGING SYSTEM (TONTO)	11-6
11.7 FIRE CONTROL COMPUTER INVESTIGATIONS	11-7
11.8 FORWARD AREA AIR DEFENSE SYSTEM SIMULATION	11-7
11.9 AIR DEFENSE SYSTEM INTEGRATION TO THE FIRE UNIT LEVEL	11-8
 <u>Appendix</u>	
A RADAR "BORESIGHT" ERRORS	A-1

TABLE OF CONTENTS (Continued)

<u>Appendix</u>		<u>Page</u>
B	TERMINAL CORRECTION OF BIAS ERRORS IN PREDICTION-CORRECTED PROJECTILE SYSTEM	B-1
C	CLOSED LOOP PERFORMANCE WITH SPECIFIED INITIAL BIAS	C-1
	REFERENCES/BIBLIOGRAPHY	Bibli 1

LIST OF ILLUSTRATIONS

<u>Figure</u>		<u>Page</u>
3-1	Components of Miss Vector	3-7
3-2	Miss Vector Projected in Sight Plane	3-7
3-3	Slant Range (Meters)	3-9
3-4	Slant Range (Meters)	3-10
3-5	Time of Flight vs. Slant Range	3-11
3-6	System "Bias" Components	3-12
3-7	System "Random" Error Components	3-12
3-8	Standard Deviation of Prediction Error Caused by Angular Tracking Error	3-14
3-9	Standard Deviation of Prediction Error Caused by Angular Tracking Error	3-14
3-10	Maneuver Miss with Linear Prediction (Smoothing Time; One Half Time of Flight)	3-1
3-11	Maneuver Miss with Linear Prediction (Smoothing Time: One Second)	3-16
3-12	Probability Density Function of Typical "Calibration Bias"	3-17
3-13	Situation Geometry and Event Times	3-18
3-14	Event vs. Range Relationships	3-20
3-15	Firing Time vs. Release Range	3-21
3-16	Target Kill Probabilities with Optimum Dispersion	3-27
3-17	Effect of Muzzle Velocity Bias	3-35
3-18	Effect of Bias in Present Range	3-36
3-19	Radar Cross Section of Sphere $a = \text{radius}$	3-42
3-20	Radar Cross Sections of Sphere and Ellipsoid	3-43
3-21	Estimated Radar Cross Section of 20-mm Projectile	3-49
3-22	Estimated Radar Cross Sections of Projectiles vs. Wavelength and Caliber	3-51

LIST OF ILLUSTRATIONS (Continued)

<u>Figure</u>		<u>Page</u>
3-23	Determination of Effective Area of Trihedral	3-53
3-24	Effect of an Error in all Three Corner Angles Upon the Performance of a Trihedral	3-53
3-25	Effect of Construction Error in Trihedral Fabrication	3-55
3-26	Hypothetical Design of Projectile with Trihedral to Maximize Laser Cross Section	3-58
3-27	Possible Method of Reducing Effect of Fabrication Errors	3-58
3-28	Comparison of Experiment and Theory for Projectiles with Trihedrals at 70 GHz	3-59
3-29	Comparison of Experimental and Theoretical Radar Cross Sections of Projectiles at 70 GHz	3-60
3-30	Comparison of Experimental and Theoretical Lobe Widths of Projectiles with Trihedrals at 70 GHz	3-61
3-31	Comparison of Experimental and Theoretical Lobe Widths of Projectiles at 70 GHz	3-63
3-32	Required Off-Axis View Angle versus Range for Oerlikon 35-mm Projectile	3-64
3-33	Geometric Relations for Shaped Projectile Base	3-66
3-34	Sections Through Projectile Base for "Power Law" Shaping	3-70
3-35	Estimated Laser Cross Section of 30-mm Projectiles with Parabolic Base	3-71
3-36	Estimated Laser Cross Section of 30-mm Projectiles with "Power Law" Base Shapes	3-72
3-37	Fraction of Radiant Emittance Below Specified Values of λT	3-74
3-38	Radiant Emittance of Black Body in 8-14 Micron Window versus Temperature	3-75
3-39	Functional Relationships for Estimating Infrared Signature	3-76
3-40	Equivalent Collector Optics and Detector Field of View Geometry	3-77
3-41	Detectivity Curves	3-78

LIST OF ILLUSTRATIONS (Continued)

<u>Figure</u>		<u>Page</u>
3-42	Schematic of Imaging Sight Field	3-78
3-43	Estimated Signal to Noise Ratio of 30 mm projectile at 3 km as Viewed by Imaging Sight versus Projectile Temperature	3-85
3-44	Data Flow in Closed Loop System to Correct for "External Biases" Excluding Target Maneuvers	3-89
3-45	Data Flow Using Vista Module to Correct for Target Maneuvers and "Internal" Biases	3-90
3-46	Fire-Observe-Correct Sequence with Observation Delay	3-94
3-47	Flow Diagram Showing "SEPARATION THEOREM"	3-103
3-48	Flow Diagram for 3-D Closed Loop Configuration	3-113
3-49	Standard Deviation of Azimuth Bias	3-122
3-50	Standard Deviation of Muzzle Velocity Bias	3-122
3-51	Standard Deviation of Elevation Bias	3-123
3-52	Standard Deviation of Total Lateral Bias	3-123
3-53	Standard Deviation of Total Elevation Bias	3-124
3-54	Coordinate System for 2-D Closed Loop System	3-126
3-55	Variation of Angle ψ With Time	3-133
3-56	Slant Range versus Time	3-136
3-57	Residual Standard Deviation of Traverse Bias	3-137
3-58	Residual Standard Deviation of Elevation Bias	3-137
3-59	Residual Standard Deviation of Vector Bias in Sight Plane	3-138
3-60	Reduction of Standard Deviation of Traverse Bias	3-139
3-61	Reduction of Standard Deviation of Elevation Bias	3-140
3-62	Comparison of Firing Doctrines: Residual Standard Deviation of Vector Bias in Sight Plane	3-141

LIST OF ILLUSTRATIONS (Continued)

<u>Figure</u>		<u>Page</u>
4-1	Heading Angle versus Time on Dive/Glide Bombing Paths Flights 1, 2	4-3
4-2	Heading Angle versus Time on Dive/Glide Bombing Paths Flights 3, 4	4-4
4-3	Superimposed Heading Traces Matched at -5.0 Seconds on Flights 1 and 2; Dive/Glide Bombing	4-6
4-4	Superimposed Heading Traces with Mean Rate Removed on Flights 1 and 2 Dive/Glide Bombing	4-7
4-5	Superimposed Heading Traces on Dive/Glide Bombing Flights 3, 4	4-8
4-6	Dive Angle versus Time on Dive/Glide Bombing Paths Flights 1, 2	4-9
4-7	Dive Angle versus Time on Dive/Glide Bomb Paths Flights	4-10
4-8	Superimposed Dive Angle Traces on Flights 1 and 2; Dive/Glide Bombing	4-11
4-9	Conservation of Energy in Dive	4-12
4-10	Comparison of Energy Conservation on Two Passes	4-13
4-11	Altitude and Total Energy on Dive/Glide Bombing Passes	4-14
4-12	Velocity on Glide/Dive Bombing Passes	4-15
4-13	Energy Conservation by P-51 WW-II Aircraft Doing "Pushups"	4-17
4-14	Energy Conservation by P-51 WW-II Aircraft over Extended Time Interval	4-17
4-15	Cross Range Prediction Errors (X) with Linear Predictor on Flights 1 and 2	4-19
4-16	Cross Range Prediction Errors (X) with Linear Predictor on Flight 4	4-20
4-17	Down Range Prediction Errors (Y) with Linear Predictor on Flight 4	4-21
4-18	Altitude Prediction Errors (Z) with Linear Predictor on Flight 4	4-22
4-19	Effect of Target Linear Acceleration in Dive on Linear Predictor Errors	4-23

LIST OF ILLUSTRATIONS (Continued)

<u>Figure</u>		<u>Page</u>
4-20	Superimposed Heading Traces on Pop-Up and Dive/Glide Bomb Passes	4-25
4-21	Superimposed Dive Angle Traces on Pop-Up and Dive/Glide Bomb Passes	4-26
4-22	Cross Range Prediction Errors on Pop-Up and Dive/Glide Bomb Passes	4-27
4-23	Down Range Prediction Errors on Pop-Up and Dive/Glide Bomb Passes	4-28
4-24	Altitude Prediction Error on Pop-Up and Dive/Glide Bomb Passes	4-29
4-25	Superimposed Heading Traces on Strafing Attacks	4-30
4-26	Superimposed Dive Angle Traces on Strafing Attacks	4-31
4-27	Cross Range Prediction Errors with Linear Predictor on Strafing Passes	4-32
4-28	Down Range Prediction Errors with Linear Predictor on Strafing Passes	4-33
4-29	Altitude Prediction Errors on Strafing Passes with Linear Predictor	4-34
4-30	Heading Traces on Laydown Passes	4-35
4-31	Superimposed Dive Angle Traces on Laydown Passes	4-36
4-32	3-sec Prediction Errors on Laydown Passes	4-37
4-33	Lateral Prediction Errors with Defense of Known Point Predictor	4-38
4-34	Elevation Prediction Errors with Defense of Known Point Predictor	4-39
4-35	Variation of Lateral Prediction Error with Time of Flight for Defense of Known Point Predictor	4-40
4-36	Defense of Known Point Predictor Errors on Dive/Glide Bomb Flights 1, 3	4-41
4-37	Defense of Known Point Predictor Errors on Dive/Glide Bomb Flight 4	4-42
4-38	Defense of Known Point Predictor Errors on Pop-up and Dive/Glide Bomb Passes	4-43

LIST OF ILLUSTRATIONS (Continued)

<u>Figure</u>		<u>Page</u>
4-39	Heading vs. Time for Data Sample	4-44
4-40	Histograms of Down-Range Prediction Error on Pass 4-6 Segment	4-45
4-41	Mean and Standard Deviations of Down Range Linear Prediction Error of Pass 4-6 Segment	4-46
4-42	Estimated Cross-Range Acceleration vs. Time	4-47
4-43	Estimated Rate of Change of Cross-Range Acceleration vs. Time	4-47
4-44	Peak Prediction Errors vs. Time of Flight for "Vigorous" Evasive Maneuvers	4-48
5-1	Specific Muzzle Energy of Guns versus Maximum Pressure and Caliber Length	5-7
5-2	Specific Muzzle Energy of Guns versus Caliber Length	5-8
5-3	Muzzle Velocity vs. Shot Weight and Caliber Length for Design Series	5-10
5-4	Propellant Weight/Projectile Weight versus Muzzle Velocity for Conventional Guns and Recoilless Rifles	5-11
5-5	Propellant Weight/Weight at Burnout versus Burnt Velocity for Rockets	5-17
5-6	Comparison of Propellant Weight Requirement for Rockets and Gun Launched Projectiles	5-18
5-7	Weight of Projectile/Weight of Complete Round vs. Muzzle Velocity for Gun Fired Projectiles	5-22
5-8	Payload Weight/Complete Round Weight vs. Burnt Velocity for Rockets	5-24
5-9	Muzzle Velocity versus Projectile Weight for Specific Guns and Projectile Design Variants	5-26
5-10	Drag Buildup of Cone Cylinder	5-27
5-11	Drag Coefficient Variation with Mach Number for Spin Projectiles	5-29
5-12	Drag Coefficient of 35-mm Projectile, Inferred From Firing Tables	5-33
5-13	Tube Life of Guns vs. Firing Rate and Firing Time Parameter	5-35

LIST OF ILLUSTRATIONS (Continued)

<u>Figure</u>		<u>Page</u>
5-14	Payload to Complete Round Weight Ratio vs. Total Velocity and Gun Boost Velocity for Conservative Rocket Case Weight	5-44
5-15	Payload to Complete Round Weight Ratio vs. Total Velocity and Gun Boost Velocity for Lightweight Rocket Case	5-44
5-16	Payload to Complete Round Weight Ratio for 2200 m/s Total Velocity vs. Gun Boost Velocity	5-45
5-17	Payload to Complete Round Weight Ratio for 1100 m/s Total Velocity vs. Gun Boost Velocity	5-45
5-18	Design Trade-offs for Boosted Rounds with Lightweight Rocket Case and Specific Payload	5-46
5-19	Design Trade-offs for Boosted Rounds with Conservative Rocket Case Weight and Specific Payload	5-47
5-20	Flow Diagram of a Predicted-Corrected Projectile Air Defense System with Mid-Course and Terminal Loop Closures	5-54
5-21	Intercept Geometry	5-60
5-22	Zones within which Required Lateral Acceleration of Line of Sight Beam Rider Exceeds Specified Values	5-63
5-23	Roland System Coverage and Effectiveness	5-63
5-24	Assumed Warhead Terminal Effectiveness	5-70
5-25	Minimum Gun Caliber to Develop Specified Muzzle Energy	5-72
5-26	Comparison of Cost/Kill vs. Incoming Target (Head-on)	5-76
5-27	Comparison of Cost/Kill vs. Passing Target (Near Midpoint)	5-76
5-28	Rounds/Kill of Conventional AA Gun Systems	5-77
5-29	Effect of Weight of Warhead plus Control Package on System Characteristics	5-77
5-30	"A Solution this Large is Not Recommended"	5-79
5-31	Sketches of L/D = 10 Configurations	5-80
5-32	Sketches of L/D = 15 Configurations	5-81

LIST OF ILLUSTRATIONS (Continued)

<u>Figure</u>		<u>Page</u>
6-1	Body Diameter and Length of Missiles versus Maximum Range	6-3
6-2	Average Missile Velocity versus Average Range	6-4
6-3	Ratio: Wall Thickness/Outside Diameter of Cylindrical Warheads versus Fraction of High Explosive by Weight	6-9
6-4	Body Diameter versus Warhead Weight of Missiles	6-10
6-5	Approximate Side Wall Thickness versus Warhead Weight	6-10
6-6	Penetration Regions	6-12
6-7	Penetration of Dural and Titanium by Ball Ammunition versus Impact Velocity	6-14
6-8	Penetration of Dural and Titanium by Ball Ammunition versus Impact Pressure	6-14
6-9	Penetration of Steel Plate versus Impact Velocity	6-15
6-10	Penetration of Steel Plate versus Impact Pressure	6-15
6-11	Penetration Capability of Shaped-Charge Antitank Missiles	6-16
6-12	Vulnerable Area of Cylindrical Warheads	6-20
6-13	Penetration Capability of AP Projectiles Scale From Oerlikon 35-mm APT	6-24
6-14	Penetration Capability of High-Density Subcaliber Penetrators versus Range	6-26
6-15	Vulnerable Area of 200 kg GP Warhead to Full Caliber 40-mm AP Projectiles	6-28
6-16	Vulnerable Area of 200 kg GP Warhead to Full Caliber 40-mm AP Projectiles versus Crossing Range	6-28
6-17	Vulnerability Regions of 200 kg GP Warhead to Full Caliber AP Projectiles	6-29
6-18	Vulnerability Regions of 200 kg GP Warhead to Subcaliber High Density Projectiles	6-30
6-19	Vulnerability Regions of 200 kg GP and SAP Warheads to Subcaliber High Density Projectiles	6-31

LIST OF ILLUSTRATIONS (Continued)

<u>Figure</u>		<u>Page</u>
6-20	Probability of Detonating 200 kg Warheads with Guns Firing High Density Subcaliber Projectiles	6-31
7-1	Geometry of Cooperating Stations	7-14
7-2	Range Error of Two Station Ranging System versus Target Position	7-16
7-3	Range Error of Two Station Ranging System with Only One Station in Error	7-18
8-1	Cost of Gun Barrels versus Weight	8-4
8-2	Weight of Gun Barrels versus Caliber	8-5
8-3	Automatic Cannon Costs versus Caliber	8-6
8-4	Cost of Vehicles for Air Defense Fire Units versus Weight Loaded	8-9
8-5	Cost of Unguided Rockets versus Weight	8-14
8-6	Cost of Conventional Bombs versus Weight	8-16
8-7	Annual Cost per Soldier on Active Duty	8-17
8-8	Cost of Antitank Missiles vs. Launch Weight	8-21
8-9	Annual Operating Costs of Missile Battalions vs. Number of Personnel	8-27
8-10	Price of 1973 Airborne Weather Radars vs. Weight	8-29
8-11	Price of 1973 Airborne Weather Radars vs. Power	8-30
8-12	Price of 1973 Radar Altimeters vs. Weight	8-30
8-13	Price of 1973 Autopilots vs. Weight	8-31
8-14	Price of 1973 Transceivers vs. Transmitter Power	8-32
B-1	Geometry	B-2
B-2	Required Tracking Beam Half Width for Terminal Correction at Midpoint of 5 Mil Bias vs. Time Lag and Range	B-3
B-3	Region Outside of Which a 5 Mil Bias Error Can be Corrected vs. Lag Time for 5° Half Beam Width	B-4

LIST OF ILLUSTRATIONS (Continued)

<u>Figure</u>		<u>Page</u>
B-4	Region Outside Which a 5 Mill Bias Error Can be Corrected vs. Lag Time for 2.5° Half Beam Width	B-5
B-5	Correctable Bias Error at Midpoint Versus Range and Beam Width	B-6

LIST OF TABLES

<u>Table</u>	<u>Page</u>
III-1 Categorization of System Error Components	3-6
III-2 Firing Time vs. Release Range	3-22
III-3 Average Range vs. Release Range	3-22
III-4 Computation of Target Kill Probability	3-23
III-5 Comparison of Kill Probabilities	3-25
III-6 Methods of Sensing Projectile Miss Distances	3-29
III-7 FLIR Types	3-32
III-8 Estimating Relationships for Radar Cross Section in the Optical Region	3-44
III-9 Estimated Optical Region Cross Section Referenced to Geometric Cross Sectional Area	3-46
III-10 Estimating Relationships for Radar Cross Section in the Rayleigh Region	3-48
III-11 Estimated Radar Cross Section of Trihedral	3-52
III-12 Measured Radar Cross Section of Projectiles (Maximum in Tail Aspect) at 70 GHz	3-59
III-13 Comparison of Estimated Radar Cross Sections of Shaped Bases versus View Angle	3-69
III-14 Comparison of Estimated Laser Cross Sections of 30-mm Projectiles versus Base Shap (db Relative to 1 Square Meter)	3-73
III-15 Assumed Characteristics of Imaging Sight	3-81
III-16 Estimated Signal/Noise Ratio of Projectiles at 3-km as Viewed by Imaging Sight	3-84
III-17 Color Scale of Temperature	3-86
III-18 Summary of Estimation and Control Algorithms	3-104
III-19 Assumed Standard Deviations	3-121
IV-1 Minimum Simultaneous Prediction Errors with Defense of Known Point Predictor on Dive/Glide Bomb Passes	4-40

LIST OF TABLES (Continued)

<u>Table</u>		<u>Page</u>
V-1	Qualitative Comparison of System Characteristics	5-4
V-2	Characteristics of Free Rockets	5-13
V-3	Characteristics of Gun-Boosted Rockets	5-14
V-4	Case Weights	5-20
V-5	Equivalent Drag Coefficients at Mach 2.0 of Operational Projectiles	5-31
V-6	Equivalent Drag Coefficients at Mach 2.0 of Developmental and Low Drag Design Projectiles	5-32
V-7	Weights of Rocket Launchers	5-41
V-8	Comparison of Characteristics of Fire Units	5-50
V-9	Effectiveness Comparison	5-51
V-10	Estimates of Cost/Kilogram of Projectile Types	5-52
V-11	Trajectory Options for SAMS	5-56
V-12	Projectile Position Sensing Options (Non-Homing Missiles)	5-57
V-13	Command Channel Options	5-59
V-14	Methods of Obtaining Control Moments	5-59
V-15	Comparison of System Characteristics	5-74
V-16	Effectiveness - Cost Estimates	5-75
VI-1	Equivalent Mirador Detection Ranges	6-6
VI-2	35-mm Oerlikon Ammunition	6-16
VI-3	Penetration Capability of Shaped Charge Antitank Warheads	6-17
VI-4	Sensitivity of Explosives to Bullet Impact	6-18
VI-5	Assumed Warhead Characteristics	6-27
VII-1	Probable Errors in Measuring Slant Range with Single and Multiple Station Passive Ranging Systems from Proving Ground Experiments	7-13
VIII-1	Cost of Antiaircraft Gun Fire Units (Towed or Fixed Installations)	8-2

LIST OF TABLES (Continued)

<u>Table</u>		<u>Page</u>
VIII-2	Cost of Antiaircraft Gun Fire Units (Self Propelled)	8-3
VIII-3	Cost of Automatic Cannon for Aircraft	8-7
VIII-4	Turret Weights of Air Defense Fire Units	8-10
VIII-5	Comparative Costs of Congreve Rockets and Mortar Shell in 1810	8-12
VIII-6	Costs of Unguided Rockets	8-13
VIII-7	Rocket Program Costs (Millions of Dollars)	8-14
VIII-8	Costs and Characteristics of Conventional Bombs	8-15
VIII-9	Costs of Surface To Air Missiles	8-18
VIII-10	Costs of Air to Surface Missiles	8-22
VIII-11	Cost of Surface to Ship Missiles	8-23
VIII-12	Costs of Antitank Missiles	8-24
VIII-13	Bullpup Price History	8-25
VIII-14	Estimated Price vs. Quantity for SRAM	8-25
VIII-15	Cost of Ownership of Sam Systems	8-26
IX-1	Velocity and Acceleration Inputs for Straight Line Test Paths	9-3
IX-2	Simulation Test Problem for Level, Constant Velocity Path	9-5
IX-3	Simulation Test Problem for Climbing, Decelerating Path	9-6
IX-4	Residual Errors on Circular Paths	9-7
IX-5	Simulation Test Problem for Circular Path	9-8
IX-6	Filter Constraints	9-10
IX-7	Least Squares Filter Coefficient Algorithms	9-10
IX-8	Example of Least Squares Filter Coefficients	9-12
IX-9	Computation of Miss Distances Resulting From Tracking Biases on Circular Path	9-15

LIST OF TABLES (Continued)

<u>Table</u>		<u>Page</u>
IX-10	Simulation Generated Miss Distances For Various Tracking Biases on Path C3	9-16
IX-11	Comparison of Simulation Results with Desk Calculator Computations on Path C3	9-16
IX-12	Projectile Inputs	9-19
IX-13	Single Shot Kill Probabilities Obtained From Simulation	9-20
IX-14	Single Shot Kill Probabilities Obtained By Desk Calculator	9-21
A-1	Bias Errors of T5 and T6 Radars in Proving Ground Tests	A-2

SECTION 1

INTRODUCTION

During the period of performance of this contract, antiaircraft automatic weapons again demonstrated their effectiveness against modern aircraft in the Mideast War. The value of guns to complement surface to air missiles in a complete defense configuration was again confirmed. Guns shot down Styx standoff missiles according to Aviation Week, maintaining a record that began when guns accounted for half of the V-1 pilotless aircraft destroyed by defenses in World War II.

The Army initiated the GLAADS prototype air defense gun system development, utilizing up to date technology. Field test and evaluation programs such as HITVAL are underway to obtain objective assessments of predicted fire systems using modern instrumentation.

Several programs have been activated to exploit an ability to measure projectile miss distances and the ingenuity of systems designers continues to generate potentially feasible sensor/data processing solutions for "closed loop" improvement of predicted fire systems.

Meanwhile the annual cost per man in uniform has escalated to a level which makes the trade-off between personnel costs and hardware costs of military systems of critical importance.

The present reports have been developed against this background of renewed activity and appreciation of guns as effective and economical components of air defense systems.

SECTION 2

SUMMARY

The purpose of the reported supplemental effort is to provide additional analyses and evaluations of potential closed loop predicted fire systems for air defense, to assess and interpret experimental data on actual aircraft flight paths in terms of predictability, to examine the potential of rocket and rocket-boost projectiles in comparison with conventional gun fired projectiles, and to consider what advantages may lie in a system using control of projectiles in flight along a predicted trajectory. Additional and timely objectives are to consider the capability of predicted fire systems against standoff munitions and ways in which predicted fire systems may be made less susceptible to enemy countermeasures. Another objective is to develop verification procedures for the Litton simulation.

An additional task, developed in considerable detail in Volume II, has the objective of determining the implications, in terms of required computer characteristics, of a modern digital computer solution of the predicted fire problem, including closed loop algorithms.

The immediately subsequent subsections summarize the major conclusions and recommendations of this work. The recommended programs are discussed in greater detail in the final sections of this report.

2.1 CONCLUSIONS AND RECOMMENDATIONS

The principal conclusions and recommendations appropriate to each major subdivision of the effort are collected in the following subsections by topic.

2.1.1 Frankford Arsenal Aircraft Capabilities Test (FACT) Data

Conclusions:

- a. The prompt acquisition of the initial data base by Mr. Stanley Goodman and Mr. Kenneth Heulitt of Frankford Arsenal with the complete and enthusiastic cooperation of the U.S. Navy is a tour de force of cost-effective experimental planning and execution.
- b. The existence of a predictable segment of useful length on all attack paths was demonstrated. Determination of its microstructure, which fell generally within the noise band of the instrumentation radar is now of high priority.

- c. Energy conservation by aircraft on diving passes was verified and algorithms employing this characteristic will improve prediction accuracy.
- d. Dive angles are not constant during an attack pass but exhibit a characteristic pattern over all attack types which may be exploited in prediction algorithms.
- e. In turns, aircraft held turn rate remarkably constant for the duration of a turn, and the rates of turn were of about the same magnitude across many passes.
- f. An unexpected characteristic of bombing passes was the existence of a segment of several seconds duration about 7 seconds prior to munition release during which the aircraft pointed its velocity vector directly at its ground target.

Recommendations:

- a. The FACT program should be continued and augmented to include accelerometer records on aircraft, and to obtain attack path data for helicopters, aircraft launching standoff controlled munitions, and the trajectories of the standoff munitions themselves.
- b. The FACT data base should be used to develop improved prediction algorithms.
- c. The FACT data base should be used to evaluate proposed prediction algorithms.

2.1.2 Closed Loop Predicted Fire Systems

Conclusions:

- a. The outstanding advantage of closed loop systems is their potential ability to provide automatic, dynamic calibration of predicted fire systems in the field and in combat. System errors which appear in the field, and cause "operational degradation" are believed to be grossly underestimated in most systems analyses.
- b. A data base on causes and magnitudes of field degradation of existing and past predicted fire systems does not exist.
- c. Prediction errors resulting from target maneuvers can be separated from errors resulting from imperfect sensor to gun calibration, wind and other exterior ballistic effects, and muzzle velocity biases, and each set of error sources in this dichotomy can be processed according to its unique characteristics.
- d. Errors resulting from target maneuver are judged to be best attacked in the open loop prediction module, since the data rate on target derivatives is higher and

tracking sensor noise is probably lower than the noise associated with projectile miss measurements.

- e. Error sources contributing to projectile miss distance can be divided into two categories, (1) those which result in miss vector components perpendicular to the flight path (azimuth and elevation bias and wind, etc.) and (2) those which result in miss vector components parallel to the flight path (range bias, muzzle velocity bias, etc.). The first category can be reduced by a "2-D" closed loop system which requires no range sensing on the projectile; for example by tracer sensing with FLIR. Reduction of the second category of error source requires miss measurements when the projectile is at the target range and, hence, requires ranging on the projectile. Within its category, a 2-D system has a lower information acquisition rate than a 3-D system, and so requires more observations for the same reduction in source errors.
- f. In order for a closed loop system to perform successfully when several fire units are engaging the same target, each system must be able to discriminate between its own projectiles in the vicinity of the target and those fired from other mounts.
- g. The optimal use of a closed loop system is judged to result from its use in a combination of precombat calibration firings and subsequent corrections during actual engagements.
- h. In order of increasing technical risk, sensors for observing the projectile miss distances are judged to be
 - (1) Radar (demonstrated) 3-D
 - (2) FLIR with projectile tracer, 2-D
 - (3) Optical Radar
 - (4) Cooperative FLIR/Laser, 3-D
- i. A conservative estimate is that if a closed loop predicted fire system is compared against an open loop system using the best current technology with on-mount muzzle velocity measurement, precise doctrinal calibration, and local, current meteorological data, the closed loop system will not show an advantage as great as a factor of 2.0. However, under realistic combat conditions improvement factors of over 4.0 are expected. Hence proving ground tests should be planned to introduce severe operational environments, and to establish the magnitude frequency and source of operational degradation.

2.1.3 Rocket and Rocket Assisted Projectile Predicted Fire Systems

Conclusions:

- a. Systems utilizing rocket propulsion elements for air defense without projectile guidance are considered to be dispersion limited.
- b. RAP projectiles may achieve shorter times of flight to specified ranges for the same warhead weight and complete round weight than conventional projectiles, but the time of flight advantage may be lost to the increased angular and time of flight dispersions.
- c. RAP projectiles may have a cost disadvantage because of their greater manufacturing complexity, and the development cost associated with any new ammunition development program.
- d. If the dispersion, and cost handicaps can be reduced, a system using RAP may have higher effectiveness beyond two or three km for given cost, and lower fire unit weight than a system using conventional projectiles.
- e. Sensor and computer requirements for RAP are essentially identical to those of conventional systems.

Recommendations:

- a. No new development activity of unguided RAP systems should be undertaken at this time.
- b. Javelot, which is reported to have the objective of achieving RAP dispersions competitive to gun fired unboosted projectiles, should be critically observed in development and demonstration firings to determine the feasibility and possible difficulties in achieving these objectives.
- c. Moderate analytical effort should be conducted possibly using Javelot as a point of departure, to fix the achievable dispersions of RAP projectiles and their probable development and production costs.

2.1.4 Predicted-Corrected Projectile Systems:

- a. The concept of a projectile controlled to fly a minimum energy path to target intercept appears to offer attractive potential for low cost per target kill at

ranges both overlapping and extending considerably beyond the effective ranges of uncontrolled predicted fire systems.

- b. A system using a gun-launched unboosted projectile has potential advantages over both RAP and rocket solutions and may be feasible using a gun of less than 75 mm caliber.
- c. Such a system would have the advantage of both conventional predicted fire at short ranges, and controlled projectile fire at medium to long ranges.
- d. A principal current uncertainty is the degree to which the cost and weight of the on-board control package can be reduced. In particular, the gun caliber required depends on the control package weight.
- e. The possibility exists of using a "closed loop" module to apply terminal corrections to eliminate the boresight errors which have plagued predicted beam riders in the past. This requires that in the terminal phase the target tracking sensor acquire and command the projectile. However, in those cases where there is insufficient time to realize the full correction on the first projectile sensed, subsequent projectiles will benefit from the error reduction in the system achieved on the first round sensed. The closed loop element would also be operative for improvement of the prediction solution for the alternate conventional projectile firings.

Recommendations:

- a. Continue and expand the systems analysis activity for this type of solution.
- b. Emphasize control package definition, sensor selection, and complete system definition.
- c. Consider the system type as a potential future replacement for Croale, Roland, Rapier types of beam riders, with range capability to the order of 7-9 km.
- d. Emphasize minimum cost of expendable munitions.
- e. Emphasize minimum weight of the fire unit consistent with muzzle energy requirements to obtain good mobility.

2.1.5 Defense Against Standoff Munitions

Conclusions:

- a. Currently operational foreign predicted fire gun systems have a demonstrated defense capability against the larger, subsonic lift-supported class of standoff unmanned vehicles. In particular, the Israeli SAAR boats, armed with 40-mm guns are reported to have shot down STYX missiles.
- b. It is desirable to extend the capability of the local defenses to include defense against smaller and faster standoff munitions.
- c. This extension is possible and does not require unacceptably large gun calibers.
- d. Target acquisition of small vehicles and tracking at high angular derivatives are considered to be the pacing problems.
- e. The objective should be to force an enemy to use more expensive and complex standoff weapons than those which he can use if the defense has no capability against them.
- f. Active defense against all standoff weapons would be prohibitively costly, and there should be a reasonable compromise between incremental defense effectiveness against the less sophisticated standoff weapons and incremental defense system cost.

Recommendations:

- a. Continue systems analyses of local defense modifications to successfully engage small standoff munitions emphasizing sensor capabilities, projectile/target terminal relationships with experimental verification, and utilizing recorded munitions trajectories to optimize prediction algorithms.

2.1.6 Countermeasures Resistance

Conclusions:

- a. Mideast War experience demonstrates that defense systems using active sensors are not easily negated by electronic countermeasures.

- b. Defense systems with multiple sensor options are both difficult to countermeasure, and induce uncertainty in the plans of the attacker. They also impose a logistics load of countermeasures on him which subtracts from his munitions delivery capability.
- c. All air defense systems should possess an operational mode, either primary or back-up, which requires only passive sensors.
- d. Since angular information can be obtained by visual tracking, by FLIR tracking, or by track on strobe of an on-board jammer, target range is the remaining sensor input required to complete a predicted fire solution. This can be obtained by exchanging passively obtained angular measurements across separated fire units.

Recommendations:

- a. Development of fire control systems for predicted fire should include data links among fire units, and a data processing module in the fire control computer to convert the separately obtained angular measurements (in continuous angular tracking at each station) into slant range to target from and for each fire unit's individual computation of its gun orders.

2.1.7 Data Acquisition and Field Test

Conclusions:

- a. Many fundamental areas of analysis of predicted fire systems are still subject to conjectural estimates as opposed to interpretations of experimental data.
- b. In addition to the FACT program, experimental determination of system component performance is necessary.
- c. The Army's air defense program includes a number of field tests of predicted fire systems, some of which are in process or completed. Current and future tests include GLAADS, Javelot, and the equipment complex employed in HITVAL.
- d. It is essential that the test data be considered not only as a means of evaluating complete systems, but also as a means for identifying sources and magnitudes of contributions to the overall miss vectors. This information will allow an appropriate direction of future development effort to the reduction of those error sources most damaging to system performance.

- e. It is essential that the test environment include a phase simulating the most difficult combat environments to approach quantitative assessments of combat degradation and its sources.

Recommendation:

- a. The Army in-house development community involved in predicted fire control system research and development should participate actively in test planning, and should initiate a separate and continued program of analysis for exploitation of the test data in the design of improved air defense systems.

2.2 OVERVIEW OF THE REPORT

This section summarizes and highlights, in order of appearance in the body of the report, the general content of the report on the separate tasks.

2.2.1 Closed Loop Predicted Fire Systems

Section 3 develops an analysis of closed loop predicted fire systems, emphasizing the computational algorithms, but also reviewing the sensor options and their effect on the types of data processing required.

Some simple computations of the gain in effectiveness which may be realized with a closed loop system suggest that under optimum conditions, closed loop may provide only a small advantage over a modern open loop system which is properly calibrated, has current meteorological inputs and can use them, and has on-mount means for measuring muzzle velocity. However, even small boresight errors (and other possible undetected bias sources) can degrade an open loop system by large factors. These error sources can be reduced and possibly eliminated by closed loop systems.

A number of sensor/projectile/system concepts are reviewed. The possibility of correcting for some bias sources without ranging on the projectiles is described. Difficulties associated with unsynchronized FLIR/Laser systems are noted. Systems using internally generated ballistics triggered by weapon firing to choose observation instants are discussed and it is shown that such systems are "blind" to biases in the direction of the target velocity vector, such as are produced by muzzle velocity and sensor range biases.

Some estimates are made of projectile cross sections in the optical region, and it is suggested that radar and laser cross sections in this region can be significantly increased

by shaping the projectile base to a smooth surface of revolution with large radius of curvature. These are termed "Callipygean" designs. The cross section achieved does not approach that of a trihedral inscribed in the base, but would involve a minor, or negligible manufacturing cost increment as compared with trihedrals.

In the development of miss distance processing algorithms, a method for separating the errors caused by target maneuver and initial solution settling time from other bias sources is detailed. It is considered that prediction for target maneuver is best handled open loop, since both open and closed loop attempts to make this correction depend on the consistency of the target maneuver. An open loop system can observe target acceleration from continuous, accurate tracking sensor data, but a closed loop system would be inferring the same variable from projectile miss measurements at a lower data rate, and with measurements contaminated by projectile dispersion, which in turn is almost inevitably larger than the sensor tracking error.

Some examples are worked for a 3-D system, using a three error-source model. Each measurement provides two angular pieces of information, hence there are more error sources to be reduced than miss coordinates on each round. A Kalman methodology is used to assign sequential measurements to sources, with the proper allocation depending on the varying geometry.

It is shown that the Kalman algorithms always operate to reduce bias as sensed, i. e., in a plane perpendicular to the sight line at the target, even though not all sources can be eliminated in a single geometrical configuration. However, as the geometry changes, the relative contributions of bias sources to miss components change, and as observations are obtained over a number of engagement geometries all sources are eventually eliminated, even though not all may be accessible in any one geometrical configuration.

Analytical solutions are obtained for the 2-D problem, in which only angular sensing of a bullet trace past the target is possible, as for a FLIR system sensing a tracer bullet. Here there is one measurement per shot, and the example assumes two bias sources. It is shown that on a complete fly-by pass, with a total of n observations, the residual variance of each of the two assumed bias sources (elevation and azimuth) is reduced approximately as

$$\sigma^2 / (n/2)$$

where σ^2 = the variance of random error associated with each measurement. For this case, the presence of two bias sources reduces the number of effective measurements against each

source to one half the total number of measurements. This result can be extended to a rough "rule of thumb" estimator of the reduction in N bias sources, when M components of miss are measured on each of n projectiles.

In view of the fact that some bias sources (for example wind and azimuth bias) have similar effects in a particular geometrical configuration, it is concluded that system calibration doctrine using a closed loop capability should include wherever possible firings of a few rounds at each of a number of selected points in space chosen to give equally weighted exposure of the most probable bias sources. This firing might be done each morning, or after moving into a new position, to obtain as much precalibration of the system as possible prior to engagement of an enemy target. This would leave variables of the hour such as wind for combat correction. Precombat calibration using internally generated artificial target paths with actual firing represent an extension of the fixed point firing mode.

2.2.2 Analysis of Frankford Aircraft Capabilities Test (FACT) Data

This data includes experimental records of five types of attack paths of aircraft delivering munitions. The data is summarized and examined from the point of view of consistent and predictable patterns. Charts of heading, dive angle and velocity do reveal patterns which can be utilized in prediction algorithms. Target velocity and rate of change of altitude are shown to be closely interdependent on a "total energy" basis, and this fact can be used in prediction. The relationship is a special case of the "state space" description of the aircraft motion, which is a promising line for additional improvement of the prediction process.

Testing of the data for predictability and use of the data to test candidate prediction algorithms is demonstrated by application of the simplest prediction algorithm, - extrapolation based on the assumption of constant target velocity in each coordinate. The computed prediction errors obtained by this simple predictor serve as an upper limit of error against which more sophisticated predictors may be compared.

Testing of a "defense of known point" predictor against the FACT paths reveals comparatively poor performance, especially in elevation, suggesting that against aircraft targets, the algorithms as originally presented should be modified if they are to be useful. However, this set of computations reveals an unexpected and possibly exploitable characteristic of the attack paths as viewed from the ground target being attacked.

A remarkable consistency appears in the turning schedules used by aircraft in the test during the turn into an attack pass, and the breakaway after weapon release. This may

or may not be exploitable in prediction, and the relatively small number of pilots involved makes it difficult to generalize from personal habits to taught doctrine.

The data obtained on aircraft flying "laydown" delivery passes indicates very high predictability of these paths, provided only that the target can be acquired and tracked at the very low altitudes involved.

2.2.3 Rocket, Rocket-Assist and Predicted Corrected Projectile Systems

In Section 5 an attempt is made to identify the potential advantages of rocket propulsion in the projectiles of predicted fire systems. Such projectiles offer the potential of shorter flight times to specified ranges and/or lighter fire unit weight for given payload delivered to the target and weight of ammunition consumed. The higher velocities may also be obtained without serious penalties in tube life of the launching gun.

Although these potential advantages are confirmed by preliminary analysis, computations indicate that the time of flight advantage and its effect on improved probability of hitting may be lost unless angular and time of flight dispersions of the RAP rounds can be brought down to values typically expected of unboosted gun launched fired projectile systems, exclusive of fire control errors.

Some computations are developed, using a simple effectiveness model to compare rocket-boost solutions against conventional solutions in 35-40 mm caliber normalized to approximately the same fire unit weight by limiting the average recoil force of firing over a one-second burst. The best RAP solutions and the best conventional solutions develop about the same target kill probability per burst and the same weight of ammunition consumed per kill. These results are obtained assuming RAP dispersions greater than gun dispersions by a factor depending on the fraction of the total projectile velocity derived from the rocket motor.

In attempting a cost comparison, it was judged that the more complex RAP rounds would cost more per kilogram to manufacture than would conventional full caliber projectiles, with unboosted sub-caliber discarding sabot rounds occupying an intermediate cost position. On this basis, none of the solutions involving rocket elements was judged to be cost competitive with unboosted solutions in terms of dollar cost per target killed.

The computations of this comparison were intentionally kept at an elementary level, so that rocket enthusiasts who feel that the assumptions regarding the RAP rounds are unduly pessimistic can easily modify the computations as they may desire.

A preliminary analysis was made of a "predicted-corrected" projectile system, in which projectiles are guided in flight, by the simplest and most inexpensive control package feasible, to fly minimum energy trajectories to the target. This concept combines a conventional prediction algorithm with a guide beam, or track and command system for the projectiles. The possibility of utilizing a "closed loop" function at the terminal end of the trajectory is also introduced to eliminate the boresight errors which habitually plague two-sensor systems.

The estimates suggest the ballistic feasibility of a gun-fired projectile without rocket boost, capable of effective performance to extended ranges (7 to 9 km). The required gun size is ultimately determined by the estimated weight of the control package on each projectile. This determines the projectile weight, together with warhead weight, and in conjunction with the muzzle velocity required to attain the desired ranges fixes the gun caliber required to produce the specified muzzle energy. Preliminary design of a control package to serve as a basis of weight estimates was beyond the scope of the present effort, but it is suggested that a solution may be obtainable in a gun smaller than 75-mm caliber. Rocket and RAP solutions are also competitive at this top level of comparison.

Since the predicted beam can be constrained to change its direction relatively slowly, the lateral acceleration requirements on the projectile are modest. In a worst case, if the target maneuvers violently, the projectile acceleration need not exceed that of the target by more than a small margin.

Some computations of the beam width required of the target tracking sensor to sense both projectile and target in the terminal phase in time to accomplish a terminal correction for bias are given in Appendix B. This function appears potentially feasible, and since bias sensings can be made and applied sequentially as in "closed loop" operation of an uncontrolled projectile system, subsequent projectiles will benefit from bias corrections made on the first shot, even in those cases where the terminal command to the first projectile is not made in sufficient time to allow realization of the first correction.

A system concept using an unboosted but controlled rocket projectile instead of an unboosted gun fired round can be similarly configured, with savings in fire unit weight, but without the gun's ability to fire either controlled, or conventional ammunition. RAP solutions are not yet excluded.

It is suggested that the general concept has sufficient attractiveness to justify more definitive systems analysis and preliminary design.

2.2.4 Defense Against Standoff Munitions

Section 6 constitutes a review of the possibility of successfully engaging standoff missiles by local defense fire units. Principal emphasis is on the problem of defeating the warheads of such munitions by penetrating the cases. For preliminary estimates, the probability of detonating the high explosive after case penetration is approximated as an additional penetration requirement.

Computations indicate that these assumed terminal requirements can be achieved at desirable ranges with guns of acceptably small caliber. This conclusion results from the assumption that although a warhead designer can make head-on case penetration very difficult by thickening the forward warhead section, he cannot similarly thicken the warhead sidewalls without drastically impairing the warhead effectiveness. Hence in an Army defense configuration, where modest angles of projectile impact off the target longitudinal axis are possible, significant terminal potential of high-density sub-caliber rounds is indicated.

Detection and tracking of small high velocity standoff missiles at high angular derivatives may be difficult, and this aspect of the problem requires further treatment, using experimentally determined standoff munitions signatures to applicable sensors. On the other hand, the trajectories flown by the munitions should be much more predictable than those of aircraft, and optimum algorithms can be determined from experimentally recorded trajectories of standoff munitions employing typical terminal guidance modes.

2.2.5 Countermeasures Resistance

The problem of system design to minimize its vulnerability to enemy countermeasures is addressed in Section 7. A surprisingly comprehensive "state of the art survey" is achieved by assembling extracts from Aviation Week reports on the Mideast war. This summary reconfirms the value of guns as elements of air defense systems which complement surface to air missile defenses. The value of multiple sensor types and operational modes of the defense complex is noted as a means of providing resistance to countermeasures, introducing uncertainty in the enemy's estimates of attack effectiveness and probable losses of attack vehicles, and imposing on him a logistic burden in combat for countermeasures equipment, and an R&D manpower burden in pursuing the "wizard war."

Since angular tracking data can be obtained passively either with FLIR or by visual tracking in a back-up mode, target range data remains as the single predicted fire element sensor input which can no longer be obtained passively since optical range finders have been abandoned. A method is therefore described for obtaining target range continuously by

exchanging angular tracking information among two or more fire units. There is a problem in accomplishing target acquisition by multiple fire units within the limited engagement time, and a method is described for reducing the search problem of cooperating stations to search in a single coordinate rather than two coordinates. The method is applicable to visual or FLIR tracking by cooperative stations, which should provide range accuracies equal to that of radar or laser range finders, and to blind "track on strobe" of a jamming aircraft, which would provide usable but less accurate range information. Generalized graphs are provided which allow standard deviation of range error in the general case to be determined as a function of angular tracking accuracies of two cooperative stations.

The German World War II conclusion that air defense units must have a self-defense capability against attack by ground forces is reconfirmed by the indications of the Aviation Week extracts that if a forward air defense cannot be neutralized from the air, it will be assigned to ground forces for direct attack.

It is also noted, with support from the FACT data, that the simplest, and final "back-up" mode of a fire unit in self defense against air attack is to shoot directly at attacking aircraft with zero angular lead except for approximate correction for gravity drop, and that this mode for this attack path will apparently continue to have its historically demonstrated effectiveness.

2.2.6 Cost Considerations

This section continues the build-up of a cost "data bank" applicable to air defense systems, initiated in a prior report in this series. The rapid and continuing increase in military personnel costs per man per year is noted. This has two major implications, (1) in peacetime there is a critical trade-off within constrained budgets between hardware costs and personnel costs, and (2) complete systems analyses, and, at a higher level, weapon system planning, must consider how to transition from peacetime constraints to wartime conditions in the event of a major conflict. These considerations are beyond the scope of this report.

Cost data of varying reliability is also assembled on missiles and missile systems to provide an approximate preliminary reference against which predicted fire system costs may be compared. The cost advantage of gun systems over missile systems, even within ranges of comparable effectiveness, tends to be reduced as the guns are given sensor packages for target acquisition and tracking at night and in inclement weather. It is considered essential that designers of predicted fire systems maintain as a primary objective the achievement of

designs that will economically and effectively complement missiles systems to yield a defense complex at lower cost than that which might be provided by missiles alone.

2.2.7 Simulation Verification

An orderly procedure for verifying the correct operation of the principal modules of the Litton simulation is developed in Section 9. The basis of the method is the choice of a series of test problems for which the correct results can be computed separately and compared against the simulation output.

2.2.8 Program Recommendations

The final sections of this report contain program recommendations for data acquisition, system test, system analysis and advanced and exploratory development. These sections develop the findings of the prior sections in more specific detail.

SECTION 3

CLOSED LOOP PREDICTED FIRE SYSTEMS

Adjustment of fire against surface and aerial targets by visual observation of the fall of shot, tracer, or burst position, has been a part of the firing doctrine of artillerymen for generations. This closure of the loop via human observers in the case of antiaircraft fire has been outpaced by the increase in target speed, the shortening of the duration of the engagement, and "blind" firing with radar under conditions when visual observation is impossible.

Three factors have brought loop closure by projectile observation back into prominence. These are (1) the ability of modern sensors to measure the projectile miss distance, (2) the ability of modern digital computers to process the miss observations and apply the corrections in a sophisticated manner, (3) demonstration that fully automatic closed loop operation is in fact feasible by the General Dynamics Phalanx system.

In this section a number of closed loop concepts are analyzed, considering sensor characteristics, projectile signatures, data processing algorithms, and system performance. The concepts considered by no means exhaust the variety of possible solutions. If current interest in this type of predicted fire system is maintained, it is probable that many additional concepts will result from the application of the inventive ingenuity of the military technological community.

3.1 RATIONALE

The most prominent characteristic of a closed loop system for predicted fire weapons is the time lag between the application of a correction, and the observation of the result of this application in terms of miss distance at the target. The lag, of course, results from the finite time of flight of the projectile.

The gun/target geometry changes so rapidly in an antiaircraft engagement that loop closure will be effective only if corrections are applied to error sources which are relatively invariant over a time interval which is long compared with projectile time of flight. Some error sources, such as boresight errors can be corrected in the coordinate system in which they are observed. Others, such as wind or muzzle velocity, require skill in extracting the probable error sources, and by data processing assigning the corrections at the proper points in the normal lead prediction process. Fortunately, the Kalman methodology provides a systematic way of doing this.

It will be obvious that the closed loop function must be superimposed on a normal open loop prediction scheme.

We note one obvious trade-off to be considered in deciding whether to pay the incremental cost of a closed loop module: the balance of external battery calibration equipment vs. closed loop correction. Muzzle velocity can be measured directly by separate equipment for this purpose, or a closed loop module can correct for muzzle velocity bias. Wind can be obtained from the Army's meteorological net, from meteorological equipment at the battery, or it can be corrected by a closed loop module. Boresighting of the fire units can be accomplished by standard doctrine, or by closed loop.

There are also internal trade-offs. The miss associated with a maneuvering target may possibly be reduced by open loop quadratic, partial quadratic or Kalman predictors, based on open loop acceleration estimates, or the equivalent acceleration measurement can be inferred from the closed loop module.

There is, therefore, a trade-off between additional battery equipment to measure bias sources directly and eliminate them from the system, and the added sensor and computer capability on the mount to infer the same bias source magnitudes from projectile observation and eliminate them. In the former case one does not incur the time of flight delay between observation and correction, in the latter, one may reduce the amount of correction to be done in combat by periodic "calibration" firings.

However the most valuable characteristic of a closed loop system, and the one most difficult to quantify in peace time, is that it provides automatic calibration of the fire unit under combat conditions. Calibration of a fire unit under proving ground conditions is qualitatively different from calibration in combat. A mobile fire unit, moving over rough terrain, and required to go into action without time for doctrinal checkout is vulnerable to boresight errors, local meteorological variations from net data, and other sources of systematic error which require time to determine and correct by conventional methods. The advantage of closed loop is that it not only provides these corrections quickly, but that it can, if necessary, develop them during the course of an actual firing engagement.

3.1.1 Historical Perspective

A form of "closed loop" operation was possible with pre-World War II vintage large caliber antiaircraft guns using a computer, stereoscopic range finder, and time fuze ammunition. A battery was initially calibrated by firing at a selected point in space, and observing the mean position of a number of bursts in angle and range with the stereoscopic

range finder. Corrections were then applied as "spot corrections" at the computer. This calibration scheme was effective: for many years it eliminated an error source which only during World War II was determined to originate in erroneous computations on which the ballistic cams of the M-4 series directors were constructed (an incorrect gear ratio had been used in the mechanical differential analyzer used to compute the 90-mm firing tables).

It was also proposed to sense miss distances at the target in combat via the stereoscopic range finder, and apply spot corrections at the computer. This combat mode was extremely difficult to implement when several batteries were firing at the same target, and was further limited by the ability of the range finder operator to accomplish the sensings in combat to a useful degree of accuracy.

An interesting characteristic of observed fire with a computer was general knowledge at that time, and reoccurs in modern closed loop considerations: if a time fuzed projectile was fired with all computer inputs correct except target altitude, the burst position would be observed to lie exactly on the line of sight to the target.

At the lowest level of sophistication, firing with tracered ammunition and no computer (Gunner's Delight), provided a useful level of effectiveness for short range weapons such as the Cal 0.50 machine gun, in situations where the angular lead required was not great.

Col. Kerrison's drill for the 40mm gun with the Kerrison predictor (adopted by the United States as the M-5) clarified a useful characteristic of the tracer "stream" as seen by an observer which we shall use in one of the closed loop concepts described later.

The gunner, with his eye fixed on the target, sees successive tracers sweep by his line of sight with a direction and magnitude of angular velocity directly opposite to that of the target. The gunner has no effective depth position at target ranges, but he can see the tracer stream as "high" or "low" relative to the target. The Kerrison doctrine was for an operator to apply a vertical spot to bring the tracer stream into the same plane as that defined by the target velocity vector and the gun, and then, hopefully, to observe whether the stream passed in front of the target, or was obscured by the target, in the former case applying a spot correction to reduce range input, in the latter, increasing range.

This concept was adapted by Weiss to the Computing Sight M7 (course and speed "Weissight") for the 40-mm gun. The sight setter adjusted the setting of the heading arrow of the sight to bring the tracer stream in line with the target, then adjusted speed depending on whether tracers were or were not obscured by the target. The relation between observation and required correction was unambiguous, and the correction schemes of both the

Kerrison system and the Weissight worked very well in proving ground firings. It is likely that neither was operable in combat with many weapons firing simultaneously.

However, the resolution of miss distances into "in plane" and "out of plane" components is fundamental to many of the modern concepts of closed loop, since the two categories of miss component are each associated with an essentially independent category of error source.

3.1.2 Miss Vector Components

In this section we discuss the error sources which contribute to the miss vectors of the individual projectiles. The discussion is limited in the present paper to projectiles which are intended to hit the target, although most of the discussion applies to proximity fuzed projectiles. Time fuzed projectiles, which are not in current use, require separate interpretations of effect versus source in some cases.

The terms "random" and "bias" will be loosely used. If one fires a series of rounds at a target, and observes the pattern of miss distances, the pattern can be described in terms of the position of its center of gravity relative to the target, and the shot distribution about this point. Now some components of the miss vector, are truly uncorrelated across rounds, for example, the angular "dispersion" of projectiles fired from a fixed gun. Other components are clearly constant during a firing sequence, for example, an angular bore-sight error. Still other components of miss may arise from a constant "source," but their magnitude measured at the target may change with the geometry of the engagement, for example, the effect of a steady wind. Finally, some miss components will vary with time in a stochastic manner, so that successive values will be correlated in time. This category is sometimes called "aim wander." If the correlation time is long compared with the projectile time of flight, some correction for "aim wander" may be possible by closed loop.

Miss components of the "aim wander" type may result from the correlation imposed on sensor tracking errors by the open loop smoothing and prediction process, or they may result from irregularities in the target path which are not in conformity with the prediction algorithms used in the open loop solution. Considered over a complete firing segment, however, the "aim wander" aggregate may be approximated by dividing it into a "systematic" and a "random" component using Tappert's method. However, we note that if the "aim wander" can be modelled as a stochastic process with fairly consistent descriptive parameters, across firing passes, and target types, and if it has a long correlation time, the "systematic" component can be reduced by Kalman, or equivalent processing in the computer.

Possible sources of miss components are listed in Table III-1. In some cases, the magnitude of the effect on projectile miss distance will depend on whether the open loop solution of the computer has access to estimates of the source, and performs the required computation. For example muzzle velocity "bias" could be relatively unimportant if the fire unit had a built-in method of measuring muzzle velocity directly, as is done on the Oerlikon 35-mm system. Similar comments apply to wind, air density, and temperature.

Each possible error source is also categorized as to whether its resulting miss component is "in" or "out" of the slant plane defined by the gun position and the target velocity vector. Figure 3-1 shows the geometry of this plane. To be precise, we should give the "in plane" sources small "out of plane" components because of their effect on gravity drop of the projectile, however this component is so small that we can ignore it in most of the corrective algorithms.

The target/projectile geometry as viewed by a sensor, or a human observer tracking the target, is as shown in Figure 3-2. If the bullet has a tracer, a human observer sees a streak across his sight which is almost parallel to the apparent target direction, the very small difference in inclination being caused by the gravity drop vector.

As discussed later, with a sufficient number of observations at different gun/target geometrical configurations, all "out of plane" sources can be resolved by measuring simply the minimum "out of plane" angle of each trajectory. However, to resolve the sources which cause "in plane" miss components, it is necessary to know when the bullet is at the same range as the target from the gun. We call these "2-D" and "3-D" systems respectively. Anticipating later results, we also note that since a 2-D system obtains less information per projectile measurement than a 3-D system, it will require a larger number of observations over a wider range of geometrical configurations to accomplish equal error source reduction, even of the out of plane sources, than is possible with a 3-D system.

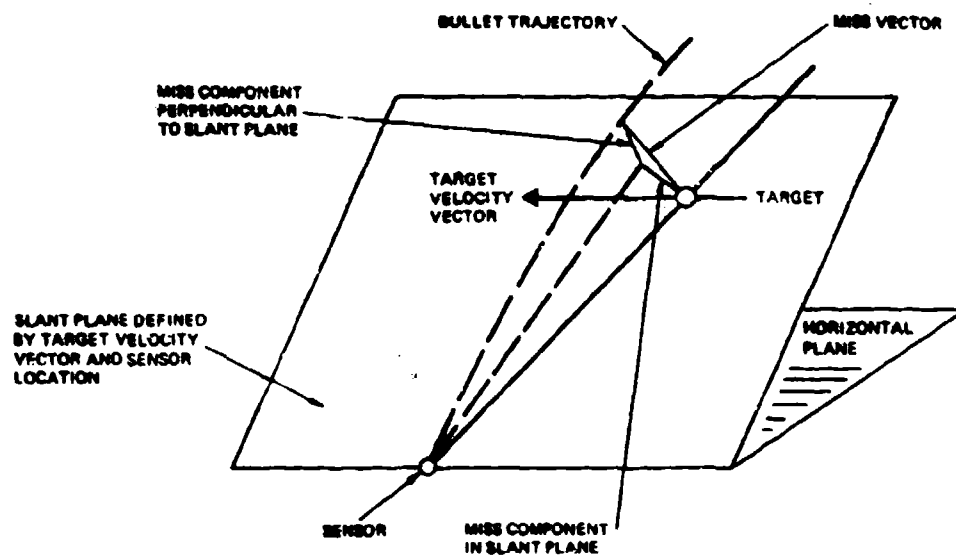
We also note that a "4-D" system is possible, if the sensor can measure bullet velocity at the target. This additional element of information will greatly improve the efficiency of the in-plane error source reduction.

3.1.3 Relative Magnitudes of Miss Vector Components

As a preliminary to estimates of the improvements which may be achieved in kill probability using a closed loop solution, a few examples are given of the miss components which may result from various sources. The examples are based on the Oerlikon 35-mm

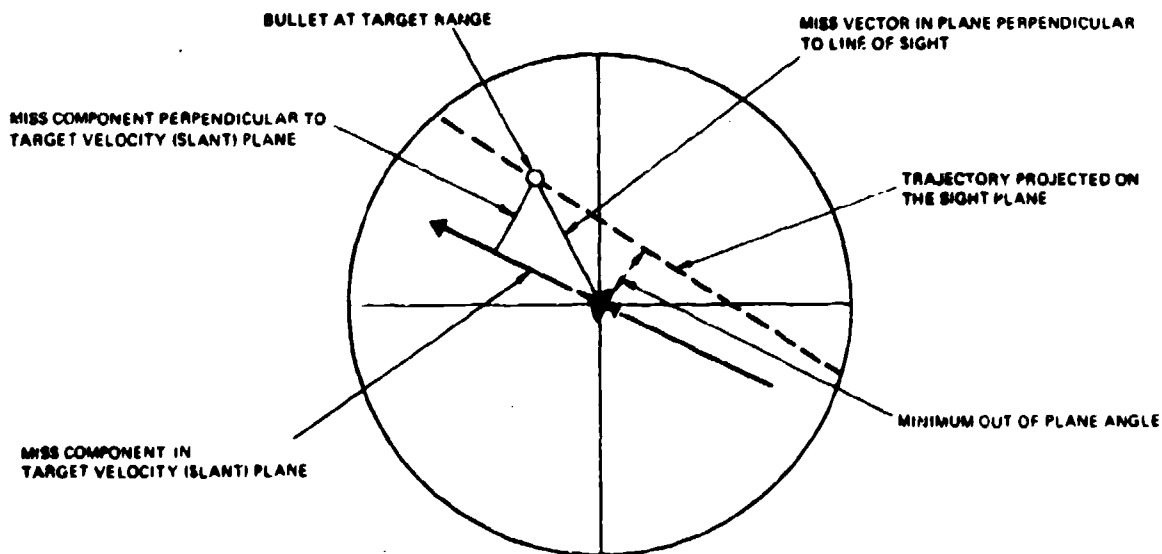
Table III-1. Categorisation of System Error Components

Source	Type of Error*		Orientation	
	Random	Systematic	"In Plane"	"Out of Plane"
Target tracking sensors	X	X	-	X
Mount levelling	-	X	-	X
Boresighting	-	X	-	X
Ammunition angular dispersion	X	-	-	X
Muzzle velocity variations	X	X	X	-
Gun vibration and tube whip	X	-	-	X
Jump and launch tip-off	X	X	-	X
Tube heating sag	-	X	-	X
Projectile weight variations	X	-	X	-
Wind	X	X	-	X
Air density	-	X	X	-
Temperature (mostly powder)	-	X	X	-
System "instrumentation" errors including servo lags, converters, computational accuracy, approximations etc.	X	X	X	X
Target path	X	X	-	X
<p>*Depending on time of flight and the length of the firing segment, error sources with X's in both components may cause miss components which may be assigned to both "random" and "bias" columns, in a proportion that can be computed once the power spectral density of the variation is known.</p>				



40001-1

Figure 3-1. Components of Miss Vector



40001 2A

Figure 3-2. Miss Vector Projected in Sight Plane

gun, since it is the only modern weapon for which a fairly complete set of ballistic tables is on hand.

Figure 3-3 shows the lateral deviation in meters caused by a 10 meter/second cross wind. The effect is relatively independent of quadrant elevation, and depends primarily on slant range. Figure 3-4 shows the change in time of flight associated with a 10 meter/second change in muzzle velocity. To convert this to miss distance at the target, it is multiplied by target velocity times the sine of the angle between the velocity vector and the trajectory direction, and is a maximum at midpoint.

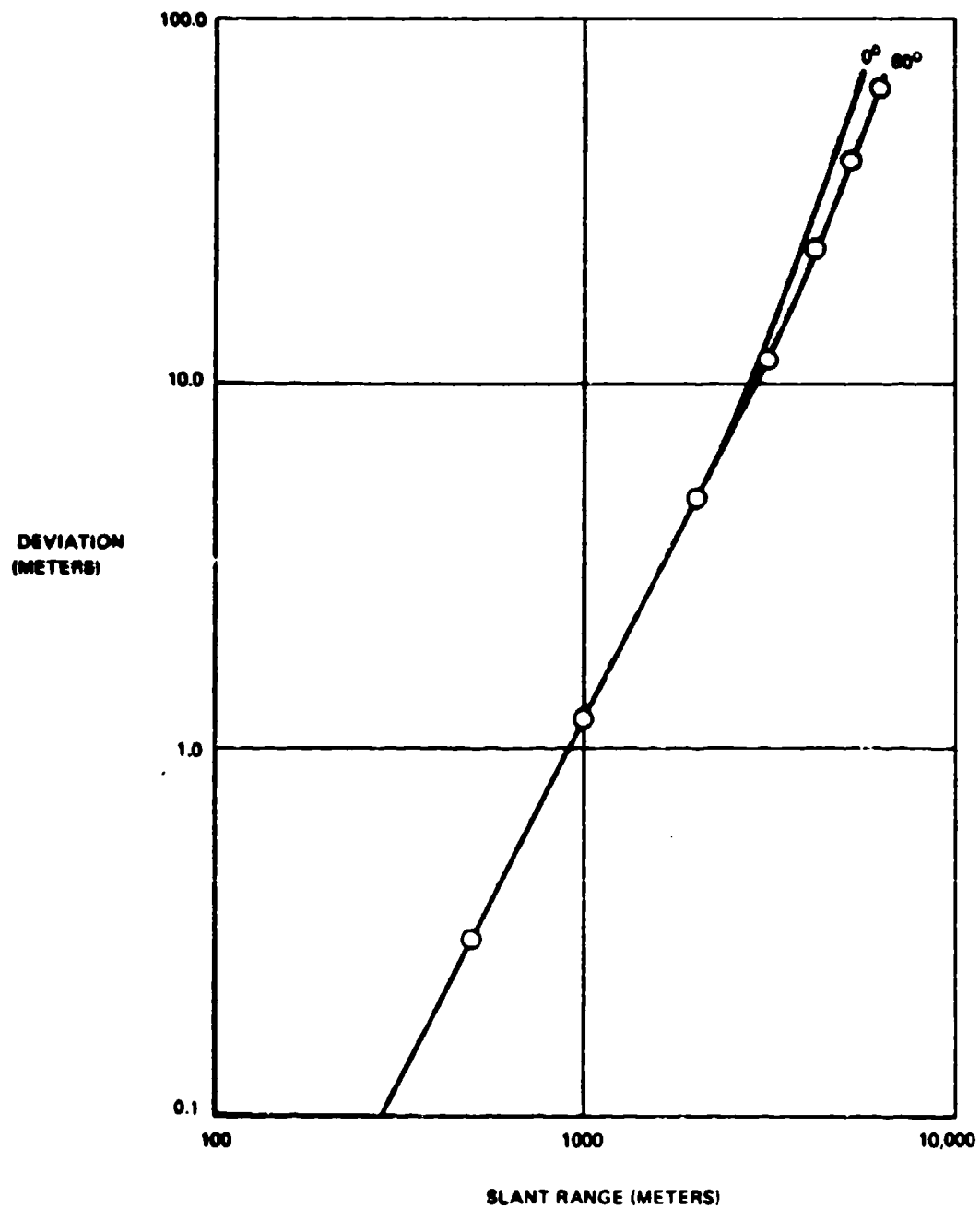
Expressions for the effect of air density, projectile weight, etc., will be found in the first AFAADS report.^① Small changes in projectile weight are probably of minor importance. A slightly underweight projectile emerges at a slightly higher muzzle velocity, but slows down more rapidly; the effects compensate in part, and there is a range at which the net effect is zero.

An average time of flight vs. range curve for the Oerlikon is shown in Figure 3-5. For present purposes, the variation with quadrant elevation can be ignored.

The effects of a number of error sources in terms of miss at the target are summarized in Figure 3-6 for "bias" components, and in Figure 3-7 for "random" components. Those components affecting time of flight ("in-plane components") are shown as computed at target path midpoint. Note that at midpoint, a 20 m/s muzzle velocity bias would have about the same effect as a constant 3-mil angular bias.

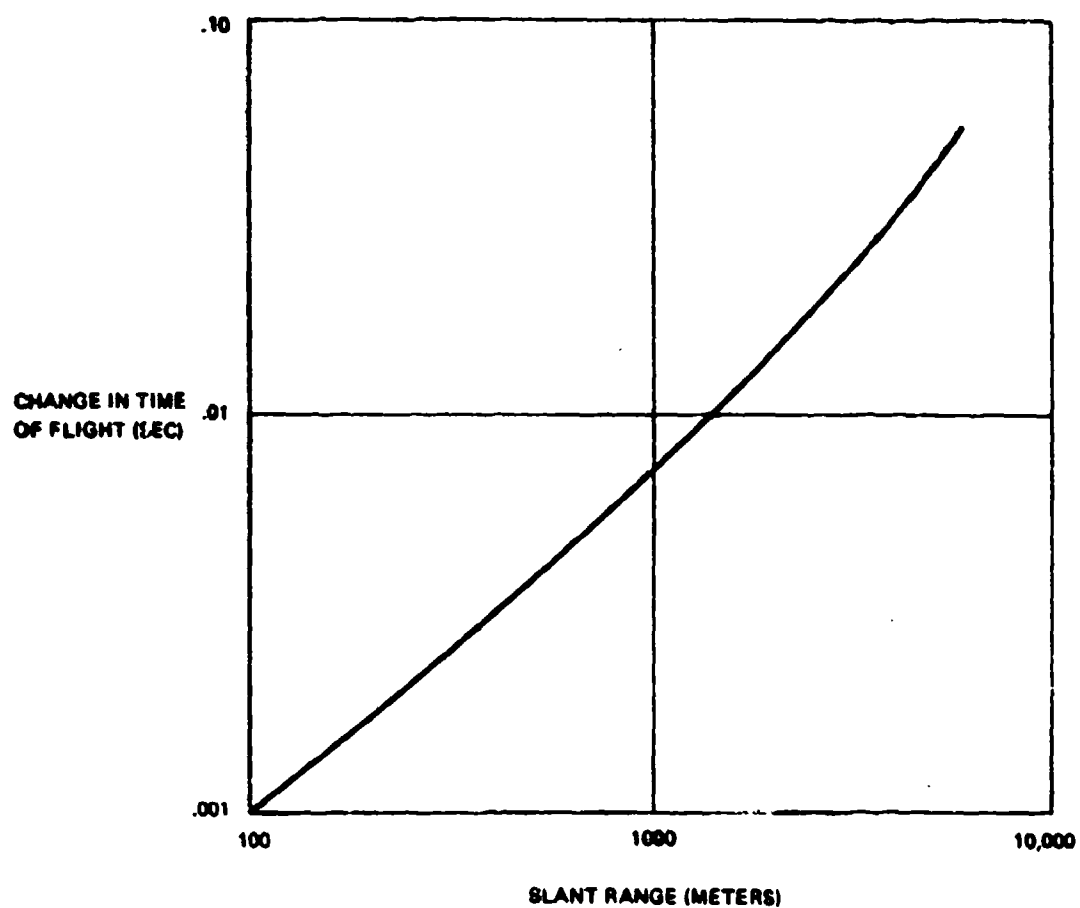
To estimate the prediction error resulting from sensor noise for radar, we assume a mean standard deviation of tracking error laterally and vertically of 1.50 meters, independent of range. For FLIR tracking, we assume a standard deviation in each angular coordinate of 0.30 mils. For the head-on paths used in later computations, range errors have a minor effect on prediction errors, and are not considered in this section. The variance of prediction error is estimated, assuming a "linear" predictor, according to the expression

$$(\sigma_p/\sigma_0)^2 = 1 + 2(t_p/T_s) + 2(t_p/T_s)^2 \quad (3.1)$$



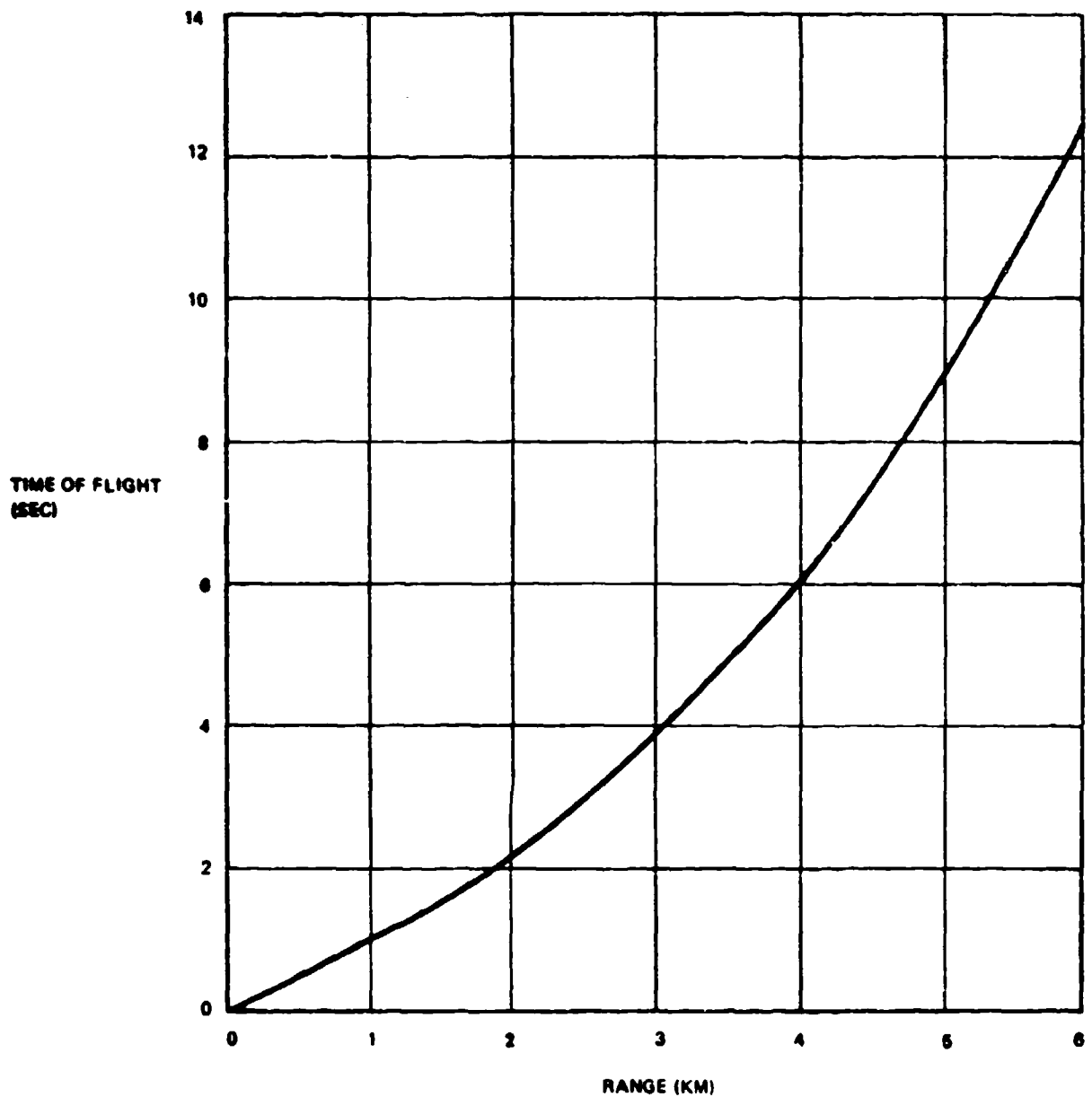
40001-3

Figure 3-3. Slant Range (Meters)



40001-4

Figure 3-4. Slant Range (Meters)



40001-5

Figure 3-5. Time of Flight vs. Slant Range

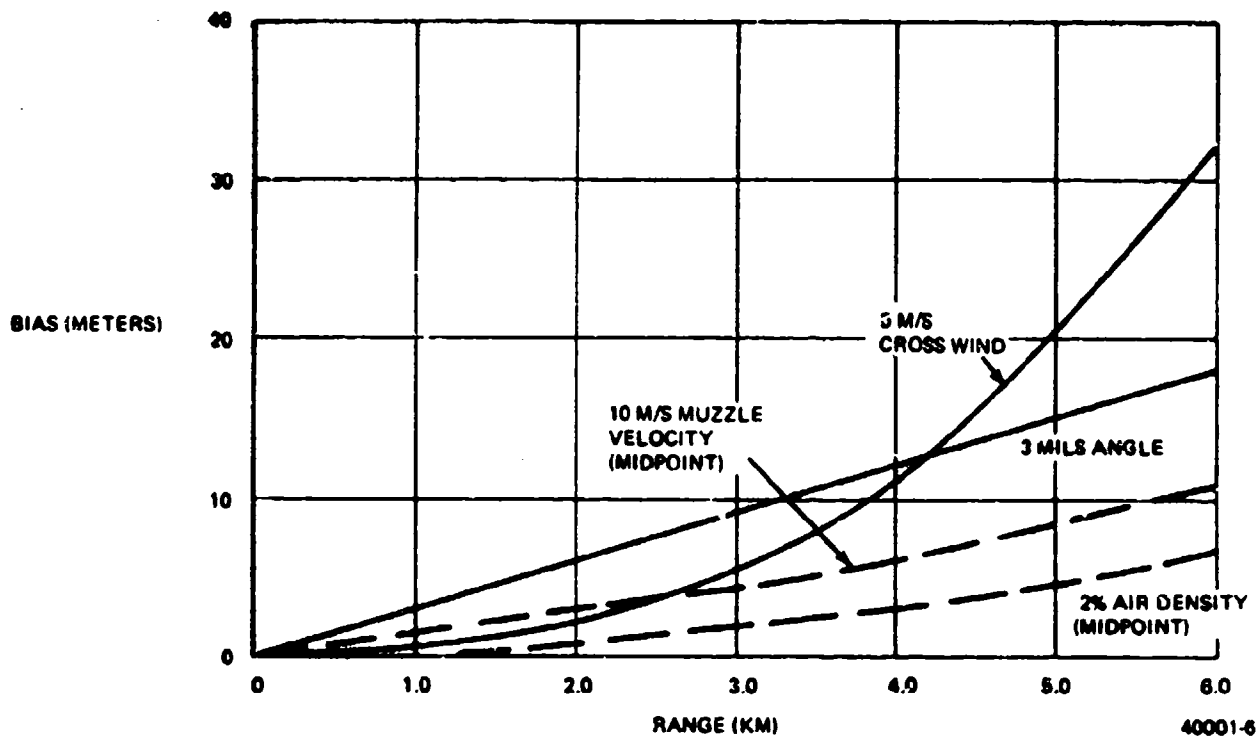


Figure 3-6. System "Bias" Components

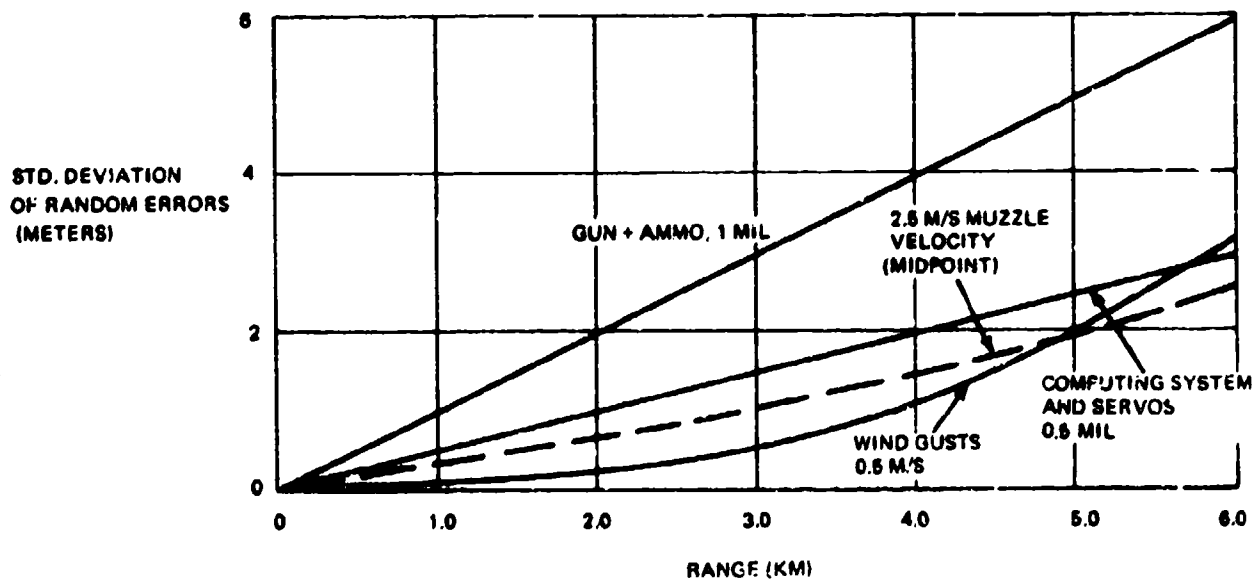


Figure 3-7. System "Random" Error Components

40001-7

where

σ_p^2 = variance of prediction error

σ_0^2 = variance of sensor error

t_p = time of flight

T_s = computer smoothing time.

Figure 3-8 shows the resulting standard deviations of prediction error from this source vs. slant range with 1-second smoothing, and Figure 3-9 shows the effect of $t_p/2$ smoothing. Note the advantage of increasing smoothing time with time of flight in minimizing this component.

The error component is correlated in time because of the finite band width of the tracker, the signature variations, and the smoothing interval. We divide it into two components using Tappert's method. The smoothing time is probably the dominating factor (narrowest band width).

If a burst of duration T_b is fired, Tappert's method gives

$$\text{"Bias" Component: } \sigma_{pb}^2 = \sigma_p^2 e^{-(2/3) T_b/T_s} \quad (3.2)$$

$$\text{"Random" Component: } \sigma_{pr}^2 = \sigma_p^2 [1 - e^{-(2/3) T_b/T_s}] \quad (3.3)$$

The characteristics of aircraft flying attack paths of various types are discussed extensively in Section 4 of this report in which the FACT experiments are summarized.

The FACT data indicates that on some target runs, the target accelerations perpendicular to the target path are so small that their effect is difficult to separate from the measurement errors of the tracking radar employed, about a 3 -5 meter standard deviation. The velocity increase on a diving path is just about that which would be expected from the projected component of gravity, and is correctable in the computer.

In considering the components of miss which should be associated with "bias" as compared with "random errors" over a firing segment, a proper analysis requires a more precise determination of target accelerations, with tracking noise removed. It is hoped that this data will be available in the near future.

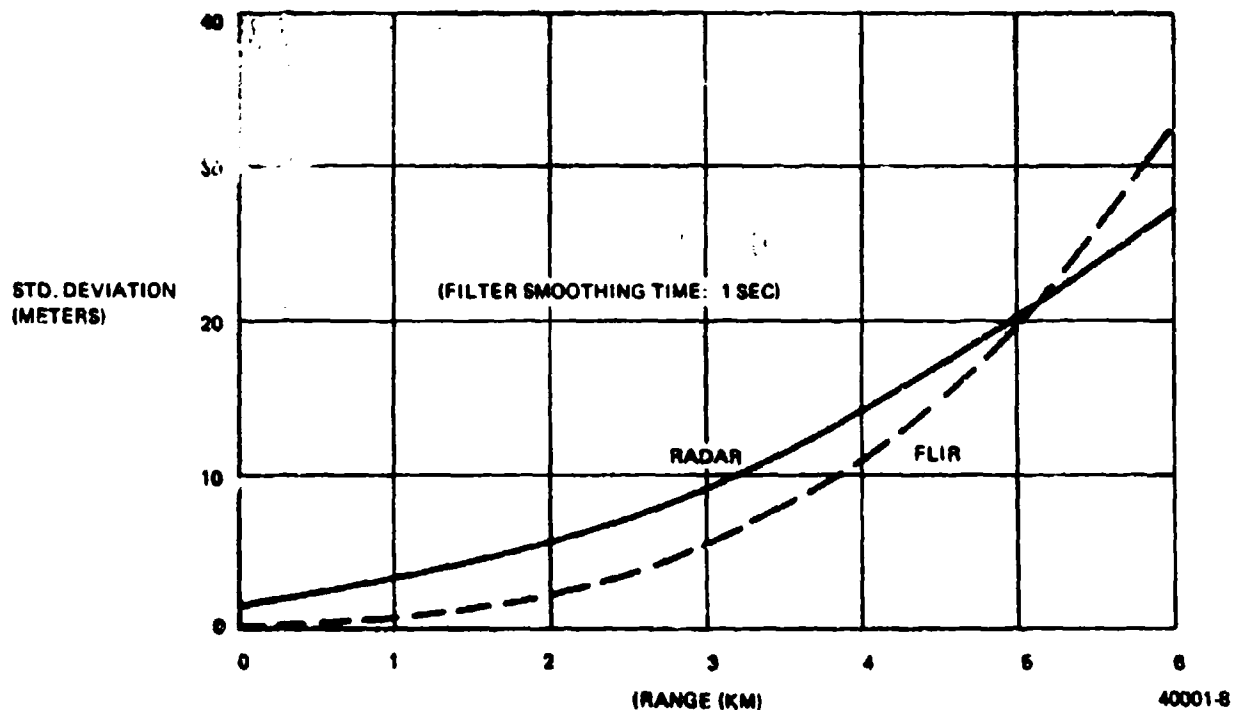


Figure 3-8. Standard Deviation of Prediction Error Caused by Angular Tracking Error

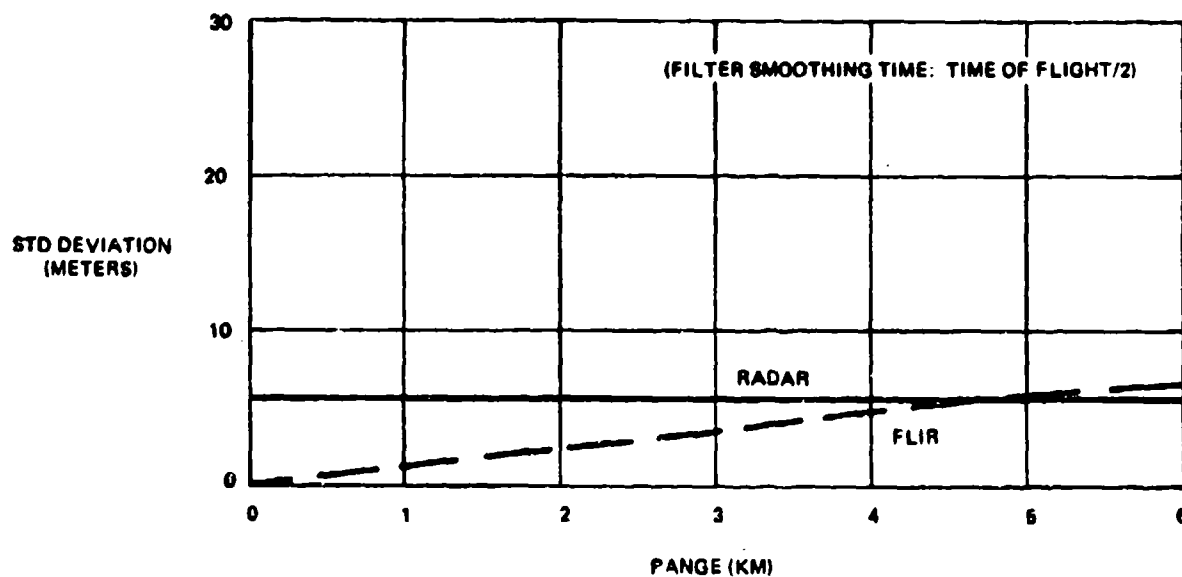


Figure 3-9. Standard Deviation of Prediction Error Caused by Angular Tracking Error

For the present assessment, we assume that the target path is characterized by a mean acceleration which lies between about 0.0 and 0.4 g; (0 to 4 meters/sec²). Variations about this mean are assumed to be slow, so that there is no increase in the random component of miss from this source. With autocorrelations of the target acceleration available, one could consider the effect of using quadratic or Kalman prediction, both of which would reduce the mean acceleration, and increase the random component.

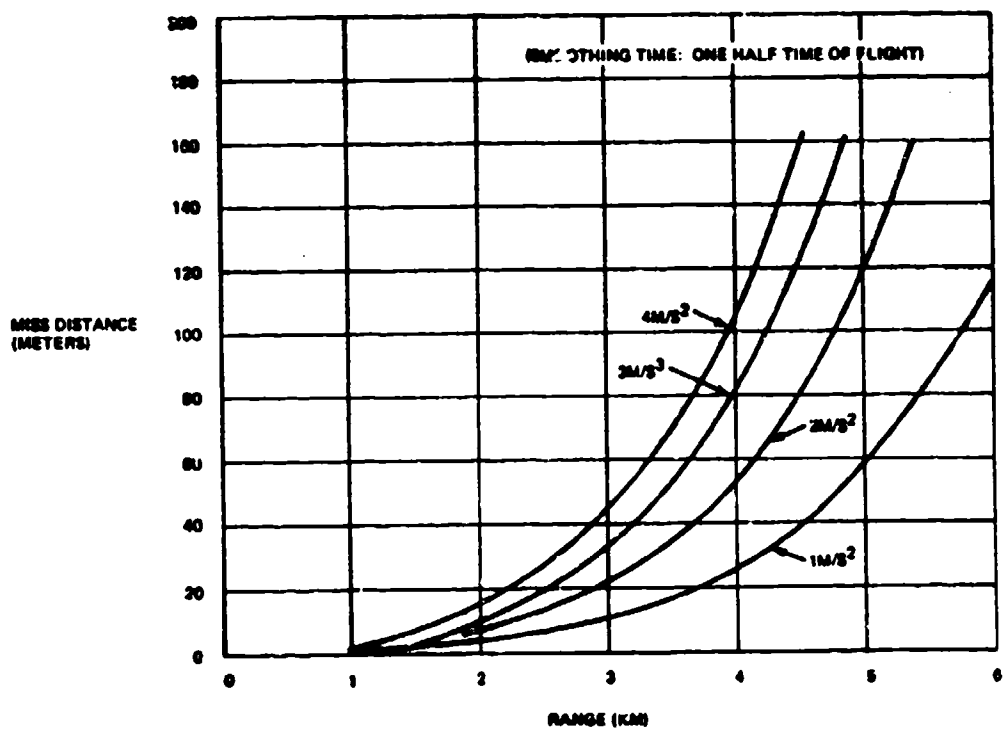
Figures 3-10 and 3-11 show the "maneuver bias" vs. range, under the above assumptions, and for the two smoothing types considered. Obviously, the shorter the smoothing time, the less lag there is in following the maneuver, but at the expense of sensor noise.

At about 3 km, maneuver miss dominates the other bias components shown on previous figures. Beyond a range of about 3 km. An optimistic view is that (1) on many attack paths, the mean acceleration during the attack pass is less than 0.10 g, and (2) the acceleration itself changes slowly enough (5 to 10 second half period) so that either a Kalman algorithm or a partial-quadratic correction will eliminate the bias, with acceptable increase in the random component. A pessimistic view is that the best pilots with the most modern "maneuver bombsights" will be able to generate an acceleration pattern during the attack pass that will not permit acceptable hit probability with any prediction scheme beyond about 4 km. However, based on data now available, it does appear that this is an unduly pessimistic view of the problem of hitting targets on dive bombing passes, delivering unguided bombs. The FACT program will, it is hoped, soon place this conjecture on a factual basis.

Finally, we consider "boresight" or "system calibration" errors. This is a major unknown at the present time. When a fire unit moves into position, if the crew goes through the established boresighting and system calibration doctrine, errors of this type should be very small. In fact, considering the "fog of war" and its associated adverse weather, emergencies and stresses on the crew, it would seem unduly optimistic to count on proving ground precision of system calibration, under all operational circumstances. Figure 3-12 suggests how the probability density of boresighting and other calibration biases might change under adverse conditions. A few observations informally reported on predicted fire systems under peacetime conditions suggest that even in this benign environment, proving ground boresighting accuracies are not met uniformly in the field.

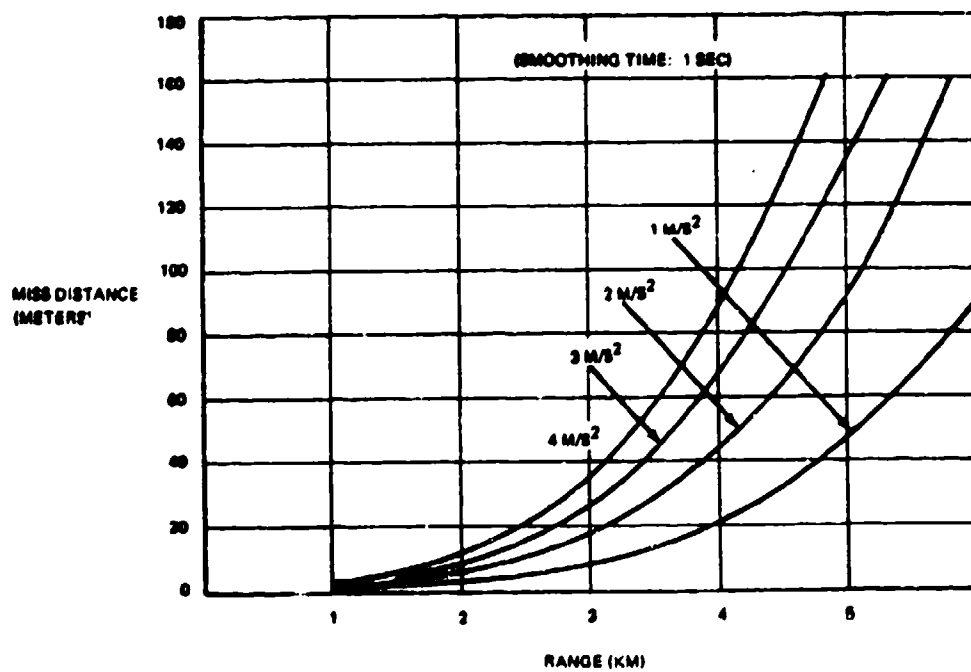
3.1.4 Is a Closed Loop System Worthwhile?

A closed loop system can reduce only those "bias" sources which persist for a time interval which is long compared with the projectile time of flight. As noted above, the target may be a major source of displacement of the center of the shot pattern. Hence a



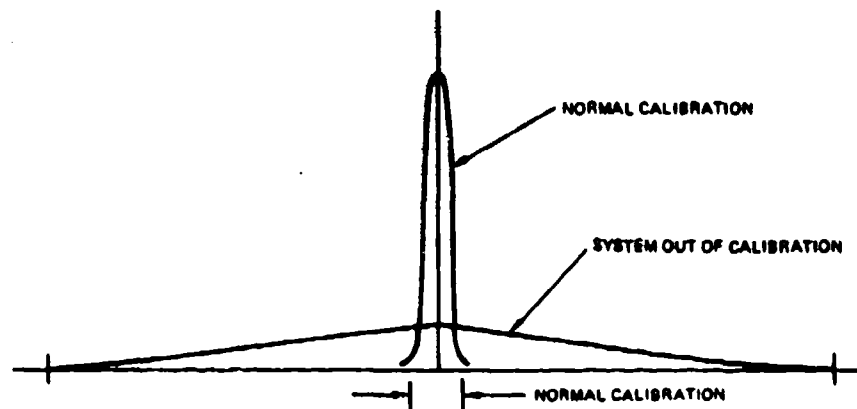
40001-10

Figure 3-10. Maneuver Miss with Linear Prediction (Smoothing Time: One Half Time of Flight)



40001-11

Figure 3-11. Maneuver Miss with Linear Prediction (Smoothing Time: One Second)



PROBABILITY DENSITY FUNCTION OF TYPICAL "CALIBRATION BIAS"

40001-12

Figure 3-12. Probability Density Function of Typical "Calibration Bias"

reasonable question to address is: how large must a potentially correctable component of the miss vector be, in order to devote effort to its elimination?

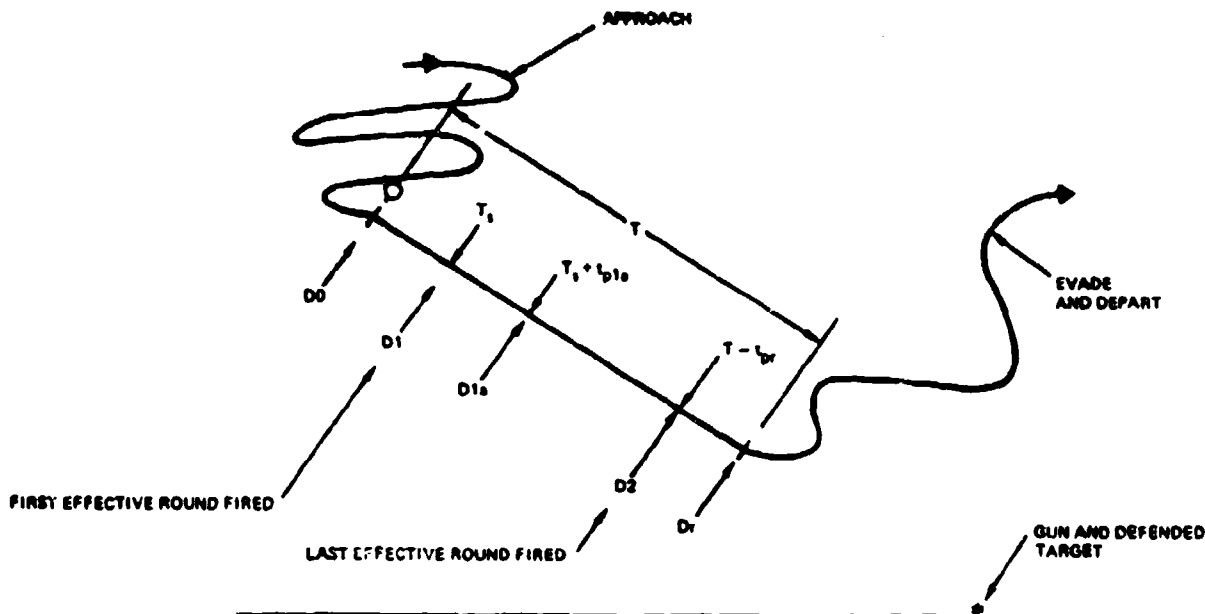
To illuminate this problem, we use a simple analytic model to compute target kill probability. Although the problem could be run on the Litton simulation, the analytic model is preferred at this point because it exposes the details of how the various parameters affect the kill probability. The model is based on Oerlikon weapon characteristics but applications to other weapons can be easily made.

The attack path is based on the FACT data, which indicates that for current dive bombers, a 10-second relatively straight path segment is expected.

For this simple analytic model we assume a target delivering an unguided bomb by conventional dive bombing. The gun is assumed to be at the ground target.

The flight path is shown in Figure 3-13. The target maneuvers into position, comes "down the chute" then breaks away. We assume that the maneuver into position and the break are at high enough accelerations so that they are low-payoff firing segments.

The maneuvers in the chute are relatively mild, and are treated as a variable parameter.



40001-13

Figure 3-13. Situation Geometry and Event Times

The fire control system has a settling time T_s , and it is assumed that this is "lost time" for the defense. T_s can be zero with a "defense of known point" algorithm. The first effective round is fired at T_s , although the gun may have begun firing earlier. The chute begins at D_0 , and ends at D_r . The last effective round reaches the target at D_r , but was fired t_{pr} earlier.

The effective firing time determines the maximum number of effective rounds that can be fired.

$$\text{Effective firing time: } T_{\text{fire}} = [(D_0 - D_r)/V_t] - T_s - t_{pr} \quad (3.4)$$

and if the average shell velocity to D_r is

$$V_{ar} = D_r/t_{pr} \quad (3.5)$$

the effective firing time is

$$T = \frac{D_0 - D_r[1 + (V_t/V_{ar})]}{V_t} - T_s \quad (3.6)$$

Although we shall not include the time-varying reduction of bias sources by closed loop in this example, we digress briefly to consider the time relationships for closed loop functioning.

Given a target release range, we can compute the range at which a round must be fired to reach the target at this point. This round is termed the "last effective round." If the target begins its attack run at less than this range, clearly there will be no effective rounds.

The closed loop correction applied at the time of firing this last effective round is based on whatever round is at the target at that instant. This is the last correction that can be effectively utilized, hence we compute the range at which it was fired to establish the target range at which the last usable round for correction is fired.

These ranges are shown in Figure 3-14, vs. release range. Also shown is the target range at the start of the firing run assuming a 10 second run, also as a function of release range.

For the assumed ballistics, "effective" firing can be conducted (subject to degradation of hit probability with range) against this assumed target, for release ranges up to 5.2 km.

However, if the closed loop operation is limited to measurements made on the firing segment, closed loop corrections will be usefully obtained only for release ranges less than 3 km.

The "10 second target path" line applies in this case only after the computer has settled, i.e., after one "smoothing time."

This illustrates the advantage of the VISTA⁽²⁶⁾ algorithm, which allows closed loop corrections to be obtained even though the target is maneuvering, and while the computer is settling. With a VISTA loop, the system should be capable of delivering effective corrected fire for release ranges out to 5.2 km. VISTA is discussed in the section of this report on closed loop algorithms.

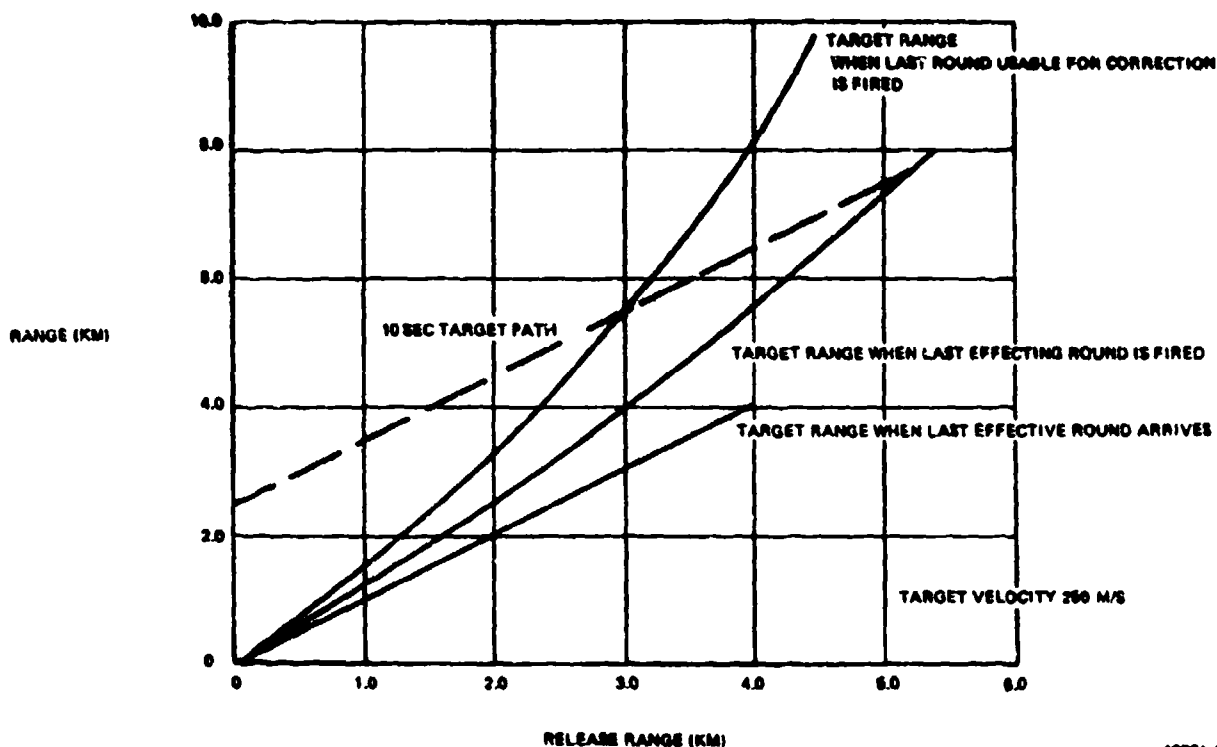


Figure 3-14. Event vs. Range Relationships

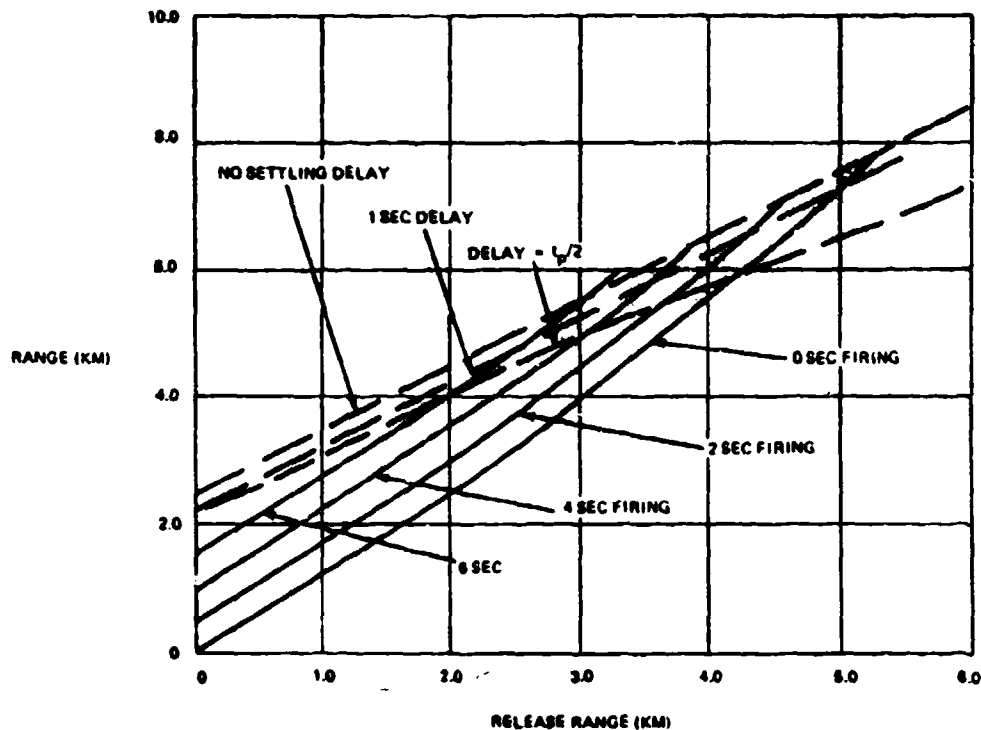
40001-14

Assuming that a VISTA loop is employed, we can plot total firing time of effective rounds, vs. release range, as in Figure 3-15, where the 10 second target path limit has been plotted for zero smoothing time, 1-second smoothing time, and smoothing time equal to one half time of flight.

From Figure 3-15 we can read, for example, that if release range is 3 km. we have 4 seconds of effective fire with a computer settling time of one half time of flight, 5 seconds with 1-second settling, and 6 seconds with zero settling. The last case may be considered to correspond to a "defense of known point" algorithm, which requires no settling.

The fact that one second settling gives more firing time than settling in one half time of flight must be balanced against the greater sensor noise amplification of the 1-second smoother, as shown in subsequent sections.

To compute kill probability, a release range is selected, and the gun firing time determined. This gives the number of rounds fired. The vulnerable area is obtained by multiplying target area by the probability that a hit produces a kill. The variances involved in the probability computation are taken as average values for simplicity, computed at the average range at which the projectiles reach the target.



40001-15

Figure 3-15. Firing Time vs. Release Range

Table III-2 shows firing time for various release ranges, and Table III-3 shows the average range at which the projectiles reach the target.

Only one release range example is worked: it is simple to extend the computations to other cases.

Computations of target kill probability are provided in Table III-4 for a release range of 2 km. The case is worked through for the radar and FLIR sensor noise assumptions, and for two filter types. The gun system is assumed to fire 20 rounds per second, each of which has a 0.50 probability of killing the target if it hits. For this head-on aspect the target area is represented by a circle of radius 1 meter.

The build up of the "random" and "bias" variances is shown.

The firing time is sufficiently greater than the predictor smoothing time, so that all of the prediction error resulting from sensor noise is assigned to the random variance budget.

The kill probabilities are computed from the following relations.

Table III-2. Firing Time vs. Release Range

Firing Time (Seconds)				
		Computer Settling Time		
D_0 (km)	D_r (km)	0 Second	1 Second	$t_p/2$
7.5	5	0.8	0	0
6.5	4	4	3	1
5.5	3	6	5	4
4.5	2	8	7	6
3.5	1	9	8	7.8

Table III-3. Average Range vs. Release Range

Average Range (km)		
D_r (km)	Computer Settling Time	
	1 Second	$t_p/2$
5	NA	NA
4	4.3	4.1
3	3.5	3.3
2	2.7	2.5
1	1.8	1.7

Table III-4. Computation of Target Kill Probability

Release Range (8 km)

Sensor	Radar		FLIR	
Smoothing	1 Second	$t_p/2$	1 Second	$t_p/2$
Firing Time (Sec)	7	6	7	6
Av. Range (km)	2.7	2.5	2.7	2.5
Av. Time of Flt.	3.3	3.0	3.3	3.0
No. of Rounds Fired	140	120	140	120
np_c ($p_c = 0.50$)	70	60	70	60
Random Variances of Prediction Error (Meter) ² Source				
Tracking	64	30	20	9
Other (2 mils)	29	25	29	25
Total (σ^2)	93	55	49	34
Variances of "Bias" (Meter) ² Source				
Tracking	0	0	0	0
Wind (5 m/s)	16	16	16	16
Boresight (1 mil)	7	6	7	6
Maneuver (1 m/s ²)	64	121	64	121
Total (σ_b^2)	87	143	87	143
Variance Ratio $(\sigma/\sigma_b)^2$	1.06	0.38	0.56	0.24
$(np_k/2\sigma_b^2)$	0.40	0.21	0.40	0.21
Target Kill Prob.	0.17	0.13	0.20	0.14
Opt. Random Variance Ratio $(\sigma^*/\sigma_b)^2$	0.36	0.25	0.36	0.25
Max. Kill Prob. with Given Bias Variances and Opt. Disp.	0.22	0.14	0.22	0.14

Arbitrary bias and dispersion variances:

$$K = \sum_{j=1}^{\infty} \frac{(-E)^j}{j!(1+\lambda)^j} \quad (3.7)$$

where

$$E = na^2 p_c / (a^2 + 2\sigma^2) \quad (3.8)$$

$$\lambda = (\sigma_b / \sigma)^2 \quad (3.9)$$

K = probability of killing the target

n = number of rounds fired

a = target radius

p_c = probability that a hit produces a kill.

σ^2 = variance of "random" miss components

σ_b^2 = variance of "bias" miss components

Approximate solution for optimum "dispersion":

$(\sigma^*)^2$ = "optimum" variance of random miss components

$$(\sigma^* / \sigma_b) = \left[(8/25) \left(\frac{na^2 p_c}{2\sigma_b^2} \right) \right]^{1/4} \quad (3.10)$$

$$K = 1 - \left[1 + \left(\frac{na^2 p_c}{\sigma_b^2} \right)^{1/2} \right] e^{- \left[\frac{na^2 p_c}{\sigma_b^2} \right]^{1/2}} \quad (3.11)$$

In all cases except one, the "optimum" random variance is not greatly different from that obtained from the variance buildup, and is, in fact, for three of the four cases slightly too large. If the random components of miss are reduced to the optimum, kill probability is improved by from .01 to .05. It will of course be recognized that the achievement of "optimum" dispersion at all firing points is unlikely.

Table III-5. Comparison of Kill Probabilities

Sensor	Radar		FLIR	
Smoothing	1 Second	$t_p/2$	1 Second	$t_p/2$
Kill Probability				
Original Parameters	0.17	0.13	0.20	0.14
Original Bias with Opt. Disp.	0.22	0.14	0.22	0.14
All Bias Except Maneuver Bias Removed, Opt. Disp.	0.28	0.16	0.28	0.16
All Bias Eliminated, Original Dispersion	0.31	0.42	0.51	0.59
Maneuver Bias and 3 mils System Bias with Opt. Disp.	0.17	0.12	0.17	0.12
Maneuver Bias and 4 mils System Bias with Opt. Disp.	0.13	0.10	0.13	0.10

In Table III-5 the results of some perturbations of the original parameters are shown. Eliminating all bias sources except target maneuver and using optimum dispersion, kill probability is improved from 0.22 to 0.28 in two cases, and from 0.14 to 0.16 in the remaining two cases.

It will be noted from Table III-4 that the $t_p/2$ smoothing results in a smaller random variance budget, but its lag increases the maneuver miss with a net effect of reducing kill probability over 1-second smoothing. However, as shown in Table III-5, if all bias sources were eliminated, and the original dispersion budgets retained, $t_p/2$ smoothing would give significantly higher kill probabilities. A generalized form of Kalman filtering could also accomplish a change of effective smoothing time with range.

Increments of system bias of 3 and 4 mils were then added as representative of "combat operational degradation" to the maneuver bias, and the kill probability was computed with optimum dispersion. There is an appreciable, and progressive reduction in kill probability, as bias is increased to these values.

Considering that a change in kill probability from 0.20 to 0.22 represents a 10% improvement in effectiveness, and that a 4 mil system bias in addition to the assumed maneuver bias can reduce kill probability from 0.22 to 0.13, there does seem to be a good justification for minimizing bias sources.

Noting that the lag associated with a linear predictor against even a mild maneuver has a more serious effect in this example than the reduction in the effects of sensor noise obtained by smoothing, there is a strong indication that a slightly more sophisticated prediction algorithm would be desirable. Depending on the autocorrelation of the target maneuver, a good compromise algorithm would reduce the maneuver bias, somewhat, at the expense of amplification of tracking noise.

Finally, we observe that in this computational example, in which the target is flying directly at the gun, the system is not degraded by muzzle velocity bias, or other "in-plane" error components. To this degree, the computed results of bias elimination are conservative.

3.1.5 General Conclusions with Regard to Bias Reduction

In Figure 3-16 we show the probability of killing a target, given the number of rounds fired, the target size, the variance of systematic error, and the probability that a hit kills the target, all for the cases where the random component of miss (dispersion) is optimized.

We can make some general observations from this curve. Its slope is close to unity over what is likely to be the operating range of any gun system.

Since the abscissa is inversely proportional to the bias variance, a reduction of a given small percentage in the standard deviation of bias will produce double this percentage increase in kill probability. Since this relation holds over the range of interest, it is independent of the magnitude of the bias variance. It holds whether target maneuver bias is large or small.

As a rough rule of thumb, if a 10% increase of probability of kill is set as a criterion, then this is equivalent to a 10% reduction in the aggregate bias variance. Hence any source which contributes more than 10% of the total becomes a candidate for elimination.

This suggests that even when the errors caused by unpredictable elements of the target path may be large, the system is still significantly improved by eliminating remediable bias sources which individually have a much smaller effect.

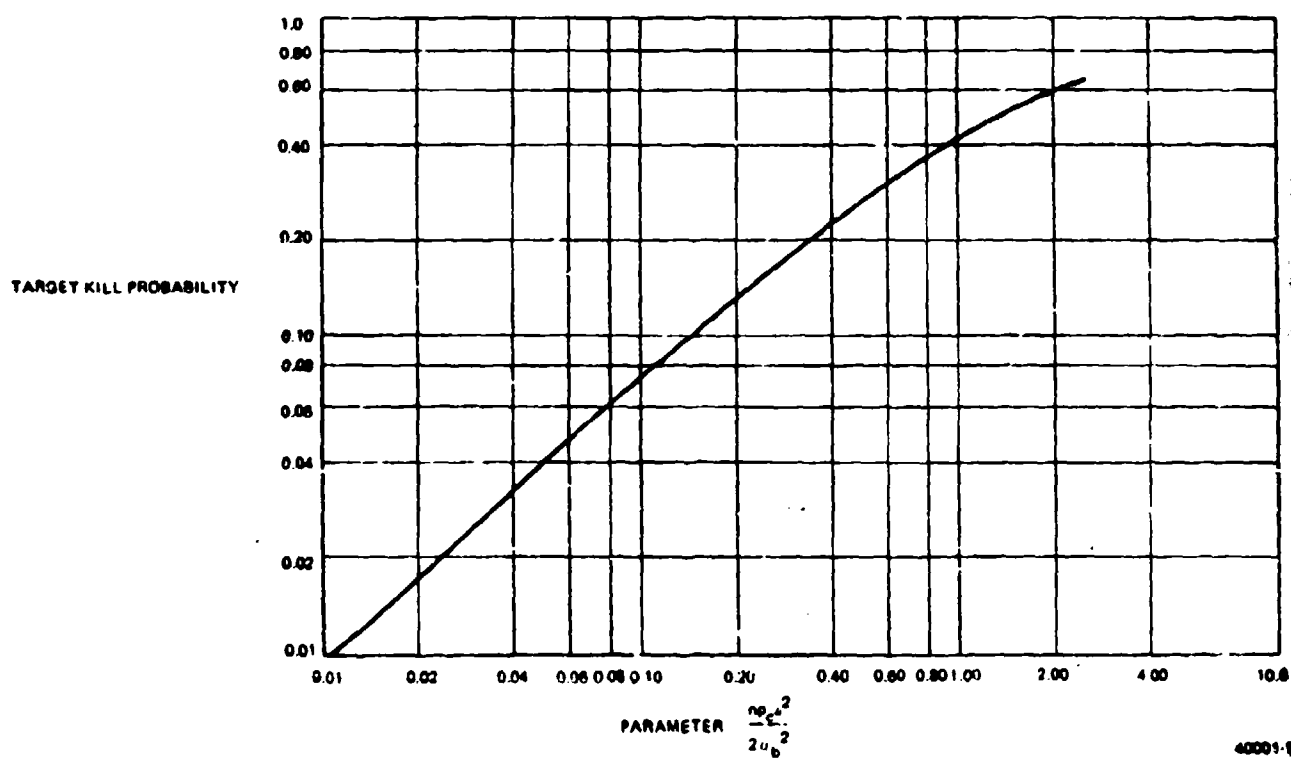


Figure 3-16. Target Kill Probabilities with Optimum Dispersion

Finally, we note that the shorter the time of flight of the weapon the less the maneuver biases will be, and the larger the proportion of the whole that will be represented by sources independent of time of flight, such as boresight errors.

The decision as to whether a closed loop system is desirable therefore seems to rest on two factors. These are (1) the predictability of the target path, and (2) the expected magnitude of the effects of correctable bias sources. The FACT data indicates that on many current dive bombing attack paths, the target maneuver component of miss variance is not greater by a factor of ten than a conservative estimate of the contributions of "normal" correctable bias sources. On this basis, closed loop offers the potential of at least 10% improvement in kill probability. On the other hand, bias sources of an "abnormal" but correctable type appearing in field operations, and, as yet, unquantified, may be much larger than "normal" expectations, so that the result of eliminating them will be a gain of much more than 10% in kill probability.

Taking a pessimistic view of the difficulty of field calibration, and assigning the remediable biases a standard deviation of 4 mils, their removal would more than double target kill probability, even if the target maneuver bias were not eliminated. Reduction of the target maneuver bias by sophisticated prediction algorithms could raise this factor to a threefold increase.

On net balance, a conservative judgement is that a closed loop system offers significant potential in improvement of system effectiveness.

3.2 SENSORS

An estimate of the state of the art in sensing projectiles by various sensor types is provided in Table III-6. This estimate is conservative; demonstrations probably exist which are not known to the writer.

The feasibility of a complete closed loop system using radar has been demonstrated by the Phalanx system. The ability of centimeter radar to measure projectile miss distances has been demonstrated by the MIDI system.

Projectiles with tracer elements are easily observed visually, since the tracer is designed for visual observation; they have also been observed in TV tracking and miss observation systems (including a miss measurement system based on angular measurements produced by Oerlikon), and there is no reason to doubt that tracer of the proper composition can be observed on a FLIR sensor. However, for a full 3-D system, tracer observation

Table III-6. Methods of Sensing Projectile Miss Distances

Sensor	Angle Sensing	Range Sensing	State of the Art Demonstration
Radar (Centimeter) Range Gates	Yes	Yes	Yes (MIDI)
Doppler plus Range Gate	Yes	Yes	Unknown
Radar (Millimeter)	Yes	Yes	Not yet
Laser Range only	No	Yes	Not yet
FLIR plus Laser	Yes	Yes	Not yet
Visual (Eyeball Mk I)	Yes	No	Yes (requires tracer)
TV/LLTV	Yes	No	Yes (requires tracer)
FLIR alone	Yes	No	Not yet (requires tracer)
Optical Radar	Yes	Yes	Not yet
Visual with Optical Rangefinder	Yes	Yes	Yes (WW-II M3A2 director) (requires tracer)

requires an associated range measurement, with correlation problems across the sensors. Some concepts for sensor configuration are discussed below. The problem of projectile signature for each sensor type is developed in a subsequent section.

3.2.1 Radar

A 3-D radar solution applicable to closed loop predicted fire systems has been demonstrated at Fort Bliss.^④ It consists of a monopulse 9-10 Ghz (3 cm) radar which tracks the target and senses projectiles near the target. The projectile signals are separated from those of the target by using two narrow slave range gates on each side of the target range gate. Pulse width is about 30 nanoseconds, and gate depth is about 5 meters, with 10 meters spacing between the three gates.

Projectile misses within about 50 mils of the target are sensed.

It is reported that the demonstration system had a beam width narrower than desired and an excessively long pulse width, so that wide misses could not be recorded, and a maximum rate of fire of 600 rounds per minute was a limit. With the objective pulse width, it was expected that the system would handle 3600 rounds per minute, with 20 strobes per projectile in each passage of a gate at a prf of 1480.

Computations of miss distance were done in real time with a minicomputer.

Since this system was intended to measure miss distances accurately as a replacement for the cumbersome existing multiple cinetheodolite optical system (originally developed in 1944), the antenna system was calibrated in 1 mil intervals before use. This precision might not be required for a closed loop fire control system.

The demonstration showed that the system was equal in accuracy to the optical system, and in this quasi-real time application, reduced data reduction time by at least a factor of 100. The limiting error source was radar glint error in tracking the target as a reference, which was estimated to be about 1 mil at 1 kilometer.

Although only a single slave gate would be required to cover miss sensings from a single fire unit, the paired gates form a fortuitously useful means of allowing each fire unit to discriminate between miss measurements on its own projectiles, and miss measurements on projectiles fired from other fire units at the same target.

An alternate system might be conceived in which a single range gate is employed, centered on the target, but with the projectile signatures separated from the target signature by a doppler velocity gate centered on the projectile expected velocity at the target as determined by the computer. This type of gate would also discriminate against projectiles fired from other fire units.

The use of radar sensors for closed loop systems would therefore appear to have a well established feasibility, the principal disadvantage being the current desire of the user to have as passive a system as possible.

3.2.2 3-D Systems with FLIR and Laser

The most attractive current system concept of this type which, however, pushes the laser state of art is considered to be one in which the bullet is illuminated by a pulsed laser, and viewed by a FLIR. The miss distance recorded on the FLIR sensing elements must pass a range gate driven by the laser, which also ranges on the target. Characteristics required for one system configuration are as follows:

Assume a FLIR with a frame rate of about 30 frames per second, operating at about 8-14 microns, with a dwell time per resolution element of about 75 μ s. The projectile is illuminated by a pulsed laser, probably CO₂ at 10.6 microns, and either has a Callypegian base⁽²³⁾ or a corner reflector in the base. It can be seen by the FLIR only if it is illuminated. It will be seen by the FLIR only if it is illuminated at the instant a scanning resolution element includes the projectile.

To ensure illumination at the instant the resolution element crosses the projectile, the laser repetition rate must be the inverse of the dwell time of the element. For this example this works out to a repetition rate of 13,000 pps. For projectiles at a range of 1 to 6 km. the round trip time of a pulse is 7 to 40 μ s. A 10 meter gate would be .03 μ s wide. In theory, therefore, one would use a 13,000 pps rate, a .03 to .05 μ sec pulse, and there would be no range ambiguity to well beyond 6 km, which is adequate for closed loop systems.

"Off the shelf" commercially available CO₂ pulsed lasers are advertised at a maximum pps of 3,000, and a pulse width no shorter than 150 μ s. However, CO₂ lasers are only at an early stage of application to the rangefinder problem. Only one CO₂ laser rangefinder has been located in the open literature.

If the above requirements on the laser can be met, there is an additional requirement on beam width, since each pulse must cover the field within which one expects to measure angular misses. The power requirements may possibly be more easily satisfied with a CO₂ laser than with current solid state lasers used for operational rangefinders.

Given the above capabilities, the provision of gates driven by the laser (which continually ranges on the target) to pass only angular sensings made within the range band about the target should be straightforward. The problem then reduces to a straightforward one of data processing, and is similar to the 3-D radar solutions.

The Army is also considering FLIRs for the 3-5 micron region. Off the shelf commercially available lasers of the solid state ND-YAG pulsed type are advertised⁶ with 50 joule output 100×10^{-6} μ s pulse width and 500×10^6 pps, at 1.06 microns. Neither the 8-14 nor the 3-5 micron FLIRs are narrow bandpass, but the detector sensitivity drops off rapidly below the design range. Hence it is not clear that illumination at 1.06 microns will provide a sufficiently strong reflection on the 1.06 micron sensitivity ordinate of either FLIR type.

Many FLIR types are under development, some of which are listed in Table III-7. The requirements of FLIR/Laser coordination will vary with the characteristics of each type but are believed to be of comparable difficulty.

Table III-7. FLIR Types

Processing Mode	Manufacturer	State of Art
Parallel Rectilinear Scan	Texas Instruments Hughes	Operational in Airborne Applications
Circular Scan	Xerox	Development for USAF Austere FLIR Army Lightweight Airborne Thermal Imaging System (LATIS) Army Advanced Circular Scan Thermal Imaging System (ACSTIS)
Serial Processing	Hughes (DISCOID) Honeywell (TV compatible)	Development

As a less attractive solution one might consider a low pps CO_2 laser with very long pulse width, i.e., a pulse width of 30,000 μs and 15 pps. This would fully illuminate the FLIR field on every other frame. There would appear to be practical difficulties in getting accurate target range data, and in synchronizing a range gate to coincide with the element exposure rate of the FLIR in order to isolate projectile sensing within a narrow range gate about the target. If one drives the laser pulse by the ballistics generated by gun firing, most of these difficulties vanish, but as noted earlier, the system is blind to errors in the direction of target motion, although it has a higher data rate against errors out of plane. The fact that it is active may make it less desirable than a simple 2-D system that simply observes tracer in the bullets with the FLIR. This use of long pulse laser illumination is discussed in more detail under "Computer Timed Solutions."

3.2.3 Unsynchronized FLIR/Laser Systems

It is possible that by careful base design, a projectile can be built with tracer that can be seen on the FLIR and with a high enough laser cross section to be ranged on by a laser rangefinder. One then acquires two sets of independent data - sequential angular measurements of bullet traces in the neighborhood of the target, and range vs. time histories

of bullets from the laser. Not all bullets will necessarily be sensed by both sensors, there is a severe problem in matching the range sensings to the angle sensings when the rate of fire is very high, as is typical of a gun air defense system.

It may be possible to use identical time windows (time gates moving in time) for the two sensors, and to develop a data processing scheme based on averages within the windows. It may also be possible to relate the sensings within these gates to the gun rate of fire and internally generated ballistics. One might in this way get an approximate 3-D solution. However, algorithms to do this have not yet been developed, and at the moment, the difficulties and approximation required seem to make this one of the less desirable approaches.

3.2.4 Other FLIR/Laser Hybrids

One might imagine a wide-beam laser, range gated short of the target, with a moderate pulse rate and narrow pulse width for range accuracy. When the laser senses a bullet in its range gate it emits a single pulse of long duration sufficient to illuminate the bullet for one FLIR frame. At a firing rate of 3000 rpm, or 50/second, and a bullet velocity of about 500 m/s, bullets will be spaced on the average 10 meters apart in range. The range gate would be set short of the target. During the subsequent long pulse of 1/30 sec. all bullets in the field at whatever range would be illuminated, but only signals returning via the FLIR within a time gate keyed to the original sensing would be processed. Since two new bullets would have passed the original range gate during the long pulse, it might be necessary to provide signal enhancement (reflectors) in say, only one out of five bullets, and accept a lower data rate.

3.2.5 Passive 3-D System

A potential solution is the use of an optical rangefinder to determine when a bullet with tracer reaches the range of the target. In its simplest configuration, an operator keeps the rangefinder on target, thereby generating range input to the computer. He can be assisted by regenerated range from the computer. As each tracers bullet passes the target he sees two intersecting tracks if he is using a coincidence rangefinder, with a stereo device he actually senses the bullet in range as it passes the target. He can then observe the miss distance, and subject to his limitations as a data processor, inputs corrections to the system.

At a higher level of sophistication, the images from the two ends of the rangefinder base are merged on a TV-type screen which matches the target position. The scanning process extracts the sensings of the bullet tracer from the two sensors at the ends of the

range-finder base, and derives the intersection points, which are transmitted to the closed loop data processing algorithms. There are obvious problems in angular resolution using a short base length.

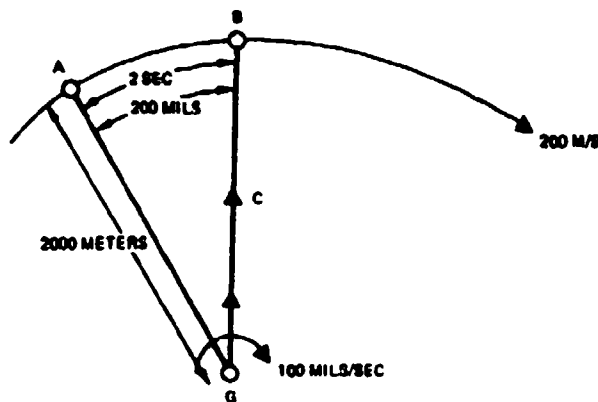
There are also problems when many traces are present in the field of view at one time. However, the system is completely passive, and is perhaps worth noting for this reason. It is, in fact identical in concept with that installed on the M5A3 director for the 40-mm gun in World War II when it was demonstrated to have some capability within about 2 km, using only a 36 inch base range-finder, visual observation, and manual insertion of corrections.

3.2.6 Computer Timed Systems

A concept which handles the miss measurement problem by observing short bursts of projectiles simultaneously is the following: A short burst of predetermined duration is fired. The fire control computer receives the firing time, and when the time of flight to the target as determined by the computer's ballistic unit has elapsed a sensor is activated. In the case of radar, the activation would be on the midpoint of the burst duration, the radar would obtain a weighted average of the positions relative to the target of all projectiles in its field, and this average would be applied as a corrective input to the closed loop processing. In the case of a FLIR system, a long laser pulse of duration equal to one frame time of the FLIR would be emitted, time centered on the burst midpoint, all FLIR sensings of projectiles during this laser pulse would be recorded and averaged according to the angular position of the recording elements, and the average would be used as an input to the closed loop processing algorithms.

These concepts may be attractive from the point of view of relative simplicity of implementation. They do require that only one burst be in the sensor field at the time of observation. The systems are also "blind" to any biases which result from differences between the computer generated ballistics and the actual bullet ballistics. Hence they do not sense miss components resulting from muzzle velocity biases, for example. We digress briefly to show why this is so.

First consider the function of a computer timed system, when there is a muzzle velocity bias. For simplicity assume a target circling the gun at a range of 2 km and a velocity of 200 meters/second, with an expected projectile average velocity of 1000 meters/second, as shown in Figure 3-17.



40001-17

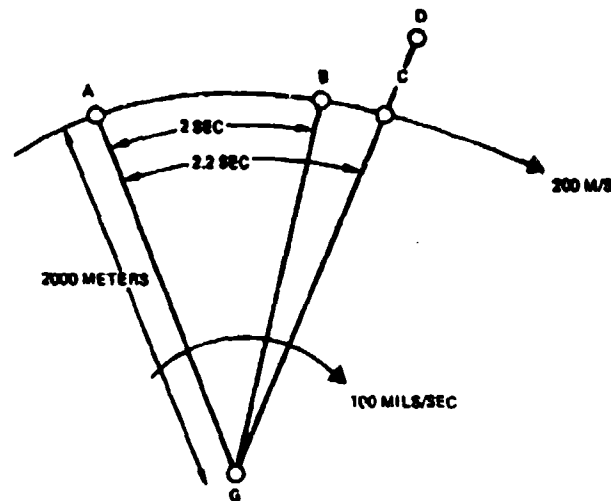
Figure 3-17. Effect of Muzzle Velocity Bias

Assume that the observation system starts a clock when a bullet is fired, computes projectile range versus time from internal ballistics (for the example assume a 1000 m/s velocity) and calls for an observation of projectile position relative to the target when estimated projectile range equals target range.

The computer computes a 200 mil lead, and the projectile is fired with a 200 mil lead when the target is at A, along the line GB. If in fact the projectile velocity is 1000 m/s it will be at the target at B when the observation is called for. For any other projectile velocity, differing from that assumed by the computer, the projectile will still be on the line GB at the time of observation, and no angular miss will be recorded. If the projectile velocity is in fact 500 m/s it will only be half way to the target when observed, and when it finally crosses the target path 2 seconds later, the target will be 500 meters away. But the observation cannot be called for 4 seconds instead of 2 seconds, since the internally generated ballistics have no way of telling that the bullet velocity differs from that assumed.

Hence we say that this system is "blind" to muzzle velocity biases.

It is also "blind" to biases in measuring target range. Consider the configuration of Figure 3-17 but introduce a rangefinder bias of +200 meters as shown in Figure 3-18. The



40001-18

Figure 3-18. Effect of Bias in Present Range

computer derives a time of flight of 2.2 seconds and generates a lead angle of 220 mils. The gun is fired when the target is at A. The bullet travels along the line GC. At 2.0 seconds the bullet is on the forward projection of the target path with a miss of 40 meters. However the computer does not call for an observation until 2.2 seconds have elapsed, at which time the bullet is at D, the target is at C, and a zero angular miss is recorded.

Since these computer timed systems do achieve measurements of two angular components of miss on each sensed projectile or "flock" (the out of plane miss vector only, since they are blind to in-plane vector components), they have twice the information rate of the 2-D systems discussed below, in correcting out of plane miss sources.

3.2.7 The "Spot" Flare

A system has been suggested in which the bullet contains an ingenious pyrotechnic component which emits a brief tracer flare at a precisely timed interval after the bullet is fired. This "spot" flare may be detected on a FLIR and the angular position relative to the target measured. Since the time is known, the range can be determined from internally computed ballistics, and the measured miss projected to miss (if any) at the target.

Since the system depends on internally generated ballistics it, like the other computer timed systems, is blind to muzzle velocity and range biases.

A few computations suggest that for the system to operate when the target has a high angular velocity (say 200 mils/second), rather high precision of timing would be required (.01 second for 2 mils). On second thought, however, it is evident that any deviations of the flare position caused by timing, will be parallel to the direction of relative target motion. Hence in a worst case of gross dispersions in timing, the system reduces to a 2-D system, and the only useful measurement per projectile is the minimum angle of the extrapolated trace relative to the target.

On net balance this concept seems to fall midway between one of the computer timed systems and the 2-D systems discussed below.

3.2.8 2-D Systems Using FLIR, TV, Etc.

As noted in Table III-6, a number of imaging sensors, including visual observation can sense a tracer bullet as the target sweeps by the tracer, and the minimum angle between the tracer and the target can be observed and measured. These are completely passive systems, requiring no ranging on the projectile, and as we show in the section on processing algorithms, this single measurement on each of a number of projectiles is capable of being processed to reduce all sources of out-of-plane error.

The information rate of such systems is lower than that of the computer timed systems, which are also blind to in-plane error sources, but their relative simplicity suggests that they be retained as candidate solutions through a complete evaluation. There appears to be little technological risk associated with these 2-D systems, as opposed to the possible problems in implementing a FLIR plus laser solution.

Performance of a 2-D system is developed in some detail in Section 3.4.6.

3.2.9 Optical Radar

An optical radar would avoid the difficulties of FLIR-Laser coordination, and would retain the advantages of the 3-D microwave radar solutions. Optical radar for this application is undoubtedly approaching state of the art, and at least one system is under development. Since details of proposed solutions are proprietary at this time, it will only be observed here that the approach is attractive, and highly competitive with the 3-D microwave radar solutions and the 2-D passive solutions previously indicated to have the highest feasibility-capability characteristics.

3.3 PROJECTILE SIGNATURES AND CROSS SECTIONS

Closed loop systems depend on the ability of a sensor to acquire the projectile signature, and to make useful measurements. We consider three cases (1) sensing of projectiles designed with no particular attention to the objective of providing an adequate signature for closed loop sensing (i.e., "off the shelf" projectiles),⁽²¹⁾ (2) projectiles with bases which have been shaped to maximize the signature for a specified sensor type ("Callipygean" designs),⁽²³⁾ these projectiles may also be given high reflectivity coatings for use with laser sensors, and (3) projectiles with some type of signature augmentation.

Methods of signature augmentation include use of tracer, and the insertion of corner reflectors in the projectile base.

The ability of radar to obtain useful sensings on some existing projectile designs is well established. This capability against projectiles without signature "augmentation" depends sensitively on the architecture of the projectile base, and on the radar frequency and the projectile size.

The ability of TV sensors to record tracers on existing projectiles is also well established. It seems to be a safe assumption that IR sensors will be able to make useful angular measurements of bullets with tracer, although it is possible that some pyrotechnic development may be needed to fit the tracer spectrum to the IR sensor spectrum. It is unlikely that an IR or TV sensor will be able to acquire a projectile without tracer or illumination.

The ability of laser systems to illuminate and sense a projectile in flight is still in process of determination.

In the following sections, estimates are developed of projectile signatures for each of the candidate sensor types.

3.3.1 Estimating Relationships for Projectile Radar and Laser Cross Sections

The radar cross section of a target and the laser cross section are defined identically. Following Weinstock,⁽⁹⁾ the signal power received by a radar is, assuming no system losses

$$S = \left(\frac{P_t G_t}{4\pi R_t^2} \right) \left(\frac{\sigma}{4\pi R_t^2} \right) A_e \quad (3.12)$$

where

S = signal power received

P_t = transmitted power

G_t = gain of transmitting antenna

R_t = target range from transmitting antenna

R_r = target range from receiving antenna

σ = radar cross section of target

A_e = collecting area of the receiving antenna

The first term gives the power density at the target. The second term gives the power density of the wave reflected by the target assuming that this reflection is isotropic.

Effect of Wavelength

The reflective characteristics of a target depend on the target dimensions (and configuration) and the wavelength of the illuminating radiation. These are conventionally discussed in three regimes:

- a. Wavelength large compared with target dimensions (Rayleigh scattering).
- b. Wavelength on the order of target dimensions (Resonance region).
- c. Wavelength small compared with dimensions (Surface and edge scattering; optical region).

According to Nathanson,⁽¹³⁾

"The optical region in which most radar targets of practical interest reside is so named since the ray techniques of geometric optics may be applied to the problem of RCS estimation. Any smooth curved surface nearly normal to the incident field will give a specular return. From a consideration of the power reduction due to the divergence of the scattered beam, the RCS is found to be

$$\sigma = \pi R_1 R_2$$

where R_1 and R_2 are the principal radii of curvature at the surface normal. In the optical region the RCS behavior with wavelength is monotonic although the RCS does not necessarily converge to a constant value. The RCS behavior with wavelength may be classified for many simple objects in terms of the principal radii of curvature at the point where the normal to the surface is parallel to the direction of incidence:"

1. λ^{-2} dependence: two infinite radii of curvature (e.g., flat plates)
2. λ^{-1} dependence: one infinite, one nonzero (e.g., a cylinder)
3. λ^0 dependence: (a) one infinite, one zero (e.g., a wedge)
(b) two nonzero finite (e.g., a spheroid)
4. λ^1 dependence: one nonzero finite, one zero (e.g., a curved edge)
5. λ^2 dependence: two zero (e.g., the apex of a cone).

For laser cross sections, we use the optical approximations, but they must be multiplied by a reduction factor for the reflectivity of the surface.

Absorption, reflection (including scattering) and transmission account for all incident radiation in a particular situation.

$$\alpha + \rho + \tau = 1 \quad (3.13)$$

If the material is opaque so that it transmits no radiation

$$\alpha + \rho = 1 \quad (3.14)$$

α = absorptivity

ρ = reflectivity

τ = transmissivity

Define

ϵ = emissivity

For a blackbody

$$\epsilon = \alpha = 1 \quad (3.15)$$

$$\rho = 0$$

$$\tau = 0$$

For passive IR viewing, a high emissivity for the target is helpful. For a laser target, a high reflectivity is desirable. If the target is opaque,

$$\rho = 1 - \epsilon \quad (3.16)$$

Sohl^⑤ reports that a titanium dioxide coating on a bullet may be expected to reflect 0.85 of the incident energy.

In the case of trihedral reflectors, for which estimating relations are given later, three surfaces are involved, hence for laser cross section estimates the estimates for unit reflectivity should be multiplied by $(\rho)^3$.

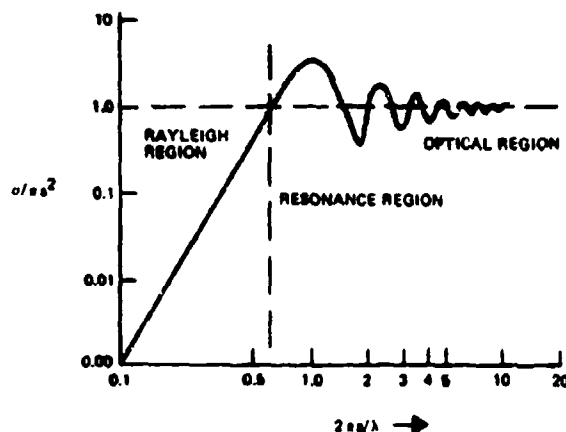
Most of the published material on radar cross sections is for objects whose principal dimensions are large compared with the wavelength of the illuminating radar. In the case of projectiles, the caliber and wavelength may be of the same order of magnitude.

In Figure 3-19 is shown the radar cross section of a perfectly conducting sphere as a function of $(2\pi a/\lambda)$ where a = radius and λ = wavelength. $2\pi a/\lambda$ is the ratio of the circumference to the wavelength. The solution was computed many years before radar, and is known exactly.

Note the three regions in Figure 3-19: (1) the Rayleigh region where the sphere is small compared with wavelength, (2) the "resonance" region where the dimensions are comparable to wavelength (the term resonance results from the oscillating behavior of cross section as wavelength changes), and (3) the optical region.

Good, simple approximations are available for the Rayleigh and the optical regions; computations for the resonance region are more difficult.

In Figure 3-20 the radar cross section for a sphere has been replotted. Also shown is the nose-on radar cross section of an elongated ellipsoid (10:1) which is given in the literature^⑫ over the section shown by the solid line, and confirmed by experiment. The



40001-19

Figure 3-19. Radar Cross Section of Sphere $a = \text{radius}$

experimental data suggests that the oscillations in the resonance region for this body persist over a wider range of $(\pi C/\lambda)$ than for the sphere.

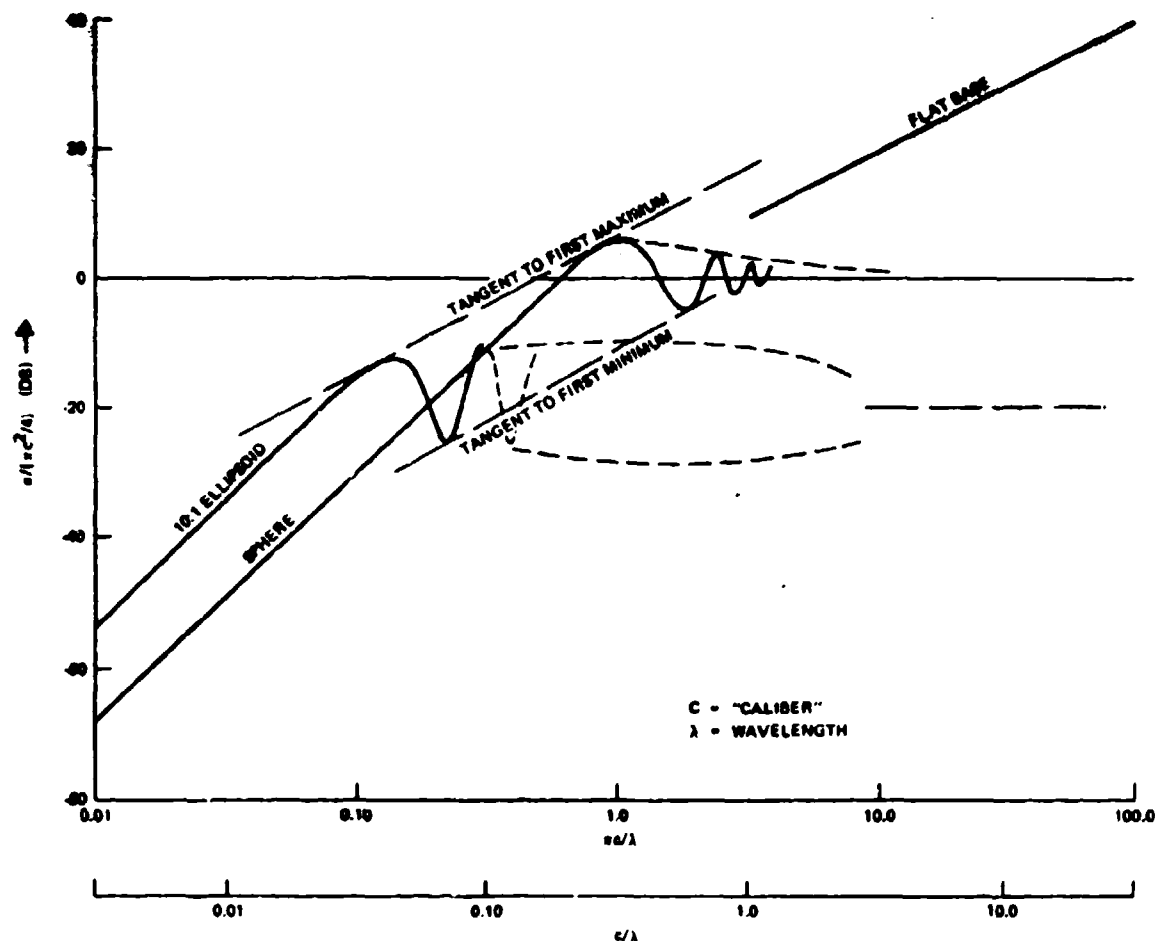
Note that the ellipsoid has a larger volume than the sphere for constant axial cross sectional area, hence the radar cross section is larger at long wavelengths. However, at short wavelengths it is less because of the smaller radius of curvature of the surface at the nose.

Bodies of intermediate elongations would be expected to fall between the two curves shown.

A cylinder of 10:1 elongation would have a slightly higher radar cross section than that of the 10:1 ellipsoid at long wavelengths because of its greater volume.

However, at short wavelengths in the axial aspect, the flat face of the cylinder would develop the cross section shown as "flat base." No experimental data has been located for a cylinder end-on in the resonance region.

The radar cross section of a projectile with a hemispherical base in the optical region would coincide with that of the sphere.



48891-20

Figure 3-20. Radar Cross Sections of Sphere and Ellipsoid

Table III-8 summarizes expressions for estimating radar cross section in the optical region. ⁽¹⁰⁾ Since we are interested in the base-on aspect of projectiles, including only relatively small angles off the tail, it is convenient to refer the radar cross section to the geometric cross sectional area of the projectile perpendicular to its longitudinal axis, and this has been done in Table III-9. The flat plate expression must be corrected for base-tail area when this is less than $\pi C^2/4$, where C = caliber. We use the ratio L/C for the ratio of the projectile length to its diameter.

Table III-8. Estimating Relationships for Radar Cross Section in the Optical Region (Sheet 1 of 2)

Shape	Aspect	Cross-Section σ	Symbols
Prolate Spheroid	Any	$\frac{\pi b^4 c^2}{(b^2 \sin^2 \theta + c^2 \cos^2 \theta)^2}$	b = minor semi-axis
	End on ($\theta = 0$)	$\pi b^2 (b^2/c^2)$	c = major semi-axis
	Side on ($\theta = 90^\circ$)	πc^2	θ = angle off long axis
	$\theta = 45^\circ$	$4\pi \frac{b^4 c^2}{(b^2 + c^2)^2}$	
Sphere	Any	πa^2	a = radius
Body of Revolution	Any	$\pi \left \frac{r}{\frac{d^2 r}{dx^2} \sin^4 \theta} \right ; r = r(z)$	θ = angle from axis of symmetry r = radius of section at z z = distance along axis of symmetry
Circular Flat Plate	Any	$\frac{\pi a^2}{\tan^2 \theta} \left[J_1 \left(\frac{4\pi a \sin \theta}{\lambda} \right) \right]^2$	a = radius θ = angle from normal λ = wavelength
	Normal, $\theta = 0$	$4\pi \left(\frac{A}{\lambda} \right)^2$	A = area

Table III-8. Estimating Relationships for Radar Cross Section in the Optical Region (Sheet 2 of 2)

Shape	Aspect	Cross-Section σ	Symbols
Tip of Thin Cone	Axis of Cone	$\frac{\lambda^2 \tan^2 \alpha}{16\pi}$	α = half cone angle

Table III-9. Estimated Optical Region Cross Section Referenced to Geometric Cross Sectional Area

Prolate Spheroid	$\sigma(\theta)/A = \frac{1}{\left[\left(\frac{C}{L} \right) \sin^2 \theta + \left(\frac{L}{C} \right) \cos^2 \theta \right]^2}$ $\sigma(0)/A = \left(\frac{C}{L} \right)^2$ $\sigma(90^\circ)/A = \left(\frac{L}{C} \right)^2$ $\sigma(45^\circ)/A = \frac{4}{\left[\left(\frac{C}{L} \right) + \left(\frac{L}{C} \right) \right]^2}$	<p><u>Symbols</u></p> <p>C = minimum diameter</p> <p>L = length</p> <p>θ = angle off longitudinal axis</p> <p>A = minimum cross sectional area</p>
Sphere	$\sigma/A = 1.0$	
Circular Flat Plate	$\sigma(0)/A = 4\pi \frac{A}{\lambda^2}$ $\sigma(\theta)/A \approx \beta^2 \cos^2 \theta e^{-\left[(\beta \sin \theta)^2 + (1/12) (\beta \sin \theta)^4 \right]}$ $\sigma(\theta)/A = 0, \beta \sin \theta = 1.95 \dots$ $\sigma(\theta)/A \approx \frac{1}{2\pi\beta\theta^3}; \beta \sin \theta \gg 2.0$	$\beta = \pi C/\lambda; \beta \sin \theta \leq 1.5$

Approximations are also given for the optical cross section of a flat plate at small angles from normal incidence. These were obtained by expanding the Bessel function as a series. The approximate expression for large angles from normal for a flat plate is given as a matter of interest, but will not be used.

Siegel's approximation^{10,12} for the radar cross section of elongated shapes is given in Table III-10. The factor "F" depends on the L/C ratio of the shape, and for projectiles viewed from the tail aspect, is very close to 1.0

If the projectile has a tracer element in the base and a tracer cavity, the radar cross section of the base at high frequencies will be affected. Siegel¹⁰ observes that the result depends on what is in the cavity. For an open ended tube, with

$$(2\pi C/\lambda) \geq 10.0 \quad (3.17)$$

he gives the expression (empirical)

$$\sigma/\lambda^2 \approx 0.05 (2\pi C/\lambda)^3 \quad (3.18)$$

or

$$\sigma/A \approx 5 (\pi C/\lambda) \quad (3.19)$$

He suggests that the variation with aspect to be taken as similar to that of a flat plate multiplied by an additional $\cos \theta$.

This estimate yields a somewhat higher cross section for normal incidence than that of a hemispherical base of equal diameter (for which $\sigma/A = 1.0$).

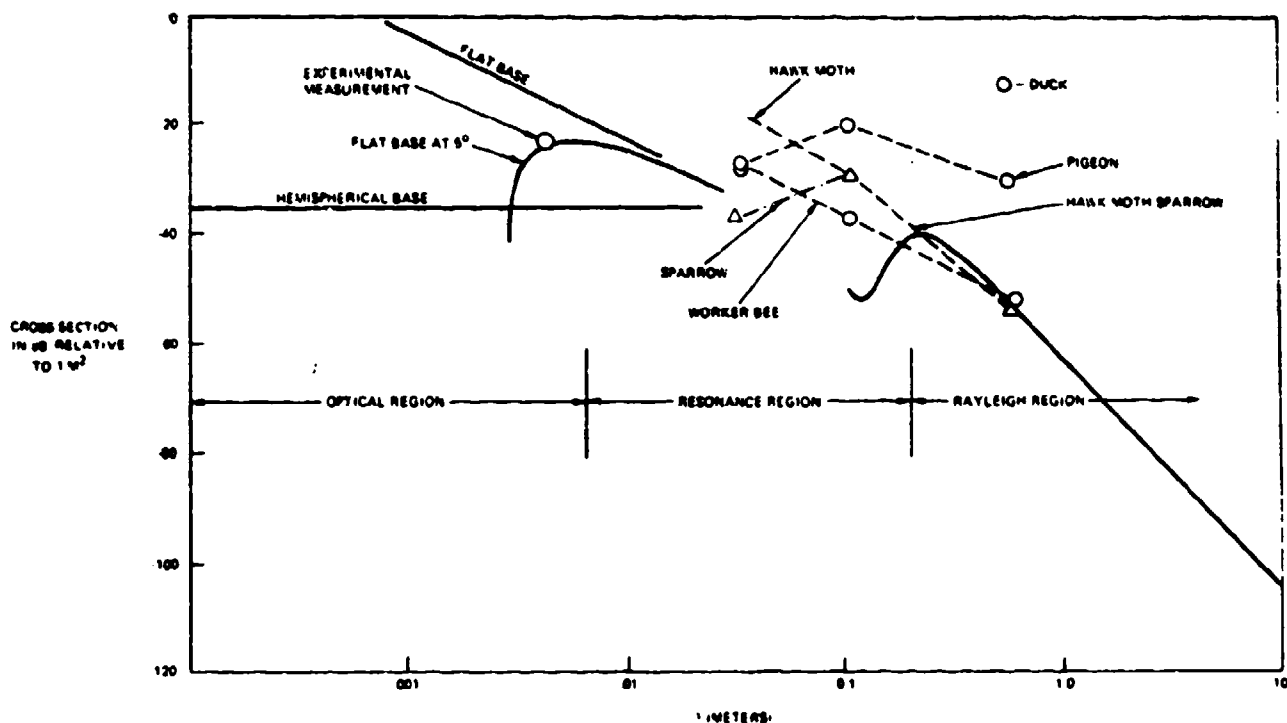
The simple estimating relationships given do not account for destructive and constructive interference among shape irregularities and anomalies in the base region, when these irregularities are of the same magnitude as the observing wavelength.

3.3.2 Estimates of Radar Cross Section of Projectiles

Using the estimating expressions given in the tables, estimates have been developed for the radar cross section of a 20-mm projectile, and these have been sketched in Figure 3-21, as a function of radar wavelength. Radar cross section is computed in db relative to 1 meter², i.e.,

Table III-10. Estimating Relationships for Radar Cross Section in the Rayleigh Region

<u>Elongated Shape</u>	$\sigma(0^\circ) = \frac{4}{\pi} k^4 V^2 F^2$ $F = 1 + (\pi y)^{-1} e^{-y}$ $k = (2\pi/\lambda)$	<u>Ellipsoid</u> $\sigma(0^\circ)/A = (64/9) (\pi C/\lambda)^4 (L/C)^2 F^2$ <u>Cylinder</u> $\sigma(0^\circ)/A = 16 (\pi C/\lambda)^4 (L/C)^2 F^2$
Estimates of Parameter "y"	<p>Spheroid:</p> <p>Cylinder:</p>	$; V = \frac{4}{3} \pi a^2 b; y = b/a = L/C$ $; V = \pi a^2 b; y = \frac{3b}{2c} = \left(\frac{3}{2}\right) \left(\frac{L}{C}\right)$
<u>Sphere</u>	$\sigma = 81 \pi^2 V^2 / \lambda^4$	
<u>All Cases:</u>	For large b/a ; $F \approx 1.0$	



40001-21A

Figure 3-21. Estimated Radar Cross Section of 20-mm Projectile

$$\text{Radar Cross Section in db rel. to } 1\text{m}^2 = 10 \log_{10} \sigma. \quad (3.20)$$

For the case of a flat based projectile, a boattail was assumed that reduced the base area to 70% of the maximum cross sectional area of the projectile.

Note the sensitivity of the solution to assumptions regarding the base shape. Also shown is one experimental point taken with a millimeter radar (discussed later).

To provide some other factual data points, the radar cross sections given in the literature⁽⁹⁾ for some wild and tame life are plotted. The points at different frequencies are connected by dashed lines, but variations between the points will be irregular, since most of them lie in the resonance region. The birds and the bees are averaged over all aspects. The worker bee is stated to have a typical dimension of 15 mm.

The measured radar cross section of a man over the range 3 cm to 70 cm averages about -5 db, and a fighter aircraft nose-on averages about +5 db.

The same method of computation has been applied to projectiles of larger and smaller calibers, and the results are shown in Figure 3-22. All of the flat base cases are computed for 70% reduction in cross sectional area at the boat tail.

Three experimental points obtained with millimeter radar are also shown.

To convert these estimates of cross section to probability of detection by a given radar, assume that one has a specified probability of target detection for the radar on a 1 m^2 target at a specified range. Then it will have at least that probability of detecting a projectile at a range given by

$$\sigma_p/R_p^4 \leq \sigma_1/R_1^4 \quad (3.21)$$

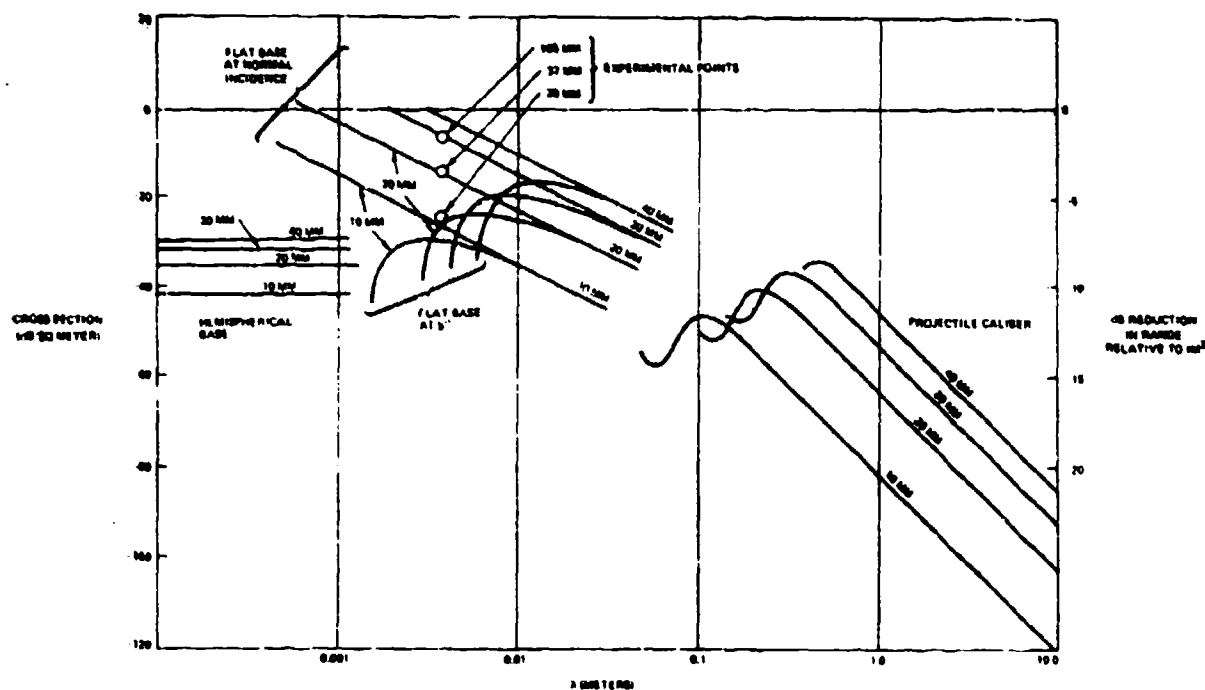
$$\log_{10}(R_p/R_1) \geq [10 \log_{10}(\sigma_p)]/4 \quad (3.22)$$

The reason for the inequality is that atmospheric attenuation will be smaller at the shorter range.

Thus if the projectile cross section is -40 db relative to 1 m^2 , the radar range is shortened to about 1/10 of its equiprobability range on 1 m^2 . The right hand scale of Figure 3-22 shows this factor, which is conservative because it does not correct for atmospheric attenuation of the signal.

3.3.3 Estimates for Corner Reflectors

One method of improving the signature of a projectile is to insert a reflector in its base. Table III-11 and Figure 3-23 summarize the estimating relationships for corner reflectors.⁽¹⁰⁾ The advantage of a corner reflector is that if it is accurately fabricated, the radar cross section is large, and changes only slowly for angles off the axis of symmetry of the reflector.



40001 72A

Figure 3-22. Estimated Radar Cross Sections of Projectiles vs. Wavelength and Caliber

On the other hand, the accuracy of fabrication required is a function of the ratio of the illuminating wavelength to the length of a side of the reflector, i.e., the angular accuracy to which the orthogonality of the three sides must be held depends on λ/b , where λ = wavelength and b = length of a side.

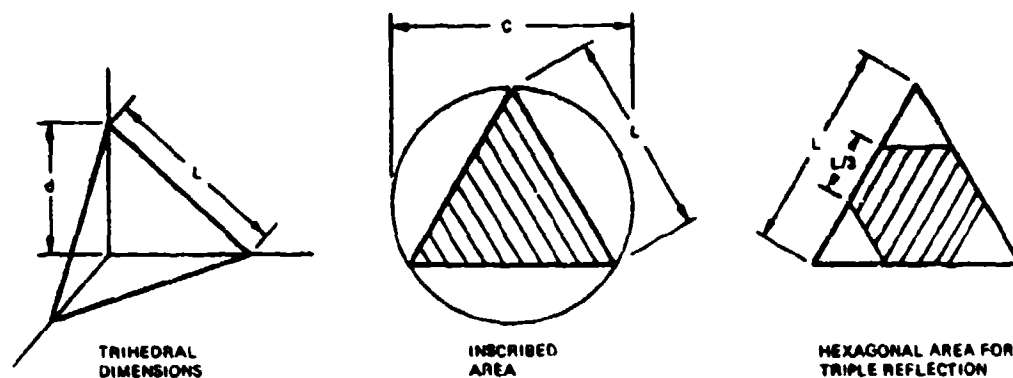
At laser wavelengths, this implies optical precision of manufacture.

Figure 3-24 shows the effect of such errors on manufacture on the radar cross section, and variation of cross section with angle from symmetry for a particular corner

Table III-11. Estimated Radar Cross Section of Trihedral

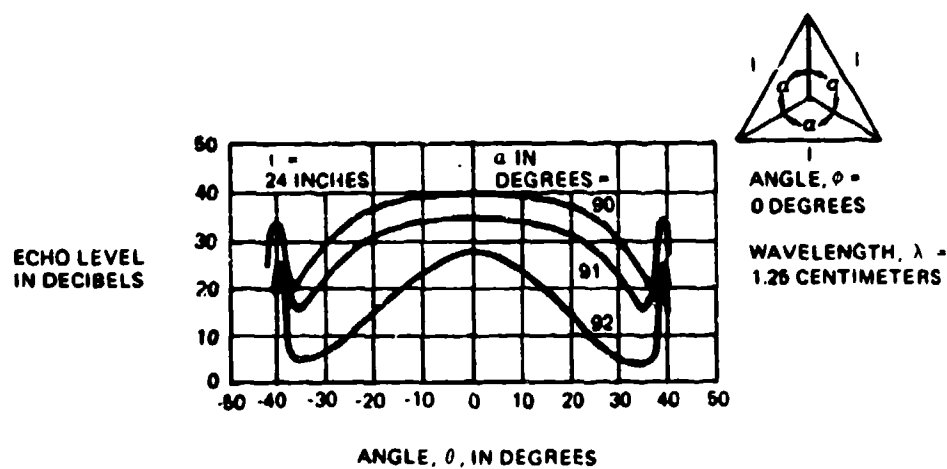
Radar Cross Section	$\sigma = \frac{4\pi(A_{\text{eff}})^2}{\lambda^2}$	<u>Symbols</u> σ = Radar Cross Section C = Caliber of Projectile Base λ = Wavelength θ = Angle off Axis of Symmetry L = Length of Edge ϵ = Angular Error of Fabrication
Inscribed Area	$A_1 = \frac{(3)^{3/2}}{16} C^2$	
Effective Area (Axis of Symmetry)	$A_{\text{eff}} = \frac{2}{3} A_1$ $= \frac{3^{1/2}}{8} C^2$	
Radar Cross Section (Axis of Symmetry)	$\sigma = 0.589 \frac{C^4}{\lambda^2}$	
Reduction for Off-Axis Viewing (θ in Degrees)	$\sigma = 0.589 \frac{C^4}{\lambda^2} (1 - .00076\theta^2)^2$	
Effect of Constructional Errors: 50% reduction in σ for: One side misaligned by angle $\epsilon = 0.70 (\lambda/L)$ Three sides each misaligned by $\epsilon = 0.35 (\lambda/L)$		

Note: For laser cross section multiply "radar" cross section by reflectivity of surfaces.



40001-23

Figure 3-23. Determination of Effective Area of Trihedral



40001-24

Figure 3-24. Effect of an Error in all Three Corner Angles Upon the Performance of a Trihedral

reflector.⁽²⁰⁾ Note that the half-power lobe width narrows much more rapidly than the cross section decreases, as error in fabrication is increased.

The estimating relationship given in Table III-11 for the reduction in cross section with angle off the axis of symmetry indicates a 50% reduction in effective cross section (-3 db) for an angle of about 19.6° off the axis of symmetry.

To estimate the laser cross section of the trihedral, the estimates of radar cross section should be corrected for the reflectivity of the surfaces of the trihedral at the laser wavelength. Since three surfaces (and three reflections) are involved, one would expect that 90% reflectivity per surface would require multiplication by 73%.

It was indicated in Table III-11 that the orthogonality of the three sides of a trihedral should be held to an angular error of somewhat less than the ratio of wavelength to edge length of the reflector. This represents optical precision at laser wavelengths, and in view of the disbelief with which this statement of requirement is sometimes greeted, it seems desirable to show how it comes about.

For simplicity, we work an example with a rectangular corner reflector, instead of the trihedral of Table III-11. The effects are nearly the same.

Consider the simple rectangular corner reflector of Figure 3-25. If the corner is a perfect right angle, the axis of an incoming beam and the reflected beam are collinear. But if the angle differs from a right angle by Δ , the axis of the reflected beam is diverted by 2Δ .

The laser cross section is

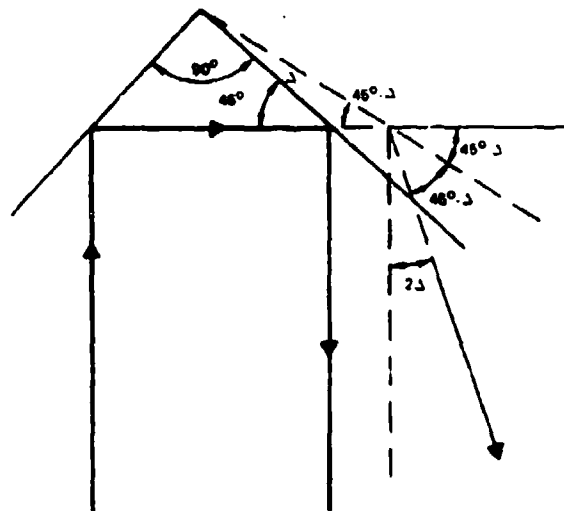
$$\sigma = GA \quad (3.23)$$

where

$$G = \text{gain} = 4\pi A/\lambda^2 = 4\pi/\Omega \quad (3.24)$$

hence Ω , the solid angle of the reflected beam is

$$\Omega = \lambda^2/A \quad (3.25)$$



40001-25

Figure 3-25. Effect of Construction Error in Trihedral Fabrication and for a rectangular corner reflector

$$A = (3)^{1/2} b^2 \quad (3.26)$$

beam input on the axis of symmetry.

The solid angle of the reflected beam is

$$\Omega = \lambda^2 / A = (3)^{-1/2} (\lambda/b)^2 \quad (3.27)$$

In one dimension

$$(\Omega)^{1/2} = 3^{-1/4} (\lambda/b) \quad (3.28)$$

The beam is not rectangular, but assuming the preceding expression as an approximation, if we deviate the axis by the specified beam width, we miss the return. If we assume that a construction error of angle is Δ so that the return beam axis is deflected by 2Δ ,

$$2\Delta < \frac{\lambda}{\sqrt{A}} \quad (3.29)$$

$$\Delta < 0.38 \frac{\lambda}{b} \quad (3.30)$$

A more accurate computation^{10, 11} gives

$$\Delta = (0.40) (\lambda/b) \quad (3.31)$$

for the half power return point.

This accounts for the beam shape and deviations from the axis of symmetry. The same source gives, for three equal angle errors in each side

$$\Delta = 0.24 (\lambda/b) \quad (3.32)$$

In the optical range, the allowable Δ is therefore very small indeed.

Multiple Reflectors

A suggestion was made that instead of a single reflector, one might have many small reflectors on the same surface.

For a single reflector, the laser cross section is

$$\sigma_1 = 4\pi A_1^2 / \lambda^2 \quad (3.33)$$

Assume that one can get n reflectors, each of area A_n , into a total area A_1 . For each of these smaller reflectors,

$$A_n = A_1/n \quad (3.34)$$

$$\sigma_n = 4\pi A_n^2 / \lambda^2 = 4\pi A_1^2 / (n\lambda)^2 \quad (3.35)$$

and they sum to

$$\Sigma \sigma_n = n \sigma_n = 4\pi A_1^2 / (n\lambda)^2 = \sigma_1 / n \quad (3.36)$$

hence it is best to have a single large reflector for a specified area A.

It is undesirable to increase the cost of a projectile by putting a trihedral in its base, and a subsequent section describes a potential, but less effective method of avoiding this. However, if a trihedral is necessary to obtain an adequate laser signature, the fabrication accuracy indicated to be necessary in the above paragraphs suggests that the trihedral might be an optical prism, manufactured by standard optical techniques, with the assembly as suggested in Figure 3-26. Cost probably is strongly related to precision of manufacture, i.e., the orthogonality of the reflecting faces. A concept for relaxing this requirement, which would broaden the return lobes at the expense of cross section, is sketched in Figure 3-27, which shows a very slight convexity (large constant radius) ground into each face.

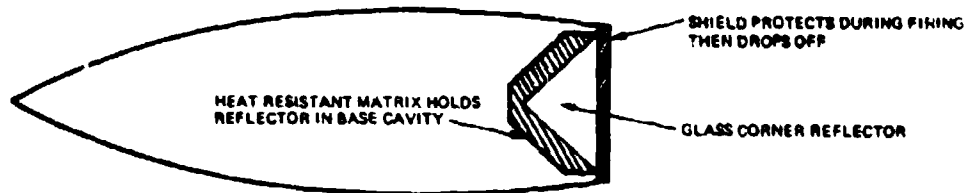
3.3.4 Comparison of Estimated Radar Cross Sections vs. Measurements

Frankford Arsenal has made available reports of measurements of radar cross section of projectiles at 70 GHz, taken by the Ballistic Research Laboratories. ⁽²²⁾

The experiments were made on projectiles ranging in caliber from 20-mm to 105-mm, both with and without trihedral reflectors in the base. For the cases discussed in this section, the projectile models with trihedrals were made of aluminum, and the trihedrals were machined into the bases.

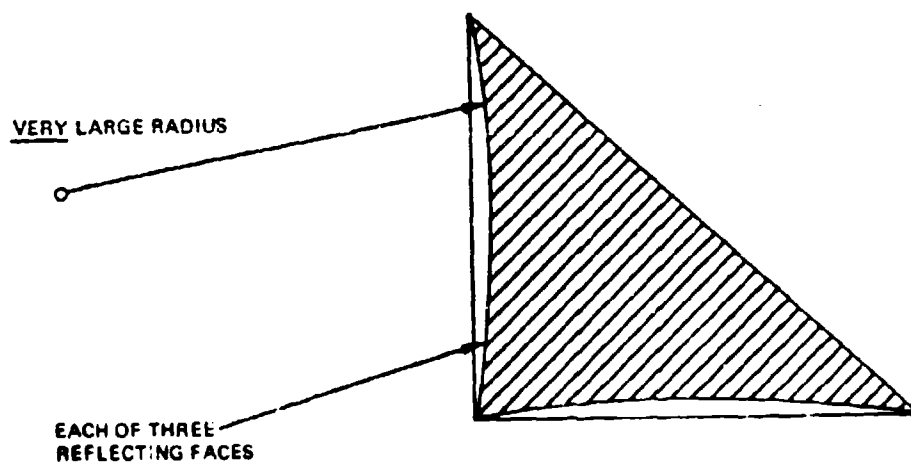
Table III-12 lists the measured radar cross sections (maximum) obtained at a tail-on aspect.

The radar cross section of the projectiles with trihedrals compares well with estimates computed by the methods given in earlier sections of this report, and the comparison is shown in Figure 3-28. The BRL report comments on the possibility of destructive interference between the reflections from the trihedral, and the residual flat base in which it is cut. Estimates of this interference require a more complex computation than the simple expressions used here.



40001-26

Figure 3-26. Hypothetical Design of Projectile with Trihedral to Maximize Laser Cross Section

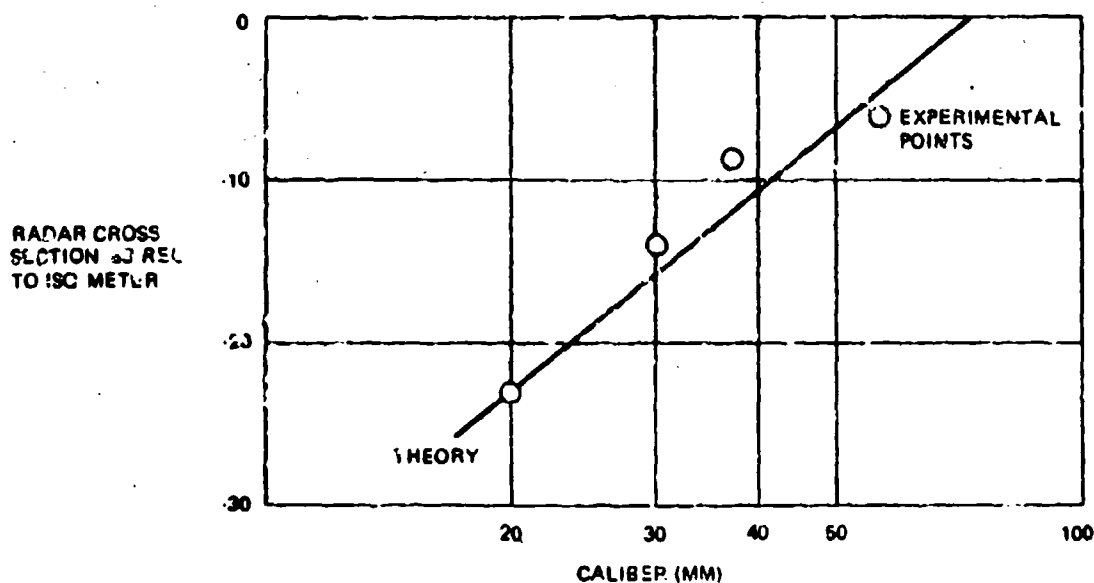


40001-27

Figure 3-27. Possible Method of Reducing Effect of Fabrication Errors

Table III-12. Measured Radar Cross Section of Projectiles (Maximum in Tail Aspect) at 70 GHz

Projectile Unmodified		Cross-Section (Peak) (m ²)	db Rel. to 1 m ²
Caliber	Base		
20 mm	?	0.005	-23
30 mm	?	<0.0001	<-40
37 mm	?	<0.0001	<-40
57 mm	"Flat"	0.041	-14
105 mm	"Flat"	0.20	-7.0
105 mm APDS	?	0.013	-19
With Trihedral Reflector			
20 mm		0.005	-23
30 mm		0.042	-14
37 mm		0.13	-8.9
57 mm		0.25	-6.0



40001-28

Figure 3-28. Comparison of Experiment and Theory for Projectiles with Trihedrals at 70 GHz

The radar cross sections of the projectiles without trihedrals (as normally used, without modification) are shown in Figure 3-29, compared against flat base theory, and against several curves for bases of constant curvature. No significant return was obtained from two of the projectiles. For the cases plotted, the variation with caliber follows a C^2 slope (base with slight curvature) rather than a C^4 slope (perfectly flat base).

The two projectiles which did not yield significant returns, (30 mm and 37 mm) were both boat-tailed down to bases of about 25 mm diameter. There is no obvious reason for their low signature, since the 20-mm projectile provided a measurable return. The 57-mm had a small base cavity (probably for tracer).

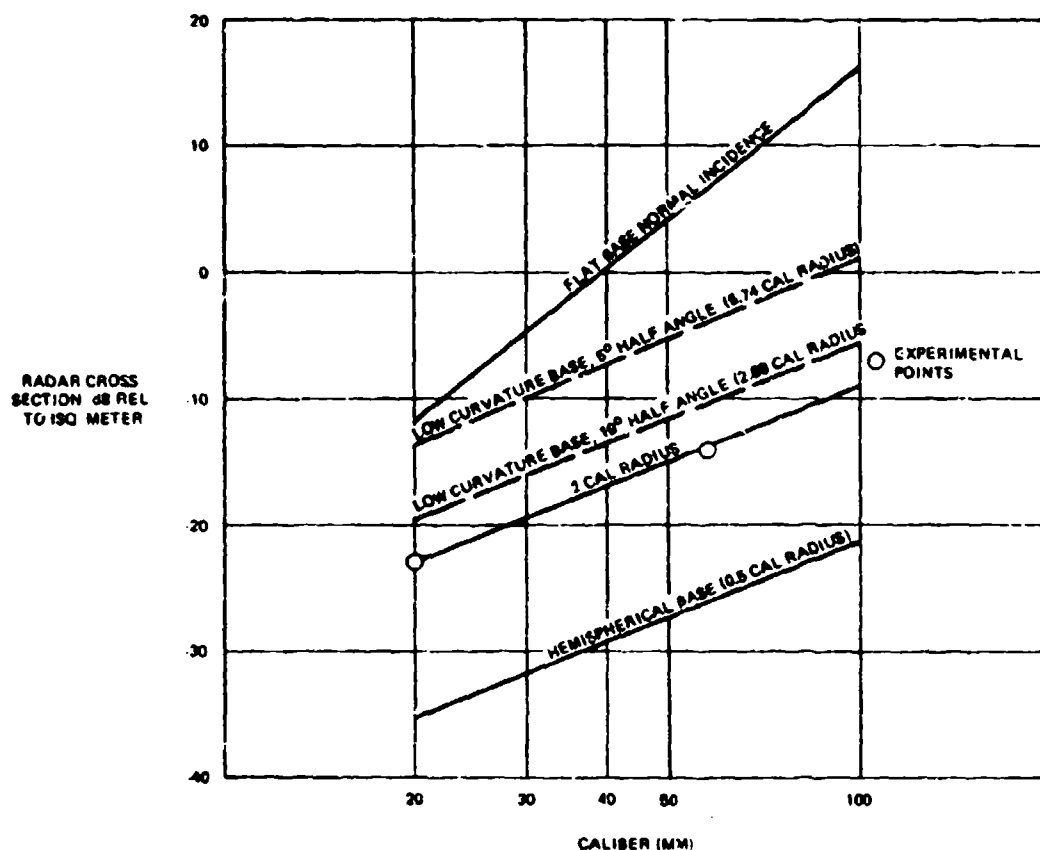
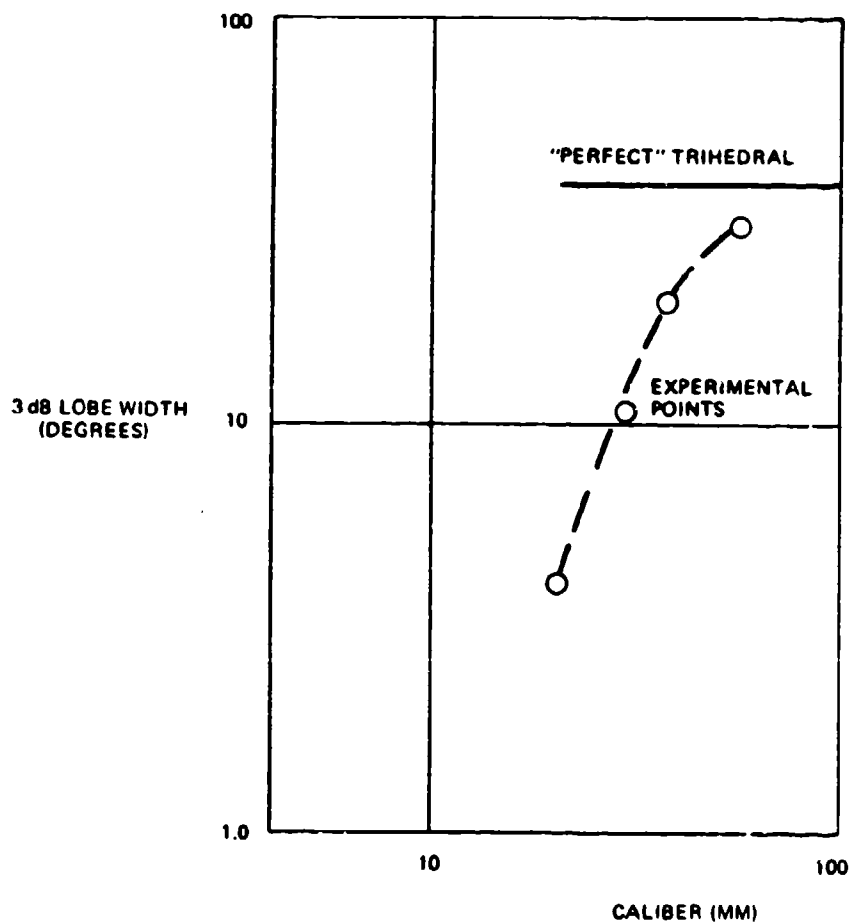


Figure 3-29. Comparison of Experimental and Theoretical Radar Cross Sections of Projectiles at 70 GHz

The measured lobe widths between half power points (-3 db) are plotted in Figure 3-30 for the projectiles with trihedrals, and compared against the expected lobe width for a perfect trihedral. BRL suggests that destructive interference between the trihedral and flat base segment reflections may be responsible for the discrepancy. However, if the accuracy of maintaining the sides of the trihedral orthogonal were imperfect to the same amount in angular measure, one would expect a similar degradation, increasing as caliber is reduced. At 70 GHz, however, fabrication errors are less likely as a source of the observed degradation.



40001-30

Figure 3-30. Comparison of Experimental and Theoretical Lobe Widths of Projectiles with Trihedrals at 70 GHz

Lobe widths for the unaugmented projectiles are shown in Figure 3-31 where they are compared against lobe width from flat base theory, and alternately on the assumption that the base has slight curvature. The best one can say is that the experimental points are bracketed by the two methods of estimation.

The maximum radar cross sections for the trihedrals agree well with the theoretical estimates. The measured lobe widths agree with theoretical estimates better for the large projectiles than for the small.

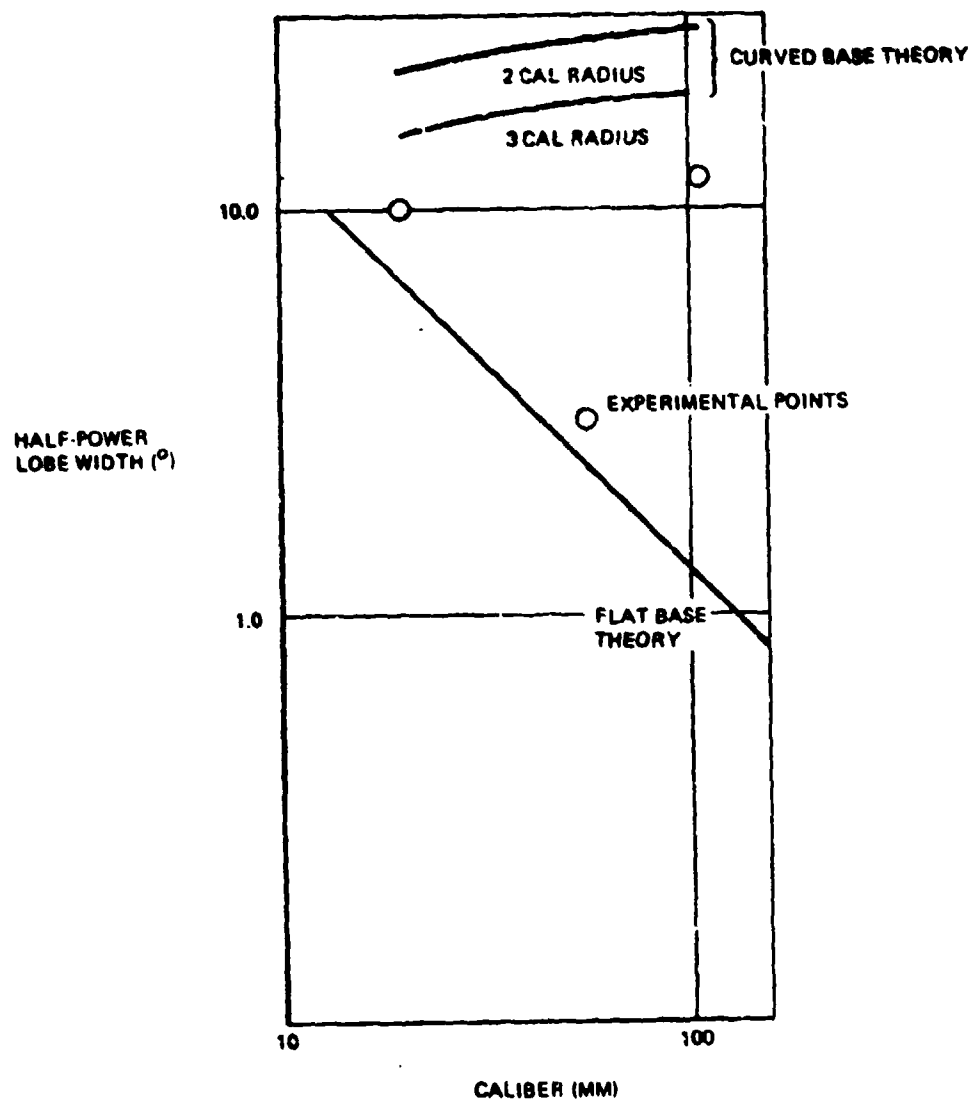
For projectiles without trihedrals, those for which signatures were measurable showed a variation of radar cross section with caliber corresponding to that which theory would indicate for projectiles with 2 caliber radius bases. They did not approach the estimates from simple flat plate theory. Lobe widths were bracketed by the two methods of estimation.

In summary, considering 70 GHz data, the simple methods of estimating radar cross section in the optical region appear to be adequate for predicting the maximum radar cross sections of trihedrals, but the discrepancy in lobe width prediction suggests the requirement for more testing and application of more refined estimation methods to determine the cause of the discrepancy.

If the discrepancy results from destructive interference between the returns from the trihedral and the residual flat base segment, the flat section may possibly be removed, using the BRL experimental designs of "square" boat-tails adapted to "triangular" boat-tails.

For projectiles without trihedrals, it appears that apparently flat bases do not reflect as theoretical flat bases, and that the steps, boat-tailing and notches in some existing projectiles may cause a complete loss of signature. However, those signatures that were obtained were large enough for limited use in closed-loop systems using this frequency of radar (70 GHz).

In this case, what is required is a series of measurements of radar cross section on projectiles whose bases are designed to give maximum signature over the expected angle of viewing, with smooth transitions from the base shape to the body contours to avoid undesirable interferences.



40001-31

Figure 3-31. Comparison of Experimental and Theoretical Lobe Widths of Projectiles at 70 GHz

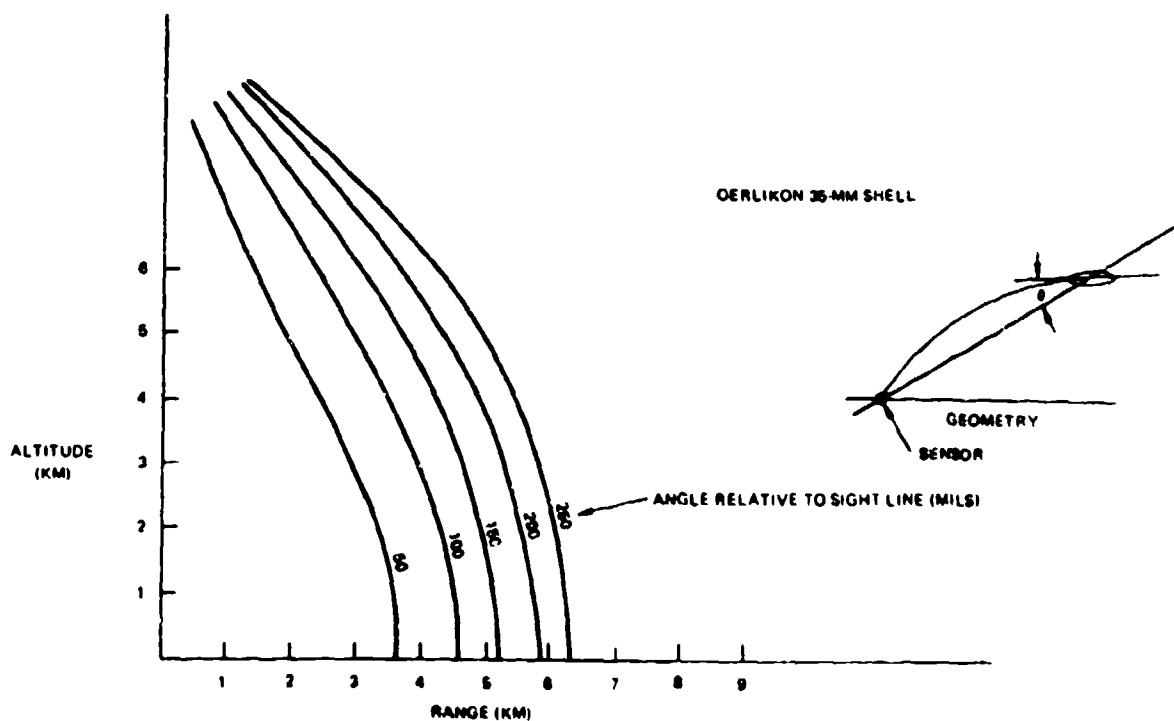
3.3.5 Callipygean Projectiles ⁽²³⁾

For very short wavelengths, from the millimeter radar to the laser/optical region, the radar/laser cross section is proportional to the product of radii of curvature at the specular point, provided that each radius of curvature is large compared with the wavelength. The lobe width of a flat base is too narrow to be useful at these frequencies, and the radar cross section of a hemispherical base is only equal to the geometric cross sectional area of the projectile.

However, by using a curved base of very large radius, one may possibly attain a radar cross section of useful magnitude, as well as a half-power lobe width sufficient to include all desired viewing angles.

Projectiles of this type, with well shaped bases, we call Callipygean. ⁽²³⁾

To obtain an estimate of the maximum angle off the projectile's longitudinal axis at which we shall desire a signature, the projectile angle relative to line of sight to the projectile has been plotted in Figure 3-32 for the Oerlikon 35-mm weapon, as a function of range and altitude of the projectile relative to the gun.



40001.32

Figure 3-32. Required Off-Axis View Angle versus Range for Oerlikon 35-mm Projectile

Note that a maximum off-axis view angle of 50 mils provides complete coverage to about 3.6 km range; 100 mils provides coverage to about 4.6 km. Hence we are interested in maximum view angles off the projectile axis of about 5° .

The projectile longitudinal axis is inclined to the line of sight (hence to the laser beam axis) by an angle which increases with range as a result of gravity drop.

Assume that the projectile base is a surface of revolution, with the shape chosen so that the product of the principal radii of curvature increases as the specular point moves off-axis. If these radii are R_1, R_2 , the radar/laser cross section is approximately

$$\sigma = \pi R_1 R_2 \rho \quad (3.37)$$

where ρ = reflectivity of the surface, unity for radar.

The specular point will be close to the longitudinal axis for short range illumination, and will move off with range by an angle increasing about as slant range. One would like σ to increase about as the fourth power of range. A section through the base might then have the shape shown in Figure 3-33, with the radius of curvature increasing rapidly with distance from the longitudinal axis.

We compute the shape approximately. ⁽¹⁰⁾ ρ is suppressed in the following to shorten notation: it is simply a multiplier.

For a body of revolution

$$r = r(z) \quad (3.38)$$

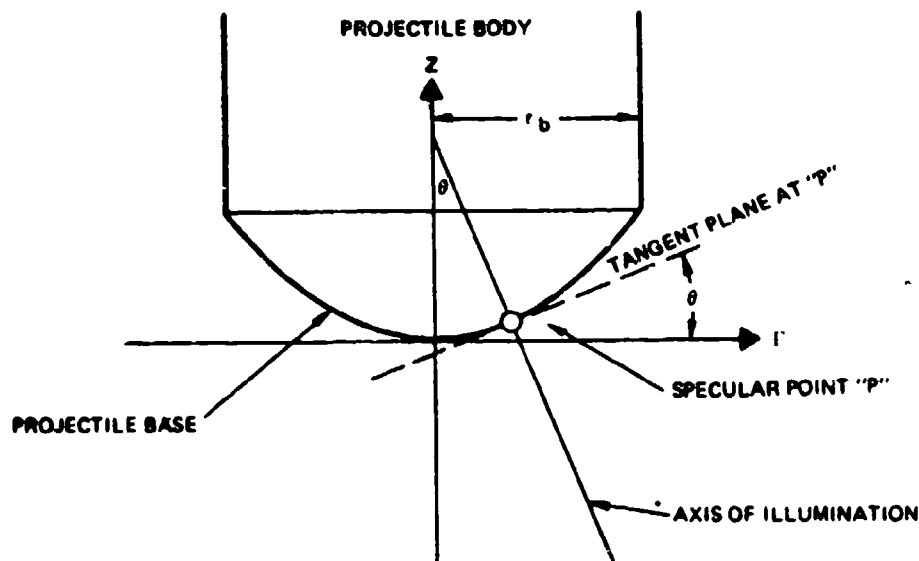
$$\sigma = \pi R_1 R_2 \quad (3.39)$$

$$\sigma = \pi \left| \frac{r}{d^2 r / dz^2 \sin^4 \theta} \right| \quad (3.40)$$

where coordinates are defined in Figure 3-33, and r, r'' are evaluated at the specular point.

The specular point is defined by

$$\tan \theta = dz/dr \quad (3.41)$$



40001-33

Figure 3-33. Geometric Relations for Shaped Projectile Base

Superelevation angle increases as about the first power of the range. For a vacuum

$$\phi_s = g/(2v_0^2) D \sin \phi \quad (3.42)$$

To this zero order approximation, the projectile off-axis view angle equals superelevation.

It would be useful if the laser cross section of the projectile increased with tilt in such a way that the power in the reflected signal was a constant with range. Since power (except for atmospheric attenuation) varies inversely as range⁻⁴, we would like the laser cross section to increase as the fourth power of the angle off the longitudinal axis.

Suppose that we shape the projectile base as a body of revolution described by

$$z = kr^a \quad (3.43)$$

$$r = z^{1/a} k^{-1/a} \quad (3.44)$$

then

$$dz/dr = kar^{a-1} = \tan \theta \quad (3.45)$$

where θ is the angle of view at which the specular point lies at r .

For maximum off-axis view angle θ_m , we place the specular point at the rim of the projectile base, which has a radius r_b

$$\tan \theta = kar^{a-1} \quad (3.46)$$

$$\tan \theta_m = kar_b^{a-1} \quad (3.47)$$

and we use these expressions to eliminate parameter k .

$$(r/r_b) = (\tan \theta / \tan \theta_m)^{1/(a-1)} \quad (3.48)$$

Now

$$dr/dz = a^{-1} z^{(1-a)/a} k^{-1/a} \quad (3.49)$$

$$d^2r/dz^2 = [(1-a)/a^2] z^{(1-2a)/a} k^{-1/a} \quad (3.50)$$

and the laser cross section for unit reflectivity is

$$\sigma = \pi \left| \frac{z^2 a^2}{(1-a) \sin^4 \theta} \right| \quad (3.51)$$

and laser cross section in terms of view angle θ , maximum view angle θ_m and r_b is

$$\sigma = \frac{\pi r_b^2}{\sin^2 \theta_m} \left| \left(\frac{\tan^2 \theta_m \sin^2 \theta_m}{(1-a) \sin^4 \theta} \right) \left(\frac{\tan \theta}{\tan \theta_m} \right)^{2a/(a-1)} \right| \quad (3.52)$$

we shall be interested only in small angles for which

$$\sin \theta \approx \tan \theta \approx \theta \quad (3.53)$$

so that finally

$$\sigma = \pi r_b^2 / \theta_m^2 \left| \frac{1}{(1-a)} (\theta / \theta_m)^{2(2-a)/(a-1)} \right| \quad (3.54)$$

If we want σ to increase with θ^4 we solve for a , and obtain $a = 4/3$
then

$$\sigma = 3\pi r_b^2 / \theta_m^2 \left(\frac{\theta}{\theta_m} \right)^4 \quad (3.55)$$

This suggests that σ would be zero for on axis viewing. However the approximation used to compute σ fails when the radius of curvature approaches the order of a wavelength. A more accurate expression is required to compute σ for $\theta = 0$, and would include λ explicitly.

For non-zero angles of view the above expression is probably adequate as a rough approximation.

We tabulate below in Table III-13 the functional form of σ for several values of a , and also give z_m . Then using these values we sketch the projectile base cross sections in Figure 3-34.

We have

$$z_m = r_b \tan \theta_m / a \quad (3.56)$$

$$z_m \approx r_b \theta_m / a$$

Note that in Figure 3-34 the vertical scale is exaggerated. All sections have the same slope at $r/r_b = 1.0$.

Table III-13. Comparison of Estimated Radar Cross Sections of Shaped Bases versus View Angle

a	$z_m/(r_b \theta_m)$	$\sigma / \left[(\pi r_b^2) / \theta_m^2 \right]$	Comments
1	1	Surface is a cone; approximation does not apply	
4/3	3/4	$3(\theta/\theta_m)^4$	not valid for very small values of θ
3/2	2/3	$2(\theta/\theta_m)^2$	
5/3	3/5	$1.5(\theta/\theta_m)$	
2	1/2	1.0	(for these small angles, the parabola is an approximation to a spherical section)
7/3	3/7	$0.75(\theta/\theta_m)^{-1/2}$	not valid for small values of θ

In Figure 3-35 we show how laser cross section varies with θ for the parabolic base, and various values of θ_m . In Figure 3-36 we compare the parabolic base and the 4/3, 5/3 law base.

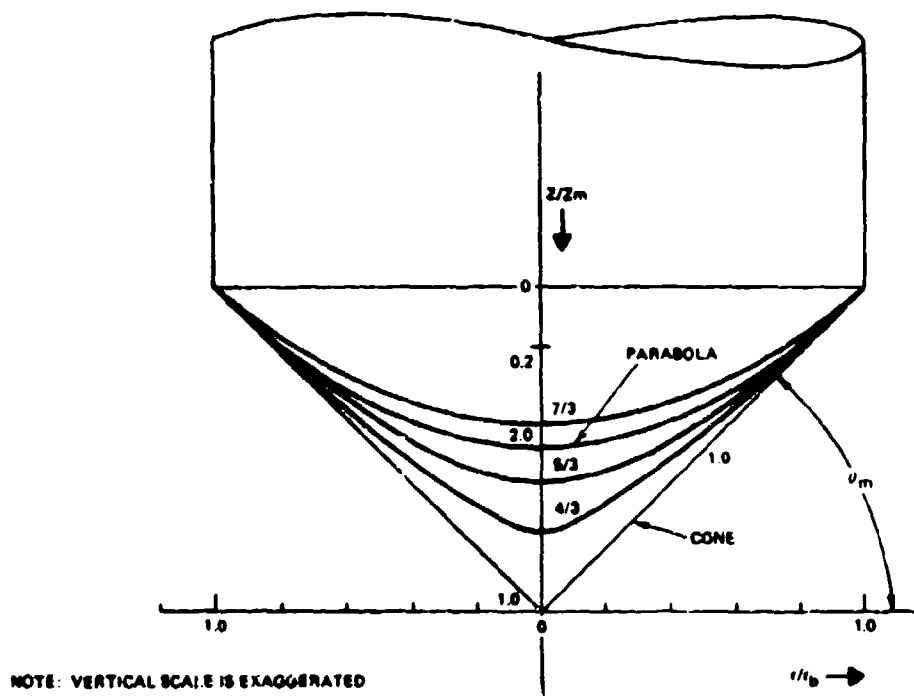
Finally in Table III-14 we compare some of the computations of laser cross section for the 30-mm projectile with various base shapes. The tables give values for unit reflectivity. Multiply the values given by about 0.20 to 0.80 depending on surface reflectivity for estimates of the realizable cross sections.

The estimate of about -2 db to 4 db for a shaped base, depending on reflectivity suggests that this simple approach, although far inferior to a possibly expensive corner reflector, deserves further analysis and experimentation.

3.3.6 Infrared Signature of the Projectiles

In this section we consider the possibility of sensing the projectile with a thermal imaging sight such as FLIR. The methodology can be used in two ways: (1) to estimate the probability of detecting a projectile with an imaging sight in view of the difference in between projectile temperature and the background (most unlikely), and (2) to determine the required radiant emission of pyrotechnics (tracer) in the sensitivity region of the sensor for reliable detection (probably achievable).

The likelihood of detecting a passive projectile with an imaging sight is indicated to be small, even under optimistic assumptions. Hence the detail presented is probably



40001-34A

Figure 3-34. Sections Through Projectile Base for "Power Law" Shaping

superfluous for signature estimation. However the characteristics of the imaging sight developed are used elsewhere in this report (Section 3.2.2) in the discussion of the problem of coordinating laser illumination and FLIR sensing of projectiles.

We consider the projectile simply as a hot body, of ill-defined temperature which must be viewed against a background, usually sky, but occasionally terrain.

A blackbody emits radiation whose spectral distribution with wavelength is given by Planck's law⁽¹⁴⁾⁽¹⁵⁾⁽²⁴⁾

$$W_{\lambda} = \left(c_1 / \lambda^5 \right) \left[e^{c_2 / \lambda T} - 1 \right]^{-1} \quad (3.57)$$

where

W_{λ} = the spectral radiant emittance (watt $\text{cm}^{-2} \mu^{-1}$)

λ = wave length (microns)

T = absolute temperature (degrees Kelvin)

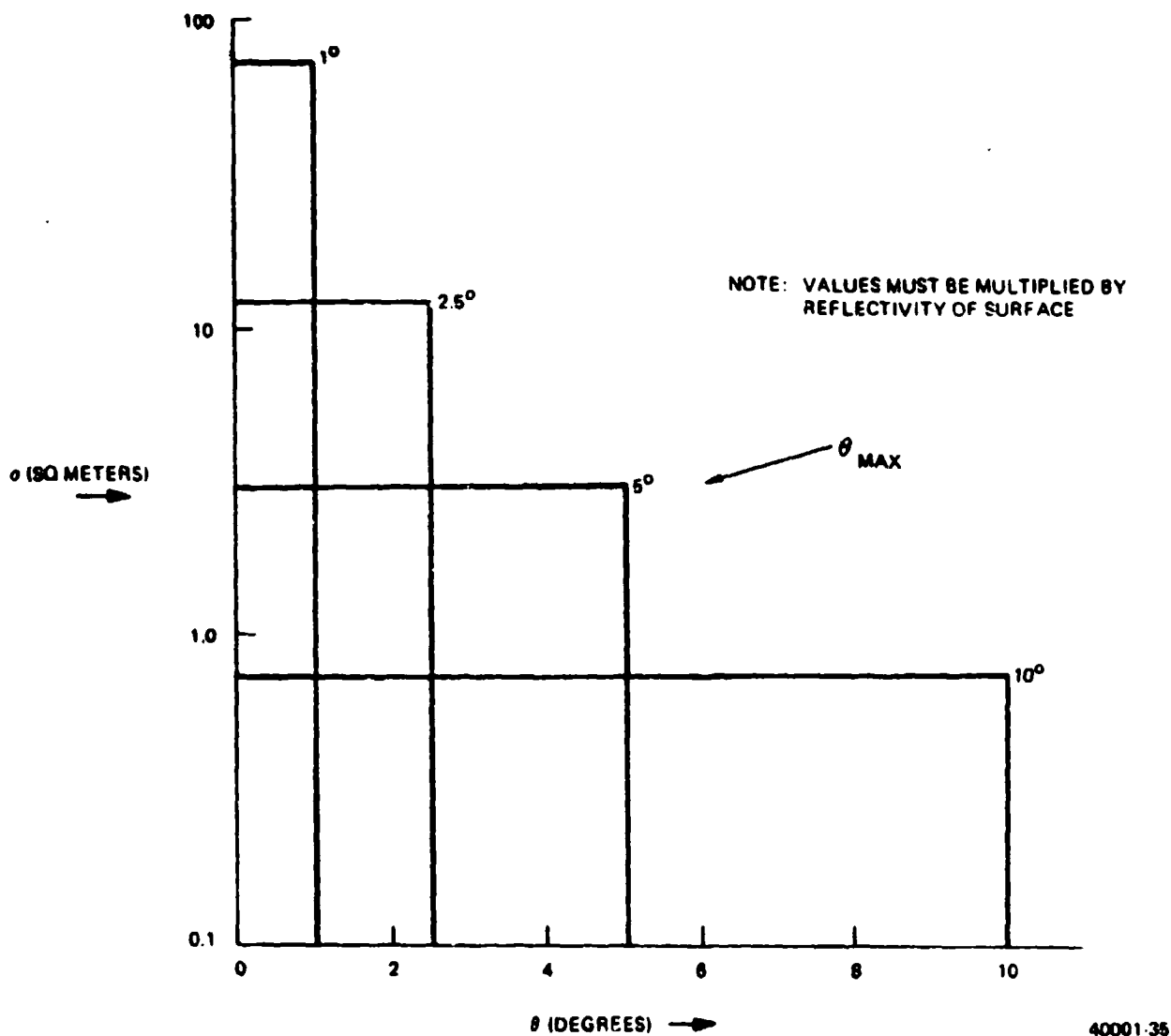


Figure 3-35. Estimated Laser Cross Section of 30-mm Projectiles with Parabolic Base

$$c_1 = \text{"first radiation constant"} = 3.742 \times 10^{-12} \text{ (watt cm}^{-2} \mu^4\text{)}$$

$$c_2 = \text{"second radiation constant"} = 1.439 \times 10^4 \text{ (}\mu^{\circ}\text{K)}$$

The total radiant emittance is obtained by integrating

$$W = \int_0^{\infty} W_{\lambda} d\lambda \quad (3.58)$$

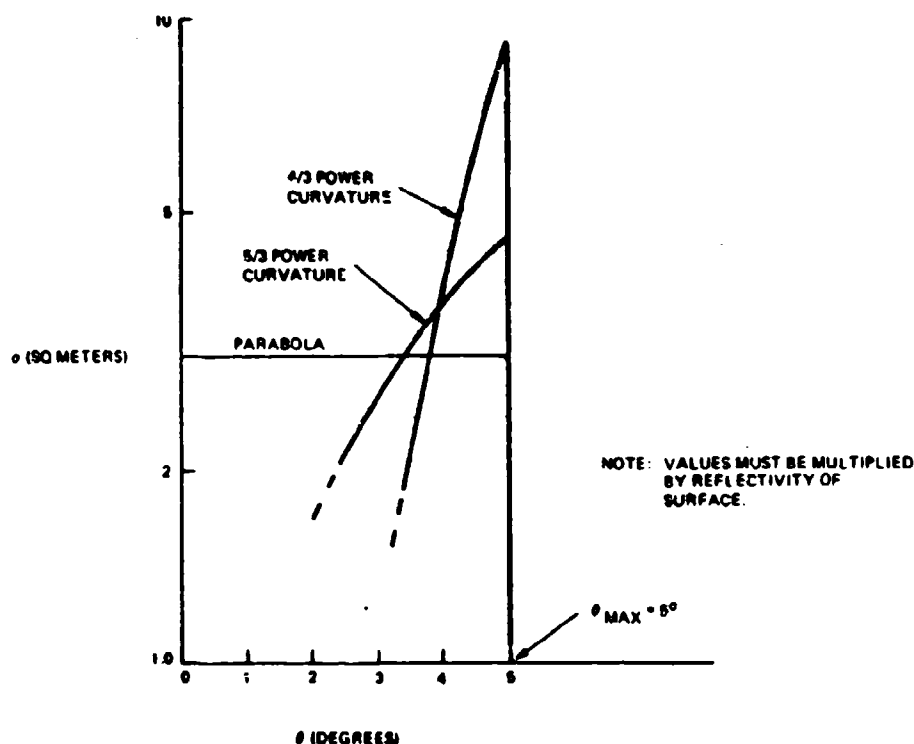


Figure 3-36. Estimated Laser Cross Section of 30-mm Projectiles with "Power Law" Base Shapes

$$W = \sigma T^4 \quad (3.59)$$

where

σ = the Stefan-Boltzmann constant = 5.67×10^{-12} (watt $\text{cm}^{-2} \text{ } ^\circ\text{K}^{-4}$)

The fraction of radiant emittance contained in the range $\Delta\lambda = (0, \lambda)$ has been computed in tabular form¹, and is also found on "radiation slide rules". It is plotted in Figure 3-37.

For the present paper we consider sensors operating in an arbitrarily assumed window from 8-14 microns and Figure 3-38 compares the total radiant emittance and the radiant emittance over 8-14 microns of blackbodies.

A projectile is not a perfect "black body" hence we must multiply the values of Figure 3-38 by an "emissivity" factor, ϵ . In particular, in the absence of experimental data, we assume $\epsilon = 0.80$.

The various quantities, symbols and their dimensions involved in computing how much of the radiant emittance at the target reaches the sensor¹⁴¹⁵²⁴ are summarized for convenience in Figures 3-39 and 3-40.

Table III-14. Comparison of Estimated Laser Cross Sections of 30-mm Projectiles versus Base Shape (db Relative to 1 Square Meter)

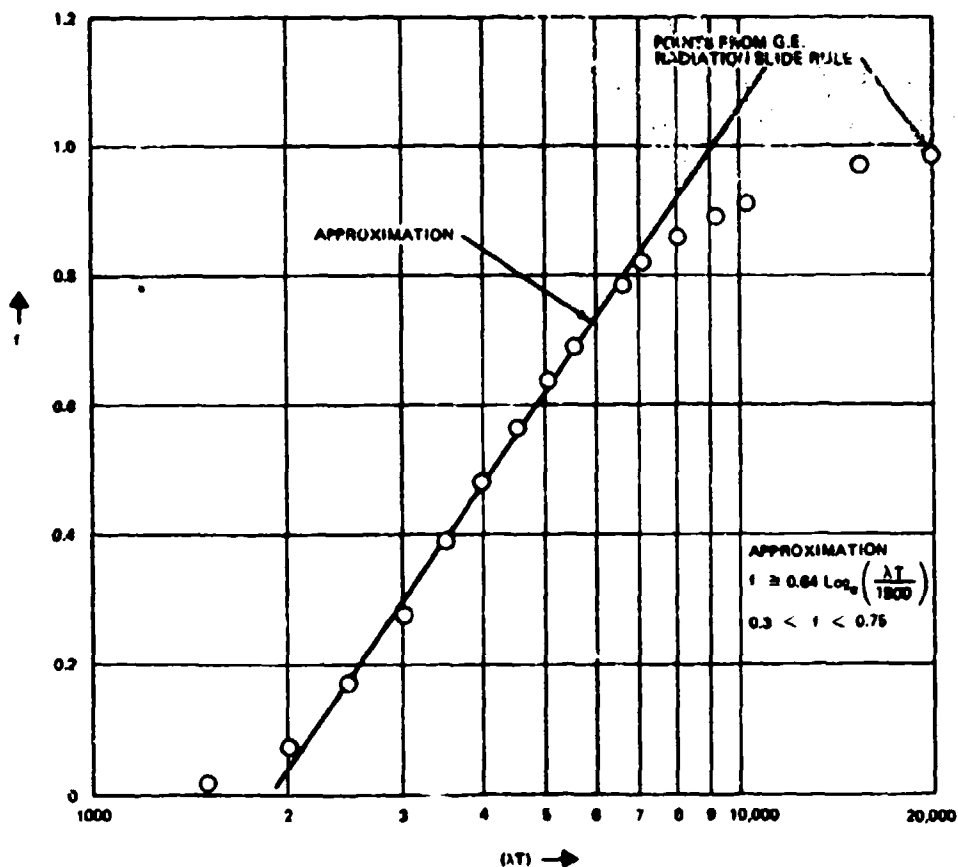
Wavelength	1 Micron			10 Microns		
Angle Off Axis	0°	5°	10°	0°	5°	10°
Base Type						
Ideal Trihedral Reflector	50.7	50.7	50.6	30.7	30.7	30.6
Flat Base	60.8	Nil	Nil	40.8	Nil	Nil
Hemispherical Base	-39.1	-39.1	-39.1	-39.1	-39.1	-39.1
Parabolic Base						
10° Max	-1.2	-1.2	-1.2	-1.2	-1.2	-1.2
5° Max	4.8	4.8	Nil	4.8	4.8	Nil
4/3 Power Law Base						
10° Max		-8.5	3.6		-8.5	3.6
5° Max		9.6	Nil		9.6	Nil
<p>NOTE: For single reflection subtract 7 db from above for 20% reflectivity 1 db for 80% reflectivity</p> <p>For trihedral subtract 21 db for 20% reflectivity 3 db for 80% reflectivity</p>						

The "spectral irradiance" at the collector lens is

$$H_{\lambda} = \frac{W_{\lambda} A_p \tau_a(\lambda)}{\pi r^2} \text{ (watt cm}^{-2} \mu^{-1}\text{)} \quad (3.60)$$

and using the subscript (_w) to designate the integral of the functions over the 8-14 micron window, with an average value of τ_a over the window

$$H_w = \frac{W_w A_p \tau_a}{\pi r^2} \text{ (watt cm}^{-2}\text{)} \quad (3.61)$$



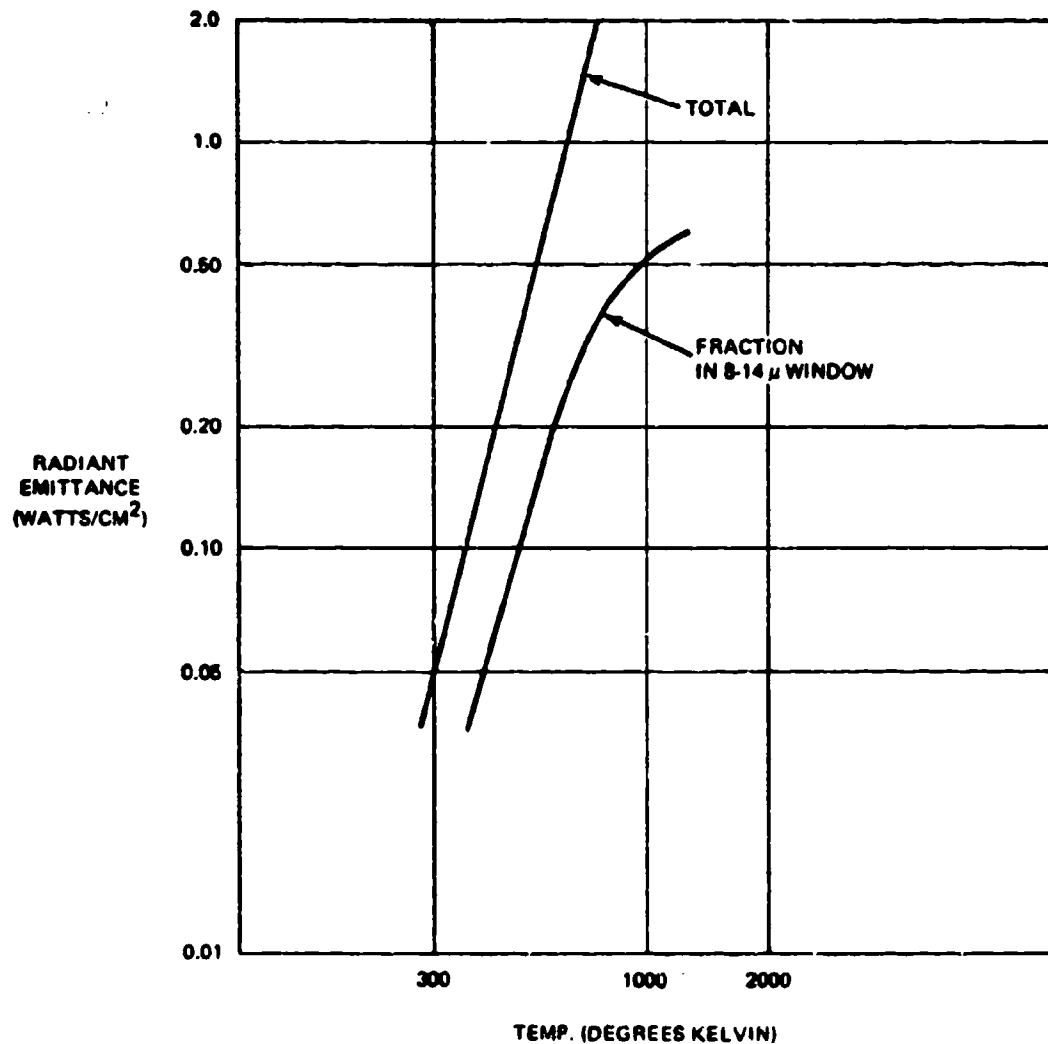
40001-37

Figure 3-37. Fraction of Radiant Emittance Below Specified Values of λT

This irradiance falls on collector optics of effective area A_o , and transmissivity (averaged over λ), τ_o , so that the "radiant flux" available at the detector element is

$$P = \frac{W_w A_o \tau_o}{\pi r^2} \quad (\text{watts}) \quad (3.62)$$

For definitions of the symbols refer to Figures 3-39 and 3-40.



40001-38

Figure 3-38. Radiant Emittance of Black Body in 8-14 Micron Window versus Temperature

The detector receives P watts and develops a voltage V_g which is then processed for display and/or computation. Symbolically

$$V_g = \int P_\lambda R_\lambda d\lambda$$

(3.63)

$$\approx P_w R_w$$

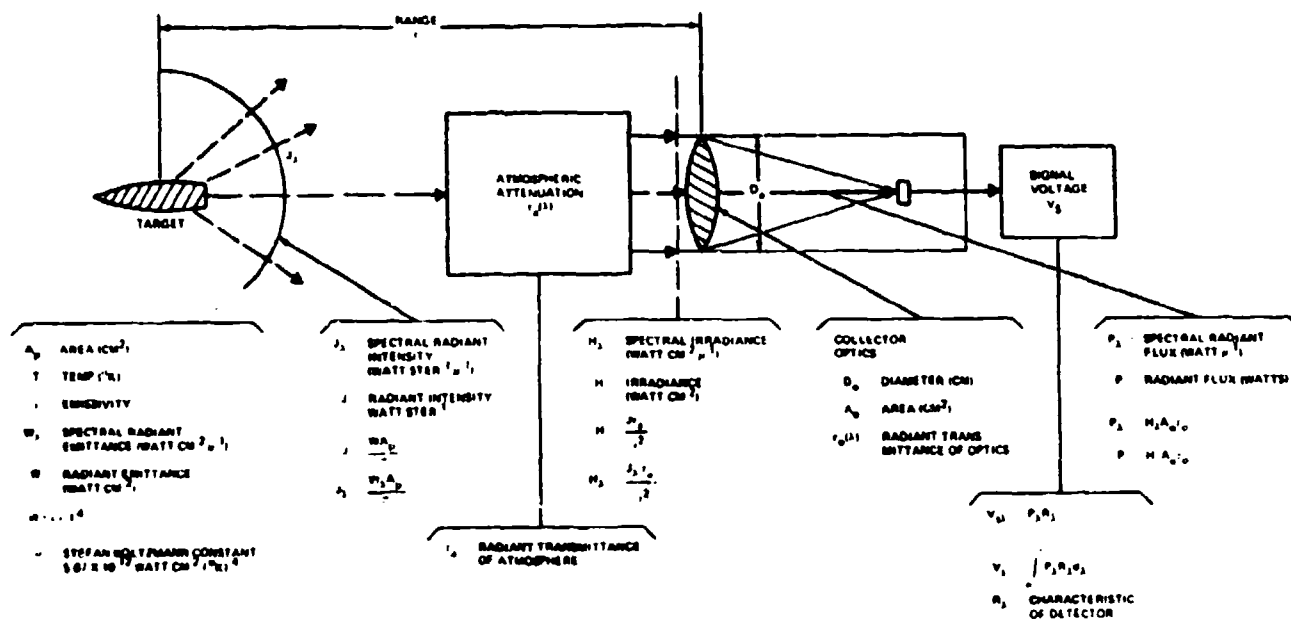
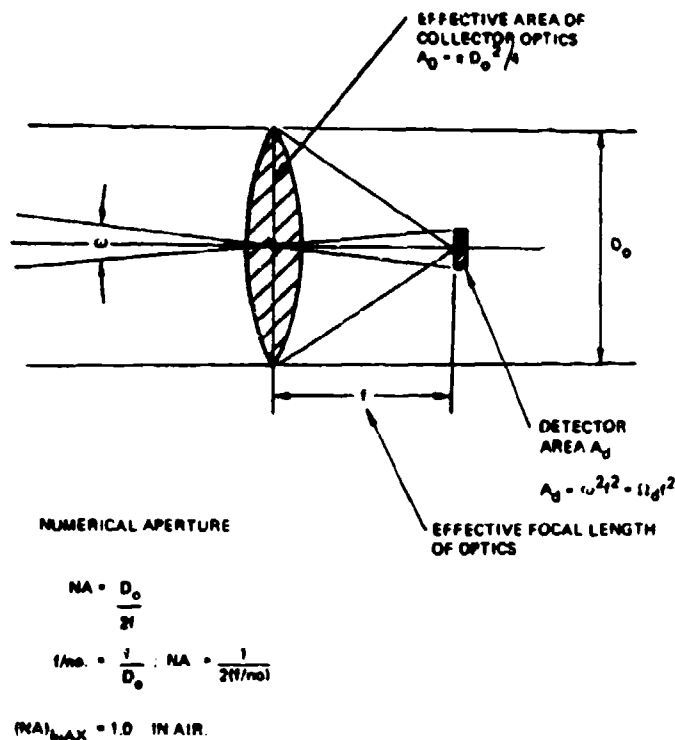


Figure 3-39. Functional Relationships for Estimating Infrared Signature

It has been found that the R_λ characteristic of the detector (voltage out/power in) can be described in terms of a "detectivity" index D_λ^* as

$$R_\lambda = \frac{V_n D_\lambda^*}{(A_d \Delta f)^{1/2}} \quad (3.64)$$



40001-40

Figure 3-40. Equivalent Collector Optics and Detector Field of View Geometry

where v_n is noise voltage developed in a bandwidth Δf , and A_d is the area of the detector element. Curves of D_λ^* versus λ allow various detector types to be compared on a common basis,¹⁶ as shown in Figure 3-41.

For the first order approximations of this paper it is assumed that the system is limited by detector noise, and signal/noise is computed using D_λ^*

Then

$$\frac{S}{N} = \left(\frac{A_p}{\tau_r^2} \right) \left(\frac{A_o \tau_o}{(A_d \Delta f)^{1/2}} \right) (\Delta W_w D_{\lambda w}^* \tau_{aw}) \quad (3.65)$$

where ΔW_w is the difference between signal and background in the window.

An imaging sight detector configuration¹⁵ is sketched in Figure 3-42. The field is rectangular of angular extent θ_a, θ_e . A linear array of detectors, n to the array, each of angular coverage (α, β) laterally and vertically is swept across the array horizontally at an azimuth scan rate S_a .

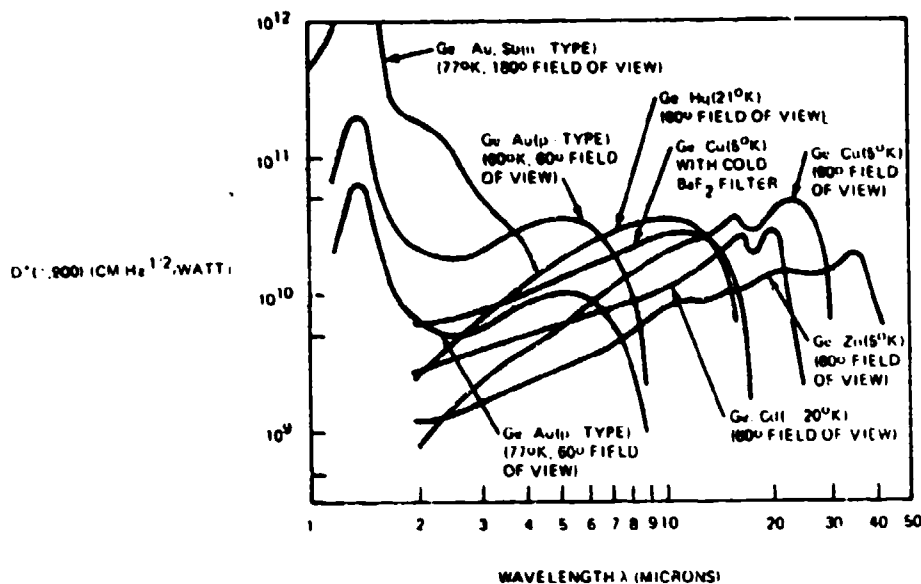


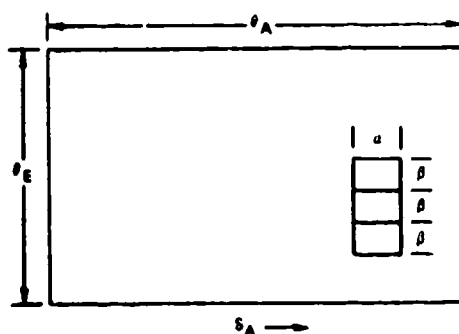
Figure 3-41. Detectivity Curves. (From Ref. 16)

4000141A

$$\text{The solid angle scanned per second} = S_a n \beta \quad (3.66)$$

$$\text{and the number of azimuth sweeps to cover the frame} = \theta_e / (n \beta) \quad (3.67)$$

$$\text{The time for one lateral scan is} = \theta_a / S_a \quad (3.68)$$



4000142

Figure 3-42. Schematic of Imaging Sight Field

Hence the time per frame is

$$T_{\text{Frame}} = \frac{\theta_a \theta_e}{S_a n \beta} \text{ sec/frame} \quad (3.69)$$

The inverse of this is the frame rate

$$F = \frac{S_a n \beta}{\theta_a \theta_e} \text{ frames/sec} \quad (3.70)$$

The "dwell time" t_d is defined as the length of time that a target smaller than the resolution of a single detector element is exposed to the element.

$$t_d = (\alpha/S_a) \quad (3.71)$$

Hence the frame rate and dwell time are related as

$$F = \frac{n(\alpha\beta)}{\theta_a \theta_e t_d} = \frac{n\omega}{\Omega t_d} \quad (3.72)$$

where ω is the solid angle viewed by one detector element and Ω is the solid angle of the field of the imaging device.

The frame rate can also be written as

$$R = (\dot{\Omega}/\Omega) \quad (3.73)$$

whence

$$\omega = (\dot{\Omega} t_d)/n \quad (3.74)$$

which is the expression given by Hudson. ⁽¹⁵⁾

Depending on the system design, there will be an interval between scans (especially with some type of mechanical/optical scan). The time between initiation of successive azimuth scans is then

$$T_{se} = T_s + T_D \quad (3.75)$$

and the average scan rate S_{ae}

$$S_{ae} = \frac{S_a}{1 + S_a t_D} \quad (3.76)$$

However, the dwell time is unchanged.

$$t_d = \alpha / S_a \quad (3.77)$$

The average frame rate is now

$$F = \frac{S_{ae}(n\beta)}{\theta_a \theta_e} \quad (3.78)$$

and substituting dwell time

$$F^{-1} = (t_d + \alpha T_D)(\Omega/n\omega) \quad (3.79)$$

If we define the "duty cycle" of the scan operation as

$$\eta = \frac{T_s}{T_s + T_D} = \frac{1}{1 + S_a t_d} \quad (3.80)$$

$$S_{ae} = S_a \eta \quad (3.81)$$

$$F = \frac{S_a \eta(n\beta)}{\theta_a \theta_e} = \eta \left(\frac{n\omega}{\Omega t_d} \right) \quad (3.82)$$

$$t_d = \eta \left(\frac{n\omega}{\Omega F} \right) \quad (3.83)$$

To estimate representative dwell times, assume a sensor sweeping a linear array of detectors horizontally across a rectangular field. The number of detector elements is chosen to equal the vertical field divided by the FOV of each detector, i.e., each horizontal sweep generates one complete frame. The number of detector elements

$$n = \theta_e / \beta \quad (3.84)$$

and the dwell time is

$$t_d = \eta \frac{n\alpha\beta}{F\theta_e\theta_A} = \frac{\eta\alpha}{F\theta_A} \quad (3.85)$$

assume a duty cycle $\eta \approx 0.80$.

The results are summarized in Table III-15.

Table III-15. Assumed Characteristics of Imaging Sight

Field*	20° x 40°	5° x 10°
FOV per element*	1 x 1 mil	1/2 x 1/2 mil
No. of elements	350	175
Duty cycle*	0.80	0.80
Frame rate*	30/sec	30/sec
Dwell time (sec)	38.2 x 10 ⁻⁶	153 x 10 ⁻⁶
Equivalent bandwidth	1.31 x 10 ⁵ Hz	3.27 x 10 ⁴ Hz
*Assumed		

If the sweep steps half the FOV of an element per sweep vertically to eliminate horizontal lines on the display (interleaving), so that there are two sweeps per frame, and if the frame rate is kept at 30/sec, the dwell times listed will be halved, and the equivalent bandwidth doubled.

The projectile occupies a small fraction of the FOV of a single detector element. Since the sight is tracking the aircraft target, and hence sweeping across the sky background (or clouds, or terrain for low angle, etc.) the signal developed by the detector will change with time even in the absence of the projectile signature. Hence there is fluctuating background signal noise in addition to background photon noise and internal system noise.

It is unlikely that the projectile will remain in the FOV of a single detector for more than one frame, i. e., a single pulse. Occupying a small fraction of the FOV the projectile must nevertheless by its presence raise the signal developed by the detector sufficiently above background and noise for reliable detection.

Limited information on the spatial power spectral density of sky⁽²⁶⁾ (the Wiener spectrum) will allow the background PSD developed by tracking to be estimated. However, for the present estimates we assume that the background is simply a 300°K sky, that detector noise as included in D^* limits signal to noise, and that detection occurs when the presence of the projectile in the FOV of a detector raises the signal above sky background sufficiently for an S/N of about 6.0.

Omissions of Wiener background noise and other possible noise sources will make the derived estimates optimistic. Even so, as will be shown, detection of a passive projectile of small caliber seems unlikely.

The signal to noise ratio of the system is

$$(S/N) = (A_p / \pi r^2) \left[\frac{A_o \tau_o}{(A_d \Delta f)^{1/2}} \right] (\Delta W D^* \tau_a)_W \quad (3.86)$$

we assume that

$$\Delta f \approx (2t_d)^{-1}; t_d = \text{"dwell time"} \quad (3.87)$$

and use the relation

$$A_o / (A_d)^{1/2} = (\pi/4) \frac{D_o}{\omega_o f / n o} \quad (3.88)$$

then

$$(S/N) = \left(\frac{A_p}{\omega^2 r^2} \right) (2t_d)^{1/2} \left(\frac{D_o \omega}{4f/no} \right) \left(\Delta W_w D_w^* \tau_{aw} \tau_o \right) \quad (3.89)$$

and for the tail-on aspect of the projectile,

$$A_p = (\pi C^2)/4; C = \text{projectile diameter} \quad (3.90)$$

From Eq. (3.89) it is easy to see how the S/N will scale with each parameter. For a reference case assume

$$C = 3 \text{ cm}$$

$$\omega = 1 \text{ mr} = 10^{-3} \text{ rad}$$

$$t_d = 5 \times 10^{-5} \text{ sec}$$

$$D_o = 15 \text{ cm}$$

$$f/no = 1.0$$

$$r = 3 \text{ km} = 3 \times 10^5 \text{ cm}$$

$$D^* = 2.5 \times 10^{10}$$

$$\tau_o = 0.80$$

$$\epsilon = 0.80$$

Transmission losses introduced by the atmosphere are introduced by the simple expression $\exp(-\lambda r)$ for τ_{aw} , with values of λ^{-1} : 14.2, 5, and 2.5 km used to represent atmospheric conditions of "clear," "humid" and "tropical haze".

Results of the computation are shown in Table III-16 and are plotted in Figure 3-43. Shown on the abscissa are some unconfirmed estimates of projectile base temperature and the temperature of a rotating band. Under 600°K, consistent detection would appear marginal for this 30-mm projectile, and most unlikely for a 20-mm round.

The signal/noise ratio would be further reduced if a factor of 0.80 was applied for non-ideal amplifier performance, with another factor of 0.7 required for 2/1 interleaving of scans. On the other hand, narrowing the FOV per sensing element (and that of the field) would improve the signal to noise ratio.

**Table III-16. Estimated Signal/Noise Ratio of Projectiles at 3-km
as Viewed by Imaging Sight**

			S/N at 3 km		
			τ_a		
			0.81	0.55	0.30
$T(^{\circ}\text{K})$	ΔW_w	S/N	Clear	Humid	Haze
300	0	0	0	0	0
366	2.15×10^{-2}	$1.0 \tau_a$	0.8	0.6	0.3
700	27.0×10^{-2}	$12.5 \tau_a$	10.1	6.9	3.8
900	43.0×10^{-2}	$20.0 \tau_a$	16.2	11.0	6.0
1200	57.2×10^{-2}	$26.6 \tau_a$	21.5	14.6	8.0

As a rough indication of the implication of the temperatures required for sensing, Table III-17 shows a "color scale" of temperature. A "red hot" projectile would appear to have a detectable signature; it seems unlikely that this temperature would be developed in firing.

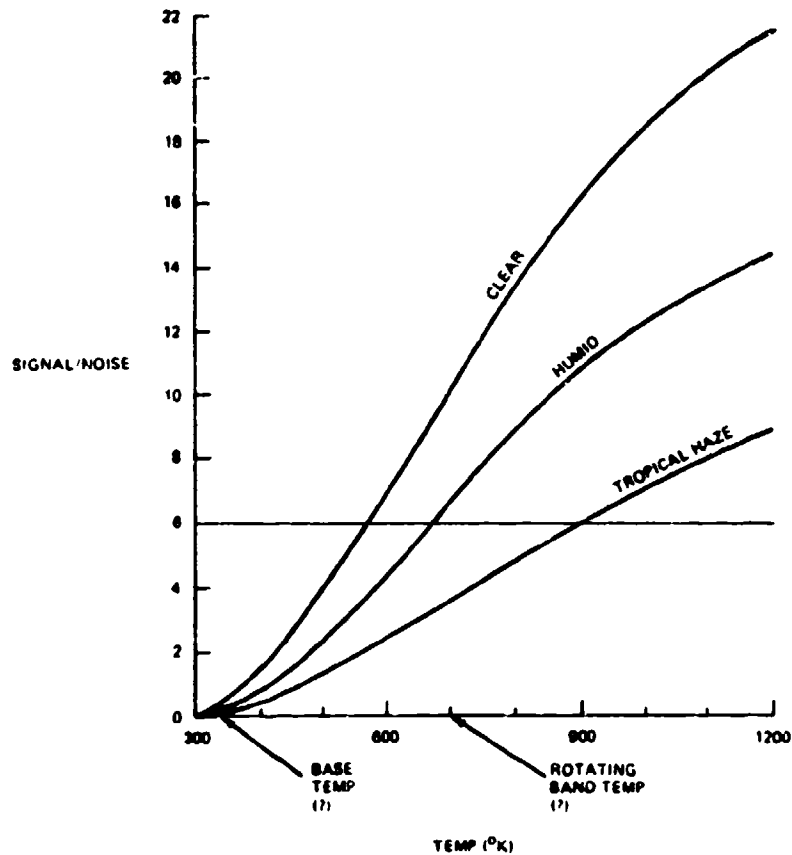
It is therefore estimated that reliable projectile sensing by FLIR will require a tracer element in the projectile.

3.4 CLOSED LOOP ALGORITHMS

3.4.1 Introduction

In Section 3.2 sensors were discussed in conjunction with the information which each sensor configuration makes available to the processing algorithms. The next decision required is how to process the miss measurements and transform them into corrections to be introduced to the gun order computations at appropriate points in the prediction process.

The point of view taken here is that there are two mutually exclusive, and qualitatively different sources of components of the "bias" miss vector. These are (1) miss components resulting from the fact that the target path differs from that assumed by the open loop prediction algorithms, and (2) miss components resulting from sources "external" to the computing system such as wind, muzzle velocity bias, and boresight biases.



4000143A

Figure 3-43. Estimated Signal to Noise Ratio of 30-mm Projectile at 3 km as Viewed by Imaging Sight versus Projectile Temperature

The first category also includes transient errors in the prediction computation after the target has been acquired, but before reliable derivatives have been computed.

Given a means for separating miss measurements into the above two categories, the processing required in each category differs both with respect to coordinate transformations, and with respect to the time-varying statistics of the inferred error sources. A method of making this separation is presented in Section 3.4.2 below.

Table III-17. Color Scale of Temperature

Color	Approximate Temperature, °K
Incipient red heat	800
Dark red heat	900
Bright red heat	1150
Yellowish red heat	1350
Incipient white heat	1550
White heat	1750

In the category of "external" miss sources, exclusive of the target, it is desirable to keep the number of significant sources small in order to reduce the computing load. It is also desirable to identify the sources in coordinates in which the source magnitude changes very slowly in order to allow the system to profit on each firing segment from the corrections made on prior passes at different geometrical gun/target configurations. For example, boresight errors can be corrected in the coordinate system in which they are observed, but wind components, to be useful for subsequent target paths, must be identified as northerly and easterly components.

Hence one may consider a wide spectrum of correction algorithms, ranging from the simplest, which might correct only in azimuth and elevation with little memory across passes, to a set of algorithms which processes the miss measurements according to the engagement geometry and assigns corrections to half a dozen sources, each chosen so that corrections derived from any firing pass are estimated to be applicable, and subject to further improvement, on subsequent firing passes.

In the following sections, the general method of data processing is developed, and numerical examples are given for limited sets of bias sources. Finally, the relatively simple extension to larger numbers of bias sources is shown.

3.4.2 VISTA Concept

One of the major sources of "bias" in a closed loop system may be target maneuvers, i.e. deviations of the target flight path from the path for which the computer's prediction algorithms are designed.

Consider the following case: the target is acquired before it begins its firing pass. Firing begins before the target settles on its firing pass. We have strong indications from FACT that the firing pass segment will be relatively predictable, but the initial turn in to the firing segment will not be predictable. It would be desirable if corrections for system "bias" exclusive of target maneuver, could be made from observations of misses before the firing pass begins.

We therefore desire a method for separating the miss components which result from target maneuver, and those which result from such sources as boresight errors, wind, etc.

This separation is accomplished by the VISTA⁽²⁶⁾⁽²⁷⁾ algorithm, as originally described in the Phase-II AFAADS Analysis Report.⁽²⁾

VISTA operates by storing gun azimuth and quadrant elevation, computing time of flight to current target position, based on ranging data, recovering gun orders that time of flight previous, correcting for superelevation, and computing the point at which the bullet should be, relative to the target. The difference

$$E_a(t) = X_t(t) - X_g(t-t_p) \quad (3.92)$$

is the "expected miss distance", and includes the effect of target maneuver. More generally, it includes the difference between the actual target motion during time of flight, and the motion predicted by whatever prediction algorithm is used in the computer.

VISTA would therefore extract the errors of an "approximate" solution such as the Vulcan gyrosight versus an unaccelerated target, since these errors are the difference between the actual target path and the algorithmic prediction.

The measurement of E_a , which is "internal" to the system, and requires no sensing of the projectiles, can be processed and used to make corrections to the predictions developed by the open loop algorithms. For example, one might correct for target accelerations by this means, instead of measuring target acceleration from the tracking sensor data by an acceleration filter.

Use of E_a to close the prediction loop internally in this manner is not discussed at length in the present report, since the process is straightforward, and in fact it is not clear that with an optimally designed open loop solution, a significant improvement is realized by closure of the inner loop.

The correction of "exterior" bias sources, which requires sensing of the projectile in flight constitutes the major technological challenge. It is therefore assumed that VISTA is used primarily to remove the error components resulting from target maneuver from the miss sensings of actual projectiles, with the possibility of using the E_a computations for correction to the open loop prediction algorithms for target maneuvers reserved for possible future consideration.

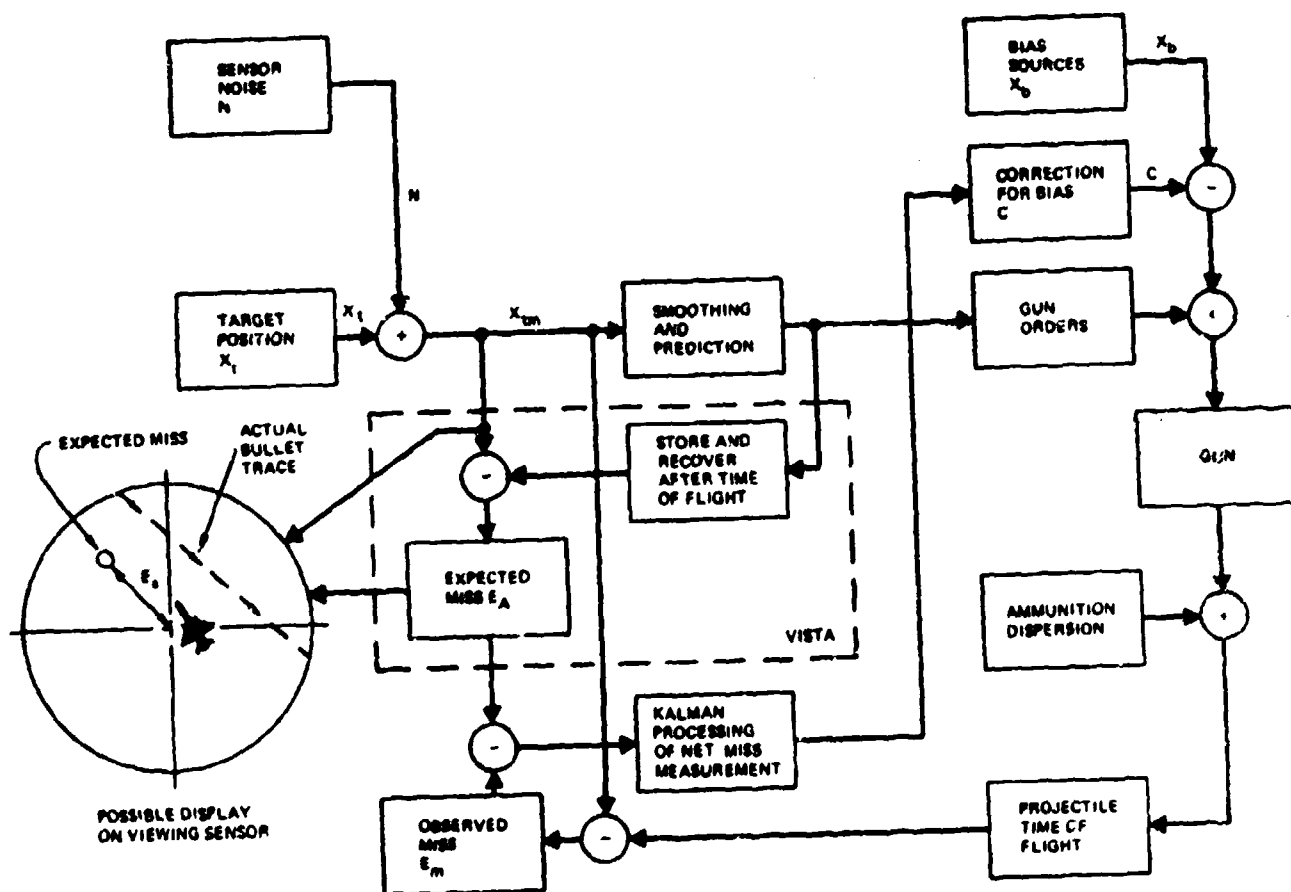
E_a does not include errors external to the computer's operation such as system boresite errors, ballistic dispersions, and projectile ballistics differing from those used in the computer. If the miss distance of a particular bullet is measured at time t , and designated $E_m(t)$, the difference between $E_m(t)$ and $E_a(t)$ is attributed to these "external" errors.

E_a would normally be computed at a high data rate, so that it would be essentially a continuous function. E_m , however, is available only when a projectile is observed. It is obtained at intervals which are not uniformly spaced.

In general, therefore, two kinds of data flow through the system, essentially continuous data based on tracking and computation of gun orders, and discrete data, based on projectile miss distance measurements.

The data flow in the closed loop system is shown in Figure 3-44. This figure is similar to Figure 6-6 of the Phase II Analysis Report,⁽²⁾ with the following important improvements:

- a. The point of injection of the bias corrections has been changed, to minimize recirculation of the corrections through the VISTA loop. As a result of this change, one may, if desired, display the VISTA "expected miss distance" on the same visual display on which the target is seen. If this display is also capable of displaying the actual bullet trace, one has a continuous indication of how much of the miss distance results from target maneuver, and how much from other error sources.
- b. The measured miss distances are processed by Kalman type algorithms, on the assumption that the "biases" can be related to specific sources, and are correctable at the source. This allows the complete system to become progressively more accurate over a series of firing passes, rather than requiring it to treat each new firing pass as a new problem.

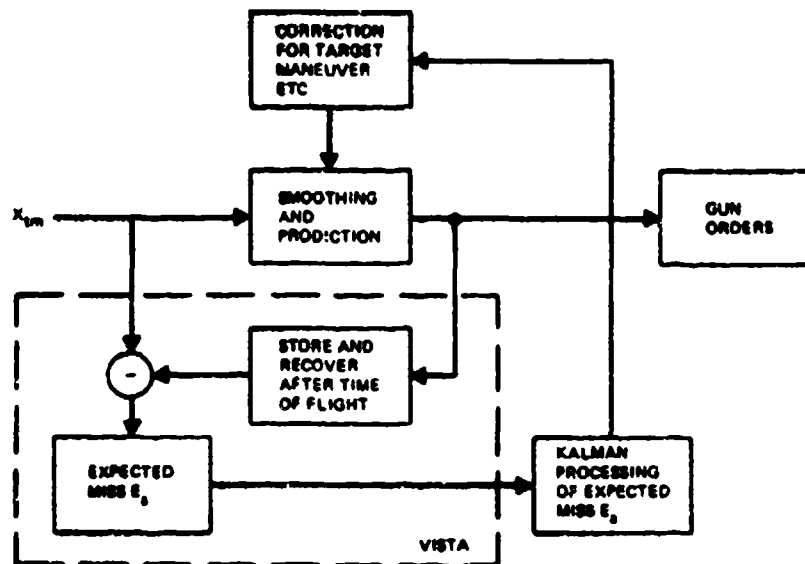


40001 44

Figure 3-44. Data Flow in Closed Loop System to Correct for "External Biases" Excluding Target Maneuvers

- c. The use of the Kalman type algorithms solves the stability problem associated with the time delay (projectile time of flight) between the instant that a correction is applied, and the instant that its effect is perceived at the target.

Data flow, if the option is exercised of using the VISTA error measurements for prediction correction, is shown in Figure 3-45 where only the modules of Figure 3-44 affected by this option are displayed.



40001-45

Figure 3-45. Data Flow Using Vista Module to Correct for Target Maneuvers and "Internal" Biases

The functional relations of the data flow in Figure 3-44 are sketched below. We use the following symbols

$$X = \begin{bmatrix} A \\ e \end{bmatrix} \quad (3.93)$$

A = azimuth angle

e = elevation angle

For this preliminary discussion, we assume that ballistic corrections for superelevation, drift, etc. have been removed from the data. Since we end up with incremental differences in X vectors, inclusion of these corrections would only complicate the discussion, without adding to the clarity. We loosely call X , target "position".

Then

X_t = true target position at time t

n = sensor noise (tracking error) at time t

X_{tm} = measured target position at time t

X_p = predicted target position made at time t by the open loop prediction and smoothing algorithms.

X_a = "expected" target position obtained by the VISTA loop

X_g = Target position aimed at by the gun at time t

X_b = "bias errors" in X , resulting from sources external to the computer, at time t

X_s = projectile position at the instant its range from the gun/sensor equals that of the target, at time t .

v = rms component of projectile miss which is random (normal distribution with zero mean) across rounds. This includes angular dispersion of ammunition, gun vibration, etc.

We use the symbology

$$X(t-t_f) = X(t)e^{-st_f}; s = d/dt \quad (3.94)$$

In addition to bias errors in X , i.e. X_b , error sources such as bias in muzzle velocity or sensor range will affect the time of flight computation. These will be dealt with in some detail in later sections. For the present discussion, we recognize the following times of flight:

t_{p0} = time of flight computed from measured target range at time t by the internal computer ballistics, and used in the VISTA algorithm

t_{pa} = actual time of flight of the projectile observed at target range at time t

t_{pc} = time of flight used in the open loop algorithms to predict target position X_p , the prediction being made at time t .

We also have the open loop prediction algorithm

$$X_p = H(s, t_{pc}, t)X_{tm} \quad (3.95)$$

The measured projectile miss vectors are

$$E_a = X_p e^{-st_{po}} - X_{tm} \quad \text{from the VISTA loop} \quad (3.96)$$

$$E_m = X_s - X_{tm} + w \quad \text{by direct sensing of the projectile} \quad (3.97)$$

w = measurement error

The net error, which is to be processed to develop a correction C , is

$$\Delta E = E_m - E_a \quad (3.98)$$

$$\Delta E = X_s - X_p e^{-st_{po}} + w \quad (3.99)$$

Since

$$X_s = (X_g + v)e^{-st_{pa}} \quad (3.100)$$

and

$$X_g = X_p + X_b + C \quad (3.101)$$

Hence

$$\Delta E = (X_p + X_b + C + v)e^{-st_{pa}} - X_p e^{-st_{po}} + w \quad (3.102)$$

We now recognize those error sources that generate a bias error in time of flight, b_t , and a random error across rounds, v_t . v_t may be interpreted to include timing errors in sensing the miss distance.

$$v_t + b_t = t_{pa} - t_{po} \quad (3.103)$$

$$\Delta E = -X_p e^{-st_{pa}} [1 - e^{-s(b_t + Kt)}] + (X_b + C + v) e^{-st_{pa}} \quad (3.104)$$

Since these errors are small, we can expand the exponential in the bracket and obtain

$$\Delta E = [-(dX_p/dt)(b_t + v_t) + (X_b + C + v)] e^{-st_{pa}} + w \quad (3.105)$$

where the first term in the brackets represents the movement of the predicted point during the error in time of flight.

We now have an expression which displays the correction problem. E is observed, on each of a series of rounds. The object is to develop a sequential algorithm for C , given a set of measurements ΔE , which will reduce the X_b and b_t miss components progressively, in spite of the random components v_t, v, w and the time lag around the loop t_{pa} .

The necessary algorithms are developed in subsequent sections of this report.

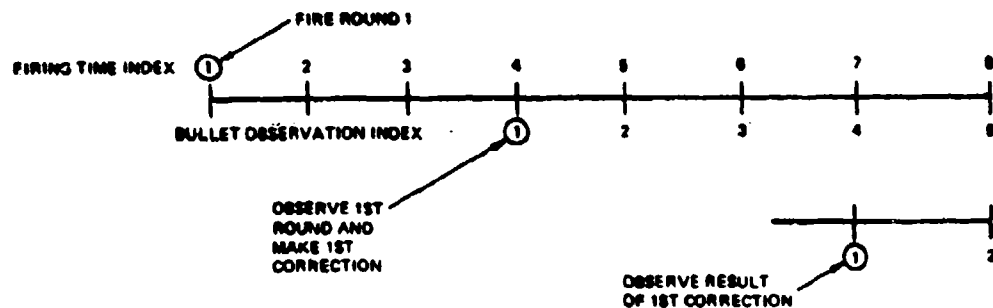
3.4.3 Development of Closed Loop Algorithms for Elementary Case

The important difference between the closed loop algorithms which we require, and those which are well established in Kalman filter theory results from the time delay between the application of a correction for an observed miss, and the observation of the result of the correction which is delayed by the time of flight of the projectile.

To show how this problem is to be handled, we work through the "optimal" correction algorithms for an elementary one-dimensional case. Having identified the necessary modification to the usual Kalman methodology, we then proceed with the known Kalman methods for the complete closed loop solution.

The elementary case considered here is defined as follows. It is one-dimensional. Bullets are fired at uniformly spaced firing times, indexed $j = 1, 2, 3, \dots$, time of flight is constant and equal to Δ , and the j 'th bullet miss is observed at index $j + \Delta$. Immediately after each observation a correction is applied to gun aim. The sequence of activities is shown in Figure 3-46 for the particular case of $\Delta = 3$.

There is an initial unknown aim bias (assumed drawn from a normal distribution with zero mean and approximately known variance), and each observation is contaminated by a random error drawn from a zero mean, normal distribution of approximately known variance.



40001-46

Figure 3-46. Fire-Observe-Correct Sequence with Observation Delay

The object is to derive processing algorithms to apply to the observations, so that the residual variance of bias after n observations is minimized, and in particular to derive recursive algorithms so that this is true for $n = 1, 2, \dots$.

The minimum variance criterion does not necessarily lead to the maximum probability of at least one target kill in n rounds, (a much more difficult criterion to apply), but it has the advantage of simplifying the analysis. In the long run, one wants to eliminate the bias error sources and the least squares criterion achieves this, even though it is not clear that it follows the optimal path at intermediate points from the criterion of cumulative kill probability.

Define

j = discrete times at which bullets are fired, $j = 1, 2, 3, \dots$

Δ = delay between firing and observation

x_j = "bias" error of the bullet fired at time j

v_j = "random" error of dispersion and observation of the bullet fired at time j

z_j = observation made at time j

u_j = correction applied at time $j+$ as a result of observations available up to time $j+$

Then

$$x_{j+1} = x_j + u_j \quad (3.106)$$

$$z_j = x_{j-\Delta} + v_{j-\Delta} \quad (3.107)$$

$$u_j = f(z_j, z_{j-1}, \dots) \quad (3.108)$$

The object is to minimize the variance in the residual "bias" after each correction.

Define

σ_b^2 = estimated a priori variance in x before any observations and corrections

x_0 = unknown initial value of bias before observations and corrections

σ_m^2 = estimated a priori variance in round to round random dispersion plus measurement error.

This would be a straightforward and trivial problem in Kalman-type filtering and control if it were not for the delay Δ between correction and observation of the result of the correction. The following solution uses only elementary mathematical techniques to clarify the method of handling the delay.

The first round is fired at $j = 1$

The first observation is available at $j = \Delta + 1$, (see Figure 4)

The first correction is made at $j = (1 + \Delta) +$

No corrections can be made before $j = 1 + \Delta$.

Then

$$x_1 = x_0$$

$$x_2 = x_0$$

$$x_{\Delta+1} = x_0$$

$$x_{\Delta+2} = x_{\Delta+1} + u_{\Delta+1} = x_0 + u_{\Delta+1}$$

$$x_{\Delta+3} = x_{\Delta+2} + u_{\Delta+2} = x_0 + (u_{\Delta+2} + u_{\Delta+1})$$

$$x_{j+\Delta} = x_0 + (u_{1+\Delta} + u_{2+\Delta} + \dots + u_{j+\Delta-1})$$

or

$$x_{j+\Delta} = x_0 + U_{j+\Delta-1}$$

where

$$\begin{aligned} U_{j+\Delta-1} &= (u_{1+\Delta} + u_{2+\Delta} + \dots + u_{j+\Delta-1}); j > 1.0 \\ &= 0 \quad ; j \leq 1.0 \end{aligned} \quad (3.109)$$

Note that we have not yet specified how the corrections u_j are to be computed but have only assumed that they are applied immediately subsequent to observations.

Now consider the observations: The first observation is available at $j = 1 + \Delta$.

Hence

$$z_1 = 0$$

$$z_2 = 0$$

.

.

$$z_{\Delta} = 0$$

$$z_{\Delta+1} = x_1 + v_1$$

.

.

$$z_{j+\Delta} = x_j + v_j$$

But, from Eq. (3.109)

$$x_j = x_0 + U_{j-1}$$

$$U_j = (u_{j-1} + u_{j-1} + \dots + u_{\Delta+1}); j > \Delta + 1$$

$$= 0 \quad ; j \leq \Delta$$

Hence

$$z_{j+\Delta} = x_0 + U_{j-1} + v_j \quad (3.110)$$

Now suppose that we have n observations, $z_{\Delta+1}, z_{\Delta+2}, \dots, z_{\Delta+n}$. Our object is to make a minimum variance estimate of x_0 using all of these observations, and then to apply a correction to x .

We have, however, allowed the possibility of making sequential corrections prior to $\Delta + n$; these total U_{j-1} . If we determine the total correction based on the whole n observations, we need apply only the increment above $j-1$.

Write

$$x_0 = (z_{j+\Delta} - u_{j-1}) + v_j \quad (3.111)$$

We have assumed v_j to have zero mean and normal distribution with variance σ_m^2 . We have n observations, and for this simple problem there is no reason to weight these differently in estimating a best value of x_0 . Hence we compute an estimated value of x_0 as

$$x_{oe} = k_n \sum_{j=1}^n (z_{j+\Delta} - u_{j-1}) \quad (3.112)$$

where k_n refers to "k" for n observations and we now wish to determine a "best" value of k_n . We have

$$x_{oe} = k_n \sum_{j=1}^n (x_0 + v_j) = nk_n x_0 + k_n \sum_{j=1}^n v_j \quad (3.113)$$

and the error in the estimate, e_n , is

$$e_n = x_{oe} - x_0 = (nk_n - 1)x_0 + k_n \sum_{j=1}^n v_j \quad (3.114)$$

The variance of e_n is

$$\sigma_e^2 = (nk_n - 1)^2 \sigma_b^2 + k_n^2 \sigma_m^2 n \quad (3.115)$$

since the measurement errors are uncorrelated across observations, and are not correlated with the bias.

Setting

$$\partial \sigma_e^2 / \partial k_n = 0 \quad (3.116)$$

we obtain

$$k_n = \frac{\sigma_b^2}{\sigma_m^2 + n\sigma_b^2} = \frac{1}{\mu + n} \quad (3.117)$$

where

$$\mu = (\sigma_m / \sigma_b)^2 \quad (3.118)$$

and substituting back into the variance expression for σ_e^2

$$\left(\frac{\sigma_e}{\sigma_b} \right)^2 = \frac{\mu}{\mu + n} \quad (3.119)$$

This expression shows the reduction in the bias variance as a function of the number of observations, and the ratio of a priori bias to observation variance.

To recapitulate, if we have n observations available, and for each compute $z_{j+\Delta} - U_{j-1}$, and sum these terms our best estimate of bias x_0 will be k_n times that sum. Our cumulative correction after seeing n rounds, i. e., after $\Delta + n$ firing intervals should therefore be the negative of this quantity, or

$$U_{n+\Delta} = -k_n \sum_{j=1}^n (z_{j+\Delta} - U_{j-1}) \quad (3.120)$$

To reduce the amount of stored data required, it is desirable to derive an expression, preferably simply recursive, for $u_{n+\Delta}$, the incremental correction to be applied at $\Delta + n$. We write

$$U_{n+1+\Delta} = -k_{n+1} \left[\sum_{j=1}^n (z_{j+\Delta} - U_{j-1}) + z_{n+\Delta+1} - u_n \right] \quad (3.121)$$

Substituting Eq. (3.120) into Eq. (3.121)

$$U_{n+1+\Delta} = -k_{n+1} [(-U_{n+\Delta}/k_n) + z_{n+\Delta+1} - U_n] \quad (3.122)$$

But

$$k_{n+1}/k_n = 1 - k_{n+1} \quad (3.123)$$

Hence

$$U_{n+1+\Delta} = U_{n+\Delta} - k_{n+1}(U_{n+\Delta} - U_n) - k_{n+1}z_{n+\Delta+1} \quad (3.124)$$

or

$$u_{n+1+\Delta} = -k_{n+1}z_{n+\Delta+1} - k_{n+1}(u_{n+\Delta} + u_{n+\Delta-1} + \dots + u_{n+1}) \quad (3.125)$$

We need to store the corrections applied during the time of flight of the most recent observation.

This expression is neater if the subscripts are written uniformly in terms of indices of successive observations, rather than firing times. If the observations are designated 1, 2, 3, ..., m,

$$u_{m+1} = -k_{m+1}z_{m+1} - k_{m+1}(u_m + u_{m-1} + \dots + u_{m+1-\Delta}); \Delta > 0 \quad (3.126)$$

$$u_{m+1} = -k_{m+1}z_{m+1} \quad ; \Delta = 0 \quad (3.122)$$

$$k_m = \frac{1}{\mu + m} \quad (3.128)$$

The expression for $\Delta = 0$ is exactly that which would be obtained from Kalmanization.

In effect, when we make a correction at $m + 1$, we recognize that the observation includes all corrections earlier than the lag interval. We have, however, made a number of corrections already in effect, the result of which we cannot yet observe, and so our new correction must depend on the difference between our most recent observation and the corrections already made and not yet observed.

The expressions given in preceding paragraphs are possibly the most straightforward to program. They may also be modified to eliminate the sum of u_j by writing

$$u_m = -k_m z_m - k_m (u_{m-1} + u_{m-2} + \dots + u_{m-\Delta}) \quad (3.129)$$

$$u_{m+1} = -k_{m+1} z_{m+1} - k_{m+1} [u_m - u_{m-\Delta} + (u_{m-1} + u_{m-2} + \dots + u_{m+1-\Delta} + u_{m-\Delta})] \quad (3.130)$$

$$u_{m+1} = -k_{m+1} z_{m+1} - k_{m+1} [u_m - u_{m-\Delta} - z_m - u_m/k_m] \quad (3.131)$$

and introducing

$$k_{m+1}/k_m = 1 - k_{m+1} \quad (3.132)$$

$$u_{m+1} = u_m (1 - 2k_{m+1}) + k_{m+1} u_{m-\Delta} - k_{m+1} (z_{m+1} - z_m) \quad (3.133)$$

or alternately

$$u_{m+1} = u_m (1 - k_{m+1}) - k_{m+1} (u_m - u_{m-\Delta}) - k_{m+1} (z_{m+1} - z_m) \quad (3.134)$$

but we still need to store all U_{m-k} over time of flight so there seems to be little advantage in this form over the preceding expressions.

Note that if we spaced the firing instants by time of flight, we would have, for the correction algorithm, simply

$$u_m = -k_m(z_m + u_{m-\Delta}) \quad (3.135)$$

This might correspond to a system that fired short bursts spaced by time of flight. As the group of rounds constituting each burst arrived at target range, their centroid would be measured and a correction based on the centroid. Insertion of this correction would then trigger the firing of the next burst.

This concept might be simpler to realize physically, although it has a very low data rate. The general method developed in this section allows closed loop operation with any firing schedule.

3.4.4 General Solution of Closed Loop Problem in Matrix Form

We now define the Kalman data processing algorithms for the closed loop system. Following the textbook solutions, ⁽²⁸⁾ we define

x = the system state vector

z = the observation vector

The system state vector consists of the "bias" sources which we hope to remove by the closed loop process. Typical elements might be azimuth boresight error, elevation boresight error, muzzle velocity bias, wind velocity and direction, etc.

The observation vector consists of the measurements that we are able to make of the projectile miss distance relative to target position. Elements might consist of the vertical and lateral miss angles measured at the instant the projectile reaches target range, if we have a 3-D system. If we are considering a 2-D system, there may be only a single element per measurement. More generally, we allow the possibility that the sensing system may be able to sense projectile velocity directly, which allows a more direct inference of muzzle velocity bias, and in this case the observation vector would contain a term for sensed velocity.

The observation vector also contains the errors of measurement and the random round to round dispersion errors of the system.

As a result of the observations z_1, z_2, \dots, z_j , a correction vector u_j is applied to x_j . Then the state vector evolves according to

$$x_{j+1} = x_j + u_j \quad (3.138)$$

and the observation vector is defined as

$$z_j = H_j x_{j-\Delta} + G_j w_{j-\Delta} \quad (3.137)$$

where Δ = time of flight, H_j is the coordinate transformation matrix relative the bias source coordinates to coordinates as seen in the projectile sensing coordinate system, and G_j is a similar matrix projecting the random error vector w into the sensing plane.

The object is to find the optimum u_j in terms of z_j, z_{j-1}, \dots

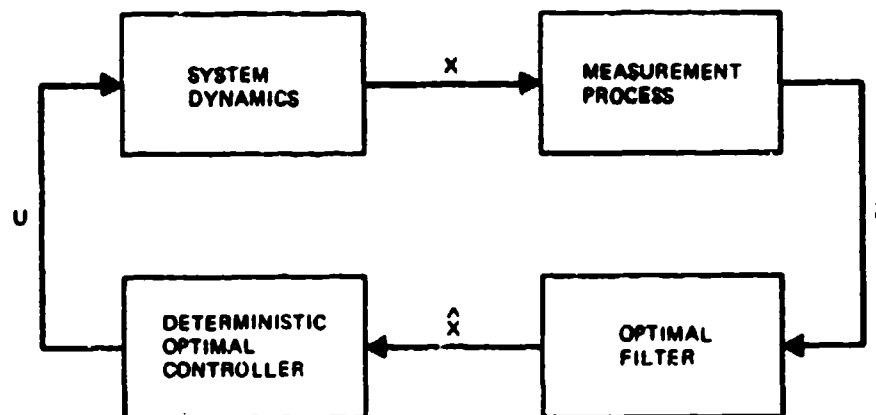
The state expression is particularly simple because we assume that the biases are constant at source unless corrected. Their effect on the observed miss distance will however depend on the geometry of the problem, and this is contained in H_j which varies with j .

The w_j vector contains all the variables that are random across rounds, including measurement errors, and G_j accounts for the way in which their effect changes with the geometry.

The criterion against which the algorithms are to be optimized is the variance of the components of the x vector, which are to be minimized. This is not necessarily equivalent to maximizing the probability of at least one lethal hit in a sequence of rounds, but it has the advantage of leading to a relatively simple solution.

In addition, the Kalman method provides a systematic way of handling the various trigonometric and other conversions involved in the data processing.

The process of determining the minimum variance solution has been determined to be separable as indicated in Figure 3-47, in which the vector x , which it is desired to minimize is generated by the system dynamics. A measurement vector z is applied to x , and from successive measurements z_j a "best estimate" of x , \hat{x} is developed in an "optimal" filter. The optimal controller has been shown to be that controller which would be optimal if x were known exactly, i.e., the "deterministic" optimal controller.



40001-47

Figure 3-47. Flow Diagram Showing "SEPARATION THEOREM"

For the present problem in which we assume the bias sources are invariant across a firing pass unless corrected, the "optimal controller" is trivial, one simply applies the control correction

$$u_j = -\hat{x}_j \quad (3.138)$$

If the biases varied in a statistical fashion with time, and if one could define the statistics as a stationary process which evolved at a rate low compared with the projectile time of flight, textbook solutions could again be applied to determine the optimum correction scheme. This extension would normally be considered in developing Kalman algorithms for processing the miss distances caused by target maneuver as isolated by the VISTA loop.

For the present problem of bias correction, excluding target maneuver by VISTA, the computational algorithms are summarized in Table III-18 for three cases:

- a. Estimation of bias without correction. Since the optimum control is equivalent to the subtraction of this estimate from the original bias, these algorithms can

Table III-18. Summary of Estimation and Control Algorithms (Sheet 1 of 2)

Process	Estimation	Control Without Observation Lag	Control With Observation Lag
System State	$x_{j+1} = x_j$	$x_{j+1} = x_j + u_j$	$x_{j+1} = x_j + u_j$
Observations	$z_j = H_j x_j + G_j w_j$ $= H_j x_j + v_j$	$z_j = H_j x_j + G_j w_j$ $= H_j x_j + v_j$	$z_j = H_j x_j + G_j w_j$ $= H_j x_j + v_j$
Best Estimate of x_j prior to z_j Best Estimate of x_j given z_j	\hat{x}_j \hat{x}_j	\hat{x}_j \hat{x}_j	\hat{x}_j \hat{x}_j
Computation of x_j Optimal Control For this problem hence	$\hat{x}_j = \hat{x}_{j-1}$ $\hat{x}_j = \hat{x}_j + K_j(z_j - \hat{x}_j)$ -----	$\hat{x}_j = \hat{x}_{j-1} + u_{j-1}$ $\hat{x}_j = \hat{x}_j + K_j(z_j - \hat{x}_j + H_j \sum u_{j-\Delta})$ $u_j = -\hat{x}_j$ $\hat{x}_j = 0$ $u_j = -K_j \hat{x}_j + H_j \sum u_{j-\Delta}$	$\hat{x}_j = \hat{x}_{j-1} + u_{j-1}$ $\hat{x}_j = \hat{x}_j + K_j(z_j - \hat{x}_j + H_j \sum u_{j-\Delta})$ $u_j = -\hat{x}_j$ $\hat{x}_j = 0$ $u_j = -K_j \hat{x}_j + H_j \sum u_{j-\Delta}$
Kalman Gain	$K_j = P_j H_j^T R_j^{-1}$ $M_j = P_{j-1}$	$K_j = M_j H_j^T [H_j M_j H_j^T + R_j]^{-1}$ $M_j = P_{j-1}$	$K_j = M_j H_j^T [H_j M_j H_j^T + R_j]^{-1}$ $M_j = P_{j-1}$

Table III-18. Summary of Estimation and Control Algorithms (Sheet 2 of 2)

Process	Estimation	Control Without Observation Lag	Control With Observation Lag
Covariance Matrix	$P_j^{-1} = M_j^{-1} + H_j^T R_j^{-1} H_j$ $P_j = M_j - M_j H_j^T [H_j M_j H_j^T + R_j]^{-1} H_j M_j$ $F_j = [I - K_j H_j] M_j [I - K_j H_j]^T + K_j R_j K_j^T$	$P_j = M_j - K_j [H_j M_j H_j^T + R_j] K_j^T$ $P_j = M_j [I - H_j^T K_j^T]$ $P_j^{-1} = M_j^{-1} + N_j^T R_j^{-1} H_j$	$P_j = M_j - K_j [H_j M_j H_j^T + R_j] K_j^T$ $P_j = M_j [I - H_j^T K_j^T]$ $P_j^{-1} = M_j^{-1} + H_j^T R_j^{-1} H_j$

be used to estimate the residual variance, and the computation is often simpler than working through the control algorithms, which yield the same result.

- b. Optimal control without observation lag. This is provided as a reference.
- c. Optimal control with observation lag. This set is identical to the previous set, except that the necessary step of storing corrections during time of flight to account for observation lag, is included.

Development of these relations will be found in Ho,⁽²⁸⁾ whose notation is used here.

We note for reference the famous matrix inversion lemma which states the equivalence of the two forms

$$P^{-1} = M^{-1} + H^T R^{-1} H \quad (3.139)$$

$$P = M - M H^T [H M H^T + R]^{-1} H M \quad (3.140)$$

For our present problem the first algorithm requires inversion of a higher order matrix than the second; if we are interested only in the evolution of P , we can often obtain more rapid insight by noting that

$$P_n^{-1} = P_0^{-1} + \sum_{j=1}^n H_j^T R_j^{-1} H_j \quad (3.141)$$

which follows from consecutive applications of (3.139). We use this form in a following section.

3.4.5 Example of 3-D Solution

We consider a system which employs sensors capable of measuring the angular errors of individual bullets as they reach target range. The sensors might be a radar system as has been demonstrated in MIDI, or a FLIR angular sensor paired with a high pulse repetition rate laser and a laser-driven range gate, as discussed in the earlier section on sensors.

It is assumed that the VISTA algorithm is employed. Three separate bias sources are assumed, but the general solution is not restricted to three.

This case, and the data flow developed for it have been used in the computer sizing estimates reported in a separate but accompanying report.

Assumptions:

- a. The sensor system is able to observe the angular miss of a bullet with respect to the target when the bullet has reached target range. The observation vector is

$$z_{jm} = \begin{bmatrix} \Delta T_m \\ \Delta e_m \end{bmatrix}_j; \quad \begin{array}{l} \Delta T_m = \text{lateral miss measurement} \\ \Delta e_m = \text{vertical miss measurement} \end{array} \quad (3.142)$$

where the observation is made on the "j'th" bullet. The time at which each observation is made is also recorded and stored with z_j for processing.

- b. The object of the system is to correct for "bias-like" error sources. The sources are assumed to be defined by the vector

$$x_j = \begin{bmatrix} A_b \\ e_b \\ V_b \end{bmatrix}_j \quad (3.143)$$

where A_b is an azimuth bias, e_b is an elevation bias, and V_b is a range-like bias, and the j subscript refers to the residual bias after the j 'th observation and correction. A_b, e_b may be considered to result from boresighting errors.

For present purposes we assume that V_b is in fact a muzzle velocity bias, and develop the correction algorithms accordingly.

- c. Since the bias sources are assumed to be constant, unless corrected, the state vector x_j evolves according to

$$x_{j+1} = x_j + u_j \quad (3.144)$$

where u_j is the correction vector applied after the j 'th observation.

- d. The effect of target maneuver on the miss distance is subtracted from the miss measurement via the VISTA algorithm before computing the correction vector u_j . In the present implementation, no attempt is made to correct via the closed loop for target maneuver.

Computational Algorithms

VISTA computations of the effect of target maneuver are performed by storing predicted azimuth and elevation (A_p, e_p, t). From the tracking sensors, ($A_{tm}, e_{tm}, D_{tm}, t$) are obtained. t is time. Time of flight to present range is obtained from the ballistic unit $t_{po}(D_{tm})$. The predicted angles this time earlier are recovered to yield

$$\Delta A(t)_v = A_{tm}(t) - A_p(t - t_{po}) \quad (3.145)$$

$$\Delta T(t)_v = \Delta A(t)_v \cos e_{tm} \quad (3.146)$$

$$\Delta e(t)_v = e_{tm}(t) - e_p(t - t_{po}) \quad (3.147)$$

The observation vector used to compute the correction is then

$$z_j = z_{jm} - z_{jv} \quad (3.148)$$

$$z_j = \begin{bmatrix} \Delta T \\ \Delta e \end{bmatrix}_j = \begin{bmatrix} \Delta T_m \\ \Delta e_m \end{bmatrix}_j - \begin{bmatrix} \Delta T_v \\ \Delta e_v \end{bmatrix}_j \quad (3.149)$$

The Kalman gain for the j 'th correction, applied immediately subsequent to the j 'th observation is

$$K_j = M_j H_j^T [H_j M_j H_j^T + R_j]^{-1} \quad (3.150)$$

where

$$M_j = P_{j-1} \quad (3.151)$$

The matrix to be inverted is only 2×2 . However, because of R_j there are never any zero elements.

The correction vector

$$u_j = \begin{bmatrix} \Delta A_b \\ \Delta a_b \\ \Delta v_b \end{bmatrix}_j \quad (3.152)$$

is computed from

$$u_j = -K_j[z_j + H_j \sum u_{j-k}] \quad (3.153)$$

It is necessary to store past corrections u_{j-k} for one time of flight. The reason is that these are corrections which have already been made, but their effect has not yet been seen. The H_j matrix applied to the sum $\sum u_{j-k}$ describes the effect which they would have on the observation at j , if they could be seen; the bracketed term represents the estimated residual miss on which the j 'th correction is to be based. Without this summation, one incurs stability problems because of the time of flight lag between correction and observation of its effect.

The algorithms for computing the correction vector u_j are Kalman-type, and are

$$u_j = -K_j[z_j + H_j \sum u_{j-k}] \quad (3.154)$$

The matrix H_j describes the projection of the assumed bias sources into the observation coordinate system,

$$H_j = \begin{bmatrix} \cos e & 0 & \sin \delta_T \\ 0 & 1 & \sin \sigma \end{bmatrix} \quad (3.155)$$

The $\cos e$ term results from the assumption that lateral angular bias originates as an azimuth boresight type error, the effect of which is reduced by $\cos e$ when observed at the target. The $\sin \delta_T$, $\sin \sigma$ terms represent the projection of the range/velocity type biases along the flight direction projected into the observation plane, and measured as lateral and vertical errors.

These latter two sine terms can be extracted from the other computations involved in prediction in several ways, since they need not be obtained with high accuracy. In view of the availability of the data used in the VISTA computation, it may be simplest to compute

$$\delta_T \approx [A_1 \dots A_n] \cos e_t \quad (3.156)$$

$$\sigma \approx e_p(t) - e_{tm}(t)$$

The state variance matrix is defined as P_j . The *a priori* estimates are

$$P_0 = \begin{bmatrix} \sigma_{Ab}^2 & 0 & 0 \\ 0 & \sigma_{eb}^2 & 0 \\ 0 & 0 & \sigma_V^2 \end{bmatrix} \quad (3.157)$$

The two variances of angle are in angular measure; the σ_V^2 term, if attributed to muzzle velocity is the variance of the fractional error in muzzle velocity.

P_0 is an initial input to the computer. In conjunction with the *a priori* matrix of expected measurement variances, it determines how much of the observed miss on each round is used in the subsequent correction.

Observations of miss are assumed to include

- a. The effect of residual bias
- b. Round to round dispersion in angle and muzzle velocity. These effects are assumed to be random across bullets, to have zero mean, and to result from the rms sum of constant standard angular deviation in angle, and constant standard deviation of fractional muzzle velocity error.
- c. Measurement errors. These are assumed to be random across measurement with zero mean, and to have the same characteristics, but not necessarily the same magnitudes as the bullet dispersion components. Timing errors cause errors along the flight direction which will vary in a different way with range from the effect of muzzle velocity dispersion. In the absence of experimental data or estimates, we do not recognize this difference in the present configuration.

We therefore combine b and c by summing squares, and obtain for the matrix of random error variances across observations

$$R_j = \begin{bmatrix} \sigma_T^2 + \sigma_V^2 \sin^2 \delta_T & \sigma_V^2 \sin \delta_T \sin \sigma \\ \sigma_V^2 \sin \delta_T \sin \sigma & \sigma_e^2 + \sigma_V^2 \sin^2 \sigma \end{bmatrix} \quad (3.158)$$

σ_T^2 , σ_V^2 and σ_e^2 are a priori estimates and are inputs. At the moment we see no reason for not setting

$$\sigma_T^2 \approx \sigma_e^2 \approx \sigma^2 \quad (3.159)$$

After each correction it is necessary to update the P_j matrix. Various forms are possible; a simple one (in notation at least) is

$$P_j = M_j [I - H_j^T K_j^T] \quad (3.160)$$

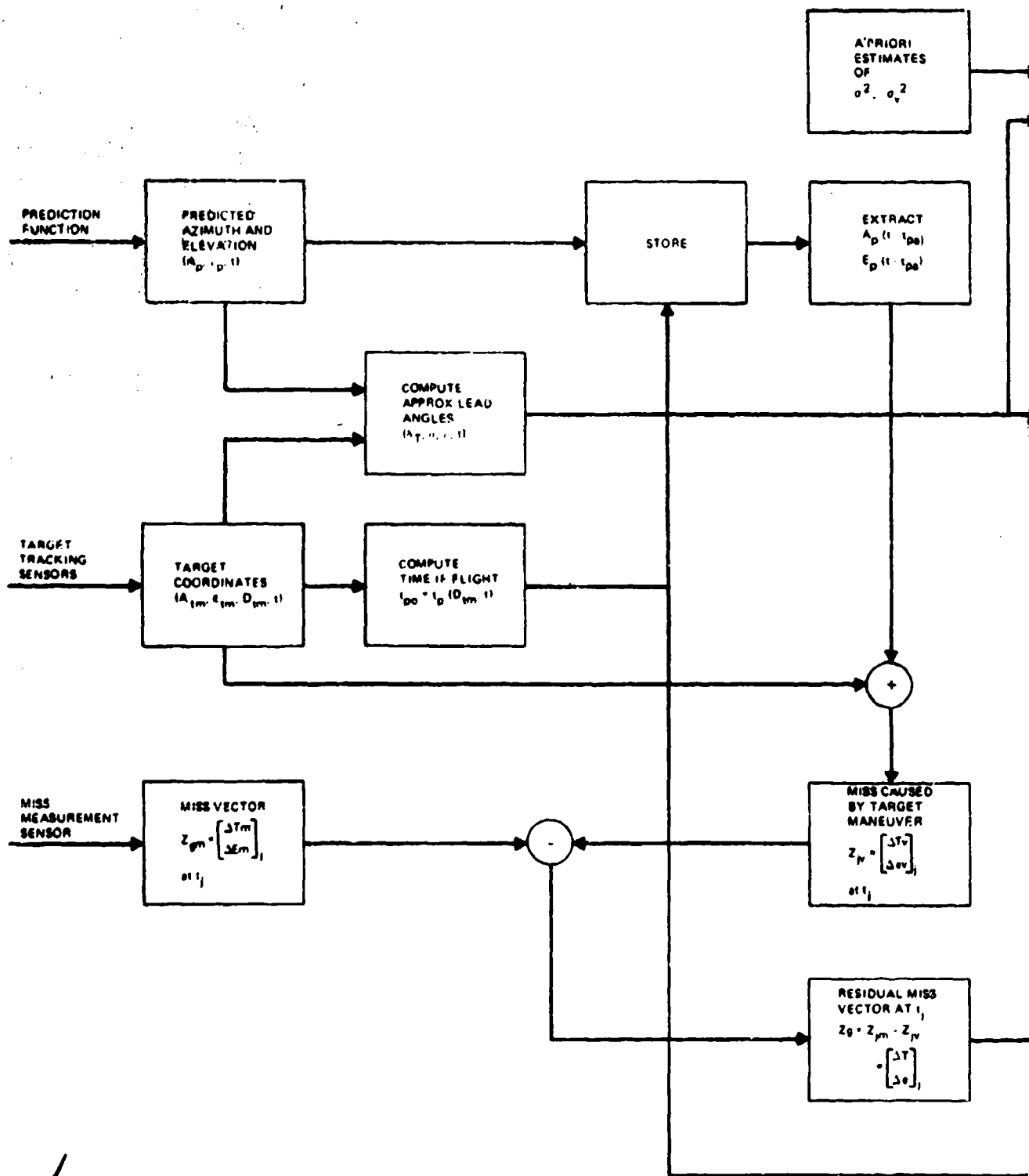
Figure 3-48 shows the flow of computations. The matrices have not been expanded to individual terms for conciseness. The expansions follow directly from the preceding material.

Note that if one is willing to abandon the correction for muzzle velocity/range bias type errors, all of the computations become extremely simple, and if one is willing to assume that the $\cos e$ term can be replaced by unity, they become even simpler.

At this point, however, it is considered preferable to size the complete 3-D configuration to determine its cost in computer capacity.

3.4.6 Estimate of 3-D System Performance

To estimate the performance of the system described above, we use the estimation relationships from Table III-18, since they allow us to go directly to the estimate of residual bias variances after n observations, without the necessity for working through the sequential computations of the control form of the algorithms. The covariance matrix of the residual biases after n observations, P_n is obtained by noting that





2

$$P_j^{-1} = M_j^{-1} + H_j^T R_j^{-1} H_j \quad (3.161)$$

$$M_j = P_{j-1} \quad (3.162)$$

hence

$$P_n^{-1} = P_0^{-1} + \sum_{j=1}^n H_j^T R_j^{-1} H_j \quad (3.163)$$

then

$$R_j^{-1} = \frac{\begin{bmatrix} \sigma^2 + \sigma_V^2 \sin^2 \sigma & -\sigma_V^2 \sin \delta_T \sin \sigma \\ -\sigma_V^2 \sin \delta_T \sin \sigma & \sigma^2 + \sigma_V^2 \sin^2 \delta_T \end{bmatrix}}{\sigma^2 (\sigma^2 + \sigma_V^2 \sin^2 L)} \quad (3.164)$$

where we use the relation that

$$\begin{aligned} \sin \delta_T &= \sin L \cos \psi \\ \sin \sigma &= \sin L \sin \psi \end{aligned} \quad (3.165)$$

and L is the total lead angle; ψ is defined by the above relation, it is the apparent direction of motion of the target projected into the sight plane.

Multiplying out the matrix product

$$H_j^T R_j^{-1} H_j = \frac{\begin{bmatrix} (1 + \lambda \sin^2 \sigma) \cos^2 e & -\lambda \sin \delta_T \sin \sigma \cos e & \sin \delta \cos e \\ -\lambda \sin \delta_T \sin \sigma \cos e & 1 + \lambda \sin^2 \delta_T & \sin \sigma \\ \sin \delta_T \cos e & \sin \sigma & \sin^2 L \end{bmatrix}}{\sigma^2 (1 + \lambda \sin^2 L)} \quad ()$$

where

$$\lambda = (\sigma_v/\sigma)^2 \quad (3.166)$$

Then performing the summation indicated by Eq. 3.163 we obtain a 3×3 matrix for P_n^{-1} which can be inverted. To do this analytically would be tedious and provide no useful insight at this time. Instead we perform the inversion for some special cases, which are relatively simple.

First however, we develop an additional expression, relating P_n (which describes source variances) to bias variances of miss distance itself, in the "sight" plane.

The previous relations given the covariance matrix of the bias sources. To see what the variances in miss distances become, note that

$$M = \begin{bmatrix} T_b \\ e_b \end{bmatrix} = \begin{bmatrix} \cos e & 0 & \sin \delta_T \\ 0 & 1 & \sin \sigma \end{bmatrix} \begin{bmatrix} A_b \\ e_b \\ v_b \end{bmatrix} \quad (3.167)$$

and denoting the covariance matrix of miss distances

$$S = \langle MM^T \rangle \quad (3.168)$$

$$S_j = H_j P_j H_j^T \quad (3.169)$$

then if the elements of the P_j matrix are p_{ij} ; where $p_{ij} = p_{ji}$

$$S_j = \begin{bmatrix} p_{11} \cos^2 e + 2p_{13} \sin \delta \cos e + p_{33} \sin^2 \delta & (p_{12} + p_{13} \sin \sigma) \cos e \\ & + (p_{32} + p_{33} \sin \sigma) \sin \delta \\ (p_{21} + p_{31} \sin \sigma) \cos e + (p_{23} + p_{33} \sin \sigma) \sin \delta & p_{22} + 2p_{23} \sin \sigma + p_{33} \sin^2 \sigma \end{bmatrix} \quad (3.170)$$

Consider a large number of rounds fired at a particular geometrical configuration of the engagement, i.e., a burst at very high rate of fire. The matrix inversion theorem gives the following alternate form for computing P_n

$$P_n = P_o - P_o H^T [H P_o H^T + Q]^{-1} H P_o; Q = R/n \quad (3.171)$$

but

$$S_n = H P_o H^T \quad (3.172)$$

so that

$$S_n = S_o - S_o [S_o + Q]^{-1} S_o \quad (3.173)$$

and as n becomes large, all of the elements of Q become small, so that

$$[S_o + Q]^{-1} = S_o^{-1} [1 - S_o^{-1} Q + \dots] \quad (3.174)$$

$$S_n \approx S_o^{-1} Q S_o \quad (3.175)$$

$$S_n \approx S_o^{-1} R S_o / n \quad (3.176)$$

hence S_n vanishes, for n very large: the algorithms will always work to reduce the observed miss vector, even though the allocation as to source may be imperfect.

We can gain some insight as to how the process evolves by considering a series of bursts fired at geometrical configurations of the target path at which the matrix elements simplify. We consider three special cases below.

CASE I: Direct Incoming Target

For this case, $\psi = 90^\circ$, $\cos \psi = 0$, $\sin \psi = 1.0$. Assume that n rounds are fired in a short interval during which the matrix elements do not change significantly. Then

$$P_n^{-1} = P_o^{-1} + n\sigma^{-2} \begin{bmatrix} \cos^2 e & 0 & 0 \\ 0 & m & m \sin L \\ 0 & m \sin L & m \sin^2 L \end{bmatrix} \quad (3.177)$$

where $m = (1 + \lambda \sin^2 L)^{-1}$

This form is easily inverted, and extracting the diagonal elements of the inverse matrix

$$\begin{aligned} (\sigma_{An}/\sigma_{Ab})^2 &= \frac{\sigma^2}{\sigma^2 + n\sigma_{Ab}^2 \cos^2 e} \\ (\sigma_{en}/\sigma_{eb})^2 &= \frac{\sigma^2 + \sigma_v^2 \sin^2 L + n\sigma_{Vb}^2 \sin^2 L}{\sigma^2 + \sigma_v^2 \sin^2 L + n(\sigma_{eb}^2 + \sigma_{Vb}^2 \sin^2 L)} \\ (\sigma_{Vn}/\sigma_{Vb})^2 &= \frac{\sigma^2 + \sigma_v^2 \sin^2 L + n\sigma_{eb}^2}{\sigma^2 + \sigma_v^2 \sin^2 L + n(\sigma_{eb}^2 + \sigma_{Vb}^2 \sin^2 L)} \end{aligned} \quad (3.178)$$

As n becomes very large, the variance of azimuth bias is reduced to zero. At this aspect, however, the system cannot discriminate uniquely between the effects of elevation bias and muzzle velocity bias, but it does reduce both, allocating the corrections according to the *a priori* estimates of their relative magnitude.

In fact the system is much cleverer than the above statement would imply. It may not know exactly where the source of the elevation bias is located, but the corrections it applies do in fact reduce the elevation bias in the sight plane, i.e. at the target to zero. We can see this by observing the covariance matrix of bias errors in the sight plane.

For this special case of a direct incoming target,

$$S_j = \begin{bmatrix} p_{11} \cos^2 e & 0 \\ 0 & p_{22} + 2p_{23} \sin \sigma + p_{32} \sin^2 \sigma \end{bmatrix} \quad (3.179)$$

or in terms of the P_j^{-1} matrix elements m_{ij} before inversion,

$$S_j = \begin{bmatrix} m_{11}^{-1} \cos^2 e & 0 \\ 0 & \frac{m_{33} - 2m_{23} \sin \sigma + m_{22} \sin^2 \sigma}{m_{33}m_{22} - m_{23}m_{32}} \end{bmatrix} \quad (3.180)$$

since $\sigma = L$ for this geometry.

Substituting the values of the m_{ij} , we obtain

$$\sigma_{Ab}^2 = \frac{\sigma^2 \sigma_{Ab}^2 \cos^2 e}{\sigma^2 + n \sigma_{Ab}^2 \cos^2 e} - \sigma^2/n \quad (3.181)$$

$$\sigma_{eb}^2 = \frac{(\sigma_{eb}^2 + \sigma_{vb}^2 \sin^2 \sigma)(\sigma^2 + \sigma_v^2 \sin^2 \sigma)}{(\sigma^2 + \sigma_v^2 \sin^2 \sigma) + n(\sigma_{eb}^2 + \sigma_{vb}^2 \sin^2 \sigma)} - \frac{(\sigma^2 + \sigma_v^2 \sin^2 \sigma)}{n} \quad (3.182)$$

This is a remarkable characteristic of the Kalman solution. At various times, and various positions of the target, the algorithms will be able to identify bias sources (which may be numerous) to varying degrees of reliability. But the computed corrections are always apportioned in a way that reduces the resultant biases projected into the sight plane.

Elimination of all biases at their source depends on the comprehensiveness of the sample sets over the firing region, and the accuracy with which the model represents the actual bias sources. However this learning process, which can continue over many paths, does not reduce the rate of reduction in bias at the target on any one course.

CASE II: Target Attacking Down Line of Sight

For this case, the above relations hold, with $L = 0$. The algorithms unambiguously recognize azimuth and elevation bias, and apply corrections for both.

The residual variances in the sight plane are obtained from the expressions given above, setting $L = 0$.

Case III: Target at midpoint of a passing, level course

$$\psi = 0, \cos \psi = 1.0, \sin \psi = 0$$

Then

$$P_n^{-1} = P_0^{-1} + n\sigma^{-2} \begin{bmatrix} m \cos^2 e & 0 & m \sin L \cos e \\ 0 & 1.0 & 0 \\ m \sin L \cos e & 0 & m \sin^2 L \end{bmatrix} \quad (3.183)$$

This expression inverts easily and we obtain

$$(\sigma_{An}/\sigma_{Ab})^2 = \frac{\sigma^2 + \sin^2 L (\sigma_v^2 + n\sigma_{Vo}^2)}{\sigma^2 + \sin^2 L (\sigma_v^2 + n\sigma_{Vo}^2) + n\sigma_{Ab}^2 \cos^2 e}$$

$$(\sigma_{en}/\sigma_{eb})^2 = \frac{\sigma^2}{\sigma^2 + n\sigma_{eo}^2} \quad (3.184)$$

$$(\sigma_{Vn}/\sigma_{vb})^2 = \frac{\sigma^2 + \sigma_v^2 \sin^2 L + n\sigma_{Ab}^2 \cos^2 e}{\sigma^2 + \sin^2 L (\sigma_v^2 + n\sigma_{Vo}^2) + n\sigma_{Ab}^2 \cos^2 e}$$

Now if we allow "n" to become very large, we see that the algorithm eliminates the elevation bias, and reduces the azimuth and muzzle velocity biases somewhat. Since the algorithm cannot discriminate ambiguously between the azimuth and muzzle velocity bias sources, however, the best it can do is to apportion the correction according to the ^apriori estimates of the relative variance magnitudes. This is the ^apriori estimate of muzzle velocity bias variance is very small, the algorithm will eliminate the azimuth bias, and vice versa. However if we projected the residual biases into the sight plane we would again observe the total elimination of their effects as n becomes large.

To simplify the calculations, we consider the bias correction process resulting from firing two bursts, one when the target is almost directly incoming, and one when it is at "midpoint". The following parametric values are assumed as shown in Table III-19.

For the incoming position $\sin \sigma = 0.10$; $\delta = 0$, $\cos e = 0.90$ and at midpoint $\sin \delta = 0.50$, $\cos e = 0.707$, $\sigma = 0$.

The "normalized values" are simply the actual values divided by 5.0. The resulting standard deviations may be multiplied by 5.0 to obtain mils, in the case of angular computations, and by 0.5 to obtain % in the case of muzzle velocity.

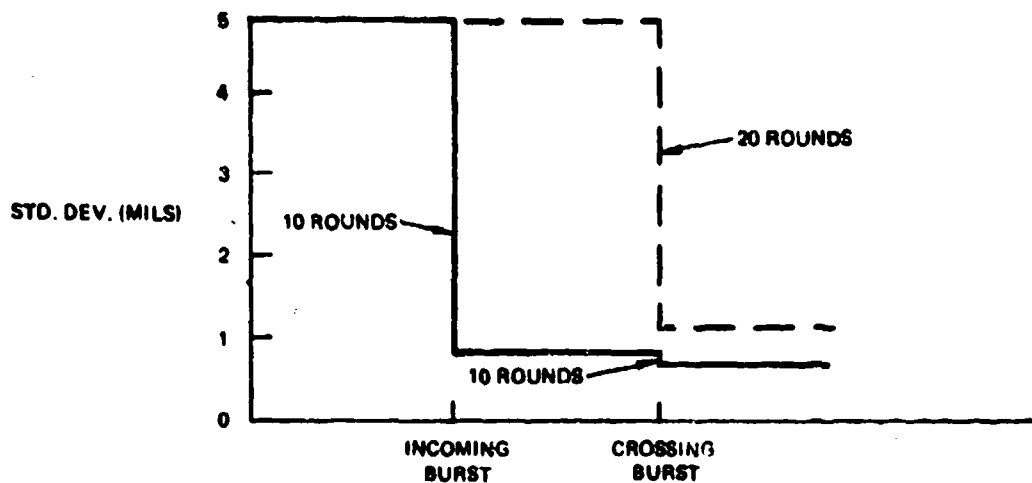
For this case we require the residual variance matrix from the first burst as an input to the second, and the matrix inversion is slightly more tedious.

On any particular course, of course, one has specific initial biases to be reduced, whereas the computation shows only the reduction in the variance of the expected residual bias, averaged over many paths. One could, however perform analogous computations for specific assumed initial bias values; after n rounds had been observed, the fractional reduction in bias would be the same as the fractional reduction in standard deviation of bias, averaged over many courses.

Figures 3-49 through 3-53 show the results of two firing sequences. In one, 10 rounds are fired as the target is almost directly incoming, then another 10 rounds at "midpoint". In the second, 20 rounds are fired at midpoint.

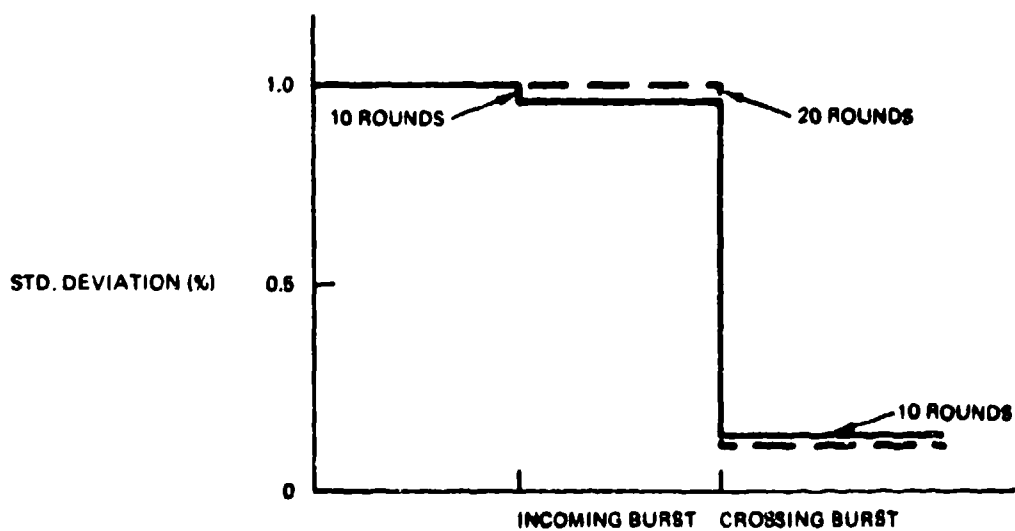
Table III-19. Assumed Standard Deviations

Actual	Normalized
$\sigma_{Ab} = 5 \text{ mils}$	1.0
$\sigma_{eb} = 5 \text{ mils}$	1.0
$\sigma_{Vb} = 1\%$	2.0
$\sigma = 2.5 \text{ mils}$	0.5
$\sigma_V = 0.25\%$	0.5



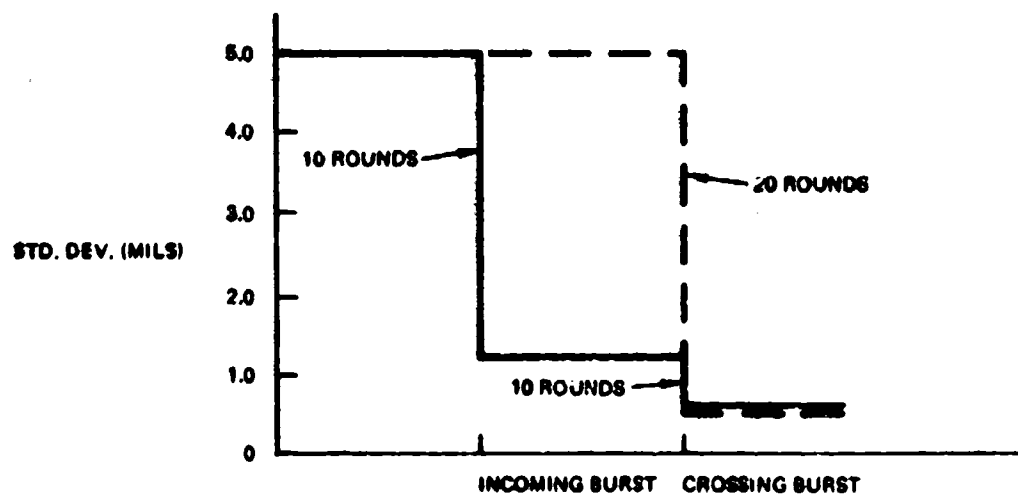
40001-49

Figure 3-49. Standard Deviation of Azimuth Bias



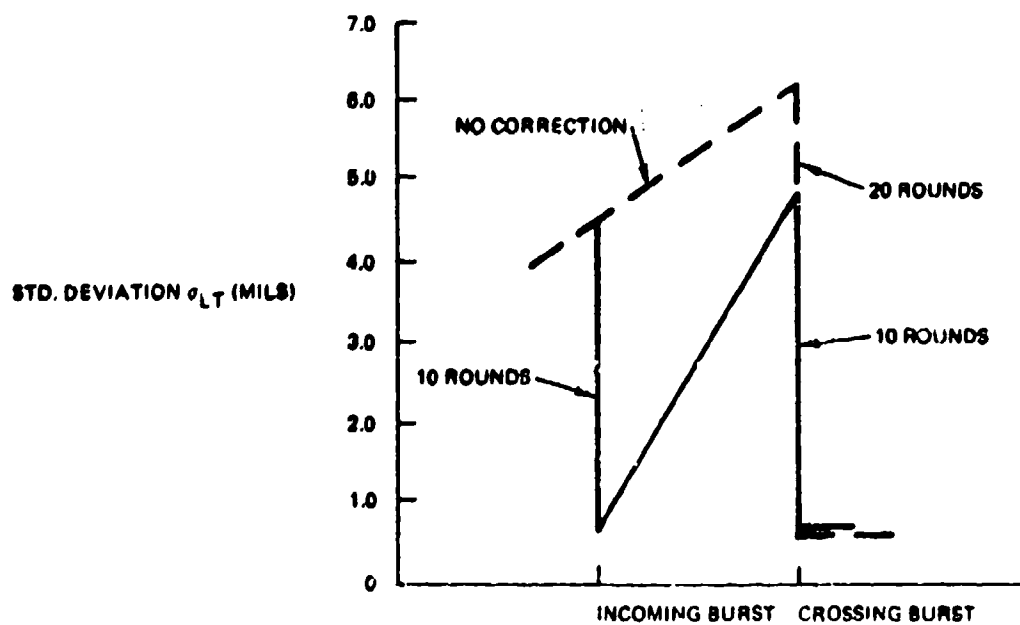
40001-50

Figure 3-50. Standard Deviation of Muzzle Velocity Bias



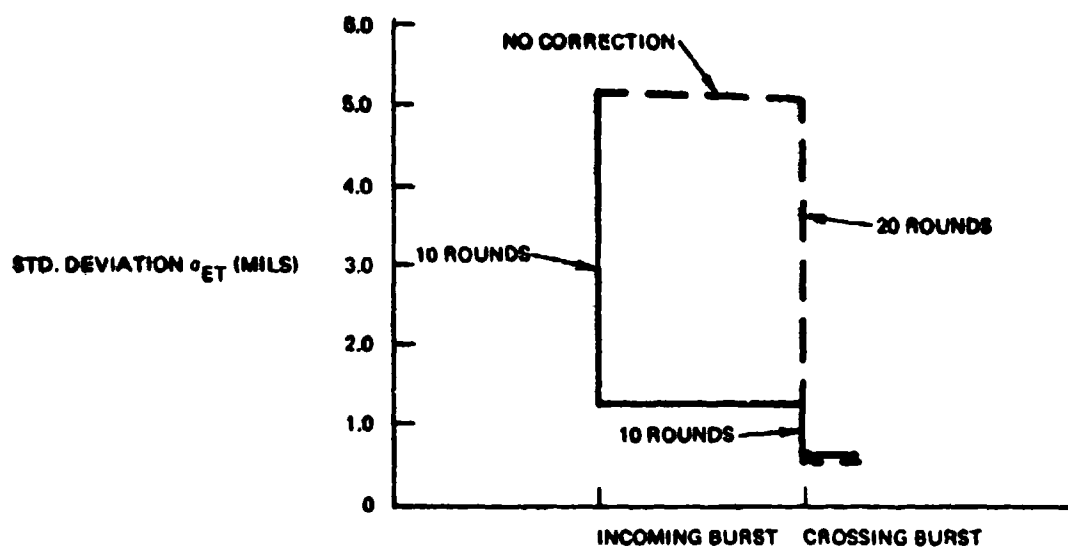
40001-51

Figure 3-51. Standard Deviation of Elevation Bias



40001-52

Figure 3-52. Standard Deviation of Total Lateral Bias



40001-53

Figure 3-53. Standard Deviation of Total Elevation Bias

Figure 3-49 shows the reduction in the standard deviation of azimuth bias. There is no ambiguity in source of the azimuth miss for the incoming burst, and all the corrections are applied to azimuth bias. At midpoint, however, the lateral miss includes components of both the residual azimuth bias and the muzzle velocity bias, and the algorithms produce only a small reduction in azimuth bias, but a large one in muzzle velocity bias, as seen from Figure 3-50.

For the initial burst, elevation and muzzle velocity biases interact, but the geometry is such that very little of the observed miss is attributed to muzzle velocity bias, and most of the correction is applied in elevation, as shown in Figure 3-51. There is no ambiguity in elevation at midpoint, where the whole correction is applied.

When 20 rounds are fired at midpoint only, the lateral miss observations generate corrections which are applied to both azimuth and muzzle velocity. Since the *a priori* estimates of muzzle velocity variance were larger than those of azimuth, the algorithms apply a larger correction to muzzle velocity than to azimuth.

When these standard deviations are combined and projected into the sight plane, to show bias of lateral and vertical miss at the target from all three sources, the results obtained are as shown in Figures 3-52 and 3-53.

The initial 10 rounds reduce azimuth bias, and at the incoming point muzzle velocity is relatively unimportant as a bias source. However, as the target angle increases, the lateral bias increases because of the increasing prominence of muzzle velocity. The 10 rounds at midpoint then reduce this source, and the total lateral vector.

It might appear that one would be better off, as far as bias reduction is concerned, to fire the 20 rounds at midpoint instead of in two parcels of 10. Note that if one does this, one is left with a larger residual azimuth bias (Figure 3-49) which will affect the incoming leg of the next target path.

For this simple case, one could probably do better with some other mix than a 10/10 to minimize the residual biases, and more generally, given n rounds, and a cooperative target, one could work out an optimum distribution of firing points. This can hardly be done with combat paths, but should be considered in setting up "calibration" firing doctrines, using internally generated target paths with actual shooting.

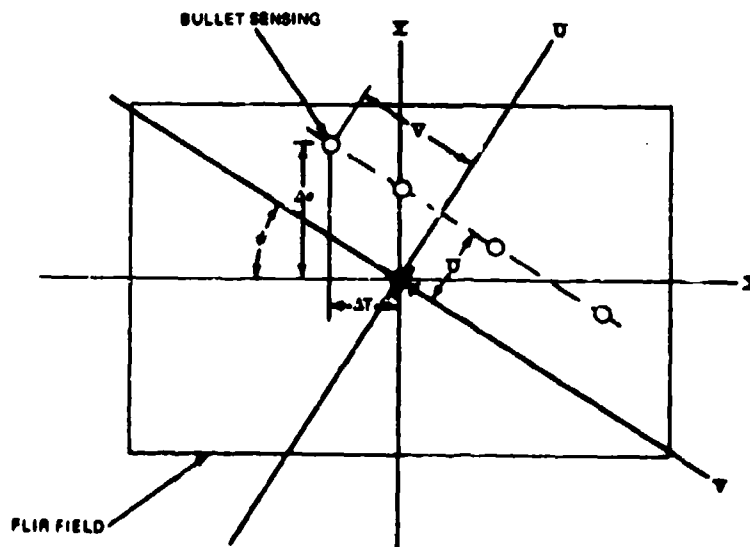
3.4.7 Example of 2-D Solution

A relatively simple method of obtaining closed loop operation of a predicted fire system, using an imaging sight, is one that depends only on the viewing of the tracer of a bullet, without range sensing.

This sensing allows out of plane bias sources to be corrected, even though it is not known when the bullet is at target range. Corrections for in-plane biases such as muzzle velocity bias cannot be made by this method, but importance of out of plane bias corrections and the probable simplicity of implementation of the method make it of interest.

The concept is as follows: the bullet is assumed to have a tracer element which is easily visible on the imaging sight. The method applies to TV systems as well as IR, but will be discussed here in terms of the FLIR.

The FLIR is centered on the target, within angular tracking accuracy, hence sweeps across a bullet trajectory with an angular velocity of magnitude and orientation determined by the angular velocity of tracking. This is shown in Figure 3-54.



40001-54

Figure 3-54. Coordinate System for 2-D Closed Loop System

Normally, a single bullet will be sensed by more than one FLIR element sequentially, as the field of view of the FLIR sweeps across the trajectory.

The angle ψ is defined by

$$\tan \psi = \frac{de/dt + d\theta/dt}{(dA/dt) \cos e} \quad (3.185)$$

where de/dt and dA/dt are elevation and azimuth angular tracking velocities, e is target elevation angle, $d\theta/dt$ is the vertical velocity resulting from gravity drop of the bullet. Approximately,

$$d\theta/dt \approx -(g/v_a) \cos e \quad (3.186)$$

where v_a is average bullet velocity to the target. This term can possibly approximate using constant values for g/v_a . It may amount to about 20 mils/second, at low elevations.

The bias errors which is desired to extract are $\Delta A = \Delta T \sec e$, and Δe .

ΔT and Δe are shown in Figure 3-54.

Since the bullet position at the target range cannot be determined, the only useful information bit which can be derived from sensings on a single bullet is U_m , the minimum angular approach of the bullet trace to the target. Using the U, V , rotated coordinate system, for the j 'th sensing on a particular bullet

$$\begin{bmatrix} U \\ V \end{bmatrix}_j = \begin{bmatrix} \sin \psi & \cos \psi \\ \cos \psi & -\sin \psi \end{bmatrix}_j \begin{bmatrix} \Delta T \\ \Delta e \end{bmatrix}_j \quad (3.187)$$

Multiple sensings on the same bullet should all yield the same value of U , from the above computation, within the accuracy of the several measurements of the $(\Delta T, \Delta e)_j$ pairs.

If there were no bullet dispersion, and no measurement errors, one could obtain ΔT , Δe from two measurements of U_j at different values of ψ_j .

The basis for the system concept is the use of a Kalman type of filter to allow sensings over many bullets, at different values of ψ to be properly averaged to obtain estimates of ΔT and Δe .

Multiple Sensings of the Same Bullet

As the FLIR sweeps across the bullet trajectory, there will in general be multiple sensings of the same bullet. These can be handled in two ways.

- a. Process all sensings, but weigh each sensing by $1/n$

where

$$n = (\text{FLIR field angular extent}/\text{element angular extent})p_d$$

p_d = probability of sensing, given that the bullet is in the field of an element.

This allows the measurement error to be averaged.

- b. If p_d is essentially unity, and the measurement error is negligible, process only those sensings for which

$$|V| < |\omega|F \quad (3.188)$$

where

ω = the vector angular velocity

$$\omega = \left[(de/dt + d\theta/dt)^2 + (dA/dt \cos e)^2 \right]^{1/2} \quad (3.189)$$

and F is the FLIR frame time.

The following example considers only azimuth and elevation bias sources. It can be extended to include all "out-of-plane" sources in a straightforward way. To derive the processing algorithms it is first desired to correct for target maneuver via the VISTA algorithm. In the general case, a sensing yields the triad $(U, V, t)_j$. When the bullet is first sensed it is probably not yet at the target range, and in fact the equirange point cannot be determined. However, this lack of range information affects only changes in the angle ψ between the sensing point and the equirange point. To estimate the magnitude of the effect note that

$$d\psi/dt = -(dA/dt) \sin e$$

$$dA/dt = \omega \cos e \quad (3.190)$$

If the bullet is sensed at an angle V from its point of minimum angular separation, the change in ψ during this interval is obtained from

$$T = V/\omega$$

$$\Delta\psi = (d\psi/dt)T$$

$$\Delta\psi = V \tan e_0. \quad (3.191)$$

Thus even if the sensing is as much as 5° from the equirange point, the change in ψ will have only a very small effect on the values of the $\sin\psi$ and $\cos\psi$ in the algorithms. If V is limited as in case b above, the effect is negligible.

a sensing, then, we use the VISTA algorithm to determine the ΔT and Δe against which the actual sensing is to be compared. Since the only sensing element we use in processing is U , we receive only U_v from the VISTA loop.

The measurement "vector" is then the scalar

$$z_j = U_j - U_v \quad (3.192)$$

Restating the Kalman algorithms, to derive the Kalman gain

$$z_j = \begin{bmatrix} \sin\psi & \cos e & \cos\psi \end{bmatrix}_j \begin{bmatrix} A_b \\ e_b \end{bmatrix}_j + w_j \quad (3.193)$$

$$z_j = H_j x_j + w_j; w_j = \text{random round to round noise from all sources} \quad (3.194)$$

The state equation is

$$x_{j+1} = x_j + u_j \quad (3.195)$$

The Kalman gain K_j is

$$K_j = M_j H_j^T [H_j M_j H_j^T + R_j]^{-1}$$

$$R_j = \langle w_j^2 \rangle$$

$$R_j = \sigma^2 \quad (3.196)$$

M_j is the variance matrix of the residual bias, $M_j = P_j - 1$

P_0 is the a priori matrix of bias variances.

$$P_0 = \begin{bmatrix} \sigma_A^2 & 0 \\ 0 & \sigma_e^2 \end{bmatrix} \quad (3.197)$$

M_j is 2×2 ; the bracketed term to be inverted is a scalar.

The correction to be applied for bias is

$$u_j = -K_j \left[z_j + H_j \sum_{\mu} u_{j-k} \right] \quad (3.198)$$

where the sum is taken over corrections applied in the past but not yet observed, i.e. up to one time of flight in memory.

After each computation, the P_j matrix is updated according to

$$P_j = M_j [I - H_j^T K_j^T] \quad (3.199)$$

This completes the definition of the solution. A flow diagram is not provided, since it is very close to the 3-D data flow provided earlier, although there is great simplification in detail.

3.4.8 Estimates of 2-D System Performance

To simplify the algebra, yet retain the essential elements of the process, assume that the lateral bias is, in fact, a constant σ_{bT} , unless corrected, rather than an azimuth bias, so that the $\cos e$ term is suppressed. Then

$$U = HX$$

$$H = [\sin \psi \cos \psi]$$

$$X = \begin{bmatrix} \Delta T \\ \Delta e \end{bmatrix}$$

$$R_j = \sigma^2$$

$$P_o = \begin{bmatrix} \sigma_{Tb}^2 & 0 \\ 0 & \sigma_{eb}^2 \end{bmatrix} \quad (3.200)$$

and the covariance matrix after n observations is obtained as

$$P_n^{-1} = P_o^{-1} + \sum_j H_j^T R_j^{-1} H_j$$

$$P_n^{-1} = \begin{bmatrix} \sigma_{Tb}^{-2} + \sigma^{-2} \sum \sin^2 \psi_j & \sigma^{-2} \sum \sin \psi_j \cos \psi_j \\ \sigma^{-2} \sum \sin \psi_j \cos \psi_j & \sigma_{eb}^{-2} + \sigma^{-2} \sum \cos^2 \psi_j \end{bmatrix} \quad (3.201)$$

This matrix is easily inverted to obtain

$$P_n = \sigma^2 \frac{\begin{bmatrix} (\sigma/\sigma_{eb})^2 + \sum \cos^2 \psi & - \sum \sin \psi \cos \psi \\ - \sum \sin \psi \cos \psi & (\sigma/\sigma_{Tb})^2 + \sum \sin^2 \psi \end{bmatrix}}{(\sigma/\sigma_{eb})^2 (\sigma/\sigma_{Tb})^2 + (\sigma/\sigma_{eb})^2 \sum \sin^2 \psi + (\sigma/\sigma_{Tb})^2 \sum \cos^2 \psi + \sum \cos^2 \psi \sum \sin^2 \psi - (\sum \sin \psi \cos \psi)^2} \quad (3.202)$$

The residual variance U_b^2 in the sight plane is obtained from

$$S^2 = H_n P_n H_n^T \quad (3.203)$$

and if the elements of P_n are, (where $p_{12} = p_{21}$)

$$P_n = \begin{bmatrix} p_{11} & p_{12} \\ p_{21} & p_{22} \end{bmatrix} \quad (3.204)$$

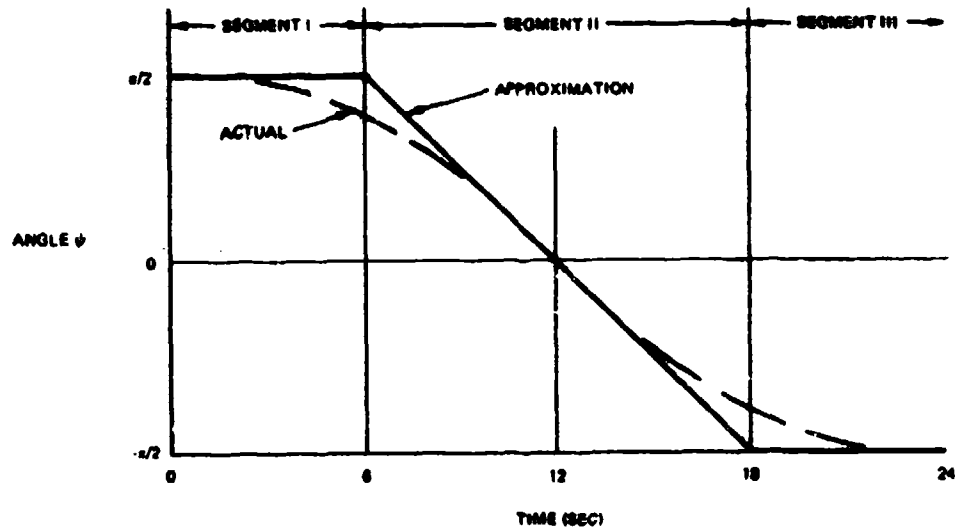
$$S_n^2 = p_{11} \sin^2 \psi_n + 2p_{12} \sin \psi_n \cos \psi_n + p_{22} \cos^2 \psi_n \quad (3.205)$$

Now consider the way in which ψ varies with time across a firing pass. This is shown in Figure 3-55. We approximate $\psi(t)$ by three straight line segments. At midpoint, for a horizontal target path

$$d\psi_o/dt \approx -dA_o/dt \sin e_o$$

$$d\psi_o/dt \approx -v_t H / (R_m D_m) \quad (3.206)$$

where v_t = target velocity, H = altitude, and R_m , D_m are horizontal and slant range to target at midpoint.



40001-55

Figure 3-55. Variation of Angle ψ With Time.

We assume a constant rate of bullet arrival at the target equal to the rate of fire of the gun,

$$dj/dt = \nu \quad (3.207)$$

Then we can approximate the trigonometric sums by integrals, for example

$$\begin{aligned} \sum \sin^2 \psi &\approx \int \sin^2 \psi dj \\ &= (dj/dt)/(d\psi/dt) \int \sin^2 \psi d\psi : d\psi/dt \leq 0 \end{aligned}$$

and

$$\int \sin^2 \psi d\psi = (\psi/2) - (1/4) \sin 2\psi$$

$$\int \cos^2 \psi d\psi = (\psi/2) + (1/4) \sin 2\psi$$

$$\int \sin \psi \cos \psi d\psi = (1/2) \sin^2 \psi \quad (3.208)$$

Over segment I, in Figure 3-55, $\psi = (\pi/2)$, hence if n_I rounds are fired

$$P_{nI} = \begin{bmatrix} \frac{\sigma_{Tb}^2 \sigma^2}{\sigma^2 + n_I \sigma_{Tb}^2} & 0 \\ 0 & \sigma_{eb}^2 \end{bmatrix} \quad (3.209)$$

and the lateral bias is reduced, but the elevation bias is unchanged.

The variance reduction over segment II begins with elements of the P_{nI} matrix, and we designate the reduced σ_{Tb}^2 by σ_{TI}^2 .

Substituting the trigonometric integrals from $(\pi/2)$ to ψ

$$\begin{aligned} \int_{\pi/2}^{\psi} \sin^2 \psi d\psi &\approx (\nu/\dot{\psi}_0) \left[\left(\frac{2\psi - \pi}{4} \right) - \left(\frac{\sin 2\psi}{4} \right) \right] \\ &\approx (\nu/4\dot{\psi}_0) [(2\psi - \pi) - (\sin 2\psi)] \end{aligned} \quad (3.210)$$

$$\int_{\pi/2}^{\psi} \cos^2 \psi d\psi \approx (\nu/4\dot{\psi}_0) [(2\psi - \pi) + (\sin 2\psi)]$$

$$\int_{\pi/2}^{\psi} \sin \psi \cos \psi d\psi \approx -(\nu/2\dot{\psi}_0) \cos^2 \psi$$

If n = total number of rounds fired over the ramp approximation to ψ , the total observation time over the ramp is

$$T = -\pi/\dot{\psi}_0, \text{ and the total number of rounds observed during } T \text{ is} \quad (3.211)$$

$$n = -(\pi\nu)/\dot{\psi}_0$$

If the observation interval begins at $\psi = \pi/2$.

$$\Sigma \sin^2 \psi \approx \left(\frac{n}{4\pi}\right)[(\pi - 2\psi) + \sin 2\psi]$$

$$\Sigma \cos^2 \psi \approx \left(\frac{n}{4\pi}\right)[(\pi - 2\psi) - \sin 2\psi] \quad (3.212)$$

$$\Sigma \sin \psi \cos \psi \approx \left(\frac{n}{2\pi}\right) \cos^2 \psi$$

At the end of segment II we have

$$P_{nI} = \begin{bmatrix} \frac{\sigma^2 \sigma_{TI}^2}{\sigma^2 + (n_{II}/2)\sigma_{TI}^2} & 0 \\ 0 & \frac{\sigma^2 \sigma_{eb}^2}{\sigma^2 + (n_{II}/2)\sigma_{eb}^2} \end{bmatrix} \quad (3.213)$$

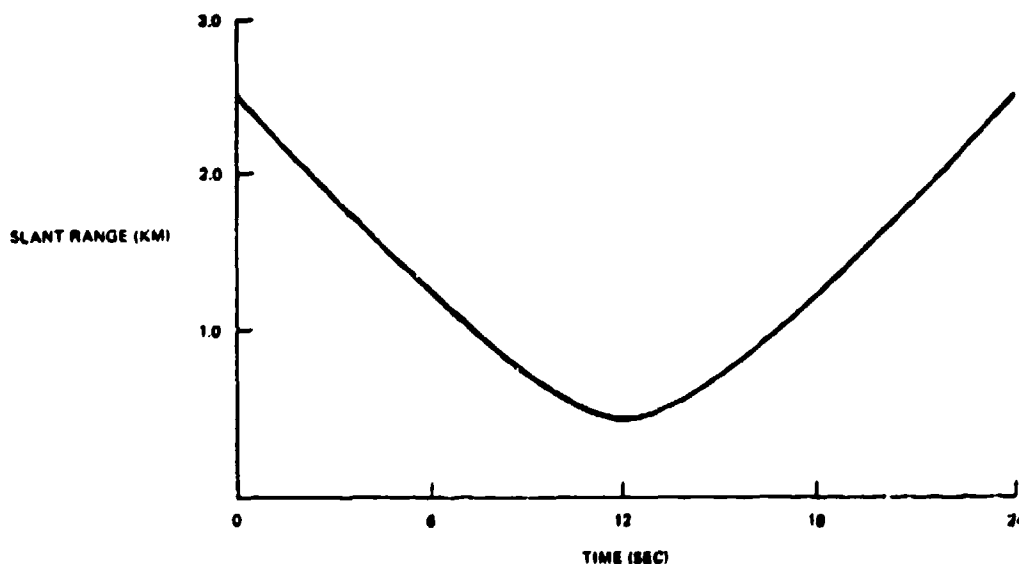
At the end of segment II, $\psi = -\pi/2$ and at this point

$$S_{nII} = \frac{\sigma^2 \sigma_{TI}^2}{\sigma^2 + (n_{II}/2)\sigma_{TI}^2} \quad (3.214)$$

where n_{II} = the number of rounds fired observed during this segment.

We observe that the end result of having two bias sources to correct is to reduce the number of observations effective against each by a factor of two.

For a numerical example, we choose a target velocity of 209 m/s, a horizontal range at midpoint of 400 meters, and an altitude such that the ratio $H/D = 0.50$ at midpoint. This makes the length of the ramp segment 12 seconds. The variation of slant range with time is shown in Figure 3-56. We assume a low average rate of fire (as an approximation to spaced bursts at a higher rate), such that 10 miss distance observations per second are obtained.



40001 66

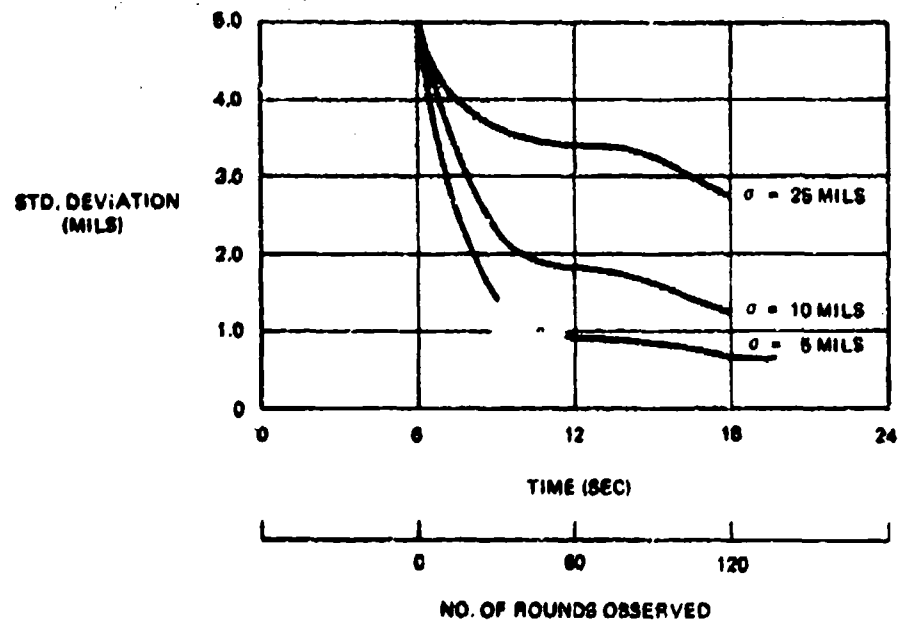
Figure 3-56. Slant Range versus Time

We assume that the standard deviations in elevation and traverse bias, (these are, of course, the averages over many cases) are 5 mils each initially.

The combination of random round to round dispersion and observation errors are assumed to have large values, namely standard deviations of 5, 10 and 25 mils in three sets of computations. In reality we would hope to have values of 3 mils or less, hence these numerical examples are definitely worst cases.

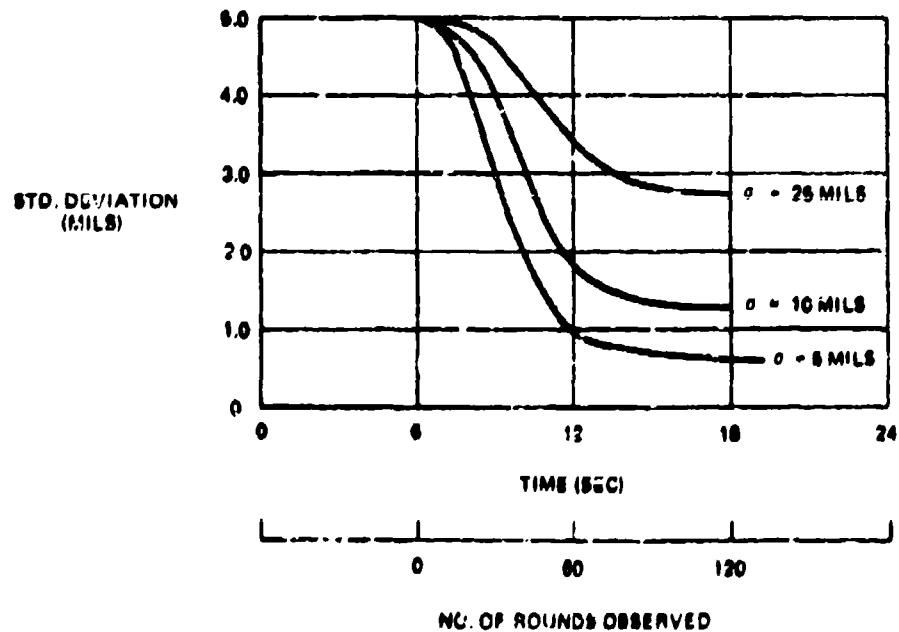
First consider firing only on the ramp segment of the target path, Segment II. Figure 3-57 shows the reduction in the residual traverse bias (averaged over many cases, as noted above), and Figure 3-58 shows the reduction in elevation bias. Note that the algorithms reduce traverse bias most rapidly initially, but make no corrections in traverse at midpoint, where this component cannot be separated by this 2-D system. On the other hand, the correction to elevation bias is initially slight, but has a maximum effect at midpoint.

It is interesting that even with 25 mils random and observation error, both bias sources are about halved after 120 observations.



40001-57

Figure 3-57. Residual Standard Deviation of Traverse Bias

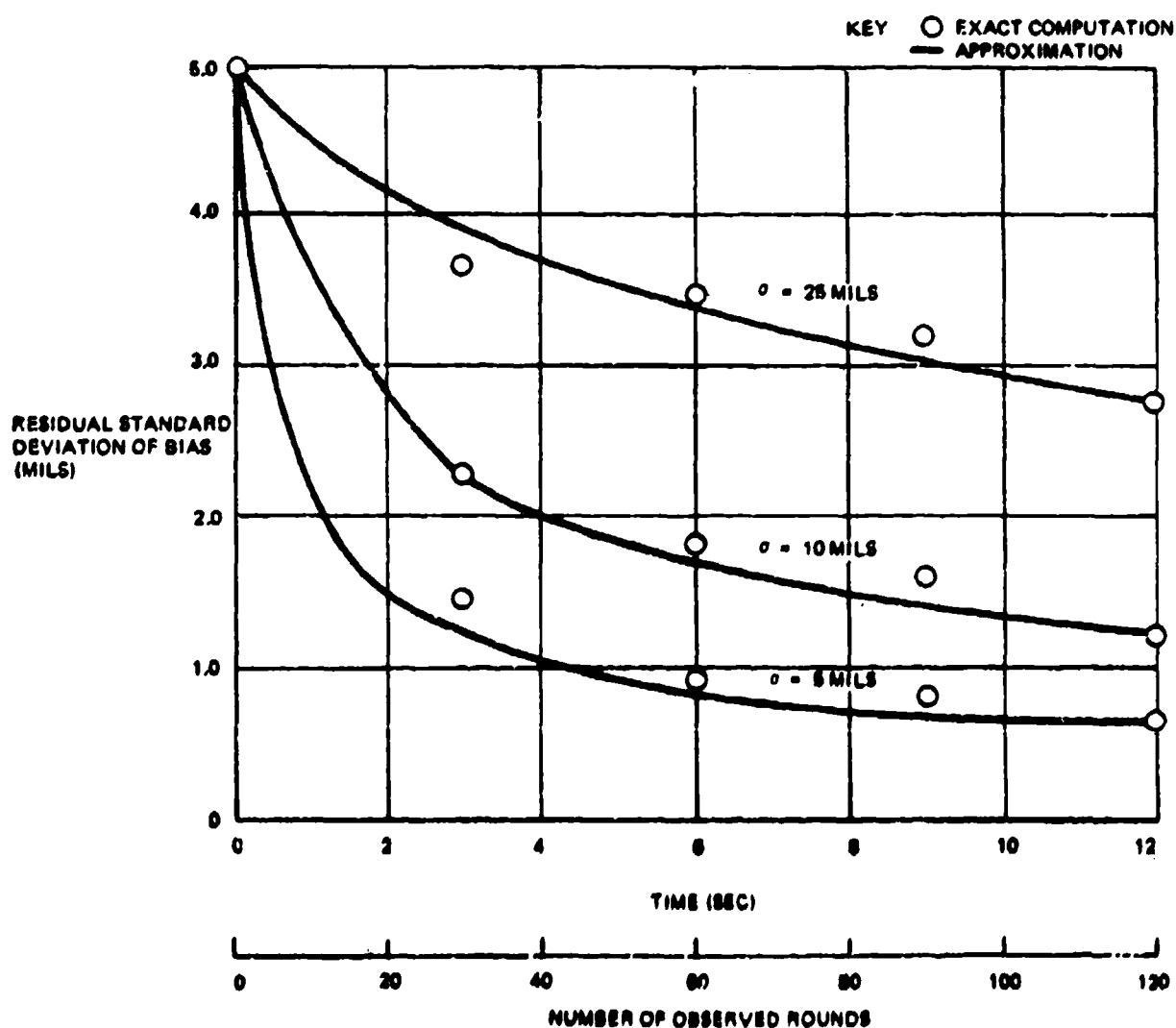


40001-58

Figure 3-58. Residual Standard Deviation of Elevation Bias

The residual bias in the sight plane (the vector sum of the two components, corrected for correlation introduced by the algorithms) is shown in Figure 3-59 and compared with the simple approximation

$$\sigma_{br}^2 = \sigma_{bo}^2 \left[1 + (n/2)(\sigma_{bo}/\sigma)^2 \right]^{-1/2} \quad (3.215)$$



47001-60

Figure 3-59. Residual Standard Deviation of Vector Bias in Sight Plane

Note that with random and observation standard deviations of 5 mils, the system has accomplished a reduction of about 80% in the initial bias after 40 observations have been made.

We next consider the effect of initially firing and obtaining observations on Path Segment I. On this segment, only lateral bias can be corrected, according to the approximate form of the computation. We allow six seconds of observations, then enter Segment II as described above, and finally continue with observations on Segment III, where, again, only traverse corrections are possible.

Figure 3-60 shows the reduction in traverse bias. There is a significant reduction on Segment I, after which reduction is lower, first because of the dual assignment of the measurements, and second, because of the $n^{-1/2}$ effect as the bias becomes smaller than the random components.

The reduction in elevation bias is as shown in Figure 3-61. Midpoint and the end of Segment II are identical with the previous computations, since elevation bias has not been reduced in Segment I.

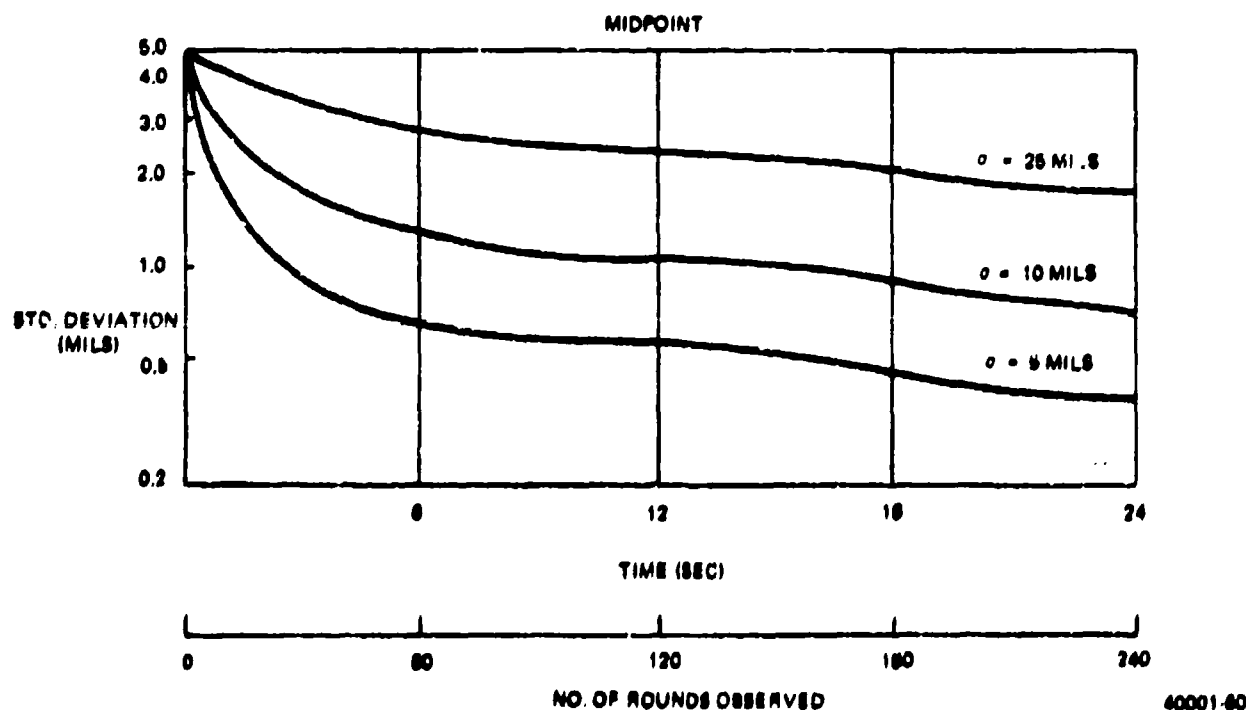
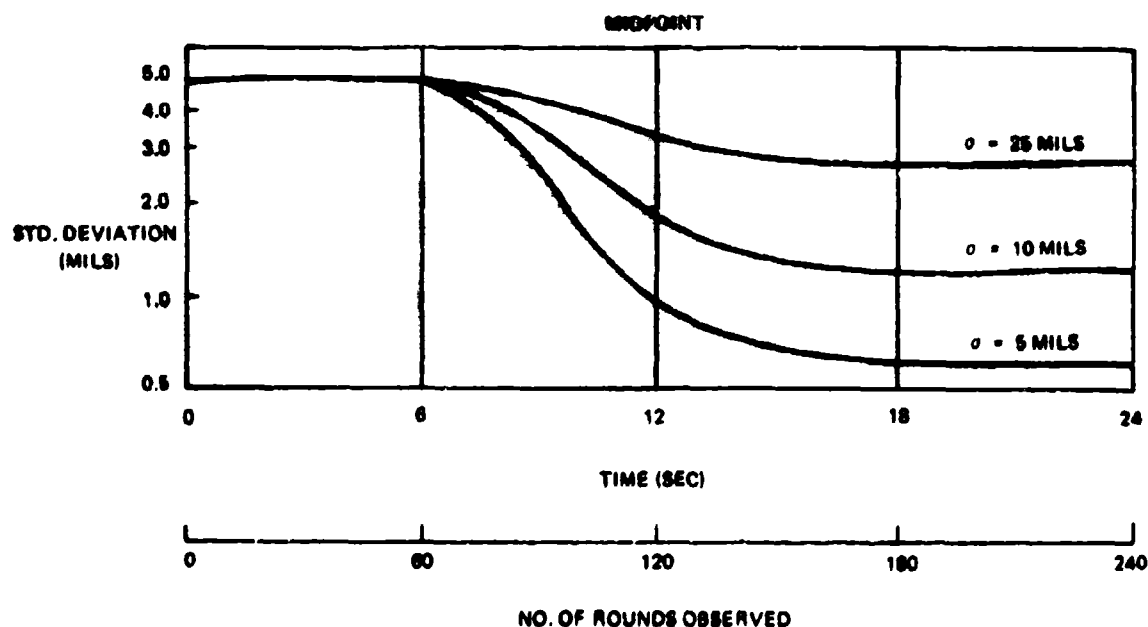


Figure 3-60. Reduction of Standard Deviation of Traverse Bias

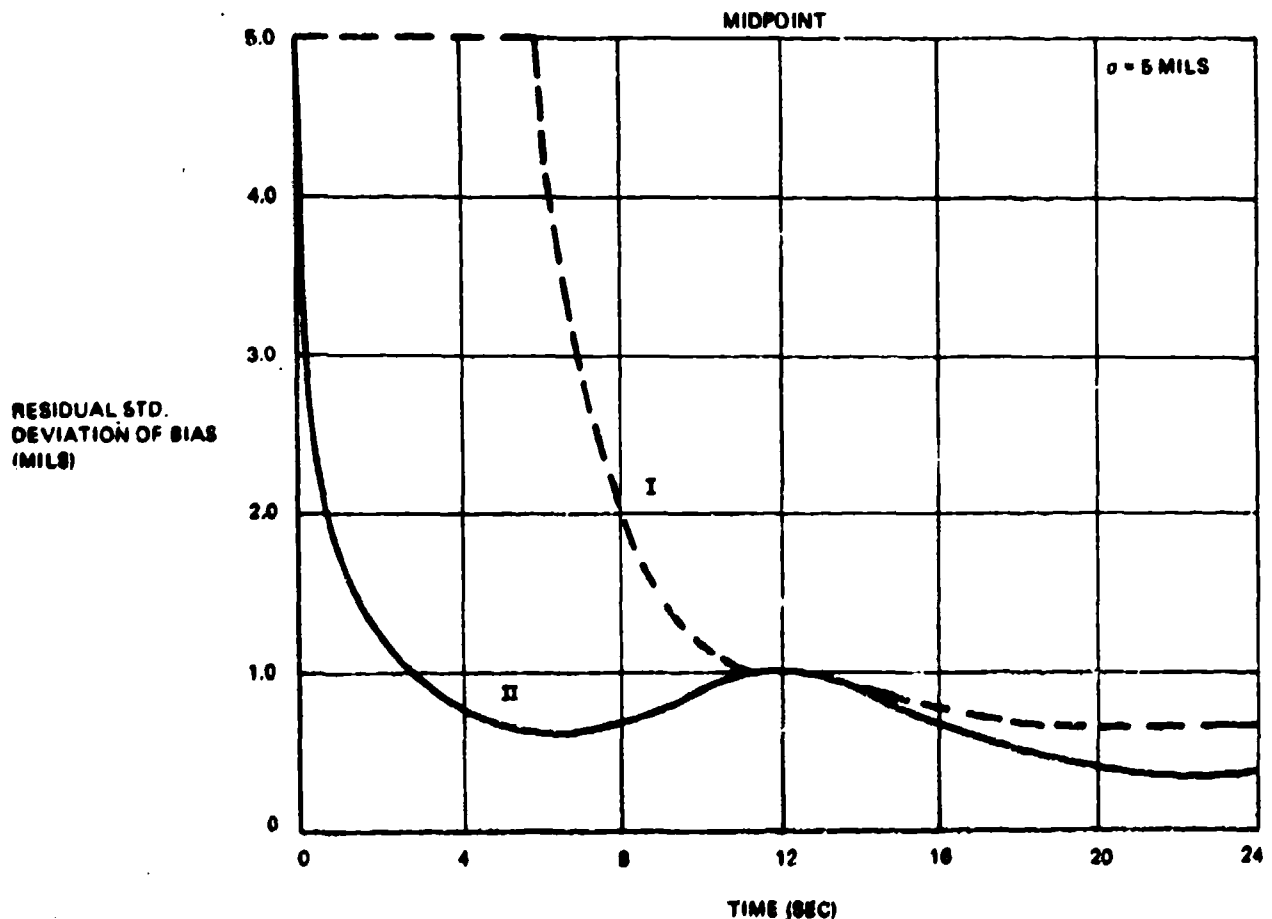


40001-61

Figure 3-61. Reduction of Standard Deviation of Elevation Bias

Figure 3-62 shows the comparison of the two firing doctrines in terms of the bias variance in the sight plane (which is what counts in hitting the target). Only the 5 mil case is shown. The system benefits everywhere except at midpoint from the prior reduction in traverse bias. As the coordinate system rotates, for the case of prior firing on segment I, the residual elevation bias increases in importance at a rate which initially is larger than the rate of reduction by the correction algorithms, so that the vector bias increases, then decreases. However the elevation loop is, as in the first case considered, effective enough to reduce the initial 5 mil elevation bias to less than 1 mil at midpoint.

This simple case shows some of the characteristics of the closed loop algorithms which are developed more generally in this report. When the number of bias sources identified in the model on which the algorithms are based exceeds the number of components of miss measurement, the algorithms allocate the miss observations to sources, according to the geometry of the engagement at each measurement. Hence all bias sources will not be eliminated until a sufficient number of observations has been processed from a mix of geometric configurations.



40001-42

Figure 3-62. Comparison of Firing Doctrines: Residual Standard Deviation of Vector Bias in Sight Plane

The algorithms, however, always make the allocation in such a way that the miss vector resulting from all bias sources, as seen at each instant of measurement, is reduced.

As a limiting case, if fire were conducted against a hovering helicopter, and a large number of rounds was observed, the resultant bias vector from all sources would be reduced to zero for that geometric configuration, even though not all of the individual bias sources would have been zeroed.

As the geometry changes, the unroduced biases may acquire prominence, and will in turn be reduced.

3.4.9 General Solution with Expanded Bias Source Vector

The two system configurations described above (3-D and 2-D) were described in terms of bias vectors having three and two elements, respectively. As observed by several persons, in particular, Dr. Richard Moore, the most bothersome systematic cause of projectile miss may be wind.

The principal objection to increasing the number of elements in the bias source vector is the increase in the size of the matrices that must be handled by the computer. All things considered, however, the incremental cost of adding computer capability may be small compared with the cost of providing a local meteorological station at each firing battery.

We therefore suggest that the following bias vector may be considered.

$$X = \begin{bmatrix} A_b \\ e_b \\ W_N \\ W_E \\ V_b \\ \rho_b \end{bmatrix} \quad (3.216)$$

where

- A_b - azimuth bias
- e_b - elevation bias
- W_N - Northerly component of wind
- W_E - Easterly component of wind
- V_b - muzzle velocity bias
- ρ_b - deviation of air density from standard (includes all systematic sources which affect time of flight other than muzzle velocity)

The first four elements of this vector can be corrected with a 2-D system (but somewhat less rapidly than with a 3-D system) since they move the projectile "out of plane". The last two require a 3-D sensor system. ρ_b may not be of sufficient magnitude to justify its inclusion. However it is shown because, like V_b , its effect is principally in the plane of the target vector and the sensor. V_b has a large effect at all ranges, ρ_b has a small effect at short range, and its effect increases with range. The different functional dependence on range offers, in theory at least, the potential of discriminating between the sources over a mix of geometries.

The elements of the H vector include this geometry. For example, the effect of wind on the observed lateral miss would be represented by H elements which would be approximately proportional to $t_p \sin A_g$ and $t_p \cos A_g$ respectively, where A_g is azimuth measured from North, and t_p is time of flight.

Since the unique value of the Kalman type of processing is that corrections applied during one configuration of a target path can be used and further improved on subsequent passes, a bias source such as wind which is only approximately constant in magnitude and direction (in earth coordinates) over limited durations of time, must be considered in a separate category from a "boresight" error, for example.

One could formally write the system state equation in the general form

$$X_{j+1} = \Phi_j X_j + u_j + w_j \quad (3.217)$$

and absorb a stochastic model of wind variation with time, the Φ_j elements allowing for some persistence, and the w_j for random disturbances which cause the mean wind to vary with time. However, system operating time, and elapsed time during which the wind may change are not the same, and rather than attempt to approximate wind statistics, and associate them with clock time in the computer, it may be adequate simply to assume that wind is constant during any continuous interval during which the system is activated, but that the a priori variances of wind be restored from their reduced values to initial values whenever the system is turned off, and then reactivated.

On the above assumption, the processing algorithms for the expanded bias source vector are identical in matrix form with those developed for the simpler bias vectors, and will not be repeated here.

3.4.10 Use of Closed Loop for System Pre-Combat Calibration Firings

The first four elements of the expanded bias matrix shown in Eq. (3.216) can be corrected by a closed loop system by firing a series of bursts at fixed points in space. These points would be located along two azimuths separated by 90° , and at two ranges, relatively short and relatively long. The two azimuths allow the algorithms to identify and correct the two wind components, the two ranges allow the wind effects (greatest at the longer ranges) to be separated from the angular biases.

The last two elements of the matrix require that the system develop a lead vector. This can be done with an internally generated "canned course". Again, range variations allow the two remaining bias sources to be separated and eliminated.

All corrections can be made simultaneously by firing "canned courses" (constant speed, constant altitude), with different orientations of the target velocity vector.

If a series of calibration firings of this type is laid on after the battery has moved into position, biases should be eliminated or effectively reduced prior to the appearance of an enemy target. By that time wind may have changed, but it will be the only remaining bias source, and the algorithms will operate to reduce its effect during the firing pass.

How much of the "learning" on each firing phase to carry over to successive phases can be established by investigation with the system itself after the initial calibration firings, one might be willing to assume that only wind will change as a bias source, hence the wind "learned" components only would be reduced to zero between enemy attacks (not necessarily between passes during a given attack).

3.5 CONCLUSIONS

3.5.1 Feasibility

Since a closed loop predicted fire system has been demonstrated with Phalanx, and MIDI has demonstrated the ability of a radar system of different configuration to obtain individual projectile miss sensings in real time at a high rate, the feasibility of these specific 3-D radar configurations may be considered to be established. The principal unknown is the sophistication which can reasonably be utilized in the processing algorithms.

There seems to be little technical risk associated with a 2-D system using FLIR or TV sensings of projectiles with tracers. 2-D systems cannot obtain access to all potential bias sources, (observability and controllability theorems apply) but with separate on-carriage muzzle velocity measurement as employed by Oerlikon, the in-plane biases may

possibly be reduced to acceptable magnitudes without the intervention of a closed loop for these bias components. It may be relatively simple to add a 2-D loop closure to the GLAADS prototype. However, the lower information rate of a 2-D system has been noted.

A 3-D FLIR plus laser configuration depends on the ability of the system to correlate illumination and angular sensings on individual projectiles (or less desirably on short bursts in aggregate), and may push the laser state of art somewhat. Feasibility remains to be determined.

Optical radar may in fact be the strongest "light horse" contender. These configurations appear to be the most attractive of those reviewed. Many others are possible, of varying degrees of technological risk, and the longer one considers the problem, the greater the variety of possible solutions that present themselves.

3.5.2 Advantages and Disadvantages of Closed Loop Systems

The concept of loop closure by projectile sensing is intriguing, both as to concept and with regard to the technological challenge. Unfortunately, its principal justification may be the serious misgivings of many persons, including the present writer, which cannot yet be supported by data, regarding the ability of operational units to maintain their equipment at a proving ground calibration level of excellence during combat conditions. Closed loop should provide a calibrated system in combat whether the crew has had time to periodically go through their calibration drill or not.

If a predicted fire system of the best modern technology, tuned and calibrated, with excellent met inputs, is fired in proving ground tests, and compared with closed loop operation of the same system, this writer would expect only marginal differences in effectiveness between the operational modes. On the other hand, in combat, with delayed, or nonexistent meteorological data, moves from travel into firing position without time to calibrate (and a desire to avoid firing until attacked so that the position will not be revealed), closed loop may have a high payoff. The simple computations of Table III-5 indicate a 50% reduction in system effectiveness if aggregate bias sources of only 4 mils are allowed to creep into the system without correction.

The disadvantages of closed loop are associated with the special performance capabilities which may be required of the sensors to measure bullet miss in addition to target tracking, and with the added computer requirements to process the data. These costs must be assessed for each candidate closed loop configuration. However, they can be balanced against the cost of additional battery equipment to provide bias source data which would be used in an open loop system.

It is regrettable that the case for or against closed loop is not an obvious one. It would be even more regrettable if this method of fire improvement were not pursued to its objective evaluation.

3.5.3 Program Recommendations

Closed loop concepts can be roughly divided into two classes, those concepts which can be implemented with some assurance of success, based on current state of the art, and those which are attractive, but require development and component validation. Effort should be applied in both categories.

Since GLAADS is usually considered a "test bed" system, a closed loop system compatible with the GLAADS sensors should be fabricated and tested on GLAADS. A specific solution, chosen for production capability consistent with possible GLAADS production should be given highest priority, but solutions of higher risk which can be tested in live fire with GLAADS should be carried in exploratory development.

A comprehensive program of projectile signature determination should be pursued, covering all potentially usable sensor types, and including signature augmentation schemes ranging from simple shaping of the projectile base to the use of trihedral reflectors. Cost of making these projectiles with improved signatures should be an important part of this investigation, and in particular the trade-off between cost of augmenting the signature versus cost of providing enough sensor power to acquire an unaugmented signature should be made explicit.

The Army's continuing program of exploratory and advanced research in predicted fire technology should not be limited to GLAADS or existing radar sensors. It is not yet clear that the partial passivity of a system with FLIR and laser, for example is greatly less susceptible to detection and countermeasures than one using millimeter radar, or that differences are significant considering the operational environment.

SECTION 4

FRANKFORD AIRCRAFT CAPABILITIES TEST (FACT)

The lack of accurate, realistic data on aircraft targets flying munitions delivery passes has been a serious limitation on the development of algorithms for predicted fire systems. Many studies have been made using assumed and plausible flight path characteristics, but attempts to go beyond simple constant velocity prediction algorithms are so critically dependent on actual target path deviations from straight line, constant velocity paths both in choosing the algorithms and in assessing their effectiveness, that these investigations have only marginal payoffs unless tested against actual flight trajectories.

4.1 SCOPE OF DATA

The FACT (Frankford Aircraft Capabilities Tests) data was obtained to provide an accurate description of target paths flown by typical attack aircraft in munitions delivery. The flights and data acquisition were performed by the U.S. Navy at the Naval Weapons Center, China Lake on 26 and 27 July 1973, and the plan of experiment and objectives were developed jointly between Frankford Arsenal personnel, Stan Goodman and Ken Heulitt, and personnel at Naval Weapons Center. The experiment is remarkable in the extremely short elapsed time between original discussions with China Lake, and the availability of experimental data.

Raw radar tracking data was obtained on tape at 0.1 second intervals. In addition, the Navy provided printouts of computer processed data and real-time graphs of horizontal track and altitude which were of great value in initial studies of the data. Preliminary analyses of a few pass records were made by Litton to establish a method of analysis, and a corresponding analysis of all of the recorded passes was made by Frankford Arsenal.

Path data was recorded on attack aircraft types flying the following types of attack paths:

Glide/dive bombing

Pop-up and glide bombing

Laydown bombing

High level bombing

Strafing

On most of the bombing passes, the aircraft released munitions and the impact points were recorded. Pilots had combat experience in Vietnam and chose their tactics in accordance with their experience. Aircraft and pilot identification, types of aircraft fire control employed, bomb impact records, and additional data regarding the experiments and results will be found in a report under preparation by Frankford Arsenal.

All of the recorded data, computer processing, and computer-generated graphs and plots are on file at Frankford Arsenal.

The aircraft were tracked by radar, using a beacon in the target aircraft on most passes. The estimated radar accuracy and its effect on record interpretation is discussed in a later section. Tracking accuracy was sufficient to satisfy the main purpose of the experiments, namely to confirm that the attack paths observed had relatively predictable segments over which a predicted fire defense system could function. Tracking accuracy was insufficient to separate the mild target maneuvers during these segments from the tracking noise, an important conclusion in itself.

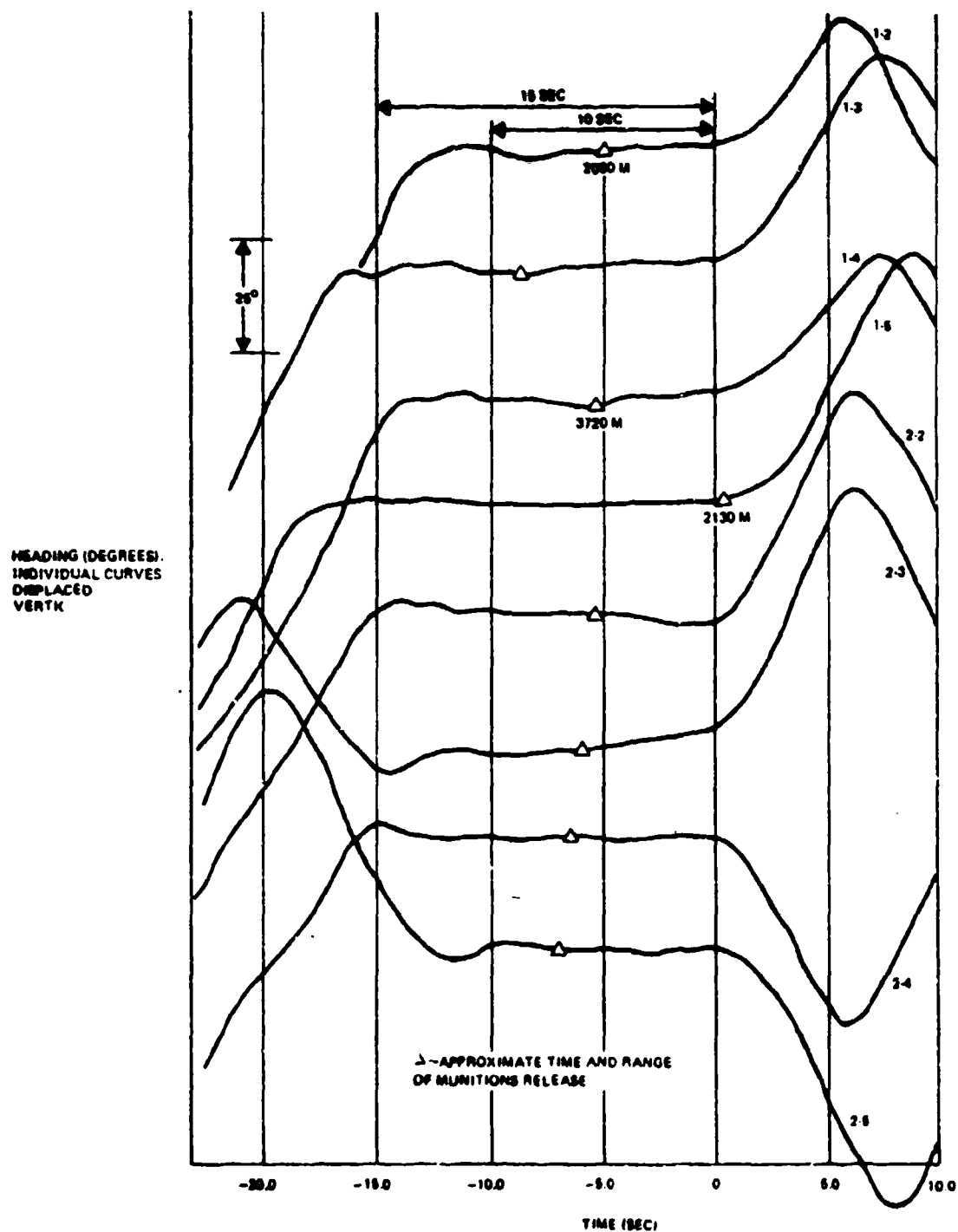
It should be noted that for the purpose of these tests, a constant, or slowly varying bias in the radar data is unimportant. However, rapid variations of the radar error about its mean does limit the analysis by preventing the reliable extraction of true aircraft accelerations, when these accelerations are small (less than a few tenths of a g).

In the present analysis of the FACT data, the parameters chosen to display the path characteristics are target heading in a horizontal plane, dive angle and velocity along the flight path. If all of these parameters are constant for an appreciable length of time, a very simple linear predictor will be highly effective. In fact, the three parameters are rarely simultaneously constant, and so the data records set a challenge to the designer of prediction algorithms.

4.2 DIVE/GLIDE BOMBING PASSES

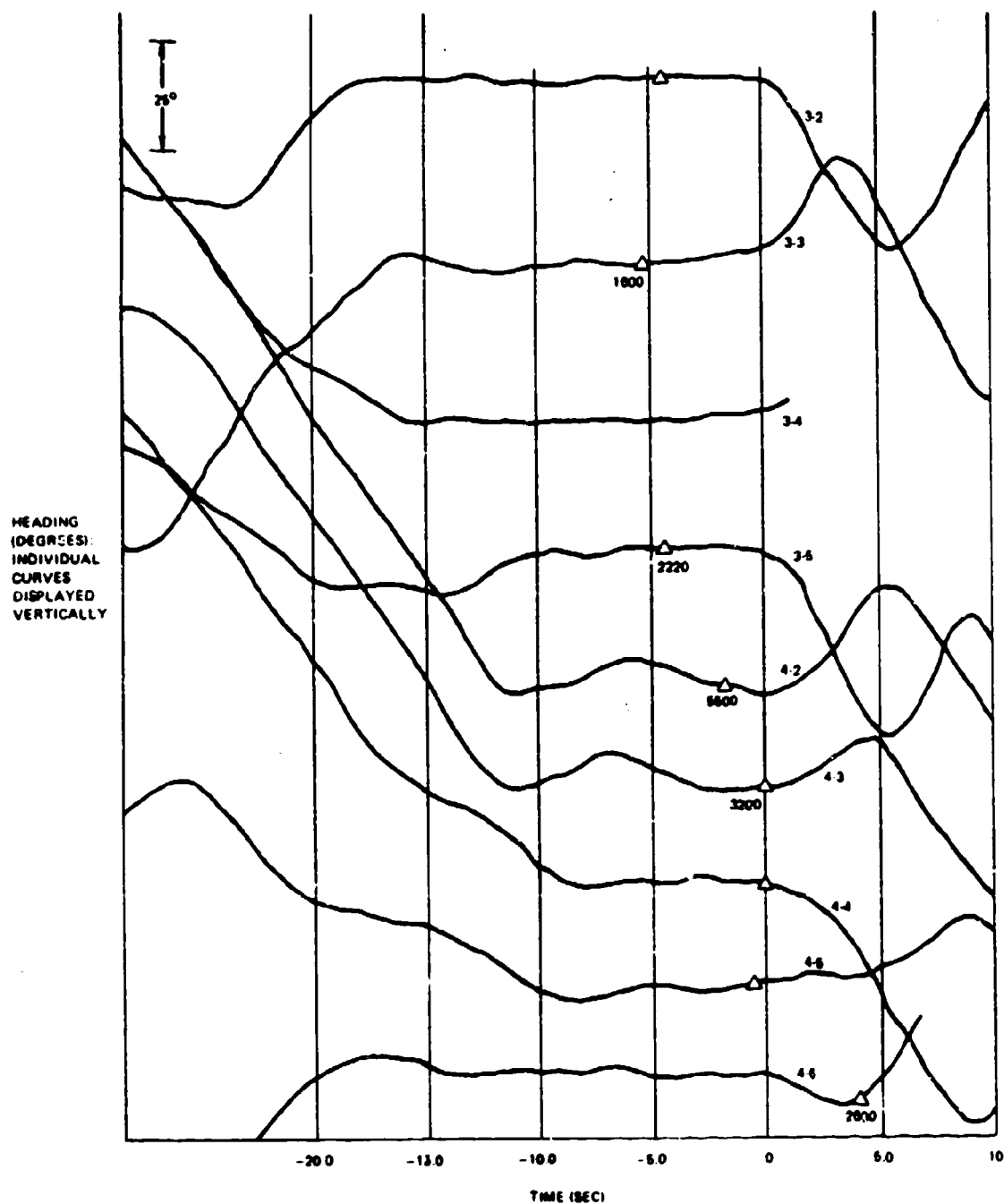
4.2.1 Aircraft Heading

The Frankford processed traces of heading angle versus time have been plotted in Figures 4-1 and 4-2 for dive/glide bombing passes. In these figures the traces have been displaced vertically to avoid overlap. Small triangles on some of the paths show the estimated time of munition release, and in some cases the munition release range from the target is also shown. According to K. Heulitt the indication of munitions release tended not to be precise, hence in these figures the traces were not aligned by point of weapons release, but rather by the approximate end of the relatively straight heading segment.



40001 63

Figure 4-1. Heading Angle versus Time on Dive/Glide Bombing Paths Flights 1, 2



40001-64

Figure 4-2. Heading Angle versus Time on Dive/Glide Bombing Paths Flights 3, 4

An immediate observation is that heading is either relatively constant, or has a relatively low mean rate of change on these passes for from 10 to 15 seconds. There is no apparent correlation between these time durations and the release range. The turn to the attack segment and the breakaway display very high turn rates, and work out to about 4g lateral acceleration.

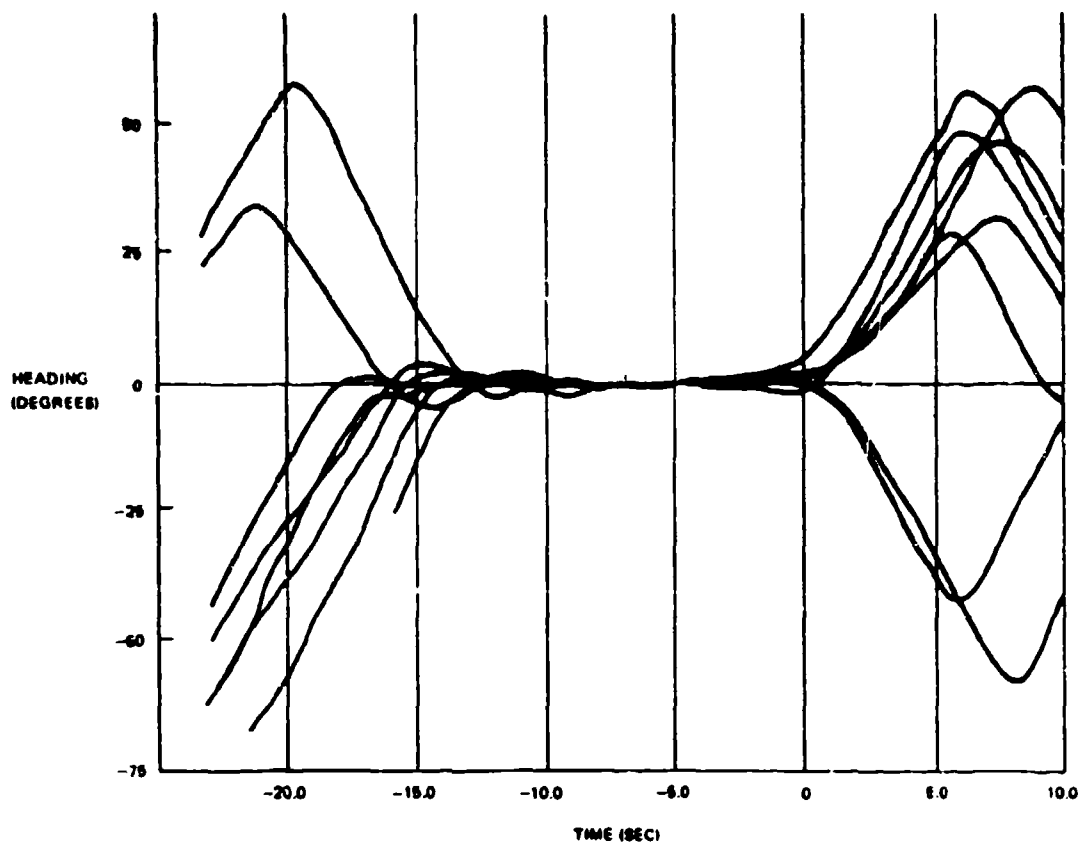
In Figure 4-3 the traces of Figure 4-1 have been superimposed to coincide at 5 seconds from the end of the path segment. This plot emphasizes the existence of the relatively predictable heading segment. In Figure 4-4 the same traces have been superimposed and rotated slightly to eliminate the small mean heading rate of the attack segments. This could be accomplished by an acceleration term in the prediction module. The turn into the attack and the breakaway have been changed in sign in some cases to allow a direct comparison of these patterns. It is remarkable that heading rate for turn into the attack is almost identical for the passes shown, and there is a surprising amount of consistency in the breakaway patterns. In part, this results from the small number of pilots represented. On the other hand, the similarity may result from training and operational doctrine. If this consistency can be exploited in the defense computer, and exists in the case of enemy pilots (who may have a more rigid doctrinal training than U. S. pilots) it will be important to provide means for recording enemy tracks in combat and adjusting defense computer algorithms in the field to match enemy attack patterns. Figure 4-5 shows superimposed heading traces on flights 3 and 4 on which the pilots were able to introduce some lateral weave.

4.2.2 Aircraft Dive Angle

Figures 4-6 and 4-7 are traces of dive angle versus time of the passes for which heading was previously displayed. Again, the traces are displaced vertically in these figures. In addition to triangles indicating approximate time of weapon release, circles are added to indicate the point at which dive angle is zero. This allows the maximum dive angle to be estimated from the charts in each case.

Unlike heading, dive angle shows no relatively constant segments, although for about 10 seconds, on the average, the rate of change of dive angle is low. Note that in almost all cases, the last 5 seconds of the constant heading segment corresponds to a high-g pullup on the dive angle curve, i.e., the aircraft does a constant heading pullup. There are, however, a few cases of climbing turns beginning immediately from weapon release.

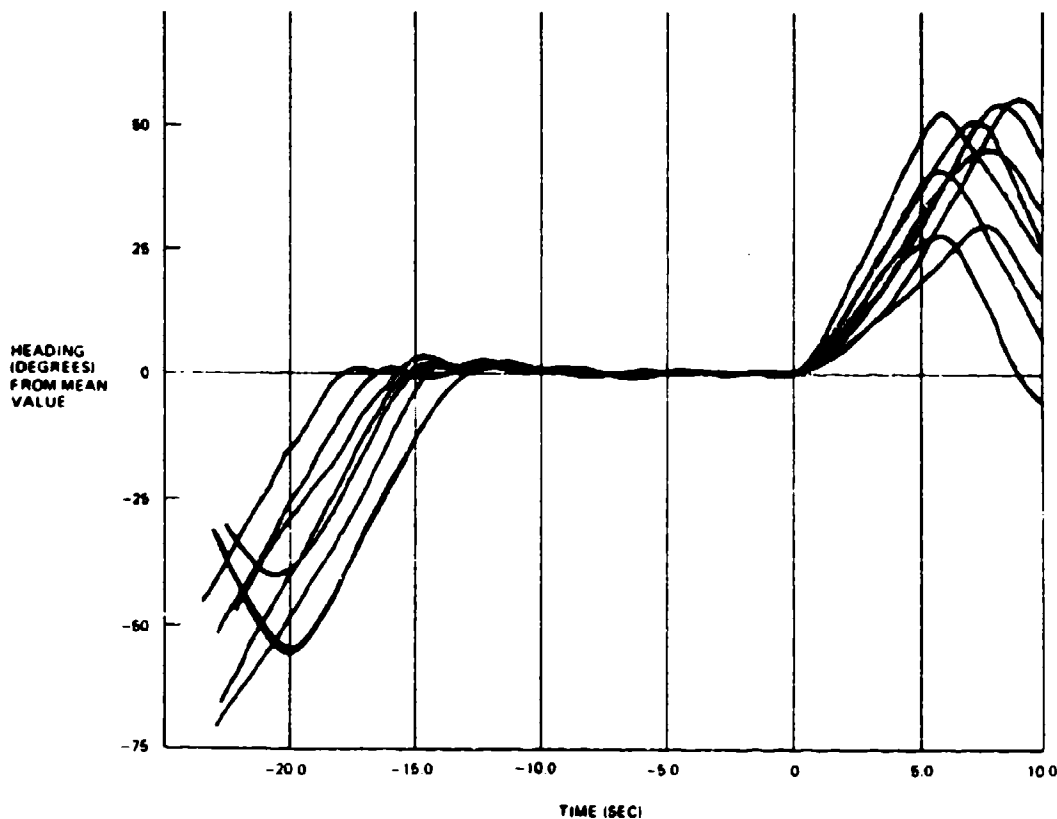
Some of the dive angle traces have been superimposed to the same dive angle scale in Figure 4-8. A characteristic pattern is apparent which might be exploited in prediction algorithms. The aircraft pushes over into its dive (inverted for eyeballs-in acceleration) at a fairly constant rate of change of dive angle, which corresponds to constant g force. It then



40001-65

Figure 4-3. Superimposed Heading Traces Matched at -5.0 Seconds on Flights 1 and 2; Dive/Glide Bombing

rolls out and pulls up fairly sharply to a positive rate of change of dive angle. This rate is then slacked off causing a characteristic concave-downward segment until weapon release. Pull-up is then at high g, with a rate of increase of angle that is about the same across passes, i.e., about the same positive acceleration in pullup. When the aircraft axis rises above horizontal there is a good deal of variability in patterns, undoubtedly associated with the concomitant lateral maneuvers in each case.

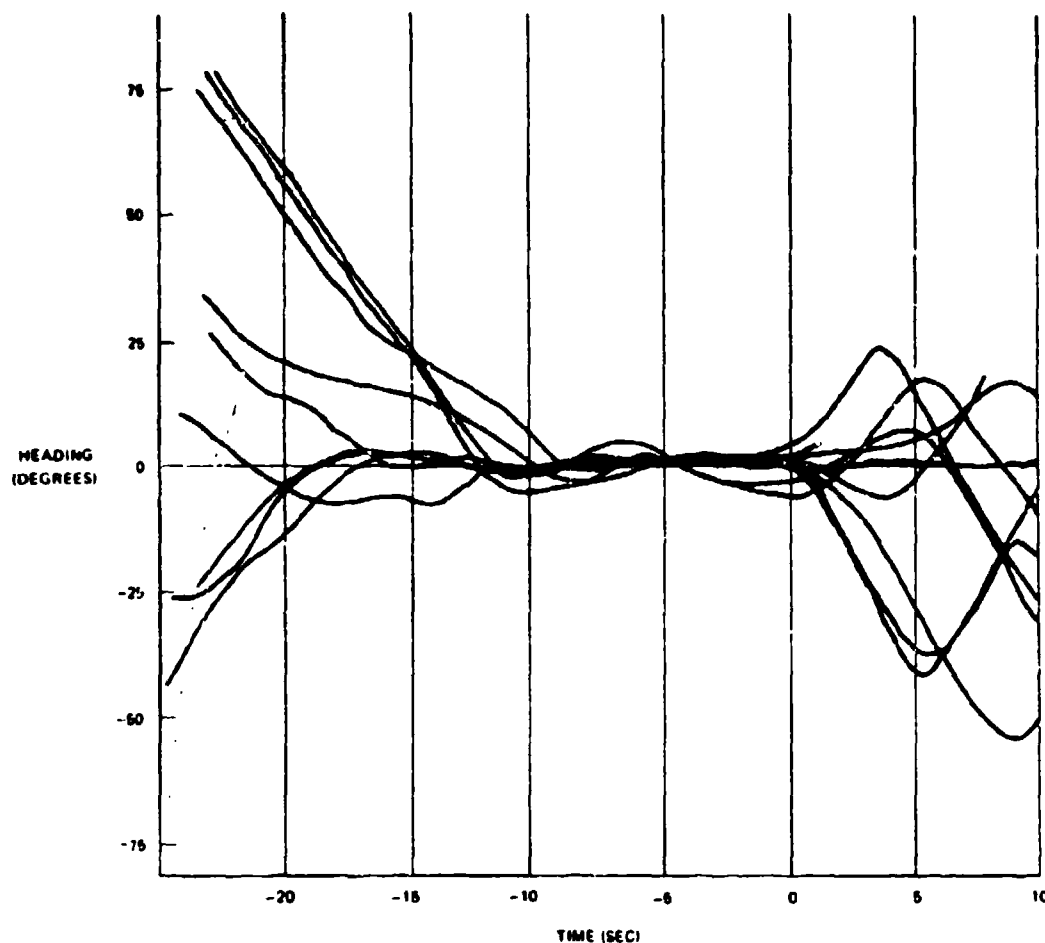


40001 66

Figure 4-4. Superimposed Heading Traces with Mean Rate Removed on Flights 1 and 2 Dive/Glide Bombing

4.2.3 Energy Conservation

It was originally conjectured (based on WW-II analyses by H. K. Weiss)¹ that the velocity of aircraft during altitude changes would change in such a way that the sum of kinetic and potential energy remained fairly constant, or at worst changed very slowly. Figure 4-9 shows that this is indeed the case. The "total energy" is computed as "energy altitude" Z_E ,



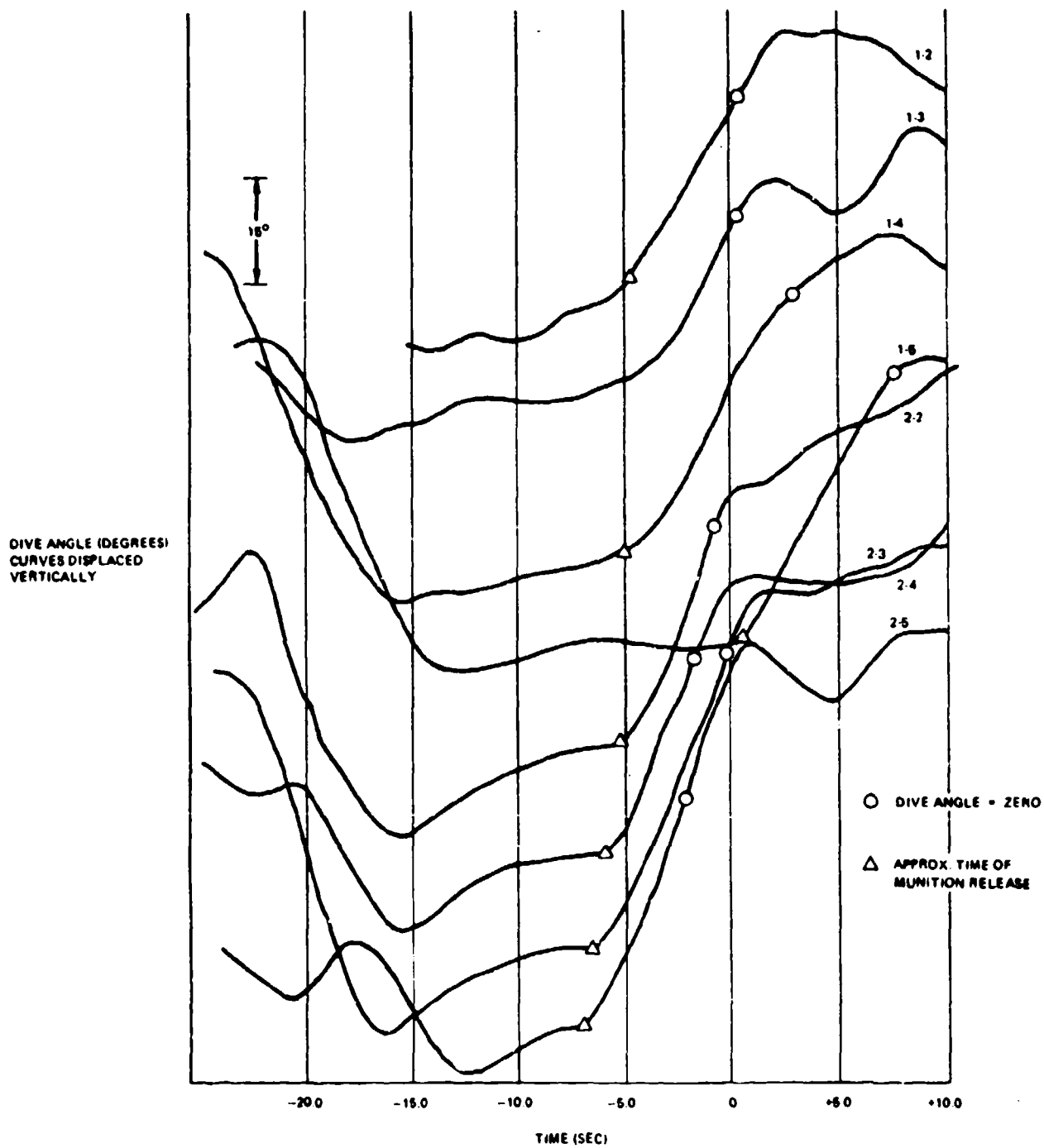
40001-67

Figure 4-5. Superimposed Heading Traces on Dive/Glide Bombing Flights 3, 4

$$Z_E = Z + v^2/2g \quad (4.1)$$

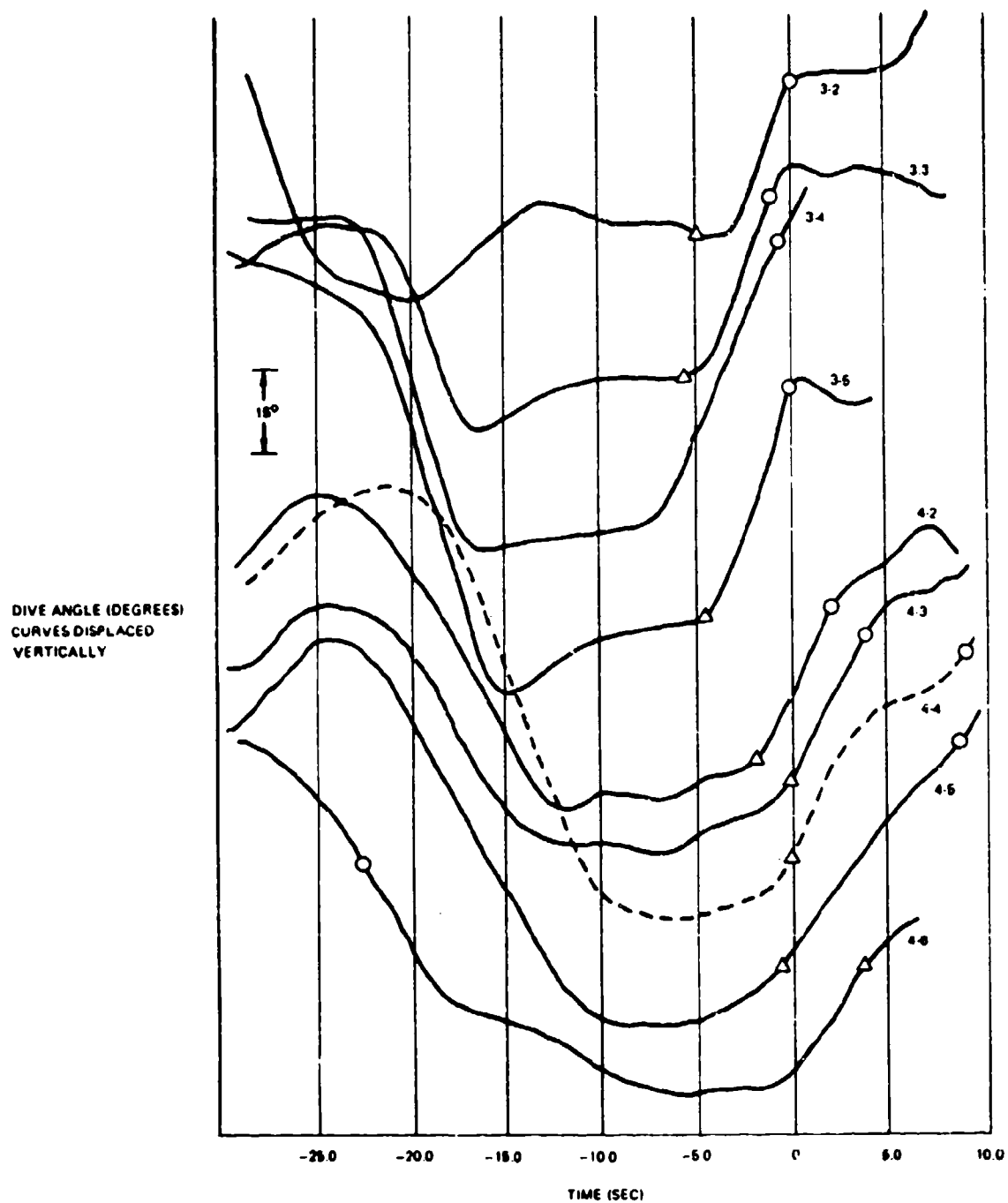
where Z = actual altitude, v = velocity along the flight path, and g is the acceleration of gravity.

Over a time segment of about 20 seconds, on this pass, during which aircraft altitude is reduced from 3000 to 1000 meters and velocity increases from 160 to 250 m/s, energy altitude changes by only about 120 meters. This relationship allows the aircraft acceleration along its flight path to be computed from



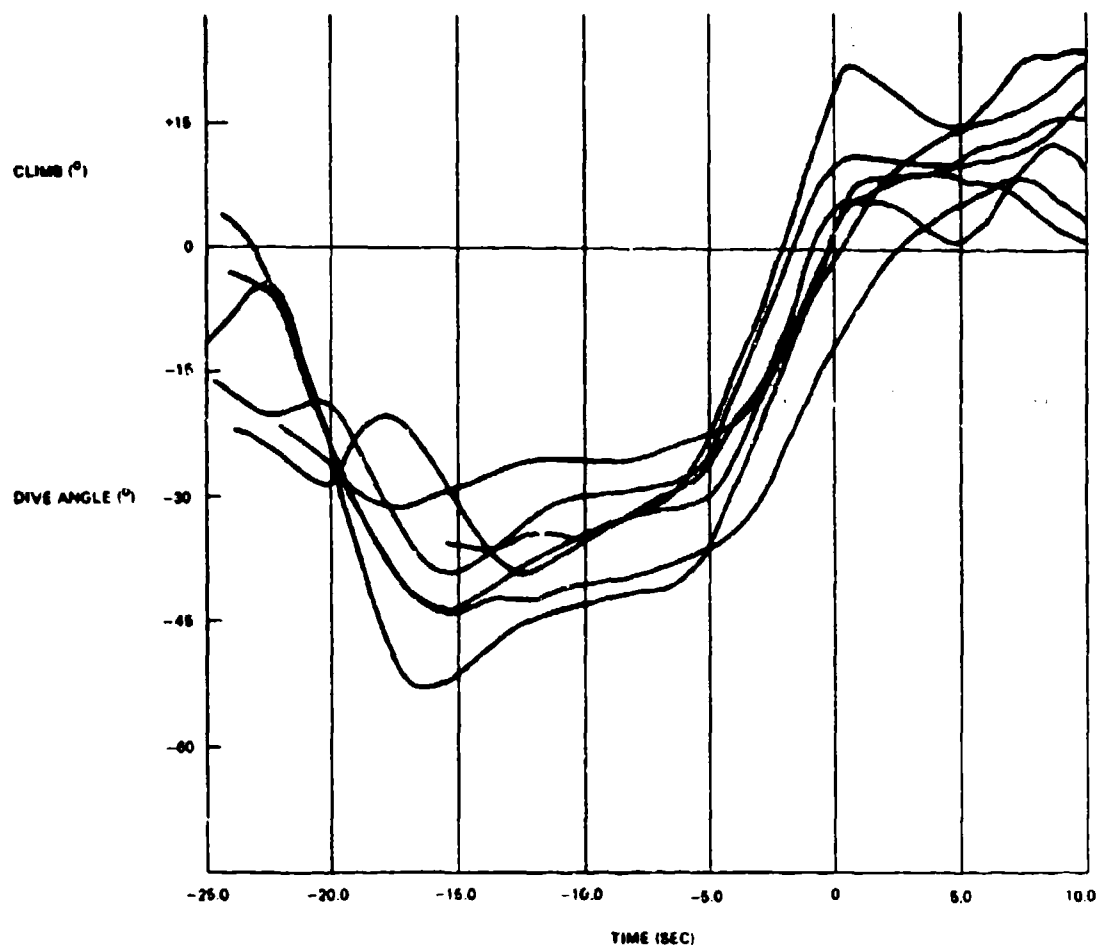
40001 68

Figure 4-6. Dive Angle versus Time on Dive/Glide Bombing Paths Flights 1, 2



40001-02

Figure 4-7. Dive Angle versus Time on Dive/Glide Bomb Paths Flights



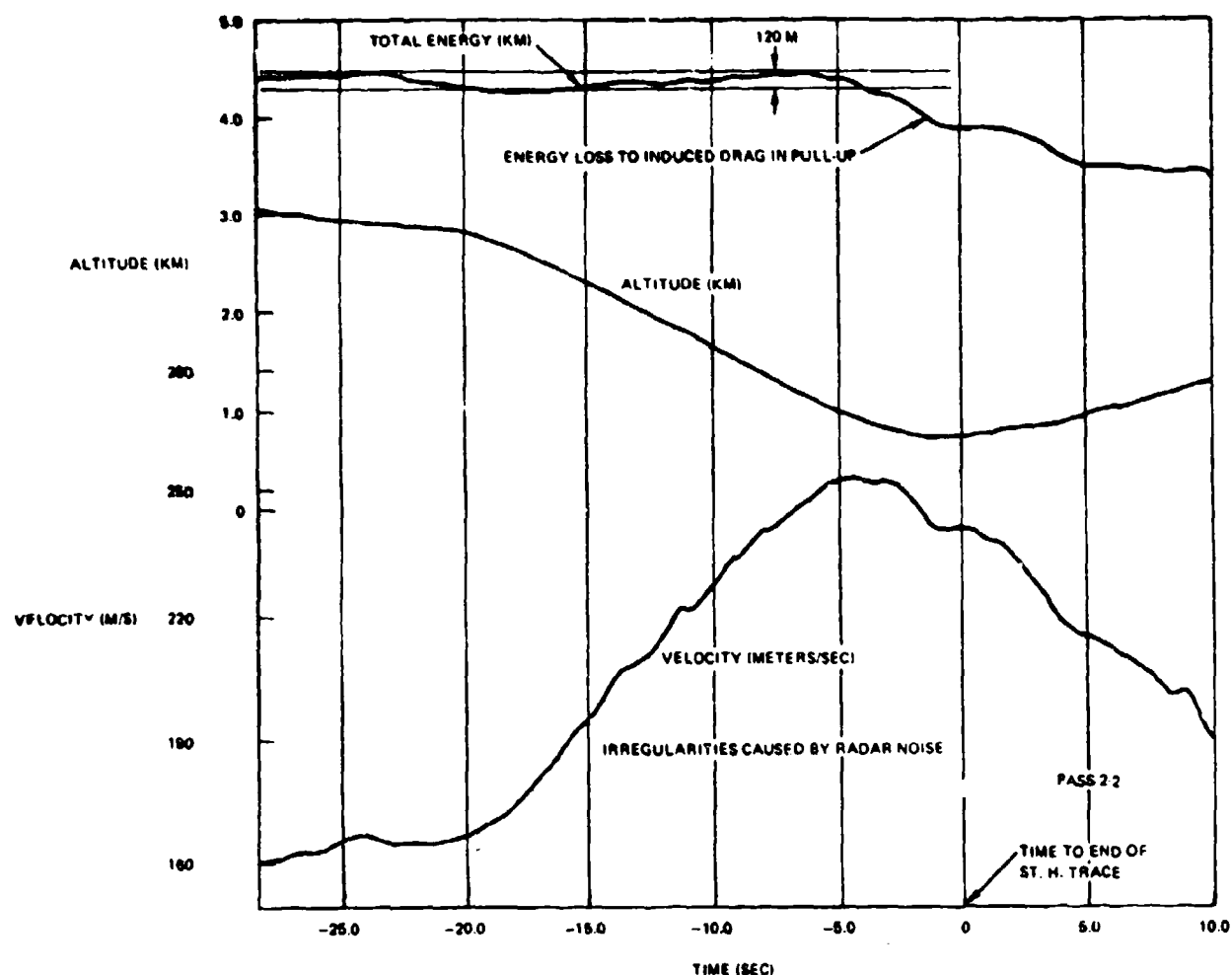
40601 70

Figure 4-8. Superimposed Dive Angle Traces on Flights 1 and 2; Dive/Glide Bombing

$$dv/dt = -(dZ/dt)/v \quad (4.2)$$

i.e., the acceleration along the flight path is obtainable from velocity measurements only, hence, one avoids the noise amplification of an acceleration measuring filter in this coordinate.

In the pull-up the high lift developed by the aircraft has a very large increase in induced drag associated with it, and energy is lost to this sources, as is clear in Figure 4-10. Equation 4.2 is, in fact, a special case of the "state space" equations of the aircraft, and in developing improved prediction algorithms to test against the FACT data, one should

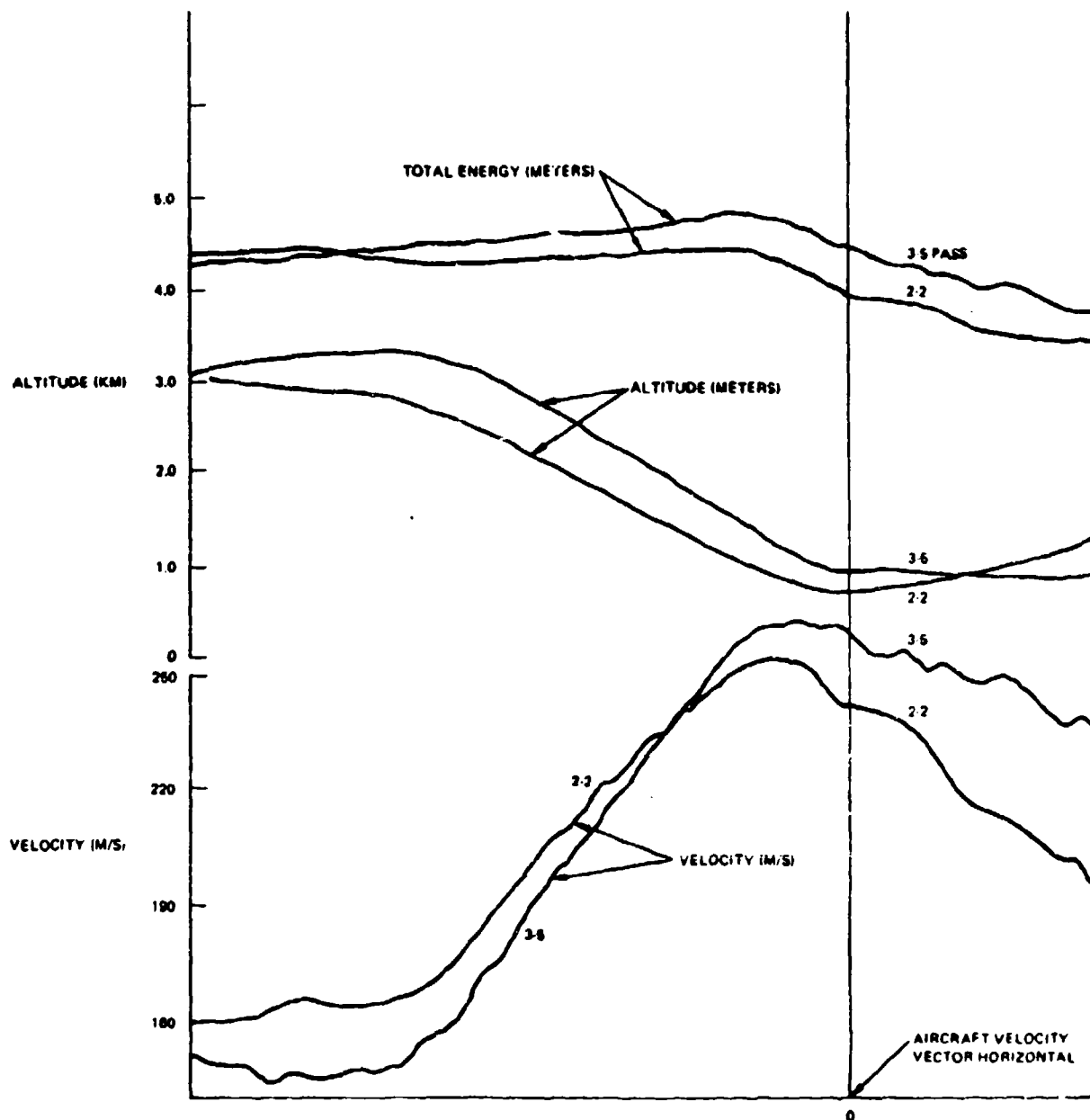


40001-71

Figure 4-9. Conservation of Energy in Dive

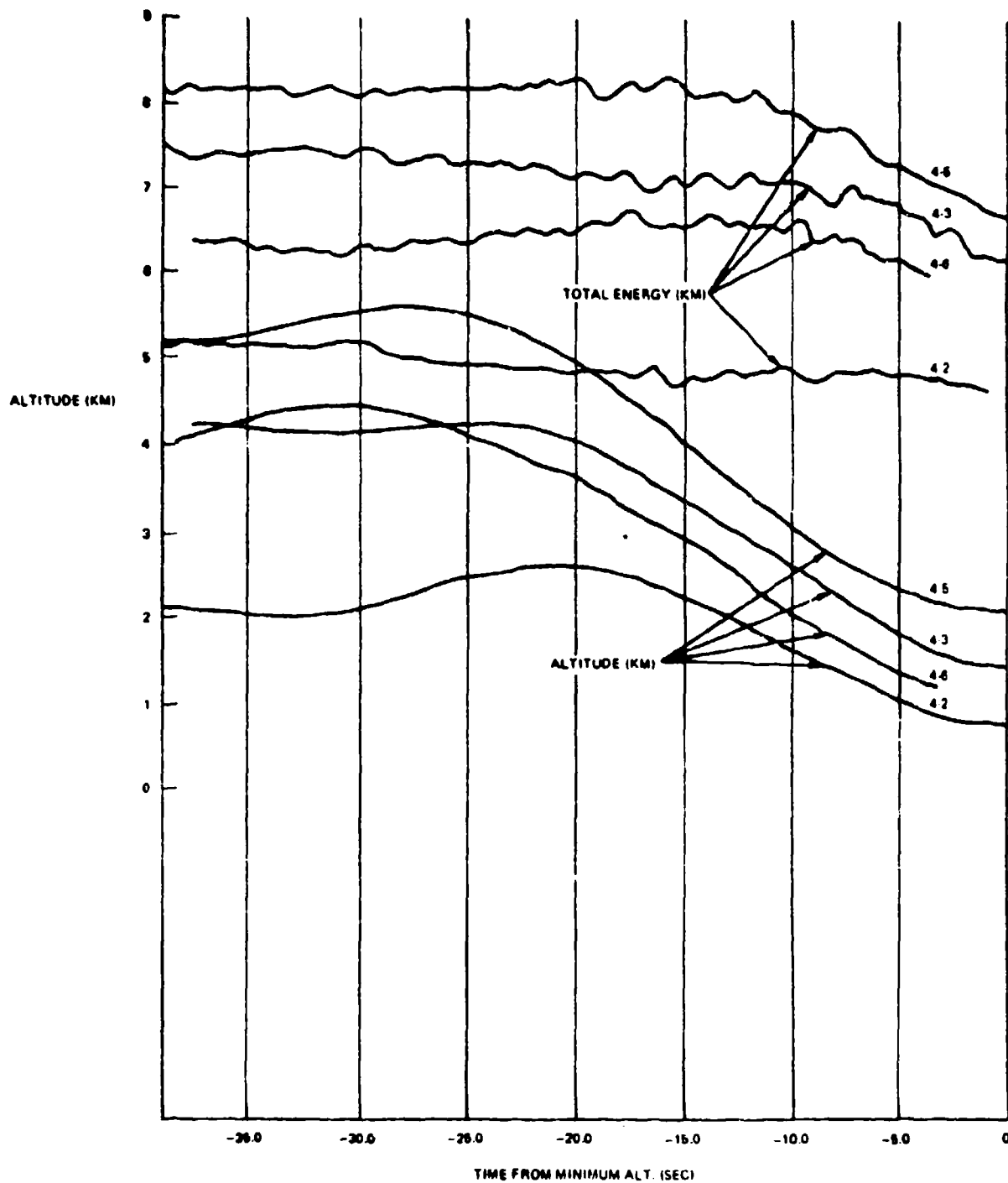
certainly incorporate a state space formulation of the aircraft dynamics. The fact that this approach is inherent in a general development of Kalman filter methodology should make it of interest to Kalman enthusiasts.

Figure 4-10 compares the path data of Figure 4-9 against the data from another dive/glide bombs pass, and a similar constancy of energy altitude is observed. Finally, Figures 4-11 and 4-12 provide comparable data on four more dive/glide bombs passes, and the same conclusion is reached.



40001 72

Figure 4-10. Comparison of Energy Conservation on Two Passes



40001 73

Figure 4-11. Altitude and Total Energy on Dive/Glide Bombing Passes

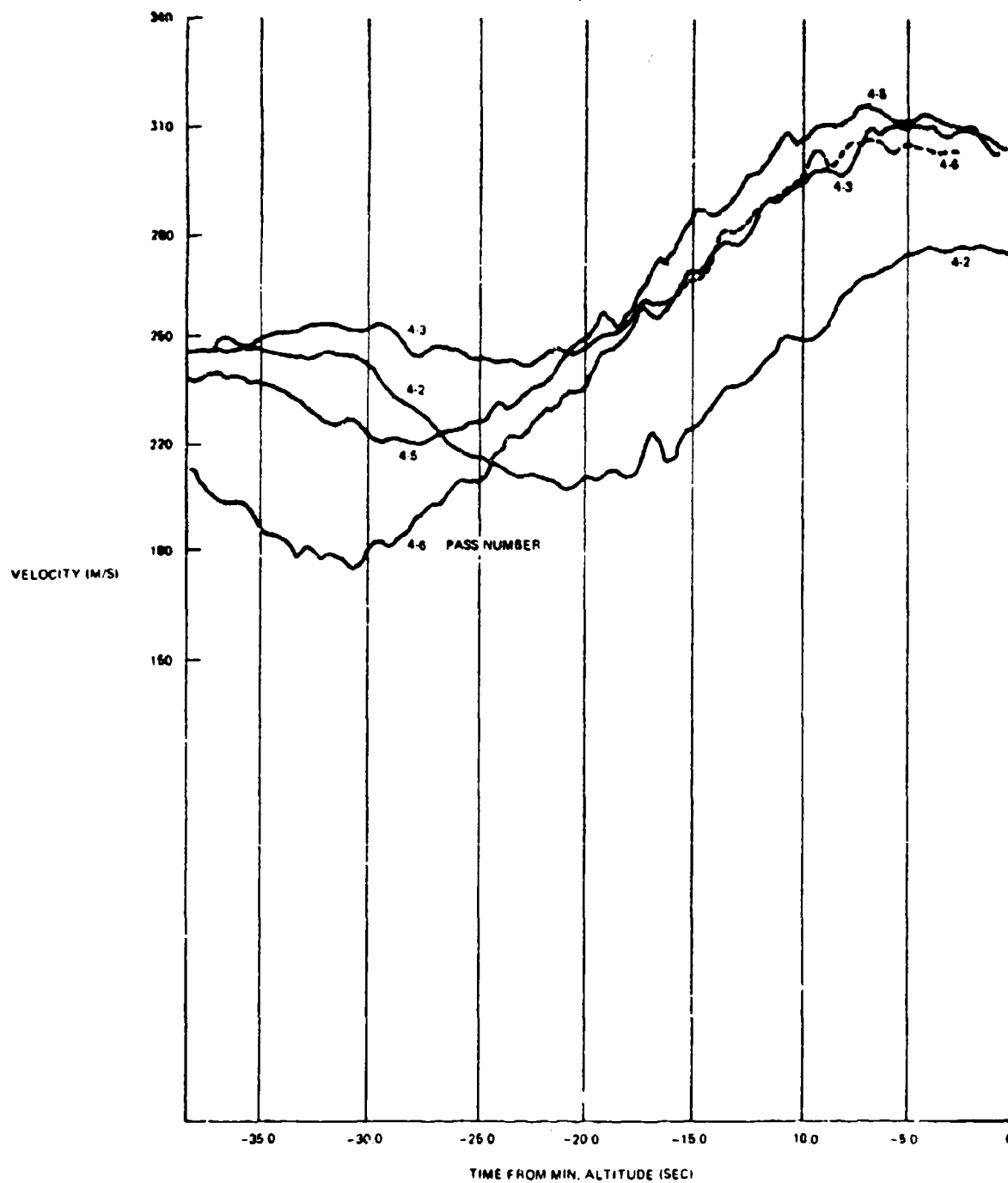


Figure 4-12. Velocity on Glide/Dive Bombing Passes

In all of these figures, the time axis has been zeroed against the minimum altitude in the pull-up. Note that pass 4-2 which has a relatively shallow dive and mild pull-up indicates very little energy loss in pullup.

The irregularities of the velocity traces results from radar noise, even after smoothing has been applied to the data in the Frankford data reduction. The unfavorable effect of these irregularities on direct acceleration measurements is clear, and emphasizes the great advantage in using Equation (4.2) to derive the rate of change of aircraft velocity without acceleration measurements.

Jet aircraft are much cleaner aerodynamically than World War II propeller driven aircraft, and the simple expression (4.1) holds more closely for them. Figures 4-13 and 4-14 show the effect on energy altitude of altitude and velocity changes in the case of a World War II fighter, the P-51, as originally reported by Weiss.

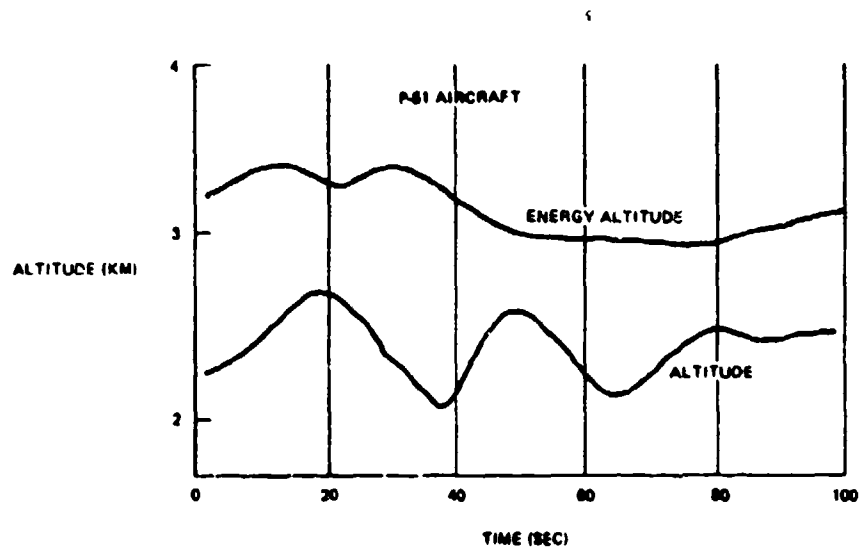
4.2.4 Linear Prediction Errors

Although the traces of heading angle, dive angle and velocity versus time provide an excellent qualitative indication of the path predictabilities, a quantitative estimate is also valuable. This was obtained by reducing the path data to rectangular coordinates (altitude, down range and cross range. Down range is approximately parallel to the aircraft ground track on its attack segment and cross range is approximately perpendicular to this coordinate.

Prediction was made by applying a simple 1-second smoothed constant velocity predictor to each of the X, Y, Z coordinates of the data which had been previously smoothed to reduce the perturbations of tracking noise. The result of this presmoothing is also to reduce the magnitude of high frequency perturbations of the actual aircraft flight path, if any, but the moderate to large deviations remain.

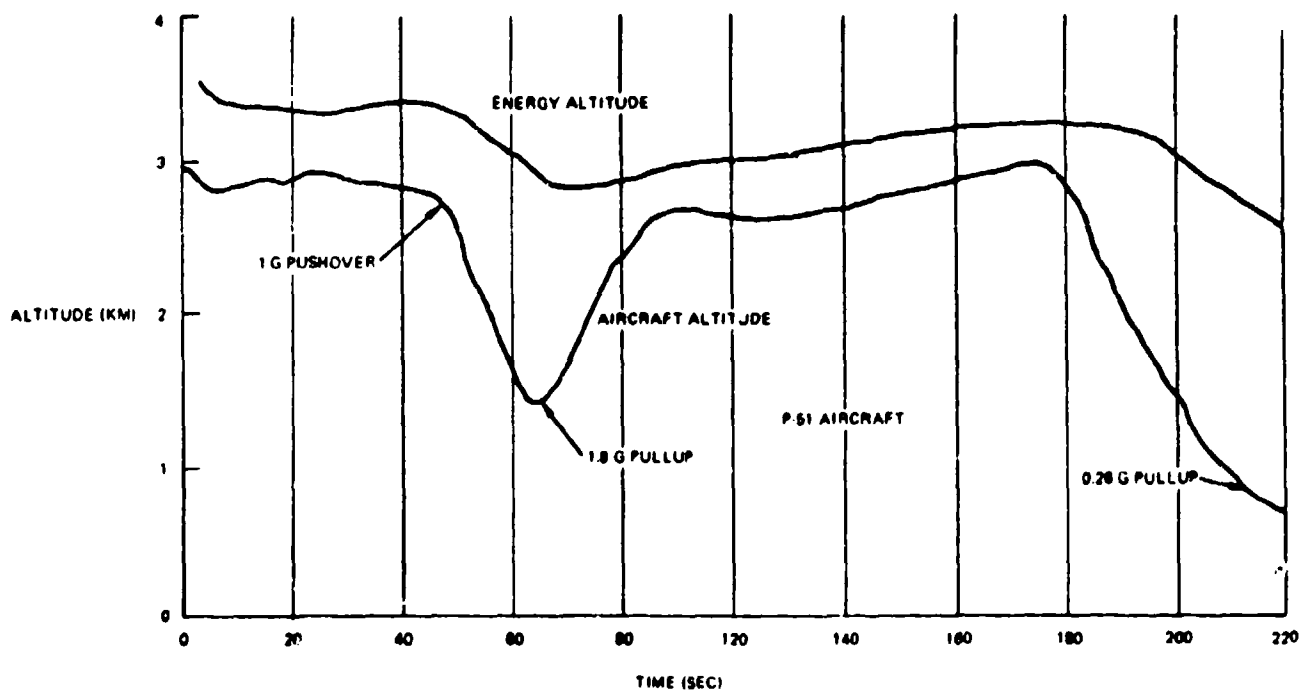
Ideally, one would prefer noiseless records of the target path to determine its "intrinsic predictability" and these may be developed in the future from accelerometer records taken onboard the aircraft.

Rather than introduce the complications of target geometry relative to a specified ground defense position, a set of computations was made with time of flight held constant at 1.0, 2.0 and 3.0 seconds over each path. For small error regions, the error increased approximately linearly with time of flight. For high acceleration segments, the error increased about as time of flight squared.



40001-75

Figure 4-13. Energy Conservation by P-51 WW-II Aircraft Doing "Pushups"



40701-76

Figure 4-14. Energy Conservation by P-51 WW-II Aircraft over Extended Time Interval

For the 3.0 second time of flight prediction Figures 4-15, 4-16, 4-17 and 4-18 show cross range, down range and altitude prediction errors for several dive/glide bombing paths. The small perturbations in the error traces are probably the result of the residual radar noise. Note in the traces of cross range prediction error that the lateral weave of the aircraft on two passes is effective in generating fairly large prediction errors. The 3-second time of flight also subtracts 3 seconds from the predictable segments of all passes.

The linear predictor is fairly effective on most, but not all of these passes in the cross range coordinate.

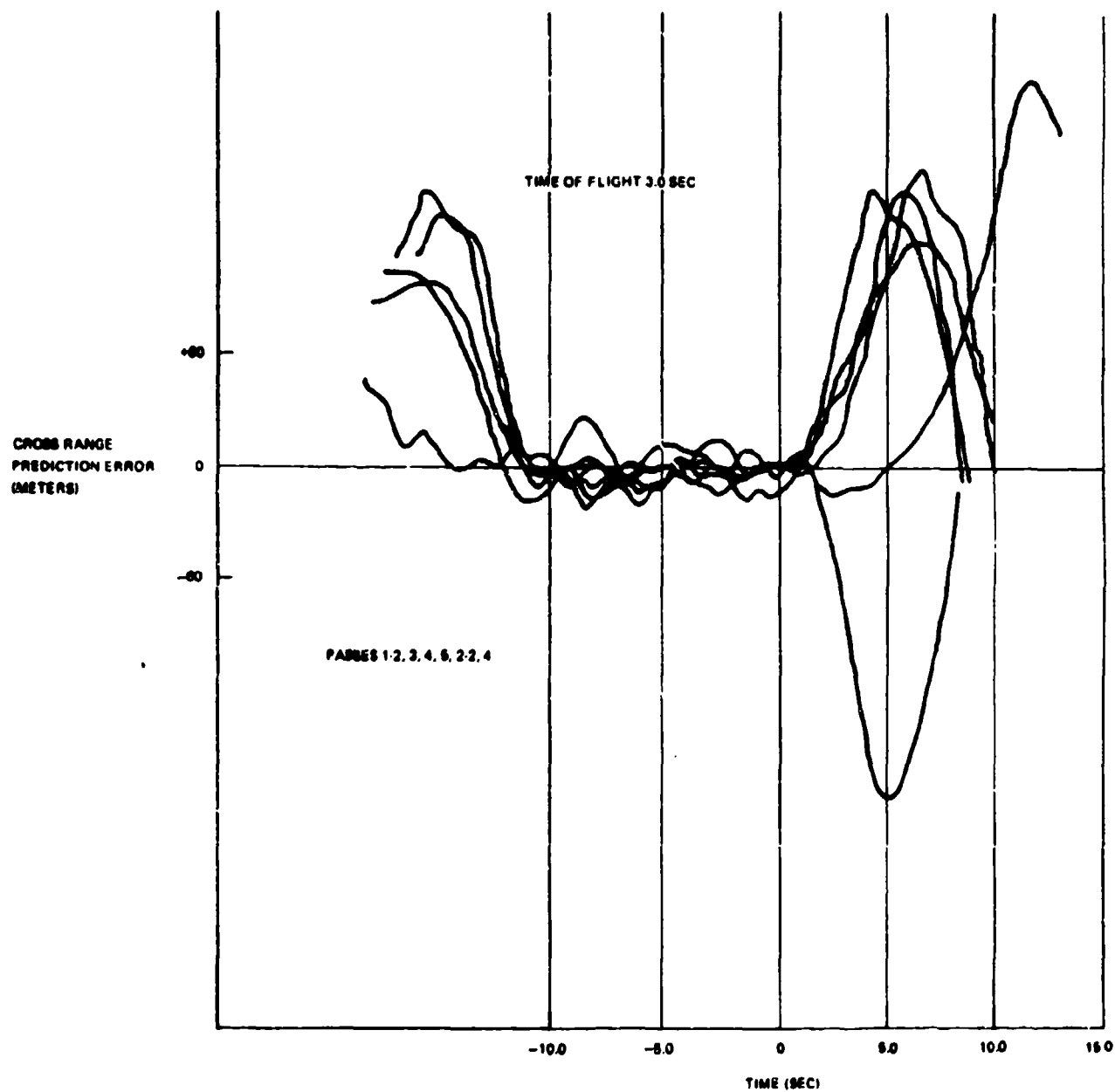
The down range prediction errors, on the other hand, shows a consistent mean error across all passes, and a deviation about the mean corresponding about to that expected from tracking error. The mean error can be eliminated entirely by the "total energy" prediction algorithm, hence in this coordinate, for about 10 seconds, one can obtain a prediction accuracy limited only by sensor tracking error. Down range prediction is almost parallel to the target velocity vector, and one expects very little change in velocity except that associated with gravity acceleration. The scatter across paths is probably almost completely the result of the residual radar noise.

Altitude prediction error traces show a less well defined bias during the firing segment, which can be attributed to the change in target velocity, and which would be eliminated by the "total energy" algorithm. However, there is a significant residue attributable to rate of change of dive angle, and more sophisticated prediction algorithms would be needed to reduce this component.

For the dive/glide bomb passes, therefore, it is clear that a total energy algorithm is desirable in the prediction module. It may be possible to exploit the characteristic shape of the dive angle variation with time to reduce the residual errors in altitude prediction. Cross range prediction errors associated with heading changes during the firing run may represent the most difficult component to reduce, although it is noted that on only a few passes was the pilot able to develop a magnitude of weave that would cause large errors in prediction.

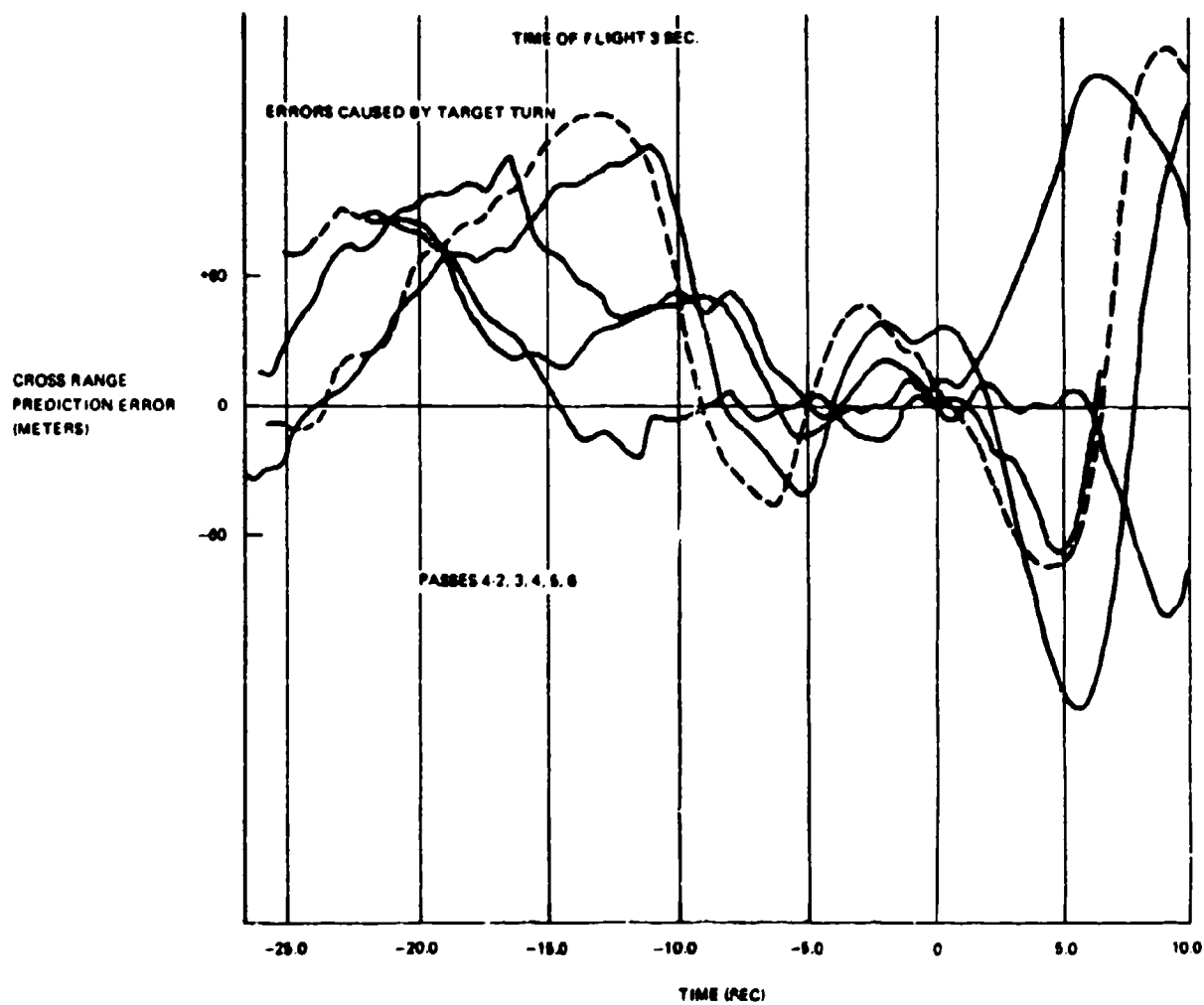
To quantify the relation between linear target acceleration and the resulting errors in altitude, and down range coordinates, Figure 4-19 shows the geometry for a target accelerating along a straight line in a dive. The increase in velocity is

$$dv/dt = -g \sin \theta \quad (\theta \text{ is negative for a dive}) \quad (4.3)$$



60001 77

Figure 4-15. Cross Range Prediction Errors (X) with Linear Predictor on Flights 1 and 2



40001 79

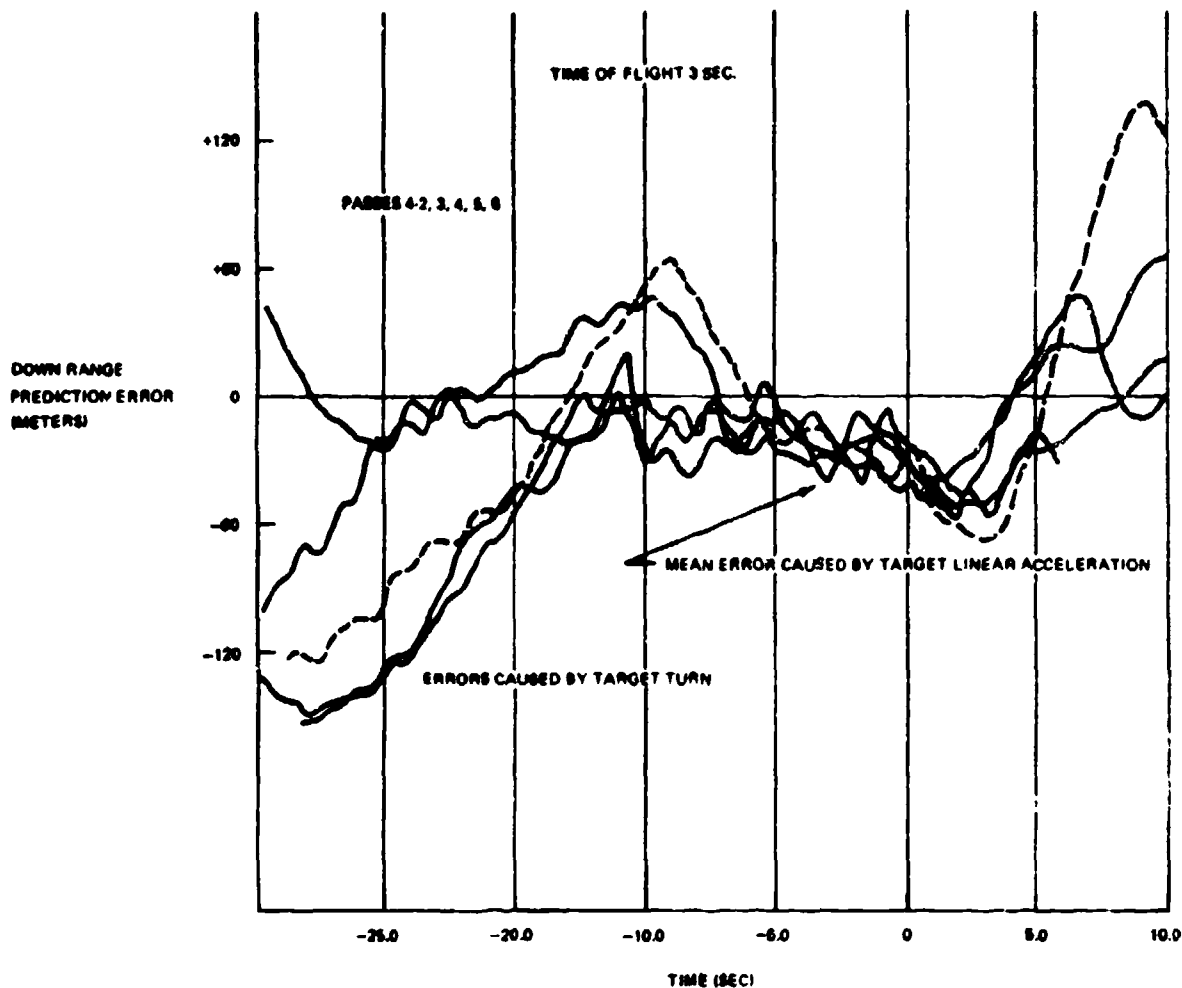
Figure 4-16. Cross Range Prediction Errors (X) with Linear Predictor on Flight 4

Then the vertical acceleration is

$$dv_z/dt = -g \sin^2 \theta \quad (4.4)$$

and the acceleration in a horizontal direction is

$$dv_h/dt = -g \sin \theta \cos \theta \quad (4.5)$$



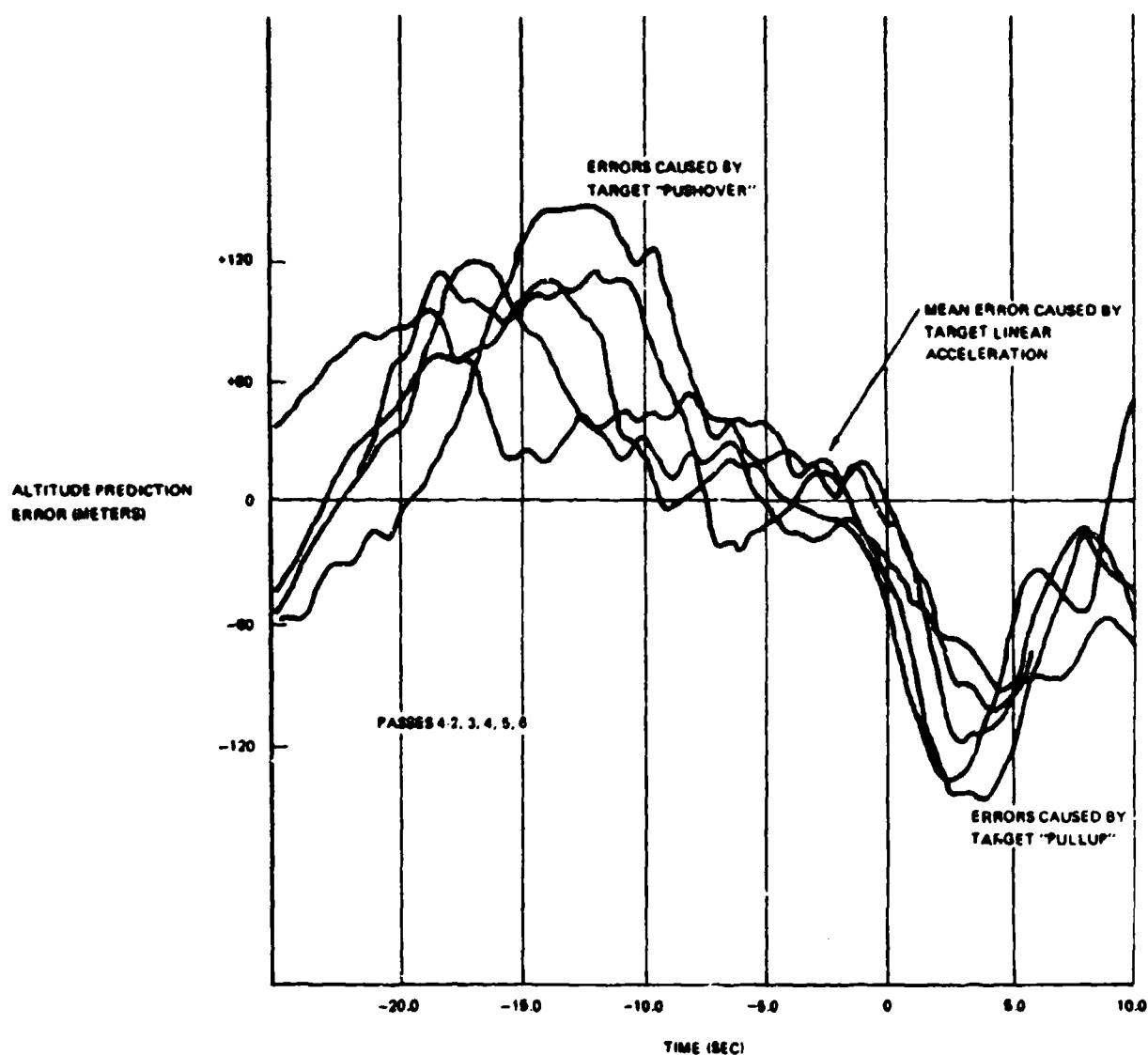
44701-70

Figure 4-17. Down Range Prediction Errors (Y) with Linear Predictor on Flight 4

The resulting errors (ignoring lag in the smoothing filter, which will increase the effective time of flight) are

$$E_z = (g/2) \sin^2 \theta t_p^2 \text{ (always positive)} \quad (4.6)$$

$$E_h = (g/2) \sin \theta \cos \theta t_p^2 \text{ (negative in dive)} \quad (4.7)$$

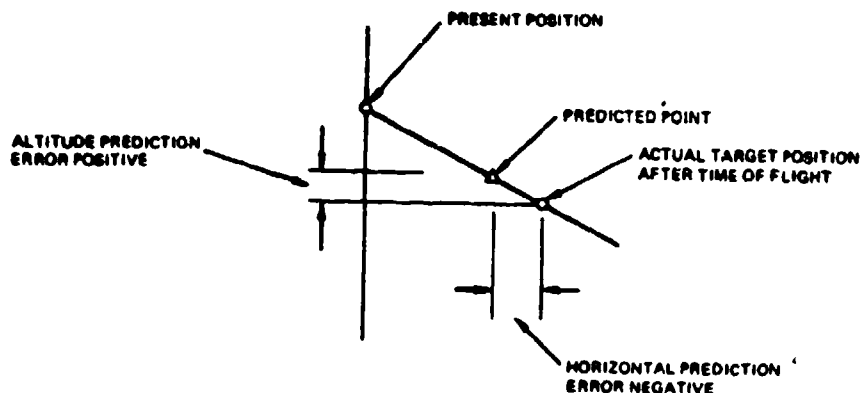


40001-80

Figure 4-18. Altitude Prediction Errors (Z) with Linear Predictor on Flight 4

If one wants to correct for rate of change of dive angle, a method is to compute rate of change of dive angle from measured linear accelerations in altitude and in the horizontal plane, by the relation

$$d\theta/dt = (\dot{v}_z v_h - v_z \dot{v}_h) / v^2; v = \text{total velocity} \quad (4.8)$$



40801-81

Figure 4-19. Effect of Target Linear Acceleration in Dive on Linear Predictor Errors

The acceleration normal to the flight path in a vertical plane is

$$A_n = v \dot{\theta} \quad (4.9)$$

This is multiplied by $t_p^2/2$ and then resolved into components to add to the prediction vector. Ignoring corrections for filter lags, which must be added in practice, the complete altitude prediction algorithm is

$$Z_p = Z_o + v_z t_p - (t_p^2/2) (g \sin^2 \theta - v \dot{\theta} \cos \theta) \quad (4.10)$$

and the prediction algorithm in the horizontal plane (which in realization would be resolved into X and Y components) is

$$H_p = H_o + v_h t_p - (t_p^2/2) (g \sin \theta \cos \theta + v \dot{\theta} \sin \theta) \quad (4.11)$$

This sequence allows the noise associated with acceleration measurements to appear only in one coordinate, normal to the flight path, and does not cause any degradation in the prediction along the flight path direction, hence should be superior to naive acceleration and prediction in each of three rectangular coordinates.

A more sophisticated curvature predictor might utilize the consistency in the dive-angle versus time pattern.

4.3 POP-UP AND DIVE/GLIDE BOMBING PASSES

On these passes, the pilots made a low level approach, then "popped-up" and made a conventional dive/glide bomb attack. Figure 4-20 shows the superimposed heading traces, and Figure 4-21 shows the superimposed dive angle traces.

With the exception of the pop-up climb-dive segment, the traces are very much like those of the attacks without pop-up reviewed in the preceding section. The predictable segments are somewhat shorter, but in an actual defense situation this would be partly compensated for by the fact that the release ranges (not shown) were on the average, somewhat shorter than for the attacks without pop-up.

Traces of computed total energy show the same constancy previously observed, and so are not reproduced.

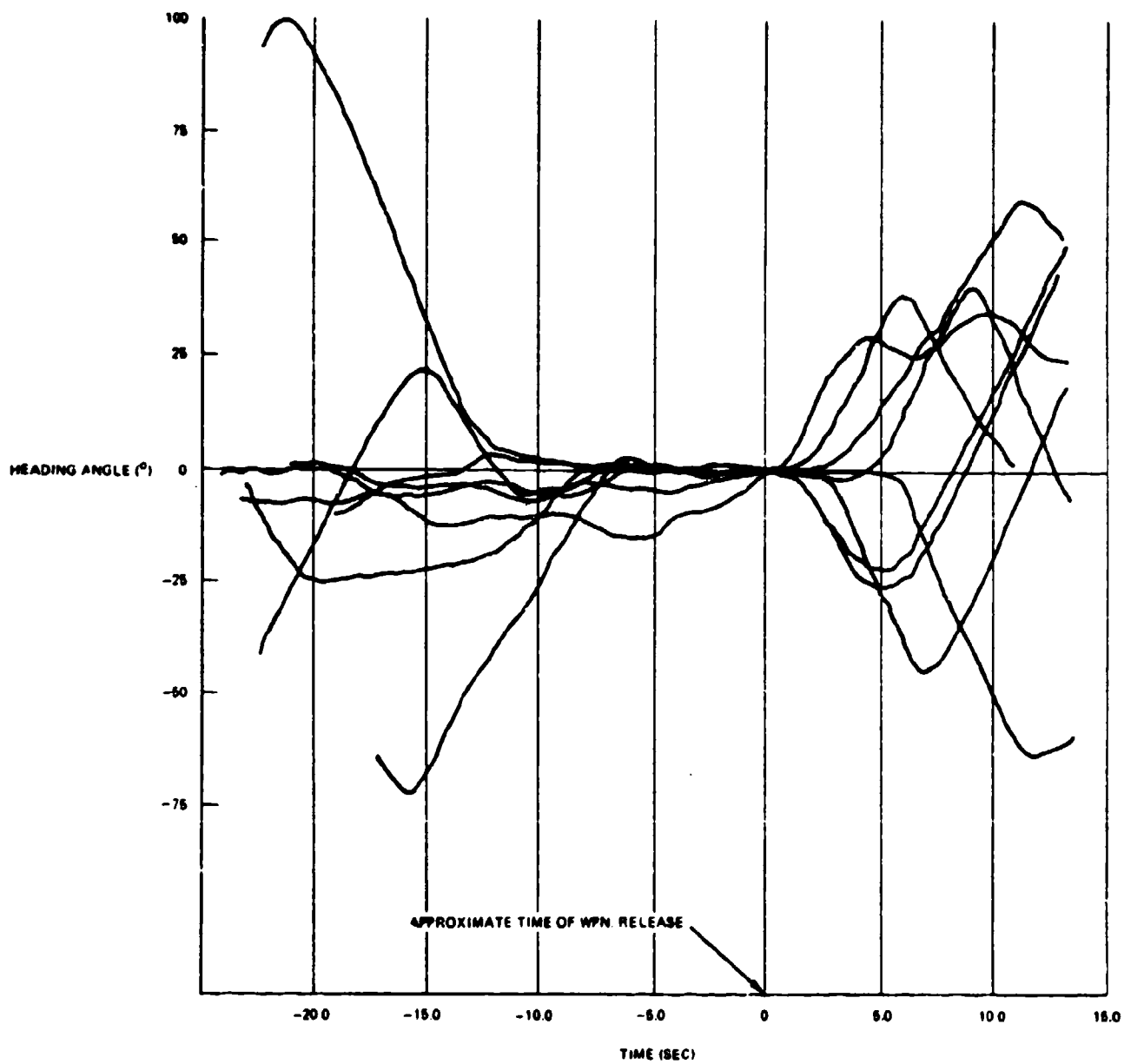
Traces of the prediction errors with a simple linear predictor in each of the three coordinates are shown in Figures 4-22, 23 and 24. The down range prediction error shows the acceleration bias, previously noted. The corresponding altitude bias is not conspicuous, and is submerged in the effects of dive angle change.

In general, this class of attack path shortens the length of the predictable segment somewhat over the previous dive/glide passes, but the heading, dive angle and speed variations are similar.

4.4 STRAFING PASSES

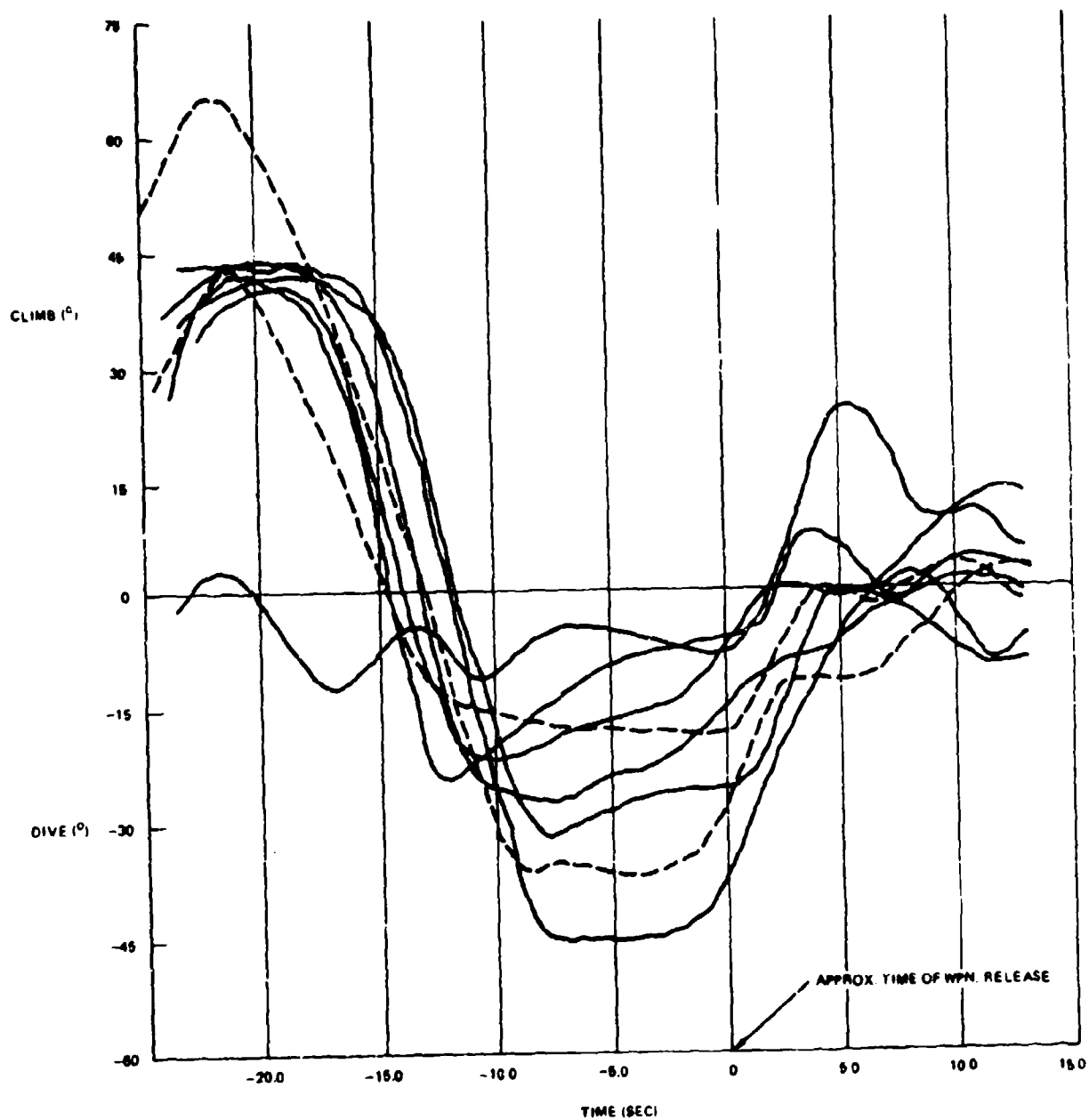
Heading traces on strafing passes are shown in Figure 4-25. The predictable segment is very short, only about 5.0 seconds. Dive angle is less than in prior attack types and is shown in Figure 4-26. The relative constancy of energy during the altitude changes (not shown) is again confirmed.

The traces of 3-second time of flight prediction errors with the linear predictor are shown in Figures 4-27, 28 and 29. The characteristic bias in down range error resulting from acceleration is again noted. The prediction error in the cross course direction is small for only about 3.0 seconds (the 5-6 second heading constancy segment less time of flight) and the same is true of altitude. Again, however, strafing involves weapon release at relatively short ranges, which tends to compensate (in the eyes of the defense) for the shortened effective firing time.



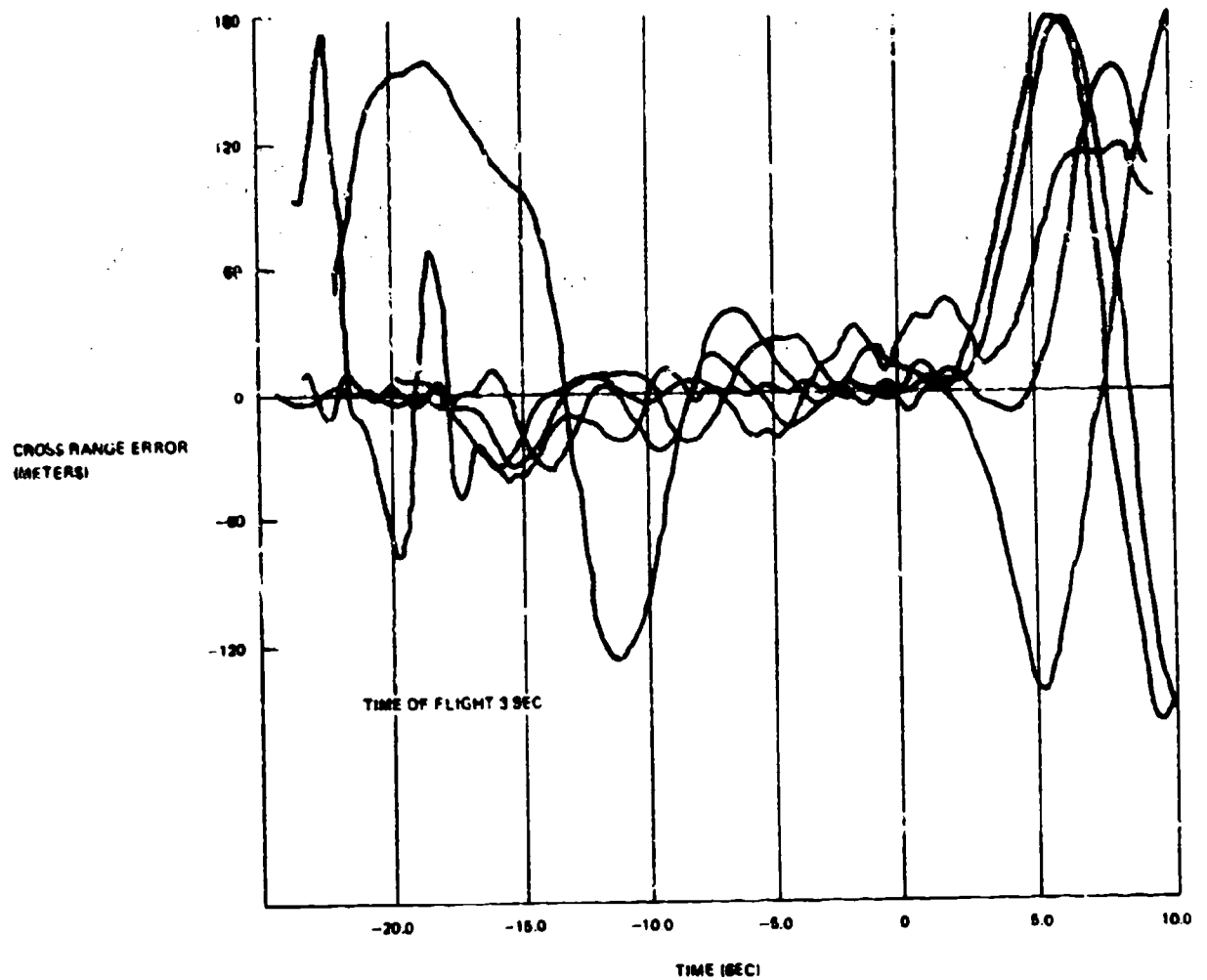
40001-82

Figure 4-20. Superimposed Heading Traces on Pop-Up and Dive/Glide Bomb Passes



40001 83

Figure 4-21. Superimposed Dive Angle Traces on Pop-Up and Dive/Glide Bomb Passes

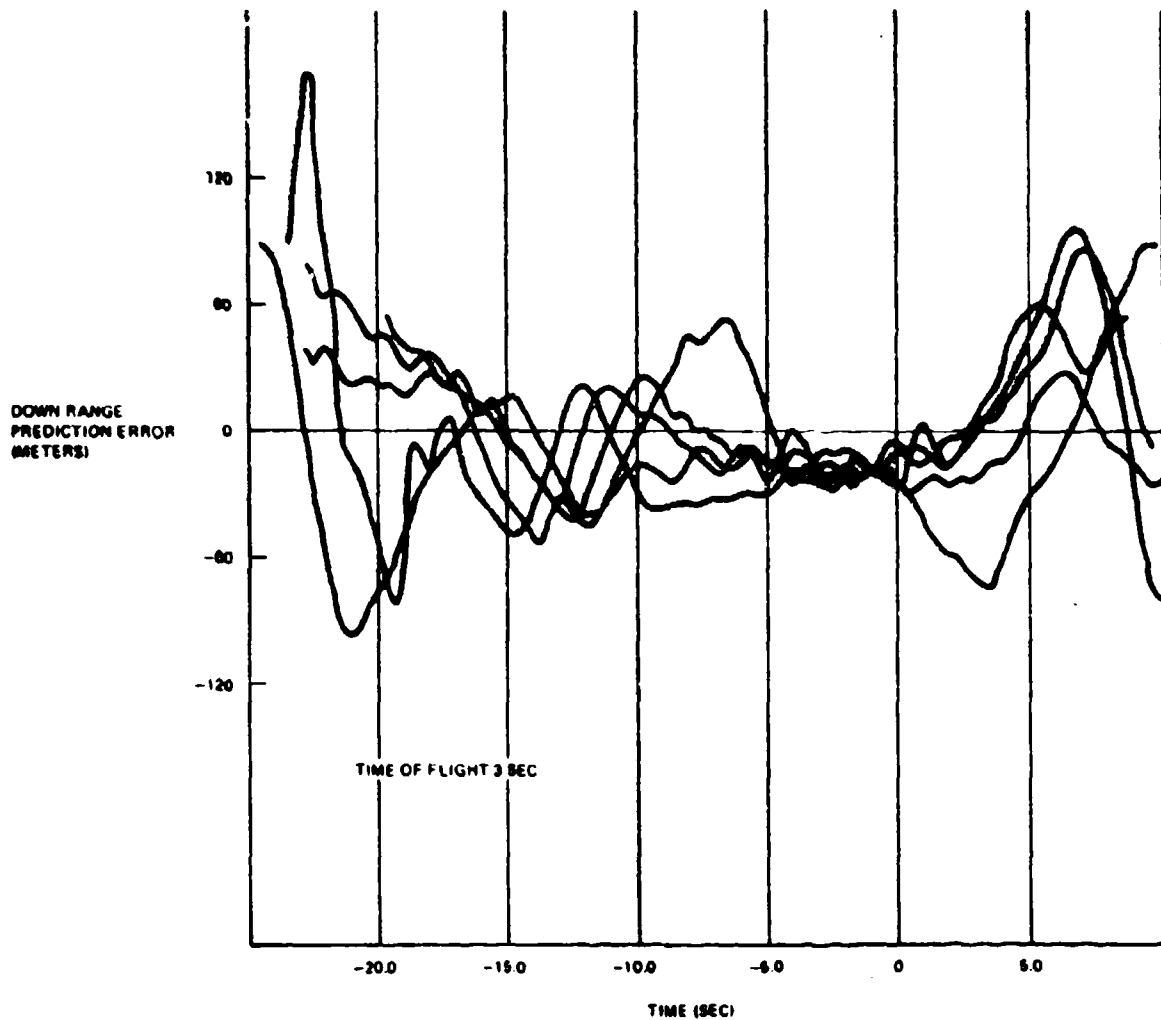


40001-84

Figure 4-22. Cross Range Prediction Errors on Pop-Up and Dive/Glide Bomb Passes

4.5 HIGH LEVEL BOMBING

There was only one high level bombing pass. The aircraft developed a moderate amount of maneuver before and after weapon release. The various traces and prediction errors displayed no new characteristics beyond those observed on the other types of passes, hence are not reproduced.

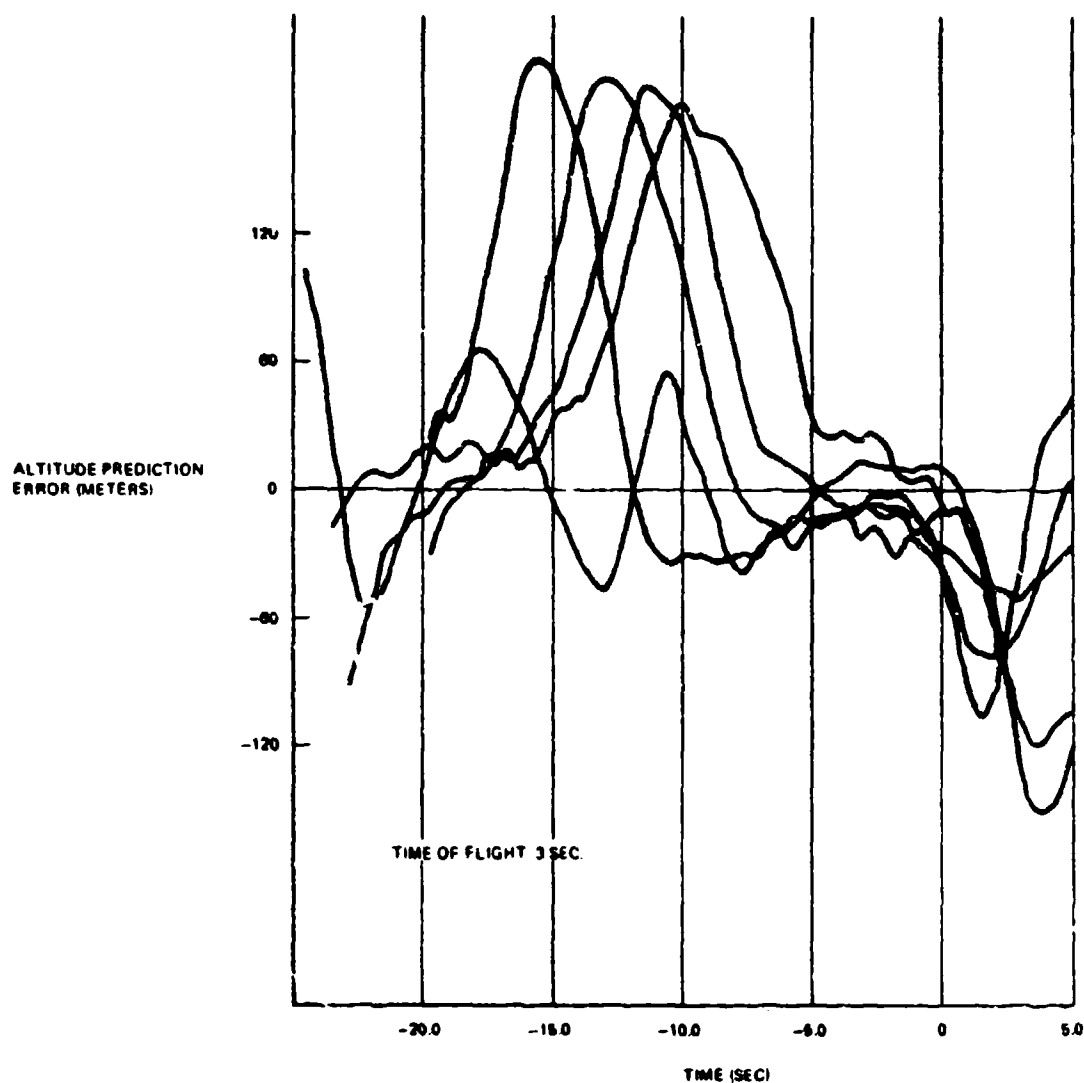


40001-86

Figure 4-23. Down Range Prediction Errors on Pop-Up and Dive/Glide Bomb Passes

4.6 LAYDOWN PASSES

Laydown passes involved a run-in at very low altitude. Three heading traces are shown in Figure 4-30 with the corresponding dive angle traces in Figure 4-31. Altitudes were about 450 meters in two cases, and under 150 meters in the third. The radar had difficulty in tracking the very low altitude target, and the large fluctuations observed are probably radar error.

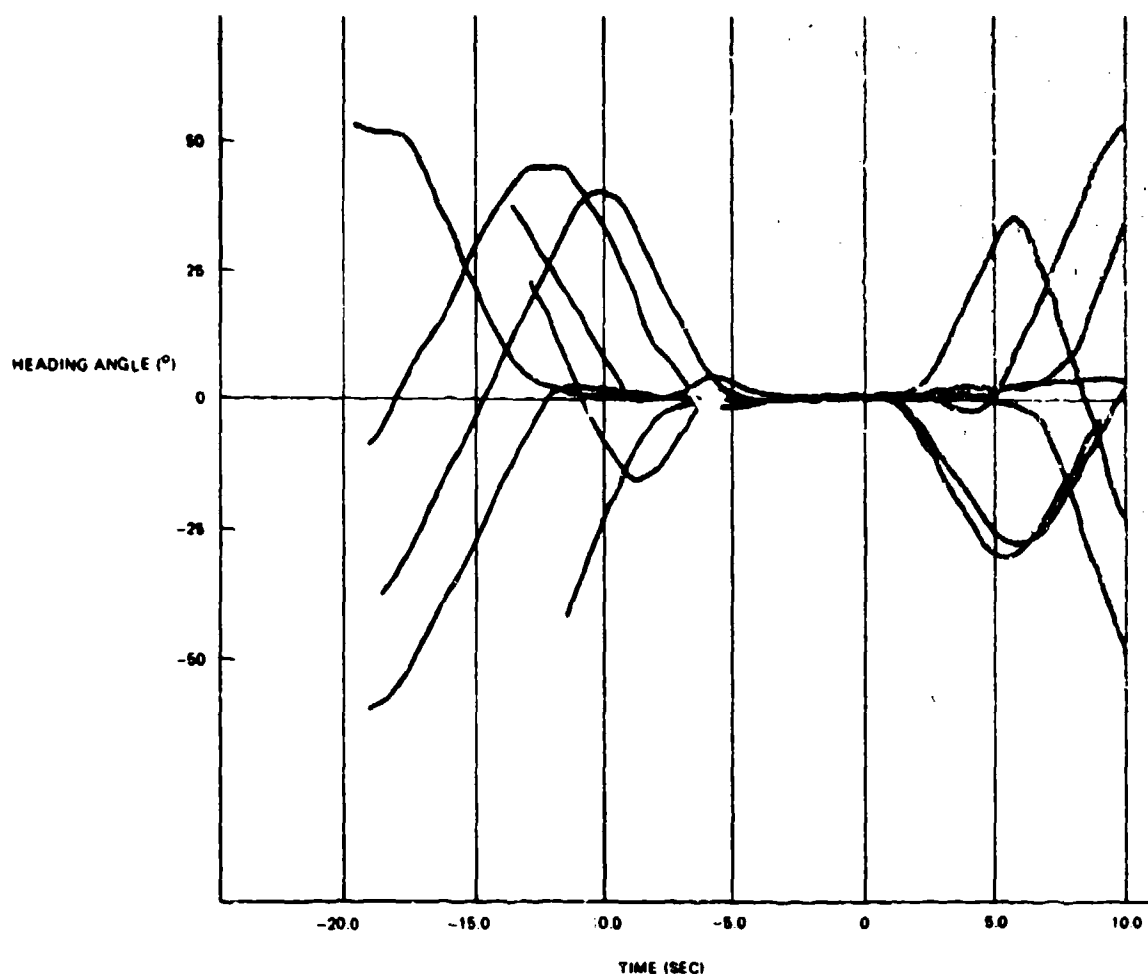


40001 86

Figure 4-24. Altitude Prediction Error on Pop-Up and Dive/Glide Bomb Passes

The errors obtained with the linear predictor are shown in Figure 4-32. They are remarkably small, and are probably entirely the result of residual radar noise in the smoothed data, except for the errors at breadaway.

From the point of view of the attacker, laydown would appear to be an extremely dangerous attack mode, provided that the defense is able to acquire and accurately track the aircraft.

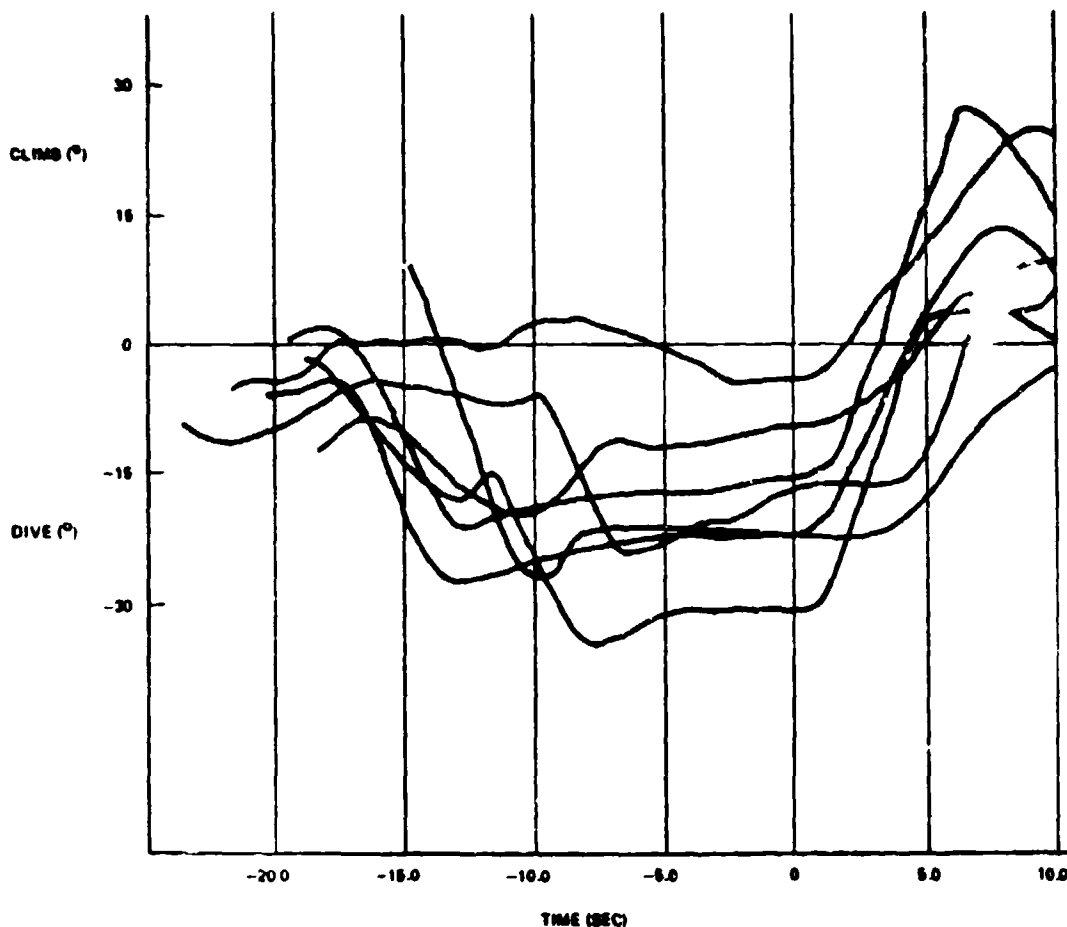


40001.07

Figure 4-25. Superimposed Heading Traces on Strafing Attacks

4.7 DEFENSE OF KNOWN POINT ALGORITHMS

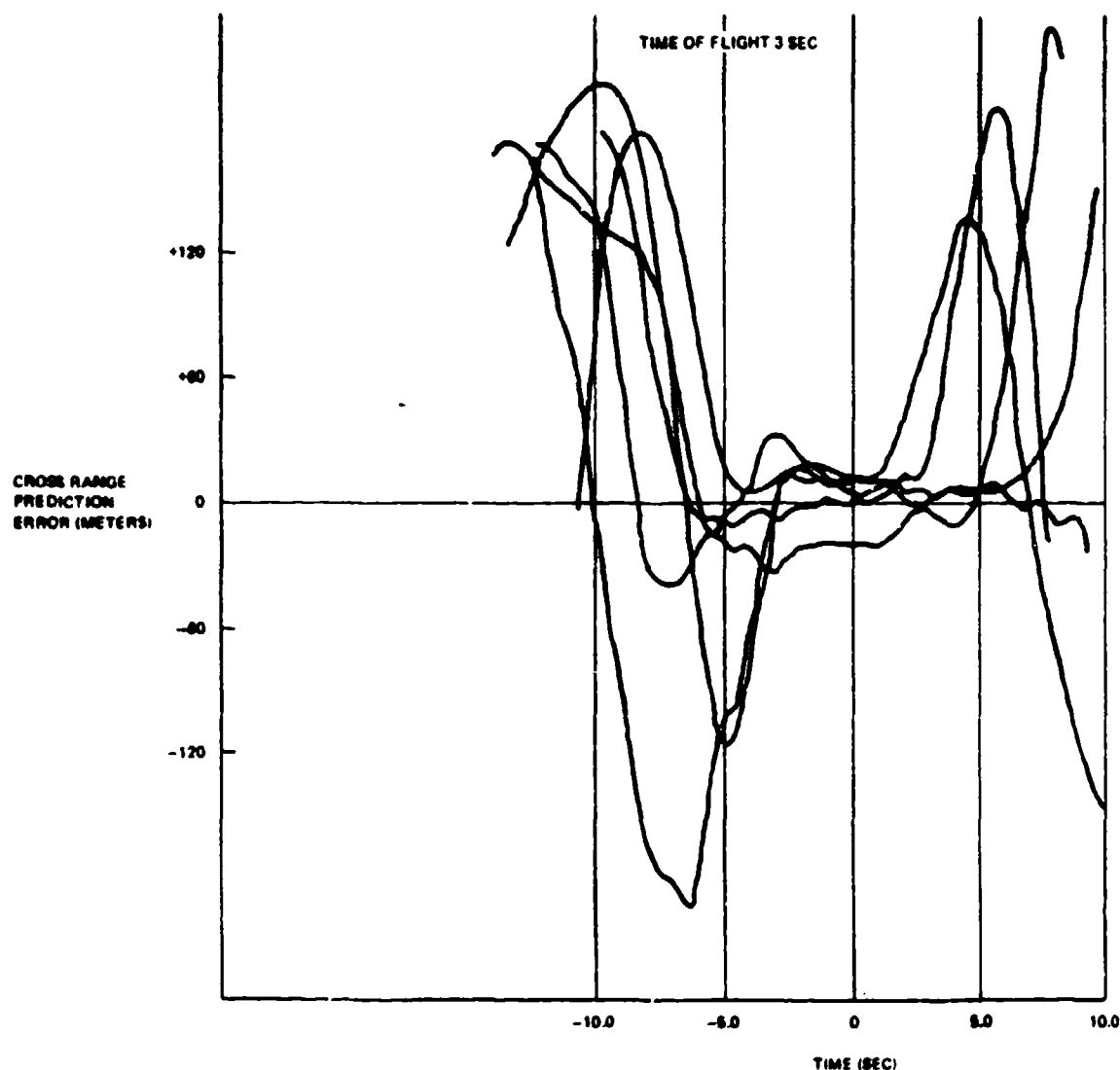
The prediction algorithms termed "defense of known point" are based on the assumption that the target on an attack pass can be predicted by simply extrapolating along a line between target present position and its target. The only prediction involved is then along this line, and as observed in all the data to this point, the accuracy of prediction in the direction of the flight path is limited only by sensor accuracy, once the correction for gravity acceleration has been applied.



40001-00

Figure 4-26. Superimposed Dive Angle Traces on Strafing Attacks

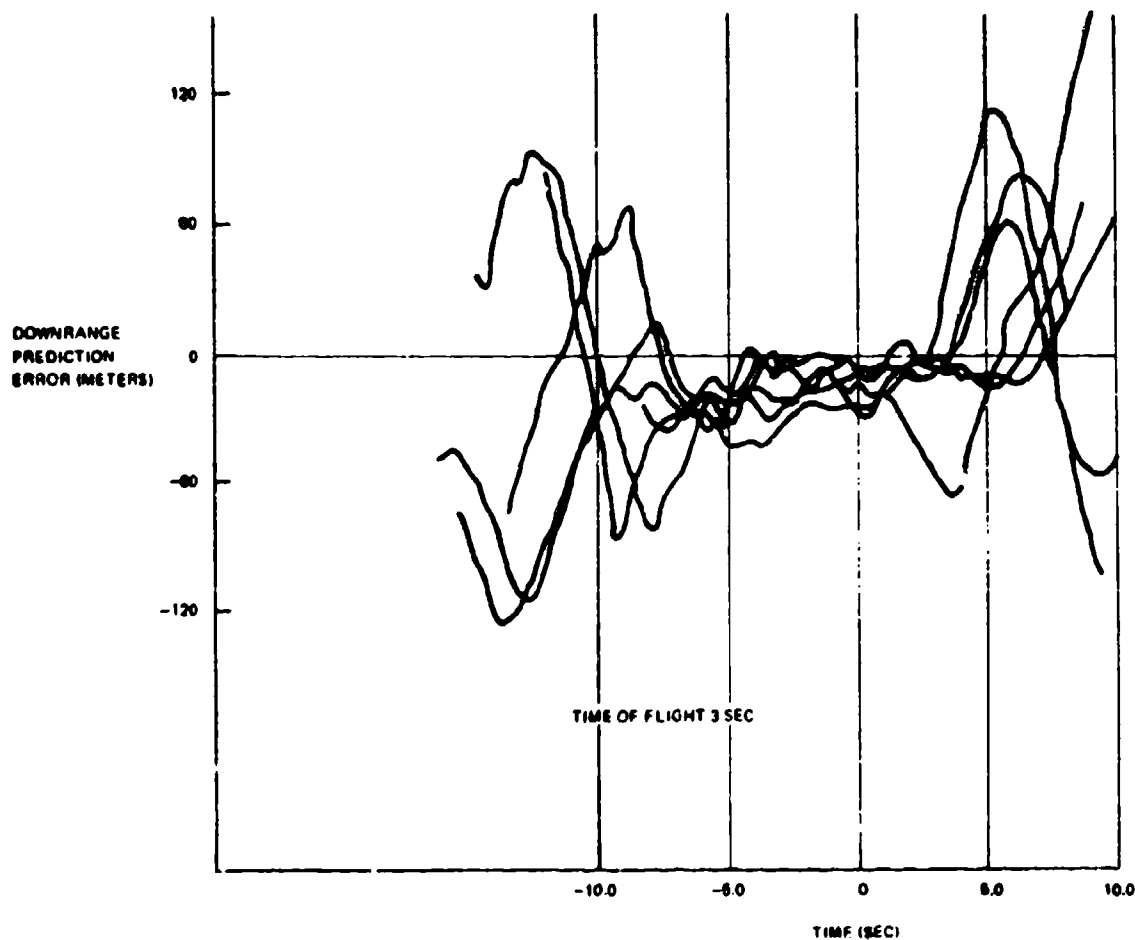
Figure 4-33 shows lateral prediction errors using this algorithm, as viewed from a position on the target, and Figure 4-34 shows elevation prediction errors. On some paths the lateral error is small over extended time intervals. The elevation error has a characteristic bowl-shape associated with the characteristic dive angle patterns. Unlike the linear prediction errors, the known point predictor is relatively insensitive to time of flight, as shown in Figure 4-35, and its errors result from the fact that the target in reality does not fly a path corresponding to that assumed by the algorithm. (These errors are opposite in sign to those shown for the prior linear predictors.)



40001-88

Figure 4-27. Cross Range Prediction Errors with Linear Predictor on Strafing Passes

To this point it would appear that the algorithm has little to recommend it, unless it is incorporated in a more general prediction scheme, or otherwise improved. However, when the variation of lateral and elevation errors by this algorithm are examined simultaneously, as shown in Figures 4-36, 37 and 38 a remarkable characteristic emerges: both error components become zero or near zero at the same time at at least one point on the attack path. In those cases where the error does not reduce simultaneously to zero, the residuals are within the expected accuracy of the data.

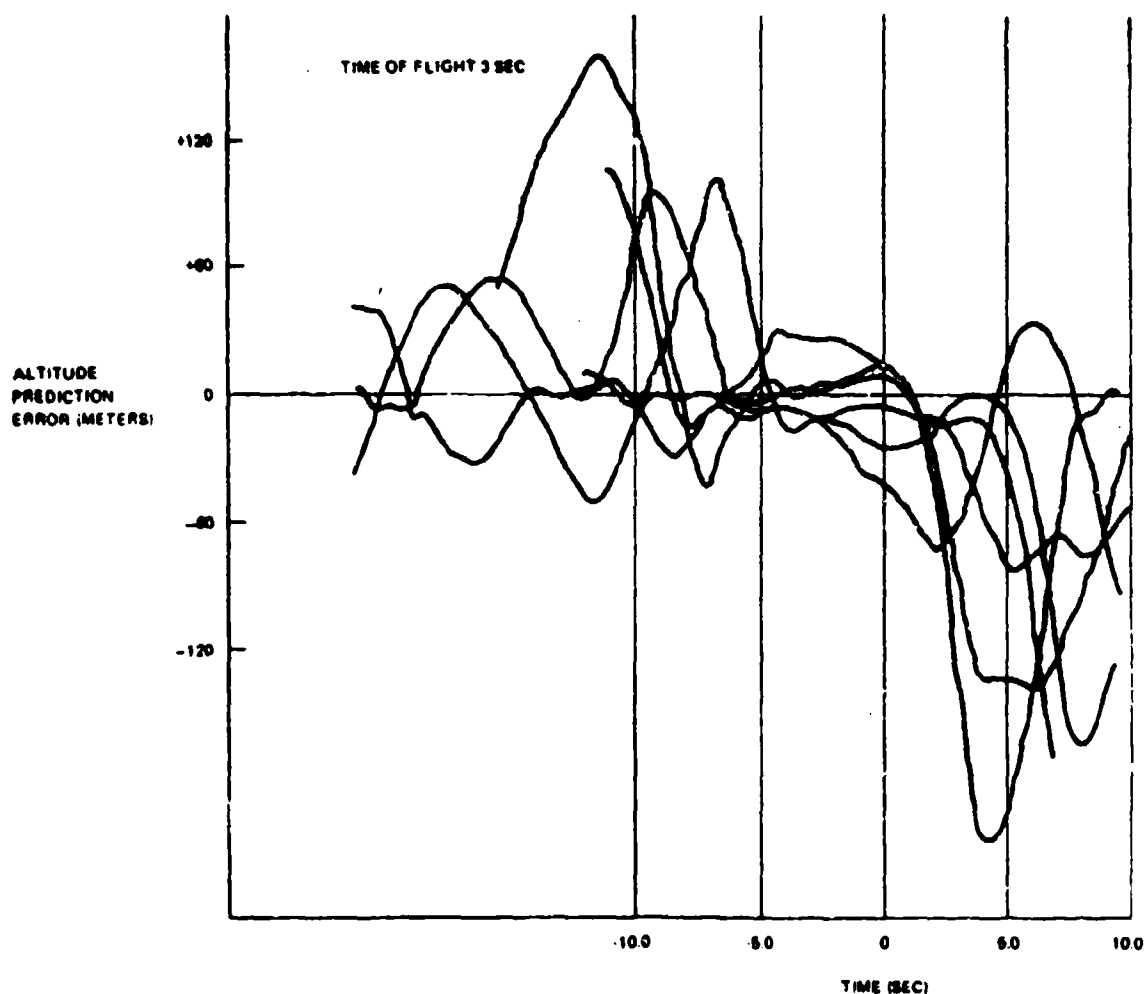


40001-90

Figure 4-28. Down Range Prediction Errors with Linear Predictor on Strafing Passes

With a more conventional predictor, the probability that the aim error will be "on target" simultaneously in two dimensions is roughly the product of the probabilities that it will be on in each coordinate, and one hopes that simultaneity of small errors will occur if the firing pass is long enough. With the "known point" predictor, simultaneity of zero error in two coordinates once on each pass appears to be guaranteed.

This effect, which has an obvious explanation, deserves further investigation. The implications for simple fire control of a gun situated on the defended target are



40001-01

Figure 4-29. Altitude Prediction Errors on Strafing Passes with Linear Predictor

straightforward, - correct for gravity drop, then fire directly at the aircraft with zero lead angle. This would explain the historical effectiveness of guns with simple tracer fire control in self-defense.

Note that the error scales are different for vertical and lateral errors, - one of the minor problems of using computer generated traces for unforeseen applications. However, zero is always zero. The simultaneous minima have been read off and are listed in Table IV-1.

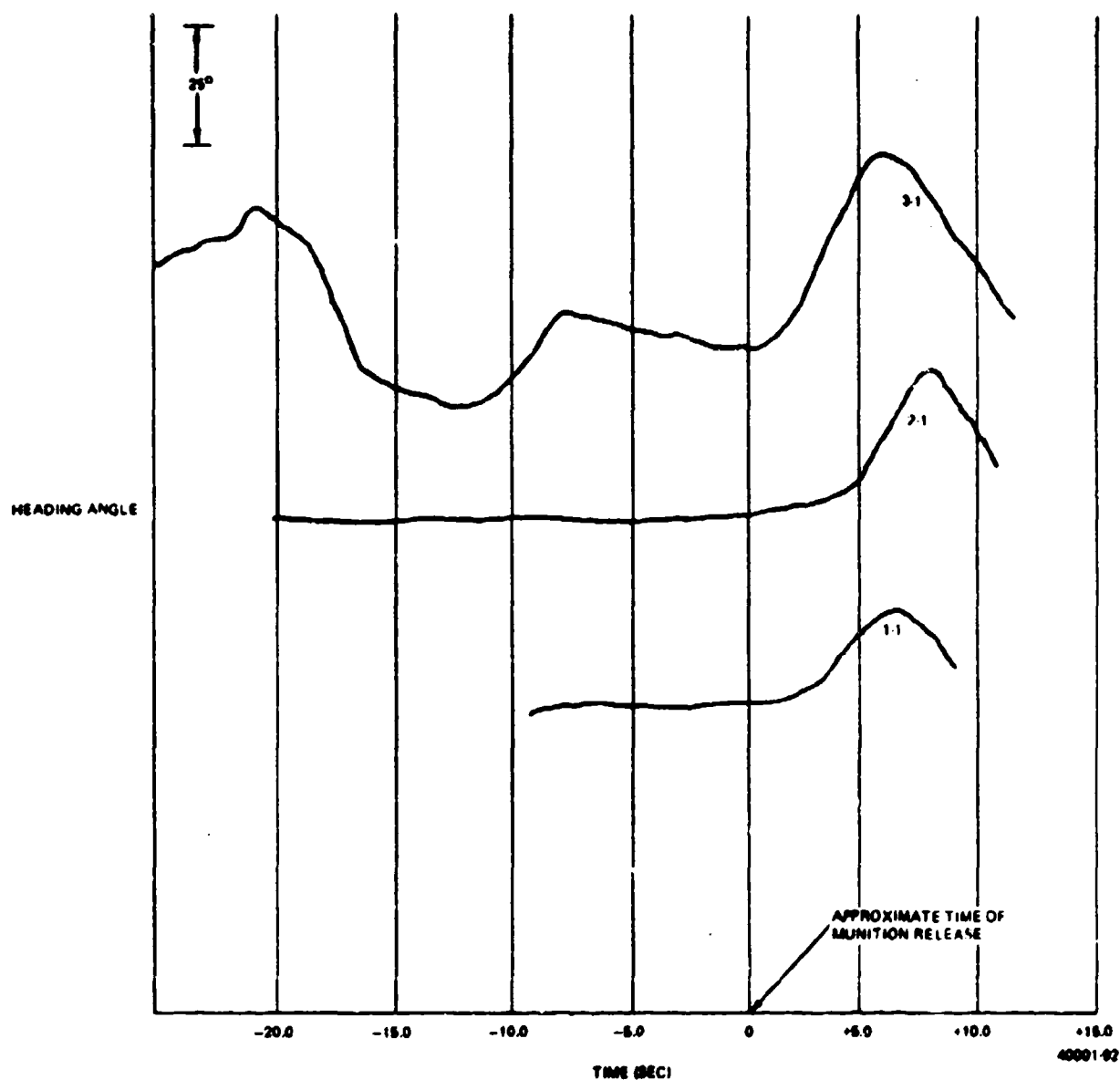
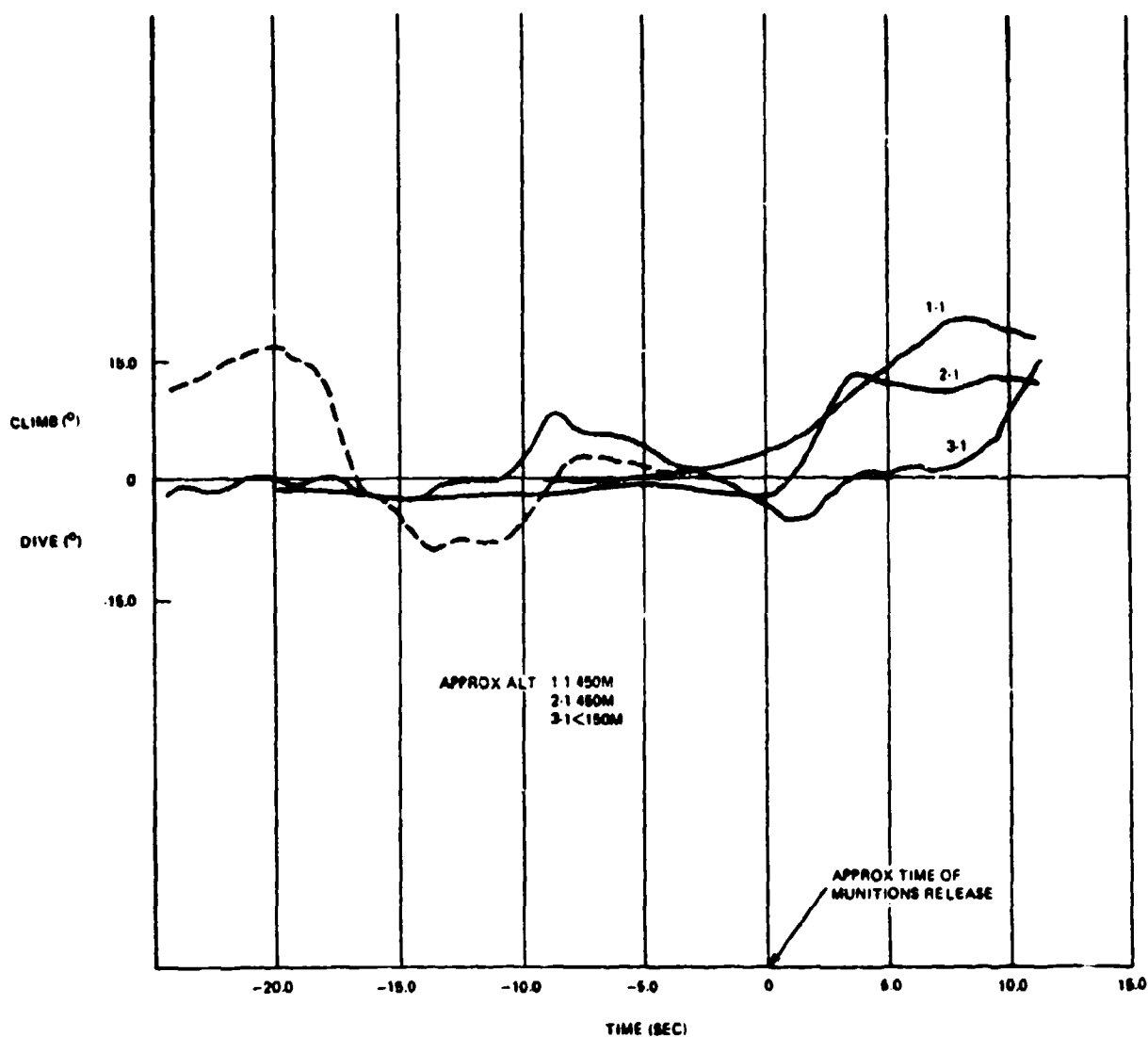


Figure 4-30. Heading Traces on Laydown Passes

4.8 DATA STATISTICS

4.8.1 Standard Deviation and Autocorrelation of Radar Noise

Some initial attempts to estimate the standard deviation of radar tracking error on these passes were made along the following lines: The raw tracking data was converted to rectangular coordinates, and the differences in computed down-range positions at 0.10 second intervals was used to obtain a variance in velocity about the mean. The down range velocity



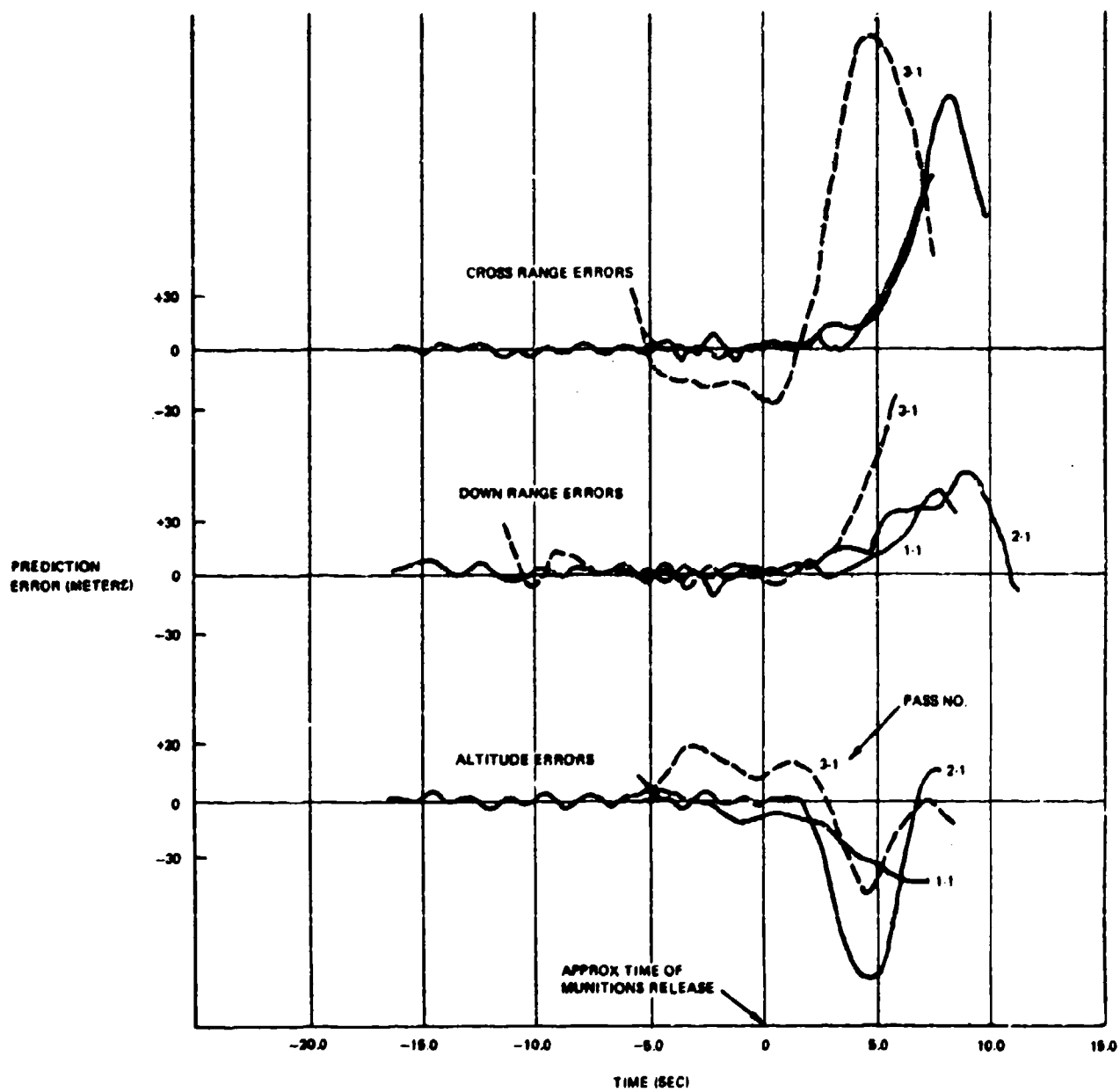
40001-83

Figure 4-31. Superimposed Dive Angle Traces on Laydown Passes

of the aircraft is expected to have only long term variations, hence the computed velocity variances could be attributed entirely to the radar. If the noise were white, the position variance could be computed as

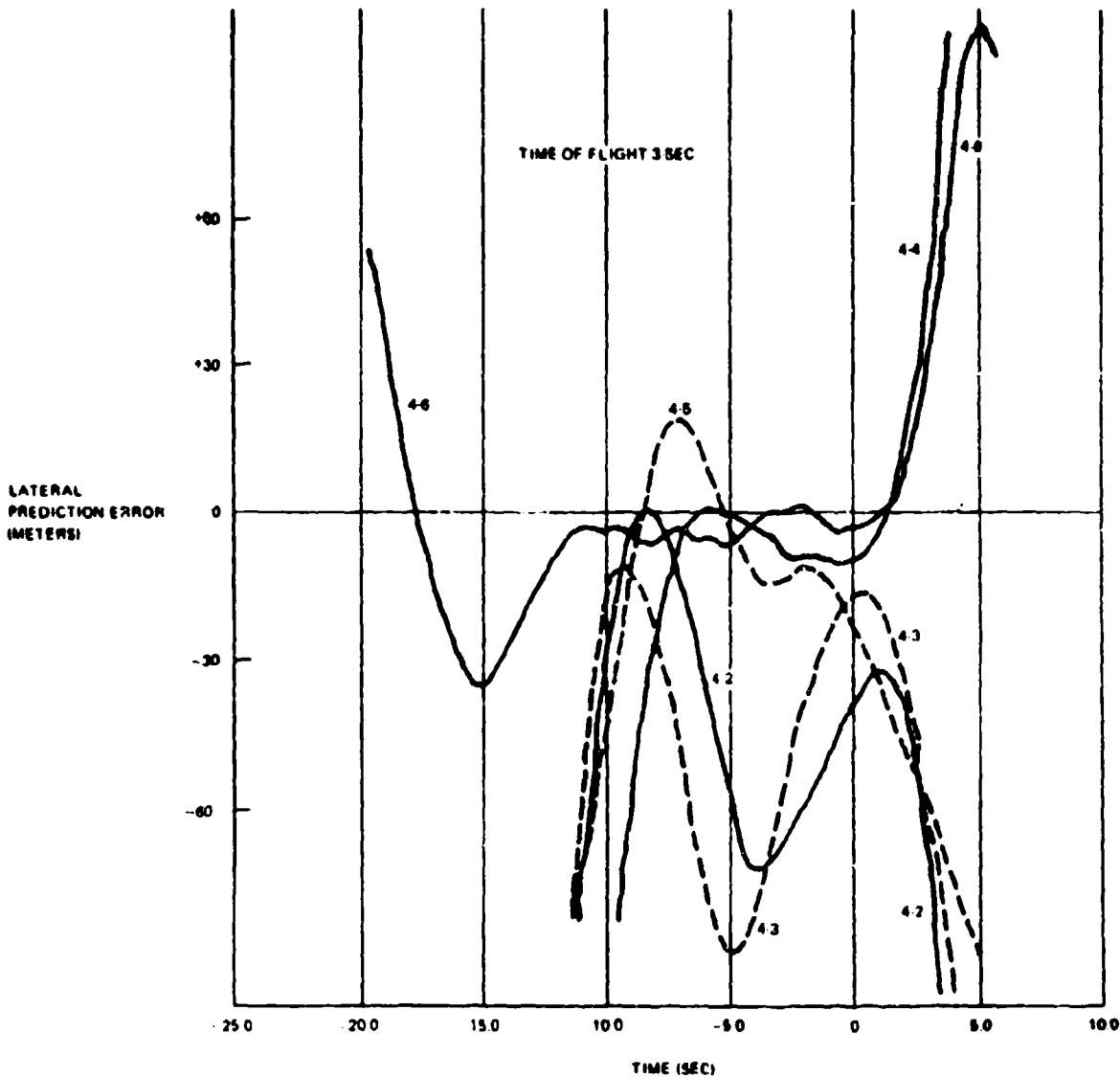
$$\sigma_x^2 = (\sigma_v \Delta)^2 / 2 \quad (4.12)$$

where Δ is the sample interval. For a few sample path segments, this method gave estimates of $\sigma_x = 1.9$ to 2.4 meters. Slowly varying radar bias is irrelevant to the present investigation, and its presence is unimportant.



40001 94

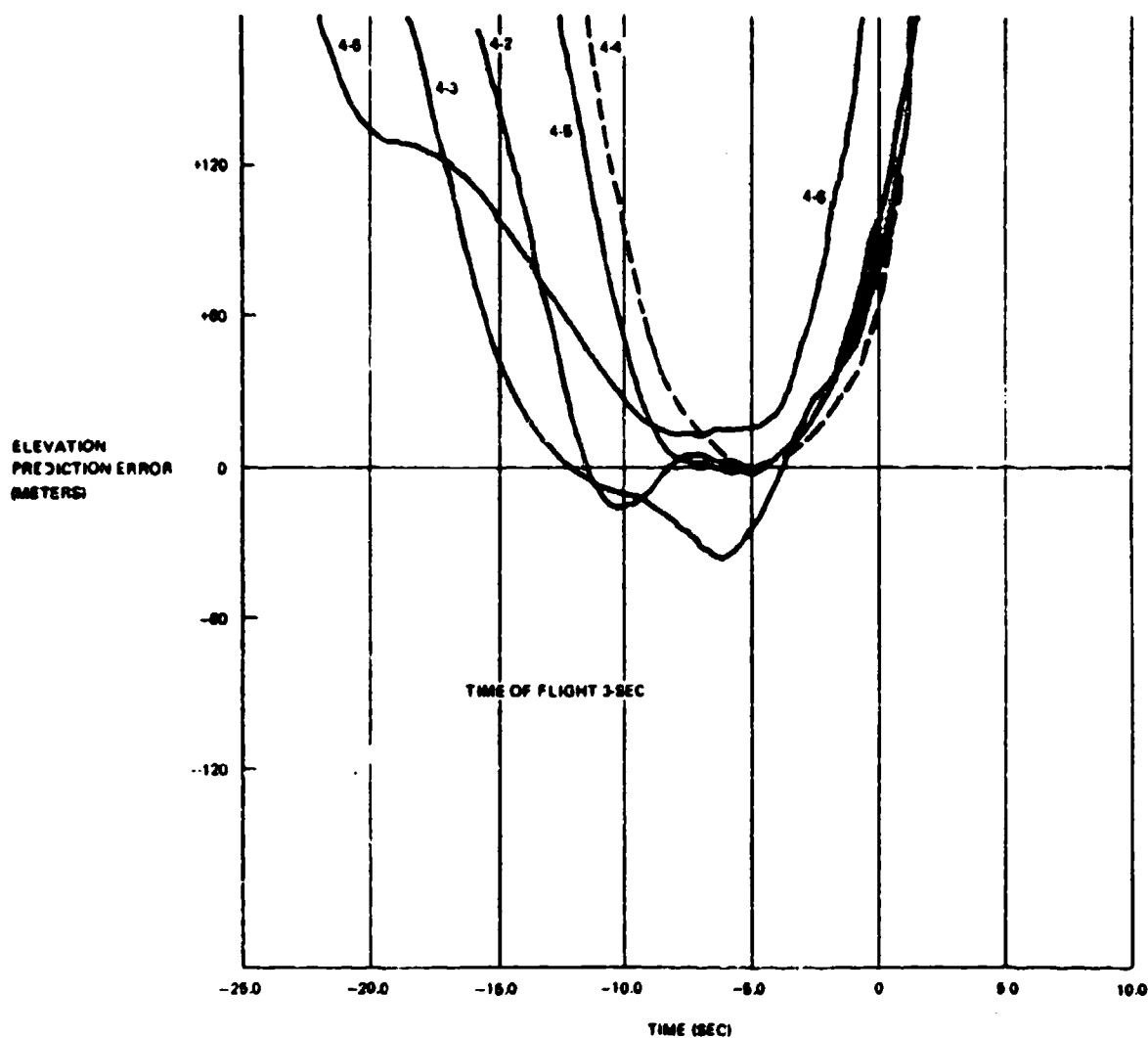
Figure 4-32. 3-Sec Prediction Errors on Laydown Passes



40001 95

Figure 4-33. Lateral Prediction Errors with Defense of Known Point Predictor

For correlated noise, the estimates made by this method are too low. For an attack segment (Pass 4-6) 10 seconds long a mean quadratic curve was next fitted, and deviations from the mean were processed to develop an autocovariance function in down range and cross range components. The curvature of the quadratics corresponded to a mean cross range acceleration of 0.12 g and a down range acceleration of 0.43 g.



40001-98

Figure 4-34. Elevation Prediction Errors with Defense of Known Point Predictor

The cross range standard deviation of position error was about 3.4 meters, and the down range standard deviation was about 3.7 meters. Both autocorrelation functions had identical shapes, indicating that they described the noise and not target path perturbations. The shape was a lightly damped oscillatory form, and for this single set of data the noise structure could be described as the sum of a white noise component of standard deviation 0.8 meter, a damped exponential with standard deviation 2.6 meters and time constant 0.8 seconds, and an undamped sinewave with standard deviation 1.6 meters and period about 5 seconds.

Vertical Error

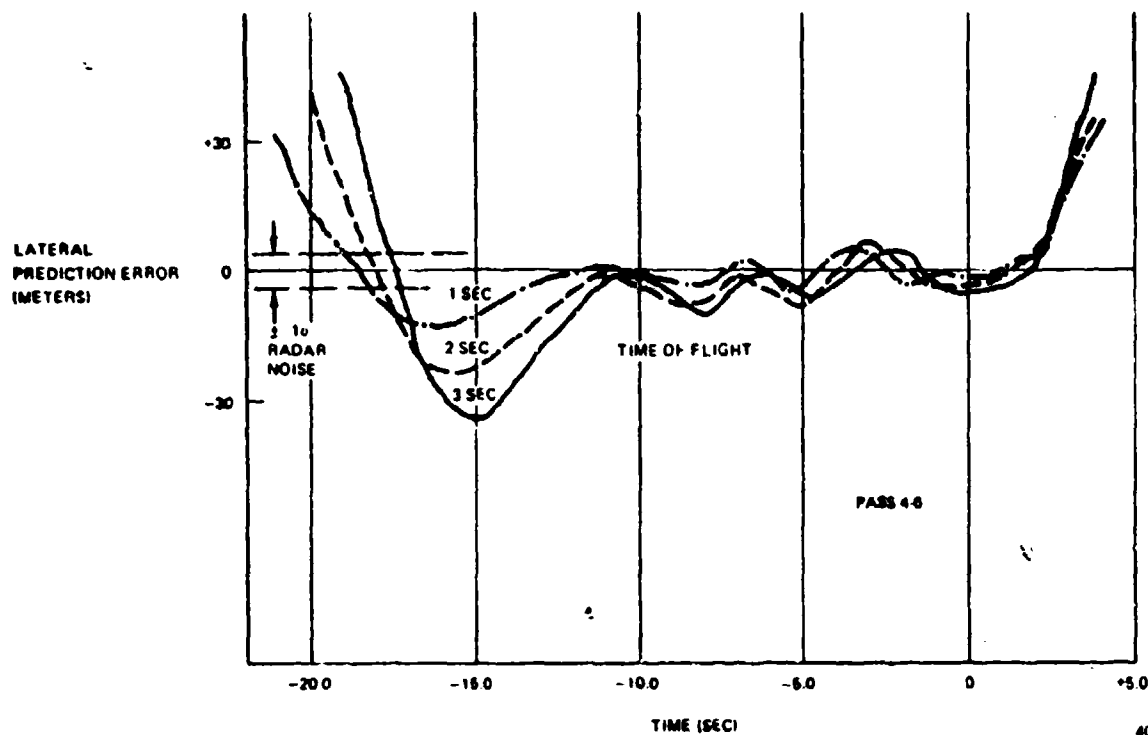
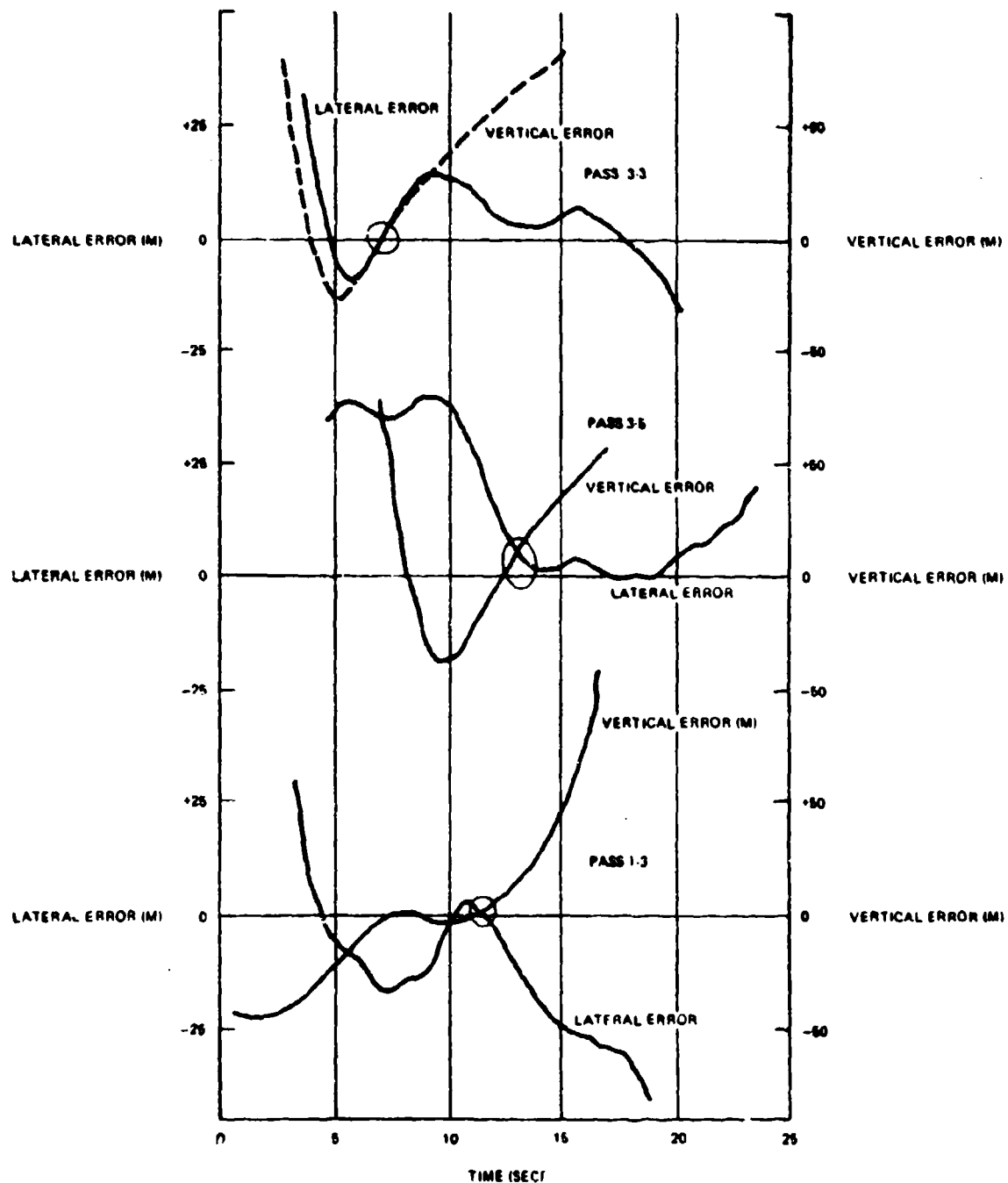


Figure 4-35. Variation of Lateral Prediction Error with Time of Flight for Defense of Known Point Predictor

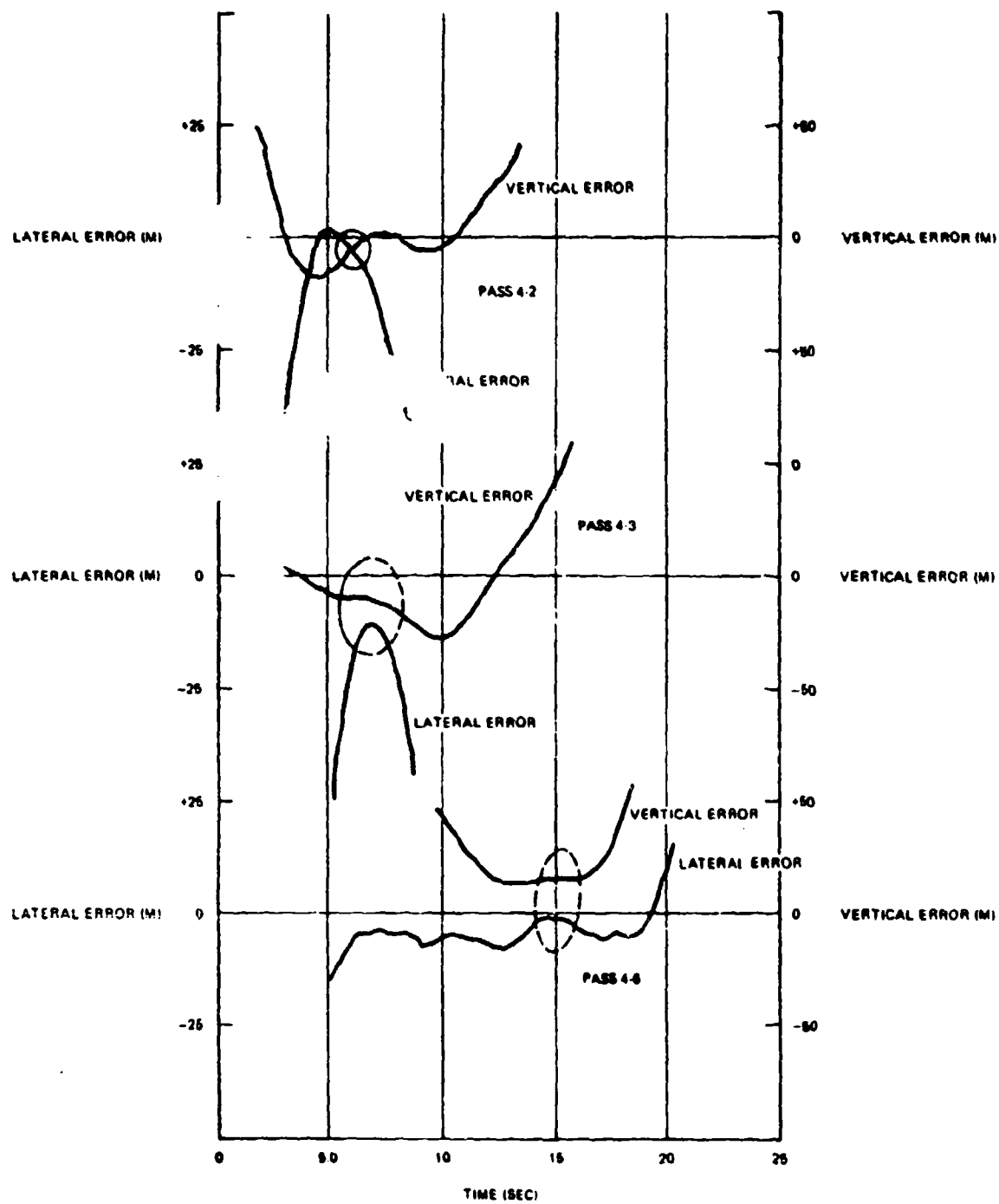
Table IV-1. Minimum Simultaneous Prediction Errors with Defense of Known Point Predictor on Dive/Glide Bomb Passes

Pass	Latitude Error (m)	Vertical Error (m)
1-3	0	0
3-3	0	0
3-5	+5	+5
3-6	+3	+3
3-7	+5	+5
4-2	-5	-5
4-3	-10	-10
4-6	+15	-2
4-8	5	5



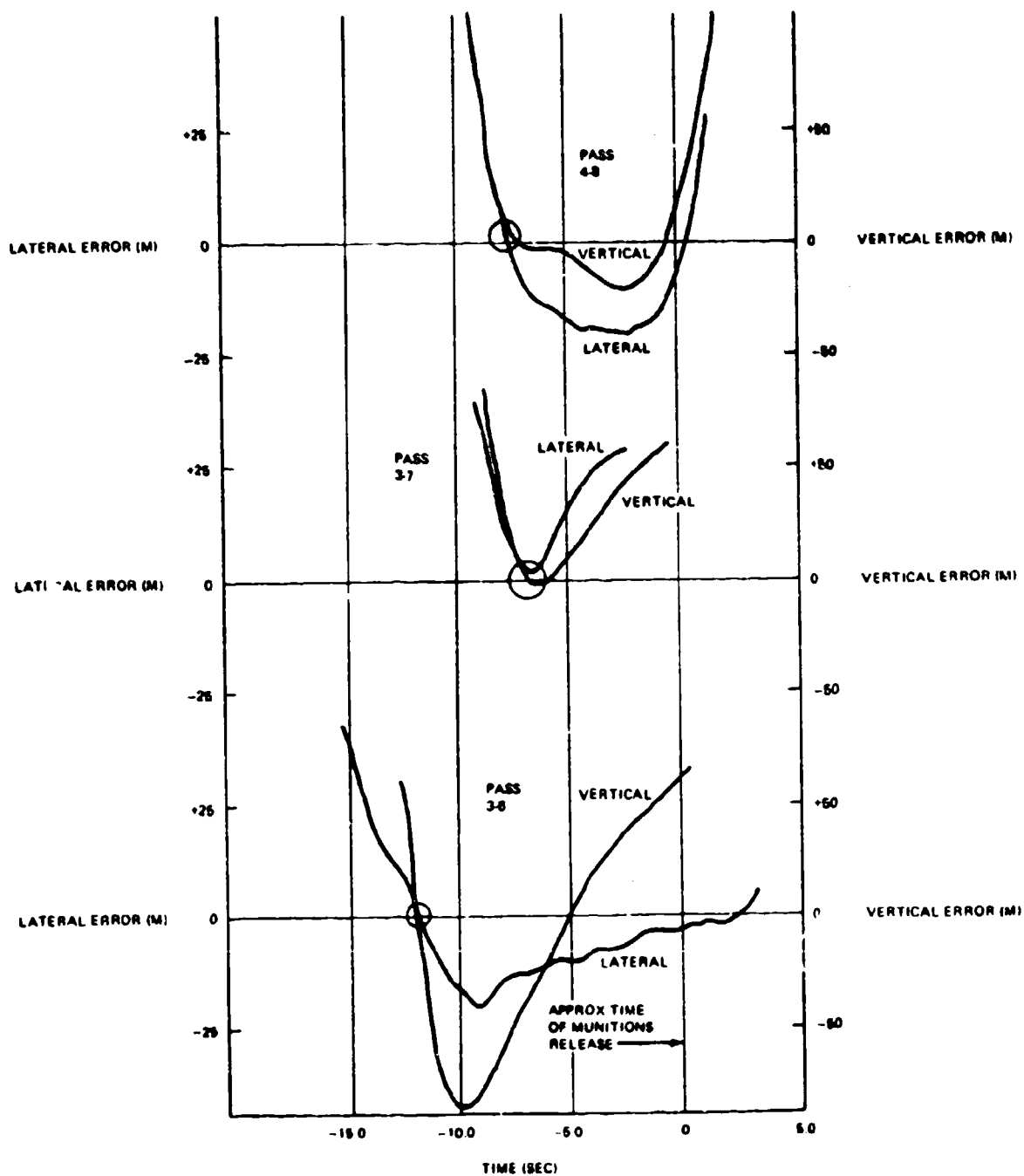
40001 08

Figure 4-36. Defense of Known Point Predictor Errors on Dive/Glide Bomb Flights 1, 3



40001-98

Figure 4-37. Defense of Known Point Predictor Errors on Dive/Glide Bomb Flight 4



40001 100

Figure 4-38. Defense of Known Point Predictor Errors on Pop-Up and Dive/Glide Bomb Passes

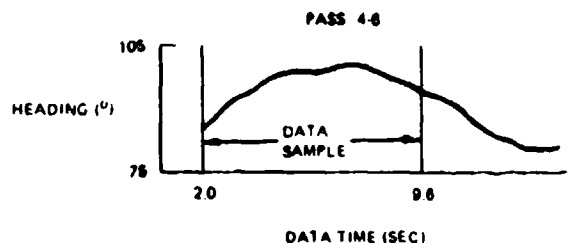
Subsequent computations by Frankford Arsenal localized the oscillatory component to angle tracking. On most paths, range noise was essentially white. The source of the oscillatory component is not known, and its period and magnitude were large enough to interfere with attempts to examine the "microstructure" of the target path perturbations.

The raw radar data was smoothed by Frankford, but the smoothing was insufficient to remove all of the radar noise. A rough estimate is that the residual radar noise had an amplitude and spectral content sufficient to prevent reliable inferences about target accelerations less than about 0.20 g.

4.8.2 Effect on Prediction Error Statistics

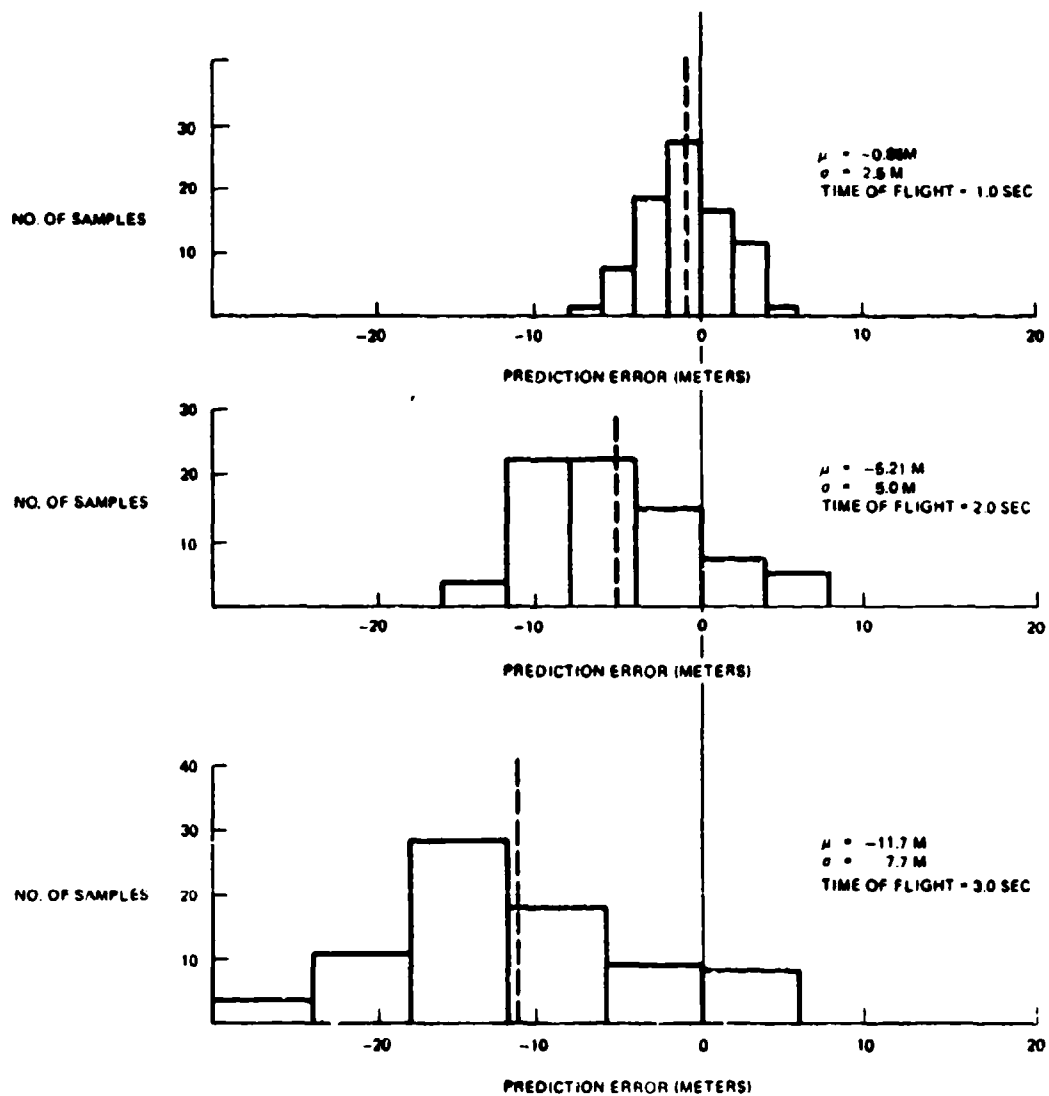
For a short segment of Pass 4-6 during which heading changed as shown in Figure 4-39, the Frankford computations of downrange prediction error over a 7.6 second segment at 0.1 second intervals were developed as histograms for 1, 2, and 3 second times of flight. These are shown in Figure 4-40. Figure 4-41 shows the mean and standard deviation about the mean for this data set as a function of time of flight. The mean increases as the square of time of flight. The standard deviation is proportional to time of flight, which would be expected if it resulted from radar noise. The corresponding estimate of standard deviation of velocity is 2.5 meters/second.

If this value of 2.5 meters/second is assumed characteristic of any data point, the standard deviation resulting from residual radar noise would equal the displacement of the mean prediction error caused by target maneuver, when the maneuver equalled about 0.18 g, and maneuvers up to 0.36 g would be imbedded in the 2σ band.



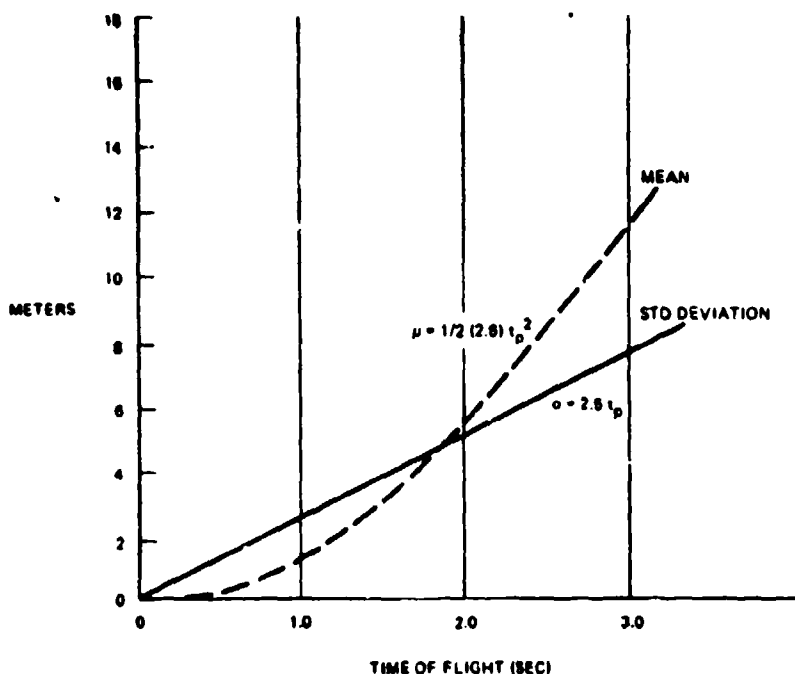
40001-101

Figure 4-39. Heading vs. Time for Data Sample



40001 102

Figure 4-40. Histograms of Down-Range Prediction Error on Pass 4-6 Segment



40001-103

Figure 4-41. Mean and Standard Deviations of Down Range Linear Prediction Error of Pass 4-6 Segment

On the other hand, during evasive maneuvers the target accelerations are many times greater than those associated with sensor noise. Figure 4-42 shows how the major accelerations rise above the noise (but with a shape distorted by noise), and Figure 4-43 shows corresponding estimates of rate of change of acceleration. "White noise" is sometimes used as an approximation to rate of change of target acceleration. This is clearly not correct for high acceleration regions, and the question of whether it is a fair representation for the very low acceleration segments cannot be resolved from this set of FACT data because of the radar noise.

The prediction errors associated with the major acceleration peaks have been examined by reading error peak magnitudes at each of three times of flight for a number of error peaks. The results are shown in Figure 4-44. Each line corresponds to the same acceleration maximum on a particular pass. For each line, the maximum error is very closely proportional to the square of time of flight, as would be expected.

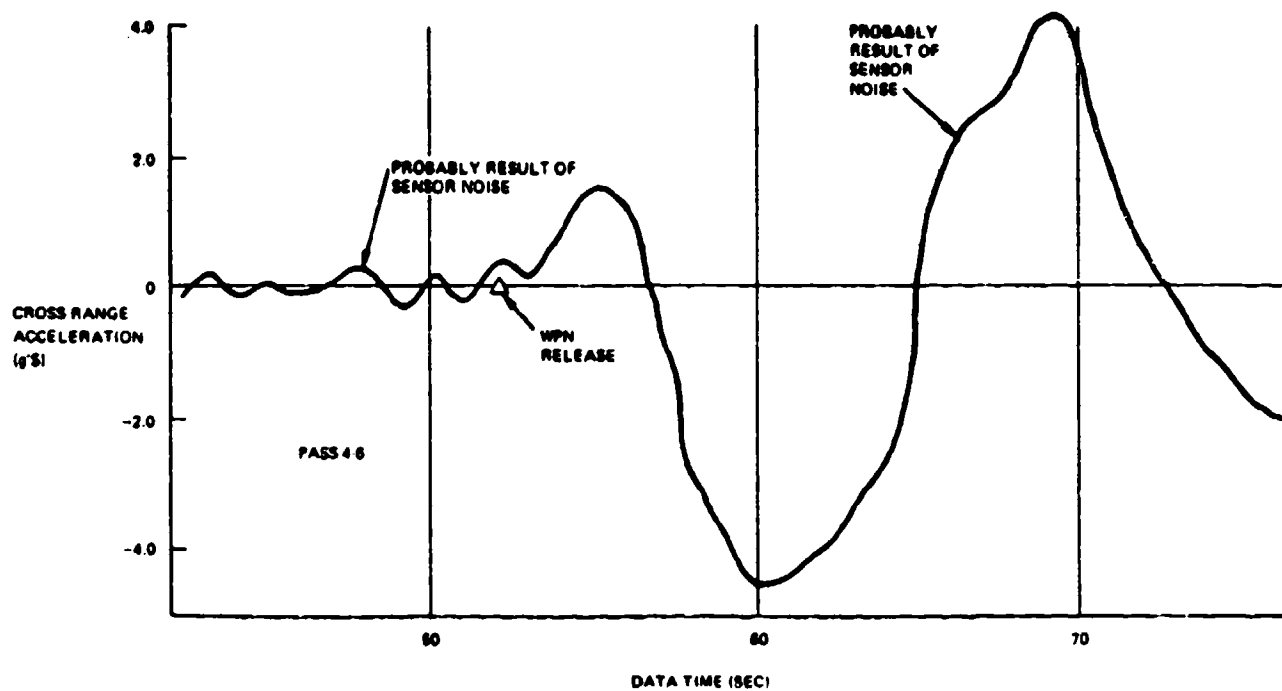


Figure 4-42. Estimated Cross-Range Acceleration vs. Time

40001.104

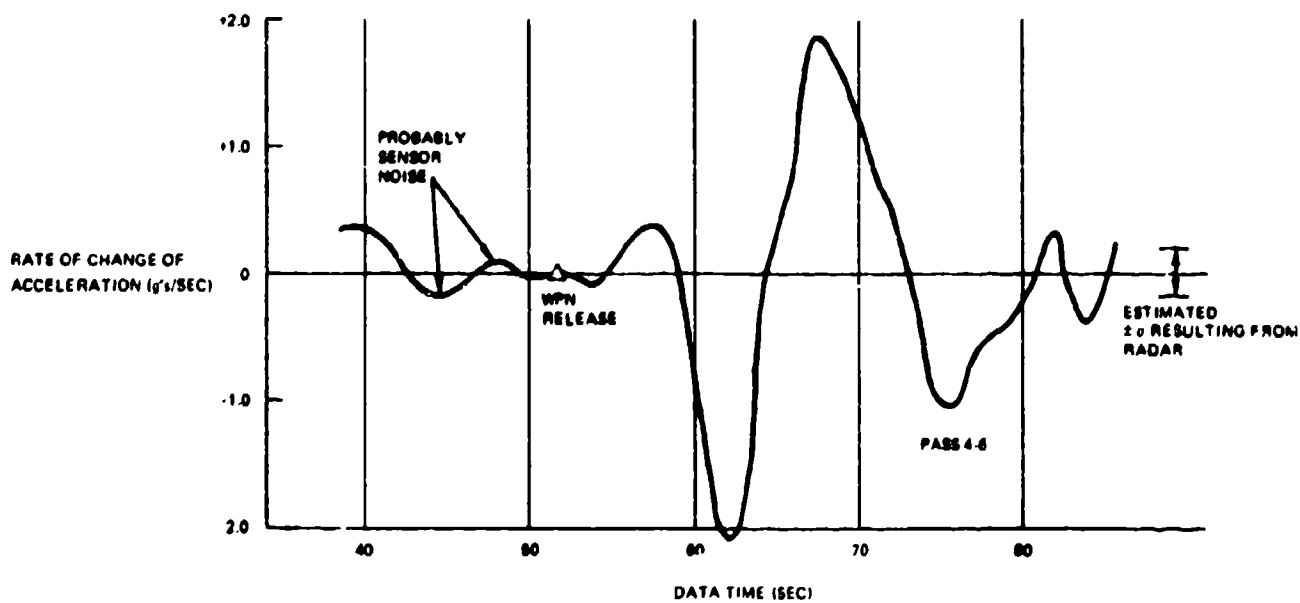
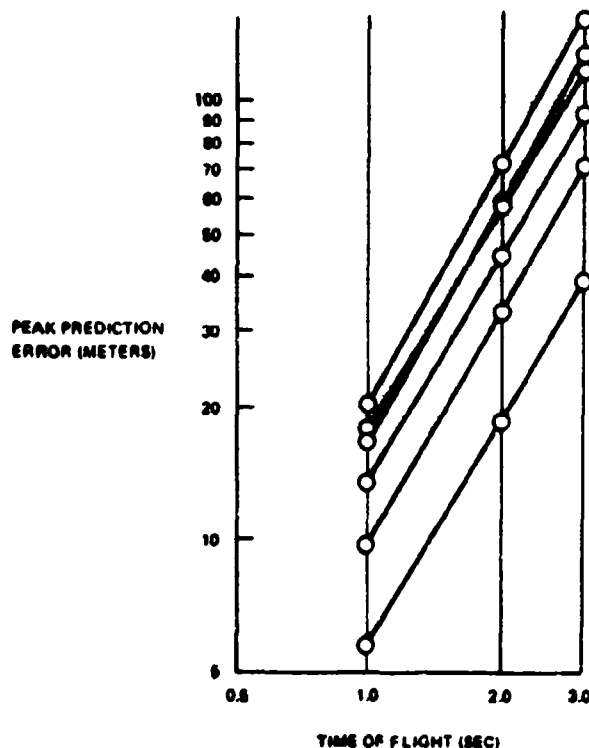


Figure 4-43. Estimated Rate of Change of Cross-Range Acceleration vs. Time

40001.106



40001-108

Figure 4-44. Peak Prediction Errors vs. Time of Flight for "Vigorous" Evasive Maneuvers

4.9 CONCLUSIONS

The FACT data currently available allows a number of important conclusions to be derived. Among these are

- (1) All of the attack modes on which data was taken contain relatively predictable, low maneuver segments, ranging in length from about 5 seconds to over 15 seconds. Hence one may be optimistic about the usefulness of predicted fire air defense systems.
- (2) The change of dive angle with time has a characteristic pattern, previously unknown (to the present writer at any rate) which may possibly be exploited in prediction algorithms.
- (3) The change of target velocity with time is closely related to the change of altitude with time in verification of the "conservation of energy" concept. Exploitation of this relation allows prediction errors along the flight direction caused by target acceleration to be removed without incurring the penalties of using an acceleration measuring filter.

- (4) Laydown delivery modes appear deadly to the attacker, if the defense can acquire and track the aircraft at low altitudes.
- (5) On the average, the "defense of a known point" algorithm in its simplest form is inferior to conventional prediction. However, it appears to possess a unique and unexpected capability of being almost exactly right in both coordinates (looking up the sight line) simultaneously at one point on each target path. Possible exploitation of this capability suggests further investigation.
- (6) High acceleration path segments show a surprising similarity across passes, in that turns tends to be at about the same rate on almost all passes for as long as 5 to 10 seconds, and rate of change of dive angle in the pull-up after weapons delivery is likewise at about the same value across passes. This consistency may be eliminated by special instructions to the pilots, but a pilot has so many functions to perform in an attack that elimination of these patterns may be difficult.

The major deficiency of the current data is that the sensor radar tracking noise prevents examination of small target accelerations during the relatively predictable flight segments. It was anticipated that this might be the case in setting up the experiments, but the risk was acceptable since the important question at that time was whether such segments existed at all. Existence having been confirmed, the microstructure is next in importance.

4.10 RECOMMENDATIONS

The FACT program should be a continuing effort as long as the military services retain an interest in air defense, since the data is basic to missile systems. The data is a requirement for the optimum design of predicted fire systems. It is also of value to missile designers.

The following data categories are recommended for acquisition and augmentations

- (1) Accelerometer records taken on-board aircraft flying attack paths similar to those reported on in this section. These records will allow analysis of the small aircraft accelerations which are masked by radar noise in the present data set.
- (2) Flight path records on attack helicopters. Aviation Week reports Soviet activity in this type of weapon system. The helicopter paths are expected to be quite different from jet aircraft paths.

- (3) Flight path records on aircraft delivering stand-off weapons, and the subsequent trajectories of the stand-off weapons. The launch aircraft path will depend on the type of weapon guidance, (guide all the way, launch and leave, etc.) and samples of each available type should be recorded. The stand-off weapons themselves are expected to have highly predictable trajectories, and if this is confirmed, definitive estimates of the probability of countering them directly with local defenses can be made.

Field evaluations of predicted fire systems, of which a number are now planned (HITVAL, GLAADS evaluations and others) should be exploited, both to augment the data base on flight trajectories and because the evaluation in each case can be improved by determining what fraction of the system error is attributable to flight path characteristics alone.

Finally, a standard set of FACT paths should be maintained and continuously updated for use in developing and demonstrating new prediction algorithms. The simple linear predictors used in the present report suggest an approach that may be developed. The data can, in FACT, be issued as a challenge to prediction algorithm designers to provide an objective means of comparing the effectiveness of any candidate prediction algorithm.

SECTION 5

COMPARISON OF GUN, ROCKET AND PREDICTED-CORRECTED ROCKET-ASSISTED PROJECTILE SYSTEMS

5.1 INTRODUCTION

Unguided rockets have a long history of successful application in surface to surface, air to surface and air to air roles. The origins of successful ground to ground applications lie centuries in the past, and "the rocket's red glare" refers to the use of Congreve rockets in the siege of Fort McHenry in 1814.⁽⁵⁾

Unguided rockets in air defense applications have a combat history of relative ineffectiveness, beginning with World War II. Limitations on production rate of antiaircraft guns caused the British to turn to rocket batteries to supplement the home defense against bombers. An anecdote, unverified, regarding this use of UP (unrotated projectile) batteries is that the first experimental battery shot down a German raider over London with its first salvo. UP batteries were then produced in large quantities, and were never again credited with kills.

It was reported⁽¹⁰⁾ that a 3.7" antiaircraft gun battery required 332 men to service 8 barrels, but a rocket battery required only 274 men to service 128 barrels. Hence one got a lot of action with limited manpower, and equipment which was considered to require less precise manufacturing facilities.

The principal disadvantage of the unguided rocket in the air defense role has been its large angular and time of flight dispersion, as compared with gun fired projectiles. It has a unique advantage in its ability to project a warhead at very high velocities from relatively lightweight ground launch equipment. The rocket also develops a lower maximum acceleration for a given burnt velocity than that experienced by a gun fired projectile with equivalent muzzle velocity, and in the early days of proximity fuzes and guidance electronics, more fuze options were available to rockets, and of course, the first few decades of guided missilery used rocket vehicles.

A natural line of development is to attempt a compromise between the rocket and the gun, utilizing the efficiency of the gun for an initial boost, and the fact that rocket velocity is additive, to obtain high velocities with relatively lightweight launch equipment. The range of options extends from simple closed-end tubes for rocket launch through gun-boosted rockets to rocket-assisted projectiles, with the fraction of total velocity provided by the

rocket decreasing in the same order. Currently, rocket assisted projectiles (RAP) to extend the maximum range of existing artillery pieces in surface to surface fire are operational.

One should also include the "travelling charge" concept in conventional guns as a sort of gun-boosted rocket. In this concept the propellant charge is attached to the projectile base and more of the propellant energy is acquired by the projectile, rather than being lost to acceleration of the propellant gases, than is the case with propellant burning in the chamber of the gun. Apparently this concept has not yet attained operational feasibility.

Gun boosted rockets experienced a short period of developmental activity in the 1940-1950 period, and among the developments which attained field test stature was a system firing 2.75" spin rounds from a gun with moderately high rate of fire. This weapon was installed in an aircraft and tested in combat in Korea. A field artillery application was also field tested. These developments stopped when it was believed that guided missiles would be a preferred solution.

Currently the Javelot gun-boosted rocket system represents the sole entry of its type in the competition for predicted fire antiaircraft defense systems.

A system type that is occasionally proposed utilizes a battery of rockets, all of which are fired in salvo at a single predicted point. Porcupine apparently included this type of launcher as one of its weapons options. An advantage is that the rate and acceleration requirements on the servos to lay the mount can be relatively low, and the launcher may be relatively low cost. A disadvantage is that there is a limited flexibility in choosing the firing point, and no opportunity to average across unfavorable target path segments, as a continuous fire system does. This system type will not be considered further in the subsequent paragraphs.

In the following paragraphs, an attempt is made to appraise the relative advantages and limitations of guns, gun boosted rockets, and rockets in an air defense role. The major uncertainty is the degree to which the original rocket handicaps of angular and time of flight dispersion can be reduced using the best modern technology. It turns out to be difficult to make a case for the gun-boosted rocket until these values can be made competitive with those attainable with conventional guns.

A relatively unexploited system type for air defense, however, consists of a gun fired projectile with in flight trajectory correction. Occasional attempts to activate a system of this type in the past have been negated by the success of guided rockets. However, the costs of air defense guided missile systems, as reviewed in Section 8, have escalated

to the point where a reexamination of this system type seem appropriate, and an outline of possible concepts and potential is developed in the final paragraphs of this section.

A qualitative comparison of system characteristics is provided in Table V-1. Subsequent sections provide quantitative data on the listed parameters, to the degree such data is available, as well as simple estimating relationships for parametric comparison.

5.2 COMPARISON OF CHARACTERISTICS

In the following paragraphs, some of the constraints and performance capabilities of gun, rockets and hybrids are compared, to attempt to identify unique advantages of rocket and hybrid systems.

5.2.1 Muzzle Energy of Guns

This index is of value in comparing guns, since there is a rather well defined upper limit to the muzzle energy that can be developed in a specified gun tube.

Define:

E_0 = muzzle energy

C = caliber

P_{max} = maximum design pressure

L/n = gun length in calibers.

P_{max} has increased from about 38,000 psi in 1900 to present day values of about 60,000 psi. L/N over the same period has increased from about $L/35$ to the $L/90$ of the Oerlikon 35mm AA weapon. The increase in muzzle energy associated with these improvements is about the same as that associated with a 1.5 increase in caliber.

The acceleration of the projectile in the tube is given by

$$m \, dv/dt = p(t) \, A \quad (5.1)$$

where

m = projectile mass

v = velocity

p = pressure on the projectile's base

A = sectional area of the projectile (tube bore)

Table V-1. Qualitative Comparison of System Characteristics

System	Gun	Rocket Assisted Projectiles to Gun Boosted Rockets	Rocket
Angular Dispersion of Projectile (mils)	<1.0	Intermediate	4-7
Velocity Dispersion (%)	<0.5	Intermediate	1-3
Maximum Practical Velocity (m/s)	1200 (Full Caliber) 2000 (Sub-Caliber)	4500 m/s	3000 m/s (Without Staging)
Erosion of Tube at High Velocity	High	Intermediate	Very Low
Heating of Tube	High	Intermediate	Very Low
Complete Round Wt. for Very High Velocity and Effective Payload	High	Lowest	High
Cost per Round of Ammunition	Moderate	Highest	Moderate
Recoil Force	High	Intermediate	Low
Weight of Gun or Launcher and Platform with Servos	High	Intermediate	Moderate
Rate of Fire	Very High	Depends more on design ingenuity than on system type	
Reload Time	Depends more on design ingenuity than on system type		
Fire Control and Sensors	Same requirement for all predicted fire systems		
Crew	Probably same requirement for all predicted fire systems		

Integrating this expression, muzzle energy E_0 is obtained as

$$E_0 = \eta p_{\max} (\pi/4) C^3 (L/n) \quad (5.2)$$

where

$$\eta = p_{\text{average}}/p_{\max} \quad (5.3)$$

$$\eta = (L p_{\max})^{-1} \int_0^L p(x) dx \quad (5.4)$$

and

C = caliber

L/n = gun length in calibers

L/n is normally measured from the face of the breech to the muzzle, hence it is greater than the actual projectile travel. However it is remarkable that values of η in the neighborhood of 0.50 are obtained for guns of all vintages of this century, implying a maximum potential future gain of a factor of only 2.0 in muzzle energy if p_{\max} could be held constant and the full caliber length L/n were available for its application.

The energy expression can be written in the form

$$(4/\pi) E_0 / C^3 = \eta p_{\max} (L/n) \quad (5.5)$$

in which case both sides have the dimensions of pressure.

Data have been assembled from open sources ① ② ③ ⑦ on a large number of guns whose parameters span the following ranges

- a. Design vintage: 1890 to modern
- b. Caliber: 0.30" to 16.0"
- c. Muzzle velocity: 1500 f/s to 5300 f/s

- c. Length in calibers: $L/10$ to $L/140$ (two heavy 12" seacoast mortars of 1890 vintage are included to fill in the low end of the L/n range)
- d. Projectile weight: 0.0007 lb to 2340 lb
- e. p_{\max} : 33,000 psi to 70,000 psi
- f. Muzzle energy: 2246 ft lbs to 264,900,000,000 ft lbs.

Figure 5-1 shows $(4/\pi)E_0/C^3$ plotted vs $p_{\max}(L/n)$ as a scatter diagram for the data collected. Considering the range of individual parameters, the small scatter shown by the points is remarkable.

An estimating relationship which fits the trend of the data is

$$E_0/C^3 = 0.912 \left[\left(\frac{p_{\max}}{40,000} \right) \left(\frac{L/n}{80} \right) \right]^{0.82} \times 10^6 \text{ psi} \quad (5.6)$$

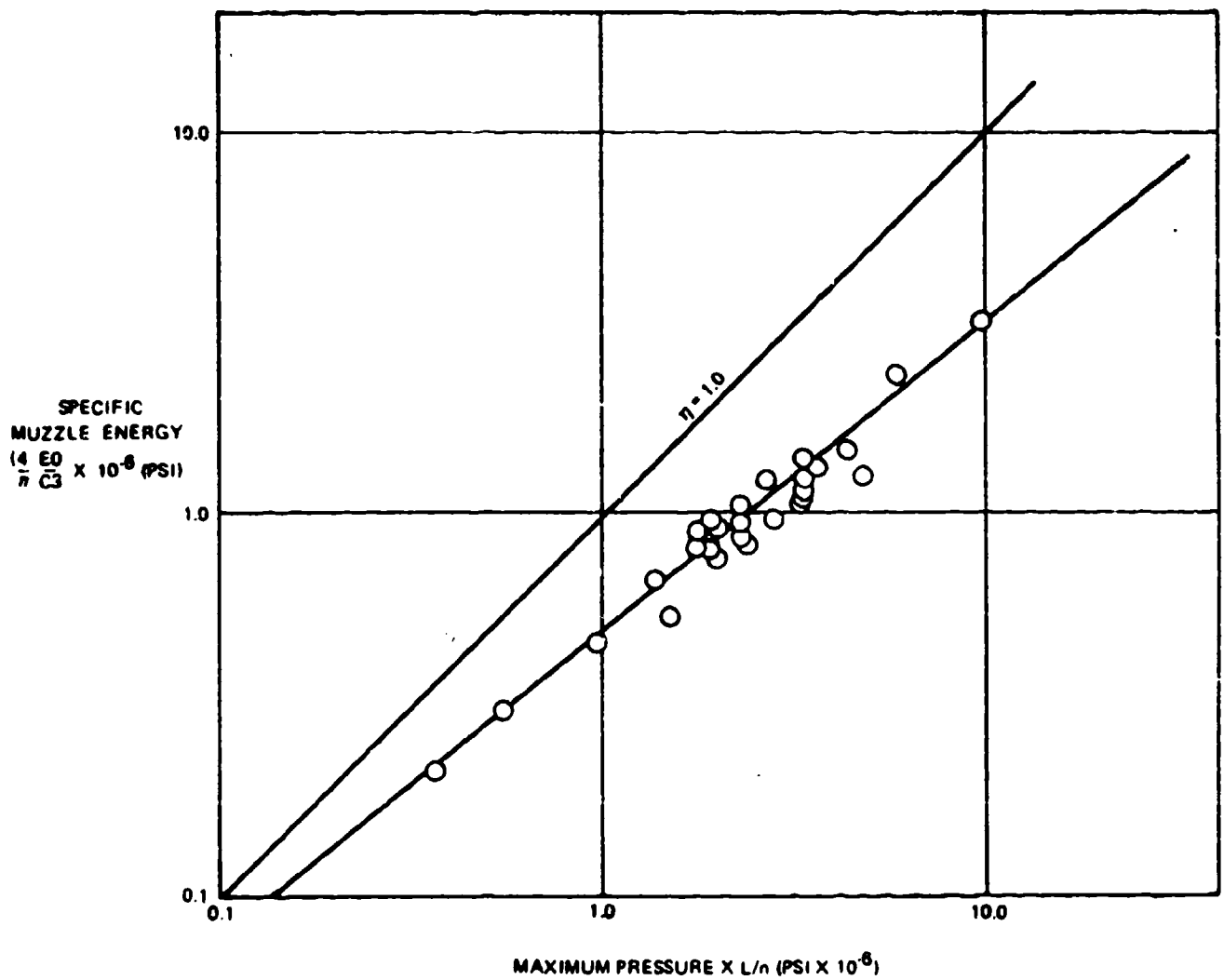
where L/n is dimensionless and p_{\max} is in psi.

All of the points are for guns firing full caliber rounds; the highest velocities represented are 3855 f/s (Oerlikon) and 5200-5500 f/s (German $L/140$ Paris Gun of WWI). Above about 4000 f/s one should probably apply a correction for the loss of energy to the powder gases, in which case the estimating relationship would be slightly modified. On the other hand, no such trend was observed to rise above the scatter in a separate computation, within the velocities available.

The important observation is that given a p_{\max} , a caliber length, L/n , and a caliber C , the muzzle energy which the designer has available to allocate between projectile weight and muzzle velocity is constrained within fairly well defined boundaries. The easiest way to get more muzzle energy is to increase the caliber; on the other hand, advances in materials and design and construction methods over the years have allowed a steady improvement in p_{\max} in usable L/n , hence in muzzle energy in a given caliber.

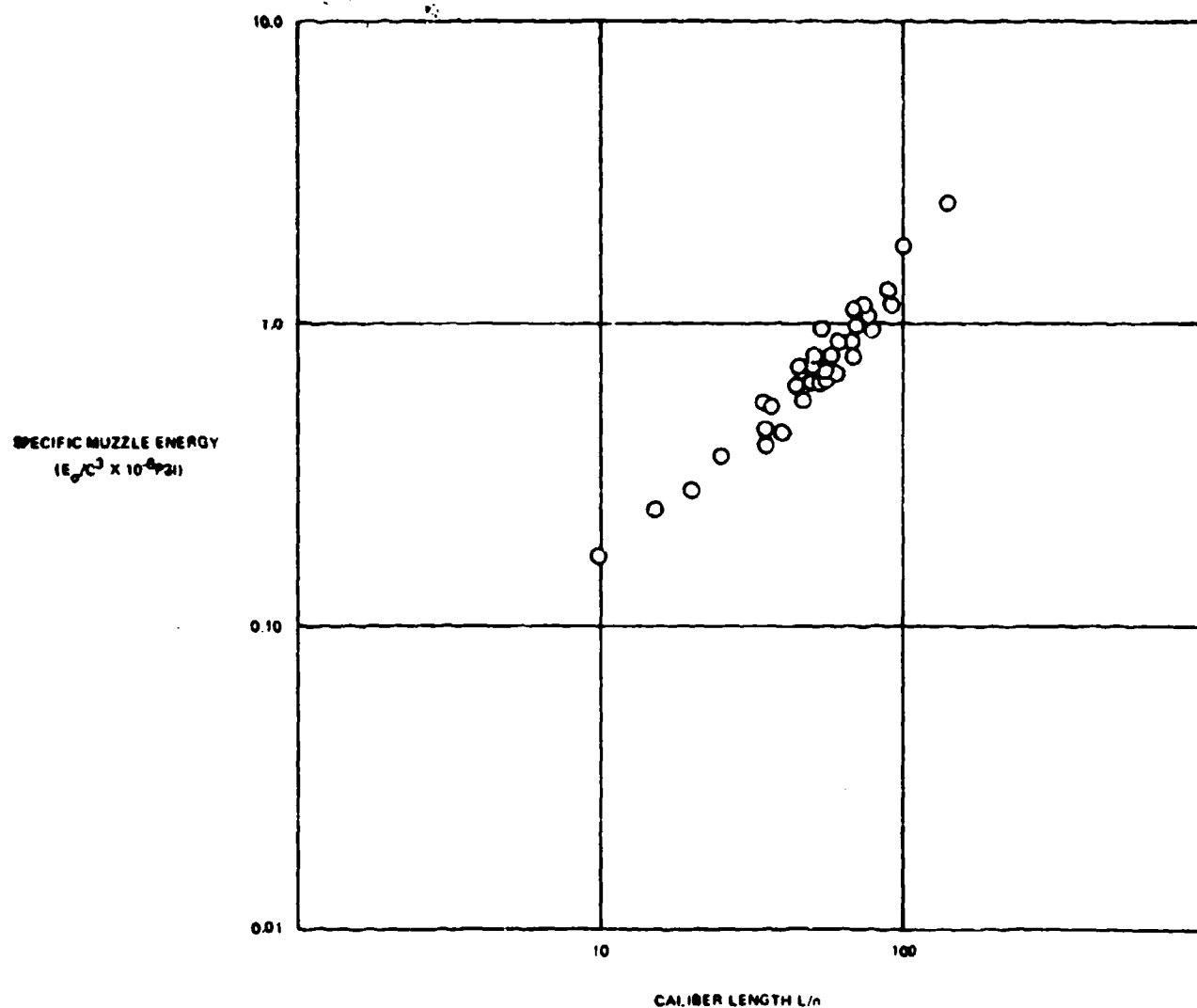
Increase in p_{\max} is correlated with increase in L/n because of interior ballistic constraints. As a result of this correlation it is possible to show E_0/C^3 vs L/n alone with small scatter, as in Figure 5-2.

The really great advances in gun tube design do not appear in these scatter diagrams, they appear in the great reduction in tube weight over the years, in spite of the increase in p_{\max} , and in increased tube life.



40001-107A

Figure 5-1. Specific Muzzle Energy of Guns versus Maximum Pressure and Caliber Length



40001-108

Figure 5-2. Specific Muzzle Energy of Guns versus Caliber Length

To a non gun designer, it would be interesting to fit the data points by least squares to the estimating relationship

$$v_0 = w_p^{\alpha} C^{\beta} p_{\max}^{\gamma} (L/n)^{\delta} \quad (5.7)$$

and the scatter would be reduced somewhat. Gun designers would no doubt prefer to do a proper design analysis.

The results of some design studies for gun-launch of multi-stage meteorological rockets by Murphy,⁽⁹⁾ are shown in Figure 5-3 for caliber lengths up to $L/300$, and muzzle velocities exceeding 6500 f/s. The gun assumed as a 16.7" smoothbore. Experimental results of firing in this program with a smaller caliber gun will be found in reports on the HARP program.

5.2.2 Velocity vs. Propellant Weight

An approximate relationship among propellant weight, projectile weight, and muzzle velocity for guns is obtained by defining a specific energy E_s (ft lbs/lb) for the propellant, and assuming that this is divided between the projectile and propellant gases, with other losses to friction, heating, etc., absorbed in the second term.

At the muzzle

$$w_{\text{prop}}(gE_s) = (1/2)w_p v_0^2 + k_2 w_{\text{prop}} v_0^2 \quad (5.8)$$

The coefficient k_2 is sometimes taken as $1/6$, or pessimistically, as high as $1/4$. Using the value $1/6$

$$w_{\text{prop}}/w_p = \frac{v_0^2}{v_s^2 - (v_0^2/3)} \quad (5.9)$$

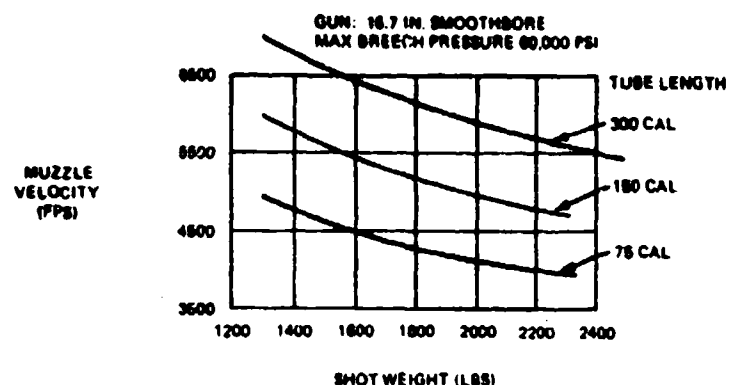
where

w_{prop} = weight of propellant

w_p = weight of projectile (including sabot weight for subcaliber rounds)

v_0 = muzzle velocity

$v_s = (2gE_s)^{1/2}$



40001-100

Figure 5-3. Muzzle Velocity vs. Shot Weight and Caliber Length for Design Series

This expression implies a maximum muzzle velocity of

$$v_{\max} \approx (3)^{1/2} v_g \quad (5.10)$$

for very light projectiles.

Figure 5-4 shows the ratio of propellant weight to projectile weight for a large number of gun/propellant combinations. All are full caliber solutions with the exception of the Dardick HIVAP "Tround".

The low velocity points are for howitzers where there is no great emphasis on minimizing the already small propellant weight. The points close to the lower boundary of the sketched envelopes are for modern high performance automatic weapons. The Dardick HIVAP gun⁽¹³⁾⁽¹⁴⁾⁽¹⁷⁾ is of a radically different design from the other guns. It is an experimental model with extremely high rate of fire, and "open breech" configuration. The Hutton 0.22-378⁽¹¹⁾ is a hobbyist's single shot weapon built to demonstrate to disbelievers that adding powder always increases velocity, until the tube blows up. (Known in the hobby press as the Hutton "Eargeshplitten Loudenboomer" it used 108 grains of powder and a 15 grain Cal 0.22 bullet to get 7200 f/s, 'until the barrel burned out'.)

The muzzle energy developed by a projectile, as a fraction of the total obtained from the propellant is obtained from (5.8) as

$$E_0/E_m = [(1/2)w_p v_0^2] / (gE_s w_{\text{prop}}) \quad (5.11)$$

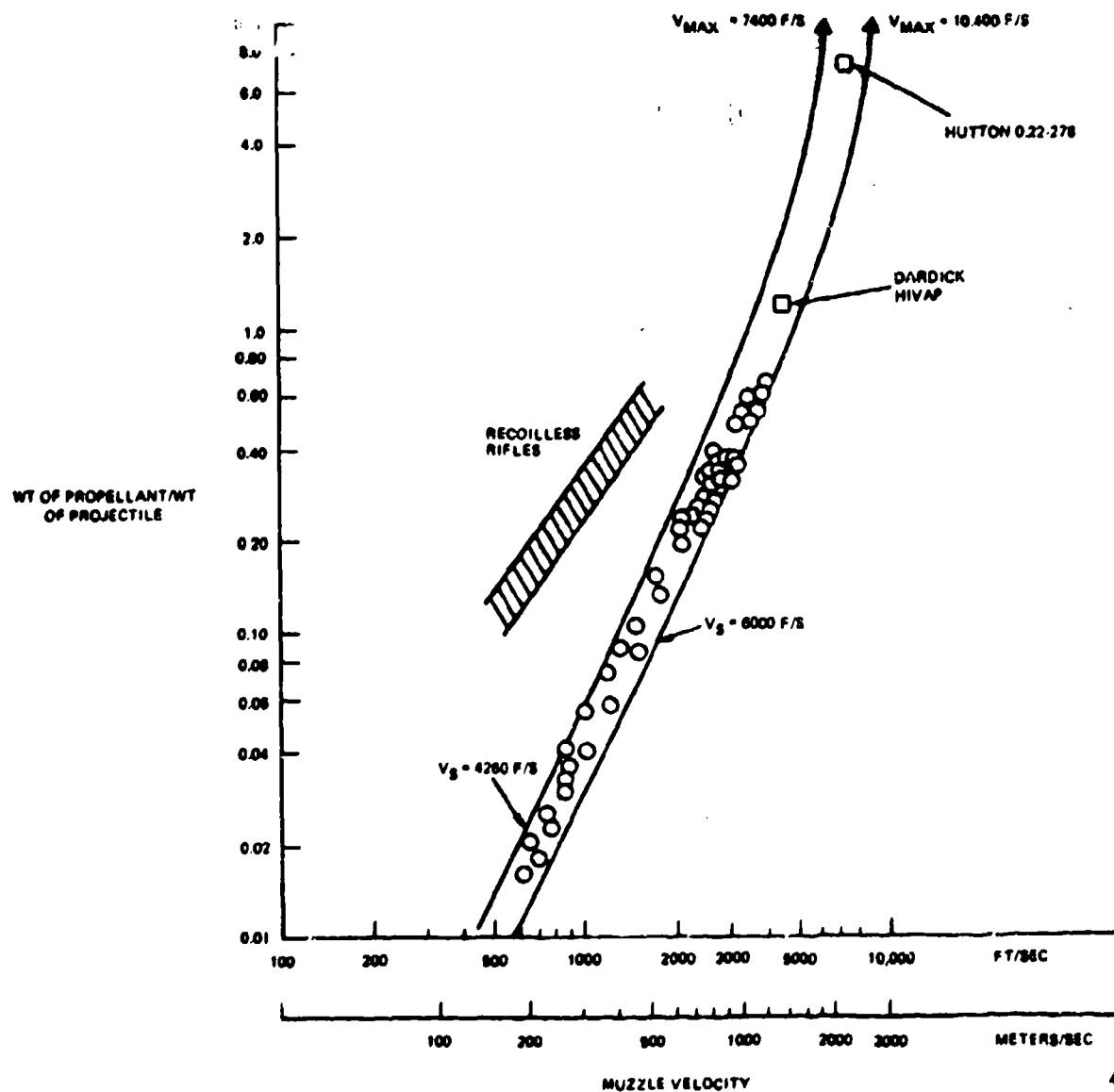


Figure 5-4. Propellant Weight/Projectile Weight versus Muzzle Velocity for Conventional Guns and Recoilless Rifles

$$E_0/E_m = 1 - (v_0/v_{\max})^2 \quad (5.12)$$

The band sketched in Figure 5-4 for recoilless rifles shows the penalty paid in propellant/projectile ratio for diversion of some of the propellant gases to recoil reduction.

Rocket data are more tedious to assemble from open sources than gun data because of the off and on vagaries of rocket development programs. Table V-2 summarizes a limited amount of data generally from Jane's Weapon Systems and the International Defense Review. ⁽¹²⁾⁽⁷⁾⁽¹⁹⁾

Note the entry for the German WWII "Fliegerfaust". ⁽²⁷⁾ This relatively unknown weapon consisted of a shoulder fired launcher containing nine 20-mm rockets which were intended to be fired in air defense in two salvos of five and four rounds each, spaced by one-tenth second.

Data on gun boosted rockets are even more limited, and a few examples are given in Table V-3. Javelot and ACRA ⁽¹⁾⁽³⁰⁾ are modern systems, the latter employing both unguided and guided projectiles with gun boost and rocket sustainer. The artillery RAPs are also modern, intended to extend the range of conventional artillery pieces. The T131 is a member of a family of weapons designed along gun lines in the 1940-50 era.

The differential equation for rocket acceleration during burning may be written approximately as

$$m dv/dt = v_e dm/dt - D(v) \quad (5.13)$$

where

m = rocket mass (time varying)

v = velocity

v_e = a "characteristic" velocity of the propellant gases

$D(v)$ = drag force

v_e is defined in terms of a "specific impulse" I_{sp} (sec) of the propellant by

$$v_e = g I_{sp} \quad (5.14)$$

Table V-2. Characteristics of Free Rockets

Rocket	Dia (mm)	Length (mm)	L/D	Launch Wt (Kg)	Propellant Wt (Kg)	Warhead or Payload Wt (Kg)	Burnt Velocity (m/s)	Burnt Wt (Kg)	Burn Time (Sec)	Payload or WHD/Initial Wt	Burst/Initial Wt	Imp (Sec)	Accuracy	Sub-Blastion
Bofors	135	3226	24	43.5		19	600		2.0	0.436				
Hispano-Derithon R-80	80	1060	13	14	3	3 (HE)	5-12	11	0.56	0.214	0.79	240	10 Mils CEP	Fin
Sura	80			11		3							2 Mils	Fin
Hatchless Brandt	100	2480	25	38		14	760			0.368				Fin
Saab 251P	68	834	12	4.3		1.05	800			0.244				Fin
253	68	911	13	5.06		1.8	600			0.356				Fin
256P	68	911	13	6.25		3.0	450			0.480				Fin
Rap-14	140	2000	14	54		19 (5.5 HE)	~700		2.0				~5 Mils	Fin
Sammari	76	1200	16	10.8		3	1100			0.292		300 (LJQ)		Fin
Tafun (W-11)	100	1917	19	29.5	9.4	0.5 (HE)	975	19.3	2.5		0.66	(LJQ)		Fin
Super Loki Booster	102	1988	19	Booster 23.1	17.1		3040E	6.1	2.11	0	0.283	232		Fin
Robin Dart	41			29.3		6.14	1815	12.2	2.11	0.210	0.417	232		Fin
Inst Dart	54			31.1		8.30	1830	14.0	2.11	0.266	0.452	232		Fin
S' Hvar	127	1828	14	64	10.9	3.3 (HE)	421	53.1	0.18					Fin
Zuni	127	2794	22	48.6			~900							Fin
Nighty Mouse	70	1219	17	6.2		4.5	884		1.5	0.555				Fin
R-115	115			17.5	3.1	1.35 (HE)	~460	14.4	0.5		0.823			Spia
FB R-127	127			44	8.3		~460	35.7	0.8		0.811			Spia
Fliegerfaust	20			0.24			310							Spia

Table V-3. Characteristics of Gum-Boosted Rockets

Type	Cal (mm)	Complete Round Wt (Kg)	Projectile (Rockets) Wt (Kg)	W. proj W. round	Missile Velocity (m/s)	Rocket Velocity Increment (m/s)	Burst Velocity (m/s)	Stab	Fire Doctrine	Launch Load (Rounds)	Wtd (KG)	CDI	Country
T212 (2.75) (T110 Gun)	70		2.4		345	400	765	Spin	Automatic Cannon			0.40	US
Javelot AA	40				Super Sonic			Fin	Salvo of 4, 8, 12	24 tubes			France
ACRA Anti Tank Unguided Round Caliber Round	142	21	15	0.71	550	150	700 at 1KM 506 AV	Fin			2.0 (DE) 2.5 (DE)		France
T212					2 Mile Dispersion Estimate					24 tubes			US
5"/50 5"/54 (US Navy)	127							Spin Spin	Arty Arty				US Navy
XM549 Artillery	155							Spin	Arty				US Army
XM548 Artillery	105				550		0.45 Kg of Propellant	Spin	Arty		2.5 (DE)		US Army

The effective value of I_{sp} to use in this approximation depends on air density. For a particular solid propellant rocket, $I_{sp} = 245$ seconds at sea level, as compared with 280 seconds in a vacuum.

Stutz, in a book dated 1959 suggests that for solid propellant I_{sp} may be in the range 150 to 240 seconds, and that liquid propellants may have I_{sp} in the range 200 to 350 seconds. A great deal of propellant research and development has been done in the space and anti-ballistic missile programs which may not have been yet exploited for application to more mundane rockets. Hence the Stutz figures are probably quite conservative.

Eq. 5.13 can be integrated in closed form for only a few functional approximations to the drag function. Performing the integration formally, one obtain

$$w_b/w_o = e^{-(v_b + \Delta v)/v_e} \quad (5.15)$$

where

w_b = rocket weight at end of burn

w_o = initial weight

v_b = incremental velocity over initial velocity (initial velocity is zero if fired from rest, positive if fired from gun-boost)

Δv = velocity loss to drag

$$\Delta v = \int_0^{t_b} \frac{D(v)}{m(t)} dt \quad (5.16)$$

where

t_b = burn time

Δv will be small for short burn times. For the "Super-Loki Dart" listed in the table, it reduces the burnt velocity by about 10% from the zero drag value.

The weight of propellant is

$$w_{\text{prop}} = w_o - w_b \quad (5.17)$$

Hence

$$w_{\text{prop}}/w_b = e^{(v_b + v)/v_e} - 1 \quad (5.18)$$

and ignoring Δv , for small values of w_{prop}/w_b

$$w_{\text{prop}}/w_p \approx v_b/v_e \quad (5.19)$$

Compare this with the corresponding gun expression

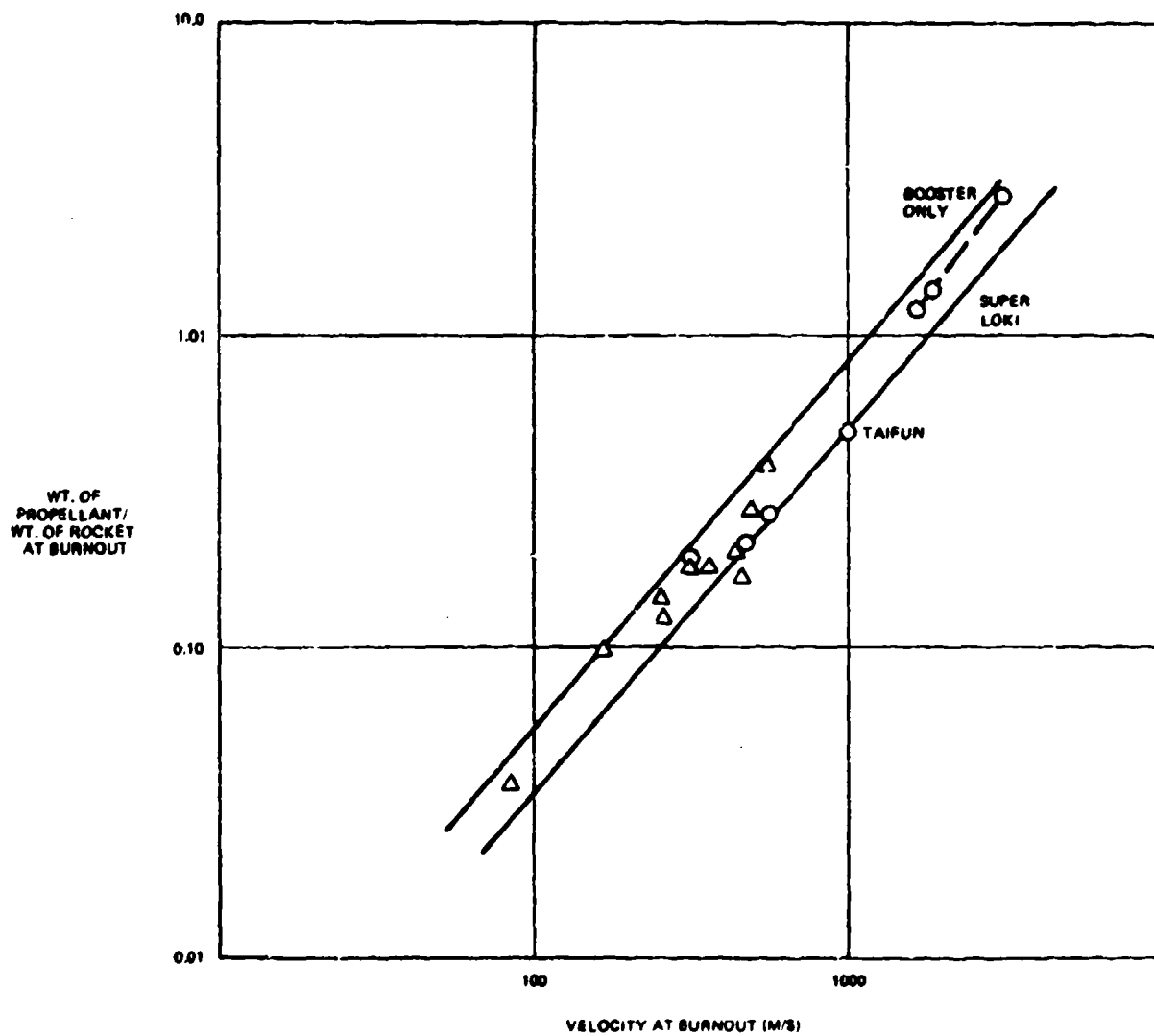
$$w_{\text{prop}}/w_p = (v_o/v_s)^2 \quad (5.20)$$

Clearly, for low muzzle or burnt velocities, the gun uses propellant far more efficiently. On the other hand, for high velocities, the square law overtakes the linear law, and the rocket uses propellant more efficiently. Moreover, since the rocket expression applies to incremental velocity, a combination gun plus rocket can in principle take advantage of gun efficiency for boost, and rocket efficiency for the final velocity increase.

Figure 5-5 shows a scatter diagram of the ratio of propellant weight to weight of the projectile at burnout for a number of rockets as a function of velocity at burnout. The triangles are World War II rockets not listed in Table V-2. The approximately linear variation of the ratio with burnt velocity is clear.

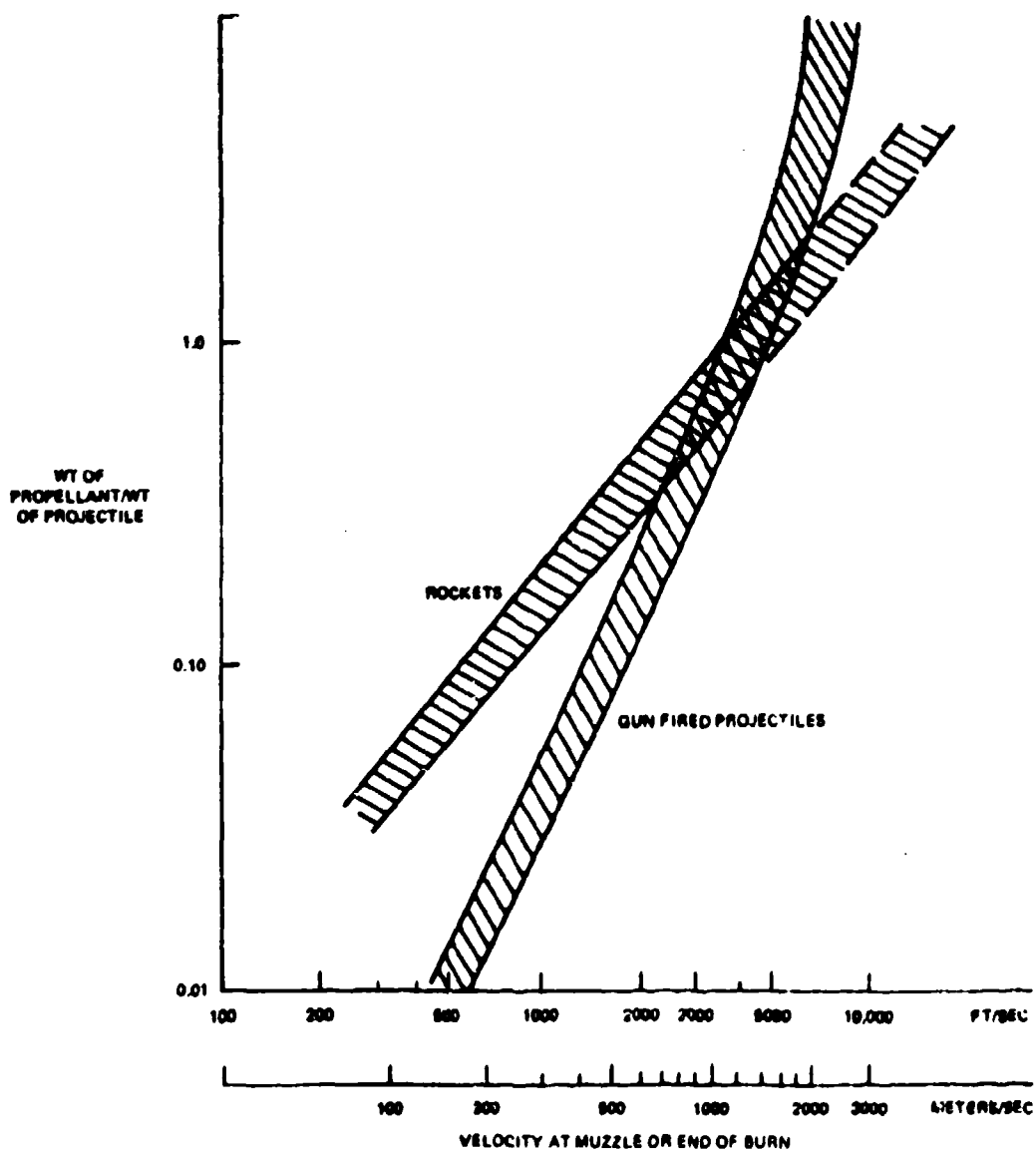
In Figure 5-6 gun fired projectiles and rockets are compared with regard to efficiency of using propellant as a function of velocity. The bands cross at about 4000 f/s.

However this index overemphasizes the comparative efficiency of the rocket, since burnt weight is used as a parameter. Burnt weight includes the weight of the motor case,



40001-111

Figure 5-5. Propellant Weight/Weight at Burnout versus Burnt Velocity for Rockets



40001-112

Figure 5-6. Comparison of Propellant Weight Requirement for Rockets and Gun Launched Projectiles

which probably contributes little to terminal effect. The gun fired projectile, on the other hand is practically all "effective weight". On the other hand, the index does not penalize the gun fired projectile for the weight of the cartridge case where one is used to contain the powder.

The efficiency of the gun's use of propellant can be further increased by attaching the propellant to the base of the projectile. This is known as the "travelling charge" and has been investigated at least as far back as German work in World War II. To the present date no practical solution of the associated design problems has been achieved.

Effective utilization of very high propellant to projectile weight in guns by conventional solutions require sophisticated interior ballistic design. Muzzle velocity dispersion is adversely affected by relatively short travel in the tube after the all-burnt point is reached. Angular dispersion and projectile yaw at launch are adversely affected by exhaust pressures which are very high above atmospheric. Burning which persists too long increases muzzle flash, - the gun is sometimes said to "spit powder". Small arms hobbyists often use relatively high charge to projectile weight ratios to obtain high velocities and if one plots charge to weight ratio vs. muzzle velocity from such sources one notes that the associated comment "excessive flash" is associated with ratios lying outside the band of Figure 5-8.

5.2.3 Complete Round Weight vs. Velocity

Use of a cartridge case for gun fired projectiles, and a motor case and nozzles for a rocket impose weight penalties. A few values are given in Table V-4.

Cartridge cases have become progressively lighter over the years. Aluminum cases allow about a 30% weight reduction, but there have been design and operational problems which have retarded their adoption. Caseless ammunition for guns has been under development at least since the German work in World War II, and a modern application is to the GAU 7A gun system for aircraft. ⁽¹⁶⁾

Caseless motors for rockets represent an interesting challenge. No feasible solution appears to have been proposed.

If one assumes that the cartridge case weight for gun fired projectiles, including igniter, is about proportional to the weight of the charge, so that

$$w_{\text{case}} = \lambda_g w_{\text{prop}} \quad (5.21)$$

Table V-4. Case Weights

Gun	Caliber (mm)	Propellant Charge Weight(kg)	Case Weight(kg)	Case Weight/ Charge Weight
Oerlikon	35	0.340	0.672 (steel)	1.976
Rarden	30	0.14	0.350	2.50
HS 831L	30	1.16	0.350	2.50
<u>Rocket</u>				
Super Loki Booster	102	17.1	6.1	0.36

one obtains an estimating expression for the ratio of projectile weight to complete round weight as follows:

$$w_{cr} = w_p + w_{prop} + w_{case} \quad (5.22)$$

as obtained previously

$$w_{prop}/w_p = (v_0/v_s)^2 / [1 - (v_0/v_{max})^2] \quad (5.23)$$

hence

$$w_p/w_{cr} = \frac{1 - (v_0/v_{max})^2}{1 - (v_0/v_{max})^2 + (v_0/v_x)^2} \quad (5.24)$$

where

$$v_x^2 = v_s^2 / (1 + \lambda_g) \quad (5.25)$$

and

$$v_s^2 = 2gE_s \quad (5.26)$$

To terms in v_0^4 this expression can be simplified as

$$w_p/w_{cr} \approx \frac{1}{1 + (v_0/v_x)^2 [1 + (v_0/v_m)^2]} \quad (5.27)$$

and $v_x \ll v_m$

For rockets, if the motor case and nozzles are assumed to be about proportional to the weight of the propellant

$$w_{case} = \lambda_r w_{prop} \quad (5.28)$$

and w_{hd} = weight of warhead

$$w_{cr} = w_{hd} + w_{prop} + w_{case} \quad (5.29)$$

Then

$$w_{hd}/w_{cr} = (1 + \lambda_r) e^{-(v_b + \Delta v)/v_e} - \lambda_r \quad (5.30)$$

and for small values of v_b/v_e this may be approximated as

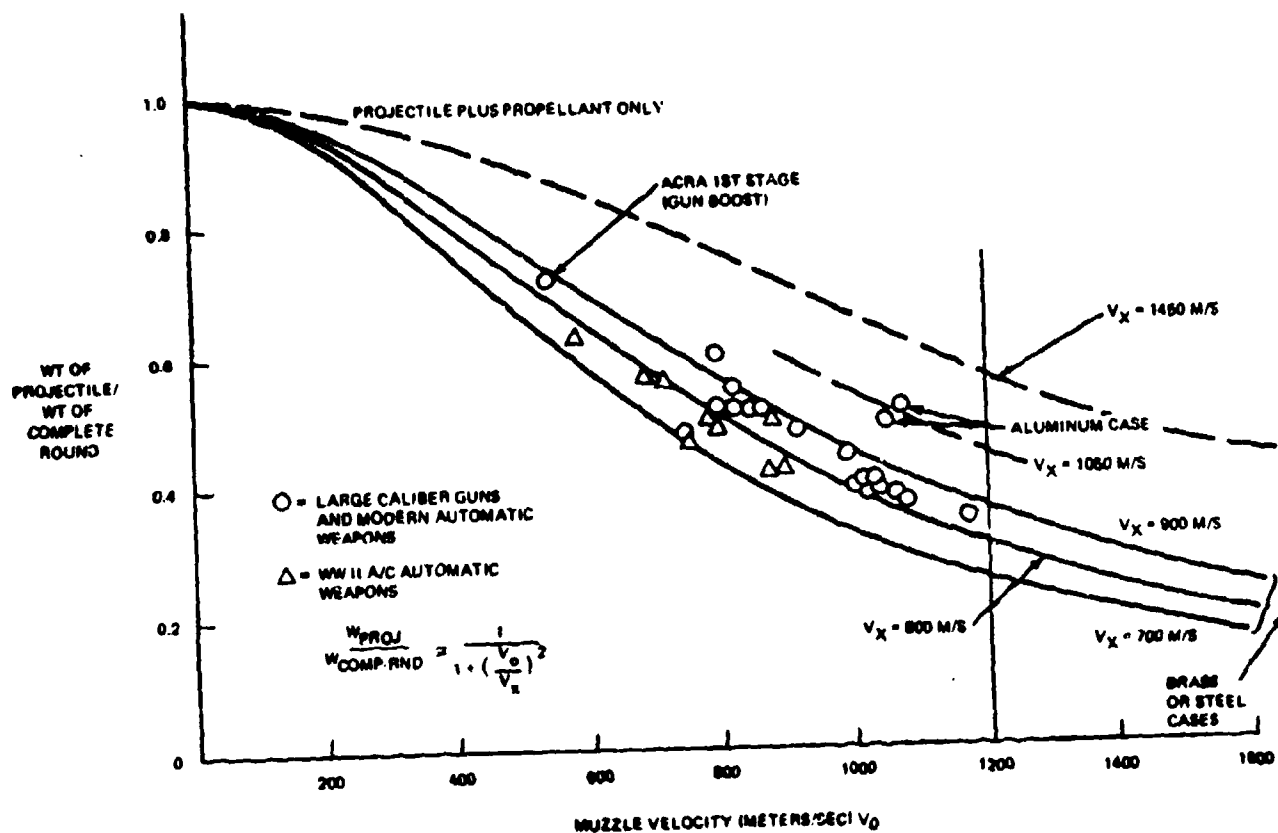
$$w_{hd}/w_{cr} = e^{-(1 + \lambda_r)(v_b + \Delta v)/v_e} \quad (5.31)$$

The maximum velocity that can be attained as payload is reduced to zero is limited by λ_r , and

$$e^{(v_b + \Delta v) \max/v_e} - 1 + (1/\lambda_r) \quad (5.32)$$

The ratio of projectile weight to complete round weight is shown vs. muzzle velocity for a number of gun fired projectiles in Figure 5-7. The more modern the design, the higher the payload fraction at a given muzzle velocity. No data is at hand to plot the GAU 7A round, but an upper limit curve is sketched, assuming that $\lambda_g = 0$, and $v_s = 6000$ f/s.

The gun boost stage of ACRA is also shown.



40001 113

Figure 5-7. Weight of Projectile/Weight of Complete Round vs. Muzzle Velocity for Gun Fired Projectiles

In published data on rocket characteristics, there is an unfortunate tendency to list only the HE content of the warhead, sometimes simply designating this weight as "warhead". It is believed that the warhead weights used in this report are complete including metal and fuze, unless HE content is specifically designated.

Figure 5-8 plots warhead weight as a fraction of rocket launch weight for some modern air to ground and surface to surface rockets. Also shown is the trend from Figures 5-7 for gun fired projectiles with brass/steel and with aluminum cases. By this index of effectiveness the operational rockets do not show up well at velocities below about 1000 m/s. For aircraft applications this disadvantage is more than compensated for by the relatively small installation weight and reaction forces compared with guns.

The advantage of the rocket for very high velocities is indicated by the points for the Super Loki Booster plus Dart payload, ⁽¹⁹⁾ which has been developed for meteorological soundings. Super Loki is a development of the Loki antiaircraft rocket, which was, in turn, a much modified descendent of the German Taifun. ⁽²⁷⁾ The Super Loki booster case is aluminum and its weight plus nozzles, payload attachment fitting etc. is about 36% of the weight of the solid propellant. This is a high ratio, compared with the corresponding ratios achieved in ICBM and space rocket designs, but is evidently much lower than the ratios achieved by the other rockets plotted in the Figure.

5.2.4 Projectile Weight vs. Muzzle Velocity and the Use of Subcaliber Projectiles

With a given gun, muzzle velocity can be increased by lightening the projectile. Stutz ⁽¹⁶⁾ suggests that perturbations about a standard projectile weight-muzzle velocity pair can be made assuming constant muzzle energy. This is optimistic for very high projectile muzzle velocities, and AMCP 706-140 ⁽²¹⁾ suggests an approximation for limited changes based on the assumption that $mv^a = \text{constant}$ with $a > 2.0$ (2.5 to 3.3 depending on propellant type).

Comparing this power law with Eq. 5.12

$$E_{01} = E_m [1 - (v_0/v_m)^2] \quad (5.12)$$

$$E_{02} = E_s (v_0/v_{0s})^{2-a} \quad (5.33)$$

where $E_{01,02}$ are muzzle energy by each expression, v_0 is muzzle velocity, v_{0s} is muzzle velocity at a "design point" about which perturbations are to be taken, E_s is muzzle

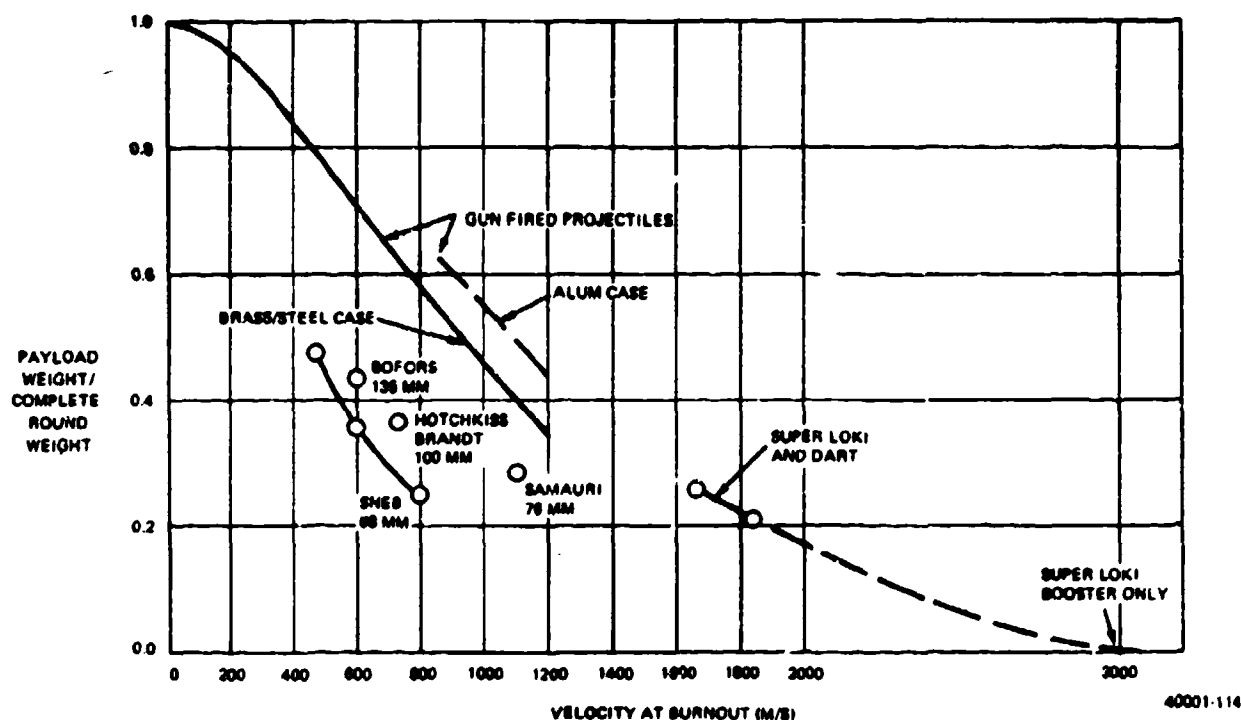


Figure 5-8. Payload Weight/Complete Round Weight vs. Burnt Velocity for Rockets

energy of the projectile at that point, and E_m and v_m are maximum muzzle energies and maximum muzzle velocities as defined for Eq. (5.12). If we equate the energies $E_{01,02}$ and the first derivatives with respect to v_0 at the design point, we obtain a local match of the two equations for

$$(v_{0s}/v_e)^2 = \frac{s-2}{s} \quad (5.34)$$

When a subcaliber round is fired, the incremental weight of a sabot is incurred, and a portion of the available muzzle energy is used in accelerating the sabot. Modern sabot designs are relatively light, when compared with those first used in anti-tank projectiles, for example, but since the sabot must seal the tube, it is an increasing ratio to projectile weight as projectile weight is reduced. An APDS design (possible Bofors) used as an example by Stutz suggests that sabot weight should be taken as equal to projectile weight for a 37.5 mm core fired from a 75 mm gun. The modern Dardick HIVAP experimental gun however required only a 15 grain sabot for a 35 grain flechette projectile fired from a cal 0.30 tube.

The series of modern gun/projectile designs referred to in Section 5.2.5 have been plotted in Figure 5-9 showing muzzle velocity vs. projectile weight, referred to a "standard" pair of reference values. The points for both full caliber rounds and subcaliber rounds of both spin and fin stabilized types follow a power law up to muzzle velocity increases of 50% above standard. Both the 40-mm and 30-mm points fall on the same curve, "Standard" velocities used as reference for the two weapons are 3396 f/s and 3300 f/s respectively. The Bofors point from Stutz is shown; it is relatively inefficient. A point is shown for the Dardick, referenced (perhaps unreasonably) against a conventional cal 0.30 gun with the same L/n .

Note that the full caliber points fall on the same curve as the subcaliber points for the design weapons up to 50% velocity increments, suggesting that the sabot weights are very small for these points.

From Eq. 5.34 with $a = 2.60$, the corresponding value of v_{\max} for the straight line segment is about $2.1 v_{0s}$, or about 7,000 f/s, with $E_s/E_m = 0.77$ at the design point.

Figure 5-9 also shows Eq. computed as

$$w_p/w_{ps} = 1.3 [(v_{0s}/v_0)^2 - 0.23] \quad (5.36)$$

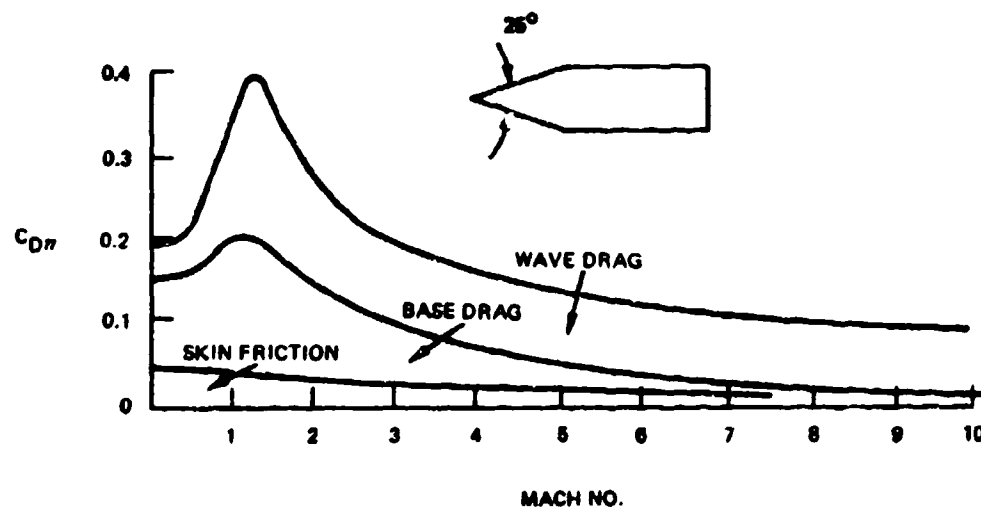
In summary, it appears that even with subcaliber projectiles, and the best of modern conventional gun design, muzzle velocities of the order of 7000 f/s will be difficult to achieve in practical designs.

5.2.5 Exterior Ballistics

Projectile drag force can be considered as composed of

- (1) Wave drag
- (2) Base drag
- (3) Skin friction

Figure 5-10 shows how these compare for a cone-cylinder shape as a function of Mach number. The nose shape for this form determines the wave drag. The drag coefficient $C_{D\pi}$ is referred to the maximum cross sectional area of the shape, perpendicular to its long axis, A_π .



40001-116

Figure 5-10. Drag Buildup of Cone Cylinder

There are several systems of notation for drag coefficient in use. They are

$$D = C_{D\pi} (\rho/2) A_{\pi} V^2 \quad (\text{U.S. aerodynamicists})$$

$$D = K_D \rho C^2 V^2 \quad (\text{U.S. ballisticians})$$

$$D = K_W (\rho g) V^2 A \quad (\text{German ballisticians}) \quad (5.37)$$

Here D = drag force

ρ = air density in mass units/volume

$A = A_{\pi}$ = maximum cross section area of projectile

V = velocity

g = gravitational acceleration

C_D AND K_D are dimensionless, K_W is not.

Conversions are

$$C_D = (8/\pi)K_D = 2.54 K_D$$

$$C_D = 2gK_W \quad (5.38)$$

Some of the aerodynamics references use $C_{D\pi}$ and A_π to refer to the projectile cross sectional area. This is a convenient index to distinguish $C_{D\pi}$ from C_D referred to wing and fin areas of missiles.

Referring to Figure 5-10, wave drag depends primarily on the apex angle of the nose; the smaller the angle, the lower the wave drag component. Base drag can be reduced by boattailing. For extremely long, thin shapes, with very small nose angles, skin friction limits drag reduction by elongation for a given internal volume.

Figure 5-11 compares drag coefficient vs. Mach number of three spin stabilized projectile shapes, as given by Stutz^⑥. It is convenient to have a single number to compare projectile drag, and this will be taken as drag coefficient at Mach 2: C_{D2} . Figure 5-11 suggests that $C_{D2} = 0.20$ is attainable with spin stabilized projectiles.

Above about Mach 1.2 for low drag spin stabilized projectiles, the variation of C_D with Mach number can be approximated by a power law. For approximate computations it is convenient to assume a square root variation,

$$C_D = C_{D2} (2/M)^{1/2} \quad (5.39)$$

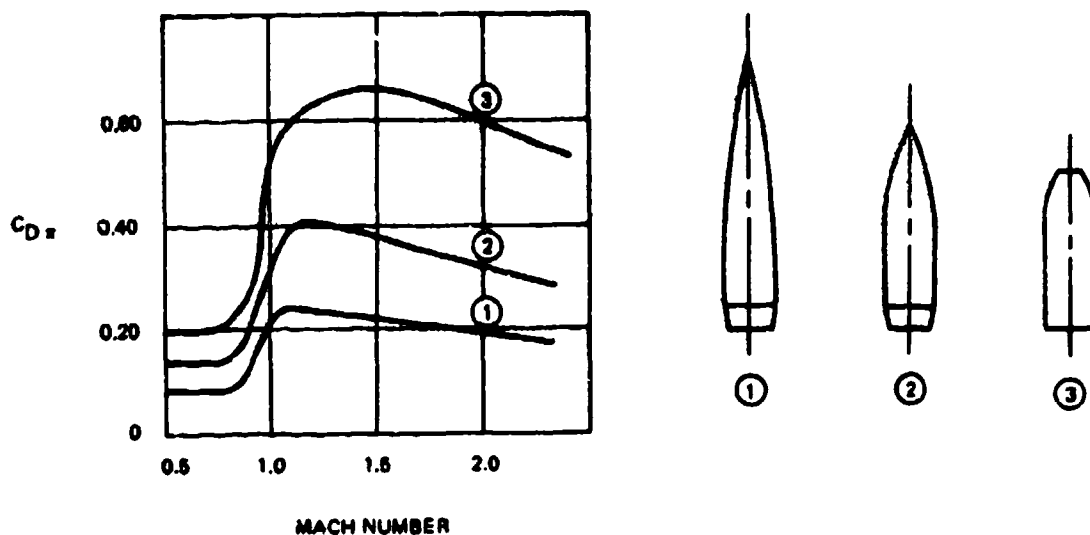
The projectile acceleration is then given by

$$dv/dt = -D/M \quad (5.40)$$

where D = drag force

m = projectile mass

$$\text{and using the square root approximation } dv/dt = -2kv^{3/2} \quad (5.41)$$



40001-117

Figure 5-11. Drag Coefficient Variation with Mach Number for Spin Projectiles

$$\text{where } k = C_{D2}(A/w_p) (2v_s)^{1/2} (\rho g/4) \quad (5.42)$$

A = projectile cross sectional area

w_p = projectile weight

v_s = velocity of sound

ρ = air density

Time of flight t , and remaining velocity v at a range D are then obtained as

$$D/t = v_0 (1 - kv_0^{-1/2} D) \quad (5.43)$$

$$v = v_0 (1 - kv_0^{-1/2} D)^2 \quad (5.44)$$

Projectile ballistic data in the literature on new weapons is often given in terms of time of flight to one or two arbitrary ranges.

A collection of such published data was provided in the report of the Phase II AFAADS contract.

The above relations can be used with such scattered data to obtain an estimate of the value of C_{D2} which, with the "3/2 power" drag law would match the published points. The computational equation is

$$C_{D2} = 0.1589 \left\{ \frac{w_p v_0^{1/2}}{DC^2} \right\} \left[1 - (D/v_0 t) \right] \quad (5.45)$$

where w_p = projectile weight (kg)
 v_0 = muzzle velocity (meters/sec)
 D = slant range (meters)
 t = time of flight to D (sec)
 C = caliber (meters)
 C_{D2} = projectile drag coefficient at Mach 2

On applying this expression to the projectiles of the referenced AFAADS list, we find that with few exceptions, when several range/time pairs are given, the computed values of C_{D2} differ by no more than about .03, and in some cases are identical to two decimal places. The result of this computation for a few current operational weapons and projectiles are shown in Table V-5.

Compared against an objective of $C_{D2} = 0.20$ it is clear that there is potential for improvement.

Data on a series of advanced design projectiles by the U.S. Army Armament Command has been made available by Mr. S. Goodman. The computations of equivalent C_{D2} at 3-km range are listed in Table V-6. It will be noted that a value of $C_{D2} = 0.21$ is inferred for the SRC designs of spin stabilized projectiles, - an achievement for which someone deserves a commendation.

Table V-5. Equivalent Drag Coefficients at Mach 2.0 of Operational Projectiles

WPN	CAL (mm)	C_{D2}
RH202	20	0.30
AMC 621	20	0.42
HS 831	30	0.30
OERLIKON	35	0.27
BOFORS	40	0.27
BOFORS	57	0.29
BOFORS	120	0.28

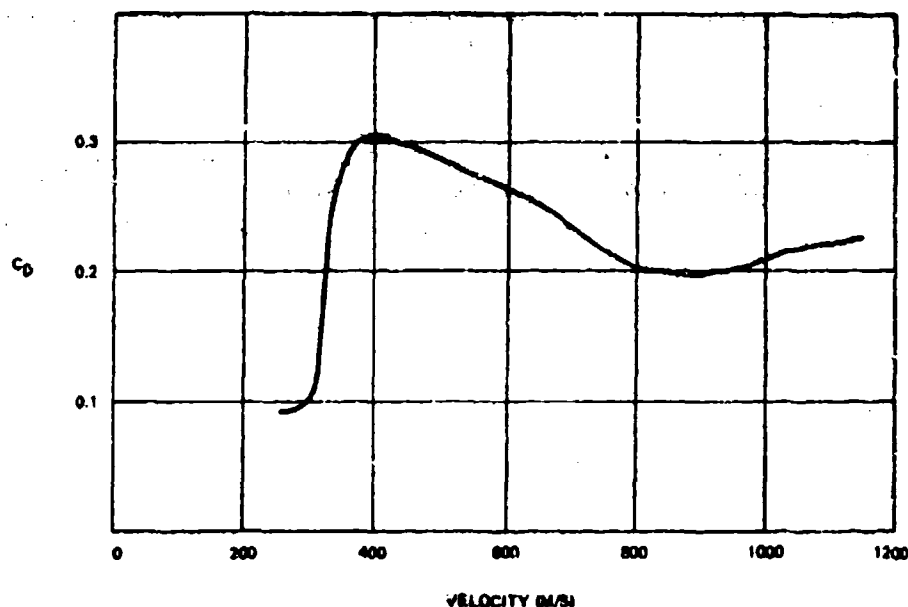
The inferred C_{D2} values for the fin stabilized rounds are in the range 0.13 to 0.15. These excellent values present a startling contrast to the C_D values for fin stabilized rounds of WW II vintage as listed in AMCP 706-242.

Also listed in Table V-6 are the fraction of weight of the projectiles devoted to HE. Improvements by factors of 2 and 3 over the HE content of current standard rounds should, in conjunction with the low drag shapes, provide order of magnitude improvements of effectiveness of the complete system from projectile design alone.

Having achieved a low drag design, the projectile/gun designers are still not home free, however. Figure 5-12 shows C_D for the Oerlikon round as inferred from Oerlikon firing tables. This round does indeed have a very low drag. Note the drag rise near muzzle velocity, however. Assuming that the inferences from the firing tables have been computed correctly, one may possibly attribute this drag increment to the initial projectile yaw, at the muzzle, produced by the destabilizing effect of propellant gases, or by vibration of the L/90 tube so that the full advantage of the low drag shape is not realized until the initial yaw rate has damped out.

Table V-6. Equivalent Drag Coefficients at Mach 2.0 of Developmental and Low Drag Design Projectiles

SPIN Stabilized Rounds				
No.	Type	CAL/SUB (mm)	C_{D2}	Fraction of Weight in HE
2	STD	40	0.33	0.10
4	SRC	40	0.21	0.24
6	SRC	40/30	0.21	0.14
2A	STD	30	0.25	0.12
3A	SRC	30	0.21	0.26
5A	SRC	30/22.5	0.21	0.19
2B	STD	20	0.30	0.07
3B	SRC	20	0.21	0.15
FIN Stabilized Rounds				
No.	CAL/SUB (mm)		C_{D2}	Fraction of Weight in HE
1	40		0.14	0.30
3	40		0.15	0.31
5	40/30		0.14	0.17
7	40/20		0.13	0.16
1A	30		0.15	0.25
4A	30/20		0.14	0.33
1B	20		0.15	0.24



40001-118

Figure 5-12. Drag Coefficient of 35-mm Projectile, Inferred From Firing Tables

With regard to drag of rockets, a survey of WWII estimates on then current designs as given in AMCP 706242⁽²⁰⁾ shows extremely high drag coefficients. No modern data is on hand. However considering what modern aerodynamic theory has contributed to projectiles, as shown in Table V-6 one might hope that comparable low values can now be achieved for both spin and fin stabilized rockets and rocket-boost projectiles.

Rockets with finite burn time derive a drag advantage in that they need not penetrate the very high velocity, high drag regions. Studies of optimum burn schedules for rockets according to various criteria such as minimum time to specified range show that the optimum paths are composed of only the following three types of segments (1) burn at maximum rate, (2) burn at constant velocity, (3) coast. Depending on the terminal criteria, from one to all three types of segments may be utilized.⁽²²⁾⁽³³⁾

Unfortunately time does not permit the development of typical optimal solutions in the present report.

5.2.6 Tube Life of Guns

Some of the most spectacular achievements of the gun designers in recent years have been in the increase in the life of gun tubes. The new M110E2 203-mm artillery piece is expected to have a tube life of 3000-4000 rounds at maximum charge, compared with 1100-1200 for the 175-mm M107 and M110. ⁽³⁴⁾

These values may be compared with the estimates given by Stutz ⁽⁶⁾ for older artillery pieces (105 mm) which can be approximated by the expression

$$L \text{ (rounds)} = 400 (1000/v_0)^5 \quad (5.46)$$

where v_0 = muzzle velocity in meters/second.

AMCP 706-150 ⁽²²⁾ cites an empirical expression by Riel for artillery weapons with low rate of fire which can be interpreted to give relative tube life as

$$(L/L_1) = (P/P_1)^{0.4} (W_{\text{prop}}/W_{\text{prop},1})^2 (V/V_1) (E/E_1) \quad (5.47)$$

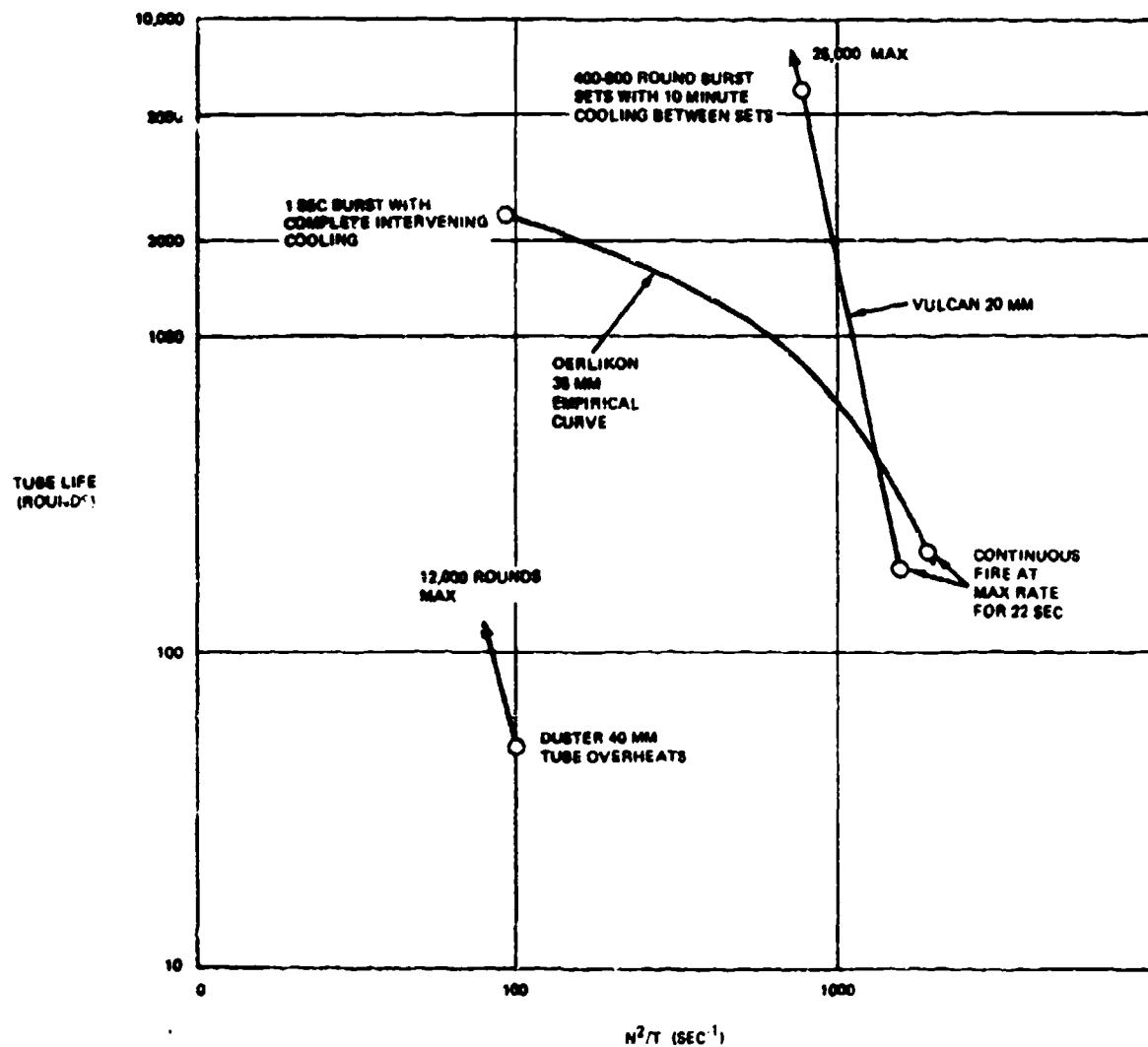
where

- P = maximum chamber pressure
- W_{prop} = weight of propellant
- V = muzzle velocity
- E = specific energy of propellant

and the subscript (₁) relates to a given gun on which the changes are superimposed. Since $W_{\text{prop}} \sim V^2$, this would make tube life inversely proportional to the fifth power of muzzle velocity for full caliber rounds, but only inversely proportional to muzzle velocity for sub-caliber rounds.

However, for antiaircraft guns, the most severe limitation associated with tube life is that imposed by sustained fire at very high rates of fire, and the associated barrel heating.

An empirical curve for the Oerlikon 35-mm gun relates tube life to the number of rounds N fired in a time T , with complete cooling between such sequences. This curve is replotted in Figure 5-13.



40001-119

Figure 5-13. Tube Life of Guns vs. Firing Rate and Firing Time Parameter

The FM's on Duster and Vulcan give the following information on tube life.

Vulcan: Tube life has been increased with time (according to published figures). The gun fires at a maximum rate of 3000 rounds per minute with 6 tubes. Muzzle velocity is 3350 f/s. If the whole load of 1100 rounds is fired in one burst, the tube heats to 1000°F, is still safe, but is warped and must be replaced. The firing time is $1100/3000 \approx 22$ sec. It takes 5 minutes to change a barrel,

If the gun is fired in bursts of 2 x 200 rounds or 3 x 300 rounds, then allowed to cool for 10 minutes, the temperatures reach a maximum of 520°F, 680°F respectively, but the tubes are not warped, and do not need to be changed. At this regime, the life is 36,000 rounds per gun, or 6000 rounds per tube. A later reference gives a life of 145,000 rounds per gun.

Duster: Each 40-mm gun fires at 120 rounds per minute. If 100 rounds are fired at this rate, the tube overheats and must be changed. It takes 3 minutes to change a tube. The life of each tube under normal operation is 12,000 rounds.

These data have been superimposed on the Oerlikon curve in Figure 5-13.

Davis¹⁸ observes that most tubes are now chrome-plated to reduce erosion, and that of the efforts now underway to reduce the problem of erosion.

"One of the most promising is to use erosion-resistant refractory metal liners, separated from a high-strength-steel outer tube by an insulator which permits the bore to operate at high temperature without excessive loss in barrel strength. This technique, together with cooler burning propellants, should permit the building of lightweight barrels with virtually unrestricted duty cycles".

Most modern antiaircraft automatic cannon do not employ liquid cooling of the tube. However, the latest Bofors 57-mm weapon is liquid cooled. Considering the capital investment involved in a modern mobile air defense weapon, of which the cost of the gun is a very small fraction, it may also be desirable to reexamine the matter of forced tube cooling, with the object of increasing permissible burst lengths, and increasing tube life of very high muzzle velocity weapons.

Considering the relative consumption and cost of tubes and ammunition for Vulcan, as an example, one tube costs about as much as 50 rounds of ammunition (conventional), and one tube weighs about as much as 30 rounds. If we assume a life per tube of about 6000 rounds we need add only 1/2% to the weight logistics for tubes and about 1% to cost. However, all other parameters assumed constant, if muzzle velocity were increased by 50%

(this is, of course, not possible without major gun redesign) we should add 38% to the weight total, and over 50% to cost of tubes plus ammunition.

The time to change all 6 tubes on Vulcan is 20 minutes. The ammunition reload time is 8 minutes for 1100 rounds. Hence as an upper limit, one need add only about 3% to reload time for time to change tubes: this need not be done sequentially, depending on the crew, and is a minor limit. However if muzzle velocity were increased 50% tubes would have a life of only about 800 rounds and about as much time would be spent in changing tubes as in reloading ammunition.

Depending on how rapidly the development of long life tubes for very high muzzle velocities progresses, tube life may be one of the important factors in choosing between high velocity guns, and lower muzzle velocity gun-boosted rockets with equal or shorter times of flight.

5.2.7 Dispersion

The angular dispersion associated with antiaircraft guns can be very small, and estimates of standard deviation of the shot pattern (linear) for a gun fired from a hard mount are of the order of 0.5 to 1.5 mils. On "soft" mounts, such as aircraft installations, corresponding estimates for automatic cannon in the 20-35 mm range may be as high as 2.0 to 4.0 mils. It may be possible to achieve angular dispersions of gun boosted rockets somewhere between these extremes.

The dispersion in muzzle velocity about its mean value has a standard deviation of from 0.25% to 0.50% of velocity for antiaircraft guns. AMCP 706-242⁽²⁰⁾ lists typical probable errors for rocket-assisted projectile parameters, with values of 1% for specific impulse of fuel, .3% for burning rate, and .5% for propellant weight. (A 1.3% σ of propellant weight was recorded for 25 Super Loki boosters⁽¹⁹⁾). The standard deviation is about 1.5 times the probable error; hence values of 1 to 2% in standard deviation of velocity might be expected. The effect on total velocity would be less than this, since the gun boost velocity would be expected to have less than 0.5% standard deviation.

The effect of muzzle velocity dispersion on hit probability depends on the lead angle, and is a maximum at rldpoint, where lead is a maximum. For a target velocity v_t , an error in time of flight ϵ_t causes a linear miss

$$M = v_t \epsilon_t \quad (5.48)$$

To a first approximation, the percent error in time of flight equals the percent error in muzzle (or burnt) velocity, hence the linear miss is proportional to

$$M = v_t t_p (e_v / v_o) \quad (5.49)$$

However, an increase in projectile velocity will reduce time of flight, so that for a given range D

$$M \sim v_t D (e_v / v_o^2) \quad (5.50)$$

One might therefore accept an increase in muzzle velocity dispersion which is no greater than the square of the increase in velocity, -i. e. for a 10% increase in average velocity, one might accept a 20% increase in muzzle velocity dispersion. A 400% increase, however, as suggested above for free rockets would be unfavorable.

Conjecturing that both the angular and the muzzle velocity dispersions of boosted rockets depend on the velocity increment outside the tube, as compared with the boost velocity, the following estimating relationship is suggested, until enough data accrues to replace it with a better one:

$$\sigma^2 = \sigma_g^2 (v_g / v_t)^2 + \sigma_r^2 (v_r / v_t)^2 \quad (5.51)$$

Where σ_g^2 is variance of either angular or % muzzle velocity dispersion for a gun system, σ_r^2 is the corresponding variance for a "pure" rocket system, v_g is the boost velocity provided by the gun, v_r is the velocity increment added by the rocket, and

$$v_t = v_g + v_r \quad (5.52)$$

In later computations we use the numerical values

$$\sigma_a^2 = (1.25)^2 [(v_g / v_t)^2 + 16(v_r / v_t)^2] \quad (5.53)$$

for angular dispersion in mills, and

$$\sigma_v^2 = (0.5)^2 (v_g/v_t)^2 + 16(v_r/v_t)^2 \quad (5.54)$$

for the % variance in muzzle velocity.

AMCP 706-242 observes that long burning rockets with thrust approximately equal to drag (sustainer) can have a proving ground accuracy very little worse than that of a conventional round fired from the same gun. It is observed also that long-burning rockets are less affected by wind than conventional projectiles.

For antiaircraft applications, however, range to burnout is preferably short (times of the order of 1 second) in order to realize the value of the rocket boost over as much of the expected engagement volume as possible, and the noted possible advantage may not be realized.

5.2.8 Rate of Fire of Gun Boosted Rockets

Two different design concepts are possible for rocket boost projectiles. One is to fire the projectiles sequentially by a conventional gun mechanism. Presumably the Navy 5" RAP rounds are fired in this way, with the rocket element employed to obtain additional range with a given gun. The T110 gun, firing the T131 RAP round, as developed in the 1940s was of this type, and various versions were built, including an aircraft mounted weapon, and a larger caliber field artillery piece. Alternately, as noted in the tables, the unguided, unboosted RAP-14 solution can be reloaded by replacing a loaded container of 22 rockets on the mount, with 1 minute required for the reload.

Javelot employs an ingenious compromise. Sketches show a battery of 96 tubes, backed by a container with 96 rockets. The system is reloaded simply by replacing the container. The tubes provide the equivalent of gun boost, but their weight is not involved in the reload package. Subject to the time delay in replacing the ersatz "breeches", one can continue to fire as long as one has loaded replacement breeches.

The trend in guns is to fire sub-caliber rounds at very high velocity. In a given gun, the impulse per round is reduced as weight of projectile is reduced, even though muzzle velocity is increased. The RAP weapon, however, obtains some of its velocity increment from rocket burn after launch, hence the gun must fire the whole rocket, with the warhead weight increased by the weight of propellant in the rocket, and by the weight of the rocket motor case. Thus even though the gun velocity may be reduced, the muzzle momentum per

round may be rate of fire increased, and for extremely high velocity objectives, the system/ may be limited by recoil force, within a mobile design.

5.2.9 Installation Weight

The low recoil force associated with rockets has made them attractive for aircraft installations. However, the launcher weights for use on supersonic aircraft represent much higher fractions of the weight of the rocket load than was possible with the subsonic WW-II aircraft.

The weight of launchers for surface fired rockets depends on the sophistication of the laying mechanism. Table V-7 shows a few examples of launcher weight and the weight of rockets carried. The RAP-14^① launcher weighs about three times as much as its load, it has hydraulic laying, and is designed for field artillery use. The SCLAR (Italian)^① launcher for fixed installation on vessels is notable for its relatively high angular velocity and acceleration capabilities, which approach those of an antiaircraft system.

By comparison, a 105-155 mm Field Artillery howitzer weighs about 20,000 kg, and the towed version of the Oerlikon twin 35-mm antiaircraft mount weighs about 4200 kg.

A field version of the SCLAR might weigh at least as much as the RAP-14 launcher, exclusive of fire control and sensors hence as much as the towed Oerlikon. However, if its 20 rockets were fired in 2 seconds, with a warhead weight 20% of rocket weight, it would project 70 kg. of warhead per second. The Oerlikon mount at about the same weight fires about 10 kg of projectiles per second. This unreliable comparison does suggest possible weight savings in fire unit weight of rocket systems compared with gun systems, some of which may carry over into intermediate gun-boosted rocket systems.

Unfortunately the Javelot weight estimates which would make this conjecture more reliable are not available at this time.

5.3 SUB-OPTIMIZATIONS OF GUN-BOOSTED ROCKETS

In this section we consider trade-offs between gun boost and rocket burning to achieve a specified total velocity at the end of burn. The basis for the comparison is minimization of the complete round weight. A secondary consideration is the reaction impulse on the mount for each round fired. An alternate basis of comparison which should be investigated is fire unit effectiveness for a given all-up weight of fire unit.

Table V-7. Weights of Rocket Launchers

	Rocket Caliber (mm)	Rocket Wt (kg)	No.	Wt of Load (kg)	Wt Empty (kg)	Wt Loaded (kg)	Launcher Wt / Load	Comments
Surface Mounts								
SCLAR Naval Mt for 105 MM SNIA Rockets	105	35E	20	700	1000	1800	1.43	Hydraulic lay (power wt 220 kg) A" 60°/S²; A 60°/S E" 50°/S²; E 30°/S I _A = 110 kg-sec²; I _E = 70 kg-sec²
	140	54	22	1188	Container 1300	4800	3.08	Hydraulic lay 10 sec for 22 round salvo 1 min container reload 4 min manual reload
US M-91 M-21	115	25.9	45	1166	545		0.47	15 sec for 45 round salvo
	114	18.2	24	437	694		1.59	
A/C Mounts								
BOFORS R4M	155	43.5	6	261	104	365	0.40	0.1 sec between rockets World War II
	55	3.52	60	211	25	236	0.12	
Shoulder Fired AA Rockets								
Fiegerfaust	20	0.24	9	2.17				German WW-II development

5.3.1 Parameters-Trade-offs

To estimate the weight of a complete round in terms of the weight fired from the gun, the expression used is

$$w_{\text{fired}}/w_{\text{cr}} = \frac{1 - (v_o/v_{\text{max}})^2}{1 - (v_o/v_{\text{max}})^2 + (v_o/v_x)^2} \quad (5.55)$$

For unboosted projectiles, the weight fired is simply the projectile weight. When a rocket shell is fired, the expression relating warhead weight to weight fired (rocket weight) is

$$w_{\text{hd}}/w_{\text{fired}} = (1 + \lambda_r) e^{-v_b/v_e - \lambda_r} \quad (5.56)$$

and in this section we ignore the small correction to v_b for velocity loss to drag during burn, and assume short burn time.

The product of these two expressions gives warhead weight as a ratio to complete round weight in terms of muzzle velocity v_o at the gun, and the velocity increment v_b . The sum of these is the velocity at the end of burn

$$v_{\text{ot}} = v_b + v_o \quad (5.57)$$

We assume a conservative value of rocket specific impulse, $I_{\text{sp}} = 225$ sec; $v_e = 2200$ m/s. For the gun, v_x which depends on the propellant specific energy and the material of the cartridge case is taken optimistically as 1100 m/s. The maximum velocity for the gun alone v_{max} is treated parametrically, with a conservative value of 2200 m/s and a very optimistic value of 3300 m/s. The parameter λ_r defining the weight of the rocket motor case and nozzles as a fraction of the propellant weight is treated parametrically, with an optimistic value of 0.25, and a conservative value of 1.0. These values limit the maximum burnt velocity increments that can be attained by the rocket to 3540 and 1525 m/s respectively. The maximum velocity for a combination of gun and boosted rocket is the sum of the two maxima.

As noted earlier, the gun alone is always the most efficient means of projecting a bullet at low muzzle velocities, in terms of complete round weight. As the desired velocity

is increased, however, there is a velocity beyond which the velocity increment is most efficiently obtained by a rocket.

In Figure 5-14 we show warhead weight/complete round weight vs. boost (muzzle) velocity for various total velocity objectives. The pessimistic rocket parameters $\lambda_r = 1.0$ and the conservative gun parameter $v_{\max} = 2200$ m/s have been used.

Below about 600 m/s the gun alone is the preferred solution, above 600 m/s the gun boosted solution is preferred. For all cases the rocket alone is inferior to the gun alone.

The maximum total velocity which can be achieved with the combination gun-boost is the sum of the separate maximum velocities, which for this case is 2200 m/s + 1525 m/s = 3725 m/s. However the combination can in fact attain velocities not achievable by either alone.

Figure 5-15 shows a similar set of curves, but with the optimistic value $\lambda_r = 0.25$ assumed for the rocket. In this case the maximum rocket velocity is 3540 m/s and there are conditions under which the rocket alone is superior to the gun alone. For these cases, however the combination is superior to either.

In Figure 5-16 we show the effect of varying the maximum gun velocity v_{\max} for a total velocity of 2200 m/s. With an efficient rocket the position of the optimum is unchanged, most of the velocity increment is provided by the rocket. With a less efficient rocket, more is required of the gun, and a small increment of effectiveness is obtained with the 3300 m/s maximum assumed for the gun.

When the total velocity objective is reduced to 1100 m/s there is very little difference in payload/complete round weight between the two values of v_{\max} for the gun, as shown in Figure 5-17.

To make the examples more specific, we assume a total velocity objective of 2200 m/s, and a warhead weight of 1 kg. For the gun alone this is, of course, the projectile weight. Figure 5-18 shows the weight of a complete round, the weight fired (rocket, or projectile for the gun alone) and the impulse of firing, defined as mass fired \times boost velocity. The efficient rocket parameter $\lambda_r = 0.25$ is used, and most optimistic gun velocity $v_{\max} = 3300$ m/s is used to allow a comparison across the spectrum. In estimating the momentum of recoil (impulse) the weight fired has been increased by an amount proportional to propellant weight required at each boost velocity.

Figure 5-18 indicates that the boost velocity which gives a minimum complete round weight is about 550 m/s, at which point the impulse per round is less than half that of the gun

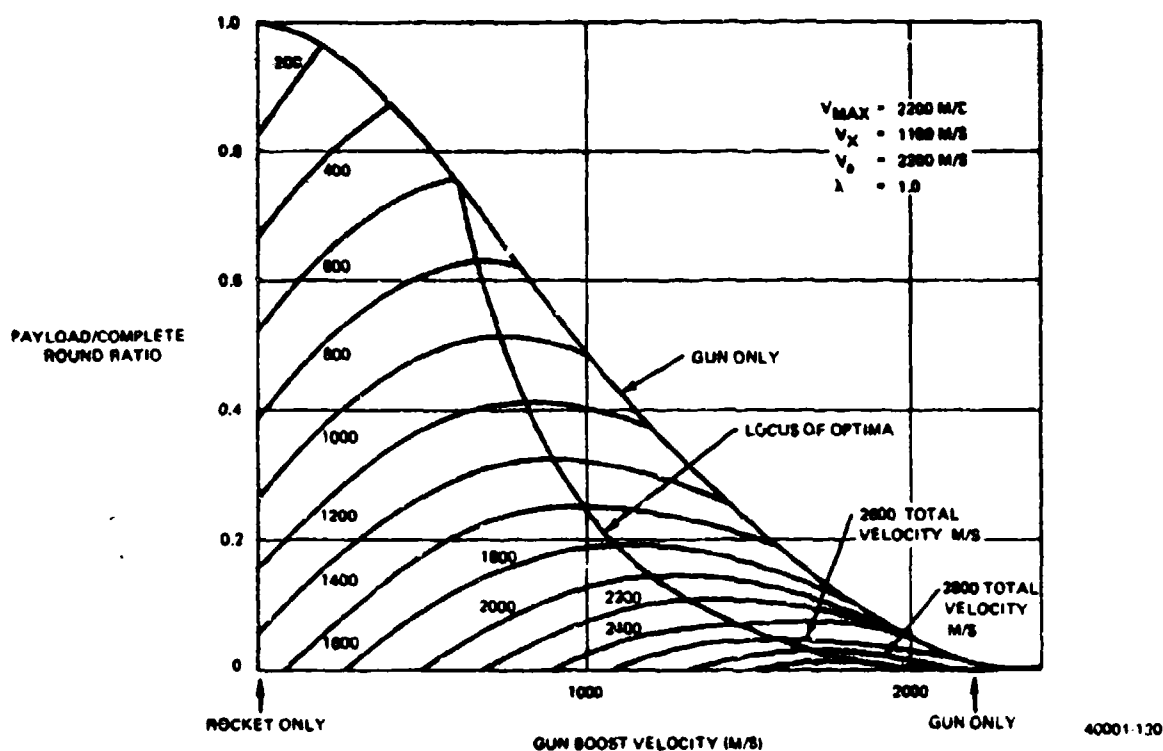


Figure 5-14. Payload to Complete Round Weight Ratio vs. Total Velocity and Gun Boost Velocity for Conservative Rocket Case Weight

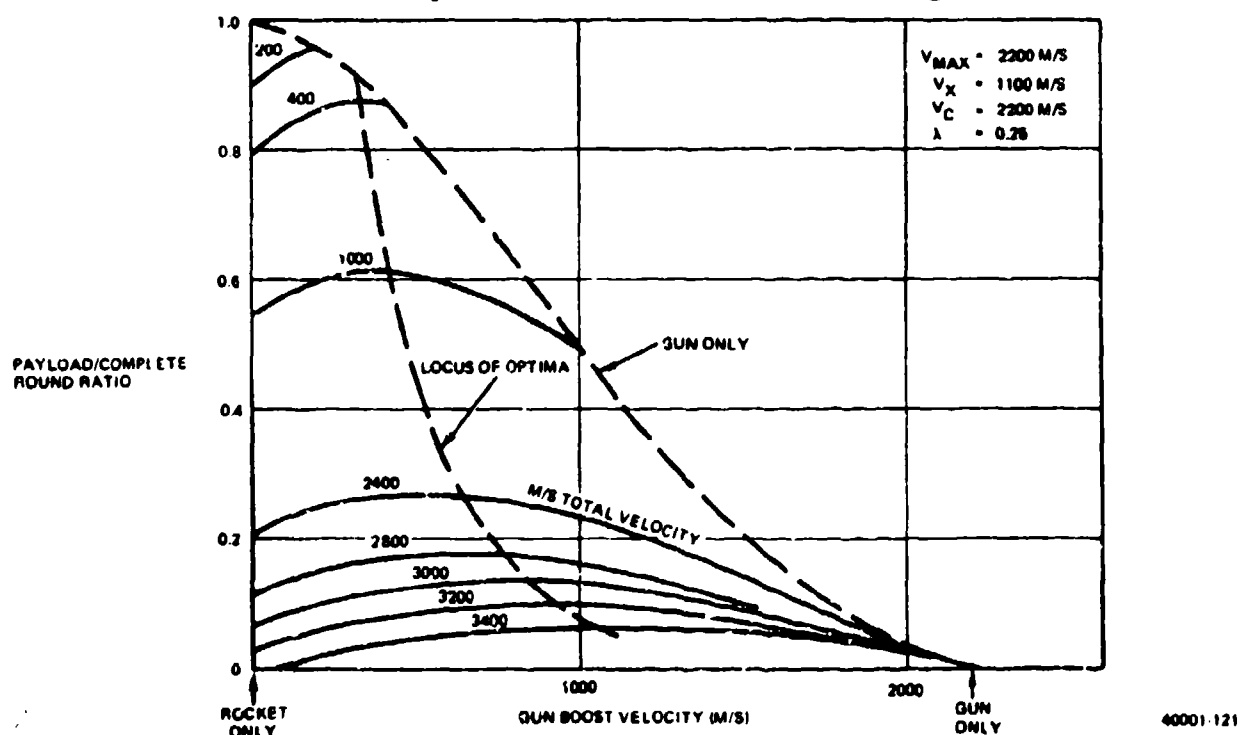
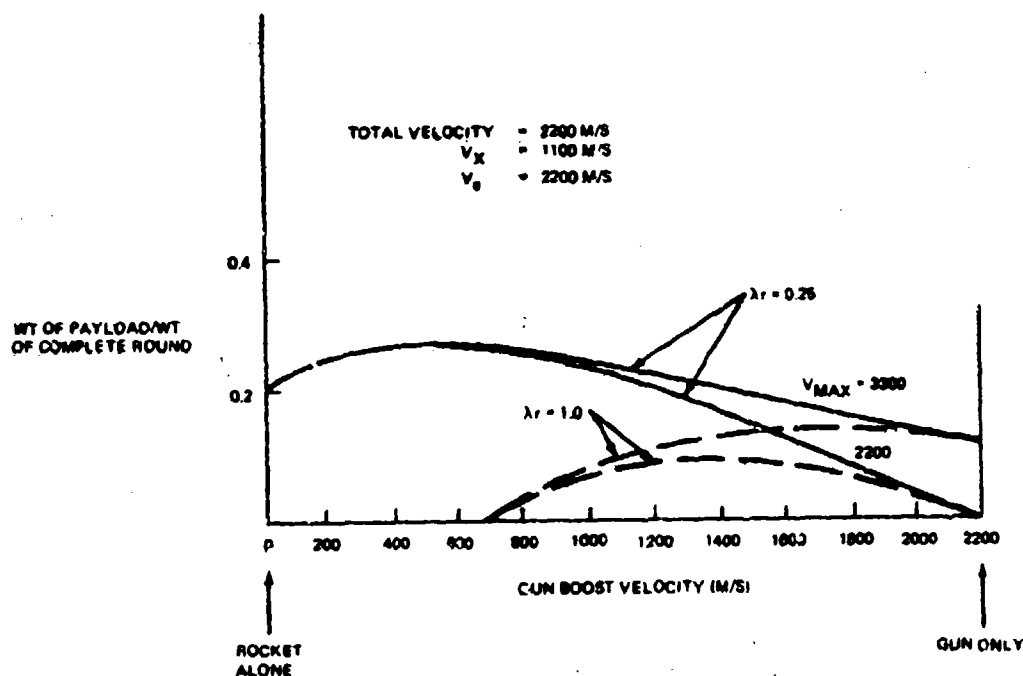
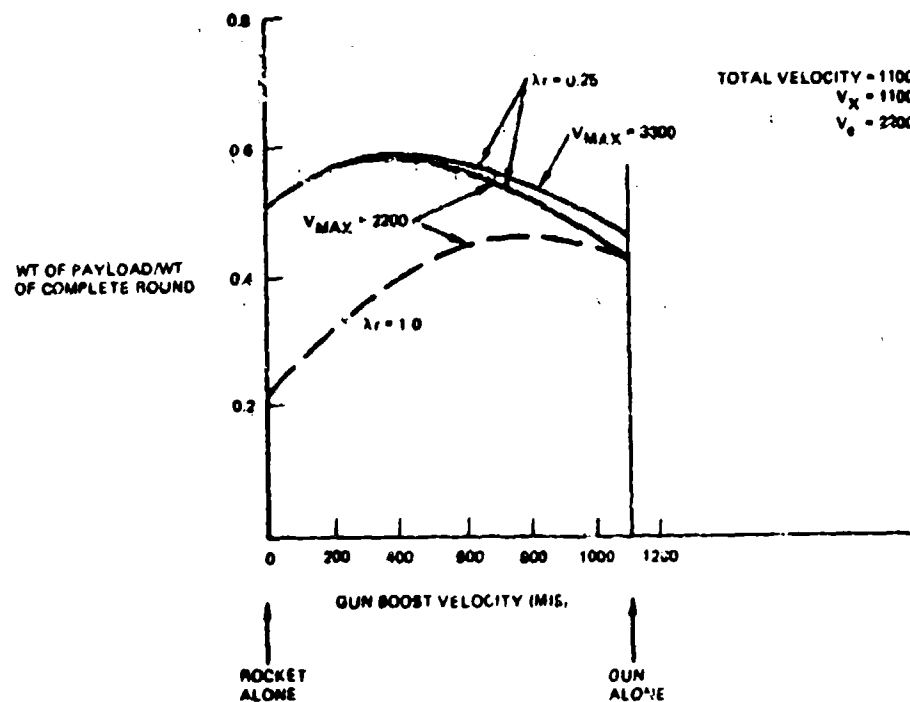


Figure 5-15. Payload to Complete Round Weight Ratio vs. Total Velocity and Gun Boost Velocity for Lightweight Rocket Case



40001-122

Figure 5-16. Payload to Complete Round Weight Ratio for 2200 m/s Total Velocity vs. Gun Boost Velocity



40001-123

Figure 5-17. Payload to Complete Round Weight Ratio for 1100 m/s Total Velocity vs. Gun Boost Velocity

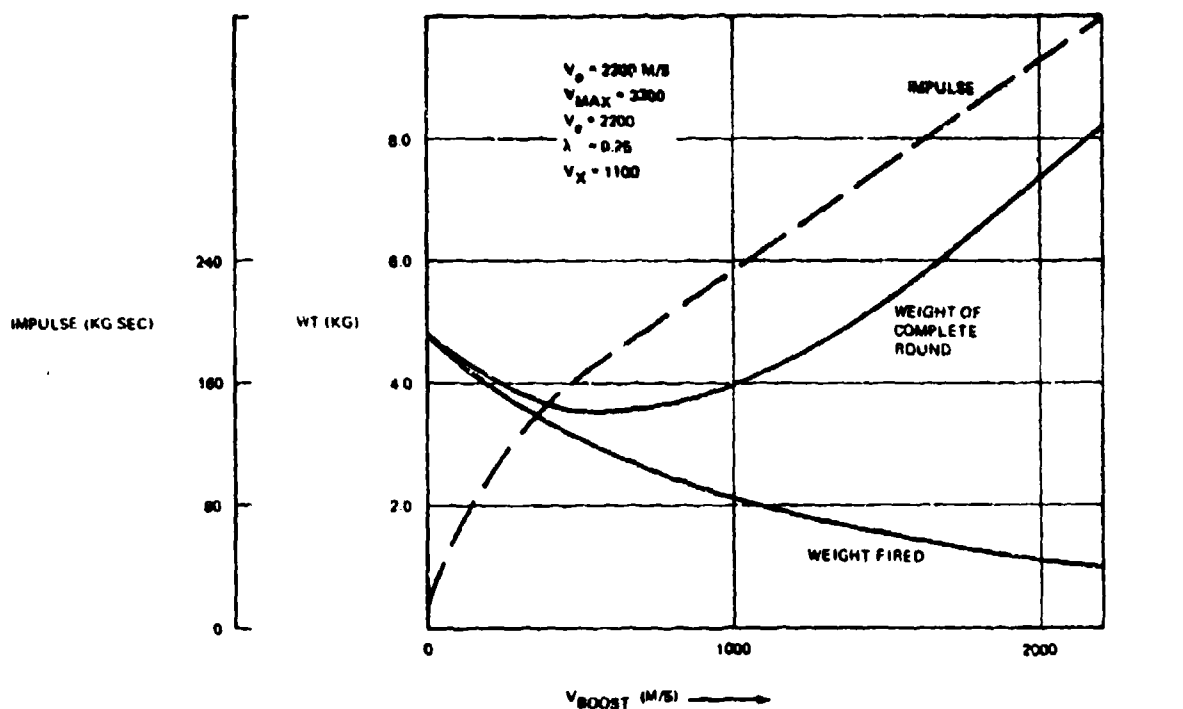


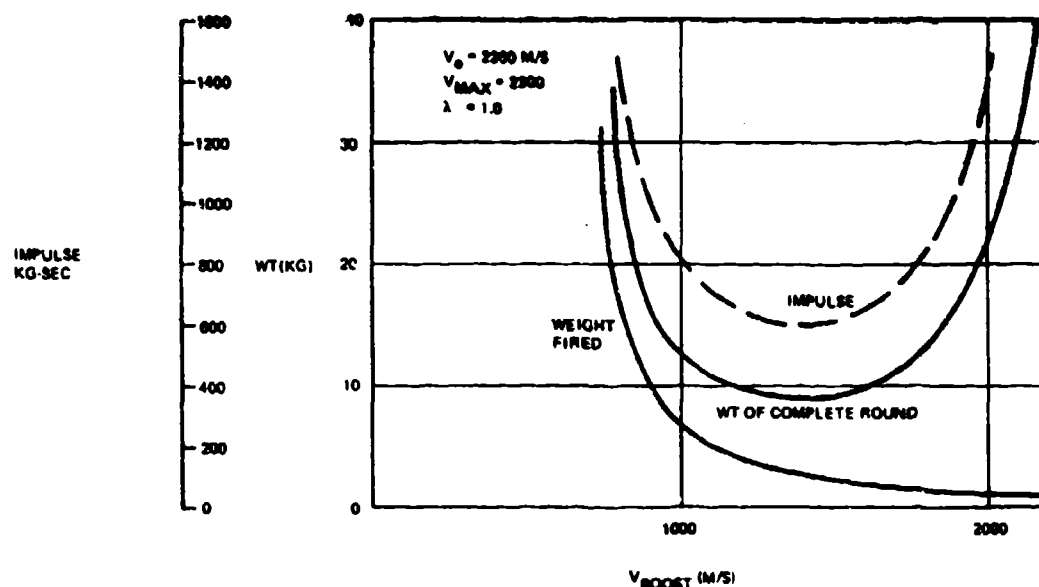
Figure 5-18. Design Tradeoffs for Boosted Rounds with Conservative Rocket Case and Specific Payload

solution. With only slight increase in complete round weight, the boost velocity could be reduced to 300 m/s and the impulse would be about 1/3 that of the gun alone.

Figure 5-19 shows the same parameters for a total velocity objective of 2200 m/s and $\lambda_F = 1.0$; $v_{max} = 2200$ m/s. In this case neither the gun nor the rocket alone can meet the objective with a finite warhead and the estimated impulse per round has a minimum at about the same boost velocity at which the weight of complete round has a minimum of 1400 m/s. However, the complete round has ten times the weight of the warhead it projects.

The simple approximating relationships used in this section suggest that a gun-boosted rocket solution may have significant advantages in reducing the recoil force on the launcher and in meeting a warhead/velocity objective with minimum round weight, as compared with gun or rocket solutions alone. The reduced recoil force can result in a lighter mount than that required for a gun solution.

It would seem desirable to continue with more exact computation for this type of system, emphasizing the application of advanced propellant and materials technology to



40001-125

Figure 5-19. Design Tradeoffs for Boosted Rounds with Lightweight Rocket Case Weight and Specific Payload

design studies of the rocket element, and with more reliable dispersion estimates, preferably based on experimental data.

5.3.2 Effectiveness Comparisons

There are so many unknowns with regard to realistic design parameters for advanced gun-boosted rocket systems, that comparisons on a systems basis must be considered highly conjectural. Hence the following estimates should be considered mainly as an effort to organize some of the estimates in an orderly way. The methodology is so simple that the reader disagreeing with any individual parameter can easily change it, and quickly determine its effect on the result.

The fire units considered are (1) a "free" rocket system, (2) four gun-boosted rocket systems using optimistic and pessimistic values of the rocket parameters, (3) the Oerlikon 35-mm system as a reference for which firm weight information exists,⁽¹²⁾⁽²³⁾ and (4) three hypothetical 40-mm systems based on the advanced 40-mm low drag projectile data.

The comparison is based on the assumption that the payoff of a gun-boost system will be realized in short time of flight, hence a total boost plus burn velocity of these systems is

set at 2300 m/s. An alternate basis for comparison would be to keep time of flight equal to that of a gun system, and determine whether a lighter fire unit could be realized.

The gun boost and rocket systems are estimated for a warhead weight equal to the Oerlikon projectile weight (0.55 kg) but with a slightly higher fraction of the weight in HE. The terminal effect defined as the probability that a hit causes a kill is taken as increasing with the square root of the weight of HE.

Average recoil force is assumed to be proportional to the number of rounds fired in one second multiplied by the muzzle momentum per round with one half the propellant weight for boost added to the weight of the projectile fired. For the gun boosted systems the number of rounds fired in one second has been adjusted to keep this value below 6500 kg. The average recoil force of Vigilante was about 7500 kg, so that the systems compared are considered to be capable of mounting on a single self-propelled vehicle.

The tactical situation consists simply of firing a one second burst against an incoming target with presented area represented as a circle of 1-meter radius. This is a relatively small target area. Average range is assumed to be 3 km.

For the gun-boost systems the random dispersion was estimated by the expression given earlier, depending on the velocity increment given by the rocket burn.

Since the object is to highlight the advantage of short time of flight, a slightly maneuvering target was assumed which produced an aim bias constant during a burst, random across bursts, with computations for acceleration variances of 1 and 2 m/s².

Table V-8 compares the system characteristics, and Table V-9 shows the results of the kill computations.

To estimate ammunition costs, the approximate values given in Table V-10 were used.

Some basis for these cost estimates is given in Section 8 "Cost Considerations."

The rocket and gun boost systems are limited by the random round to round dispersions as estimated. The gun systems are limited by the target maneuver. Hence the gun systems would be benefited by a more sophisticated prediction scheme which reduced bias at the expense of random dispersion, but the gun-boost systems would require dispersion reduction to benefit from such improvements.

For the systems as defined, the burst kill probability of the best gun-boost system is about equal to that of the best gun system, to within the reliability of this simple computation,

and this holds true for both levels of target maneuver. This is also true for the estimated number of rounds of ammunition expended per kill.

Since it has been assumed that the more complex RAP rounds would cost from 2 to 3 times as much per kilogram of weight as the simpler unboosted rounds, the estimated cost per kill with the rocket-assist weapons is from two to three times that of the gun system.

Note that since in all cases, for this 1-second burst, kill probability is under 0.10, there is only a minor gain in increasing the random dispersion of the gun systems to an optimum value. If firing were continued to, say 3 seconds, there would be a small incremental advantage for this situation of the guns over the RAP systems, from this source.

From these crude estimates it would appear, therefore, that for the situation considered, and with the assumptions made, there is no advantage in gun boosted rocket systems over the best gun designs. The fact that they work out to approximate equality in effectiveness, however, suggests that it would be desirable to continue with limited design studies and evaluations to estimate the possibility of reducing dispersion of the gun boosted systems to smaller values than those assumed, and to make production cost of the ammunition approach that of conventional and APDS projectiles of equal all-up weight.

The computations should be considered only as a means of comparing the systems represented, rather than absolute values characteristic of predicted fire antiaircraft systems. The geometric situation is one in which the target presents its smallest aspect. At the same range of 3km, but at 30° approach aspect, the kill probabilities would increase over those shown by factors of from 2.0 to 3.0 as a result of increased presented target area alone, and the rounds per kill and cost per kill would be reduced by similar factors.

5.3.3 Controlled Dispersion

Javelot proposes an ingenious method of last-second control of projectile direction by using "splayed" tubes, each of which is installed at a small, but different deviation from the mean axis of the launcher. Beginning with a full load, one could then

- (1) Fire a salvo biased in the direction of an observed target maneuver
- (2) Fire a salvo with predetermined angular dispersion

The usefulness of this concept depends on how small the inherent dispersion of individual rounds can be made. If the gun-booster rocket dispersions can in fact be brought down to magnitudes comparable to those of conventional guns, the method would provide a simple way of controlling dispersion in successive salvos against a target as a function of range.

Table V-8. Comparison of Characteristics of Fire Units

System Type	Free Rocket	Boosted Rockets				Oerlikon L/90 2x35mm	40mm Low Drag 2/70 Designs		
		A	B	C	D		#4 SpIn	#6 SpIn 40/30	#7 Fin 40/20
Parameter Ar	0.25	0.25	0.25	1.00	1.00	-	-	-	-
Total Velocity (m/s)	2200	2200	2200	2200	2200	1175	1125	1473	1667
Gun Boost (m/s)	0	550	1000	1400	1200	1175	1125	1473	1667
Rocket Velocity Increment (m/s)	2200	1650	1200	800	1000	-	-	-	-
Burn Time (sec)	2	1.5	1.5	1.5	1.5	-	-	-	-
Warhead or Proj. Wt (kg)	0.55	0.55	0.55	0.55	0.55	0.55	0.73	0.35	0.11
HE Fraction	0.30	0.24	0.24	0.24	0.24	0.21	0.24	0.14	0.16
Wt. of HE (kg)	0.17	0.13	0.13	0.13	0.13	0.11	0.16	0.05	0.02
Wt. of Rocket (kg)	3.02	1.65	1.16	1.65	2.30	-	-	-	-
Wt. of Complete Rnd.	3.02	1.93	2.20	4.95	5.50	1.56	1.52	1.52	1.52
Muzzle Momentum (kg-sec)	0	98	145	357	378	86'	109	84	35
Rate of Fire (RPM) for 1-Sec.	3000	3000	2400	1000	1000	1100	3000	3000	2500
Av. Recoil Force (kg)	0	4900	5800	6000	6300	1600	5500	4200	1200
Time to 3KM	2.0	2.0	2.0	2.0	2.0	3.8	3.6	2.8	2.7
σ_A (mils)	5.0	3.8	2.9	2.2	2.5	1.25	1.25	1.25	1.25
σ_V (')	2.0	1.5	1.2	0.9	1.0	0.5	0.5	0.5	0.5
σ_V (m/s)	44	33	26	19	22	6	6	7	8

Table V-9. Effectiveness Comparison

System Type	Free Rocket	Boosted Rockets				Oerlikon L/90 2x35mm	40mm Low Drag L/70		
		A	B	C	D		#4 SpIn	#6 SpIn 40/30	#7 Fin 40/20
No. of Rounds in 1-Sec.	50	50	40	17	17	18	50	50	42
Wt. of Complete Round (kg)	3.02	1.93	2.20	4.95	5.50	1.56	1.52E	1.52E	1.52E
Terminal Effect (Prob.)	0.45	0.41	0.41	0.41	0.41	0.34	0.46	0.33	0.20
Time of Flt (Sec)	2.0	2.0	2.0	2.0	2.0	3.8	3.6	2.8	2.7
np_c^2 (m ²)	22.5	20.5	16.4	7.0	7.0	6.1	23.0	16.5	8.4
Random Variances (m ²)									
Angular Dispersion	225	133	77	42	58	14	14	14	14
Prediction Noise Component	29	29	29	29	29	38	34	22	21
Total Random Variance σ_r^2	254	162	106	71	87	52	48	36	35
Bias Variances (m ²)									
Boresight (1 mil)	9	9	9	9	9	9	9	9	9
Wind (3 m/s)	16	12	9	9	9	36	25	16	25
Tgt (2 m/s ²)	36	36	36	36	36	333	274	113	100
Total Bias Variance σ_b^2 (2 m/s ² Tgt)	61	57	54	54	54	378	308	138	134
Ratio σ_r^2/σ_b^2 Opt σ_r^2/σ_b^2	4.2	2.8	2.0	1.3	1.6	0.14	0.16	0.26	0.26
$\sigma_r^2 \cdot \sigma_b^2$	315	219	160	125	141	430	356	174	169
Kill Prob. K	0.036	0.047	0.051	0.028	0.024	0.007	0.032	0.047	0.025
Rounds/Kill	1390	1065	785	610	710	2570	1560	1060	1680
Ammo wt./kill (kg)	4200	2055	1720	3020	3900	4010	2400	1610	2550
Ammo Cost/(kg) (Dollars)	8	14	14	12	12	6	6	8	8
Ammo Cost/Kill (Dollars)	31,000	29,000	24,000	36,000	47,000	24,000	14,000	13,000	20,000
1 M/S ² (Tgt)									
Total Bias Variance	34	30	27	27	27	128	111	53	67
Total Random Variance	254	162	106	71	87	52	48	36	35
Total Variance	288	192	133	93	114	180	159	89	102
Kill Prob K	0.039	0.053	0.077	0.036	0.031	0.017	0.072	0.092	0.041
Rounds/Kill	1240	935	520	475	555	1060	690	540	1020
Ammo Wt./kill (kg)	3870	1805	1140	2360	3040	1655	1050	820	1550
Ammo Cost/Kill (Dollars)	31,000	25,000	16,000	28,000	36,000	10,000	6300	6600	12,400

Table V-10**Estimates of Cost/Kilogram of Projectile Types**

Ammunition Type	Cost per kilogram of Complete Round Weight (\$/kg)
Full Caliber HE	6.0
APDS HE	8.0
Rocket Assist (conservative)	12.0
Rocket Assist (advanced design)	14.0
Free Rocket	8.0

It is not clear that an attempt to counter systematic target maneuver by this means would be superior to simply shifting the whole mount in response to an acceleration measurement. It would appear that one has to measure acceleration in either case, and it is not obvious to the present writer that simply aiming the launcher in the best estimated predicted direction, including a curvature component of prediction is not the best solution.

As the number of rounds in the launch package is depleted, the number of choices of preselected deviations decreases. One would expect that against incoming targets, one could predetermine an approximately optimal dispersion pattern as a function of range, and so the use of splayed tubes could provide a changing pattern size working through the options sequentially, until all rounds are fired. This mode does appear useful, provided that individual round dispersion is not so large as to make it irrelevant. Many computations indicate that in any case, the optimum dispersion pattern is relatively small, and too much dispersion is likely to be developed unintentionally, rather than too little.

5.4 PREDICTED-CORRECTED PROJECTILE FORWARD AREA AIR DEFENSE SYSTEM

Given an air defense fire unit with accurate sensors, and the potential of sensing projectile miss distance at the target with loop closure through the prediction scheme, a natural question is whether the system performance might be further improved at acceptable cost by providing a mid-loop closure either with or without terminal miss closure. Such a mid-loop closure would correct the trajectory of the projectile in flight, and by using the open loop prediction as initial firing orders to the projectile, would minimize the maneuver requirements on the projectile.

Conceivably, such a system would achieve kill probabilities equal to those of the best terminal homing missiles, but at a lower cost in ammunition expended per kill because of the relative simplicity of the equipment on-board the projectile.

In the following paragraphs, some of the characteristics which may be contemplated for a solution of this type are developed.

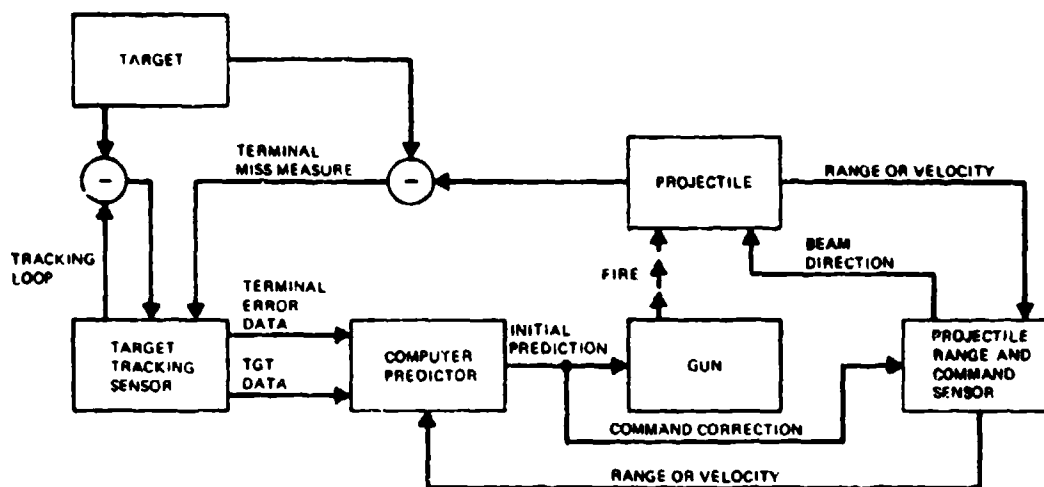
It should be emphasized that the object of this section is not to do a concept analysis of an optimum guided missile air defense system, but rather to explore the interface between conventional air defense gun systems and air defense gun systems with mid-loop closure providing trajectory correction in flight. In view of the highly productive cooperation between the Army Armament Command and the Army Missile Command on the Cannon Launched Guided Projectile for field artillery employment, a similar cooperative venture in the air defense field would seem worth developing.

5.4.1 Concept Objectives

As a general objective, we seek to configure a feasible system exploiting predicted fire technology to the maximum extent, and minimizing the incremental cost of on-board equipment to be added to the projectile. We exclude terminal homing systems from the present investigation on the grounds that this field is extremely active and well covered. We do emphasize projectiles fired at the predicted position of the target on minimum energy paths, as offering a priori the expectation of minimizing the in-flight correction requirements and, hopefully the cost of munitions expended per target kill.

We also consider the possibility of employing terminal loop closure related to the "closed-loop predicted fire systems" discussed in Section 3.0 of this report. Here the idea is to reference the projectile trajectory against the target in the terminal phase to eliminate "boresight" errors which might arise in the mid-course loop closure.

The elements of this objective system are sketched in Figure 5-20. There are three loop closures. Target tracking, of course, always is closed loop, whether the loop closure is automatic or manual. A normal open loop prediction is developed by the computer defining gun orders at which the projectile is fired. Once fired, the projectile is either tracked, and commanded or given a beam to ride which defines a minimum energy path to the target. This is a mid-course loop closure. Once the projectile is underway the computer maintains an updated prediction of the intercept point and adjusts the projectile trajectory as the lead angle to the target collapses to zero. To avoid the equivalent of "muzzle velocity bias and dispersion" for this type of predicted path, the computer must receive in-flight measurements of either range or velocity of the projectile, since the time of flight vs. range characteristics



40001 126

Figure 5-20. Flow Diagram of a Predicted-Corrected Projectile Air Defense System with Mid-Course and Terminal Loop Closures

will vary in a stochastic fashion with the drag loss to control perturbations. Hence the prediction is continuously updated to correspond to projectile computed "time to go" as well as to correct for target maneuvers during time of flight.

When both projectile and target can be seen by either the target tracking sensor or the projectile tracking or directing beam, the computer is given differential measurements between target and projectile from either source, and terminal corrections are based on these differences. This is "terminal-loop closure". Its feasibility depends on the beam width of the sensor and the angular velocity of the beam at the target. Terminal loop closure is most likely to be feasible when targets are incoming and angular velocities are low. This is also the time at which the presented area of the target is smallest, and the accuracy requirement is highest. The time for terminal loop corrections at midpoint on a passing target may be too short for significant correction, but at this point the target presented area is largest, the target is closest, and extreme accuracy may not be required.

The configurations examined will be restricted to projectiles with contact fuzes, in the interest of minimizing the projectile weight, and hence the gun caliber.

The material developed in this section should be considered only as a preliminary exploration of the possible potential of this type of system. It may serve as a point of departure for more definitive preliminary designs, systems analysis and evaluation.

5.4.2 Functional Options

In order to place the system described in the previous paragraph in a broader context, and to provide some basis for comparison of the estimates to be developed, a brief survey is offered of the solutions employed in operational and developmental guided missile and (projectile) systems for each of a number of functions required to be performed by these systems.

In Table V-11 the trajectory characteristics that have been employed for air defense missiles are summarized. The simplest solution, in many ways, is simply to require the projectile to fly up the line of sight to the target. Against aircraft targets this trajectory unfortunately places the highest requirement of any solution (except the unused "pure pursuit") on the lateral acceleration required of the projectile to remain on the line of sight. It does have the advantage that many projectiles may simultaneously ride the beam simultaneously.

The most attractive trajectory for present purposes is the "minimum energy" path. This was used by Nike Ajax. The trajectory is basically that of an unguided projectile with the inclination of the control line continually adjusted so that the projectile does not expend maneuver acceleration against gravity drop, as would be the case with a straight line to the predicted position. With this trajectory the projectile expends maneuver energy only to follow the beam adjustments for target acceleration, and with noiseless tracking, the maximum acceleration required of the projectile never exceeds that of its target. However the directing beam is subject to sensor noise, as analysed later, and this requires a joint optimization of the sensor characteristics, prediction algorithms and projectile maneuver dynamics.

A wide variety of methods have been implemented for sensing a projectile and commanding it in flight. Table V-12 summarizes the methods which have been used for sensing the projectile. Many of the first generation SAMs were radar beam riders, and this mode is used on some current systems. The missile carries on-board equipment to sense its position relative to the beam and correct its position accordingly. Rapid advances in laser technology suggest the use of a laser beam rider, and this mode has been investigated with ACRA.

A more widely employed solution, especially for relatively short range weapons, is to track the projectile with a sensor at the launch station, and command it via a separate command link. The table shows the great variety of solutions of this type that have been implemented. In part the popularity of this mode, which requires in general one tracking

Table V-11. Trajectory Options for SAMS

General Type	Projectile Path	Trajectory Generated Lateral Acceleration	Multiple Projectile Capability	Ground Computer Requirements	Air Defense Example
Beam riders	Target line of sight	High and sustained except for small angles of approach	Yes	Low	Rapier Roland
	Line to predicted position	Low	No	High	None
	Minimum energy	Least	No	High	Nike
Homing systems	Pursuit	Extremely high near target except in tail chase	Yes	Low	None
	Prop. navigation	Low	Yes	Low	Redeye
Mixed	Beam rider with mid-course conversion to prop. navigation homing. Beam may be line of sight or predicted.	Moderate to low	Yes	Moderate	Talos

Table V-12. Projectile Position Sensing Options (Non-Homing Missiles)

Type	Examples
Beam Rider Radar Beam	Masurca Mod 2 TALOS/Terrier (Initial Flight Segment) Indigo Primary Mode
Laser Beam	ACRA
Launch Station Tracking and Command Tracking Sensor Radar	Crotale** (Mid & Terminal Phase) Rapier - II
IR-Flare*	Crotale (Boost Phase) $\pm 5^\circ$ Field Roland Indigo (backup mode vs. ECM) Tow, Dragon, etc.
TV-Flare*	Rapier - I Slam
Visual-Flare*	Blowpipe Seacat (day mode)
Optical Radar	None yet operational
<p>*Flare may be sustainer rocket, special pyrotechnics or other IR/Visual source.</p> <p>**Crotale uses a Ku band monopulse radar, 1.2° beam width with 3-beam receiver. to track target Ku 2 missiles simultaneously.</p>	

sensor per bird in flight, may have resulted from the progressive improvement in missile reliability, accuracy, and terminal effect so that multiple missiles need not be fired against single targets.

Command channel options associated with the track and command system configuration are listed in Table V-13. Since the command channel is a primary consideration to the enemy for ECM, open sources tend not to describe the details of the command coding and the frequencies employed. The wire link is of course least vulnerable to countermeasures, but is limited in application to ranges of a few kilometers.

Many ingenious methods have been devised for maneuvering the projectile in flight, and these are summarized in Table V-14. Some are applicable only to missiles with sustainer rocket motors, such as rocket exhaust deflectors. Others such as gas jets require an on-board source of reaction gas. Aerodynamic sources of maneuver acceleration tend to lead to large lift surfaces if high lateral accelerations are required. To some degree relatively small projectiles benefit from the "square-cube" law, - weight varies about as the cube of a dimension, life as the square, and if acceleration requirements are not high, a small bird may develop enough lateral acceleration from the turning moment of a small tail plus body lift. However for terminal correction the use of small "bonkers" may be feasible within weight and size constraints.

The on-board equipment for sensing the projectile position in the beam and applying corrections, or for receiving commands and applying corrections varies widely with the desired range and application. A few early anti-tank missiles used no gyroscopic references; current designs use at least a single gyroscope for roll stabilization. How far beyond this to go in providing an "autopilot" depends on the projectile dynamics and the response time desired of the projectile. Crotale is reported to employ a position gyro and three rate gyros. Vigilant is reported to employ a "twin-gyro autopilot", - this is not necessarily a very high cost item, since the whole Vigilant missile (14 kg weight) is reported to cost about \$2000. The electronics package designed for ACRA to sense position in the laser beam and provide commands to the control servos is reported to weigh only 1.2 kg and weight-wise is a small part of the control package.

In some systems the missile and the ground station exchange information which can be used to modify the characteristics of the control loop. Apparently this link exists in Crotale, and Roland and is an essential element of the SAM-D system. For birds riding a line of sight beam an anticipating command can be provided of required (large) lateral accelerations to prevent the bird from lagging the beam. This type of assistance is believed to be provided in Crotale and Roland.

Table V-13. Command Channel Options

Link	Examples
Wire	Tow, SS-10, 11, Dragon
Radio to Microwave Frequencies	Blowpipe, Indigo, Slam, Nike, Crotale*, Roland, Rapier *Crotale receives digital coded commands via X-band
Optical Frequencies Infra-red, Laser	
Note: Loop may be closed automatically or via manual control (Blowpipe, Seacat, Slam)	

Table V-14. Methods of Obtaining Control Moments

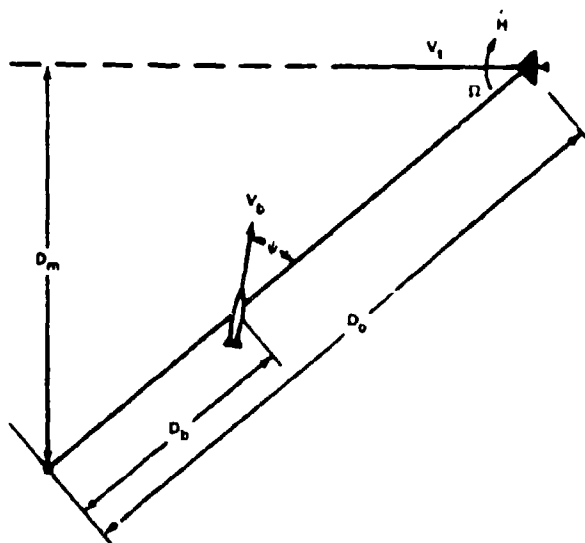
Generic Type		Examples
Aerodynamic	Tail Fins and Wings Tail Fins and Body Lift Tail and Nose Fins	Rapier ACRA Redeye, Blowpipe, Tow
Reaction	Tail, Fins plus Gas Jets Discharge Pellets Rocket Exhaust Deflection Side Thrusters "Bonkers"	Shillelagh, Chaparral Polecat Milan, Swingfire, Hot Dragon

A low drag projectile has limited intrinsic aerodynamic damping for rapid settling after a control perturbation. The simplest solution is to provide rate gyros. To determine whether other sources of a damping signal are feasible, such as differentiation of the sensed position in the beam (which gives no angular information) would require detailed dynamic analysis. The extensive use of rate gyros suggests that these represent the more "cost-effective" solution as determined by experience.

5.4.3 Line of Sight Beam Rider Limitations

Since the medium range air defense missile systems of greatest current interest in the U.S. (Crotale, Rapier and Roland) are all line of sight beam riders, as a point of departure we consider some of the dynamics of line of sight beam riding, and, in particular, the lateral acceleration requirements which this type of system imposes on the controlled projectile.

The computations are done for the simple case of motion in a plane. The geometry is shown in Figure 5-21, which also defines the notation. It is assumed that the missile simply flies up the line of sight to the target, adjusting its heading vector to remain on the line of sight.



40001 127

Figure 5-21. Intercept Geometry

We write the required lateral acceleration of the beam rider in terms of an aircraft turning at a constant rate of turn dH/dt in space, not concentric with the launch point.

The motion of the line of sight to the target, and the rate of change of slant range are defined by

$$\begin{aligned} D_0 \dot{\Omega} &= V_t \sin \Omega \\ \dot{D}_0 &= -V_t \cos \Omega \end{aligned} \quad (5.58)$$

In order to remain on the axis of the line of sight, the projectile must have a lateral velocity equal to that of the line of sight, hence

$$\begin{aligned} V_b \sin \psi &= \dot{\Omega} D_b \\ V_b \cos \psi &= \dot{D}_b \end{aligned} \quad (5.59)$$

The lateral acceleration of the projectile is (constant velocity assumed)

$$A_b = V_b (\dot{\Omega} + \dot{\psi}) \quad (5.60)$$

hence

$$\begin{aligned} V_b \cos \psi \dot{\psi} &= \dot{\Omega} D_b + \dot{\Omega} \dot{D}_b \\ &= \dot{\Omega} D_b + \dot{\Omega} V_b \cos \psi \end{aligned} \quad (5.61)$$

and

$$\dot{\psi} = \dot{\Omega} + \frac{\dot{\Omega} D_b}{V_b \cos \psi} \quad (5.62)$$

and

$$A_b = 2 V_b \dot{\Omega} + \frac{\dot{\Omega} D_b^2}{V_b \cos \psi} \quad (5.63)$$

If the target were flying a circle concentric with the tracking point, the second term in this expression would be zero.

We assume that the target is flying at constant velocity, but may have a constant rate of turn in space. Then

$$\dot{D}_0 \dot{\Omega} + D_0 \ddot{\Omega} = V_t \cos \Omega (\dot{\Omega} + \dot{H}) \quad (5.64)$$

$$D_0 \ddot{\Omega} = 2V_t \cos \Omega + V_t \cos \Omega \dot{H} \quad (5.65)$$

The target radial acceleration is

$$A_t = V_t \dot{H} \quad (5.66)$$

and so, finally,

$$A_b = 2 \Omega \left[V_b + \frac{V_t \cos \Omega D_b}{\cos \psi D_0} \right] + A_t \frac{\cos \Omega D_b}{\cos \psi D_0} \quad (5.67)$$

$$A_b = \frac{2V_t \sin \Omega}{D_0} \left[V_b + V_t \frac{D_b \cos \Omega}{D_0 \cos \psi} \right] + A_t \frac{D_b \cos \Omega}{D_0 \cos \psi} \quad (5.68)$$

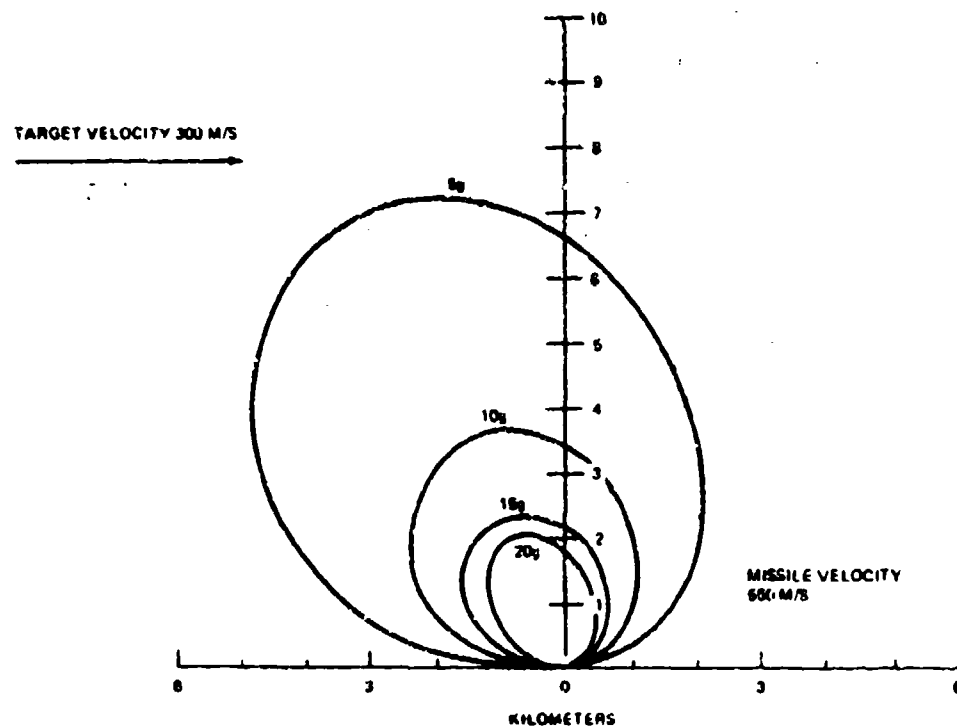
At midpoint on a passing course, $\Omega = 90^\circ$, and

$$A_{bm} = \frac{2V_t V_b}{D_m} \quad (5.69)$$

For a target flying an unaccelerated pass course, Figure 5-22 shows the regions within which the acceleration required to stay on the line of sight exceeds the values specified. Target velocity is taken as 300 m/s and projectile velocity at the target is taken as 550 m/s, approximately that of the Roland, Rapier, Crotale systems.

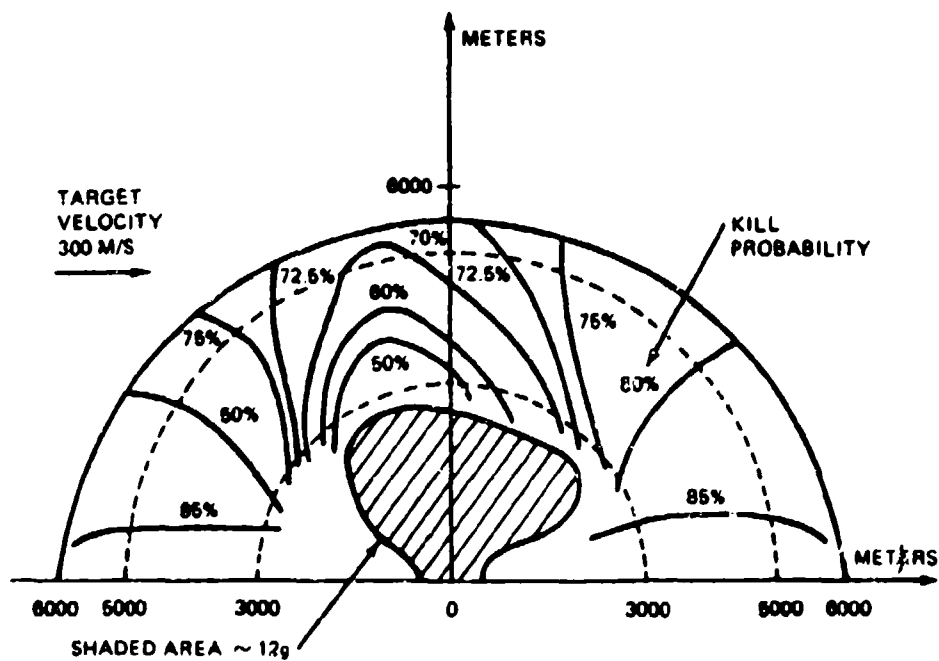
To lend some support to these simple computations, Figure 5-23 shows the Roland operational limits as released by Aerospatiale. ⁽²⁹⁾ The "hole" in the center corresponds to a maximum maneuver acceleration of about 12 g. Note that its diameter of about 3 km corresponds to the 3km design point range of the GLAADS gun system.

For directly incoming targets, the acceleration requirements are not severe in the forward region. A number of SAM systems are believed to have combined initial beam riding with terminal homing, using the beam riding in the low acceleration region to get the bird close enough to the target to acquire it with a homing head. After



40001 128

Figure 5-22. Zones within which Required Lateral Acceleration of Line of Sight Beam Rider Exceeds Specified Values



40001 129

Figure 5-23. Roland System Coverage and Effectiveness

acquisition the projectile converts to a proportional navigation type of path, with reduced acceleration requirements after conversion.

If a projectile is flying the line of sight beam, its required look angle to see the target is, from the above expressions,

$$\begin{aligned}\sin \psi &= \dot{\Omega} D_b / v_b \\ &\approx \dot{\Omega} t_b\end{aligned}\tag{5.70}$$

where t_b is the projectile flight time. A possible implementation of this concept is for, the ground station to transmit $\dot{\Omega}$ to the projectile, which has an internally generated measure of its flight time. With this information, ψ is computed on board, and the homing head can be properly directed. Since $\dot{\Omega}$ is common to any projectile in the beam, there is no limit to the number of projectiles that can be in flight in the beam simultaneously.

This system could be applied to projectiles with homing heads responsive to target illumination by a laser spot, and would avoid both the acceleration problem, and the rate of fire limitations of systems which tie up one control unit per projectile as long as the projectile is in flight.

5.4.4 Predicted-Corrected Air Defense System Considerations

In this section we outline some of the considerations in configuring an air defense system using projectiles with trajectory in-flight correction based on a predicted beam. Although not explicitly mentioned, it will be understood that the predicted beam is corrected in elevation by the computer for gravity drop as well as target motion, so that the projectile need not expend maneuver energy against gravity.

In most of the discussion we make no distinction between a configuration in which the projectile rides a beam with self alignment and a configuration in which the projectile is tracked and commanded to follow a minimum energy path to intercept by the computer. In both cases there is an effective "predicted beam".

We consider briefly the dynamics of the predicted beam. The angular perturbations of the beam will initially be relatively large, resulting from the amplification of sensor noise and target accelerations via the prediction process. However at the launch end of the beam, these perturbations cause only small linear deviations for the projectile to follow. As the projectile approaches the target, the lead angle collapses to zero, and beam motion reduces essentially to tracking noise. When the missile is midway to the target the linear

perturbations of the beam tend to be largest, unless the prediction process is designed to have a narrow band pass at this time.

The filter/prediction process in an actual design would be optimized, in view of the above considerations, and Kalman type filters would seem to be a reasonable way to optimize. It seems probable that the filter gains for this system could be pre-computed with resulting savings in ground computer requirements.

To be specific about the beam perturbations, consider the propagation of small errors in tracking. Define e_0 , \dot{e}_0 as the errors in position and velocity in tracking the target, in linear measure. Then the aim wander of the predicted beam at the predicted target range is

$$e_p = e_0 + \dot{e}_0 t_g \quad (5.71)$$

where t_g = the "time to go" of the projectile, i.e. the remaining time to intercept. Assuming a constant velocity of the projectile, with an initial estimate of flight time t_{p0} at launch, the linear motion required of the projectile perpendicular to the beam axis is

$$e_b = e_p (t_b/t_{p0}) \quad (5.72)$$

where t_b is the time from launch, and

$$t_{p0} = t_b + t_g \quad (5.73)$$

Hence

$$e_b = e_0 (t_b/t_{p0}) + \dot{e}_0 t_{p0} [1 - (t_b/t_{p0})] (t_b/t_{p0}) \quad (5.74)$$

If the position tracking error has a variance σ_t^2 at the target, and velocity smoothing is over an interval T_s , the velocity variance would be approximately $2\sigma_t^2/T_s^2$, and the variance of beam position at the projectile would be approximately

$$\sigma_b^2 = \sigma_t^2 \left[1 + 2 (t_g/T_s) + 2 (t_g/T_s)^2 \right] (t_b/t_{p0})^2; T_s \ll t_{p0} \quad (5.75)$$

For constant T_s , σ_b^2 has a maximum at about

$$t_g = t_{po}/2 - (7/8) T_s \quad (5.76)$$

at which point

$$\sigma_b^2 / \sigma_t^2 \approx (1/8) (t_{po}/T_s)^2 \quad (5.77)$$

This value could be rather large if T_s were held constant and small, hence it is clear that the dynamics of the prediction element and the control dynamics of the projectile must be worked through for an optimum time-varying solution.

In fact the position data must be smoothed also, and the criteria at the terminal end of the trajectory depend on a balancing between averaging to reduce sensor noise and improve the terminal accuracy, and the desire to have a tight loop to follow target maneuvers.

If one works through the noiseless dynamics of the predicted beam rider against a maneuvering target with constant acceleration, it can be shown that even with a "linear" predictor, the projectile is not required to develop an average acceleration exceeding that of the target. However, the ability to follow the accelerating target through sensor noise requires a compromise. A rough estimate of this trade-off may be derived as follows:

Assume that tracking noise is white, with spectral magnitude

$$\phi_n = \sigma_n^2 T_n (2/\pi) \quad (5.78)$$

flat to $\pi/2 T_n^{-1}$.

Assume that the corresponding power spectral density of target acceleration is

$$\phi_a = \left(\sigma_a^2 / \omega^4 \right) \frac{T_a}{1 + \omega^2 T_a^2} (2/\pi) \quad (5.79)$$

where σ_a is the rms value of acceleration.

Approximate the tracking, control, projectile dynamics loop by a band pass filter which follows the target and noise perfectly below B, and passes no information above B with $\lambda_n^{-1} \gg B$. Then the variance of miss is given by

$$\sigma_m^2 = \int_0^B \phi_n d\omega + \int_B^\infty \phi_a d\omega \quad (5.80)$$

$$= \sigma_n^2 T_n B (2/\pi) + \sigma_a^2 / (5B^5 T_a) (2/\pi) \quad (5.81)$$

Choosing B to minimize σ_m^2 , the optimum bandwidth is found to be

$$B^* = \left(\frac{\sigma_a^2}{\sigma_n^2 T_a T_n} \right)^{1/6} \text{ rad/sec} \quad (5.82)$$

with corresponding

$$(\sigma_m^2)_{\min} = 0.76 \sigma_n^2 T_n B^* \quad (5.83)$$

This simply derived expression turns out to be almost identical with one derived as a minimal error variance by Wiener theory in an early study of beam rider optimization. (24) (25)

For a numerical example, assume sensor noise $\sigma_n = 5$ m (half the target span) with a band width of 3 Hz so that $T_n = 0.05$ sec. Assume a jinking target with $\sigma_a = 5 \text{ m/s}^2$, which is rather high for a target attempting to deliver munitions and $T_a = 5$ sec. Then

$$B^* = 1.26 \text{ rad/sec}$$

$$\sigma_m = 1.2 \text{ meters}$$

of which tracking noise alone contributes 1.0 meter.

An actual design would require consideration of acceleration limits on projectile maneuver, and would in fact involve optimization of the system over the whole trajectory. However, the value of B^* suggested above does not seem to impose difficult requirements on the system.

Unfortunately, the use of a guidance or projectile tracking beam which is separately located from the target tracking sensor introduces boresight problems. There are a number of ways of circumventing this problem. One is to calibrate the system dynamically, with zero prediction, and both sensors tracking the same target (friendly or otherwise). It may be possible also to close the loop through the tracking sensor when the projectile comes within its beam, introducing the projectile position relative to the target to the end game computation. The computer in the end game would then receive and apply to the predicted beam a correction equal to the difference between the observed missile-target deviation, and that internally computed. Analysis is required to determine the amount of improvement possible, considering the short time that the target tracking beam will contain both target and missile. Preliminary estimates are given in appendix B.

Considering exterior ballistics, a major advantage of a predicted beam rider is that the lateral accelerations required are very small, except possibly in the end game when target acceleration normal to the projectile trajectory must be matched. We review briefly the consequences in terms of the projectile drag increment associated with lateral acceleration.

Consider the drag penalty for generating maneuver acceleration. The projectile lift is given by

$$L = C_{L\alpha}(\rho/2)V^2A\alpha^2 \quad (5.84)$$

where

$C_{L\alpha}$ = lift curve slope (radians⁻¹)

ρ = air density

V = velocity

A = area on which $C_{L\alpha}$ is based (cross sectional area for projectiles without wings or fins)

α = angle of attack of projectile relative to direction of motion

Then the lateral acceleration N_y in g's is

$$N_y = L/W \quad (5.85)$$

where W = projectile weight

$$N_y = C_{L\alpha} (\rho/2) V^2 (A/W) \alpha \quad (5.86)$$

The drag coefficient is

$$C_D = C_{D0} + (C_{D\delta 2}) \alpha^2 \quad (5.87)$$

where C_{D0} = drag coefficient for zero angle of attack (zero yaw)

$C_{D\delta 2}$ = drag coefficient slope with square of yaw angle

If a family of projectiles homologously scaled in caliber is considered, the angle of attack required to produce a given lateral acceleration varies inversely with W/A . Hence small projectiles may require less angle of attack, and the rise in their drag coefficient is less. For a given acceleration, one is less likely to require additional lift surfaces than with large projectiles, and body lift alone may be sufficient.

All of the coefficients vary with Mach number, but we may consider average values in the supersonic region for an estimate of magnitudes. For a numerical example, consider a projectile similar to the ACRA round, with 142 mm diameter, 44 lb weight, and a velocity of about 1800 f/s. Assume $C_{L\alpha} \cong 3.0$; $C_{D\delta 2} \cong 8$. Then

$$\alpha = .023 \text{ radians/g}$$

and the drag increment is about

$$\Delta C_D \cong .004 N_y^2$$

ACRA is not a low drag projectile; hence C_{D0} might be about 0.50. At any rate, lateral accelerations below about 3 g would not add significantly to the zero lift drag. However, a requirement for 10 g, as in the case of line of sight beam riders, would about double the drag. Since, in a general case,

$$C_D = (W/A)^2 N_y^2 \quad (5.88)$$

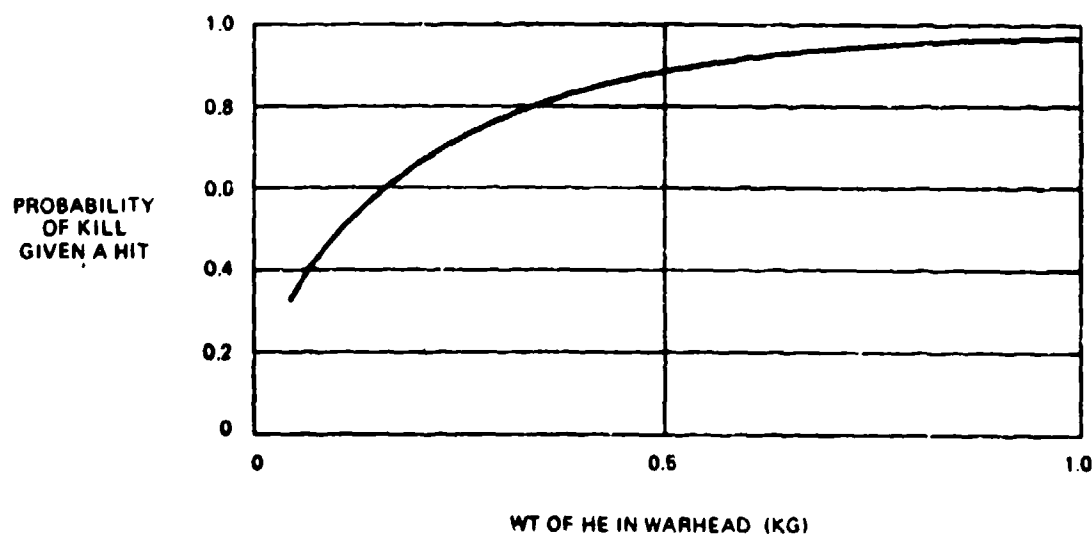
if weight scales as the cube of diameter, and area as the square, the smaller the projectile, the less will be the drag penalty.

However, since the drag loss to beam following corrections introduces a random variation on time of flight, time to go, etc., this source of dispersion will cause a miss component similar to that of a conventional uncorrected projectile with muzzle velocity dispersion. To eliminate this error source it would seem to be necessary to track the projectile in range or velocity, and continually update the estimated time to go in the prediction equations. This error source does not arise, of course, with line of sight beam riders.

5.4.5 Estimated Characteristics and Cost-Effectiveness

To estimate what one might optimistically expect from a guided-predicted projectile system, four gun/projectile combinations have been considered.

The four systems each carry 0.8 kg of HE in the warhead. It is estimated that this weight of HE will produce an 0.95 probability of kill given a hit. The assumed variation with weight of HE in the warhead is shown in Figure 5-24 and is based on estimates developed in prior reports in this series. The weight of warhead case plus contact fuze is estimated to bring total warhead weight to 3.0 kg.



40001 130

Figure 5-24. Assumed Warhead Terminal Effectiveness

5.0 kg is allocated to the control package, including fins. The only basis for this estimate at this time is the published difference between all-up weight of the ACRA guided and conventional rounds.

The warhead plus control package then totals 8.0 kg. This "payload" is to be boosted to 700 m/s by various combinations of gun and rocket boost. An initial set of computations at 1000 m/s indicated that the projectiles would have more range than is required, and the gun boost systems would require larger caliber guns than seemed desirable.

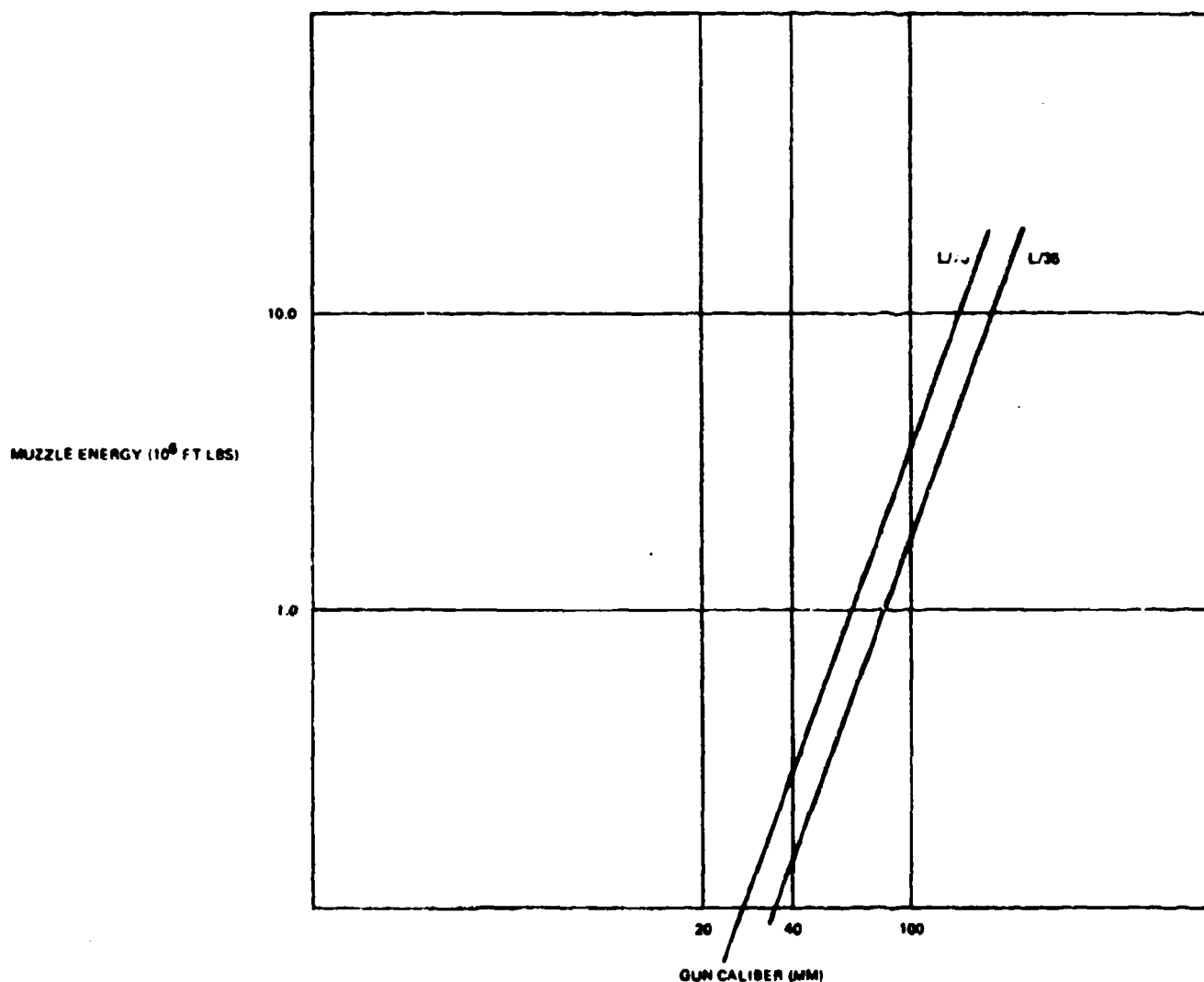
The gun boost increment is computed at 700 m/s (no rocket), 500 m/s, 300 m/s and zero (no gun). For rounds with rocket boost, aluminum cases and Loki propellant are assumed, the gun boost case fractions being slightly higher than for the rocket alone. This gives the weight of projectile fired from the gun, and together with the required gun boost velocity defines the muzzle energy required of the gun. Given a caliber length L/λ for the gun, the gun caliber is then determined within narrow limits as shown in Figure 5-25. For an $L/70$ gun, the caliber ranges from 75 mm for a gun boost alone, to 42 mm for only 300 m/s gun boost. The assumed relation between muzzle energy and minimum gun caliber is shown in Figure 5-25.

The principal determinants of projectile size are assumed to be the low density components, the HE in the warhead, and the rocket propellant. These volumes are estimated in each case, an optimistic shape factor is applied, and projectile length and diameter estimates were derived for $L/D = 10$ and 15 . A high L/D is desirable to reduce drag coefficient, but the range to sonic velocity for the cases considered seemed adequate for L/D as low as 10 , and these values are shown in the subsequent tables.

The cartridge case volume was estimated roughly from gun propellant weight, and sized to the gun chosen for each projectile. Aluminum or equivalent lightweight cartridge case material was assumed.

For the gun only solution, the required gun caliber turns out to be larger than the projectile diameter, for example, a 75/46 solution. As more of the boost is provided by the rocket, the projectile diameter increases for a specific L/D , and the required gun caliber to provide the boost energy decreases, until the solution is a full-caliber round.

The high payload weight in the projectile tends to give the solutions a relatively high value of w/C^2 . Drag coefficient at Mach 2 has been assumed to be 0.50 for an L/D of 10 , including some allowance for fin drag and the mild maneuvers required by this type of system. On this assumption, all four solutions exceed sonic velocity at least to 9 km.



40001-121

Figure 5-25. Minimum Gun Caliber to Develop Specified Muzzle Energy

The cost of a complete round is optimistically assumed to consist of \$1200 for the control package, plus \$20, \$40, \$30/kg of complete round weight for the gun, gun-boost, and rocket solutions respectively. The cost per round then sums to about \$1500-1600, hence is determined almost entirely by the assumed control module cost.

The numerical values developed are listed in Table V-15, where they are referenced against Crotae, Roland, Zuni (a simple unguided rocket) and ACRA. The gun boosted rocket rounds are somewhat more optimistic than ACRA in terms of the rocket motor and

case weight required to boost the assumed payload, but are roughly comparable to ZUNI in this regard.

The major uncertainties have to do with the volume, weight and cost of the control package. It would seem desirable, therefore, to do a good preliminary design of this module for several command and control concepts to establish reliably what can be done within the state of the art, with regard to both weight and cost. Emphasis should be on minimizing the weight, sophistication, and cost of the on-board equipment, even at the expense of some added cost in the ground station.

With regard to the derived lengths of the complete rounds, one may note that the complete round length of a conventional round of ammunition is from 10 to 12 times the gun caliber. Hence the gun boost-only solution works out to about the same length as the conventional round for a 75-mm gun.

Assuming optimistically that the design problems of the control package and projectile command can be solved, we show in Table V-16 some effectiveness-cost estimates, and in Figures 5-26 and 5-27 compare them against ammunition cost per kill with conventional gun systems and Crotales.

The curves for the conventional guns should not be considered definitive; the lower limit is defined as a "3-mil system", and can be adjusted if one believes that a "2-mil system" is achievable. The conventional gun curves are also shown as rising rapidly as the projectile drops to sonic velocity; this limit for a 30-mm weapon would occur at about 3/4 of the range shown for 40-mm.

The values used for reference for the "conventional" predicted fire system are, in fact rather favorable to this system. Figure 5-28 sketches the corresponding "rounds per kill" and compares them against the rounds per kill achieved with 40-mm guns below about 2 km in World War II.

Obviously the cost comparison depends entirely on the assumed cost of the control package for the predicted-corrected system, hence the importance in developing accurate estimates of this cost.

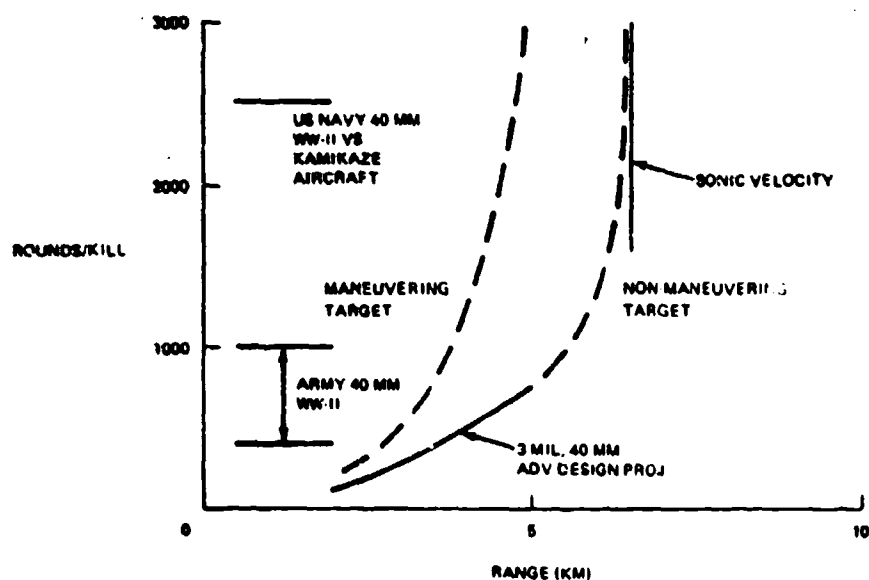
Since the solutions scale with the weight of the warhead plus control package, we show in Figure 5-29 the result of changes in this parameter on the caliber of gun required, and the projectile body diameter for L/D values of 10 and 15. It has been assumed that the L/D 15 projectile would have slightly lower drag coefficient because of the smaller nose apex angle.

Table V-15. Comparison of System Characteristics

	Gun	Gun/Rocket	Gun/Rocket	Rocket	Crotale	Roland	Zuni	ACRA	
								Guided	Unguided
Wt. of HE in WHD (kg)	0.8	0.8	0.8	0.8		3.5	22	2.8	2.6
Wt. of WHD + Fuze (kg)	3.0	3.0	3.0	3.0	15.0	6.5			
Wt. of Control Package + Fins (kg)	3.0	5.0	5.0	5.0					
Total "Payload" Wt. (kg)	8.0	8.0	8.0	8.0					
Gun Boost Velocity (m/s)	700	500	300	0	-	-	-	550	550
Rocket Boost Increment (m/s)	0	200	400	700	900	580	900	~150	150
Sum of Velocity (m/s)	700	700	700	700	800	580	900	~700	700
Rocket Case Parameter $\lambda \sigma$	-	0.35	0.30	0.25					
Projectile/Rocket Wt. (kg)	8.0	9.1	10.2	12.1	80	62.5	49	20	15
Rocket Propellant Wt. (kg)	0	0.8	1.7	3.3					
"Burnt" Weight of Proj. (kg)	8.0	8.3	8.5	8.8					
Wt. of Complete Round (kg)	11.9	11.3	11.1	12.1	80	62.5	49	26	21
Wt. of Gun Propellant (kg)	1.8	1.0	0.4	-	-	-	-		
Volume of HE + Rocket Prop (cm ³)	482	958	1500	2042					
Volume of Cartridge Case (cm ³)	2510	1000	410	-					
Gun Muzzle Energy/Ft Lb x 10 ⁻⁶	1.57	0.83	0.34	0	-	-	-	4.45	
Min. Gun Caliber (mm) L/70	75	60	42	-	-	-	-	110	
L/35	90	75	54	-	-	-	-	140	
Projectile L/D	10	10	10	10	19	15	22	8.8	
Projectile Dia (mm)	46	58	67	74	150	160	137	142	
Projectile Length (mm)	460	580	670	740	2890	2400	2800		640
Gun Cal (mm)	75	60	67	-	-	-	-	142	
Complete Round Length (mm)	720	820	750	740	2890	2400	2800	1245	900
C _{D2}	0.5	0.5	0.5	0.5					
Range to Sonic Vel (km)	21	14	10	9	8.5				
Cost./Round (\$)	1500	1650	1650	1600	17,000	17,000	400		

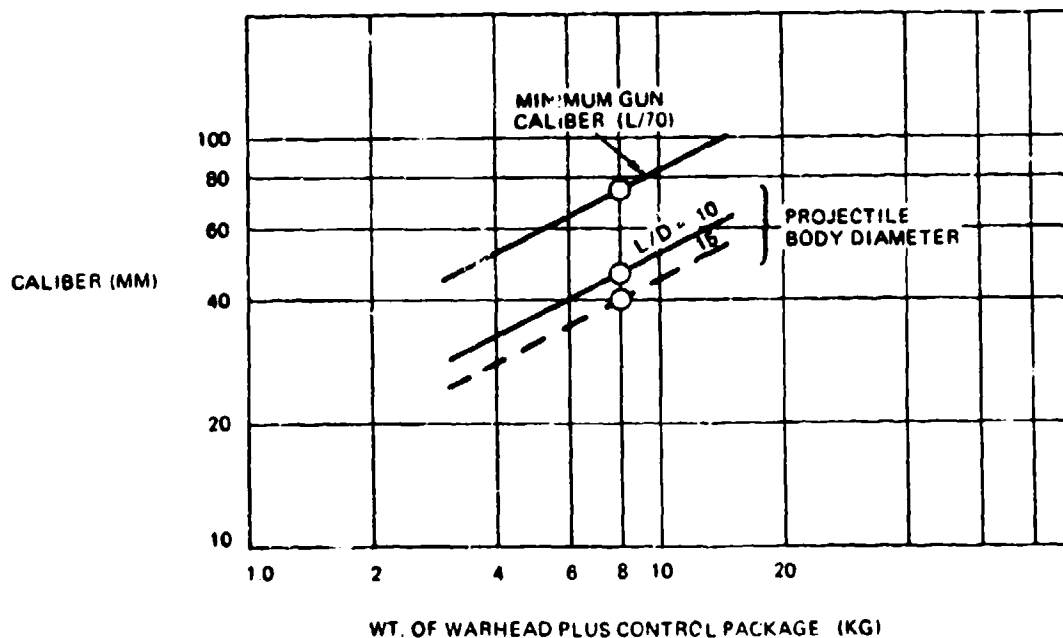
Table V-16. Effectiveness - Cost Estimates

	System	Predicted/Corrected Projectile System				3-Mil 40-mm Conv. Gun Non-Maneuvering	Crotale All Cases	
		Target	Non-Maneuvering		Maneuvering			
			Head-on	Side-on	Head-on			Side-on
Without Terminal Loop Closure	Aspect							
	Target Radius (m)	1.0	3.0	1.0	3.0	1.0	3.0	
	System Std. Dev. (m)	1.0	1.0	1.2	1.2	3D (km)	3D (km)	
	Prob. of Hit	0.39	0.99	0.29	0.96	$(18D^2)^{-1}$	$(2D^2)^{-1}$	
	Prob. of Kill/Hit	0.95	0.95	0.95	0.95	0.60	0.60	
	Prob. of Kill/Round	0.37	0.94	0.28	0.91	$0.033D^{-2}$	$0.30D^{-2}$	
	Rounds/Kill	2.7	1.1	3.6	1.1	$30D^2$	$3.3D^2$	
	Cost/Complete Round	1500	1500	1500	1500	10	10	
	Cost/Kill	4450	1650	5400	1650	$300D^2$	$33D^2$	
With Terminal Loop Closure	System Std. Dev. (m)	0.5	0.5	0.6	0.6			
	Prob. of Hit	0.86	1.00	0.75	1.00			
	Prob. of Kill/Rnd	0.82	0.95	0.71	0.95			
	Cost/Kill	1650	1600	2100	1600			



40001-134

Figure 5-28. Rounds/Kill of Conventional AA Gun Systems



40001 135 A

Figure 5-29. Effect of Weight of Warhead plus Control Package on System Characteristics

The estimated ranges to sonic velocity are all in excess of those probably required to match the sensor ranges. This suggests that additional perturbations might be performed in a more comprehensive study in which the muzzle velocity developed by the gun is reduced. The required gun caliber for a given weight of projectile varies as $v_0^{2/3}$ where v_0 = muzzle velocity, and the 75-mm solution would then reduce to a gun caliber of 60-mm. If in addition the warhead weight were reduced, (Figure 5-29) and the control package weight also to a total of 5 kg., the gun caliber required might be only 50-mm. It is doubtful however, that cost per round would be reduced.

For the reader who may be alarmed by a self-propelled antiaircraft fire unit mounting a gun as large in caliber as 75mm, we offer Figure 5-30 which shows a 94 mm gun (WW II) on a self propelled chassis. A solution of this magnitude is not indicated by the optimistic estimates developed above.

As an aid in visualizing the projectile and complete round configurations resulting from the estimates of Table V-15, projectile plus cartridge case outlines have been sketched in Figure 5-31 for $L/D = 10$ solutions and in Figure 5-32 for $L/D = 15$ solutions. They are optimistic in terms of the volume provided for both the low density components and the control elements. The sketches suggest that the excessive projectile length of the intermediate gun-boost-rocket solutions compared with conventional round length in the listed minimum gun calibers may be undesirable.

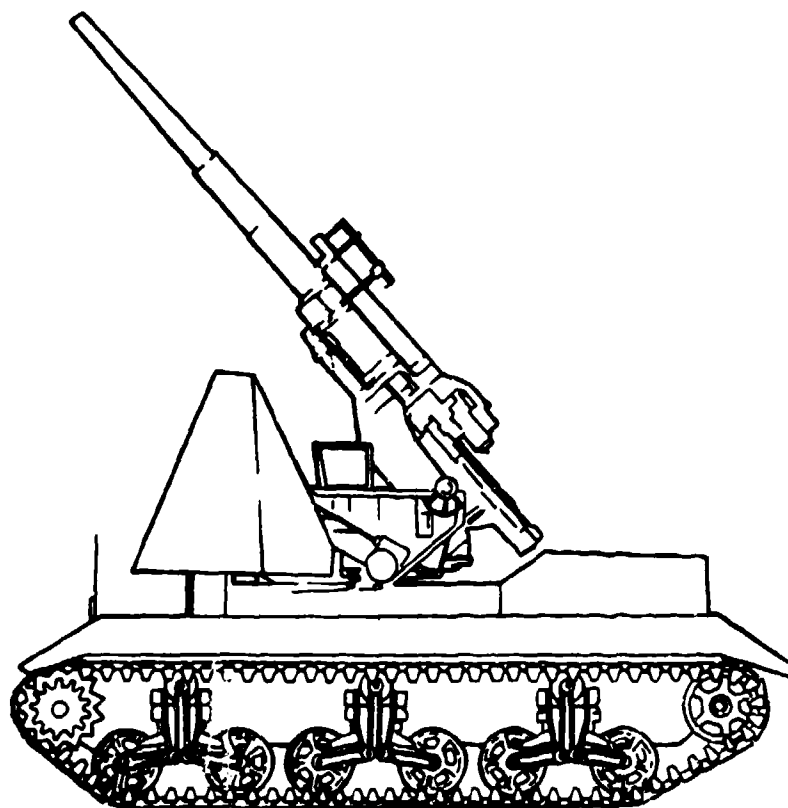
The gun-only solutions have the advantage that the round length about matches that of a conventional round, and leaves the base of the projectile unbroken by a nozzle opening, hence available for a trihedral reflector and signal receptors.

The estimated lengths of the projectiles without rocket boost may be too short considering the weight balance, and the fact that almost the full length is required to accommodate the warhead.

These sketches should not be considered definitive, since they are not supported by a proper preliminary design analysis.

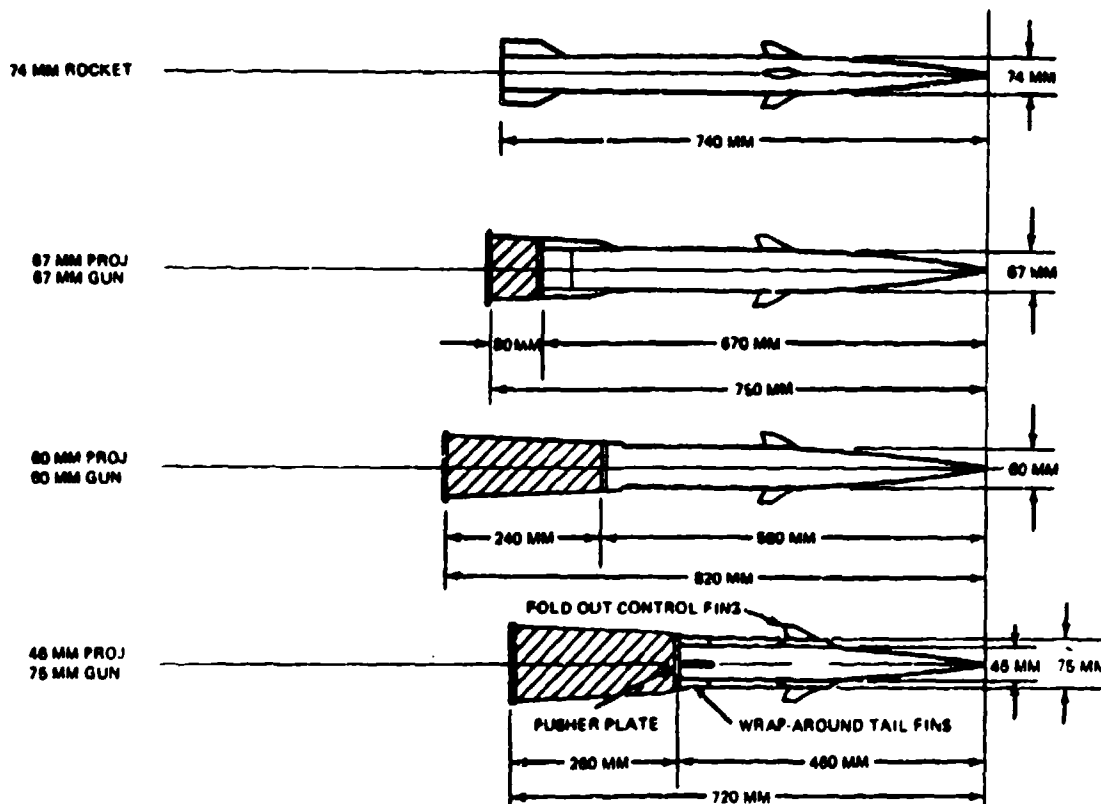
5.5 CONCLUSIONS

Gun boosted rockets appear to offer the possibility of substantially shorter time of flight than can be achieved with unboosted projectiles. Exploitation of this potential requires that angular and velocity dispersion of the boosted projectiles be held close to those values achievable with unboosted rounds. Some of the system advantage may be taken in reduced fire unit weight, although this potential was not analysed in the present review.



40001-138

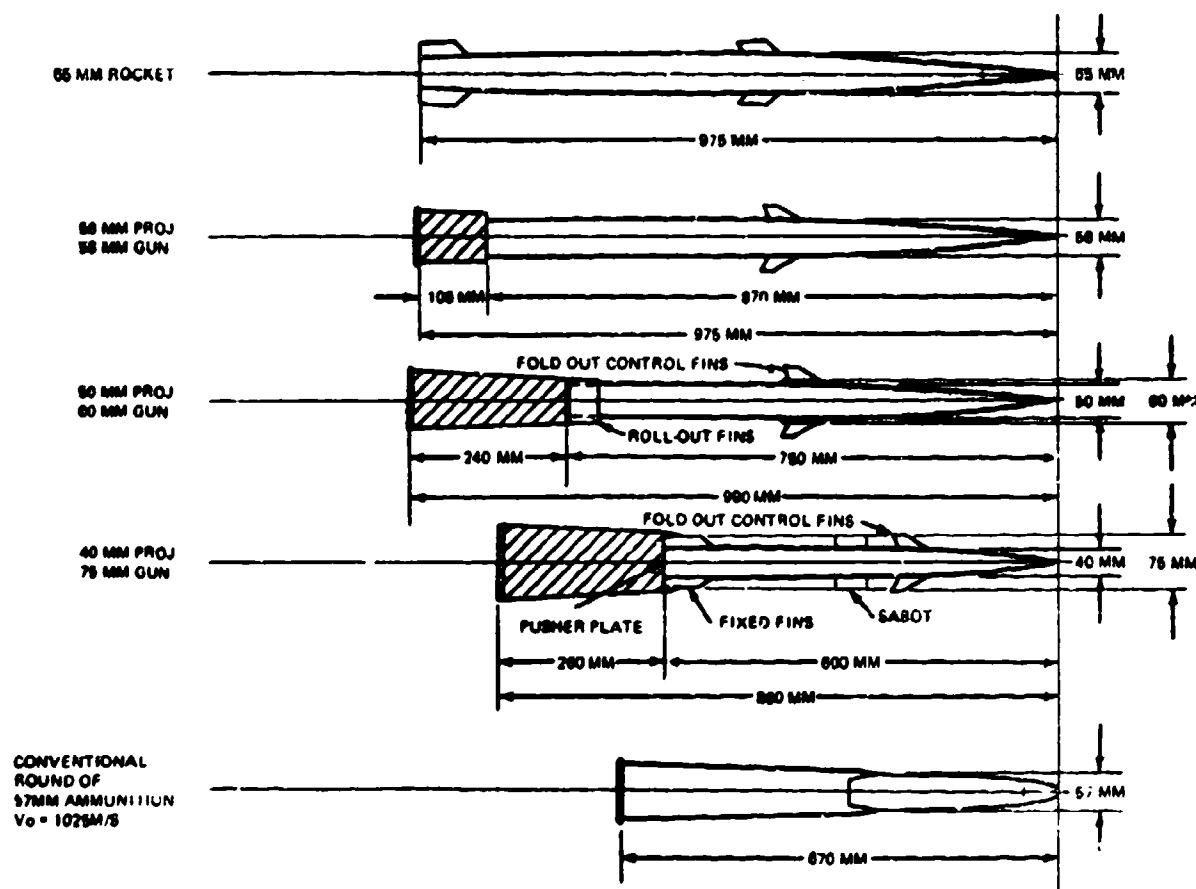
Figure 5-30. "A Solution this Large is Not Recommended"



40001-137

Figure 5-31. Sketches of $L/D = 10$ Configurations

Combination rounds may suffer a cost disadvantage in cost of ammunition per target killed, unless the cost per kilogram of the complete round can be brought down to be competitive with that of conventional projectiles. The few RAP rounds now being procured, admittedly at an early point on the cost-quantity curve, suggest that the more complex design may involve inherent cost disadvantages in situations where the boosted rounds are competitive in effectiveness with conventional full caliber or subcaliber rounds. However, conventional rockets are in fact competitive with conventional gun fired projectiles on a cost/kilogram basis, so that better cost estimates are desirable.



40001 128

Figure 5-32. Sketches of L/D = 15 Configurations

It is concluded that rocket-boost projectiles should not be excluded from further evaluation as an air defense weapon.

An air defense weapon solution utilizing projectiles controlled to fly a predicted beam appears highly attractive, in spite of the many current unknowns. The brief examination of this section suggests that a solution may be feasible utilizing a gun-fired unboosted projectile and a gun in the caliber range 50 to 75 mm, depending on the weight of the control package required. For a number of reasons detailed in the text such a solution appears preferable to a gun-boosted rocket solution, although a simple guided rocket may be competitive. The

relatively low maneuver accelerations required of a predicted beam solution suggest substantial payoffs in reduced weight and cost of the guided projectiles. However, this possible gain must be traded against the possibly increased cost of the sensor packages on the fire unit.

5.6 RECOMMENDATIONS

It is recommended that the Army maintain an interest in gun-boosted rocket solutions, with further supporting analyses emphasizing very high velocity solutions, reduction in projectile angular and velocity dispersion and reduction in ammunition costs. This effort should not be postponed until the Javelot shoot-out, although it should incorporate experience as gained with Javelot. Javelot should provide information on reduction in fire unit weight with projectiles of moderate velocity, and on the problems of reducing dispersion, but it is not believed that the present design of Javelot will indicate the potential of very short time of flight solutions.

It is recommended that the Army Armament Command develop a joint effort with the Missile Command to explore the potential of predicted-corrected solutions, emphasizing gun-fired controlled projectiles.

SECTION 6

DEFENSE AGAINST STANDOFF MUNITIONS

" - a Styx missile heading your way can be a disconcerting sight, the Israeli sailors report

" 'That missile looks like a ball of fire when its headed your way, 'said Capt. Yumi. 'You better dodge it or shoot it down'."

L A Times, 31 Oct 1973

The problem of how much air defense to provide against aircraft and how much to provide against surface to surface ballistic missiles has often been treated as a dichotomy of targets. Meanwhile, the relatively short range air to surface guided munitions have increased in range, in size, and in effectiveness to constitute a significant threat lying between these extremes. Surface to surface lift supported missiles continue to be used. This middle portion of the threat spectrum will be additionally populated by remotely piloted vehicles, some of which will serve as unmanned weapons platforms delivering their own air to surface guided munitions.

Currently air to surface guided munitions have reached a level of effectiveness such that they can destroy a small hard ground target at less total cost than would be possible with conventional bombing, even in the absence of local defenses.

Hence it is important to examine the degree to which the capability of local air defenses designed primarily for use against aircraft, can be augmented to deal with at least a portion of the threat of standoff munitions.

In such an examination, it is considered important to avoid the trap of trying to deal with all standoff weapons, however launched, since this seems to lead to unacceptably expensive "junior antiballistic missile" defenses.

In the following paragraphs we attempt to hold the view that the object of augmenting the defense capability is to deny the enemy the use of his simpler, less costly standoff weapons, thereby raising his cost and logistics requirements to accomplish a given level of damage.

The future use of cannon launched guided projectiles (CLGP) must be noted. These are not considered in the present study, as they represent a threat which, like medium range ballistic missiles may be too costly to counter by active defenses. The advances of technology, even under conditions of austerity, have however, a way of outpacing conservative objectives, and such defenses may not be economically impossible in time.

Beginning with the simpler air delivered standoff munitions, we note that the first generation of designs required that the launch aircraft maintain a line of sight to the ground target, down which the munition was directed. Such munitions are still used by helicopters. Aviation Week notes¹

"Armament of the Soviet Hind A helicopter gunship consists of a gun and alternate missile configurations, including two rocket pods. The pods can be swivelled to aim the unguided weapons without pitching the helicopter. Hind A can be armed with guided antitank missiles. The helicopter, which also can carry troops, is operational with Red Army units".

However, standoff munitions of second generation design, now operational provide partial to complete relaxation from the continuous line of sight requirement.

Systems range from munitions that home on a target designated by a laser spot, to munitions that acquire ground targets in flight via a television head with automatic homing after target designation by a remote observer. They include various types of antiradiation homing systems.

The current generation of air to surface missiles has sufficient maximum range to allow the launch aircraft to remain outside the local defenses of a ground target. How much of the maximum standoff range can be utilized operationally depends on the target acquisition sensors, weather, and the degree to which the ground target acquisition and designation process must be complete before the munition is released from its carrier aircraft.

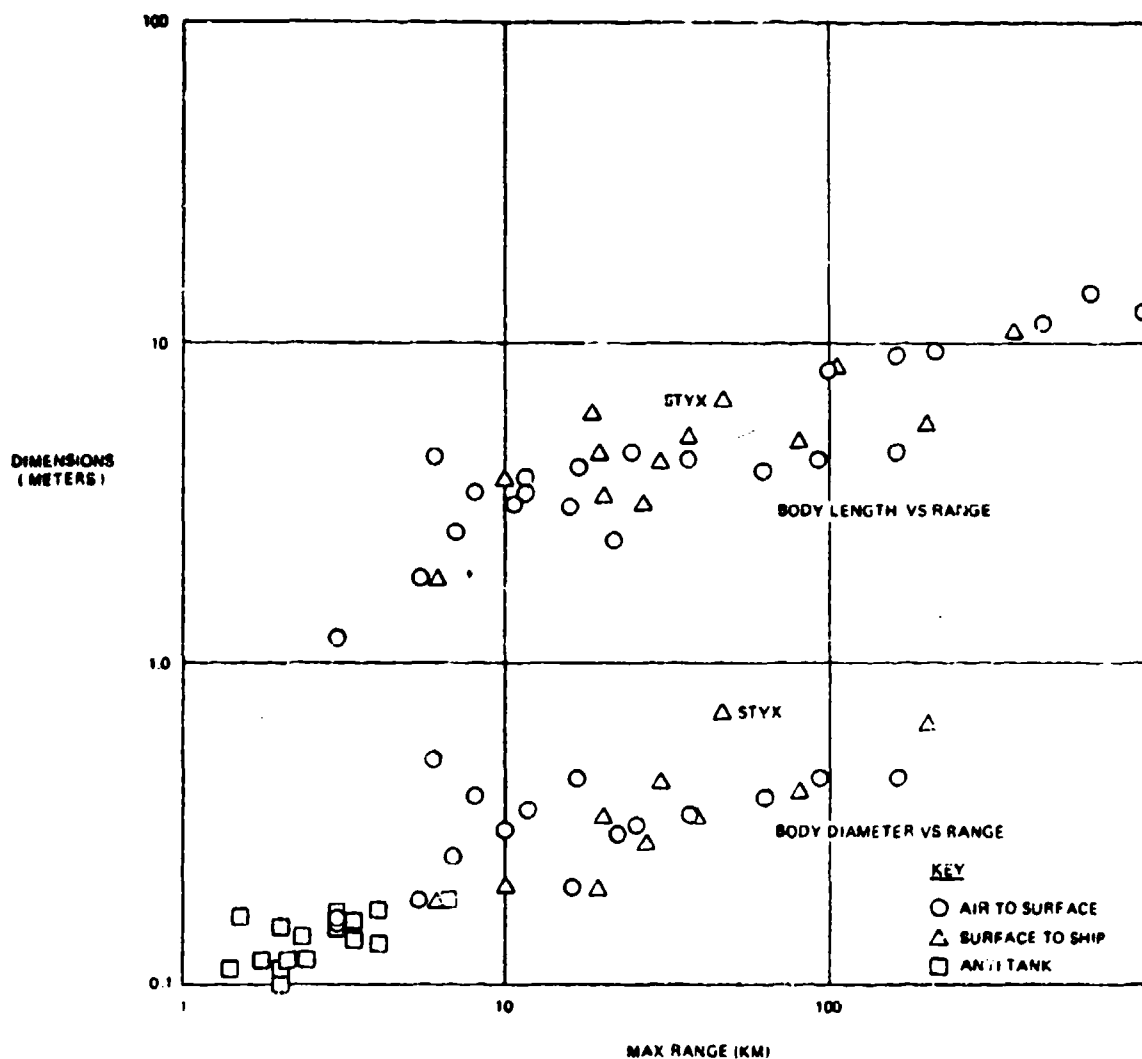
Clearly, the defense would prefer to engage the parent aircraft prior to munitions release. The trend of development however, is to place the launch aircraft outside the defenses (or below them if there is good SAM cover) in which case it becomes important to consider the capabilities of the defense against the standoff munitions themselves.

6.1 STANDOFF MUNITIONS CHARACTERISTICS

Characteristics of standoff munitions are summarized in Section 8, along with some estimated costs. In this section we consider the munitions characteristics affecting the capability of an active defense against them. We do not consider the possibility of electronic and optical countermeasures.

6.1.1 Munitions Size and Velocity vs. Standoff Range

Body diameter and length of stand-off munitions are shown as a scatter diagram in Figure 6-1. The points represent operational and developmental air to surface munitions, surface to ship missiles, and to fill in the lower end of the spectrum, small antitank surface to surface missiles.



40001-140A

Figure 6-1. Body Diameter and Length of Missiles versus Maximum Range

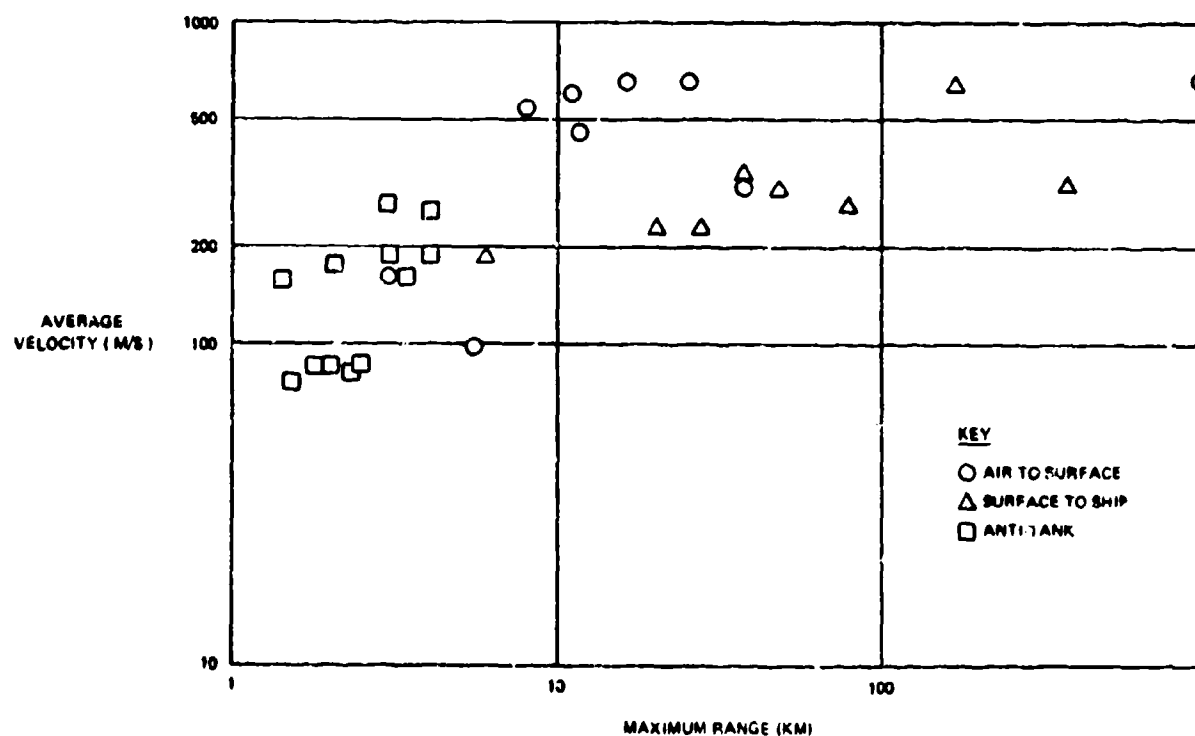
Some of the points represent early subsonic vehicles which were essentially pilotless aircraft, and these have relatively large dimensions. The trend is to faster weapons which have smaller aerodynamic surfaces, and increased body length to diameter ratio.

The maximum range given is that which is associated with the munition in open sources. Maximum range is difficult to quantify in any case, and is as likely to be fixed by the guidance mode as by the vehicle propulsion and aerodynamics. For present purposes however, it is a useful rough indicator of the likelihood that the launch aircraft or platform will be outside the range of the local defenses.

It will be noted that few of the air to surface munitions are indicated to have a maximum range of under 6 kilometers. In the absence of local defenses, shorter ranges would no doubt be utilized, however there does appear to be a general capability of launch beyond the range of the local predicted fired defenses.

All of the munitions shown are small, compared with fighter aircraft, even those of ranges exceeding 100 km. The anti-ship Styx, an early design, is relatively large and hence should not be used as a basis for estimates of defense effectiveness against future standoff munitions.

The average velocity of the missiles is shown as a scatter diagram in Figure 6-2. Except for the small antitank missiles, velocities tend to fall into two categories, - high subsonic and about Mach 2.0. The slow missiles tend to have larger wings or fins, for a given weight and range, however the aerodynamic surfaces contribute little to detection probability in a head on aspect, and, as discussed later, are only of secondary interest with regard to vulnerability.



40001 141

Figure 6-2. Average Missile Velocity versus Average Range

6.1.2 Detectability

It is difficult to make reliable, generalized estimates of the detectability of stand-off munitions with various sensor types without resorting to experimental measurements. The nose shape of the munitions in particular, varies widely across types. More importantly, the material of which it is fabricated varies from metal (line of sight beam riders) to dielectric Radomes and Irdomes for homing missiles and optical lens closures for TV guidance.

For high frequency microwave radar and for optical radar, one may derive a rough lower bound to cross section by representing the missile body as an ellipsoid with the same L/D . On this basis (which yields a limit far too low for radar versus dielectric nose ogives) one obtains head-on radar cross sections of -25 to -40 dB relative to 1 square meter, and optical cross sections when corrected for surface reflectivity which are slightly less.

A possible upper limit for microwave radar might be obtained by assuming that the inner structure and equipment reflect about as a hemisphere of missile diameter. On this basis one would obtain head-on radar cross sections of -7 to -15 dB, for diameters 0.5 to 0.2 meters.

As the aspect of the missile changes, and one approaches a side-on view, the metal body behind the radome assumes prominence, and estimates may become more reliable. An ellipsoid with an L/D of 10.0 has a side on radar cross section about 20 dB above the head-on cross section, hence one might expect a cross section of -5 to -20 dB in the optical range in this aspect. In addition, for narrow angles about the beam one would obtain substantial increments from the fins, wings, strakes, etc.

As the radar wavelength becomes large compared with the missile dimensions, the radar cross section at a given wavelength is proportional to the square of the volume of the missile. The volume of a 10-20 km missile may be less than 1/100 that of a small fighter aircraft; hence its radar cross section in the Rayleigh region would be down 40 dB from that of the fighter.

Surveillance radars associated with local air defense systems claim ranges approaching 20 km on a 1 meter² target. The Mirador¹⁰, for example, is stated to have a 17 kilometer range on a 1 m² target, and 11 km on 0.10m² target (probability criterion not specified). The 11 km range works out as equivalent to the following ranges, versus target cross section in dB as shown in Table VI-1.

Table VI-1. F-4 Mirador Detection Ranges

Target Radar Cross dB rel to 1m ²		Range (km)
-10.0		11
-20.0		6
-30.0		4
-40.0		2

If the launch aircraft can be acquired before munitions release, the weapon separation may be observed. This could simplify the missile acquisition problem. However, if the launch aircraft need not maintain a line of sight to its target during acquisition, but can fire its bird from low altitude under "defilade" the problem is more difficult.

Radars for counter mortar and artillery use do acquire and locate much smaller projectiles in flight, and at artillery ranges, hence the problem is not insoluble. However, it does require a more definitive analysis of the sensor equipment required for acquisition and tracking than time permits in the present paper.

6.1.3 Warhead Characteristics

Warheads of stand-off munitions with which the Army will have to cope will be those intended for use against personnel, vehicles, structures (bridges) and in the near future, heavy armor.

The high explosive contained in a warhead has only about 1/5 the density of steel, hence the warhead tends to be one of the largest components of a missile, exceeded only by the volume of rocket propellant (also low density) for weapons with large stand-off ranges.

For most of the above applications, a high ratio of HE to metal is desired to maximize warhead effectiveness. Warheads for attacking heavy armor and employing the Monroe effect likewise have a high HE content by volume.

AP projectiles used in Naval gunfire have very low HE content, since the object is to perforate heavy armor and then detonate inside an enemy vessel. The very low effectiveness of such projectiles against most land targets suggests that they would be unlikely to be used for such purposes.

It is therefore suggested that the following warhead types are of principal interest in considering the vulnerability of stand-off munitions.

- (1) Simple high explosive type, with high fraction of HE by weight, thin wall, intended to project many small fragments at very high velocities, and alternately to deliver high blast effect on impact. These warheads might be considered roughly similar to conventional GP bombs. Warheads with "shaped charge" heads would have similarly high HE content.
- (2) Semi-armor-piercing warheads. These have a heavier nose, ogival shaped, thicker walls, lower fraction of HE by weight than (1) and are intended to penetrate target armor before detonating. Some present missiles already claim the availability of this type of head as an option. Ship to ship missiles would be expected to use this type of head, since most combat ships are designed to resist externally bursting fragmenting projectiles.
- (3) "Cluster" type warheads which contain many small bomblets. These are strewn over the target area, and increase the effects coverage against men and light vehicles.

Of the three types indicated, the first is probably the most vulnerable, the second is relatively invulnerable from the forward aspect. The third is home free once it has ejected its cloud of bomblets, but if penetrated before this point, there is some hope that detonating one bomblet will produce a chain reaction among the others.

Note that an effective defense against type (1) will cause the enemy to make an easy change to type (2).

In particular, with the exception of the shaped charge head, the warhead effectiveness will not be significantly reduced if the forward section is made quite thick to prevent penetration of defensive projectiles in the nose-on aspect.

Because of the low density of HE, warheads in stand-off munitions tend to use the full diameter of the missile body. The ratio of case thickness to diameter then depends on the fraction of weight of body plus HE (except for the nose ogive) devoted to HE. Figure 6-3 shows this ratio, which varies only slightly with the ratio of explosive to metal densities.

Figure 6-4 shows warhead weight versus body diameter for a large number of missiles for use against ground targets. Also shown are obsolescent GP and SAP bombs, and some low-drag bombs. The most efficient packaging of the warhead tends to cause it to follow the L/D ratio of WWII GP bombs. The semi-armor piercing bomb, with higher relative case weight, has a slightly smaller diameter for given weight. The low drag bombs pack HE into the ogive, an inefficient arrangement for missiles.

Using Figures 6-3 and 6-4 as a guide some rough estimates of typical side-wall thicknesses of warhead types are shown in Figure 6-5 as a function of warhead weight. Principal interest should probably be directed to the SAP and GP range, and wall thicknesses of from 10 to 30 mm of steel.

These values are not greatly different from the armor plate thicknesses which may be used to armor ground attack aircraft. The Soviet IL-2 aircraft in WWII used 8 to 13 mm steel plate to protect the pilot. The current AX aircraft has been reported to protect the pilot and vital components with from 1600 to 1700 lbs of armor, variously reported⁽⁸⁾ as aluminum or titanium, with thicknesses up to 50 mm. 50 mm of titanium would work out to roughly 30 mm of steel equivalent, on a density basis. It is interesting to compare these values with the pre-WWII aircraft vulnerability estimates given by Rougeron.⁽⁶⁾

6.2 WARHEAD VULNERABILITY

As noted earlier, the largest single component of a standoff missile, with the possible exception of the rocket propellant, is the warhead. This is evident on inspection of the many inboard profiles which have been published for the various missile designs.

The control systems: gyros, homing heads, servos, power supplies, etc. are becoming smaller with advancing technology and as the velocities of missiles are increased, the wing and fin areas become smaller. To affect the missile's impact point by damaging its controls requires that the damage take place at an appreciable range from the missile's target. These considerations suggest that the primary objective of defensive fire should be to destroy the warhead of the attacking missile. Any related damage to controls would be bonus.

We therefore discuss only warhead vulnerability in succeeding paragraphs.

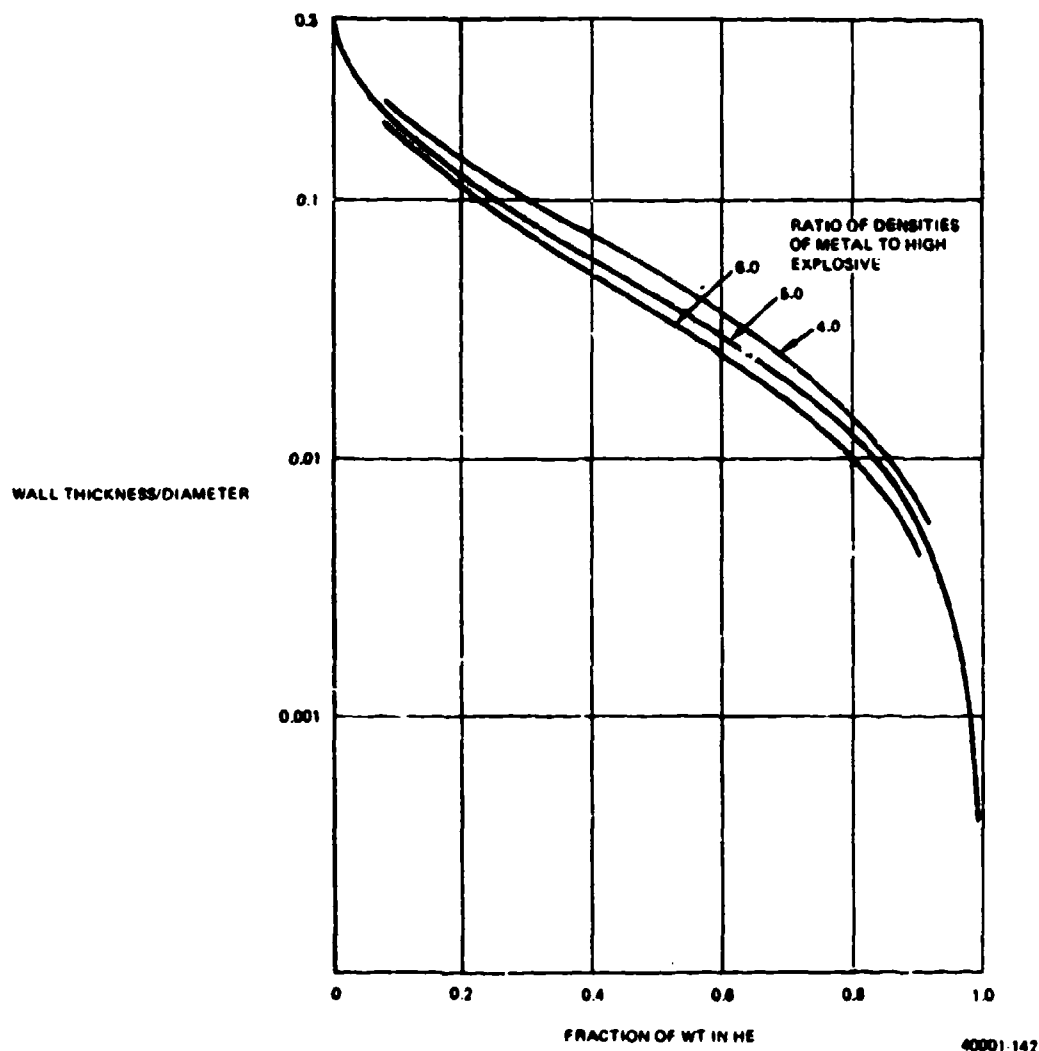


Figure 6-3. Ratio: Wall Thickness/Outside Diameter of Cylindrical Warheads versus Fraction of High Explosive by Weight

Most warheads can be detonated by projectiles which penetrate the case to the high explosive with adequate residual velocity. The combination of residual mass, velocity, caliber, and shape that will cause a detonation varies with the type of high explosive used in the warhead, and the requirement can be varied widely by combining the HE with various additives.

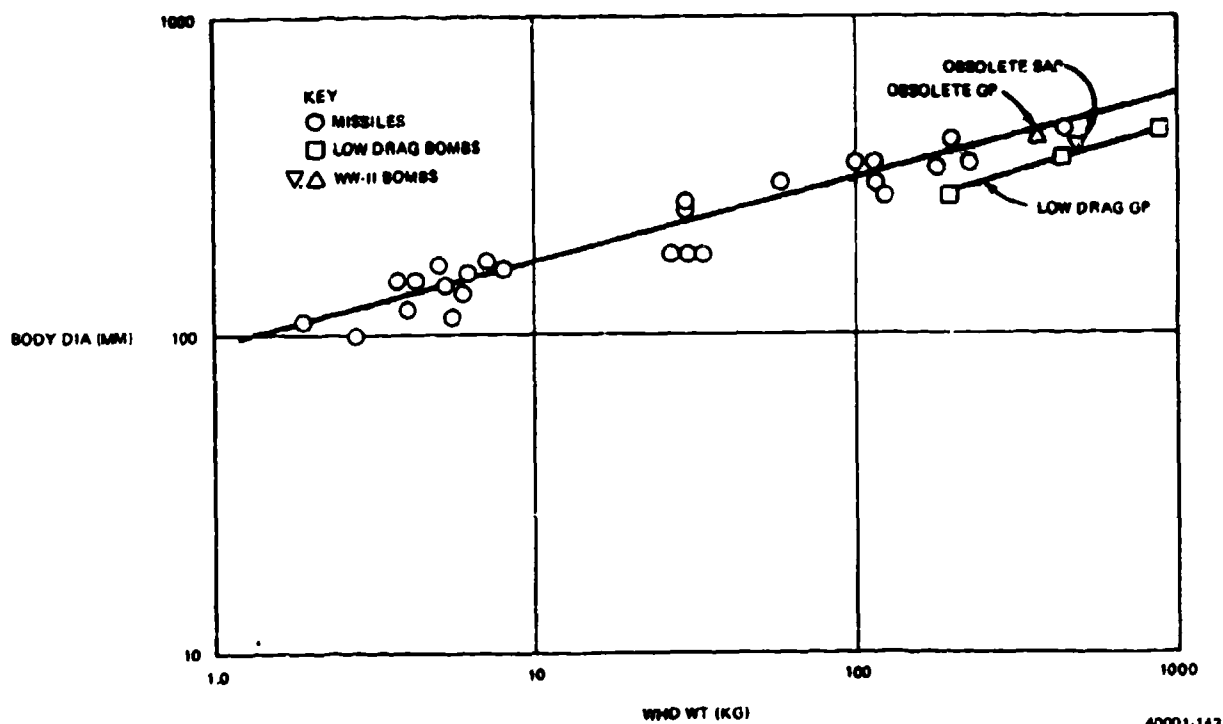


Figure 6-4. Body Diameter versus Warhead Weight of Missiles

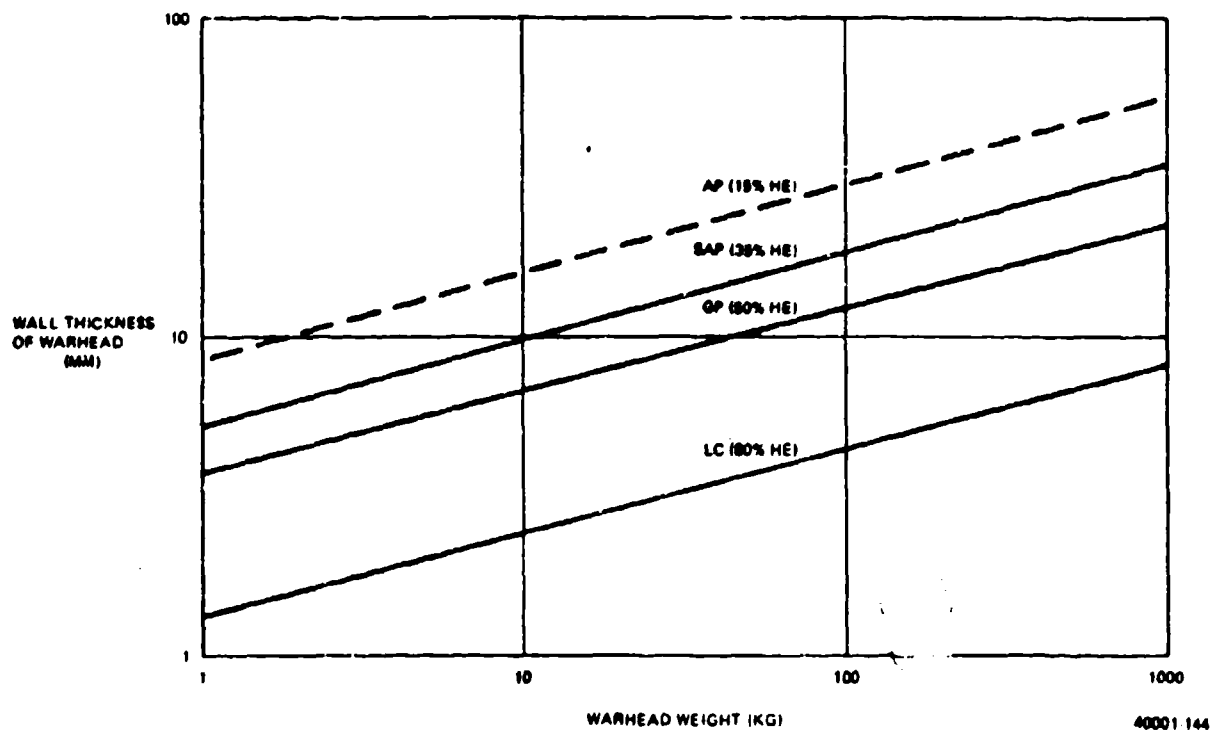


Figure 6-5. Approximate Side Wall Thickness versus Warhead Weight

To hold the classification of the present material to a minimum, we assume that to detonate a warhead, an impacting projectile must perforate the case, with a residual velocity which can be expressed in terms of equivalent penetration of a specific thickness of steel. We note in general, that any terminal effect criterion can be approximated in the neighborhood of a reference point as the product of relevant parameters to various powers, with coefficients and exponents chosen to match the value at the reference point and its first derivatives with respect to each parameter. In the case of two consecutive requirements, i.e. penetrate, then detonate, if the first criterion is the more difficult, the approximation to the joint function will be dominated by, and approach the first in functional form and parametric values.

6.2.1 Penetration Expressions for Projectiles

Since the problem of warhead detonation is first one of penetration of the case, we begin by remarking on the various penetration laws that have been developed for projectiles attacking plate. An admirably concise review of the penetration problem has been developed by Dunn and Huang^⑦ and Figure 6-6 is reproduced from their paper. Note that there are four regions, divided into two sets of perforation and non-perforation regions and two sets depending on whether or not the projectile shatters on impact. The shatter criterion tends to limit the projectile designer in the degree to which he can achieve penetration by very high striking velocities.

Almost all of the many empirical functions that have been developed over generations for penetration can be written in the following form, sufficiently accurately for present purposes.

$$T/C = k (wv^2/C^3)^a f(\theta) \quad (6.1)$$

where T = thickness of plate perforated

C = caliber (diameter) of impacting projectile

w = weight of impacting projectile

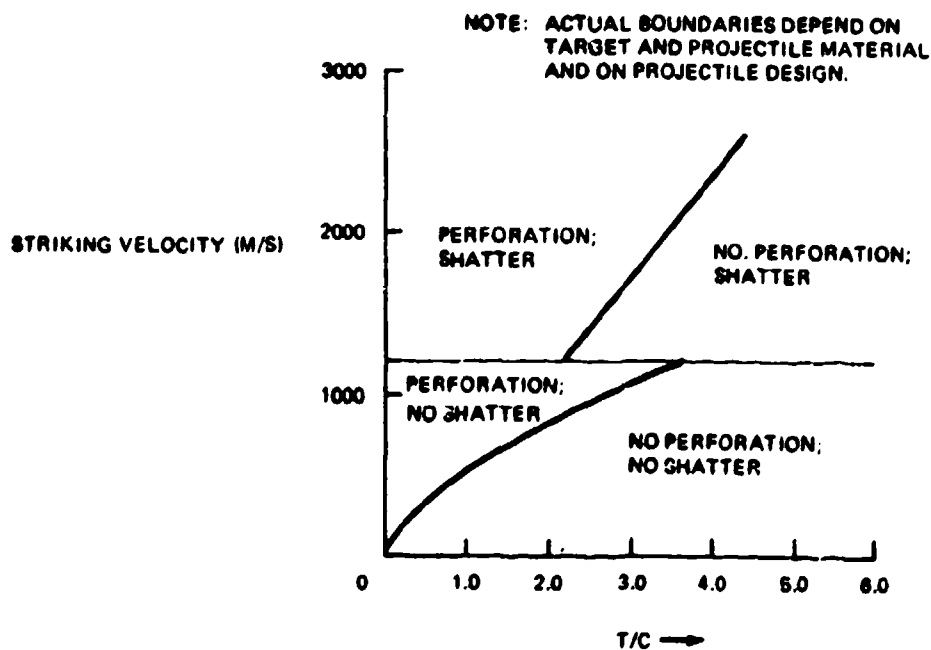
v = impact velocity

k = a dimensional coefficient depending on the plate material and projectile design

a = a coefficient somewhere in the range $0.5 \leq a \leq 1.0$ also depending on plate material and projectile design

We shall find it convenient to use the notation

$$P = [(wv^2)/(2gC^3)] \quad (\text{dimensions of pressure}) \quad (6.2)$$



40001-145

Figure 6-6. Penetration Regions

since this relates directly to the corresponding estimates of "specific muzzle energy" if guns developed in Section 5.0.

Then

$$T/C = (P/P_1)^a \quad (6.3)$$

where T/C is penetration in calibers at an impact pressure P , and P_1 is the impact pressure required at the same angle θ for a T/C value of unity.

Stutz⁽⁹⁾ suggests a form for penetration based on the de Marre formula which we can write, with only minor liberties taken with the exponents, as

$$T/C = k [wv^2 \cos \theta / (2gC^3)]^{0.7} \quad (6.4)$$

for penetrators that do not have "too high" an L/C ratio, and we use this form in later computations. This works out to a dependence on striking velocity of about $v^{1.5}$.

In Figure 6-7 we replot some data⁽⁶⁾ on penetration of aluminum and titanium wing spars by ball ammunition, showing that the $v^{1.5}$ relation is approximately followed. Figure 6-8 replots the data against P and we note that this tends to normalize the separate calibers to the same mean.

Figure 6-9 shows the caliber penetration of a large number of anti-tank projectiles of WWII vintage from several open sources.⁽²⁾⁽³⁾ Also included is a modern APT round used by the Oerlikon 35-mm⁽¹²⁾ automatic cannon. The relatively small dispersion in the points, considering that only velocity is a parameter, is remarkable. In Figure 6-10 the same data is plotted against impact pressure P, and much wider scatter appears. The German "squeezebore" rounds are believed to have had tungsten cores, hence should preferably be rated against the core characteristics. The 0.30 and 0.50 AP rounds and some of the Soviet WWII rounds appear to be relatively inefficient. Performance of the Oerlikon round, for which design details are not available, is outstanding.

For present purposes, we have not attempted to separate out the effect of plate type in each case (homogeneous steel, face hardened, etc.), since this is rarely given in the sources. The difference, although vital to the tank-anti-tank duel has a relatively small effect on the present estimates.

Table VI-2 summarizes published characteristics of the Oerlikon ammunition.⁽¹²⁾ The penetration estimates at 1 km and 60° impact angle have been converted to estimates for normal impact by Stutz's formula.

Note the availability of a HEAT (shaped charge head) round. HEAT penetration falls off only as the cosine of the impact angle. Since these are spin stabilized rounds, HEAT penetration is substantially less than that which could be achieved with a non-spinning round.

Table VI-3 and Figure 6-11 summarize the claimed penetrating abilities of some of the anti-tank missiles.⁽¹⁰⁾⁽¹¹⁾ Penetration at a given obliquity tends to be proportional to warhead diameter, in a ratio as high as 5/1. With the availability of unrotated fin-stabilized projectiles to be fired from guns in air defense, the option of a HEAT projectile, unrotated, for attacking warheads should be considered.

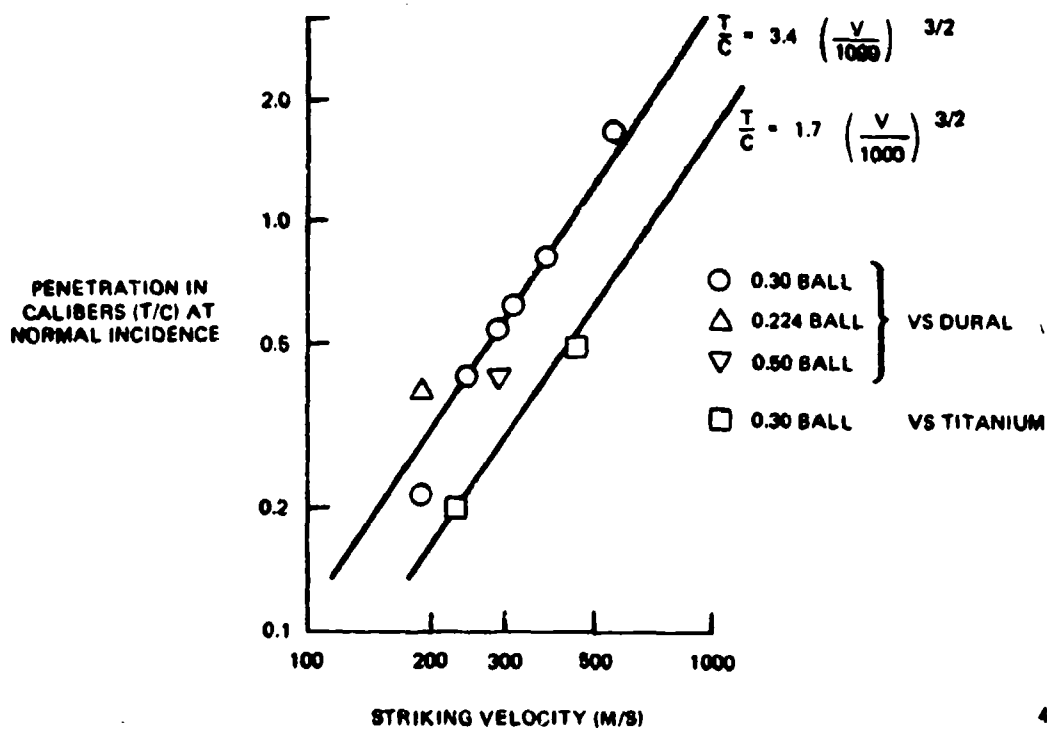


Figure 6-7. Penetration of Dural and Titanium by Ball Ammunition versus Impact Velocity

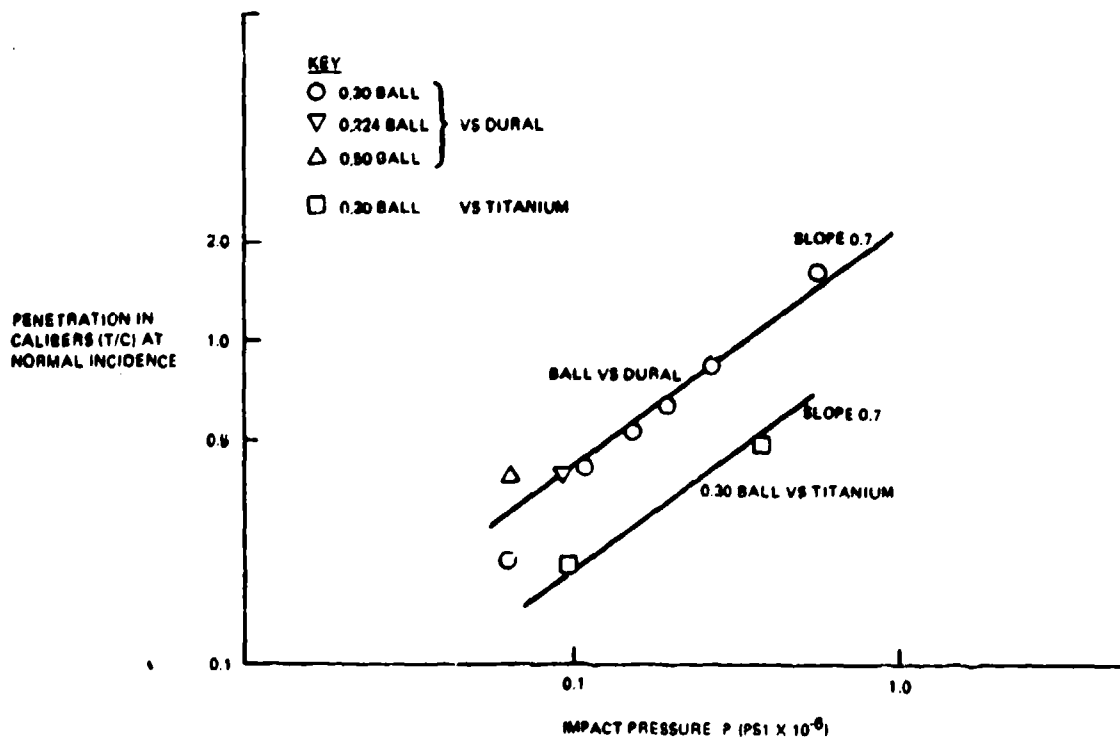
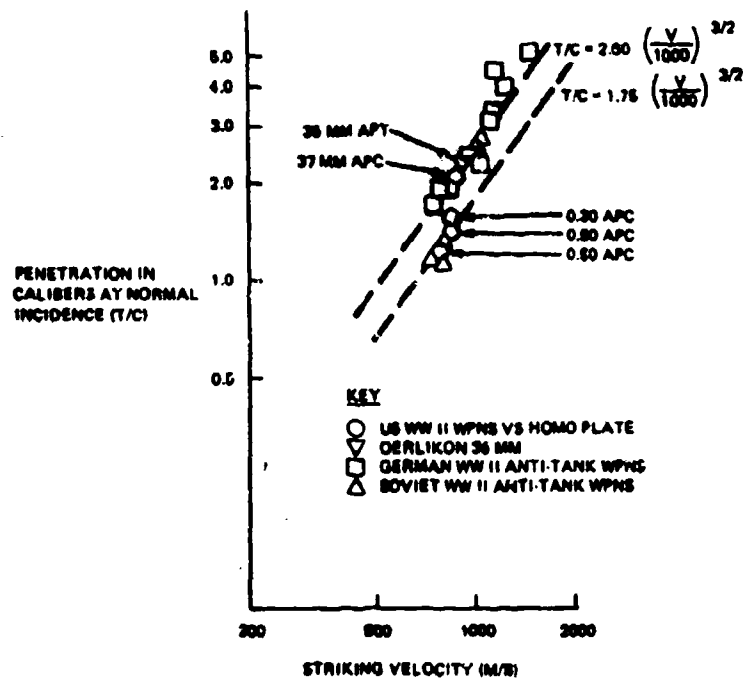
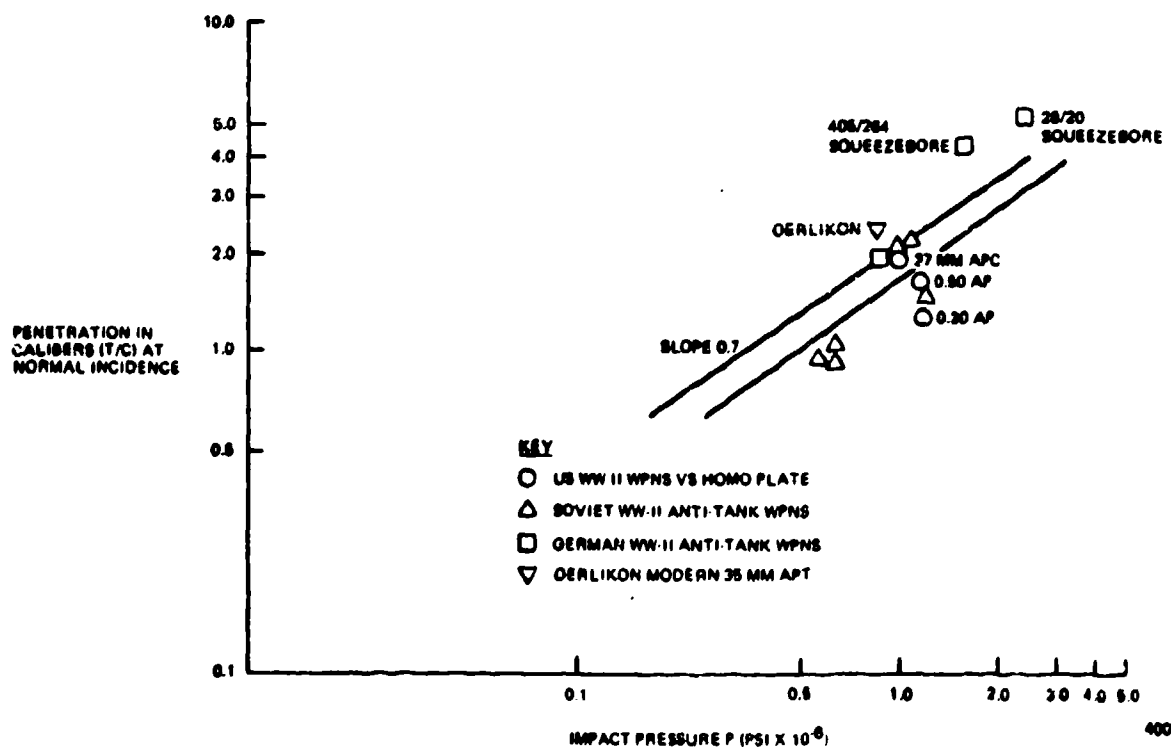


Figure 6-8. Penetration of Dural and Titanium by Ball Ammunition versus Impact Pressure



40001-148

Figure 6-9. Penetration of Steel Plate versus Impact Velocity



40001-149

Figure 6-10. Penetration of Steel Plate versus Impact Pressure

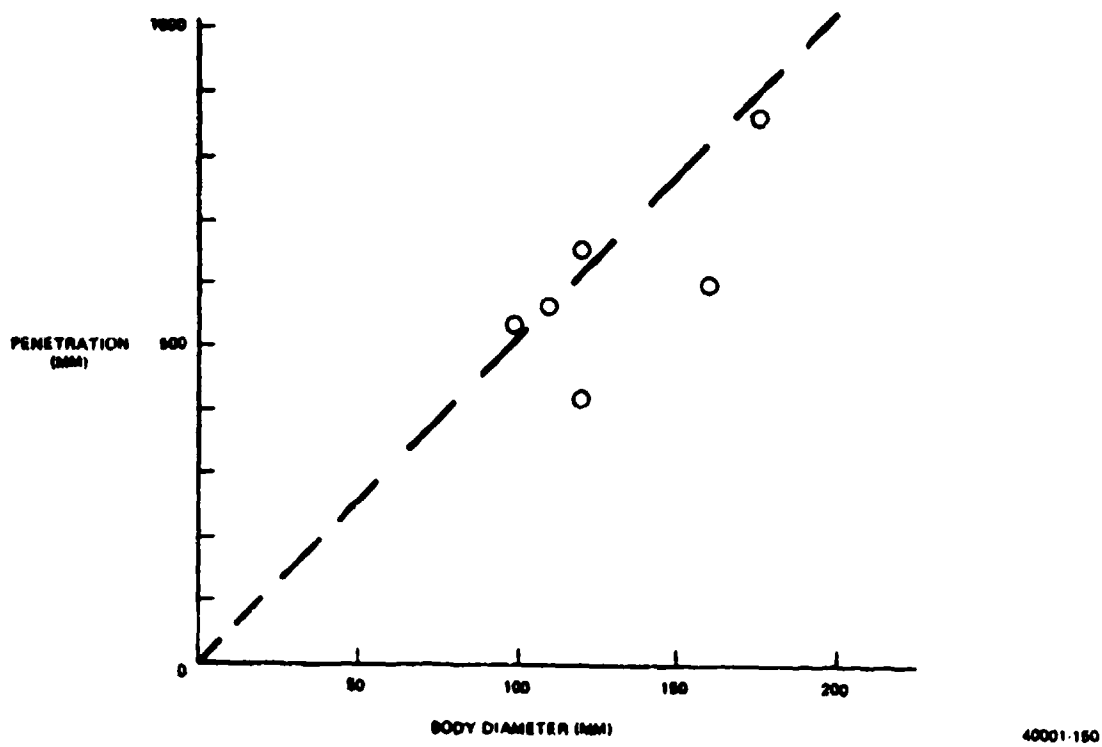


Figure 6-11. Penetration Capability of Shaped-Charge Antitank Missiles

Table VI-2. 35-mm Oerlikon Ammunition

Type	APHE/K	HEAT/B	APT
Complete Round Weight (kg)	1.562	1.562	1.562
Projectile Weight (kg)	0.550	0.550	0.550
Weight of HE Filler (kg)	0.120	0.022	--
Muzzle Velocity (in/s)	1175	1175	1200
Velocity at 1000 m (m/s)	920	920E	940E
Penetration at 1000 m; 60° impact angle (mm)	--	35	66
Penetration at 1000 m; normal impact (mm) (EST)	--	41	82
T/C at 1000 m; normal impact (EST)	--	1.16	2.35

Table VI-3. Penetration Capability of Shaped Charge Antitank Warheads

Missile	Body Diameter (mm)	WHD Weight (kg)	HE Weight (kg)	Penetration
VIGILANT	110	8		558 mm (normal incidence)
HOT	175	6	3	377 mm @ 65° over 800 mm normal incidence
SS-11	160	8		600 mm (normal incidence)
COBRA	100	2.5	1.5	545 mm
MOSQUITO	120	4		660 mm
CONTRAVES/ OERLIKON (original MOSQUITO)	120	3.3	1.6	405 mm

6.2.2 Residual Velocity After Plate Perforation

The minimum velocity to perforate a plate can be estimated from Stutz's expression, or equivalent. ⑦ Above this velocity, the penetrator retains a velocity which is approximately

$$v_r^2 = k (v_i^2 - v_b^2) \quad (6.5)$$

where k depends on the relative masses of penetrator and plate material displaced, and is close to unity for present considerations. Here

v_r = velocity after perforation

v_i = impact velocity

v_b = minimum velocity to perforate (essentially the "ballistic limit", - the velocity at which a projectile will perforate half the time in a series of controlled experiments)

6.2.3 Detonation of Warhead

As a minimum, it is assumed that the warhead case must be completely perforated by the bullet in order to detonate the high explosive. The residual bullet velocity after perforation required for detonation can be a thousand feet per second or more. High explosives vary in their sensitivity to impact, and the sensitivity can be changed over a wide margin by additives. ⑧

The Encyclopedia on Explosives gives the maximum velocity at which no detonation was obtained and the minimum velocity at which complete detonation was obtained for a brass

bullet (8 mm, 8.1 gram) fired against 300 to 500 grams of uncased explosive, 30 mm in depth in some French experiments. A few sample results are extracted in Table VI-4 to show the range of variation in velocities.

Table VI-4. Sensitivity of Explosives to Bullet Impact

Explosive	Max Velocity for No Detonation (m/s)	Min Velocity for Complete Detonation (m/s)
TNT/Cast	1042	none
RDX	274	327
RDX/TNT 50/50	396	400
same with 1% wax	616	641
RDX/Paraffin 97.5/2.5	714	724
same 90/10	1063	1110
RDA/Beeswax 92.5/7.5	833	847

As would be expected, the probability of detonation is stated in the reference to increase with the bullet caliber in firings against HE. The reference also cites Hercules Powder firings against TNT in steel containers, "even cast TNT could be made to detonate fairly consistently with a 220 grain bullet but less consistently with a 172 grain (soft point) or 166 grain AP bullet".

Rather than raise the classification of this note, it is suggested that the requirement to detonate the HE may be approximated as an additional thickness of case. Assuming that the detonation probability is insensitive to the bullet material, after case penetration, and depends only on caliber, mass and velocity, we note that at 600 m/s a projectile should perforate a thickness of steel about equal to its own caliber. For the French data on RDX/TNT with 1% wax, this would be an equivalent thickness of steel of about 8 mm. 1000 m/s would correspond to about twice this, or 16 mm.

The present writer observed at first hand, the ability of bullets from a cal 0.45 pistol to detonate 100 lb GP "dud" bombs at short range while lying behind some Fort Bliss "boon-docks" in 1945 in company with an NDRC scientist who had undertaken the dud disposal job for the day to keep his hand in at small arms varmint "plinking".

6.2.4 Perforation of Warhead Case versus Angle of Impact

It is desirable to perforate the warhead case while the missile is at some distance from the gun. Hence the bullet will impact at less than the optimum angle for perforation. In addition, if the missile is entered from the forward direction, there may be a considerable amount of equipment (homing head for example) and structure to be perforated before the bullet gets to the warhead.

The warhead is here represented as a cylinder, and we consider perforation only of the cylindrical wall. The warhead may have a relatively thick ogival nose, if it is designed for some penetration ability, and the reduced angle of impact caused by the ogive would help penetration; on the other hand the nose section of bombs tends to be thicker than the side walls, possibly more than compensating for the improvement in impact angle. As noted earlier, if, for anti-personnel effect, the warhead had thin ends, the presence of bullets designed to perforate the ends could easily be guarded against by thickening the nose structure.

First consider impact normal to the longitudinal axis of the warhead. Assume that the bullet can perforate a thickness T_0 , and that the warhead wall thickness is T . The warhead cylindrical portion is assumed to have a diameter D and a length L . From the de Marre formula, as given in Stutz^②, bullets striking the case will be able to perforate out to an angle at which

$$T = T_0 \cos^{3/2} \theta \quad (6.6)$$

The "vulnerable width" of the cylinder is defined as

$$W_v = D \sin \theta \quad (6.7)$$

and the "vulnerable area" is

$$A_v = W_v L = DL \sin \theta \quad (6.8)$$

$$A_v = DL \left[1 - (T/T_0)^{4/3} \right]^{1/2} \quad (6.9)$$

Next assume that the average bullet trajectory makes an angle Ω with the warhead longitudinal axis. This reduces the ability of a bullet striking the cylinder at a given point to perforate. Retaining θ as the angle of impact projected into a plane normal to the warhead axis, we have the angle of impact relative to the surface at impact as

$$\cos \beta = \cos \theta \cos \Omega \quad (6.10)$$

and the bullet will perforate only to an angle

$$\cos \theta = (T/T_0)^{2/3} / \cos \Omega \quad (6.11)$$

We now have a vulnerable area, correcting Γ for foreshortening with Ω

$$A_v = DL \left[1 - \sec^2 \Omega \left(T/T_0 \right)^{4/3} \right]^{1/2} \sin \Omega \quad (6.12)$$

Vulnerable area becomes zero when

$$\cos \theta = \left(T/T_0 \right)^{2/3} \quad (6.13)$$

The resulting vulnerable area as shown in Figure 6-12 increases only slowly with T/T_0 above about 3.0. For the assumptions of this model it is clear that it will not be possible to perforate the warhead head-on. There may be warheads in use that can be so perforated, but it is such an easy design change for the warhead designer to prevent this, that head-on perforation is not considered to be a safe design assumption for defense weapons. On the other hand, if the enemy increases the wall side thickness of his warhead, he reduces its effectiveness for almost every application.

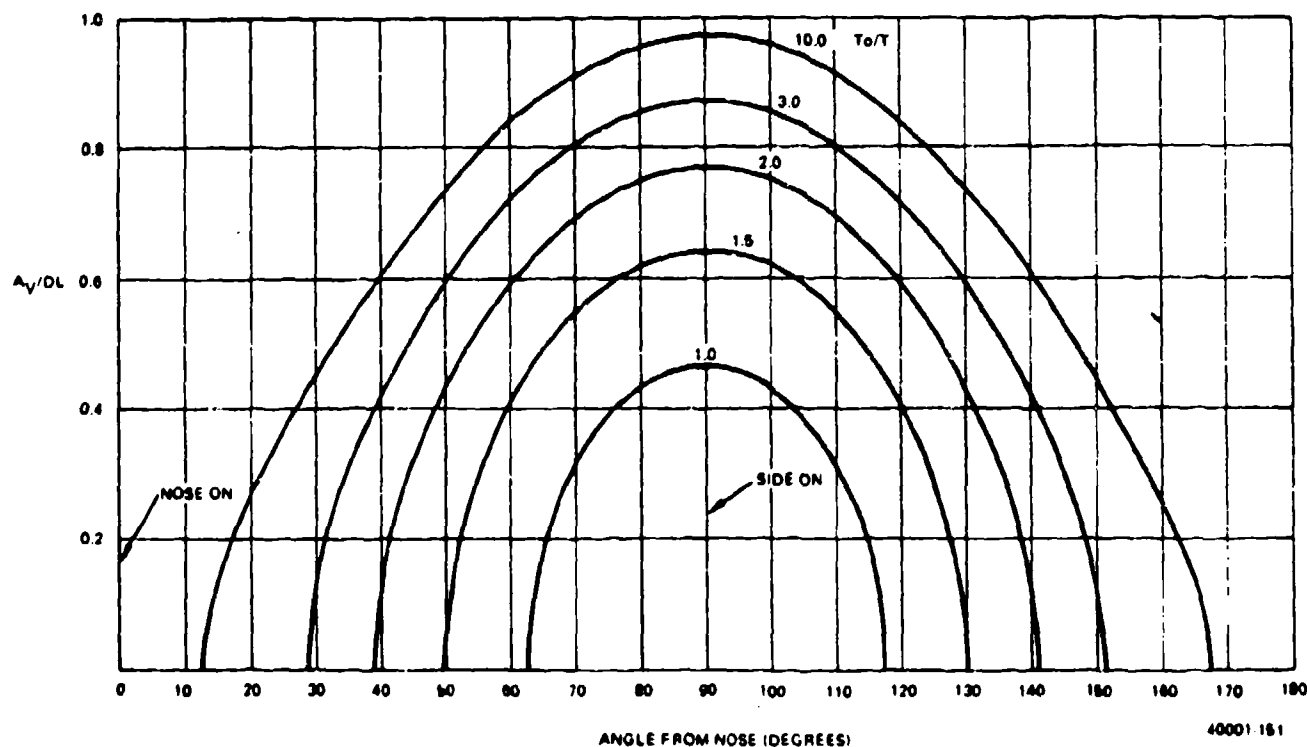


Figure 6-12. Vulnerable Area of Cylindrical Warheads

6.3 DEFENSE EFFECTIVENESS

6.3.1 Gun/Projectile Characteristics

Beginning with the gun, we consider the following sequence of conditions. The gun, with a specified maximum pressure and caliber length, develops a "specific muzzle energy" at some reference muzzle velocity, such as 1100 m/s. Light projectiles, fired above this value, are projected at a lesser muzzle energy, determined by one of the estimating relations given in Section 5 (or by a proper interior ballistic solution).

The weight of projectile fired includes the sabot, if one is used, in the computation of the muzzle velocity. The projectile in flight, however, if it is subcaliber, is lighter because the sabot has dropped off, and its diameter is less. At impact on the target, penetration may be accomplished by the projectile as flown, or by a hard core of still smaller diameter.

For the following estimates the "3/2 power" drag assumption is used as a first approximation.

To make the computation specific, it is assumed that the preliminary computation of flight projectile weight and muzzle velocity has been completed. Then the following notation is used.

Define w = projectile weight
 v = velocity
 C = caliber
 ρ = density = w/C^3

and use the subscripts

(_o) = characteristics at muzzle
(_f) = characteristics in flight
(_t) = characteristics on impact at target

Assume 3/2 power drag: ballistics so that

$$v_t = v_o (1 - k v_o^{-1/2} D)^2 \quad (6.14)$$

Penetration in calibers will be approximated as a function of $w_t v_t^2 / C_t^3$ and to be consistent with the gun computations we use the combination of terms

$$P = (w v^2) / (2g C^3) \quad (\text{dimensions of pressure}) \quad (6.15)$$

The k coefficient in the velocity expression is

$$k = C_{D2} (A_f / w_f) (2v_s)^{1/2} (\rho_{\text{air}} g / 4) \quad (6.16)$$

which we use in the form

$$k = k_1 C_{D2} (C_f^2 / W_f)$$

$$k = k_1 C_{D2} / (\rho_f C_f) \quad (6.17)$$

$$\text{Then } P_t = P_o (\rho_t / \rho_o) \left[1 - \left(\frac{k_1 C_{D2}}{\rho_f v_o^{1/2}} \right) (D/c_f) \right]^4 \quad (6.18)$$

and since

$$v_o = (2gP_o / \rho_o)^{1/2} \quad (6.19)$$

$$P_t = P_o (\rho_t / \rho_o) \left[1 - k_1 C_{D2} \left(\frac{\rho_o}{2gP_o} \right)^{1/4} \left(\frac{D}{\rho_f C_f} \right) \right]^4 \quad (6.20)$$

Now if we consider guns of a given caliber length L/n , and given maximum chamber pressure, P_o will be essentially constant over caliber changes. If we fire full caliber APC type of ammunition, all of the ρ_j will be equal, and

$$P_t = P_o \left[1 - \left(\frac{k_1 C_{D2}}{(2gP_o)^{1/4} \rho_o^{3/4}} \right) \left(\frac{D}{C_o} \right) \right]^4 \quad (6.21)$$

The thickness of metal perforated is

$$T/C_t = (P_t/P_1)^a \quad (6.22)$$

where P_1 is the value of P for perforation of a plate one caliber thick, and the exponent depends on the approximation used. Stutz suggests the value 0.7. Then

$$T = k_o C_o \left[1 - k_2 (D/C_o) \right]^{2.8} \quad (6.23)$$

and given a required penetration thickness T , and a range D , the minimum acceptable caliber of gun firing a full caliber APC round can be determined.

It can easily be seen that lightening the round to obtain higher muzzle velocity would have only an adverse effect since ρ_o would be reduced, and none of the other parameters would change, even if muzzle energy could be kept constant. In fact one loses muzzle energy as the round is lightened. However there is a tradeoff against time of flight.

Given a penetration capability of a specific gun at a specified range and striking velocity, it will be convenient to have a simple method of scaling this result to similar guns of different calibers without working through the dimensional coefficients. If D_s , v_{os} , v_{ts} are the values at the reference point,

$$k_s = (v_{os}^{1/2}/D_s) \left[1 - (v_{ts}/v_{os})^{1/2} \right] \quad (6.24)$$

and for any other weapon approximated by the same "3/2 power" drag law,

$$v_t = v_o \left\{ 1 - (k/k_s) (v_{os}/v_o)^{1/2} (D/D_s) \left[1 - (v_{ts}/v_{os})^{1/2} \right] \right\} \quad (6.25)$$

The ratio of k for any other weapon to k_s is then expressable as the ratio

$$k/k_s = (C_{D2}/C_{D2s}) \left[(\rho_{fs} C_{fs}) / (\rho_f C_f) \right] \quad (6.26)$$

so that the effects of changing drag coefficient, projectile density and calibers may be introduced as ratios to the reference weapon.

Impact pressures are related as

$$P_t/P_{ts} = (\rho_t/\rho_{ts}) (v_t/v_{ts})^2 \quad (6.27)$$

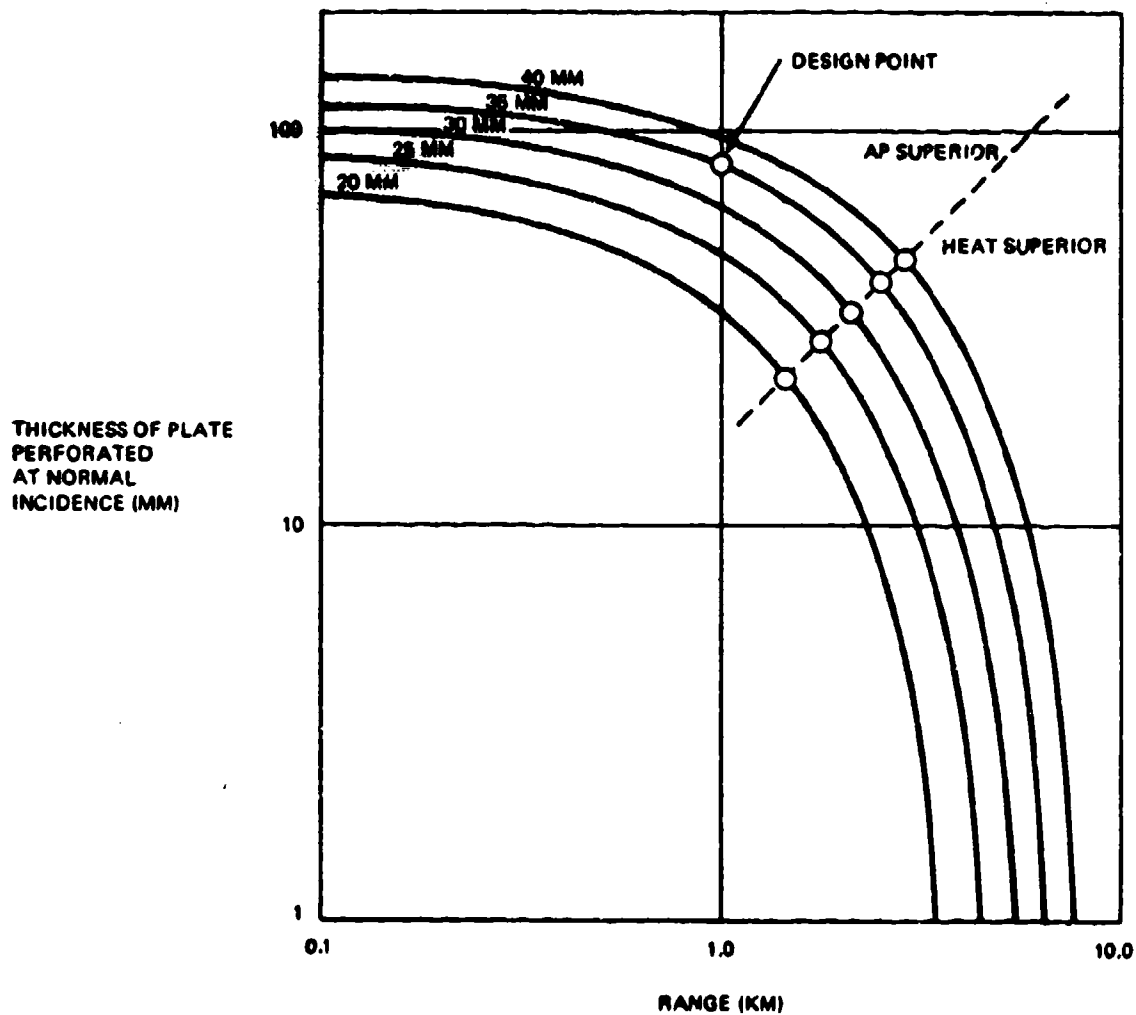
and penetrations as

$$T/T_s = (C_{ts}/C_t) (P_t/P_{ts})^a \quad (6.28)$$

6.3.2 Penetration Capability is Range and Caliber

Figure 6-13 shows the result of scaling the 35-mm APT round in caliber, and extending the penetration value to greater and lesser ranges. Note that for this type of full caliber round, the penetration curve versus slant range is identical in shape for all calibers, and is simply shifted on a 45° slope. A boundary has been shown indicating the region where penetration by the spin stabilized HEAT round is expected to be superior to that of the kinetic energy round.

Some estimates were next made for a high-density subcaliber round, the characteristics of which develop as follows.



40001-152

Figure 6-13. Penetration Capability of AP Projectiles Scale From Oerlikon 35-mm APT

We assume again for the reference weapon, characteristics corresponding to the Oerlikon 35-mm, i.e.,

$$v_{0s} = 1170 \text{ m/s}$$

$$\rho_o = 13 \text{ grams/cm}^3$$

For the subcaliber round, we assume a spin stabilized uranium core, held in a sabot which drops off at the muzzle. The core diameter is taken as half the gun caliber

$$C_{core} = C_{os}/2$$

and

$$\rho_{core} = 39 \text{ grams/cm}^3$$

The ratio of core weight to standard round weight is

$$\begin{aligned} w_{core}/w_{os} &= (\rho_c C_c^3)/(\rho_{os} C_{os}^3) \\ &= 3/8 \end{aligned} \quad (6.29)$$

We assume that the sabot has 1/3 the weight of the core, so that the weight fired is

$$w_{fired}/w_{os} = (4/3) (3/8) = 1/2$$

It is assumed that the change in weight fired is related to muzzle velocity by

$$wv^{2.6} = \text{constant}$$

Then the muzzle velocity of the subcaliber round is related to the reference muzzle velocity as

$$\begin{aligned} v_{osc}/v_{os} &= 1.30 \\ v_{osc} &= 1528 \text{ m/s} \end{aligned}$$

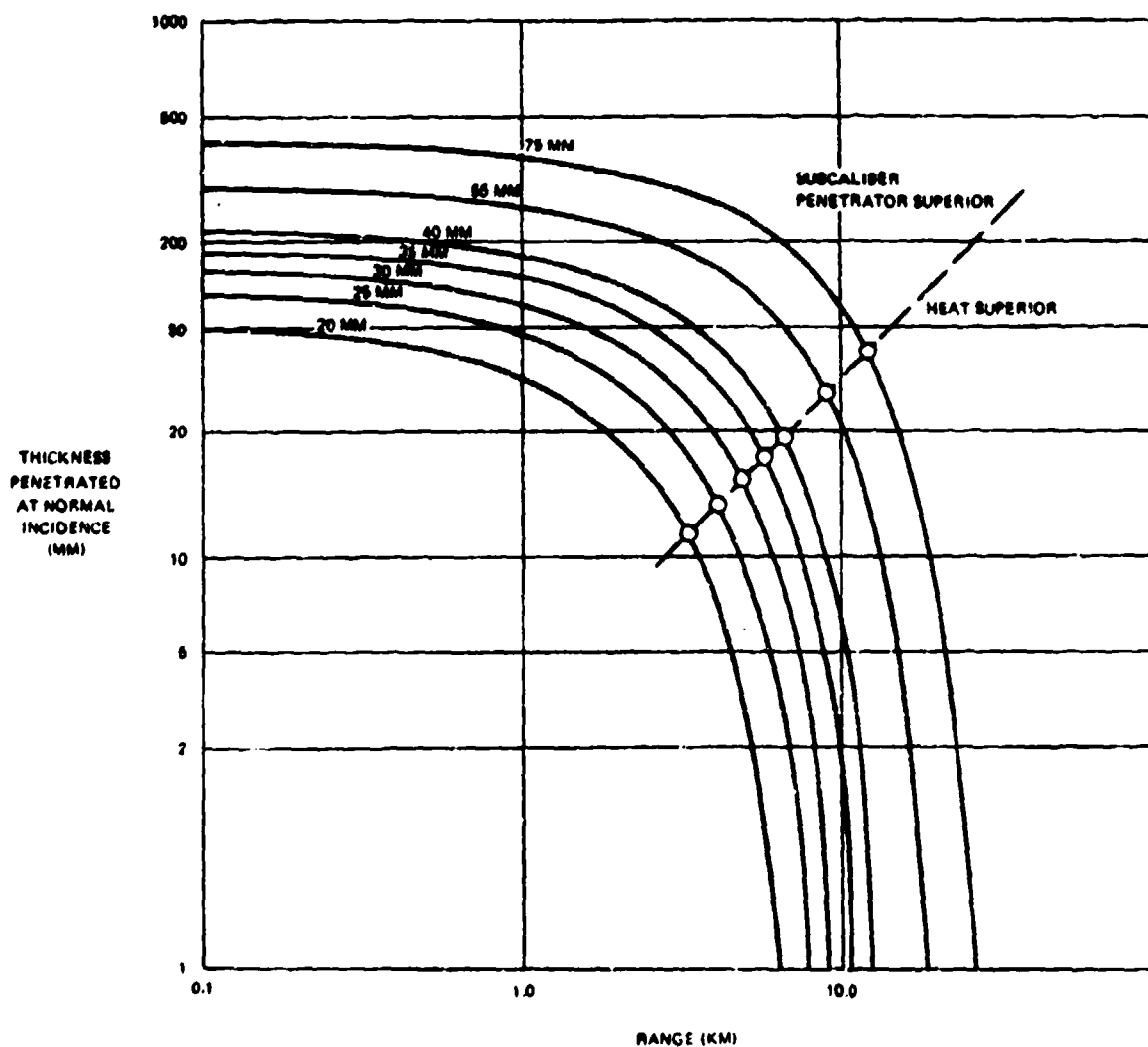
The relative penetration capabilities at the muzzle are determined from

$$\begin{aligned} (P_{osc}/P_o) &= (\rho_c/\rho_o) (v_{osc}/v_{os})^2 \\ &= 5.18 \end{aligned} \quad (6.30)$$

$$\begin{aligned} (T_{sc}/T_o)_{\text{muzzle}} &= (C_c/C_{os}) (P_{osc}/P_o)^{0.7} \\ &= 1.58 \end{aligned} \quad (6.31)$$

Results are shown in Figure 6-14 as penetration capability versus slant range for a number of gun calibers. The subcaliber rounds extend the penetration capabilities of the guns substantially.

Since the subcaliber round in each caliber has both a higher muzzle velocity and a higher value of w/C^2 than the full caliber round, its time of flight is less to any specified range, providing an additional payoff in hit probability.



40001 152

Figure 6-14. Penetration Capability of High-Density Subcaliber Penetrators versus Range

6.3.3 Vulnerability Contours

From the vulnerable area curves of Figure 6-12 and the penetration versus range curves of Figures 6-13 and 6-14, contours of constant vulnerable area of a warhead can be drawn in terms of its position and orientation relative to the gun, and in a slant plane containing the longitudinal axis of the warhead, and the gun.

Two warheads are considered with characteristics listed in Table VI-5.

Table VI-5. Assumed Warhead Characteristics

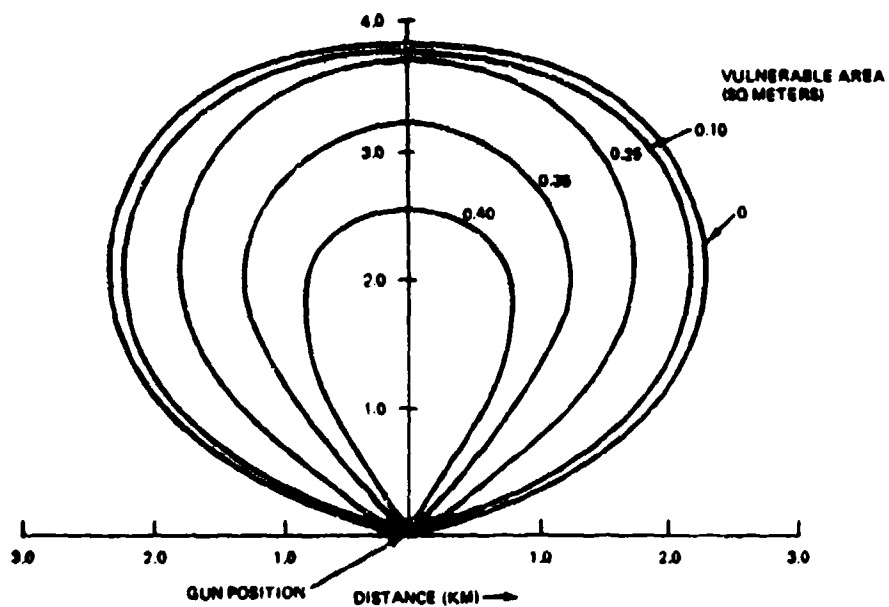
Warhead Types		
Type	"GP"	"SAP"
Weight (kg)	200	200
Percent HE	50	35
Diameter (m)	0.35	0.30
Length (m)	1.4	1.3
Wall Thickness (mm)	15	22
Side Area (m ²)	0.5	0.4

Figure 6-15 shows contours of constant vulnerable area of the GP warhead to a full caliber 40-mm AP projectile. Note that the contour on which 1/4 of the maximum vulnerable area is realized lies very close to the zero area boundary of the region.

Figure 6-16 shows how vulnerable area varies with distance down range for specified crossing ranges. The very sharp rise from zero suggests that the zero boundary is a sufficient descriptor of the vulnerability region by itself, and Figure 6-17 shows how it varies with projectile caliber.

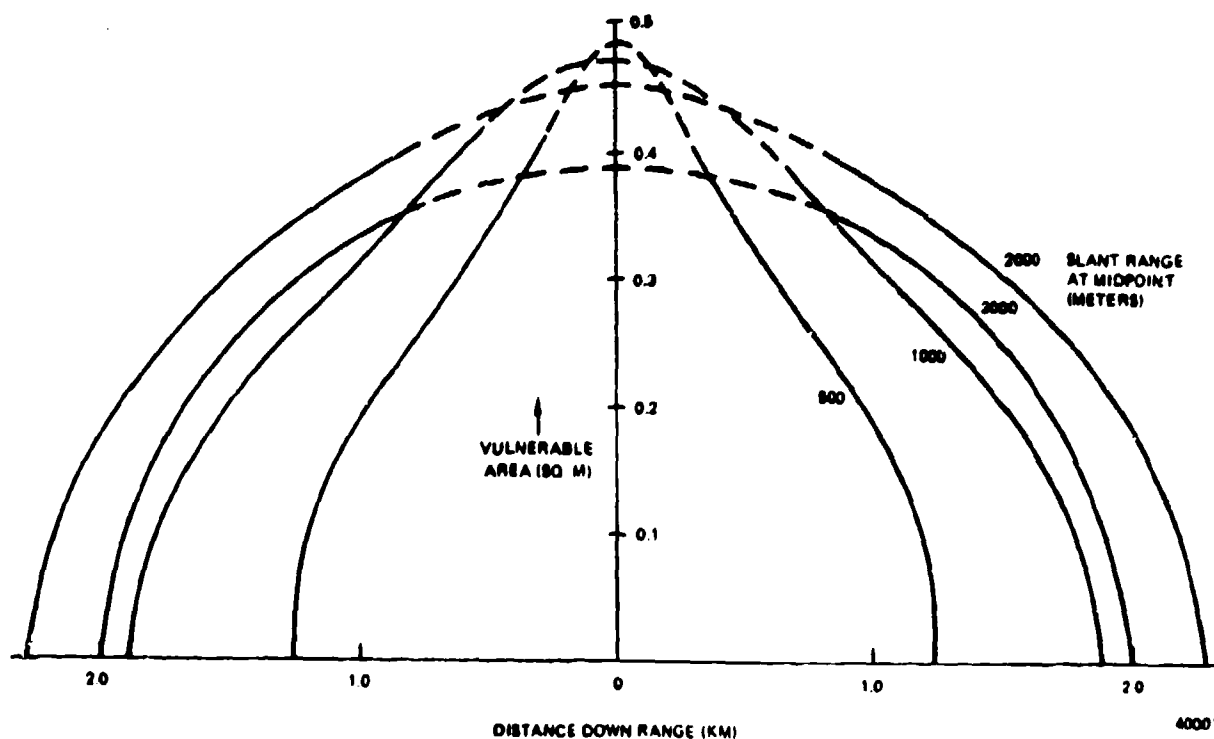
Figure 6-18 shows similar contours for the subcaliber projectiles, and Figure 6-19 compares the vulnerability regions of the GP and SAP warheads to two subcaliber solutions.

If one could be confident of the opportunity to fire in the $\pm 45^\circ$ region about midpoint against standoff missiles, one could be optimistic about the effectiveness of guns as small as 20-mm. However against almost directly incoming targets, the high angles of obliquity on warhead sides, and the uncertainty in the vulnerability estimates in this region, suggest the need for more refined estimates supported by experimental firings.



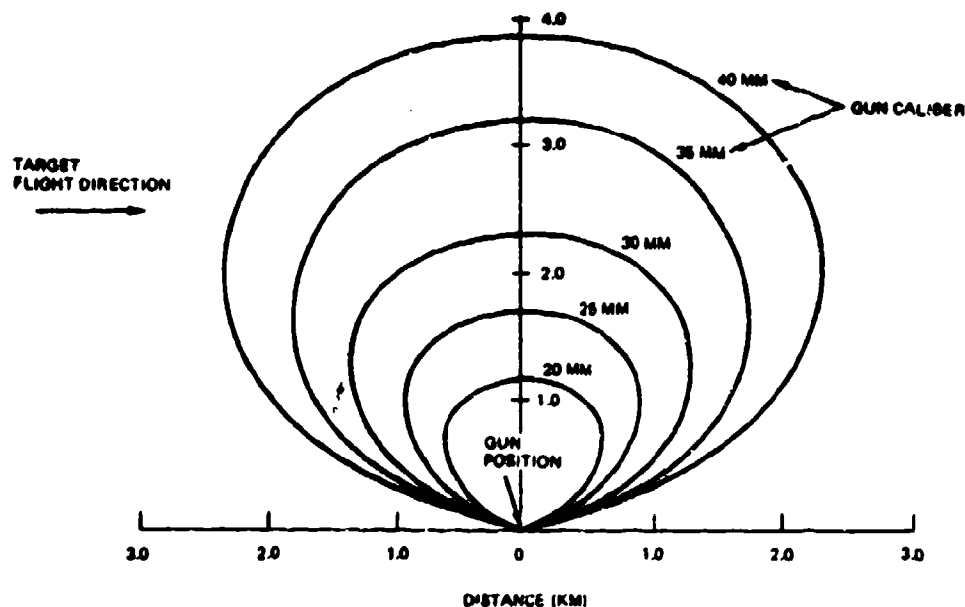
40001-154

Figure 6-15. Vulnerable Area of 200 kg GP Warhead to Full Caliber 40-mm AP Projectiles



40001-155

Figure 6-16. Vulnerable Area of 200 kg GP Warhead to Full Caliber 40-mm AP Projectiles versus Crossing Range



40001-156

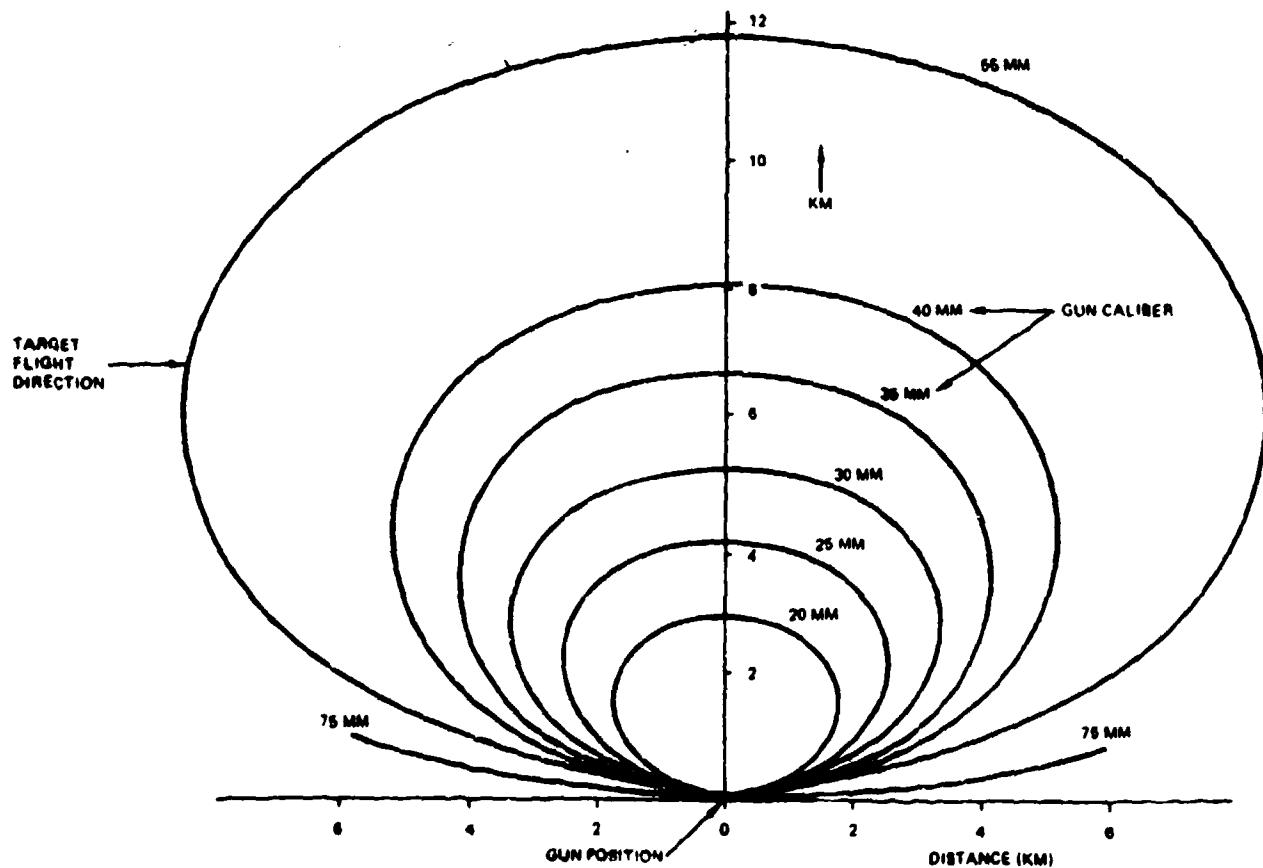
Figure 6-17. Vulnerability Regions of 200 kg GP Warhead to Full Caliber AP Projectiles

The Army's position, in any case may be somewhat better than that of the Navy, since the guns can be disposed about a defended target to improve the angles at which they can engage a standoff munition before it impacts.

6.3.4 Kill Probabilities

Some elementary computations have been made using the vulnerability region contours and a scaled family of guns. It was assumed that rate of fire of the guns varied inversely as caliber, that acquisition and tracking allowed each gun to fire as long as the warhead was within the respective vulnerability region, that an average vulnerable area equal to half the maximum could be used through this region, that missile velocity was 560 m/s and that the defense system had an overall accuracy of 2 mils.

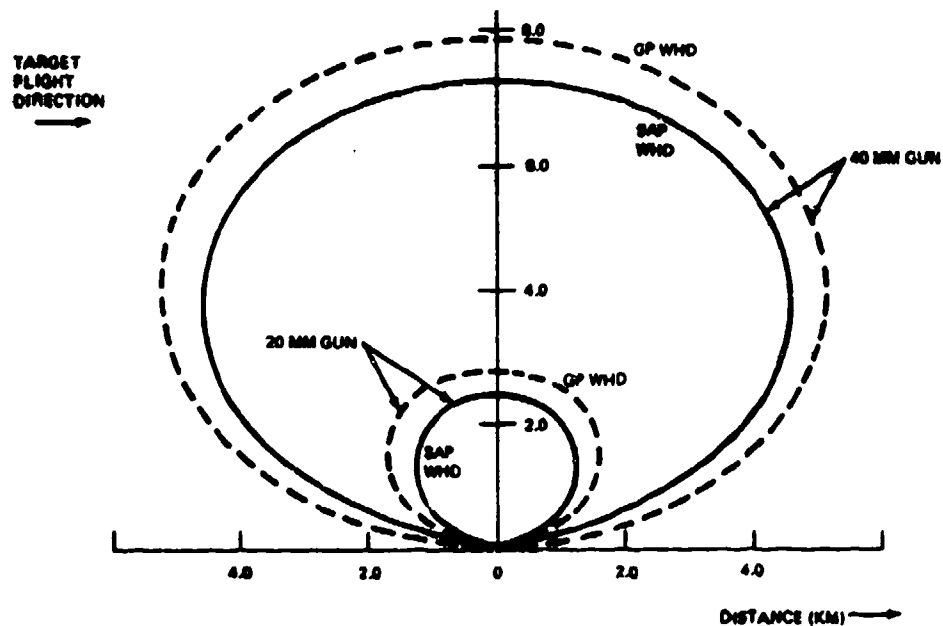
The minimum slant range of the warhead trajectory was taken as 500 meters, but it was assumed that kills must be obtained before the warhead reached a 45° angle from its projected midpoint.



40001 157

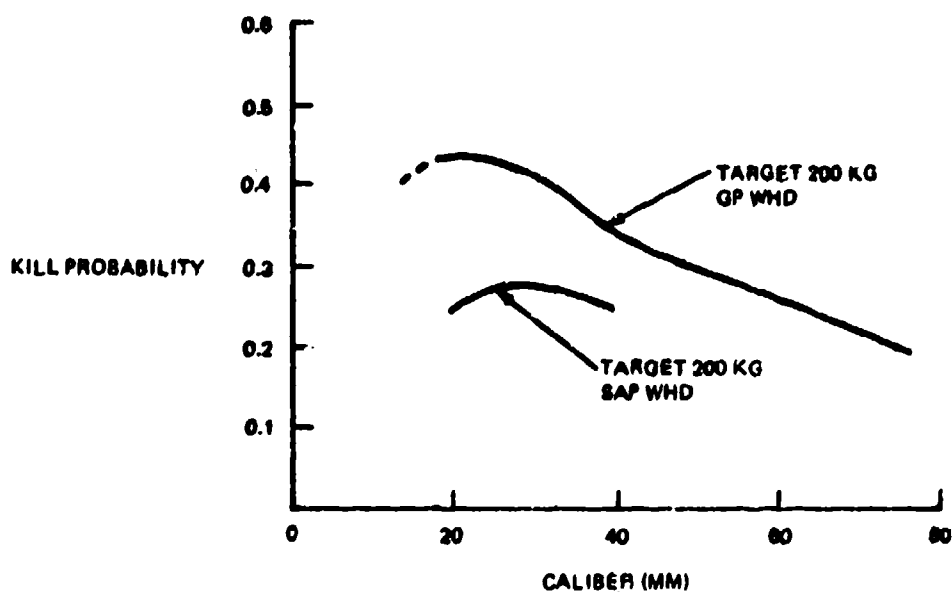
Figure 6-18. Vulnerability Regions of 200 kg GP Warhead to Subcaliber High Density Projectiles

Figure 6-20 shows the resulting kill probabilities plotted against caliber. The geometric scaling of the problem causes the number of rounds fired by each gun to increase slightly with caliber. If firing continued to midpoint the number of rounds fired would be independent of caliber. However the small caliber guns fire more rounds at short range where single shot hit probability is higher.



40001-154

Figure 6-19. Vulnerability Regions of 200 kg GP and SAP Warheads to Subcaliber High Density Projectiles



40001-154

Figure 6-20. Probability of Detonating 200 kg Warheads with Guns Firing High Density Subcaliber Projectiles

Shortening the crossing range below 500 meters moves the apparent optima of Figure 6-20 in the direction of larger calibers. So does increasing the thickness of the warhead case.

If the defense system accuracy varies less rapidly with range than is implied by a constant mil sigma assumption, the relative effectiveness of the larger calibers will be further increased.

Reducing the warhead weight would reduce the kill probability roughly in proportion to the presented area, but the thinner walls for a given percent HE content would increase the vulnerable regions slightly, for a net lowering of kill probability, and a slight relative improvement of the effectiveness of the smaller caliber weapons.

With regard to fire control system accuracy, the small size of the standoff weapon should result in accurate radar tracking, provided that it can be tracked at all, and the standard deviation in each coordinate should be about proportional to the projected missile dimension. How FLIR tracking accuracy varies with target size, range and angular velocity remains to be determined experimentally.

The missile trajectories should be highly predictable, relative to those of a manned aircraft, although FACT data is required to support this conjecture. If valid, one should expect prediction errors much smaller than those obtained against manned aircraft, and increasing less rapidly with time of flight. The prediction algorithms should, of course, make use of whatever predictable dynamics can be associated with the missile trajectory. In particular, closed loop algorithms with the missile trajectory included in the primary loop may be highly effective.

Finally, we note that the vulnerability regions associated with unrotated, fin stabilized HEAT rounds will probably be larger in a given caliber, than those shown for the sub-caliber penetrators, if the same detonation criteria can be assumed to apply. This type of defensive projectile is considered to deserve particular attention in further investigations.

6.4 CONCLUSIONS

It is concluded that predicted fire, air defense gun weapons can have an effective capability against the warheads of standoff missiles. The acquisition and tracking problem may be difficult and requires investigation on an experimental/analytical basis. Conditions required of penetrators and HEAT rounds to detonate the warhead on impact should be made specific, using the best classified data, and considering the possible future reduction in warhead sensitivity by use of additives in the HE. The preferred gun caliber is estimated to lie closer to 30-mm than to 20-mm.

6.5 RECOMMENDATIONS

It is recommended that the Army continue a program of experiment analysis, and exploratory development to establish a capability against standoff munitions for future predicted fire air defense weapons. Emphasis should be on extending the capability of systems designed for defense against manned aircraft at acceptable incremental cost, and not on the design of a small scale antiballistic missile system. The object should be to provide an effective capability against the simpler forms of standoff weapons, thereby forcing an enemy to resort to still more expensive solutions.

SECTION 7

SYSTEM CONFIGURATIONS TO MINIMIZE THE EFFECT OF ENEMY COUNTERMEASURES

All systems are vulnerable to enemy countermeasures to some degree, ranging from interference with the operation of sensors to direct attack on the system. In this section we do not attempt to analyze electronic and optical CM and CCM technology, which proceeds under high security and whose practitioners doubtless have much to Crow (Black that is) about. Instead we present a view of the "wizard" war extracted from the open pages of Aviation Week, and then review possible methods of obtaining range on air targets with passive ranging systems, since most current predicted fire air defense systems have a passive angular tracking mode, but no U.S. or friendly foreign systems are known to have a passive backup mode for ranging, other than estimated range.

It should be emphasized that active sensors are not necessarily to be avoided, even if the possibility exists that an enemy can degrade their effectiveness by countermeasures. A complex air defense network using a wide range of frequency bands imposes a severe technical and logistic load on an enemy, and if its full capability can be concealed until initiation of hostilities, it ties up his research and development resources. Furthermore, every pound of payload devoted to jammers of various types subtracts from munitions delivery capability.

At the same time, the ability to use passive modes of operation with effectiveness comparable to that of active modes (even if only under more limited weather and visibility conditions) is considered essential to good system design.

7.1 STATE OF THE ART IN THE WIZARD WAR AS REPORTED BY AVIATION WEEK

The simplest way to present an unclassified survey of the current state of the art in the "wizard war" of countermeasure vs. counter-countermeasure is to abstract verbatim from the Aviation Week articles on the Middle East War. Almost every type of countermeasure is there discussed in what is practically textbook fashion. The only change in the Aviation Week extracts reproduced in this section has been the deletion of material not directly relevant to the present objective, and assembly of sections from various articles under common topics.

7.1.1 Initial Actions ②

"Bitter battle for survival and eventual victory in the renewed Middle East war is being waged between the aircraft of the Israeli air force and the heavy, interlocking belts of

Egyptian and Syrian surface-to-air missiles (SAMs). The outcome still is in doubt, with Israel and its U.S ally urgently seeking effective electronic countermeasures (ECM) to use against the newest Soviet-supplied SAM, the low-altitude SA-6 Gainful, being used in combat for the first time.

"During the first week of the war, Israel lost 78 aircraft, almost all to SAMs and conventional anti-aircraft fire. By late last week, the total had climbed to 105 aircraft and also two helicopters.

"The toll of aircraft flying close support missions was high, with both the Egyptians and Syrian troops operating beneath the defensive umbrella of SAM belts based in Egypt and Syria proper. Syrian SAMs and anti-aircraft fire accounted for more than 30 Israeli aircraft flying over the Golan Heights in a single day.

"As a consequence, a concerted SAM suppression effort was launched by Israeli aircraft against Syria. The results were immediate. Only one Israeli aircraft loss was recorded over the Heights during the 8-hour period after the strikes. The Israeli air force, however, was unable to sustain such an effort, the SAMs were replaced, and the losses began to mount again.

"Now, the Israelis are relying heavily on ECM and other countermeasures such as chaff in an effort to blunt the SAM threat. Both fighter aircraft and helicopters are being equipped with ECM pods. Helicopters also have been assigned an airborne battlefield surveillance role to provide SAM launch warnings to Israeli strike aircraft.

"Warning time for a low-altitude SA-6 launch is minimal at best — a puff of white smoke and then the Gainful striking its target at a speed of Mach 2.8. Losses have been reduced by the Israelis to some extent, however, by:

- o Changing ordnance delivery modes and altitudes. The Israelis believe the SA-6 has such a low launch trajectory that its mobile launchers can be successfully attacked from high altitude with steep angle bombing runs.
- o Increasing use of ECM.
- o Adjusting flight profiles in order to avoid the threat environment whenever possible.
- o Making violent and rapid changes in course, a tactic that is proving successful when the white smoke puff at launch is detected instantly.

"In a further effort to blunt the SAM threat and open the way for Israeli aircraft to strike across the Suez Canal, the Israeli army last week established a bridgehead across the Egyptian-occupied east bank of the canal to the Egyptian west bank.

"Primary mission of the task force was the destruction of SAM missile radars and missile launch control sites.

"In the absence of more effective countermeasures, the Israelis have been relying on chaff to shield aircraft from radar-directed weapons. Chaff can be dispensed as a radar screen by attacking aircraft - in the case of the A-4 Skyhawks from the dispenser installed in most U.S. Navy aircraft. Israelis were loading the McDonnell Douglas F-4 Phantom speed brake recesses with chaff because the aircraft do not have dispensers. At the appropriate time, the speed brakes were opened, dumping the chaff load.

"To spoof the heat-seeking SA-7 Strellas, Israelis have been using flares, ejected from the A-4's ALE-29 dispenser, and tactics, a combination which worked with some effectiveness for American helicopters in Vietnam. Israeli reluctance to use a pylon chaff dispenser for flares out of fear of fire hazards may have accounted for their delay in picking a system for the F-4.

"Other steps were being taken last week to enable the Israelis to use chaff for large protective veils for aircraft, not simply as self-protection screens."

7.1.2 Air Defense Weapons Used by the Arabs

7.1.2.1 The 23-mm ZSU-23-4 Self Propelled Gun System^②

"The 23-mm. ZSU-23-4 SP anti-aircraft vehicle consists of four guns mounted on a single fixture and fired together. A dish-type radar in the 15.56-gc. frequency called Gun Dish is mounted with the guns. The radar has a very narrow beam providing excellent tracking of aircraft and is difficult to detect or evade, according to U.S. officials."

7.1.2.2 The SA-6 Gainful Surface to Air Missile^{①②④}

"New Soviet-built SA-6 Gainful low-altitude surface-to-air missile used effectively by both the Syrian and Egyptian forces against Israeli air force aircraft in the renewed Middle East conflict was primarily designed for rapid deployment.

"It was derived from the earlier SA-3 Goa/Low Blow system. Deployment and use of the SA-6 apparently caught the Israelis by surprise, with no immediate electronic countermeasures or tactics to blunt its effectiveness.

"The system includes several radars for tracking, guidance and command, operating in conjunction with an acquisition radar such as Flap Track. Basically, the weapon operates on command guidance, as does the SA-3, but there may be alternative backup systems, including infrared or active radar.

"Once a target is detected and acquired, the SA-6 tracking radar is capable of full radar track. Initially, the tracking dish locks onto the target and, after firing, a second radar tracks the missile based on signals from a beacon located in the rear of the weapon. The radar then can send course change commands to the SA-6 to bring the target-tracking and missile radars into coincidence and to lock onto the target.

"The SA-6 system is mounted on two tracked vehicles, one for weapons, the other for radar. Slant range of the SA-6 is approximately 20 mi. Gainful is providing evidence of USSR applications of advanced integral rocket/ramjet technology propulsion system and guidance in at least four frequencies extremely difficult to counter. The SA-6 is a command-guided missile but the specific frequency for the command system has not yet been determined, according to U.S. officials. Three frequencies have been determined for tracking/detection, and they are:

- o Five gc. in the G-band range for low altitude acquisition.
- o Six gc. in the H-band range for high altitude detection/acquisition.
- o Eight gc. in the I-band range used to track targets once a lock-on is obtained with the high or low altitude bands.

"The G-band frequency is capable of low-altitude detection to a range of approximately 15 mi. and the high-frequency/high-altitude band to about 25 mi. Detection is possible at a range of 50 mi. at high altitudes.

"The Gainful is a missile similar in design to U.S. Navy and Air Force integral rocket/ramjet missiles that will not be operational until the 1980s under present funding constraints.

"The missile's integral rocket/ramjet system is considered limited only by the range of the radar employed with it.

"While the four frequency bands in which the SA-6 operates are no mystery, the detailed characteristics of SA-6 radar performance were not widely known two weeks ago. The lack of knowledge about the radar modulation characteristics precluded one of the most successful SA-2 countermeasures -- the ability of an aircraft radar warning system to detect and alert the aircraft crew to the missile launch. The missile launch warning capability,

available now for both the SA-2 and SA-3, enables the crew to take evasive maneuvers when an aircraft is targeted, not simply when it is illuminated by acquisition or tracking radar.

"Jamming the SA-6 also poses problems, although the weapon's four bands have previously been used by Russian radars. Much of the Israeli ECM equipment supplied by late 1970 were either insufficient toward the S-band (SA-2 and AAA) threats of Vietnam or are insufficient for the SA-6. Some equipment was adapted to meet higher-frequency threats, posed by the SA-3's I-band Low Blow radar, but not the J-band Gun Dish radar on Soviet self-propelled short-range quad 23 mm. AAAs.

"None of these jammers has the broadband jamming capability needed to counter completely SA-6, which stretches in spectrum from as low as E-band up to as high as L-band.

"The missiles and Quad 23-mm. ZSU-23-4 SP anti-aircraft gun systems are proving more difficult to counter than anything U.S. aircraft have faced in the past.

"Since the SA-6 is dual-mode and uses a heat-seeking IR guidance system for terminal homing in addition to its command guidance, decoys are being developed.

"Filters can be used on IR missiles to cause them to avoid homing on flares dispensed for that purpose. Another method has been tested in U.S. research and development dubbed Hot Brick, in which JP-4 or JP-5 fuel is dumped out the rear of the aircraft and ignited at timed intervals to cause the missile to home on a heat source very similar to the exhaust of the aircraft."

7.1.2.3 The Strella SA-7 Surface to Air Missile ^④

"Soviet-built SA-7 Strella infrared-seeking, low-altitude, surface-to-air missile used by the Egyptians and Syrians from tracked vehicles against Israeli aircraft have avoided homing on flares used to decoy the heat-seeking system by operating in various infrared wavelengths, Defense officials said.

"Changing the frequency could cause the missile to avoid the bright energy of decoy flares. The flares were developed and used effectively to counter the system in Vietnam.

"Another method to permit the missile to avoid decoy flares is to add a filter to the heat-seeking guidance system so that it will screen out sources of heat not similar to that emitted by an aircraft's exhaust.

"One reason that SA-7s may have avoided Israeli decoy flares is that the heat intensity of the flares may not match the exhaust heat of the aircraft. If filters are used and wavelengths set for the aircraft's exhaust, the missile will avoid the flares, which may be at a higher wavelength, and seek the aircraft.

"One method that can be used to continue to decoy the SA-7 is to dump aircraft fuel in the air for ignition to provide a signature similar to the aircraft's exhaust plume.

"Pentagon said the missile's avoidance of flares in the Arab-Israeli war indicates the troops using the weapon possessed advanced technical expertise.

"The SA-7 was used for the first time on tracked vehicles with eight SA-7s per vehicle. These could be fired in salvos of four or in a salvo of eight. A radar for acquiring the target and directing the missiles in the azimuth of the target was also used."

7.1.3 Use of Stand-Off Munitions (1567)

"An Egyptian air force Tupolev Tu-16 flying over the Mediterranean fired a Russian AS-6 Kelt air-to-surface missile towards Tel Aviv on the opening day of the war. The Kelt was intercepted and shot down by an Israeli air force F-4. Soviet Styx surface-to-surface missiles also have been launched in the sea war.

"The Israeli air force attacked several Egyptian airfields, but runway cratering was only temporarily effective, and some attackers were lost to flak. For some time, Egyptian air force offensive action was limited to sorties by Tu-16 Badger bombers launching Kelt transonic cruise missiles. Badgers launched 25 Kelts during the war, of which all but five were destroyed by Israeli fighters and flak. One Badger was shot down. Kelts struck two Israeli radar sites and a supply depot in the Sinai.

"The (Israeli) Gabriel proved more than a match for the Soviet Styx, which arms Egyptian Osa and Komar types of attack ships, also supplied by the Russians. Officials said Israel developed a jamming device which effectively counteracted Styx as an attack weapon.

"Some were shot down by gunfire from the Israeli-built Reshef and Israeli-designed Saar boats. Israelis claim the Gabriel sank 13 Osa and Komar ships.

"Styx was effective in one early battle of the war. On October 7, Egyptian Komar patrol boats fought the Israeli Saars to a standoff. In the missile exchange, three Saar and three Komar patrol boats were sunk.

"On October 6, the first day of this year's war, Israeli Saar-class patrol boats engaged several Syrian Osa-class patrol boats near the Syrian port of Latakia. Three of the Osa-class boats were sunk, with no Israeli losses.

"In the October battles, Styx was jammed on its ballistic curve. Gabriel operated as a sea skimmer. Waves provided a clutter that confounded Soviet jamming systems. Gabriel

also carries electronic countermeasures equipment. Gabriel used in the sea-skimming mode provides a low-profile target. The Gabriel has automatic homing. It can operate in rough weather and heavy seas with little or no on-board maintenance.

"The strike force against both Egyptian and Syrian navies was the Saar, built in Cherbourg, France, to an Israeli design and armed with eight Gabriels and a 40-mm. cannon.

"Saar worked in tandem with two Israeli-built Reshef boats, equipped with eight Gabriels and two cannon fore and aft.

"The Israeli Skyhawks protected by their Mirage and Phantom top cover did a devastating job of eliminating pockets of enemy armor. The British 30-mm. Aden gun, which the Israelis had substituted for the normal U.S. 20-mm. cannon on the Skyhawk, proved extremely effective at punching out Soviet tanks and armored personnel carriers.

"In the later phase of the war, the 30-mm. Aden was supplemented by U.S. supplied-standoff weapons, including the Hughes Maverick, Rockwell International Hobos and Navy Rockeye, that scored an amazing 95 percent of hits and obliterated the tanks they struck."

7.1.4 Use of Dummy SAM Installations ⑦

"Egyptians also are establishing numerous dummy anti-aircraft missile sites on both sides of the Suez Canal. Observers who toured Egyptian military positions in mid-November estimated that dummy missile positions, complete with dummy radars, outnumbered real sites by two to one.

"Those ratios may have increased by now, because truckloads of dummy wooden missiles without fins could be seen leaving Cairo earlier this month on routes leading northeast to the Suez Canal area.

"At Qantara, one of the northernmost Israeli outposts on the east bank of the Canal, Egyptian commanders said 21 Israeli aircraft were knocked down between October 6 and October 21 in some of the fiercest fighting of the war. Seven of the aircraft were said to have been downed by small arms fire.

"This battle took place while Egyptian forces were still operating under the protective umbrella of anti-aircraft missiles on the west side of the canal. Since that time, Soviet-built SAMs have been set up on the east side of the canal by the Egyptians, together with several dummy missile sites. At one point just across the canal from Ismailiya and about a quarter mile inland, a battery of eight dummy SA-3 missiles, together with a counterfeit

radar, sits beside a road paralleling the canal. Less than a mile to the south, a real missile site is hidden between sand dunes."

7.1.5 Command and Control (5)(7)

"One of the key ingredients in the Israeli air force's ability to perform such a variety of roles over two fronts was its surveillance, command and control system.

"The Israeli air force was controlled from a single command post equipped with excellent battlefield data and communications that enabled the on-duty commander to deploy and shift his forces quickly and effectively in response to a variety of battle situations.

"Because there is little direct liaison between (Egyptian) air force units and ground forces (including the air defense command), air force pilots are believed to have been advised to stay out of range of Egyptian anti-aircraft missiles in order to avoid being shot down themselves. The fact that ground forces had no close air support during the crossing of the Suez tends to confirm this. Cover was instead provided by artillery and anti-aircraft missiles and guns.

"Israeli air force pilots apparently had a similar problem with their own ground forces - especially those pilots flying Dassault-Breguet Mirage fighters. Observers reported seeing Israeli Mirages operating overhead with large yellow splotches painted on the bottom and top of their wings to distinguish them from other, non-friendly Mirages believed to be operating during the war. Israeli air force also shot down several of its own Mirages with Sidewinder heat-seeking missiles early in the war. This was either due to misidentification as Libyan-Egyptian Mirages or non-discrimination of heat sources by the missiles."

7.1.6 Golan Heights Action (5)(13)(15)

"Until the Israeli armor could be marshaled and organized for a counterattack, the air force was the only effective military force opposing the Syrians in the Golan Heights. Attacking the Syrian armor protected by the mobile SAM belt of high-level SA-2s, and low-level SA-6s and SA-7s with interlacing of ZSU-23 flak guns proved extremely costly. Total of 30 A-4s and several F-4s were lost in the first afternoon of battle. The SA-2s were not effective because of Israeli ECM jamming from nearby helicopters and transports, and chaff. The SA-7 Strella - when launched in batteries from radar-equipped tracked vehicles - looked more dangerous than it was. Hundreds of Strellas were launched in short periods on both the Syrian and Suez fronts, but only a few Israeli aircraft were downed by

them although many scored tailpipe hits. Apparently the Strella warhead is too small to cause lethal damage to a modern jet fighter structure except for unusual hits. The SA-6 scored some kills during the Golan battle, but its main contribution was sending the Israeli attack planes into their standard high-g split-S evasive dive to the deck where the ZSU-23s chewed them up.

"In the face of the heavy missile fire, the Israeli air force switched its priority to attacking the batteries directly, with the guidance radars the primary target. Both Skyhawks and Phantoms sprayed the SAM batteries with rockets, bombs and cannon fire during a bitter four-day battle that destroyed half the Syrian SAMs in two days and eventually sent the rest fleeing toward Damascus. Syrian and Iraqi air forces were active over Golan with MiG-17s and Sukhoi Su-7 and Su-20 fighter-bombers attacking Israeli ground forces with great determination and Syrian MiG-21 and Iraqi Hawker Hunters tangling with the top-cover Israeli Mirages. More than 70 Arab aircraft were destroyed in air battles over the SAM sites during this period. At the peak of this battle 27 MiGs were destroyed in one day.

"During the whole war period on the Syrian front the Israeli air force destroyed over 200 Arab aircraft in the air and on the ground at airfields around Damascus, but it took its own heaviest losses of over 80 aircraft on this front."

7.1.7 Assessment in Terms of U.S. Programs ③

"U.S. services have been investing heavily in electronic countermeasures during the past two years. Their aim is to improve aircraft penetrability against the Warsaw Pact threat, in contrast to the defenses encountered in Southeast Asia. Ironically, the model of the threat was suggested by the Soviet-Egyptian buildup of interlaced SA-2 and SA-3 SAMs and quad 23-mm antiaircraft artillery on the west bank of the Suez in 1970.

"The shift largely revolves around coping with greater threat densities over broader ranges in frequency. Coverage has been extended from E/F bands and below, where most Soviet radar in Vietnam operated, to the higher frequency bands anticipated or observed in Eastern Europe. This was to take into account the SA-6 missile's Straight Flush radar, the SA-4's Pat Hand, the SA-3 Low Blow and the quad-23 Gun Dish.

"The expansion of his [Soviet] threat systems . . . has shown his tendency to introduce the new systems in a frequency band other than what his older systems were in but he keeps his older systems active . . ." Navy Cdr. M. T. Grady told the Senate Armed Services Committee last spring. "Therefore," Grady observed, "you have to address more than one frequency band simultaneously. The SA-2 is nominally at [E/F band]. SA-3 is at [I-band]. SA-4, SA-6 in the [G, H band] and the advanced SA-2 C and E is nominally [in G-band] and . . . the Gun Dish is nominally [in J-band]. So you have all these signals present in a combined environment." (Editor's insertions in censored testimony are in brackets).

"Despite improvements by the Navy and comparable ones by USAF, the services have:

No act' ve ECM to counter the quad 23-mm Gun Dish radar.

- o Inadequate or at best questionable ability to detect an SA-6 missile launch and to generate the necessary pilot warnings.
- o Only rudimentary protection from heat-seeking missiles, like the SA-7 Strella, first encountered by Army helicopters in Vietnam.

"Air Force and Navy regard missile launch warning capability as mandatory for penetrating in the European environment. Aircrews need positive knowledge of a missile launch and activation of missile guidance, which they had in Vietnam, to take necessary evasive maneuvers in avoiding a SAM intercept. The false alarm rate has to be minimal, as high-g maneuvers may prompt premature disposal of stores. Many military observers dismiss the value in having to rely on visual sightings of missile launches, especially with a high-acceleration weapon like the SA-6 Gainful, which allows only a small time from firing to intercept.

"The Soviets apparently deviated from what had been their practice of using the lower frequencies of C/D bands for the missile command frequency in SA-2 and SA-3 by jumping into I-band with SA-6. Their efforts were largely concentrated on the SA-2 Fan Song tracking radar and the downlink portion of the command loop. The techniques included:

- o Noise jamming the downlink to blot out the low-power beacon signals radiated from the SA-2 missile for tracking the ascending missile. USAF says it cut its losses to SAMs by a factor of 10 when it tuned its jamming pods to the downlink frequency.

- o Deceiving the tracking radar by returning false angular information to the Fan Song radar to create a false impression of where an illuminated aircraft was located in the tracking beam. Noise jamming of tracking radar also was used.
- o Using large quantities of bulk chaff dispersal, not simply self-protective chaff, to generate confusing radar echoes.
- o Passive radar detection and missile launch warning.
- o Defense suppression weapons like Shrike and Standard ARM.

"Ideally, USAF would like to be able to exploit the SA-6 command chain, much as the Israelis tried to do this month. The command chain is an inviting target for jamming the command-guided, beacon-tracked-through-midcourse SA-6 weapon. One prospect would be to jam the downlink, which would not require excessive jammer power to swamp the missile's low-power beacon by which Straight Flush tracks the missile. The difficulty is that while jamming effectiveness improves as the weapon approaches the target, the missile could revert from ground command to its terminal seeker for target data. Unlike the SA-2, the SA-6 and other Soviet SAMs above SA-4 have this important terminal feature.

"Within the past year, the idea of jamming a SAM missile's uplink has gained favor. This possibility has largely been overlooked on the grounds that it is too difficult to squirt relatively high jamming energy into a Soviet SAM's command receiver because the beacon-receiver is situated at the rear of the missile, facing away from a target. But the concept is attractive in certain geometric situations. A jammer carried in a jeep or tracked vehicle, readily deployable in desert warfare, could add another dimension to thwarting command-guided SAMs."

7.2 IMPLICATIONS FOR AIR DEFENSE SYSTEMS

We note from the foregoing material that:

- a. Air defense missile get the best press notices, but the guns are still as effective as they always have been.
- b. Guns can still shoot down stand-off missiles.
- c. IFF is a continuing problem.
- d. Air defense systems must be completely integrated in command, communications, control and data exchange.

- e. Well integrated gun plus SAM missile systems are more effective than either type alone.
- f. Diversity in defense operational modes, particularly with regard to sensors presents an attacker with more technical problems and greater uncertainty than reliance on a single, well known, and relatively unjammable mode.
- g. The attacker can always fall back on chaff and direct air and ground attack, but it can be costly to him.
- h. Air defense ground units must be prepared for self defense against attack by ground troops, and with armor cover against artillery fire.

7.3 PASSIVE METHODS OF OBTAINING TARGET RANGE

Regardless of the primary sensors of a predicted fire air defense fire unit, a passive mode of operation greatly complicates an enemy's problem. Provision of a back-up visual tracking mode for angular information is straightforward, and FLIR is, of course passive. However, since optical range finders were replaced by radar and the upcoming laser range finders, the ranging operation represents the only current active sensor function without passive back-up.

The GLAADS System for example will have FLIR angular tracking with an optical fall-back mode. Range is to be provided by laser, which is the only active sensor used in tracking. The computer algorithms should make it possible for the system to generate continuous gun orders based on intermittent range measurements, so that the laser need not be operated continuously (although there will be some degradation in prediction accuracy with intermittent range data).

However, if countermeasures should become available to the enemy which can deny laser ranging, or if it is desired to have a completely passive system, we note the following possible options.

7.3.1 Short Base Optical Rangefinders

Optical rangefinders were the primary method for obtaining target range in WW II prior to the availability of radar and were used with base lengths from one to nine meters, the latter in fixed seacoast defense installations. Experimental results obtained in 1937 and described in a prior AFAADS Report, indicated that stereoscopic and coincidence type optical rangefinders of four meter base length could obtain range measurements on aircraft to about

1% of range at 5 km and 2% at 10 km, as summarized in Table VII-1. Current fire control computers could provide regenerated range rate to assist the operator, but accuracy is ultimately operator limited.

Optical rangefinders are limited by visual observation to day, clear weather use. No investigations have been located reporting on the possibility of developing this type of instrument for night use by incorporating light amplification devices or infrared sensors for night operation. The angular resolution required for short base rangefinders may make such extensions difficult, and ranging accuracy equal to that of a laser is probably unattainable.

7.3.2 Extended Base, Multistation Ranging Systems

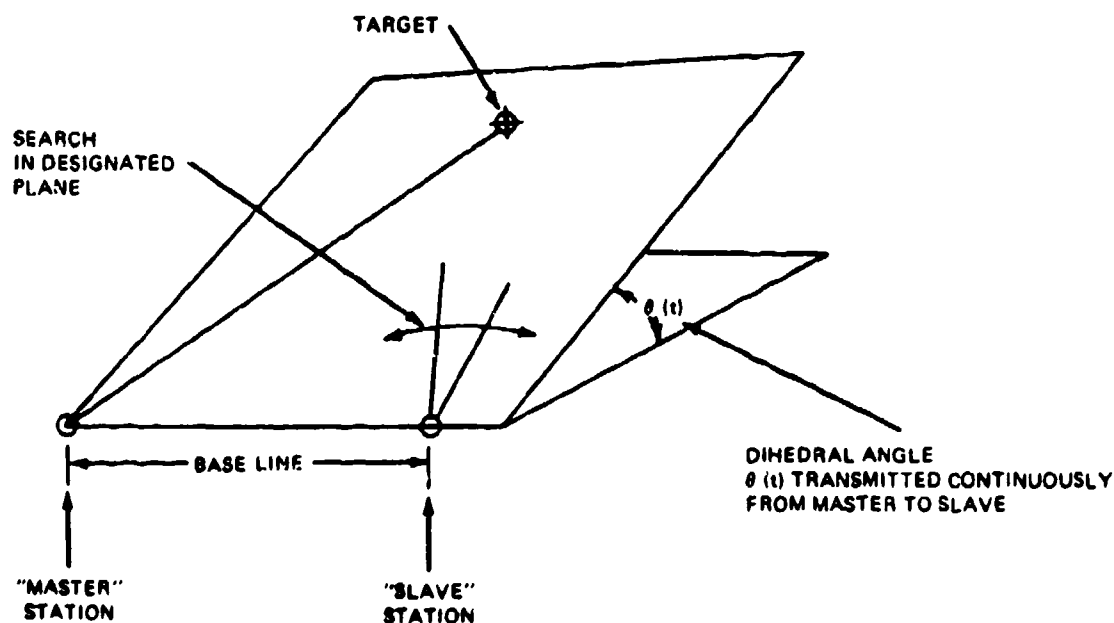
Systems of this type antedated short base rangefinders in antiaircraft applications, and were first used in World War I. "Altimeter M1920" was of this vintage. Tests in 1937 indicated that the "T-3" system with a 2 km station separation could achieve 2% range accuracy at 5 km, and the "T-14" system with 0.4 km station separation could achieve 3% range accuracy at 5 km as shown in Table VII-1. These accuracies correspond to about 5.6 and 1.6 mils angular tracking accuracy respectively at the tracking stations, however the difference in apparent tracking accuracies is probably the result of different methods of data transmission between stations.

Table VII-1. Probable Errors in Measuring Slant Range with Single and Multiple Station Passive Ranging Systems from Proving Ground Experiments

<div>Range</div> <div>System</div>	Probable Error (Meters)		
	3 km	5 km	10 km
Stereo and coincidence optical 4 meter rangefinders (best operators) T18, T9E1	30-40	70-100	200-500
Multistation Optical Systems			
T-14 (400 meter base)	70	150	500
T-3 (2000 meter base)	60	100	250

A multi-station, completely passive ranging system can be synthesized by the interchange of angular tracking information among two or more fire units of a local defense, each of which uses FLIR or visual angular tracking. A major problem is getting all participating tracking stations on the same target. A solution developed prior to WW II was to designate one station as the "master". Having acquired a target, the master station then transmits to "slaves" the dihedral angle between a horizontal plane and a plane containing the target and the base line to each slave as shown in Figure 7-1. A slave station is then required only to search in the defined slant plane until it acquires the target. The coordinate transformations are easily accomplished with modern computers. Once the master and any slave have both acquired the same target, any other slave in the net can be directed at the target without search, allowing data processing to obtain a best estimate of range for fire control, weighting each slave's input according to its position in the geometry of the whole configuration.

Although such a system must work under severe time constraints in getting at least two stations on target, the incremental computations and the data links may be acceptable with modern technology. Operational use requires that cooperating stations establish a mutual base line of known length prior to an engagement, and this can be done with the laser rangefinders, and mutual angular sighting. Intervisibility among cooperating stations is necessary.



40001 160

Figure 7-1. Geometry of Cooperating Stations

An analysis of range errors associated with multistation ranging systems has been provided by F. V. Wilson.

Figure 7-2 shows iso-error contours for two cooperating stations, in normalized form as a function of target position. "Normalization" consists of expressing all distances as ratios to the length of the base line. In this figure it is assumed that the standard deviation of angular tracking error is identical at both stations. Error contours are shown in the slant plane containing the base line of the tracking stations and the target.

To obtain the standard deviation of range error at the "master" site, the following expression is used

$$\sigma_D = \sigma_\theta bK \quad (7.1)$$

where

σ_D = standard deviation of range error (meters)

σ_θ = standard deviation of angular tracking error (radians)

b = length of base line (meters)

K = value read from Figure 7-2.

For very large values of D/b , (the ratio of slant range from the master site to the base line length), the contours approach the asymptotic expression

$$\sigma_D/b \approx (D/b)^2 (2)^{1/2} \sigma_\theta \csc \alpha \quad (7.2)$$

where α is the target angle relative to the base line, $\pi/2$ if the sight line is perpendicular to the base line.

As an example, take $b = 1.0$ km, $D = 1.5$ km, and a position normal to the base from the master station. Then $K = 4.0$ and a 1 mil standard deviation of tracking error at each

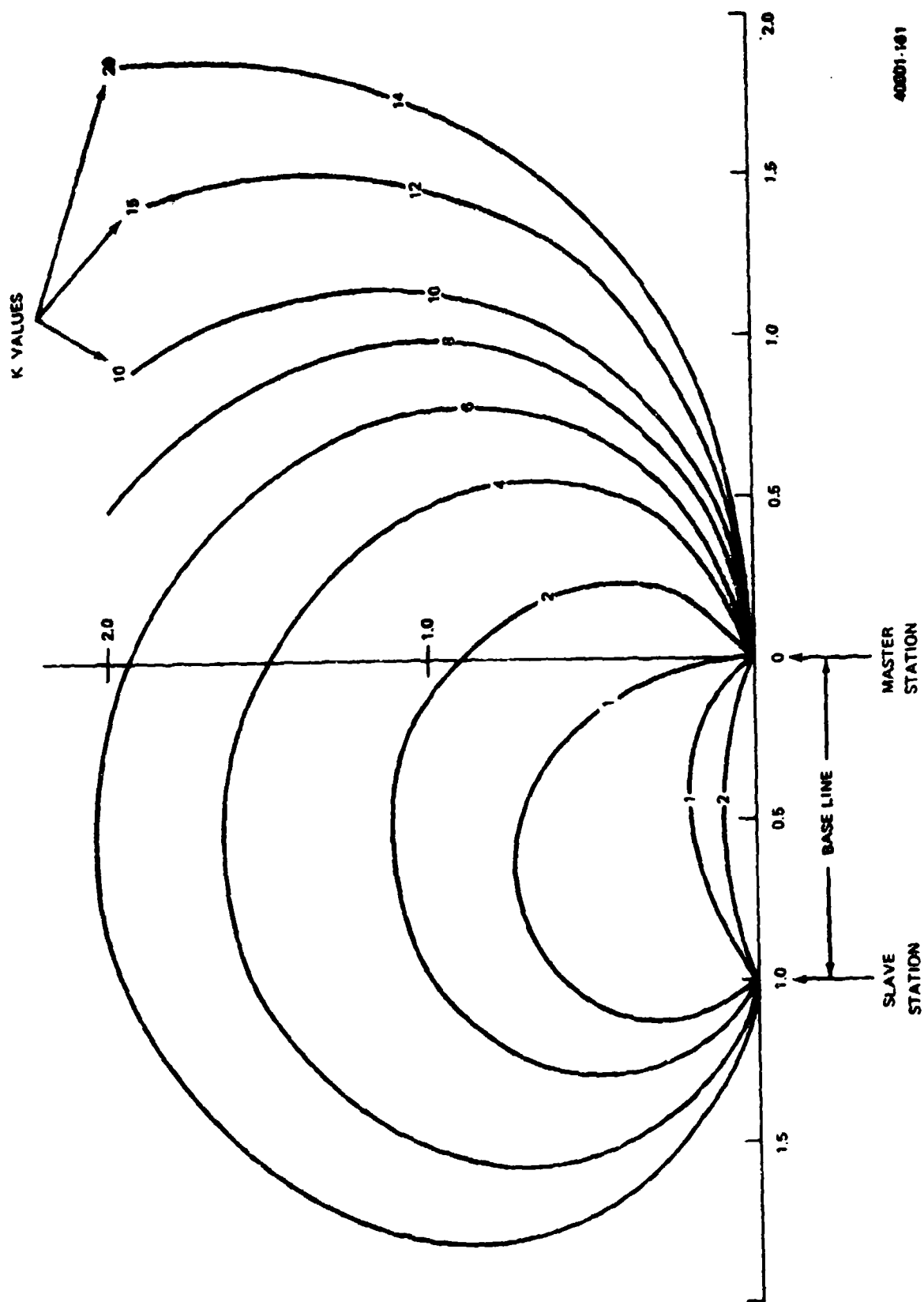


Figure 7-2. Range Error of Two Station Ranging System versus Target Position

40801-101

station will result in a 4 meter standard deviation of range error at the master station. At a range of 3 km, at the same target angle, the approximate expression (used beyond the limit of the figure) gives a standard deviation of range error of 13 meters.

Figure 7-3 is identically constructed, but shows iso-error contours of range error resulting from angular error at the slave site only.

A multistation ranging system has the additional advantage that if the target aircraft is using on-board radar jamming, and the individual fire units can track on the jamming strobe, the system can be used to obtain range on the jammer, although angular tracking errors will be much greater than with visual tracking.

7.3.3 Required Range Accuracy

To a first order approximation, the angular lead error resulting from a range error is

$$\delta\Delta = (\delta D/D)(v_t \sin \Omega / v_a) \quad (7.3)$$

where

Δ = lead angle

D = slant range

v_t = target velocity

Ω = target approach angle (90° at midpoint)

v_a = average projectile velocity

and the linear miss at midpoint (approximate maximum) is

$$M = \delta D(v_t/v_a) \quad (7.4)$$

Hence the maximum linear miss is about half the range error when $v_t/v_a = 0.5$.

Errors in range rate also affect the miss, but these may be minimized by the regenerative tracking module of the computer, which can develop range rate from angular velocities and intermittent range measurements.

At 3 km, therefore, a 2% range error would produce about a 10 meter miss at 45° before midpoint, and this might be acceptable in a "back-up" operational mode. In fact,

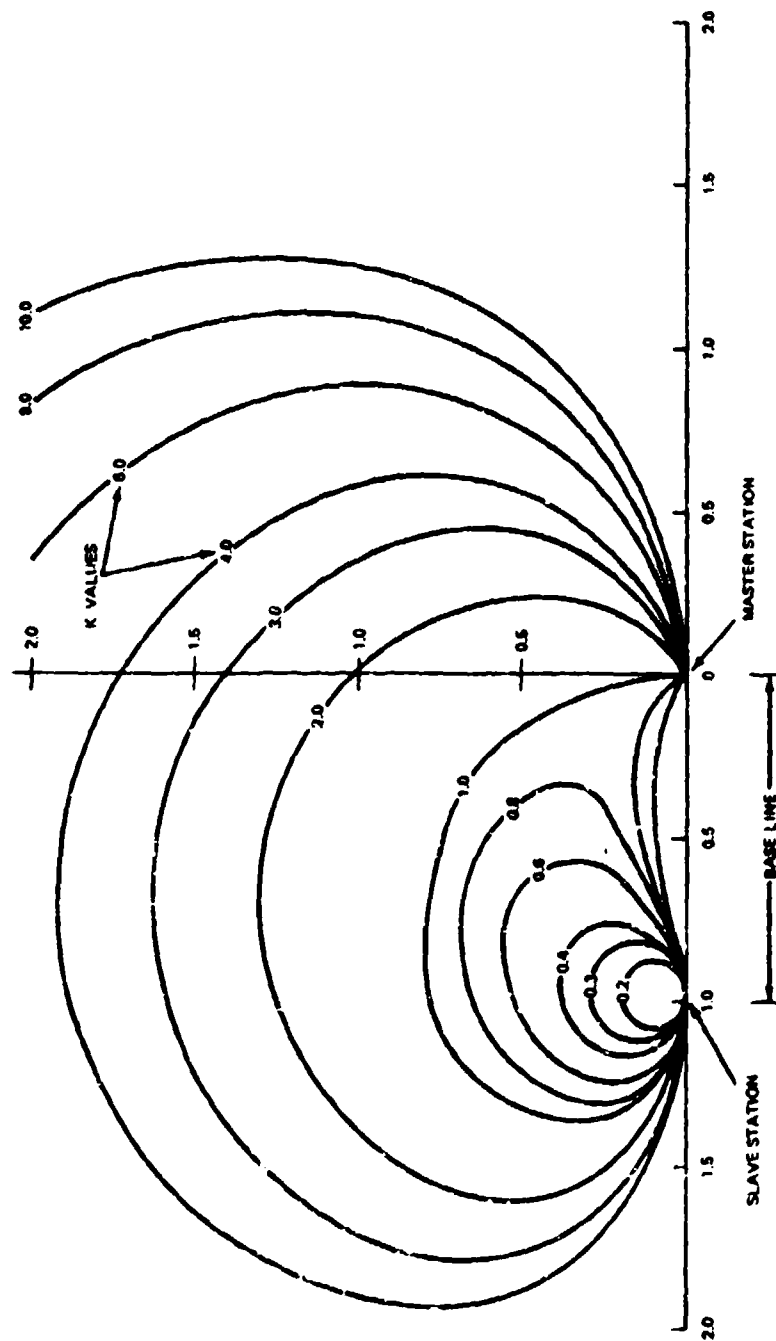


Figure 7-3. Range Error of Two Station Ranging System with Only One Station in Error

4801-102

with accurate angular tracking, data link, and computer processing of the information, very much smaller range errors can be achieved.

7.4 THE SIMPLEST "FALL-BACK" MODE

In the analysis of FACT data it was noted that on almost all attack paths with conventional weapons, there was an interval of a few seconds during which the defense required no angular lead, and only small corrections for gravity drop would be required. For guns located on or very close to a small vital target, this mode of defense has historically probably accounted for more aircraft shot down by guns of 40-mm caliber or less than any other type of fire control doctrine. Only crude estimates of range are needed for the gravity drop correction, and can be scribed on a sight. Simple tracer observation may in fact be adequate, but this should be checked out experimentally against fire without tracer, which may result in more accurate tracking. In any case, no system should be designed which prevents the use of this method of "self-defense".

7.5 CONCLUSIONS

A back-up mode for predicted fire air defense systems can be achieved by exchanging angular tracking data obtained with passive sensors among individual fire units comprising the defense. Useful accuracy should be attainable. However the problem of getting cooperative tracking stations on the same target in the short time available may be difficult.

Active sensors are not necessarily useless even though countermeasures may be conceivable which might degrade, but not necessarily negate their effectiveness. Every effort should be made, however, to have as wide a spectrum of operational characteristics of sensors in the air defense system as possible, in order to increase the logistic load of enemy countermeasures equipment, reduce his munitions delivery capability, and create uncertainty in his mind as to the probable effectiveness of his attacks. In any case, if active sensors are used in a primary role, fall-back modes of operation, using passive sensors only, should be incorporated in the defense system.

For local defense weapons located in close proximity to small vital targets, and for self-defense the effectiveness of the simplest fall-back mode, tracer fire with crude estimated range for super-elevation and zero lead angle should not be forgotten.

Finally all forward area air defense units should be prepared to resist direct attack from ground forces as well as air.

7.6 RECOMMENDATIONS

The incremental cost of providing a passive ranging back-up mode in predicted fire systems by exchanging angular tracking data across fire units should be determined. If it is favorable, brassboard field experiments should be conducted to determine the operational difficulties, and the time required for cooperating stations to acquire the same target.

SECTION 8

COST CONSIDERATIONS

This section extends the cost data "bank" provided in the prior AFAADS reports. The same ground rules are used, all cost data is from unclassified sources, and is listed without attempt to assess its validity against classified references. The object is to provide a convenient open source point of departure for more authoritative cost studies and, in particular, to raise the visibility of cost implications in early configuration considerations.

It is desired to note in particular the excellent series of reports generated at the Army Armament Command by G. W. Kalai⁽⁶⁾⁽⁸⁾⁽⁹⁾⁽¹⁰⁾⁽¹¹⁾⁽³²⁾ and associates, who are systematically developing a reliable set of cost estimating relationships for weapons, components and supporting activities for which Armament Command is responsible.

8.1 "THOSE WERE THE DAYS" (BY GENERAL "BILLY" MITCHELL)

In these days of escalating weapons system costs, it is appropriate to observe that guns still represent economical solutions to many military problems, and that over the years, the cost of guns has remained remarkably moderate in comparison with the costs of other weapons. We quote from General Mitchell's 1925 book,⁽¹⁹⁾ which furnishes an unintended commentary on how the airplane has failed to live up to its economic promise, however remarkable its performance achievements have been.

"Fighting airplanes can be built in production with their engines for from fifteen to seventy five thousand dollars, or an average of twenty-five thousand. Therefore, so far as construction is concerned, at the price of a battleship and its accessories; that is, one hundred million dollars, an average of four thousand airplanes can be built for the price of one battleship.

"The average antiaircraft gun costs anywhere from twenty to thirty thousand dollars. They will fire about twenty shots a minute with each shot costing from twenty to thirty-five dollars. The life of these guns is from about fifteen hundred to two thousand rounds when they must be replaced."

8.2 COST ELEMENTS OF GUN SYSTEMS FOR AIR DEFENSE

8.2.1 Complete Fire Units

Tables VIII-1 and VIII-2 represent extensions of those given in the prior AFADDS report, with a few weapons added. The most noteworthy addition is the cost estimate for the Phalanx system given to the Congress. ⁽³⁾⁽¹⁶⁾ Also added is the West German procurement of single 20 mm mounts ¹ ¹⁷ with minimal fire control at \$25,000 per fire unit.

We consider some of the cost elements that contribute to the listed costs.

8.2.2 Gun Barrels

Tubes are a small part of the initial fire unit acquisition cost, but in effect, a portion of each tube is expended with each round of ammunition fired, and when worn out, the tubes must be replaced. Tube wear increases with muzzle velocity. Tube cost and logistic requirements must be charged on a per-round basis against the total cost of ammunition expended, in system cost estimates.

Table VIII-1. Cost of Antiaircraft Gun Fire Units (Towed or Fixed Installations)

Caliber	Model	Weight (lb)	Cost (Dollars)	Quantity	Year
3"	US M3	7000	20-30,000		1925
75 mm	Skysweeper	20,000	313,000		1954
20 mm	West German	318	24,900		1970
2 x 20 mm	West German		76,340		1970
2 x 20 mm	Rheinmetall	3200 Firing 4600 Travel	67,000	1670	1971 for 1974 delivery
20 mm	Vulcan XM167	3150	52,000	78	1968
			90,000	120	1968
			190,000	31	1972
20 mm	CIWS Vulcan/ Phalanx Mk 15 MO	10,000	711,000 plus 3-500,000 installation cost	650E	1973
5"/54	USN Mk 45 Mount Only	78,000	825,000	54	1973

Table VIII-2. Cost of Antiaircraft Gun Fire Units (Self Propelled)

Cal	Model	Weight (lb)	Cost (Dollars)	Quantity	Year
2 x 40 mm	M42 Duster	49,500	92,840	3700	1955
20 mm	Vulcan XM163	26,000			
	Armament System		97,000	111	1968
			209,000	32	1972
	XM-741 Chassis		56,000	111	1968
			81,250	32	1972
	Total Fire Unit		153,000	111	1968
	290,000	32	1972		
2 x 35 mm	Oerlikon/Contraves	99,000	1,100,000 to 1,400,000	500-600	1972 for 1974 delivery

Figure 8-1 shows tube cost versus weight and Kalal's cost estimating relationship, ⁽⁹⁾

$$\text{Cost (1972 dollars)} = -3.49 + 20.446 (\text{weight in pounds})^{0.6} \quad (8.1)$$

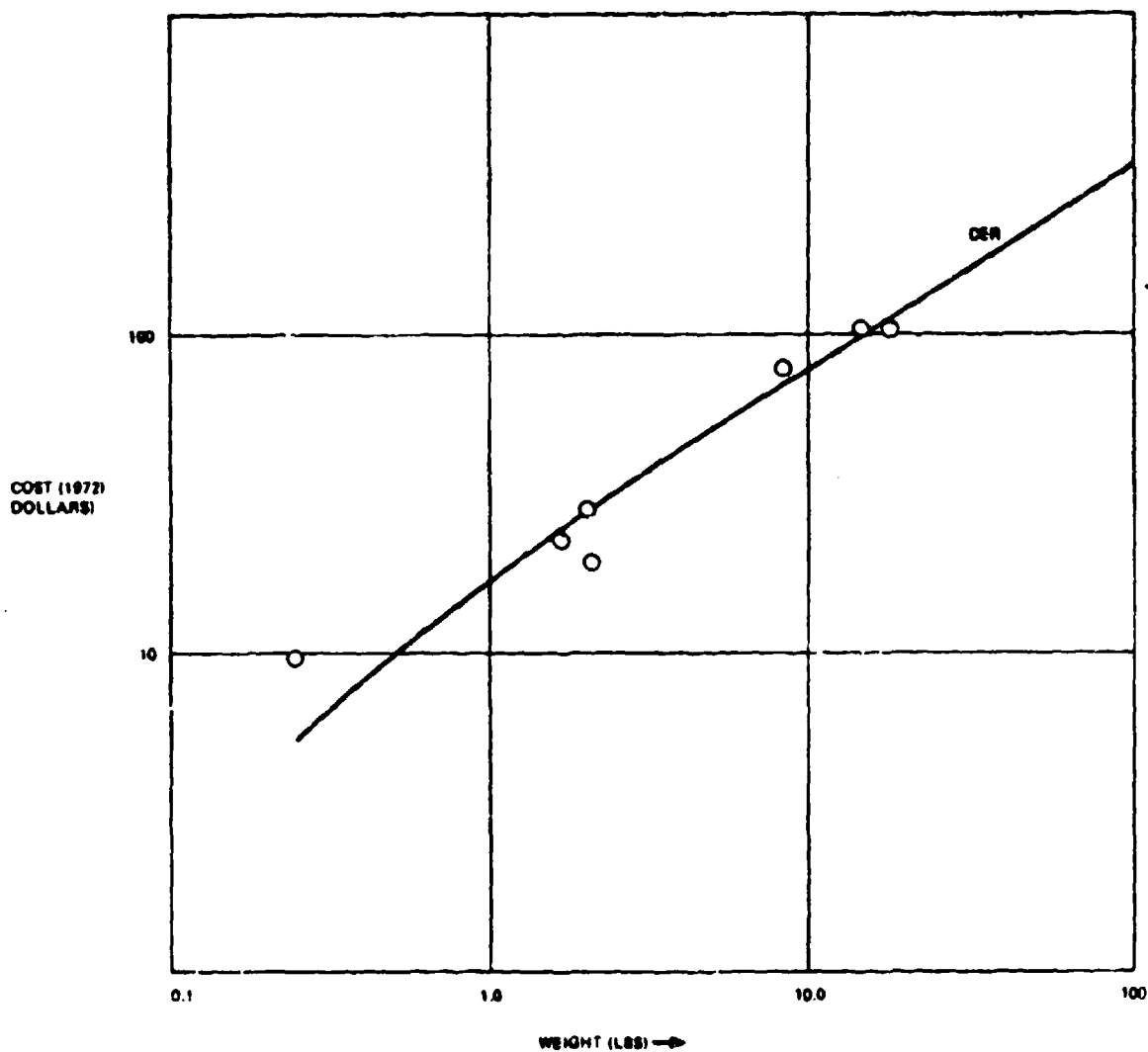
Figure 8-2 is a scatter diagram of tube weight versus caliber. The lighter tubes tend to be associated with the most modern designs, however the most significant advances are not shown by this plot, namely the great increase in muzzle energy delivered per pound of tube weight with the best modern designs and materials, and the major gains that have been achieved in tube life.

Although individual tubes are currently relatively inexpensive, they can become a significant fraction of ammunition cost for very high velocity weapons.

8.2.3 Automatic Cannon Costs

Kalal has estimated the "theoretical" first unit cost of a number of machine guns and automatic cannon. ⁽⁸⁾ His CER is

$$\text{Cost (1972 dollars)} = 8906 + 25.64 (\text{Caliber in mm})^2 \quad (8.2)$$



40001-163

Figure 8-1. Cost of Gun Barrels versus Weight

This figure shows his data base better than the simple power law shown in Figure 8-3. Also shown in Figure 8-3 are automatic cannon (single barrel) manufacturing costs, from which the CER is developed.

$$\text{Cost (1972 dollars)} = 900.10 (\text{Caliber in mm})^{0.96} \quad (8.3)$$

A few points have been added to Figure 8-3 derived from less reliable sources.

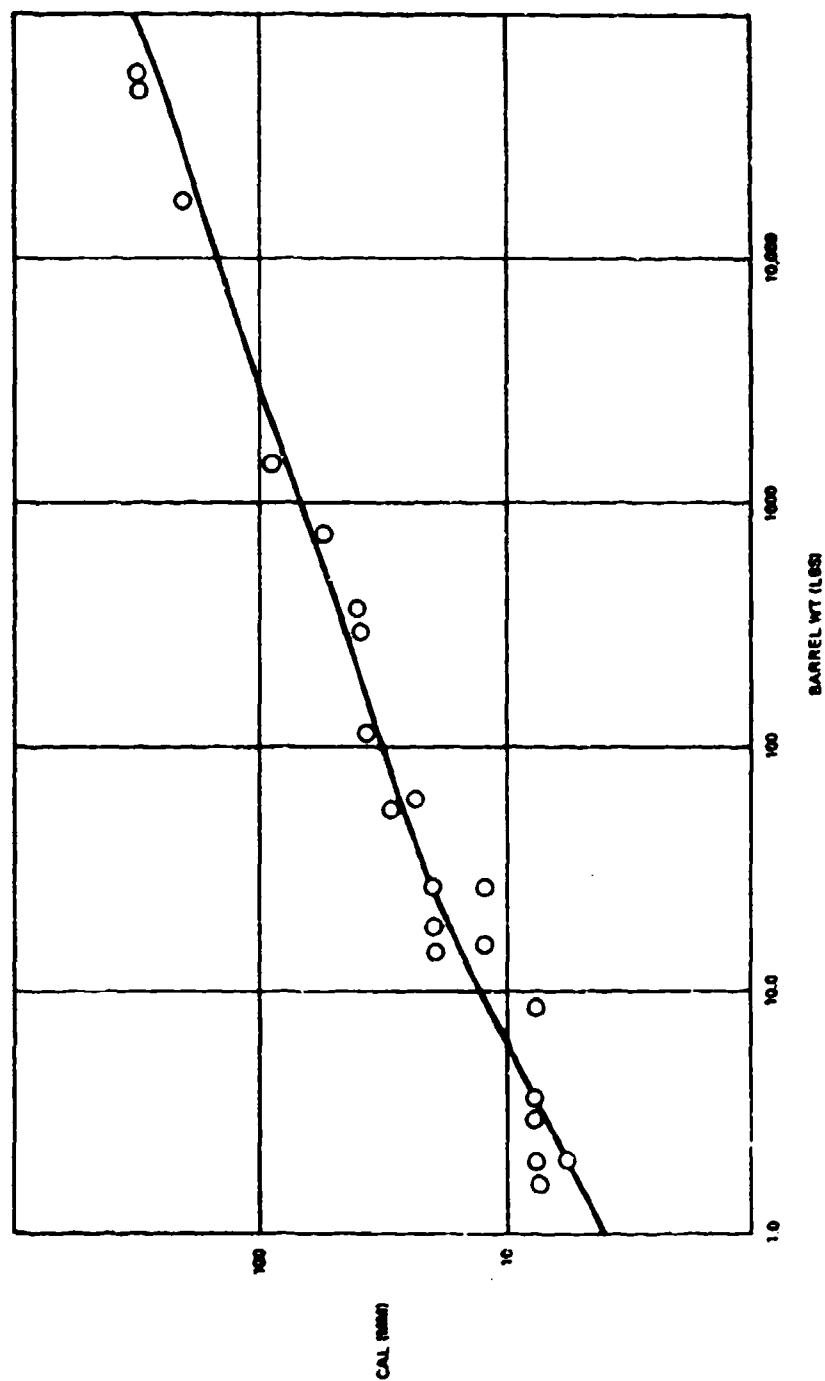


Figure 8-2. Weight of Gun Barrels versus Caliber

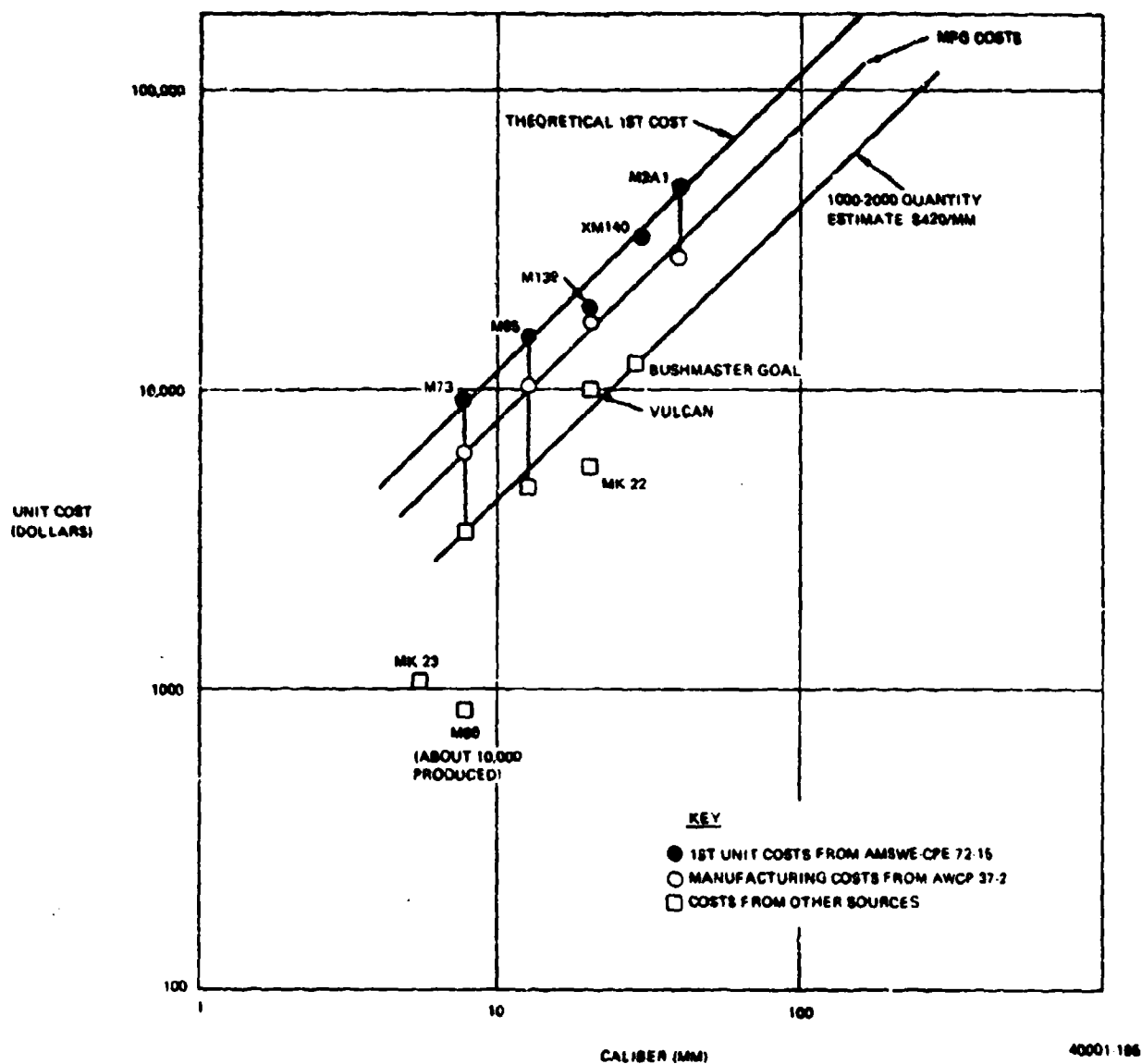


Figure 8-3. Automatic Cannon Costs versus Caliber

All of the AWCP documents describe precisely the cost elements included in the CER's and should be referenced for details.

In Table VIII-3 some unit weapon costs and program costs for aircraft automatic cannon are indicated. The cost content of the unit estimates are unknown; they are so much higher than those of the preceding data, that it is suggested that they include complete cost as installed in the aircraft.

Table VIII-3. Cost of Automatic Cannon for Aircraft

Weapon	Unit Cost (Probably as Installed)	Quantity	Program Development Cost (Million Dollars)
20 mm M61	\$47,000		
25 mm GAU-7A	\$84,500	200	\$60
30 mm GAU-8A			\$46

8.2.4 Ammunition Costs

AWCP 37-2 gives the following cost estimating relationship⁽³²⁾ for small arms (Ball type) manufacturing costs:

$$\text{Cost (1972 dollars)} = 0.01878 + 0.00007 (\text{Complete round weight in grains}) + 0.00004 (\text{Bullet weight in grains times muzzle velocity (f/s) squared times } 10^{-6}) \quad (8.4)$$

However, for present purposes, we wish to extend the estimates to other types of ammunition, for which the projectile costs will be much greater than the cost of ball projectiles. In addition, it is desired to make estimates beyond the range of the above CER which is based on ammunition in calibers from 5.56 mm to 20 mm.

From the referenced data, excluding the pistol ammunition, ball ammunition costs from \$2.6 to 3.6 per kilogram of complete round weight. From the less reliable data of the prior AFAADS report, HE ammunition in a given caliber is indicated to cost about twice as much per round as ball, hence from \$5 to \$7 per kilogram. In large calibers from 76 to 105 mm, HEAT rounds (probably in much lower production quantities) may cost two to three times as much as HE for the same gun, and anti-tank APDS ammunition at least the same multiple greater than HE.

APDS ammunition for air defense guns would be produced in much greater quantity than for anti-tank guns, and possibly would not require the same precision of manufacture; hence in the prior sections of the report we have used the estimates previously given in Table V-10, which should be improved by analyses based on more extensive cost data.

In going from ball to more sophisticated ammunition, one incurs the cost of a fuze, as well as the cost more complex manufacturing and loading operations. These costs apparently do not increase in proportion to the projectile and complete round weights, and

even for the small arms data, which are so well represented by Eq. (8.4) one can discern a dependence on weight about as the 2/3 power.

Initial indications, given in the prior report, on the cost of RAP ammunition suggests very high price multiples over non rocket-assist projectiles, but it is believed that the (unreliable) indications represent an early stage of production and lower multiples were used in Table V-10.

8.2.5 Vehicle Costs

To save vehicle development costs it is common to develop a basic chassis for a variety of applications. Vulcan, for example, is mounted on a modified APC chassis. Hence we estimate vehicle cost by comparison against costs of APC types of vehicles. Figure 8-4 shows a few data points and an estimated cost trend versus the weight of the vehicle loaded.

Vehicle cost is estimated as from \$7 to \$11/kg of loaded weight. Vehicle cost is a moderate fraction of the total system cost of SP units.

8.2.6 Turret Costs

Little data is at hand on the cost of antiaircraft gun turrets. This cost should include the servomechanisms and power supply for the turret and armament system, and probably works out to greater than the vehicle cost for the more sophisticated systems. The high cost is associated with the very high angular velocity and acceleration requirements for shooting against fast moving airplanes, and the requirement for extremely precise gun laying.

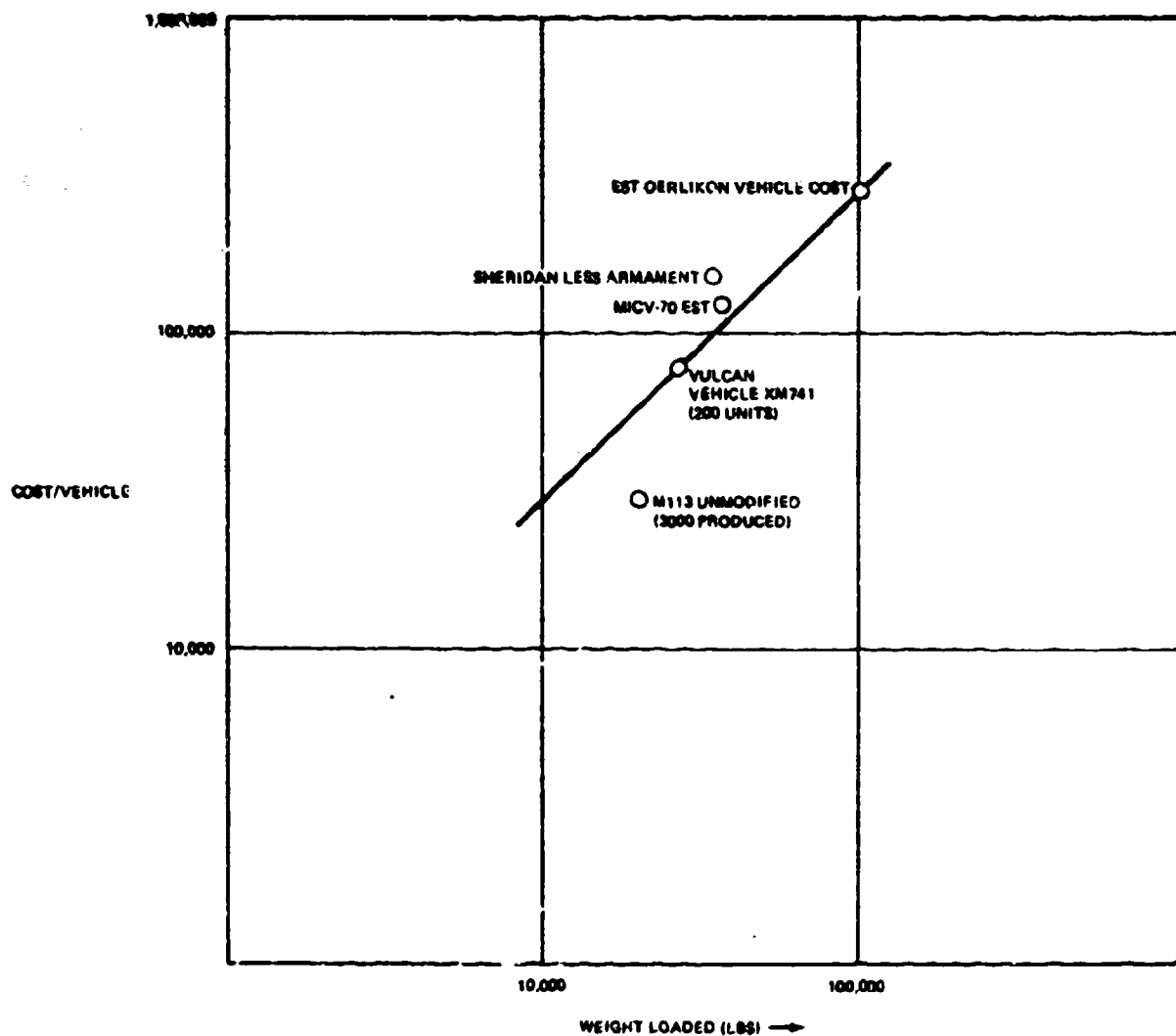
We note the indication of about \$37/kg of the Navy's 5"/54 antiaircraft gun mount (at an unknown stage of procurement), and contrast this against the \$7 to \$11/kg estimate for an Army vehicle. (The vehicle estimate would still be under \$22/kg of empty weight.)

AWCP 37-2 gives manufacturing labor costs of turret mounted aircraft armament subsystems, less guns, and derives the following CER:

Manufacturing labor cost (1972 dollars)

$$= 0.48721 (\text{weight in pounds})^{1.96450} (\text{procurement unit no})^{-0.34391} \quad (8.5)$$

and the data base indicates a range of \$20 to \$40/kg depending on the procurement quantity. The systems represented had weights of only 80-120 kg. Turret weights of a few air defense fire units are given in Table VIII-4.



40001-100

Figure 8-4. Cost of Vehicles for Air Defense Fire Units versus Weight Loaded

8.2.7 Sensor and Fire Control Costs

A build up of cost estimates based on the preceding paragraphs accounts for only about half the complete fire unit costs of Tables VIII-1 and 2 for sophisticated systems such as the Oerlikon and Phalanx. The remainder is represented by the sensors and fire control, of which the computer is a moderate cost component.

With regard to sensors, a "modular" series of airborne radars by Westinghouse is given a nomenclature associated with expected unit cost for a production run of 500 units,

Table VIII-4. Turret Weights of Air Defense Fire Units

Fire Unit	Turret Weight (kg)	Weapons
Oerlikon	14,000	2 x 35 mm
AMX	6000	2 x 30 mm
Duster	3140	2 x 40 mm
Vulcan	1320	6 x 20 mm Gatling

Much of the weight of the first two entries is represented by armor.

ranging from WX-50 (\$50,000) to WX-400 (\$400,000). It is stated that the WX-200 is for fire control in air-to-air combat. With a second data processor it gains in resolution, becomes the WX-300 and is suitable for ground mapping. With a more powerful transmitter, it can acquire targets at greater range and becomes the WX-400.

Although these are airborne radars, one may infer an estimate of about \$200,000 for a fire control radar of AFAADS ranges, i.e. a radar able to track in angle and range.

Initial FLIR costs for airborne applications were about \$500,000. Developments and production for a wider variety of applications ⁽²⁴⁾ have now made it possible to set cost goals as low as \$50,000, for "Austere" designs, and still lower cost objectives are mentioned.

Budget requests for the AN/VVG-1 laser range finder for the Sheridan vehicle indicate a unit cost of about \$31,000 midway in a procurement approaching one thousand units total.

The companion volume to this report presents computer sizing estimates for solution of the AFAADS problem on which cost estimates can be based. It may be inferred that the cost of a digital computer will be substantially less than that of a FLIR-Laser sensor combination.

Oerlikon and Phalanx utilize both acquisition and tracking radars on each fire unit. Target acquisition sensors are essential for air defense; however fire units rarely operate singly in ground operations. In considering cost versus effectiveness alternatives, one may consider two directions of concept development, - (1) share a common acquisition sensor among several fire units, with the data processing associated with the sensor given the ability to maintain multiple target tracks for assignment to fire units as they become available, and (2) increase the weapon effectiveness of each fire unit even though weapon cost is

increased, by using larger caliber hyper-velocity guns, or possibly controlled projectiles as suggested in Section 5.0.

8.3 COSTS OF UNGUIDED ROCKETS

Cost comparisons between rockets and gun fired projectiles are not new; Table VIII-5 shows a cost comparison made by Congreve in about 1810.⁽²⁸⁾

Table VIII-6 lists costs of unguided rockets of more modern origin, Table VIII-7 shows some program development costs, and Figure 8-5 is a scatter diagram of cost against weight. Current unguided rockets work out to from \$5 to \$20/kg of launch weight.

8.4 COSTS OF CONVENTIONAL BOMBS

To show that some munitions are still relatively inexpensive, we show characteristics and costs of conventional bombs in Table VIII-5 and in the diagram of Figure 8-6. The bomb dimension versus weight characteristics were previously used in Section 6.0 as a reference against missile warhead weights and dimensions.

8.5 PERSONNEL COSTS

The cost of maintaining a soldier on active duty⁽¹⁶⁾ continues to escalate, as shown in Figure 8-7. In addition, following the "Life Cycle Cost" methodology completely, one should probably charge against each year of active duty of a man in uniform, an appropriate fraction of all of the costs associated with his service, including his subsequent retirement benefits. A newspaper summary⁽²⁰⁾ indicates 20-year earnings by a soldier entering as a recruit in 1972 and retiring as a Master Sergeant in 1992 as \$325,000, or an average of \$16,000 per year. This includes cost of living increase. However subsequent retirement at half pay with a life expectancy to age 75 and built in cost of living increases in the retirement program brings the total to about \$1.7 million in pay, or about \$85,000 per year of active duty.

It is customary for economists to discount future expenditures at least at the expected inflation rate, and so one would apply a smaller annual figure against current estimates. Without working through the estimates, it does appear, however, that one might claim a "Life Cycle Personnel Cost" per year of \$30,000 to \$50,000, and on this basis one wants to hold to an absolute minimum the number of personnel required to man a weapon system.

8.6 COSTS OF MISSILE SYSTEMS

Missile system costs are relevant to evaluation of predicted fire air defense systems both with regard to comparisons as to alternate ways of solving the air defense problem, and in assessing the incremental costs forced on an enemy if he must use standoff weapons.

Table VIII-5. Comparative Costs of Congreve Rockets and Mortar Shell in 1810

Rockets				Ten-Inch Mortars			
		s.	d.		s.	d.	
Case complete	0	5	0	Carcass charge	0	15	7
Cone	0	2	11	Powder charge	0	6	0
Stick	0	2	6	Cartridge, etc.	0	1	0
Rocket charge	0	3	9				£ 1/2/7
Carcass charge	0	2	3	(Plus the cost of the mortar)			
Labor, paint, etc.	0	5	6				
		£ 1/1/11					

In addition, many of the system component costs of missile systems such as acquisition and tracking radars, are common to all air defense systems.

8.6.1 Missile Costs

Table VIII-9 lists costs of surface to air missiles, as collected from a large number of open sources. Table VIII-10 similarly lists costs of air to surface missiles, Table VIII-11 lists costs of surface to ship missiles, and Table VIII-12 lists costs of the small anti-tank missiles. One might reduce the recorded costs to a common dollar value, for example (1972 dollars), but the source data is hardly of sufficient validity to justify this modification, especially since the production quantity is rarely available.

Perhaps the most obvious conclusion with regard to surface to air missiles, is that with the exception of the shoulder-fired Blowpipe and Redeye (the latter at the end of a long production run), \$10,000 per round seems to be a rockbottom price per missile. The reported \$25,300 target cost for Stinger seems high, ⁽²⁶⁾ nevertheless, and may include the complete launch package as well as one missile on a "throwaway" basis.

The small anti-tank missiles are of interest in conjunction with estimates of the cost of controlled predicted fire air defense projectiles, since they tend to indicate a minimum cost of control package without terminal homing. Figure 8-8 indicates that there may be some possibility of building such control packages for under \$2,000, even though rate gyros may be incorporated.

Tables VIII-13, 14 show several cost-quantity histories ⁽⁶⁾ of missiles. In an initial missile (or any other weapon) buy, there are various categories of "start-up" costs which are

Table VIII-6. Costs of Unguided Rockets

Application	Designation	Diameter (mm)	Launch Weight (kg)	Cost Per Round (Dollars)	Date	Comments
Surface to Surface	Honest John	762	2700	24,800 125,000E	1960 1972	
	Little John	318	400	8000	1960	
	West German LARS			136,000	1970	(Incl. initial spares)
	LAW, M72A1	66	2.3	59 48	1972 1973	
	XM73 Practice	35		5	1973	
Air to Surface and Air to Air	ZUNI	127	49	150 E 400 300 420 321	1957 1960 1962 1970 1971	Early Product Bulk Price
	2.75" (originally Mighty Mouse)	70	8.4	60-65 43 46 22	1957 1970 1972 1973	Very large quantities
	M4 Motors only					
	SNEB 251	68	4.3	85	1972	
	GENIE AIR-2A	442	410	7000	1959	245,000 with Nuc. WHD
	Davy Crockett			1400	1960	130,000 with Nuc. WHD
Surface to Air	TAIFUN	100	29.5	RM 25 (12/6d)	WWII	An 88 mm gun projectile cost RM 80; A 20 mm round cost RM 7.50

amortized over the buy. This adds a term c_0/n to the purchase of the "n" missiles in the lot which usually dominates the "learning curve", and causes wide fluctuations in estimates of unit cost in the initial lot as the quantity is varied in initial procurement requests.

8.6.2 System Acquisition and Operating Costs

At the system level (battery or battalion), costs are likely to vary widely with the configuration of the organization, and hence the estimates recorded here are even less reliable

Table VIII-7. Rocket Program Costs (Millions of Dollars)

Weapon	Research and Development Cost	Total Procurement Cost	Year	Comments
LOKI	21.9	--	1956	Cancelled
Honest John	42.3	253.4	1960	
Little John	52.5	26.3	1960	

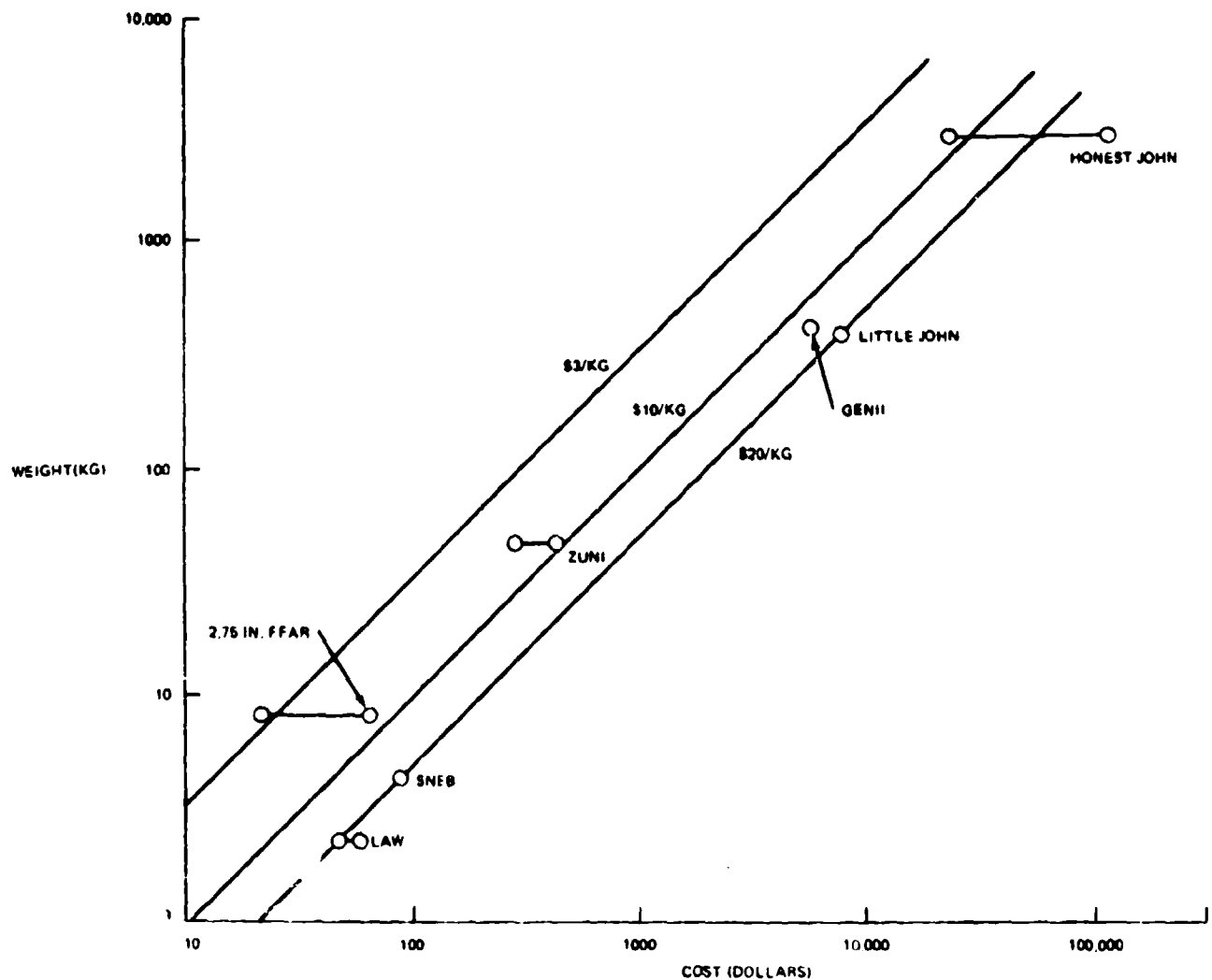


Figure 8-5. Cost of Unguided Rockets versus Weight

40001 187

Table VIII-8. Costs and Characteristics of Conventional Bombs

Nominal Wt (lb)	Type	Model	Weight (kg)	Weight of HE (kg)	Fract. of HE	Dia (M)	Length (M)	L/O	W_{HE}/D^2L^3 (grams/cm ³)	Cost (\$)	Year
750	GP	M117	374	175	0.47	0.41	2.27	5.55	45.9	212 (93 empty)	1973
500	Low Drag	MK 82 MOD 1	241	87	0.36	0.27	2.21	8.08	54.0	148 (65 empty)	1973
1,000	Low Drag	MK 83 MOD 3	448	202	0.45	0.36	3.00	8.46	52.0		
2,000	Low Drag	MK 84 MOD 1	895	430	0.48	0.46	3.85	8.42	52.8	575	1973
250	GP	M81	115							119	1973
12,000	GP	M123	6030	2262	0.38						
10,000	GP	M121	4870	3659	0.75						
4,000	GP	AN-M56A1	1984	1520	0.77						
3,000	GP	M118	1385	598	0.65					1800	1973
2,000	GP	AN-M66A2	1038	537	0.52						
1,000	GP	AN-M65A1	548	270	0.49						
500	GP	AN-M64A1	266	129	0.48						
250	GP	AN-M57A1	132	62	0.47						
100	GP	AN-M30A1	56	28	0.50						
2,000	SAP	M103	927	253	0.27						
1,000	SAP	AN-M59A	482	146	0.30	0.38	1.79	4.56	56.5		
300	SAP	AN-M58A2	250	70	0.28						
Average cost/kg of bombs dropped in Vietnam - 0.92 (\$/kg)											

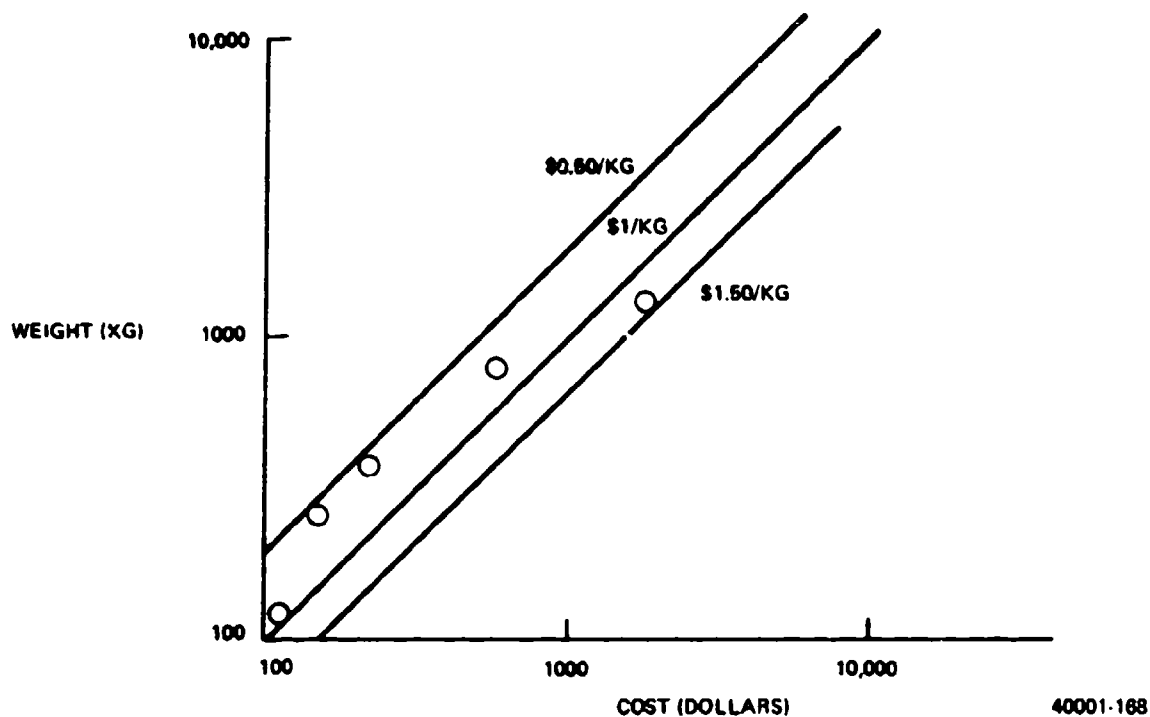
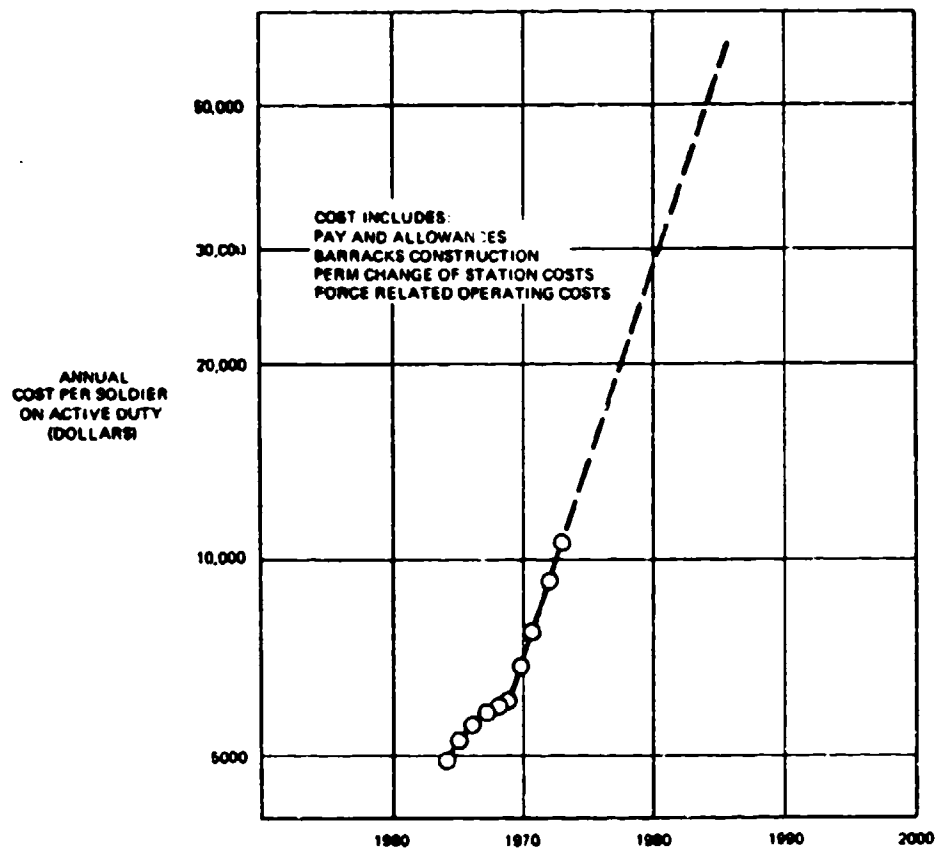


Figure 8-6. Cost of Conventional Bombs versus Weight

than those of unit missile costs. At this level, it is possible for responsible publications to confuse costs in British pounds and costs in U. S. dollars (corrected in one instance by a letter from the manufacturer) without obvious indication that the figures are in error by that large a factor. Nevertheless, we present Table VIII-15 as a framework into which an analyst with access to reliable estimates can place better data. It is suggested that an approximate way of normalizing costs across various defense configurations is in terms of the number of missiles on launchers ready to fire. One launch position of one missile is termed a "rail" for brevity. We note, however, that the time to reload a "rail" will vary widely across systems.

Figure 8-9 shows annual operating costs in USAREUR of four widely different types of missile battalions.^② The annual cost per battalion nevertheless works out to approximately twice the cost of personnel alone (including training of replacements) with an accuracy rarely achieved by cost estimating relationships. There may be a natural "law of human effort" which implies that a man is paid (in peacetime) an amount equal to the cost of material consumed per capita by the system he serves. There is a similar tendency for M&O costs of the Air Force, for example on a service wide basis, to equal personnel costs, year



40001 100

Figure 8-7. Annual Cost per Soldier on Active Duty

after year in budget requests. If the "law" works in inverse fashion as well, the escalating costs of manpower in the current Army will raise the annual operating costs of advanced weapon systems to crisis levels.

Table VIII-9. Costs of Surface To Air Missiles (Sheet 1 of 3)

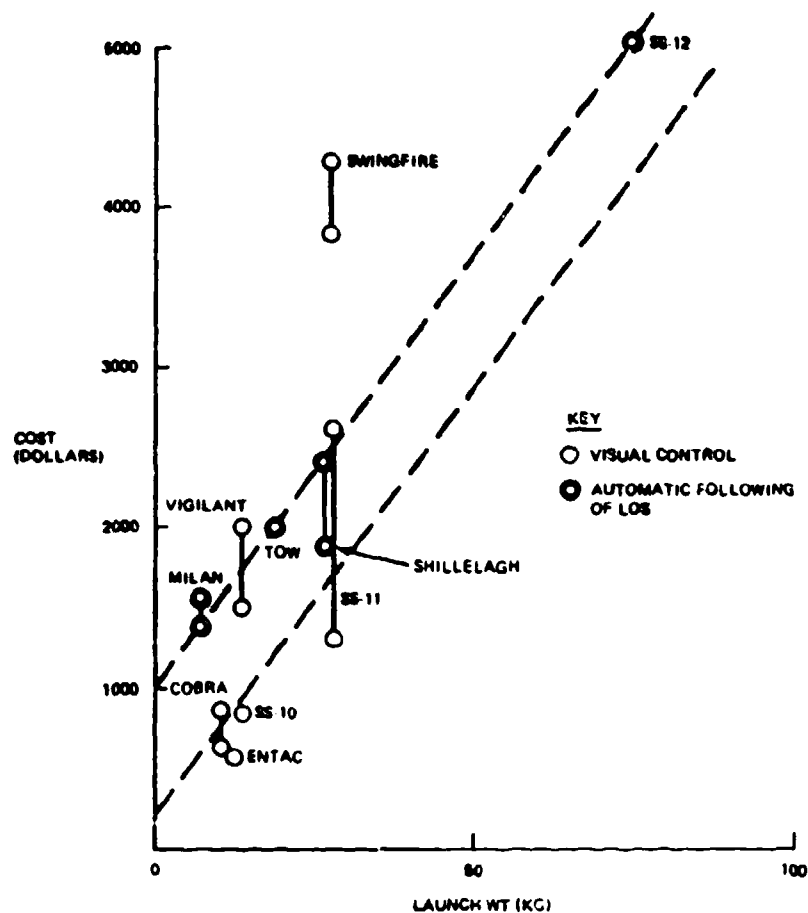
Missile	Country	Range (Km)	Launch Wt (Kg)	Wtd Wt (Kg)	Date of Introduction to Service	Cost/Missile (Dollars)	Year
Blowpipe	UK	3	12.7	1.82	1973E	2,450E 1,950	1960 1966
Chaparral	US		84	11	1969		
Crotale R440	FR	8	80	15	1973E	12,600 9,000 15-18,000	1971 1973 1973
Bomarc	US	700	7270			1,800,000 900,000	1951- 58 1958- 60
Bloodhound Mk I	UK		2000			21,840	1960
Bloodhound Mk II	UK	80			1964	35,000	1960
Hawk	US	35	587	75	1959	41,620	1965
Indigo	Italy	10	97	25			
Masurca Mk-2	FR	50	2080	48			
Oerlikon Micon	Swiss	35	800				
Nike-Ajax	US	40	1113	135	1948	20,000 19,310	1957 1962
Nike-Hercules	US	130	4720		1958	80-100,000 55,100 68,280	1967 1964 1973

Table VIII-9. Costs of Surface To Air Missiles (Sheet 2 of 3)

Missile	Country	Range (Km)	Launch Wt (Kg)	Whd Wt (Kg)	Date of Introduction to Service	Cost/Missile (Dollars)	Year
Oerlikon-56	Swiss	30	375	40		11,400	1958
Rapier-I	UK	15		5	1973E	10,000	1970-73
Rapier-II	UK						
Roland-I	Intl	6	63	6.5	1973E	12,600 15-18,000	1971 1973
Redeye	US	3	8.5		1968	6,700E (1960) 5,000 (1967)	1960 1967
SAM-D	US					90,000E	1973
Sea Cat	UK	3.5	68				
Sea Dart	UK	30	550				
Sea Slug	UK	35	1818			29,400	
Sea Sparrow	US	19	227			40,000	1973
Sparrow (Vert. Launch)	US					75,000	1973
Stinger	US		13.6			25,300 objective (1972 dollars) 31,600 max (probably for complete launch package)	1972
Tigercat	UK	3.5	68		1968	10,000	1970
Thunderbird-I	UK	35	1910			22,400	1958
Thunderbird-II	UK						

Table VIII-9. Costs of Surface To Air Missiles (Sheet 3 of 3)

Missile	Country	Range (Km)	Launch Wt (Kg)	Wtd Wt (Kg)	Date of Introduction to Service	Cost/Missile (Dollars)	Year
Tartar	US	16	545			40,000 11,000	1957 1959
Terrier-I	US	18	1450			64,000 62,000 40,000	1957 1958 1959
Adv Terrier	US	32	1360				
Talos	US	112	1542			185,000E	1958



40001-170

Figure 8-8. Cost of Antitank Missiles vs. Launch Weight

Jackson and Billings ⁽¹⁴⁾ ⁽¹⁵⁾ have presented cost estimating relationships to describe missile costs in terms of missile characteristics for a wide variety of missile types. Billings, in his later paper, concurs in Jackson's CER for propulsion costs, which is

$$\text{Cost} = a_0 P^{a_1} A^{a_2} R^{a_3} T^{a_4} e \quad (8.6)$$

Table VIII-10. Costs of Air to Surface Missiles

Designation	Model	Range (km)	Launch Wt (kg)	Warhead Weight (kg)	Approx. Av. Velocity (m/s)	Length (Meters)	Body Diameter (Meters)	Wing/Tail Span (Meters)	Cost (\$)
AS-11	AGM-22A	3	29.9		160	1.20	0.16	0.50	
AS-12		5.5	76	28.4	100	1.87	0.18	0.65	
AS-20		7	113	30	360	2.60	0.25	0.80	
AS-30		11.5	520	230	470	3.84	0.34	1.00	14,100 (1960) 13,000 (1962)
AS-30L		11.5	340	115		3.60	0.34	0.90	
Bullpup-A	AGM-12B	11	260	113	600	3.20	0.30	0.94	10,500 (1958) 2500 (1965)
Bullpup-B	AGM-12C	16.5	810	454		4.14	0.45	1.22	
Condor	AGM-53A	92	960	286		4.21	0.43	1.35	225,000 (1970) 310,000 (1973) 100,000E (Quantity Prod)
Hellcat		6	68			1.7			
Hobos	KML-353A/B KML-390/B		907 1360						
Hornet	ZAGM-64A	3.7							
Hound Dog	AGM-28	965	4350		660	12.95	0.72	3.71	
Kingsaroo	AS-3	650				14.9		9.1	
Kelt	AS-5	180				9.4		4.6	
Kennel	AS-1	100				8.2		4.90	
Kipper	AS-2	213				9.5		4.6	
Kitchen	AS-4	460				11.3			
Kormoran		37	580		315	4.40	0.34	1.00	
Nartel	AJ168 AS-371ARM)	64		30		4.00	0.38	1.12	
Naverick	AGM-65A	22	215	59		2.46	0.30	0.71	27-37,000 (1972) 19,000E (1974) 7500E (Quantity)
RB04		6	600			4.45	0.50	1.98	
RB05A			305			3.60	0.30	0.80	
SIRIKE	AGM-15A	16	182		660	3.05	0.20	0.91	21-38,000 (1972)
SRAM	AGM-69A	160	900			4.27	0.45		225,900 (1971) 3500 (1968)
Sud ARM	AGM-78B	25	816		660	4.57	0.31		13,500
Walleve	AGM-62A	5	500			3.43	0.38	1.14	20,000 (1971)

Table VIII-11. Cost of Surface to Ship Missiles

Designation	Model	Range (km)	Launch Wt (kg)	Warhead Wt (kg)	Warhead Type	Approx Av. Vel (m/s)	Length (m)	Body Diameter (m)	Wing/Fin Span (m)	Cost (\$)
-ret	MM-38	37	720	100	HIE	310	5.12	0.34	1.00	540,000 (1972)
	ZAGN-84A	20	400	180	HIE	230	3.35	0.33	1.39	91,000 (1971)
Mat		18	1300	325	Homing Torpedo	230	6.00		3.00	
Otomat		80	700	200	Semi Armor Piercing	270	4.82	0.40	1.19	200,000 (1973)
Penguin		27	330	120	HIE	230	3.05	0.28	1.40	7,000 (1971)
RB04A		200	900				5.71	0.66	3.01	
Samlet	Sea Version of Kennel	100					4.20		4.90	
Sea Dart		30	550				4.36	0.42		
Sea Killer Mk I		10	168	70	HIE	630	3.73	0.20	0.85	
Sea Killer Mk II		19	240	140	Semi Armor Piercing		4.50	0.20	1.00	134,200 (1971)
Shadlock		370				310	10.9			
SS-12M		6	75	30	AP Oxid 40-mm Steel Penetration	190	1.87	0.18	0.65	5,000 (1970)
STYX	SSN-2	46	1360			300	6.50	0.70	2.70	

Table VIII-12. Costs of Antitank Missiles

Type	Body Dia (mm)	Range (km)	Launch Wt (kg)	WHD Wt (kg)	AV. Velocity (m/s)	Cost (Dollars)	Control Type
ACRA	142	3.3	7.5	(2.8 HE)	500		Laser Beam Rider
Bantam	110	2	7.5	1.9	85		Wire + Visual
Cobra 2000	100	2	10.2	2.7	85	620 (1963) 840 (1965)	Wire - Visual
Dragon	127	1	6.1		110		Wire + Auto Los
Entac	150	2	12.2	4.1	85	600 (1962)	Wire + Visual
Harpon	164	3	30.4		190		Wire + IR Auto Los
HOT	136	4	22	6.0 (3.0 HE)	280		Wire + IR Auto Los
KAM-3D	120	1.8	16		85		Wire - Visual
KAM-9	150						Wire + Auto Los
Milan	116	2	6.3	(1.45 HE)	178	1400-1570 (1970)	Wire - IR Auto Los
Mosquito	120	2.4	14.1	4	85		Wire + Visual
Shillelagh	152	3	27	6		1906 (1967) 1295 (1968) 2400 (1970)	Auto Los
Sagger		1.8		6		1000 (1974)	Wire + Visual
Snapper	140	2.3	22.3	5	82		Wire + Visual
SS-10	165	1.5	14.8	5	79	896 (1960)	Wire + Visual
SS-11	160	3.3	29.9	8	160	1316 (1965) 2600 (1971)	Wire - Visual
SS-12	180	6	75	30	190	5050 (1965)	Wire + IR Auto Los
Swingfire	170	4	37	7	185	3840-4320 (1971)	Wire - Visual
TCW TOW	150	3	19	3.8	280	2000 (1971)	Wire - Auto Los
Vigilant	110	1.4	14	5.5	158	1560 (1961) 2020 (1962)	Wire - Visual

Table VIII-13. Bullpup Price History

Mfg	Year	Price (Dollars)
Martin	1958	10,500
	1959	6,500
	1961	4,700
Maxson	1962	4,100
	1963	3,100
	1964/5	2,500

Table VIII-14. Estimated Price vs. Quantity for SRAM

Year	Quantity	Price (Dollars)
Fy 1971	101	760,000
1972	465	330,000
1973	480	150,000

where a_0 = constant

P = payload weight/total weight

A = acceleration = thrust/launch weight

R = maximum range (nautical miles)

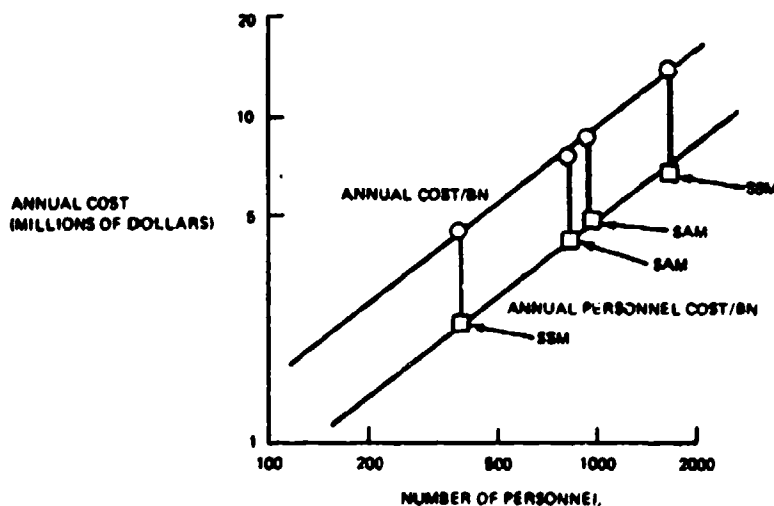
T = flight time

e = stochastic error term

and cost is cost at unit one-thousand.

Table VIII-15. Cost of Ownership of Sam Systems

Installation	Investment Cost (Millions of Dollars)	Annual Cost (Millions of Dollars)	Personnel
Hawk Battalion (4 Batteries) 6 Launchers/Battery 3 Missiles/Launcher	\$22 (1959) \$ 305,000/Rail	7.4 (Overseas) Semi- [4.5 (Continental US) Mobile [5.3 (Overseas)	827/BN 11.5/Rail
Rapier Battery 12 Fire Units 2 Field Repair Units 312 Missiles/Battery 4 Missiles/Fire Unit	\$20 (1972) \$ 417,000/Rail		28/Platoon of four fire units excluding repair personnel
Hercules Battalion 48 Launchers/Battalion	\$19.4 (1958) \$ 404,000/Rail	8.8 (Overseas)	922/BN 19.2/Rail
UK Bloodhound-2 Squadron (8 Missiles)	\$9.67 \$1,200,000/Rail		
Sam-D Battalion Estimated as 6 Fire Sections per Battalion; Battalion overhead not included	\$40.8 (1973E) \$ 250,000/Rail		



40001-171

Figure 8-9. Annual Operating Costs of Missile Battalions vs. Number of Personnel

The numerical fit yields

$$\begin{aligned} \text{Log Cost} = & 1.17 + 0.11 \text{ Log P} + 0.16 \text{ Log A} + 1.04 \text{ Log R} \\ & - 0.79 \text{ Log T} + 0.14 \text{ Log ST} - 0.05 \text{ Log SR} \end{aligned} \quad (8.7)$$

where

ST = dummy variable: unity for air launched missiles, and flight time for surface launched missiles

SR = dummy variable = unity for missiles used against air targets, and range for missiles used against surface targets.

Payload weight is defined as the total weight reaching the target, but there seems to be some doubt as to whether this was used as opposed to warhead weight in the data base.

It was stated that the model "explains" 99% of the cost of the propulsion unit. The missile is divided into two sets of components, propulsion unit and the assembly of guidance, control, airframe and warhead. Missiles included SAM, AAM, ASM and SSM types.

Billings develops a very simple CER for the non-propulsion component aggregate of radar guided missiles, based on the weight of the guidance and control section. His sample included several Falcons, Hawk, Shrike, Tartar and Terrier. His CER is

$$\text{Log } C_g = \text{Log } a - b \text{ Log } W_g \quad (8.8)$$

where

C_g = 1st unit cost in 1965 dollars per pound of guidance, control, airframe, assembly and checkout.

W_g = weight of guidance, control and airframe (pounds).

and in numerics

$$\text{Log } C_g = 3.1945 - 0.2881 \text{ Log } W_g \quad (8.9)$$

or

$$C_g = \$1565 W_g^{-0.2881} \text{ (cost per pound)} \quad (8.10)$$

$$C_1 = \$1565 W_g^{0.7119} \text{ (cost of first unit)} \quad (8.11)$$

He states that missiles in the sample followed a 92% "experience" or "learning" curve, and that this simple expression "explains" 99.7% of the first unit cost.

For 92% learning, the unit costs develop with quantity as

$$\begin{aligned} C_j &= C_1 j^{-0.120} \\ \text{so that} \quad C_{100} &= 0.575 C_1 \\ C_{200} &= 0.529 C_1 \\ C_{1000} &= 0.437 C_1 \end{aligned} \quad (8.12)$$

8.7 COSTS OF COMMERCIAL AIRCRAFT EQUIPMENT

As a supplement to the sparse data on hand on military electronics we provide some information on commercial equipment.

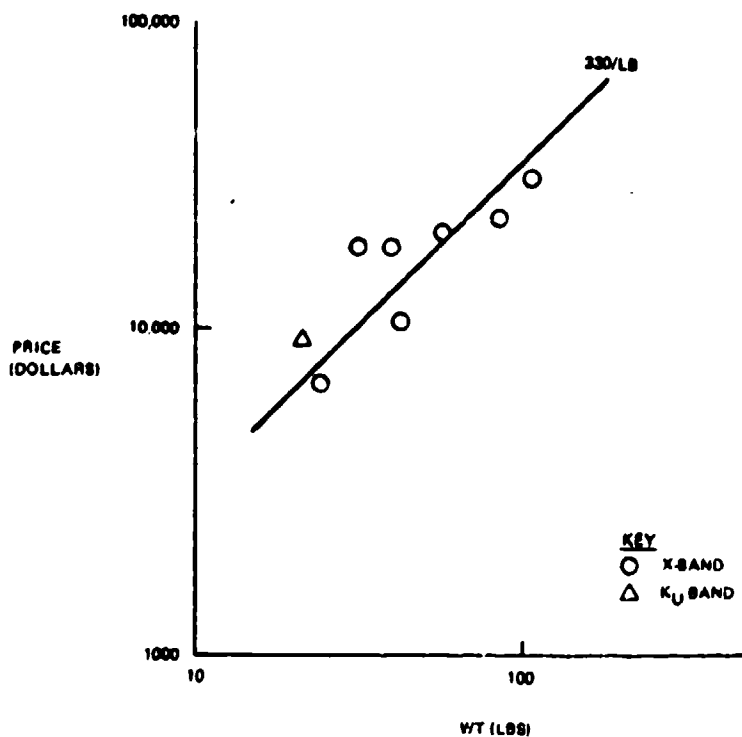
8.7.1 Radar

Figure 8-10 shows 1973 prices of airborne weather radars vs. weight, and Figure 8-11 shows price vs. power. In the latter case one needs additional descriptive parameters to account for outlying points. These radars average about \$725/kilogram of weight, but cost increases only as the $2/3$ power of power.

Radar altimeters work out to about \$1000 per kilogram, as shown in Figure 8-12.

8.7.2 Autopilots

Autopilots range in capability from light, single gyro piloting aids, to full navigational systems. Figure 8-13 shows that as weight and capability increase, cost increases from about \$250 per kilogram to \$1500 per kilogram. Again, more descriptors of function are required to reduce the scatter.



40001-172

Figure 8-10. Price of 1973 Airborne Weather Radars vs. Weight

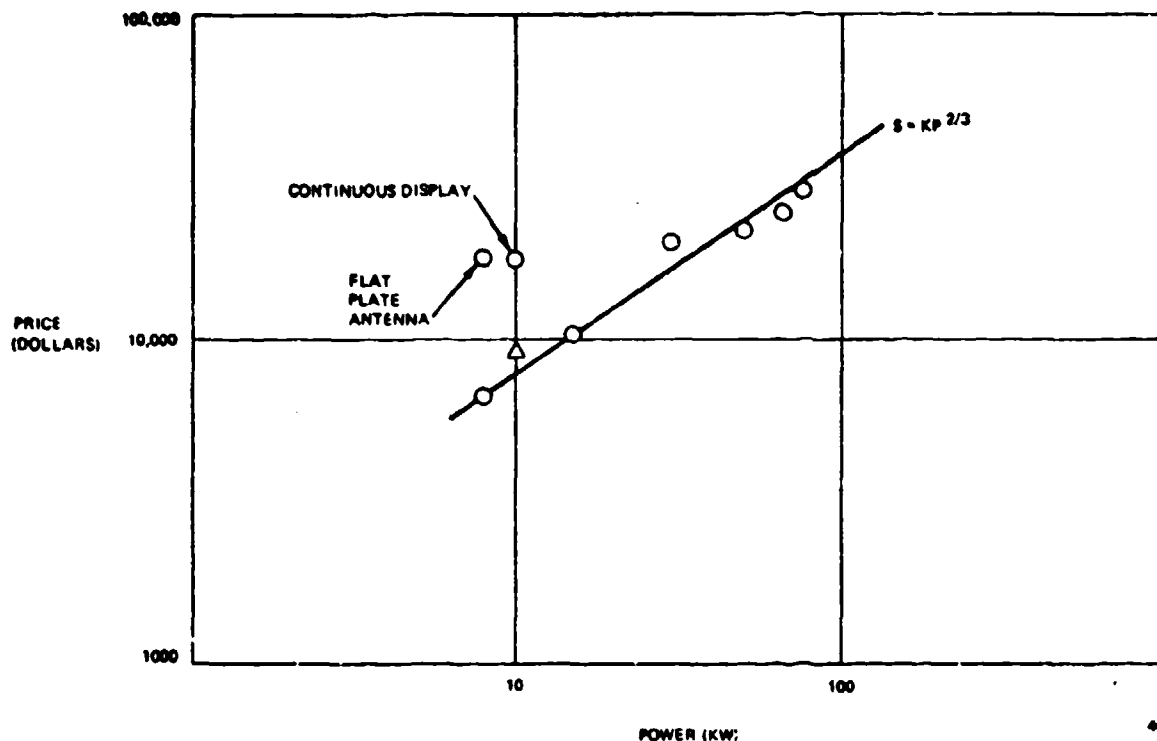


Figure 8-11. Price of 1973 Airborne Weather Radars vs. Power

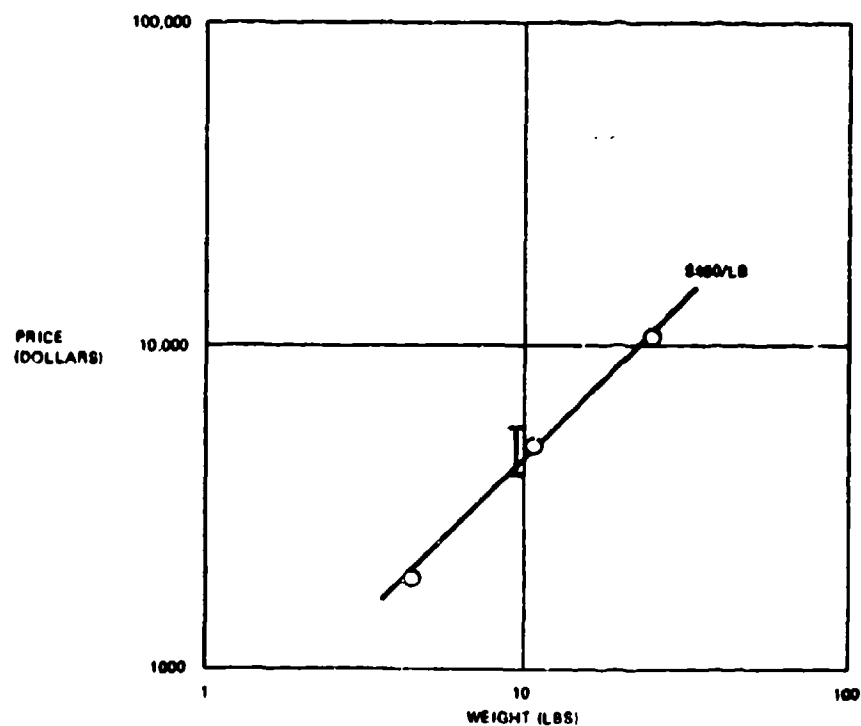


Figure 8-12. Price of 1973 Radar Altimeters vs. Weight

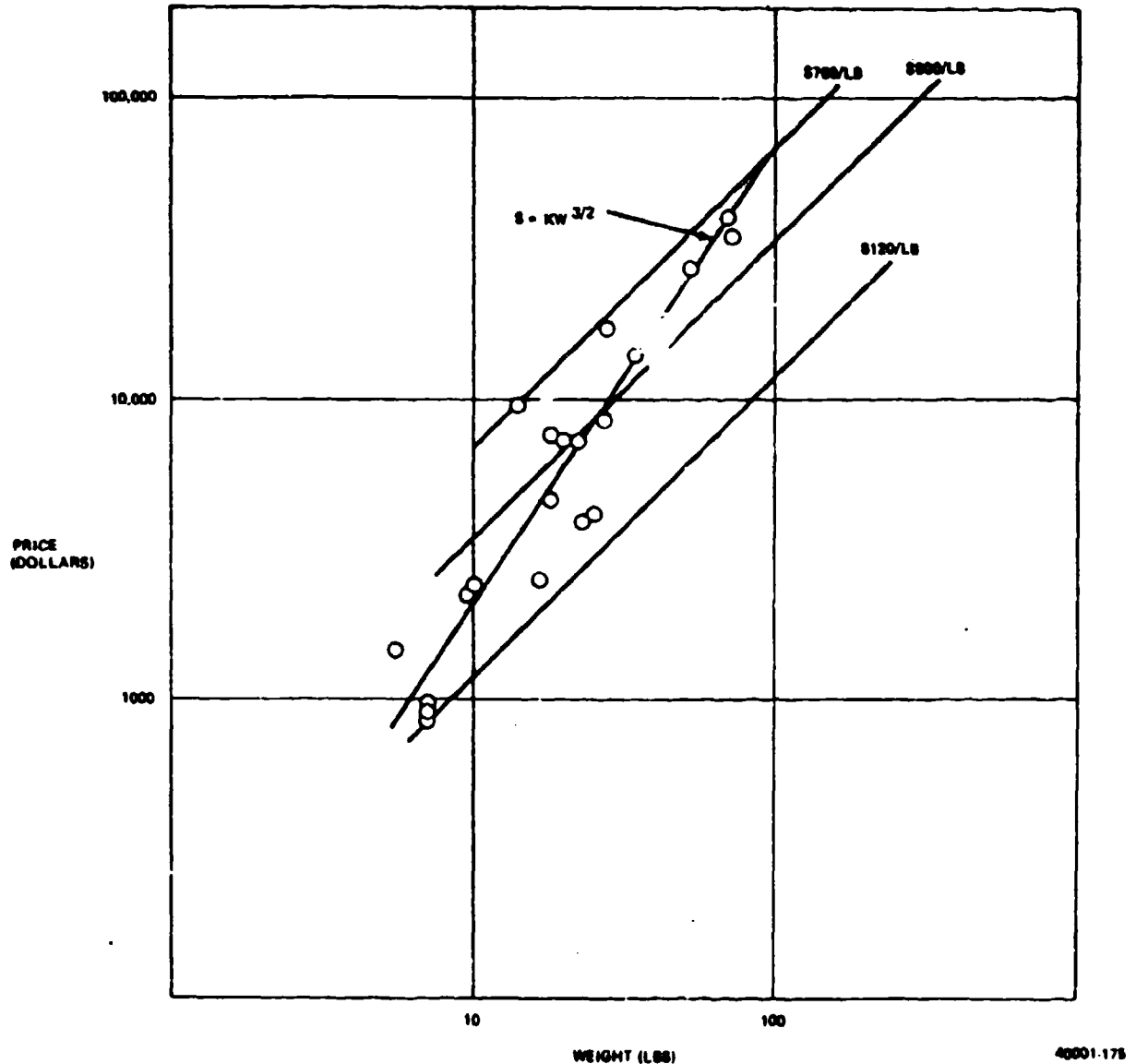
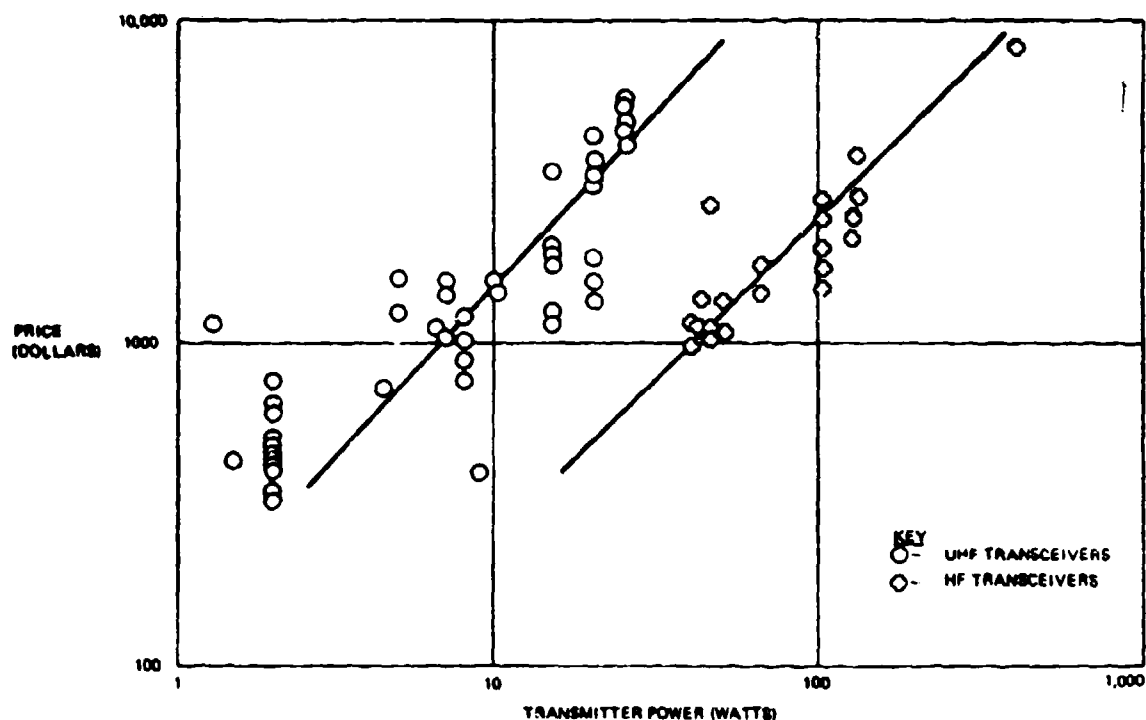


Figure 8-13. Price of 1973 Autopilots vs. Weight

8.7.3 Figure 8-14 is a scatter diagram of transceiver cost vs. transmitter power in HF and VHF. A plot against weight (not shown) indicates a cost of about \$600/kg for VHF and \$300/kg for HF, with a great deal of scatter.

8.8 COMMENTS

The costing studies and CER Development at the Army Armament Command will, as it continues, provide an excellent basis for introducing sound cost considerations to concept analysis of new systems at an early stage of concept development. Complementary work, of



40001-176

Figure 8-14. Price of 1973 Transceivers vs. Transmitter Power

a classified nature, undoubtedly exists at both the Missile Command, and the Electronics Command. It would be highly desirable if appropriate portions of these efforts on the sensor and electronics components of weapons systems could be published in unclassified extracts for ease of availability to systems designers. Classified information must, of course, remain classified, but we note that information that an industrial designer can keep on his board for immediate access has a far greater likelihood of influencing a design than information that he must charge out of document control daily, and return each night.

SECTION 9

SIMULATION VERIFICATION PROCEDURE

This section describes a series of check-out problems intended to guard against errors in the operation of the Litton simulation. Several errors in the program identified by Mr. Stanley Goodman of Frankford Arsenal were corrected in the process. The work was made possible by a comprehensive flowchart of the simulation prepared by Mr. Barry Said of Litton. Simulation runs were made by Mr. J. Onishi of Litton.

Not all of the verification procedures described are demonstrated by examples. However, the modules of principal concern in past use of the simulation have been subjected to test, and program corrections applied where necessary.

9.1 METHOD

The test procedures described and illustrated by examples are intended to verify the following functions

- a. Prediction Modules
- b. Bias Modules and Computation of Miss at Closest Approach
- c. Single Shot Kill Probability Computation

Additional tests would be required for the other functions performed by the simulation including development of statistics by replication, and the report generation program. However the above three tests should verify the three most critical sets of computations.

9.2 SIMULATION INPUTS

To avoid excessive referencing of input data which is repeated across test paths, reference is made to the informal working paper "AFAADS II-B Gun Model Input Data" by M. Ginsberg, undated, of which a copy is at Frankford Arsenal. Input data is partitioned into Groups, within each of which is a number of data cards. Content of a few of the cards has changed in later simulation modifications, but the current content can be obtained as a print-out of the program.

9.2.1 Group Content

We summarize briefly the Group content, and those cards that are relevant to the present checkout problems

- Group 1:** Study Title.
- Group 2:** Simulation Timing, including path duration and designation of special events, such as particular sensor failures and recovery
- Group 3:** Tracker Data. Includes the filter weights, the corrections for filter lags, the tracker lag coefficient regeneration command (in or out), angular tracking and range biases, radar tracking parameters, including target dimensions used in the tracking program, random number start value, correlation time for range noise, and timing of sensor failures and recovery
- Group 4:** Aircraft flight path. Contains data to construct the flight trajectory as a series of linear, circular and spiral segments with specified velocities and accelerations
- Group 5:** Ballistic Data. Contains parameters to match separately inserted reference ballistic tables against specific weapon data points, and to derive ballistics based on specific weapon caliber, muzzle velocity and ballistic coefficient. Contains terminal effect inputs to determine conditional probability of kill given a hit from projectile weight, fraction of weight in HE, vulnerability factors for target wings and fuselage
- Group 6:** Prediction Algorithms. Contains designators for type of prediction to be used, thresholds for switching prediction modes, and terminal parameters for defense of known point algorithms
- Group 7:** Gun Servos. Contains parameters for gun lag coefficients, and regeneration (in or out) command. Contains initial gun angles
- Group 8:** Report Generation. Contains instructions for number of replications. Contains parameters for angular dispersion of gun and ammunition separately input as vertical, lateral, muzzle velocity and muzzle velocity bias. Contains dimensions of target represented as ellipsoidal fuselage and wing, and coefficients to combine separate vulnerabilities of wing and fuselage to correct for overlap or shielding. Also contains specified categories for histogram-type representation of miss distance, single shot kill probability, burst kill probabilities and summarization instructions
- Group 9:** Reinitialization. Contains interface information for changes in next batch of runs

9.2.2 Common Inputs in Test Runs

For the check-out runs described in the present report, Group 2 inputs are unchanged. A 10 second flight path is used, and the first 1.6 second interval during which the filters are settling is suppressed in the print-outs. Table IX-8 shows the filter weight inputs of Group 3, Cards 1 to 4, representing least squares weighting. There is no change in these cards in the examples presented. The runs were made with zero tracker lag, which is commanded by setting $TKV = TKA = 0.0$ on Card 3-5, and $REGEN = 0.0$. A few runs were made with target dimensions identically equal to 0.001 on Card 3-8 until it was determined that the simulation would run with the three inputs equal to 0.0, providing zero tracking error. Card 3-6 contains tracking biases in angle, and range, and these inputs were varied as later specified.

All runs were made with ballistics for a 25 mm gun with 3600 f/s muzzle velocity, prediction cut-off at 1100 f/s (approximately sonic velocity) and a ballistic parameter $C = 1.1256094$.

9.3 PREDICTION MODULE VERIFICATION

9.3.1 Constant Velocity, Level Straight Line Flight

This run was made with target dimension 0.001 in each coordinate, - essentially zero. The simulation performed correctly, as shown in Table IX-2, after correction for an error in gravity drop computation identified by Mr. Goodman.

9.3.2 Dive and Climb Along Straight Line Under Gravity Acceleration

The dive/climb module of the simulation corrects for the target acceleration along a straight line, represented as the component of gravity acceleration in a vertical and horizontal coordinate.

Table IX-1. Velocity and Acceleration Inputs
for Straight Line Test Paths

Path Type	Level	Dive	Climb
VS(1)	200.00000	197.00000	197.00000
VZ(1)	0.0	-35.00000	35.00000
AZ	0.0	-0.03062	-0.03062
AS	0.0	0.17230	-0.17237

The computation of inputs is (θ = climb angle = constant)

Initial	$VZ(1) = V(1) \sin \theta$	
Values	$VS(1) = V(1) \cos \theta$	
	$AX = -g[VZ(1)/V(1)]^2$	= constant, always negative
	$AS = -g[VZ(1)VS(1)/V(1)^2]$	= constant, positive in dive (9.1)

Numerical inputs for the test problem are given in Table IX-1. Simulation errors for both dive and climb were considered satisfactory. The error printout for the climb pass is shown in Table IX-3.

9.3.3 Level, Circular Paths at Constant Velocity

A set of test problems was run with the target flying horizontal circular paths centered on the gun position. The simulation uses an approximation to a circular arc for curved flight prediction. Initial runs indicated errors exceeding a meter resulting from the approximation on a 1.0 g turn. This magnitude of error is entirely acceptable for an operational system since aircraft will not hold an exactly constant acceleration of this magnitude, however to simplify computations for subsequent test problems it was decided to add one term to the series approximation in the simulation. The modification is given in Section 9.3.4, below.

Table IX-4 summarizes the resulting simulation errors for a series of circular paths, with zero target size input. Table IX-5 is a printout of results for one of these paths. For this 1/2 g turn, the approximation has a residual error along the flight path of about 0.09 meters, and a bias perpendicular to the flight direction in a horizontal plane of -0.34 meters. Bias in a vertical direction is essentially zero.

In Table IX-5 note the variation in error with position, probably the result of the many trigonometric computations involved. Table IX-4 contains typical values from each path type.

9.3.4 Curved Flight Algorithm

The additional correction term for the curved flight approximation was obtained by a rather tedious expansion of the prediction algorithms in each coordinate up to and including terms in the square of the angular velocity of turn. The resulting expressions as derived for least squares filters are given below. For other weighting systems, the expansion should be redone.

Table IX-2. Simulation Test Problem for Level, Constant Velocity Path

TIME OF FIRE	TIME OF FLIGHT (M)	RANGE (M)	AZIMUTH (DEG)	ELEVATION (DEG)	RADIAL ACCEL. (G)	RANGE ERROR (M)	AZIMUTH ERROR (M)	ELEVATION ERROR (M)	MU (M)	MV (M)	AMS (M)
1.0	0.203	845.448	42.827	36.257	0.0	-0.000	0.0	-0.000	-0.000	-0.000	0.000
2.0	0.861	826.526	42.561	37.225	0.0	-0.000	0.0	-0.000	-0.000	-0.000	0.000
2.2	0.819	803.614	38.114	38.195	0.0	-0.000	0.0	-0.000	0.000	-0.000	0.000
2.4	0.819	791.732	35.262	39.163	0.0	-0.000	0.000	0.0	-0.000	-0.000	0.000
2.5	0.811	778.127	32.816	40.108	0.0	-0.000	-0.000	-0.000	0.000	-0.000	0.000
2.8	0.724	761.706	29.520	41.027	0.0	-0.000	0.000	-0.000	-0.000	-0.000	0.000
3.0	0.765	745.722	26.211	41.858	0.0	-0.000	-0.000	-0.000	-0.000	-0.000	0.000
3.2	0.757	727.244	22.650	42.703	0.0	-0.000	0.000	-0.000	-0.000	-0.000	0.000
3.4	0.746	727.440	18.821	43.420	0.0	-0.000	0.000	-0.000	-0.000	-0.000	0.000
3.6	0.736	715.465	14.871	44.024	0.0	-0.000	0.000	0.000	-0.000	0.000	0.000
3.8	0.729	713.343	10.660	44.501	0.0	-0.000	0.000	0.0	-0.000	-0.000	0.000
4.0	0.725	705.247	6.284	44.827	0.0	-0.000	0.000	0.000	-0.000	-0.000	0.000
4.2	0.722	707.279	1.726	44.586	0.0	-0.000	0.000	0.000	-0.000	0.000	0.000
4.4	0.723	707.534	-2.810	44.065	0.0	0.0	0.000	0.000	-0.000	0.000	0.000
4.6	0.720	710.107	-7.433	44.158	0.0	-0.000	0.000	0.000	-0.000	0.000	0.000
4.8	0.731	715.048	-11.959	44.367	0.0	-0.000	0.000	0.000	-0.000	0.000	0.000
5.0	0.740	722.416	-16.482	43.758	0.0	-0.000	0.000	0.000	-0.000	0.000	0.000
5.2	0.751	732.242	-20.328	43.066	0.0	-0.000	0.000	0.0	-0.000	0.000	0.000
5.4	0.765	744.535	-24.954	42.188	0.0	-0.000	0.000	0.000	-0.000	0.000	0.000
5.6	0.781	755.166	-28.924	41.155	0.0	-0.000	0.000	0.000	-0.000	0.000	0.000
5.8	0.801	776.241	-32.539	40.100	0.0	-0.000	0.000	0.000	-0.000	0.000	0.000
6.0	0.823	795.584	-35.102	38.937	0.0	-0.000	0.000	0.0	-0.000	-0.000	0.000
6.2	0.847	817.269	-35.326	37.723	0.0	-0.000	0.000	0.0	-0.000	-0.000	0.000
6.4	0.870	841.206	-42.344	36.469	0.0	-0.000	0.000	0.000	-0.000	0.000	0.000
6.6	0.892	867.071	-45.103	35.216	0.0	-0.000	0.000	0.000	-0.000	0.000	0.000
6.8	0.942	894.816	-47.641	32.571	0.0	-0.000	0.000	0.000	-0.000	0.000	0.000
7.0	0.977	924.430	-49.983	32.763	0.0	-0.000	0.000	0.000	-0.000	0.000	0.000
7.2	1.016	955.817	-52.126	31.541	0.0	-0.000	0.000	0.0	-0.000	0.000	0.000
7.4	1.056	988.764	-54.116	30.377	0.0	-0.000	0.000	0.0	-0.000	-0.000	0.000
7.6	1.103	1023.546	-55.555	29.242	0.0	-0.000	0.000	0.0	-0.000	-0.000	0.000
7.8	1.148	1059.563	-57.641	28.157	0.0	0.0	0.000	0.000	-0.000	-0.000	0.000
8.0	1.193	1096.904	-59.194	27.118	0.0	-0.000	0.000	-0.000	-0.000	-0.000	0.000
8.2	1.243	1135.571	-61.623	26.123	0.0	-0.000	0.000	-0.000	-0.000	-0.000	0.000
8.4	1.296	1175.674	-61.972	25.169	0.0	-0.000	0.000	-0.000	-0.000	-0.000	0.000

Table IX-3. Simulation Test Problem for Climbing, Decelerating Path

TIME OF FLIGHT	RANGE (M)	AZIMUTH (DEG)	ELEVATION (DEG)	RADIAL ACCEL. (G)	RANGE ERROR (M)	AZIMUTH ERROR (M)	ELEVATION ERROR (M)	HU (M)	HV (M)	RMS (M)
1.0	1.745	1492.539	-62.643	72.339	0.001	-0.004	0.0	0.003	0.003	0.004
2.0	1.747	1454.656	-66.723	73.030	0.001	-0.003	0.001	0.003	0.002	0.004
2.2	1.753	1455.615	-71.322	73.617	0.000	-0.003	0.001	0.002	0.002	0.003
2.4	1.757	1435.374	-76.322	74.091	0.001	-0.003	0.0	0.002	0.003	0.003
2.6	1.763	1435.671	-81.543	74.333	0.001	-0.004	0.0	0.002	0.003	0.004
2.8	1.772	1410.652	-87.570	74.634	0.001	-0.004	0.0	0.002	0.002	0.003
3.0	1.782	1317.769	-93.267	74.694	0.001	-0.004	0.0	0.003	0.002	0.004
3.2	1.754	1325.761	-98.922	74.611	0.001	-0.004	-0.001	0.003	0.002	0.004
3.4	1.803	1337.856	-103.461	74.347	0.001	-0.003	-0.001	0.002	0.002	0.003
3.6	1.823	1345.633	-105.753	74.035	0.001	-0.003	-0.001	0.003	0.002	0.004
3.8	1.843	1346.210	-114.717	73.563	0.001	-0.003	-0.001	0.003	0.002	0.004
4.0	1.859	1343.530	-119.380	72.584	0.001	-0.003	-0.001	0.004	0.001	0.004
4.2	1.881	1342.355	-122.604	72.314	0.001	-0.003	-0.001	0.004	0.001	0.004
4.4	1.901	1340.464	-127.583	71.565	0.001	-0.003	-0.001	0.004	0.001	0.004
4.6	1.925	1311.589	-131.139	70.763	0.001	-0.003	-0.002	0.003	0.001	0.004
4.8	1.952	1228.655	-134.354	65.397	0.001	-0.003	-0.005	0.006	-0.000	0.006
5.0	1.974	1245.326	-137.318	65.593	0.001	-0.002	-0.003	0.005	-0.001	0.005
5.2	2.008	1466.539	-139.621	68.771	0.001	-0.004	-0.003	0.005	-0.001	0.006
5.4	2.039	1434.632	-142.364	61.118	0.002	-0.003	-0.005	0.007	-0.001	0.007
5.6	2.073	1765.402	-144.552	66.166	0.002	-0.005	-0.005	0.007	-0.002	0.007
5.8	2.108	1727.118	-146.534	65.166	0.002	-0.005	-0.005	0.008	-0.002	0.008
6.0	2.154	1749.224	-148.326	64.190	0.002	-0.005	-0.008	0.009	-0.003	0.009
6.2	2.181	1775.014	-149.558	63.215	0.002	-0.003	-0.007	0.006	-0.003	0.006
6.4	2.222	1757.559	-151.466	62.235	0.002	-0.003	-0.007	0.005	-0.003	0.006
6.6	2.254	1822.957	-152.845	61.264	0.001	-0.003	-0.005	0.005	-0.003	0.006
6.8	2.308	1849.214	-154.112	61.333	0.001	-0.002	-0.005	0.005	-0.003	0.006
7.0	2.353	1876.270	-155.276	55.355	0.001	-0.001	-0.007	0.004	-0.004	0.006
7.2	2.400	1904.124	-156.350	53.422	0.001	-0.002	-0.005	0.004	-0.003	0.005
7.4	2.450	1932.526	-157.343	51.499	0.001	-0.001	-0.004	0.003	-0.004	0.005
7.6	2.503	1962.861	-158.273	56.587	0.001	-0.001	-0.005	0.003	-0.004	0.005
7.8	2.556	1992.956	-159.133	53.559	0.001	-0.001	-0.005	0.003	-0.004	0.005
8.0	2.612	2024.159	-159.934	54.823	0.001	-0.001	-0.004	0.003	-0.003	0.005
8.2	2.665	2059.664	-162.546	51.967	0.001	-0.002	-0.004	0.004	-0.004	0.005
8.4	2.722	2085.665	-161.355	53.119	0.001	-0.002	-0.006	0.004	-0.005	0.005
8.6	2.762	2122.333	-162.369	52.301	0.001	-0.001	-0.006	0.004	-0.005	0.005
8.8	2.858	2156.681	-162.670	51.492	0.001	-0.001	-0.006	0.003	-0.005	0.006
9.0	2.924	2174.453	-163.249	51.767	0.002	-0.001	-0.006	0.004	-0.008	0.009
9.2	2.991	2226.844	-163.793	45.941	0.002	0.0	-0.008	0.004	-0.008	0.009
9.4	3.062	2243.374	-164.300	45.191	0.002	-0.004	-0.008	0.004	-0.008	0.009
9.6	3.155	2259.503	-164.756	48.458	0.002	0.0	-0.007	0.003	-0.007	0.007
9.8	3.214	2317.623	-165.262	47.734	0.002	0.0	-0.007	0.004	-0.006	0.007
10.0	3.293	2375.617	-165.657	47.933	0.001	0.0	-0.005	0.003	-0.005	0.006

Best Available Cop

Table IX-4. Residual Errors on Circular Paths

Path	Tgt vel. (m/s)	Hor Range (m)	Alt (m)	Rad Acc (g)	Time of Flight (sec)	Errors (Meters)					
						Range	Azimuth	Elevation	MU	MV	RMS
C0	70	500	100	-1.0	0.507	0.004	0.059	0.007	-0.058	0.008	0.059
C1	98.995	2000	500	-0.5	2.680	0.001	0.005	0.011	-0.004	0.011	0.012
C2	98.995	2000	2000	-0.5	4.312	0.022	0.015	0.220	0.030	0.220	0.220
C3	98.995	2000	100	-0.5	2.572	0.000	0.004	0.000	-0.003	0.000	0.003
C4	98.995	2000	0	-0.5	2.259	0.000	0.004	-0.003	-0.003	-0.003	0.005

In the program notation, the revised instructions are

$$F = DT*(DT + TVSLA) + TSM$$

$$F1 = -0.5*DEL*F$$

$$XP = XP - DY*F1$$

$$YP = YP + DX*F1$$

$$F3 = 0.16667*DT*DT*DT + 0.250 *TVSLA * DT*DT \\ + 0.60* TSM*DT + 0.050*TVSLA*TSM$$

$$XP = XP - DEL*DEL*F3*DX$$

$$YP = YP - DEL*DEL*F3*DY \quad (9.2)$$

In algebraic notation

$$F3 = (1/6) (DT)^3 + (1/4) (TVSLA)(DT)^2 \\ + 0.60 (TSM) (DT) + 0.05 (TVSLA) (TSM) \quad (9.3)$$

9.3.5 Defense of Known Point Algorithm

No attempt was made to verify the correct operation of this algorithm (or the simple rate by time predictor) since both are of lower current interest than those modes which were selected for verification. In both cases, the method of testing would be to input flight paths conforming to the prediction algorithm assumptions and observe the errors records. The defense of known point algorithm would show transient errors for one time of flight after each change in path segment type, but if the program is correct, it should show essentially zero errors at all other points. In view of the FACT data, further work with the defense of known point algorithms should include consideration of possible modifications of the algorithms to better represent the actual attack patterns in elevation.

Table IX-5. Simulation Test Problem for Circular Path

TIME OF FIRE	TIME OF FLIGHT (s)	RANGE (m)	AZIMUTH (DEG)	ELEVATION (DEG)	RADIAL ACCEL. (G)	RANGE ERROR (m)	AZIMUTH ERROR (m)	ELEVATION ERROR (m)	ψ (m)	WV (m)	SWK (m)
1.9	4.312	2828.427	17.334	45.000	-0.500	0.021	0.018	0.213	0.127	0.214	0.215
2.1	4.312	2828.427	17.907	45.000	-0.500	0.022	0.017	0.218	0.029	0.218	0.220
2.2	4.312	2828.427	18.467	45.000	-0.500	0.022	0.019	0.217	0.027	0.218	0.220
2.3	4.312	2828.427	19.034	45.000	-0.500	0.022	0.018	0.224	0.029	0.224	0.224
2.5	4.312	2828.427	19.602	45.000	-0.500	0.022	0.018	0.224	0.030	0.227	0.229
2.8	4.312	2828.427	20.169	45.000	-0.500	0.022	0.018	0.221	0.029	0.221	0.223
3.1	4.312	2828.427	20.736	45.000	-0.500	0.021	0.017	0.218	0.029	0.219	0.221
3.2	4.312	2828.427	21.303	45.000	-0.500	0.022	0.019	0.217	0.028	0.218	0.220
3.4	4.312	2828.427	21.870	45.000	-0.500	0.021	0.017	0.217	0.029	0.217	0.219
3.6	4.312	2828.427	22.438	45.000	-0.500	0.021	0.016	0.218	0.031	0.218	0.221
3.9	4.312	2828.427	23.005	45.000	-0.500	0.021	0.014	0.217	0.032	0.217	0.220
4.1	4.312	2828.427	23.572	45.000	-0.500	0.021	0.015	0.224	0.032	0.223	0.225
4.2	4.312	2828.427	24.139	45.000	-0.500	0.021	0.016	0.216	0.029	0.216	0.218
4.4	4.312	2828.427	24.706	45.000	-0.500	0.022	0.016	0.224	0.032	0.223	0.225
4.6	4.312	2828.427	25.273	45.000	-0.500	0.021	0.015	0.221	0.031	0.220	0.223
4.8	4.312	2828.427	25.841	45.000	-0.500	0.021	0.015	0.221	0.032	0.220	0.222
5.1	4.312	2828.427	26.408	45.000	-0.500	0.022	0.018	0.217	0.028	0.217	0.219
5.2	4.312	2828.427	26.975	45.000	-0.500	0.022	0.017	0.222	0.030	0.222	0.224
5.4	4.312	2828.427	27.542	45.000	-0.500	0.022	0.017	0.224	0.030	0.224	0.224
5.6	4.312	2828.427	28.110	45.000	-0.500	0.022	0.016	0.222	0.030	0.222	0.224
5.8	4.312	2828.427	28.677	45.000	-0.500	0.021	0.014	0.221	0.034	0.226	0.229
6.1	4.312	2828.427	29.244	45.000	-0.500	0.022	0.016	0.226	0.032	0.226	0.229
6.2	4.312	2828.427	29.811	45.000	-0.500	0.022	0.015	0.225	0.033	0.225	0.227
6.4	4.312	2828.427	30.378	45.000	-0.500	0.021	0.018	0.217	0.028	0.217	0.219
6.6	4.312	2828.427	30.946	45.000	-0.500	0.021	0.016	0.218	0.030	0.219	0.221
6.8	4.312	2828.427	31.513	45.000	-0.500	0.021	0.018	0.215	0.028	0.216	0.218
7.0	4.312	2828.427	32.080	45.000	-0.500	0.021	0.017	0.215	0.029	0.215	0.217
7.2	4.312	2828.427	32.647	45.000	-0.500	0.022	0.018	0.219	0.029	0.219	0.221
7.4	4.312	2828.427	33.214	45.000	-0.500	0.021	0.016	0.219	0.031	0.219	0.221
7.6	4.312	2828.427	33.782	45.000	-0.500	0.021	0.014	0.224	0.033	0.223	0.224
7.9	4.312	2828.427	34.349	45.000	-0.500	0.021	0.013	0.227	0.035	0.224	0.229
8.0	4.312	2828.427	34.916	45.000	-0.500	0.021	0.013	0.224	0.034	0.222	0.224

9.4 COMPUTATION OF FILTER WEIGHTS AND LAG CORRECTIONS

The current simulation filter modules use finite memory weighting, and the test runs in this report were made with "least squares" weighting. However, any set of weights that satisfies certain constraints can be used. The constraints and the computation of the least squares values are summarized below.

Let

Δ = sampling interval

C_j = weighting function (coefficient) of the digital filter

j = index of the coefficient, $j = 0, 1, 2, \dots, n-1$

n = number of coefficients in the filter. ($n = 10$ for a 10 point filter)

M_r = the r 'th moment of the filter

$$M_r = \Delta^r \sum_j j^r C_j \quad (9.4)$$

The present configuration of the simulation embodies filters as follows

Position Filter: Computes a smoothed value of position. The filter is corrected for velocity lag, so that there is no lag at constant velocity.

Velocity Filter: Computes a smoothed value of velocity.

Acceleration Filter: Computes a smoothed value of acceleration.

Both the position and velocity filters develop lags against an input with a mean acceleration. These lags are corrected in the prediction algorithm.

Consider a noiseless input $E(t)$, sampled at intervals spaced Δ . The filter output is, in the most general case,

$$O(t) = M_0 E - M_1 (dE/dt) + M_2/2 (d^2 E/dt^2) - (M_3/3!) (d^3 E/dt^3) + \dots \quad (9.5)$$

where the M_r are the filter moments previously defined.

For a filter to output smoothed position without velocity lag, and a constant velocity input, all derivatives above the first of the input E are zero, and the moments must be

$$M_{0p} = 1.0$$

$$M_{1p} = 0$$

The constraints on the three levels of filter are summarized in Table IX-6 for filters uncorrected for lag to higher derivatives.

Table IX-6. Filter Constraints

Moment	Filter Type		
	Position	Velocity	Acceleration
$M_0 = \sum C_j$	1.0	0	0
$M_1 = \Delta \sum j C_j$	M_{1p}	-1.0	0
$M_2 = \Delta^2 \sum j^2 C_j$	M_{2p}	M_{2v}	2.0

To correct the position filter for velocity lag, its M_{1p} must also be zero. We can see from the above table that the way to do this is to multiply the velocity coefficients by M_{1p} and add them to the position coefficients.

Any set of coefficients that satisfies the above constraints will compute position, velocity and acceleration. Some coefficients are more effective than others, depending on the nature of the noise which contaminates E. A set of coefficients that is easy to compute is the "least squares" set. These are given in Table IX-7.

Table IX-7. Least Squares Filter Coefficient Algorithms

	Filter Type		
	Position	Velocity	Acceleration
Coefficients	$\frac{1}{n+1}$	$\frac{6}{\Delta} \frac{(n-2j)}{n(n+1)(n+2)}$	$\frac{60}{\Delta^2} \frac{[n(n-1)-6nj+6j^2]}{(n-1)(n)(n+1)(n+2)(n+3)}$
Moments			
M_0	1.0	0	0
$-M_1$	$-(n\Delta)/2$	+1.0	0
$M_2/2$	$\frac{n(2n+1)\Delta^2}{12}$	$-(n\Delta)/2$	1.0

The coefficients of the position filter corrected for velocity are

$$C_j = \frac{1}{n+1} + \left(\frac{n\Delta}{2} \right) \left(\frac{6(n-2)}{\Delta[n(n+1)(n+2)]} \right)$$

$$C_j = \frac{2(2n+1-3j)}{(n+1)(n+2)} \quad (9.7)$$

The "smoothing time" of a discrete filter is

$$T_s = n\Delta \quad (9.8)$$

This is the total interval over which data are averaged. Since the basic filter expressions for least squares filters are symmetric about their midpoints, the lag to the next higher derivative before correction is just half the smoothing time

$$(n\Delta)/2 = T_s/2 \quad (9.9)$$

The moments of the position filter corrected for velocity are then

$$M_{opc} = 1.0$$

$$-M_{1pc} = 0$$

$$M_{2pc}/2 = \frac{n(2n+1)\Delta^2}{12} - \left(\frac{n\Delta}{2} \right)^2 = -\frac{n(n-1)\Delta^2}{12}$$

When the simulation was being programmed, the programmer devised the notation

$$TVSLA = -M_{2v}$$

$$TSM = -M_{2pc} \quad (9.11)$$

For the least squares filters, therefore,

$$TVSLA = (n\Delta) = T_s$$

$$TSM = n(n-1)\Delta^2/6 \quad (9.12)$$

Table IX-8 shows the filter weights used in the present set of test runs. Note that the simulation program does an automatic check on the constraints.

Table IX-8. Example of Least Squares Filter Coefficients

Position Filter Corrected for Velocity Lag	
AP(1)	0.345455
AP(2)	0.290909
AP(3)	0.236364
AP(4)	0.181818
AP(5)	0.127273
AP(6)	0.072727
AP(7)	0.018182
AP(8)	-0.036364
AP(9)	-0.090909
AP(10)	-0.145455
Sum of Term	0.9999976
Velocity Filter	
AV(1)	0.272727
AV(2)	0.212121
AV(3)	0.151515
AV(4)	0.090909
AV(5)	0.030303
AV(6)	-0.030303
AV(7)	-0.090909
AV(8)	-0.151515
AV(9)	-0.212121
AV(10)	-0.272727
Sum of Term	-0.0000001
Sum of Term *1	-4.9999943
Acceleration Filter	
AA(1)	1.136364
AA(2)	0.378788
AA(3)	-0.189394
AA(4)	-0.568182
AA(5)	-0.757576
AA(6)	-0.757578
AA(7)	-0.568182
AA(8)	-0.189394
AA(9)	0.378788
AA(10)	1.136364
Sum of Term	0.0
Sum of Term *1	0.0
Sum of Term *1 **2	50.0000305
Lag Correction Inputs for Acceleration Lag	
TVSLA	1.80000
TEM	0.48000

9.5 EFFECT OF TRACKING BIASES

The simulation accepts azimuth and elevation tracking biases in mils and slant range bias in meters. It then computes miss distances at the point of closest approach of the shell to target in azimuth, elevation and range coordinates, and in a coordinate system rotated to alignment with the trajectory at the target. The closest approach computation changes the computed miss distances by only a few per cent in most cases, but involves a large number of program instructions.

The relations given below allow desk calculations to be done as an independent check on the simulation.

The relative shell-target position is defined in orthogonal coordinates X, Y, Z. The distance between shell and target, D is

$$D^2 = X^2 + Y^2 + Z^2 \quad (9.13)$$

This is a minimum when $dD/dt = 0$;

$$XV_x + YV_y + ZV_z = 0 \quad (9.14)$$

At a given t_0 initial, the relative coordinates are X_0, Y_0, Z_0

At a time t_c later

$$X = X_0 + V_x t_c \quad (9.15)$$

etc.

All velocities are of the projectile relative to the target, and if t_c = time to minimum approach

$$X_0 V_x + Y_0 V_y + Z_0 V_z + t_c (V_x^2 + V_y^2 + V_z^2) = 0 \quad (9.16)$$

from which we obtain t_c . Then the X, Y, Z at closest approach are

$$X_m = X_0 - (V_x/V) [X_0(V_x/V) + Y_0(V_y/V) + Z_0(V_z/V)]$$

$$Y_m = Y_0 - (V_y/V) [\text{same terms in brackets}]$$

$$Z_m = Z_0 - (V_z/V) [\text{same terms in brackets}]$$

$$\text{and } V^2 = V_x^2 + V_y^2 + V_z^2 \quad (9.17)$$

Also

$$t_c = - \left(\frac{X_o V_x + Y_o V_y + Z_o V_z}{V^2} \right) \quad (9.18)$$

$$V^2 = V_x^2 + V_y^2 + V_z^2 \quad (9.19)$$

$$X_m = X_o + V_x t_c$$

$$Y_m = Y_o + V_y t_c$$

$$Z_m = Z_o + V_z t_c \quad (9.20)$$

The slant range error at point of closest approach is

$$E_D = Z_m \sin e + Y_m \cos e \quad (9.21)$$

The elevation error in meters at point of closest approach is

$$E_e = Z_m \cos e - Y_m \sin e \quad (9.22)$$

Azimuth error in meters is

$$E_a = X_m \quad (9.23)$$

The separate computation is comparatively simple if the target flies a horizontal circular path centered on the gun. For this case, the basic computational relations are as given in Table IX-9.

The simulation determines time of flight and remaining projectile velocity at the original (biased) prediction point. It then extrapolates back to the point of closest approach assuming that velocities are constant over the interval of extrapolation. The simulation does the extrapolation based on the time of flight and projectile velocities at the uncorrected (biased) prediction point. For a separate computation these must be obtained by interpolation in the ballistic tables, and in the present case this separate interpolation probably accounts for some of the minor differences (less than 0.1 meter) between the simulation output and the separate calculation. It would be desirable to have the computer printout include these values.

**Table IX-9. Computation of Miss Distances Resulting
From Tracking Biases on Circular Path**

Azimuth Bias	Elevation Bias	Range Bias
$X_o = A_b(\text{meters})$	$X_o = 0$	$X_o = 0$
$Y_o = 0$	$Y_o = -e_b \sin e$	$Y_o = D_b \cos e$
$Z_o = 0$	$Z_o = e_b \cos e$	$Z_o = D_b \sin e$
$V_x = -V_t$	$V_x = -V_t$	$V_x = -V_t$
$V_y = V_r \cos e$	$V_y = V_r \cos e$	$V_y = V_r \cos e$
$V_z = V_r \sin e - gt_p$	$V_z = V_r \sin e - gt_p$	$V_z = V_r \sin e - gt_p$
$t_c = -A_b(V_t/V^2)$	$t_c = (e_b/V^2)(gt_p \cos e)$	$t_c = -(D_b/V^2) [V_r - gt_p \sin e]$
$E_a = A_b - V_t t_c$	$E_a = -V_t t_c$	$E_a = -V_t t_c$
$E_e = -t_c gt_p \cos e$	$E_e = e_b - t_c gt_p \cos e$	$E_e = -t_c gt_p \cos e$
$E_D = t_c(V_r - gt_p \sin e)$	$E_d = t_c(V_r - gt_p \sin e)$	$E_D = D_b + t_c(V_r - gt_p \sin e)$

NOTE: Azimuth and elevation biases are input as mils. The biases in meters are

$$A_b(\text{meters}) = A_b(\text{mils}) (2\pi/6400) D \cos e$$

$$e_b(\text{meters}) = e_b(\text{mils}) (2\pi/6400) D$$

Table IX-10 shows the computer generated miss distances for three types of tracking bias, and Table IX-11 compares these against the results of desk computation.

Note the inversion of the sign of the MU miss. Since the target dimensions are symmetrical along the MU axis the difference in sign would have no effect on the probability computations. In the desk calculations, the conversion to the U, V coordinates was done according to their original definition in a prior AFAADS report, but in the process of programming various changes were made, which apparently changed the sign of MU.

**Table IX-10. Simulation Generated Miss Distances
For Various Tracking Biases on Path C3**

Range (Meters)	Biases Azimuth (Mils)	Elevation (Mils)	Time of Flight	Miss Distances at Closest Approach (Meters)					
				Range	Azimuth	Elevation	MU	MV	RMS
100	0	0	2.577	3.413	17.698	4.816	-17.992	4.988	18.671
-100	0	0	2.564	-3.024	-16.490	-3.911	16.719	-4.052	17.203
0	+10	0	2.578	3.277	19.055	-0.147	-19.351	0.017	19.351
0	-10	0	2.566	-3.440	-19.016	0.155	19.309	-0.017	19.309
0	0	+10	2.573	0.762	-0.132	19.620	0.184	19.628	19.639
0	0	-10	2.570	-0.948	0.171	-19.611	-0.157	-19.630	19.630

Applies to all parameters:

Target Velocity 98.99493 m/s

Horizontal Range 2000.00 m

Slant Range 2002.576 m

Altitude 100.00 m

Radial Acc -0.50 g

Elevation Angle 2.862°

**Table IX-11. Comparison of Simulation Results
with Desk Calculator Computations on Path C3**

Bias Case		Miss Distances at Closest Approach (Meters)					
		Range	Azimuth	Elevation	MU	MV	RMS
+100 Meters Range Bias	Simulation	3.413	17.698	4.816	-17.992	4.998	18.671
	Manual	3.58	17.70	4.83	18.01	5.00	18.66
+10 Mils Azimuth Bias	Simulation	3.277	19.055	-0.147	-19.351	0.017	19.351
	Manual	3.35	19.04	-0.15	19.312	0.000	19.31
+10 Mils Elevation Bias	Simulation	0.762	-0.132	19.620	0.184	19.638	19.639
	Manual	0.86	-0.15	19.62	-0.177	19.64	19.64

The comparison of values indicates that the coordinate rotations give the correct absolute magnitudes and hence will lead to correct probability computations. However it would be a wise precaution to review the trigonometry of the program once again, term by term.

9.6 SINGLE SHOT KILL PROBABILITY

The circular path centered on the gun simplifies the computation of test problems, and the following relations apply to this case, except where the computation is completely general as noted.

In general, conditional kill probability, given a hit is computed in the simulation as

$$\begin{aligned} \text{Fuselage } P_{cf} &= 1 - e^{-FK(W_{he} + D W_{he}^{1/2})} \\ \text{Wing } P_{cw} &= 1 - e^{-WK(W_{he})} \\ W_{he} &= (WP)(XF) \\ WP &= \text{projectile weight} \\ XF &= \text{fraction of projectile weight devoted to HE} \end{aligned} \quad (9.24)$$

Note that by inputting XF as a very large number (999). P_{cf} and $P_{cw} \approx 1.0$, and the simulation outputs hit probability instead of kill probability. This condition is useful if one wants to separate hit probabilities of a system from the possible uncertainties in terminal effects.

In the simulation, each target dimension is multiplied by the appropriate $(p_c)^{1/2}$, reducing projected areas to "vulnerable areas".

For the special case of a circular flight path, we use the subscripts (x) and (z) to represent horizontal and vertical coordinates.

For this special case, the single shot kill probability is computed approximately as

$$P_{ss} = \frac{a_x a_z}{[(a_x^2 + 2\sigma_x^2)(a_y^2 + 2\sigma_y^2)]} \exp - \left[\frac{B_x^2}{a_x^2 + 2\sigma_x^2} + \frac{B_z^2}{a_z^2 + 2\sigma_z^2} \right] \quad (9.25)$$

where B_x , B_z are biases in the respective coordinates.

The simulation actually rotates the projected target dimensions, the dispersions and the biases into the U, V plane for this computation. This has the principal effect on the dispersion pattern of reducing σ_x to

$$\sigma_x^2 = \sigma_{xo}^2 \left[1 - (V_t/V_p)^2 \right] \quad (9.26)$$

where σ_{x0} is the input x variance in meters plus the variance resulting from muzzle velocity dispersion.

For an ellipsoidal target, the dimension in the direction of flight is foreshortened to

$$a_x^2 = a_x^2 \left[1 - (v_t/v_p)^2 \right] + a_y^2 (v_t/v_p)^2 \quad (9.27)$$

In the present special case the muzzle velocity bias and dispersion are in the x direction, the total dispersion variances are large compared with the a^2 terms, hence the exponents in the P_{ss} expression are modified by the same multipliers in numerator and denominator. The multipliers are consequently ignored, in the exponent calculation and B_z is taken as zero.

The correction for wing/fuselage overlap/shielding in the simulation is based on an area computed, for the present orthogonal case as

$$a_{fw}^2 = \frac{a_w^2 a_f^2}{a_w^2 + a_f^2} \quad (9.28)$$

Also for the present geometry, the simulation computed the miss distance resulting from muzzle velocity bias as

$$B_{MV} \text{ (meters)} = - \left(\frac{V_{MB} \text{ (m/s)} V_t}{V_p \text{ (m/s)}} \right) D \text{ (meters)} \quad (9.29)$$

and the standard deviation of dispersion resulting from muzzle velocity dispersion is identically computed. Since the computation is done in the terminal effects module, the miss distances do not appear in the miss tables previously shown in Section 9.3.

These muzzle velocity vectors are assumed to be along the flight line, and are rotated into the U, V, plane determined from the closest approach module in the simulation.

For the test problems all paths were based on a 25-mm weapon with a muzzle velocity of 1097.23 m/s and projectile characteristics leading to vulnerability factors as shown in Table IX-12. Table IX-13 shows the simulation results.

Table IX-14 shows the result of desk calculator computations of some of the cases of Table IX-13. Agreement is satisfactory. The principal cases of initial concern were paths C11 and C12, since the simulation requires a great deal of trigonometry to account for the ellipsoidal target shapes. Note that to compute the wing hit probability values in the separate

Table EX-12. Projectile Inputs

Problems	C1 to C8	C8 to C12
WP	0.51187	0.51187
XF	0.10	999. (used to obtain hit rather than kill probability)
WHE	0.051187	51.1
FK	1.0	1.0
WK	1.0	1.0
D	1.0	1.0
P _{cf}	0.24227	1.0000
P _{cw}	0.04989	1.0000
C	1.1256094	1.1256094

computation requires inclusion of the bank angle of the target as well as the relative direction of approach of the projectile.

It is considered that these results give reasonable assurance that the simulation functions properly in all computations up to and including computation of single shot probability of hit and kill. However, it is suggested that additional test problems should be developed with much wider variations in target dimensional deviations from circular, also including muzzle velocity bias for additional confirmation of the trigonometric routines.

9.7 VERIFICATION OF NOISE MODULES

No verification runs were made to determine whether the noise statistics are correctly developed. Verification can be done by the following procedures which are straightforward.

Range noise is developed in the simulation with a constant variance and constant exponential correlation time, both independent of the tactical geometry. Hence statistical tests can be run by generating range error samples of extended duration, and computing their variances and autocorrelation functions. At the same time it can be determined that the distributions are in fact gaussian with zero mean and the desired variances. Methodology is conventional.

The radar glint model can be verified by taking noise samples on circular paths concentric to the gun position. The angular velocity in azimuth is constant and the angular velocity in elevation is zero. One can therefore determine the expected variance and autocorrelation of the noise sample from the computer generated error sequences, since for this

Table DX-13. Single Shot Kill Probabilities Obtained From Simulation

Path	Target Altitude (Meters)	Dispersions σ_x (Mils) (σ_z (Mils) σ_y (M/S)	Muzzle Velocity Bias V_{OB} (M/S)	XF	Target Dimensions						Fuselage	Single Shot Probabilities			Aircraft
					Fuselage			Wing				Wing	Intersection		
					W	L	H	S	C	T					
C1	300	1.0 1.0 1.0	0.0	0.1	1.0	1.0	1.0	1.0	1.0	1.0	.0292	.00616	.00512	.0303	
C2	2000	1.0 1.0 1.0	0.0	0.1	1.0	1.0	1.0	1.0	1.0	1.0	.0160	.00334	.00277	.0166	
C3	100	1.0 1.0 0.0	0.0	0.1	1.0	1.0	1.0	1.0	1.0	1.0	.0309	.00652	.00541	.0320	
C4	0	1.0 1.0 0.0	0.0	0.1	1.0 1.0	1.0	1.0	1.0	1.0	1.0	.0310	.00654	.00543	.0321	
C5	2000	1.0 1.0 0.0	100	0.1	1.0	1.0	1.0	1.0	1.0	1.0	0	0	0	0	
C6	2000	1.0 1.0 0.0	-100	0.1	1.0	1.0	1.0	1.0	1.0	1.0	0	0	0	0	
C7	2000	2.0 2.0 0.0	0.0	0.1	2.0	2.0	2.0	2.0	2.0	2.0	.0160	.00334	.00277	.0166	
C8	2000	1.0 1.0 100	0.0	0.1	1.0	1.0	1.0	1.0	1.0	1.0	.00664	.000138	.000114	.00657	
C9	2000	2.0 2.0 0	-20	999	2.0	2.0	2.0	2.0	2.0	2.0	.00405	.00405	.00191	.00619	
C10	2000	2.0 2.0 0	20	999	2.0	2.0	2.0	2.0	2.0	2.0	.00387	.00397	.00187	.00608	
C11	2000	1.0 1.0 1.0	0	999	1.0	10.0	1.0	5.0	3.0	0.1	.239	.171	.110	.289	
C12	2000	0.5 2.0 0	0	999	1.0	2.0	1.0	2.0	1.0	0.05	.0907	.0273	.0223	.0937	

All paths circles centered on the gun

Horizontal Range = 2000 meters
 Target Velocity = 98.99493 M/S
 Radial Acceleration = -1/2 g

Table IX-14. Single Shot Kill Probabilities Obtained By Desk Calculator

Path	Fuselage	Single Shot Probabilities		Aircraft
		Wing	Intersection	
C1	.0292	.00616	.00510	.0303
C2	.0160	.00333	.00276	.0166
C8	.00071	.00015	.00012	.00074
C9	.00404	.00404	.00202	.00606
C10	.00404	.00404	.00202	.00606
C11	.2290	.1714	NW*	NW*
C12	.0905	NW	NW*	NW*
*Not Worked				

target path type both statistics will be constant, and compare them against the values expected by computing the simulation algorithms separately for variance and autocorrelation time constant.

9.8 VERIFICATION OF SERVO LAG AND REGENERATION MODULES

No verification runs were made for these modules in the present effort. They can be verified by setting in sets of values of K_v , K_a and obtaining miss distance printouts with zero tracking error. The lags are most easily computed separately for the special case of a circular target path centered on the gun. For this path, only velocity lag (K_v) should affect the output, since there is no angular acceleration and no lag should be associated with any value of K_a on this concentric circular path. Both K_v and K_a should next be verified on a straight and level constant velocity fly-by. Separate computation of the angular velocities and accelerations will be necessary for the reference lag computations, although the values are developed by the simulation and can be obtained by a separate prior printout.

To compare the separate computations accurately against the computer developed errors, the closest approach routine should be applied, but the first significant figure of the computed miss distances should match without this correction.

The regeneration correction is most accurate on a constant velocity straight fly-by path. A gross check consists of setting in low values of K_v , K_a (100, 50), observing the lags on a close-in path with high derivatives, then observing that they are substantially eliminated by the regeneration. If they are not, further checking of the program is required.

The same methodology can be applied to check the modules for tracker and gun lag and regenerative corrections.

9.9 SIMULATION MODULE FOR MANUAL TRACKING

Mr. Stanley Goodman identified an error in this module as currently programmed. The correct form is developed in the following paragraphs.

The present simulation module is intended as an interim representation of the performance of a manual tracker, until the availability of actual tracking error records allow a more accurate representation. However it contains enough disposable parameters to provide a reasonable representation.

Basic inputs are an "effective" K_v and K_a lag coefficient pair for the man, and a noise variance proportional to the target linear dimension as projected normal to the line of sight. The K_j coefficient for the man are smaller than for a good servo (the man is a 1 Hz bandwidth servo at best), and so the man will develop velocity and acceleration lag when these derivatives become of moderate to large magnitudes.

There is some indication from laboratory tests on different target path patterns that when the man is "off target" he is more concerned with getting back on than with maintaining smooth tracking, and so, in addition to lag or lead, the variance of his tracking error about its mean value increases.

In addition, the man's error has a longer autocorrelation time constant than would be typical of a good tight servo.

In the first model of the Ginsberg simulation, noise sequences were generated as

$$X_{j+1} = \alpha X_j + \beta N C; \beta = (1 - \alpha^2)^{1/2} \quad (9.30)$$

where N was a sample from an uncorrelated noise sequence of zero mean and unit standard deviation. C was set as a constant standard deviation in meters; the recursive relation generated a correlated sequence with autocorrelation

$$e^{-\alpha \Delta}; \Delta = \text{sample interval} \quad (9.31)$$

and standard deviation equal to C.

To account for the noise amplification effect of the man's perception of his lag or lead, it was intended that the term NC be replaced by

$$N(C + |L|\mu) = NC [1 + (\mu|L|)/C] \quad (9.32)$$

where μ was suggested to be about 0.25, and $|L|$ was the absolute value of lag or lead in the relevant coordinate in meters. This would have increased the noise standard deviation by one fourth of the lag or lead value.

The present form of the simulation replaces the C term by the maximum projected target dimension, lateral and vertical, in meters. A module to perform this computation is added. The target size measures are called SIGA and SIGE in the program.

The noise sequence in each coordinate is computed as

$$\begin{aligned} AZX &= AZA \cdot AZX + AZB \cdot \text{RAN}(1) \\ ELX &= ELA \cdot ELX + ELB \cdot \text{RAN}(2) \end{aligned} \quad (9.33)$$

The AZA, AZB correspond to the α, β of the original program, but for the radar glint module they depend on target angular velocity and servo coefficients, hence vary with target position. The same is true in elevation.

These linear errors (meters) are converted to mil errors, AERR, EERR, but the mil errors are apparently not used in later computation. The terms RAN(1) and RAN(2) are the N sequences of uncorrelated random noise with zero mean and unit variance.

The azimuth and elevation lag errors are computed in radians and modified by the regeneration correction when the regen flag is activated. The sum (ALAG - REGENA) and (ELAG - REGENE) is in radians, and would be zero if regeneration corrected perfectly for lag.

Multipliers SIGA2 and SIGE2, each of which is

$$1 + \text{amplification factor}$$

are applied to AZX and ELX.

The amplification factor should be dimensionless.

If correctly computed, this process should yield the intended result, consistent with the fact that this module is an approximation to the man's behavior. It might seem more reasonable to apply the multipliers at the random noise input, and process the amplifying noise through the correlating sequence, but the difference, which should be small, falls within the uncertainty of the human operator representation. It should be adequate until the human operator module is replaced by one that goes down one level of detail deeper into the representation of the human operator.

The correction amplification terms should then be

$$\begin{aligned} \text{SIGA2} &= 1.00 + (\text{ABS}(\text{ALAG}-\text{REGENA})) * \text{XMU} * \text{RO} * \text{COSEO} / \text{SIGA} \\ \text{SIGE2} &= 1.00 + (\text{ABS}(\text{ELAG}-\text{REGENE})) * \text{XMU} * \text{RO} / \text{SIGE} \end{aligned} \quad (9.34)$$

The correction to the program is in the use of the ABS value and the division by SIGA, SIGE respectively with the above changes.

The remaining expressions for the computation of tracking angle plus noise plus bias are then correct as now programmed.

$$\begin{aligned} \text{AO} &= \text{AO} + (\text{AZX} * \text{SIGA2}) / (\text{RO} * \text{COSEO}) + \text{ABIAS} \\ \text{EO} &= \text{EO} + (\text{ELX} * \text{SIGE2}) / (\text{R}) + \text{EBIAS} \end{aligned} \quad (9.35)$$

9.10 METHOD OF BY-PASSING GLINT COMPUTATION

This "quickfix" for bypassing the glint model details is not used in checkout, but is noted for reference. The glint model uses algorithms which make glint noise depend on target angular velocity. Range noise is not simulated by a glint model, but receives noise variance and characteristic time of an exponential correlation as inputs. The following remarks apply to the angular simulation.

To make the simulation operation independent of target angular velocity, as far as glint noise is concerned, set ω_w to a very large value, such as 10 rad/sec, whence

$$\Omega \cong \omega_w \quad (9.36)$$

Define σ = desired linear standard deviation of tracking error (meters)
 T = desired characteristic time of exponential autocorrelation (sec)
 K_a = servo acceleration lag coefficient (rad/sec²)
 ω_w = 10 rad/sec

$$\text{Compute } B = 2 \pi (K_a / 2.5)^{1/2} \quad (9.37)$$

Compute

$$C = \left\{ 0.7 \frac{[1 + (50/BT)]}{[1 + (100/BT)]^2} + 0.3 \frac{[1 + (0.5/BT)]}{[1 + (1/BT)]^2} \right\}^{1/2} \quad (9.38)$$

Compute $L = 2 \sigma / C$, and input to simulation (computation done identically for azimuth and elevation)

Compute $\lambda = 10 \omega_w L T$ and input λ to simulation

The desired noise sequence will then be generated.

Example

Desired Values: σ = 0.2 meters
 T = 0.5 sec
 K_a = 90 rad/sec²

Compute: B = 37
 BT = 18.5
 C = 0.36

Input: L = 1.11 meters
 λ = 55.6 cm
 K_a = 90 rad/sec²

9.11 CONCLUSIONS AND RECOMMENDATIONS

The procedures described in the foregoing paragraphs provide a systematic means for checking the major function of the simulation. In the process of producing examples, several programming errors have been corrected, and their correction has been verified. It is recommended that the verification process be continued and extended by the user.

SECTION 10

ADDITIONAL DATA REQUIREMENTS AND EXPERIMENTAL PROGRAMS

"The temptation to form premature theories upon insufficient data is the bane of our profession...I should like a few more facts..."

S. Holmes in "A Scandal in Bohemia"

This section summarizes data requirements that have become apparent in the course of the present effort as necessary for continued research and development in predicted fire systems.

10.1 FACT TRAJECTORIES

The excellent data acquisition effort initiated by Stanley Goodman and Kenneth Heullitt of Frankford Arsenal on actual flight paths of attack aircraft delivering munitions should be expanded in scope of data and type of attacking vehicle. It is hoped that the analysis of this data presented in Section 4 of this report will demonstrate the direct applicability and usefulness of this factual information. The scope of additional effort should include:

10.1.1 Accelerometer Records on Aircraft Munition Delivery Paths

The radar data answered the most important question, namely "Is there a predictable path segment?" It is now apparent that such segments exist and that their deviations from perfect predictability are small enough to be concealed in almost all cases by the radar noise in the first data set. Hence data taken with accelerometers in the aircraft are now appropriate to reveal the fine structure of the path deviations which can be used as a basis for predictor design.

10.1.2 FACT Path Data on Attack Helicopters

Attack helicopters are primary targets for the local air defense. Although flight path data on these vehicles has been taken under realistic conditions (Fort Ord) it does not seem to have been made available to the predicted fire community. Existing path data should be acquired and put into FACT format, and additional data acquired as necessary.

10.1.3 FACT Trajectory Data in Standoff Missiles and their Launch Aircraft

Aviation Week articles indicate that predicted fire gun systems accounted for a number of standoff missiles fired in the Yom Kippur war. The preliminary analyses of Section 6 indicate that guns of acceptably moderate caliber have interesting terminal effectiveness against even smaller missiles. To raise the estimation of fire control effectiveness above the level of conjecture, records of trajectories of typical standoff missiles, with the guidance modes most likely to be encountered in combat, should be obtained. In addition, the launch vehicle paths should be recorded in those cases where launch is within detection range (not necessarily firing range) of the defense. Launch vehicle paths should also be recorded for systems requiring that the launch vehicle remain on a clear line of sight to the ground target during missile flight.

10.2 PROJECTILE SIGNATURES FOR CLOSED LOOP SYSTEMS

10.2.1 Signature Measurement

The radar cross section measurements by BRL of projectiles with and without signature augmentation should be extended to other radar frequencies and to other sensors. The measurement program should be complementary to a projectile design program directed to signature improvement. It should also determine those base closures to be avoided as causing signature reduction.

In addition to radar, the program should include determination of laser cross section at several wavelengths, with and without special treatment (coating) of the projectile to improve reflectivity. A signature data base for detectability by optical radar will be required in the near future. The detectability of tracer by FLIR as a function of tracer composition should be determined.

10.2.2 Projectile Experimental Design Program

For closed loop systems, design of the projectile base to provide an adequate signature is basic. Section 3.3 suggests some low cost approaches. A program is recommended to develop projectiles with improved signatures as seen from the rear, emphasizing low cost.

10.3 OPERATIONAL DEGRADATION OF SYSTEM PERFORMANCE

The real value of closed loop predicted fire systems is believed to lie in their ability to reduce operational degradation of systems caused by loss of calibration of various sources which is certain to appear in combat. Appendix A suggests that even under proving ground

conditions, simple radar angular boresighting and range calibration may assume error values of magnitudes which would seriously degrade accurate predicted fire systems. A program of collection and analysis of proving ground and user records on simple radar calibration is recommended, to be augmented by data taking on modern predicted fire systems as they pass through the Army test procedures.

In addition to evaluations of systems properly calibrated according to doctrine, the analysis and common data base should include:

- a. Records and analysis of the loss of calibration of each system during test, and problems and likely errors in achieving calibration. These should be related to the system design to identify design approaches which tend to minimize calibration problems. This data is essential to objective assessment of the value of closed loop systems.
- b. Records and analysis of system reliability and maintainability characteristics. This data is essential in estimating the personnel support requirements of systems of different designs.
- c. The data base on operational degradation should be augmented by search for and integration into the data bank of calibration data on past tests of sensors and systems. The extensive Navy experience and record file on predicted fire systems should be exploited.

10.4 TRACKING SENSOR ACCURACIES AND POWER SPECTRAL DENSITIES VS. TARGETS OF AIR DEFENSE SYSTEMS

Test programs on new sensors of all types should be planned so that the results fit into a common data base which allows comparative evaluations in a systems context. It is believed, for example that FLIR tracking accuracies will vary with target size, range, and possibly angular derivatives in a qualitatively different way than radar. The analysis associated with test programs should be designed to establish these functional dependences on the engagement geometry, rather than being limited to average values at average ranges. The general availability of Fast Fourier Transform computer program should also allow the development of power spectral densities of tracking errors in essentially real time during the test programs. The data base should include millimeter radar, FLIR, Laser range finders and optical radar, as well as modern centimeter radar as a reference.

The spectrum of targets should include helicopters and standoff missiles of a wide range of sizes and types in addition to aircraft.

10.5 FIELD TEST PROGRAMS OF THE PERFORMANCE OF PREDICTED FIRE SYSTEMS AND COMPONENTS

Field test programs such as HITVAL, and the test programs which will be associated with GLAADS and other predicted fire gun systems provide an important means of extending the data base of "authoritative" target paths. More importantly, if the programs are properly planned in advance, and the data are analyzed appropriately, it is possible to identify the sources of the principal error components of the projectile miss vectors, and to determine whether they are inherent in the nature of the predicted fire problem, or whether they can be eliminated by system improvements.

As noted in prior AFAADS reports, it is an unfortunate characteristic of field test programs that unless the data analysis program is carefully established in detail before the field exercise begins, time constraints at the end tend to limit analysis to the minimum that will satisfy immediate requirements for decisions.

Data analysis requires a protagonist. The burden of maintaining a coherent, integrated data base that will assist the R&D community in placing its limited exploratory and advanced development effort in high payoff areas must be assumed by that community. Any data set is a potential gold mine for discovery of exploitable information for advancement of the state of the art. Unfortunately, data prospecting does not have the obviously creative attractiveness of system conception or simulation design. Establishment and maintenance of an effective data analysis effort to support systems R&D is an in-house Army management problem that has not yet been solved.

It is recommended that in addition to evaluating overall system effectiveness, field test programs be designed to support an analysis structure to:

- a. Identify and extract error components resulting from the fact that the actual target path does not conform to the prediction algorithms of the system under test.
- b. Identify and extract error components resulting from sensor noise amplitude and power spectral density.
- c. Identify residual error components and associate with sources as far as possible (ammunition dispersion, muzzle velocity bias, wind, etc.).
- d. Summarize and characterize each error class in terms of its functional dependence on tactical parameters such as range and angular velocities, and its statistical descriptors as bias-like, correlated (defined via autocorrelation function) or random round to round.

- e. Establish and maintain a uniform data base and continued program of analysis to compare systems tested both on an overall effectiveness basis, and in terms of the relative performance of components executing similar functions, such as "tracking accuracies", "prediction", and the dispersion values contributed by the mount, weapon and ammunition at various firing rates, exclusive of the errors in the prediction process.

It is recommended that this continued effort, exploiting the data obtained in equipment tests be maintained within the Armament Command.

SECTION 11

PROGRAM RECOMMENDATIONS

11.1 GENERAL

The Army now has under development the GLAADS gun low altitude air defense system. This fire unit, which is being fabricated under severe funding limitations should demonstrate the capability of modern predicted fire control technology.

In the 1970 Report on the present contract, it was noted that

"...one of the unfortunate facts of development is that brassboard experimental models tend to become standardized, contrary to plan, whenever they demonstrate significant improvements over existing equipment, or because the demonstrated improvement reduces the pressure on further expenditures for development. Brassboard items are essential to orderly development, but they should be conceived with the foresight that if they are pulled out of a program and standardized, the planned future growth is consistent with their interim implementation."

Without attempting to prejudge the question of whether or not GLAADS as now configured is an optimum solution to the Army's low altitude air defense problem, it is suggested that the early selection of improved air defense equipment for production may be of some urgency. Fortunately, the technological data base has been greatly improved in the past several years, through the GLAADS program, by the more basic program for Automatic Cannon Technology, and by other related programs of exploratory development and system improvement.

It is now essential that the overall Army program for predicted fire air defense systems be planned and scheduled in such a way that

- a. The value of predicted fire systems as components of the overall air defense system can be objectively assessed in the complete air defense context so that requirements for operational systems can be established.
- b. Prototype, brassboard, and component developments, testing and field experiments and "shootouts" are scheduled as part of the master plan of early definition of the system to be developed for operational implementation.

- c. On-going programs can be modified if necessary to provide an early solution to the complete operational requirement.
- d. Chosen solutions can be designed to have growth capability in terms of the continued progress and expected results of the exploratory and advanced development effort.

In brief, the Army's overall air defense program should be designed to provide an early operational system of high capability, with supporting effort to provide continued growth in effectiveness in an economical manner.

11.2 CLOSED LOOP PREDICTED FIRE SYSTEMS

It is recommended that the Army continue the advanced and exploratory development of closed loop systems, carrying several of the most promising solutions to the point of operational demonstration. In parallel with this effort, plans should be made for the expeditious incorporation of a closed loop capability in an operational system, dependent on the success of field demonstrations.

It is suggested that at least the following sensor options should be considered

- a. Radar (3-D)
- b. FLIR (2-D)
- c. FLIR with Cooperative Laser Illuminator (3-D)
- d. Optical Radar

A preliminary assessment of the radar potential can be made using the Phalanx system observed performance as a point of departure, supported by the MIDI performance data. The FLIR (2-D) option may possibly be tested with the GLADS prototype. The FLIR with cooperative laser mode requires analysis by the laser/FLIR development community. Optical radar is apparently well in hand with a current contract.

It is not considered that data processing algorithms represent a problem, provided that the fire control solution utilizes a digital computer. As noted in the body of this report, it is recommended that the algorithms utilize the proposed VISTA method of separating miss vector components resulting from target maneuvers from those resulting from other bias sources, so that each source can be processed optimally according to its inherent characteristics. It is recommended that the FACT data base be employed to determine whether open loop or closed loop operation is a preferred means of correcting for the miss component caused by target maneuver.

Validation of the closed loop processing algorithms by computer simulation is recommended. However this should be a continuing effort, since there are still many unknowns with regard to sensor performance and accuracy of the miss measurements and as these are resolved, the processing algorithms will be affected. Proposed system concepts should plan for the modification of the processing algorithms as indicated by experimental results.

The need for a separate supporting effort in the economical improvement of projectile design to improve projectile signatures to the candidate sensors has been noted in the preceding section. A valid data base of sensor/projectile signatures should be developed.

The most important supporting activity of the closed loop program is that of determining the magnitudes and frequency of occurrence under combat conditions of error sources which are susceptible to elimination by a closed loop system. The requirement for this data base was noted in the previous section. Imposition of severe environmental conditions, comparable to combat operation, should be a part of any field test of predicted fire systems to objectively identify and quantify these error sources.

11.3 GUN-BOOSTED PREDICTED FIRE ROCKET SYSTEMS

The preliminary analysis in the present report of predicted fire systems using rockets or rocket-assisted, gun fired projectiles (RAP) suggests that the principal problems to be overcome by this type of system, in order to be competitive with conventional guns, are (1) angular and velocity dispersion, and (2) the cost disadvantage of RAP projectiles compared with the simpler conventional projectiles. No basis to encourage development of a new RAP system at this time has been generated. However a detailed assessment of the technological possibilities of reducing RAP dispersions has not been made in the present study, nor have definitive production cost estimates been obtained.

Since the Javelot program apparently has the objective of achieving very low dispersion RAP rounds, and Javelot will be tested in the near future, this program should provide the objective data needed for objective assessment of the current RAP dispersion state of the art. In parallel with Javelot, however, it is suggested that a limited in house effort by the Army to establish minimum achievable dispersions of RAP rounds, and minimum production costs for designs other than the particular Javelot projectile would be useful in determining the degree to which Javelot answers all questions.

11.4 PROJECTILE PREDICTED-CORRECTED SYSTEMS

It is recommended that the Army continue and expand its effort on the concept and systems analysis of predicted-corrected projectile air defense systems. The preliminary analysis of possible characteristics of such a system in the present report are considered to be sufficiently attractive to justify a more detailed investigation.

As noted in the present report, the basic concept is to fire a controlled projectile along a minimum energy path directed at the predicted position of an air target. This concept is similar to that of the original Nike system. A new element however, is the possibility of eliminating the boresight errors which are habitually a problem with dual sensor systems by using projectile sensing by the target tracking sensor for final terminal correction of a projectile in flight, and elimination of boresight errors to the benefit of subsequent projectiles.

A further system advantage resulting from advancing state of the art is considered to be the possibility of fabricating an on-board projectile control package which is sufficiently small and low cost so that the cost per round is low, and for a gun fired solution, the gun caliber required is consistent with mobility requirements of the field unit. Although a solution using rocket propulsion only is a competitive approach to be investigated, a gun-fire unboosted projectile solution offers the advantages of both controlled and conventional projectile firing (both with "closed loop" elimination of systematic system error sources).

It is suggested that the program content for the next phase of investigation of this program would be as follows:

- a. Define competitive configurations, including rocket, RAP, and unboosted gun fired projectiles.
- b. Define sensor options.
- c. Define projectile configurations, including aerodynamic, stability and control parameters.
- d. Determine minimum weight and cost of on-board projectile control packages.
- e. Define fire unit characteristics of competitive options.
- f. Determine computational algorithms, data processing and computer requirements for fire control, including both prediction function and optimal control command processing for minimal control energy expenditure by projectile.

- g. Perform cost-effectiveness trade-offs of competitive configurations and compare against conventional predicted fire systems at short range, and Crotale, Roland and Rapier family at long ranges.
- h. Determine value of alternate capability to fire conventional rounds as well as controlled projectiles, and outline operational doctrine.
- i. Evaluate ground fire effectiveness.
- j. Identify high-risk technological areas, and high payoff areas for research and development.
- k. Recommend exploratory development program leading to concept demonstration.

The program content in most respects follows the topics considered in the present study, but is directed to resolution of the principal unknowns in the present investigation, in particular, the attainable minimum weights of the projectile control package, the gun in the case of an unboosted solution, the sensor package on the fire mount, and the control algorithms.

11.5 DEFENSE AGAINST STANDOFF WEAPONS

It is recommended that an analytical and experimental effort to expand the capability of predicted fire air defense systems against stand-off munitions be continued and expanded. Since Aviation Week reports that the Israeli SAAR boats armed with Bofors 40-mm guns were able to shoot down STYX missiles, and since stand-off missiles are in increasing operational use, this generic target type should be a part of all air defense system evaluations.

The following task content is suggested

- a. Evaluation of predicted fire systems capabilities against an expanded spectrum of stand-off munitions, emphasizing smaller and faster target vehicles.
- b. Determination of required system modifications allowing expanded capability at acceptable costs. This would include sensor acquisition and tracking characteristics.
- c. Investigation, supported by experimental data, of the terminal effectiveness of projectile options against standoff munitions warheads, including the assessment of the degree to which warhead content can be made less vulnerable to attack by changing the explosive composition. This study would require the utilization of classified experimental data.

- d. Overall assessment of the degree of improvement of system effectiveness against standoff munitions which can be attained at acceptable cost.
- e. Recommendation of system characteristics for improved defense against stand-off munitions, and research and development areas of high payoff.

A ground rule to the effort study should be that the objective is not to successfully engage all possible standoff munitions threats, since this would lead to a junior ABM system, but to deny the enemy the use of the least costly types of standoff munitions.

11.6 PASSIVE RANGING SYSTEM (TONTO)

It is recommended that a method be implemented for the passive and continuous determination of target range as input to predicted fire systems by the exchange of angular tracking information, obtained passively, among two or more fire units. This mode would serve as a back-up to the active laser or radar ranging device on each mount, and would allow accurate fire control if the primary ranging device were jammed out. It would also allow accurate fire control in a completely non-radiating mode when desired.

Since no technical difficulties are considered to exist with this mode of operation, it is suggested that a field demonstration of feasibility might be a near-term objective. The system elements required for such a demonstration would be

- a. A primary fire unit. GLAADS could be used for this purpose. Vulcan might also be a candidate.
- b. A "slave" tracking unit. This would, in operational use, be a second fire unit, but for demonstration could be any available optical or FLIR tracking unit.
- c. Digital data link between the two cooperating tracking units.
- d. A digital computer to (1) convert tracking data from the master station for transmittal to the "slave" unit so that the slave search requirements will be limited to search in one coordinate, (2) receive tracking data from the slave unit to combine with that of the master unit, and compute slant range to the target from the master unit, and, with parallax corrections to any other fire unit in the local defense.

A principal objective of the demonstration configuration would be to determine the time required for the "slave" unit to acquire a target designated by the "master".

This program would obviously be designated "TONTO" since it is a back-up for the lone ranger on each fire unit.

11.7 FIRE CONTROL COMPUTER INVESTIGATIONS

Recommendations with regard to further investigations of optimization of the computer component of predicted fire systems are made in the accompanying volume to this Report. In addition to the recommendations made there it is suggested that the following areas of investigation should be continued independently of any particular system development program.

- a. Determination of the operator-system interface most acceptable to the ultimate user as consistent with available personnel capabilities and the expected combat environment and constraints
- b. Comparison of alternate methods of performing certain basic computations, such as ballistic computations
- c. Determination of design implications of a requirement to minimize personnel for operations, and maintenance and to minimize all costs of maintenance, operations and support.

11.8 FORWARD AREA AIR DEFENSE SYSTEM SIMULATION

An optimum air defense system consists of the integrated operation of interceptor aircraft, area defense surface to air missiles and local predicted fire and/or short range surface to air missiles, controlled for minimal interference among the defense elements, and with prompt and accurate threat assessment, warning, acquisition and engagement. The system must have alternate operational modes to be resistant to enemy countermeasures.

The many parameters and options regarding system components make the design of such a system a complex task. Support of the requirements process and system evaluation by computer simulations with all known detail incorporated can, and has lead to simulations which require a long set-up time, and rather costly operations.

It is suggested that drawing on the Army's experience with TACOS for the general air defense simulation, and simulations of the local defense fire units with the Armament Command's FUE, and UNIMAP, the University of Michigan simulation, the Litton simulation, and other simulations of specific surface to air systems a useful effort could be directed to the development of a relatively simple simulation of forward area air defense, retaining those parametric relations which have been found to be most important in the existing complex library of models, and eliminating those input and parametric relations having observable, but "second order" effects on the outcomes. It is suggested that such a simulation would be

- a. Designed to minimize set-up time in response to changes in configuration and components of the forward area defense
- b. Designed to minimize running time and cost per solution
- c. Deterministic rather than probabilistic.

To achieve these objectives, a preliminary effort, principally in-house would be necessary to agree on the essential problem elements to be retaining in a "minimum-cost" simulation, and the problem elements which could be safely omitted.

11.9 AIR DEFENSE SYSTEM INTEGRATION TO THE FIRE UNIT LEVEL

In the interests of reducing predicted fire system cost, it may be possible to have a single surveillance sensor (for example a TWS radar with multiple track generation capability) serve a number of fire units. The desirability of data links among fire units for passive ranging has been noted. Data links including the common surveillance sensor would expedite prompt target acquisition by individual fire units with their respective tracking sensors.

If designed as an integrated system, the sensor computer could provide initial position and approximate target velocities to each fire unit, reducing subsequent solution time. Depending on the weight/volume of the surveillance unit, it might be mounted on one fire unit of a battery, with other fire units mounting lightweight "dummy" equipment of similar configuration to prevent enemy identification by visual observation of which fire unit carries the battery's surveillance equipment.

It is therefore recommended that the feasibility, cost and manpower advantages of utilizing one surveillance and acquisition unit for several fire units be determined, with data processing on the sensor package and data link to give reaction times and accuracy of data transfer superior to that now obtained, for example, with FAAR.

APPENDIX A

RADAR "BORESIGHT" ERRORS

During World War II, operations analysts customarily applied very large degradation factors to proving ground performance of weapons in order to estimate combat effectiveness. After World War II, the present writer participated in an extensive analysis of air to air weapon system effectiveness, in which kill probabilities per pass were computed to several decimal places by rather sophisticated vulnerability plus fire control analyses. Dr. Philip Morse in the DOD WSEG then divided all of these carefully computed estimates by 4.0 based on his WWII field experience. It is difficult, and, perhaps, impossible for a systems analyst trying to design improved weapon systems to assign combat degradation factors in his analysis as large as those which will be experienced in the field. Systems are conceived by optimists. Objective assessments of field performance are best done by pessimists.

In this Appendix we note some radar biases that were obtained in proving ground tests of fire control radars under optimum conditions. Even in the state of the art of that period (1947) biases as large as some shown in the subsequent tables "should not occur with a properly calibrated system".

In Table A-I we list bias errors obtained in tests of the T5 (10.7 cm) fire control radar, and bias errors on the same target paths with the T6 (3 cm) fire control radar.^① Also shown are the probable errors of the radars in each coordinate with biases removed. All of the runs were made on the same day. Data taken on several days is given in the referenced report; the biases changed from day to day, and the extracts shown in Table A-1 are neither the largest nor the smallest values recorded. Target speed was about 170 yards/second and the data shown are for medium to long range paths. For short range paths much larger azimuth biases (2 to 4 mils) were recorded; they were attributed to angular velocity which seems an incorrect inference, since they changed from "lead" to "lag" as the azimuth rate sign changed.

The reference states^①

"It should be mentioned that the results discussed in this report were obtained with equipment which was maintained by a competent engineer of the Sperry Corp.; under less skilled maintenance the equipment would not have performed in the manner to be discussed. This is indeed a weakness of both radar trackers but is similarly the case with complex radar equipment."

Table A-1. Bias Errors of T5 and T6 Radars in Proving Ground Tests

	T5 (10.7 cm) Biases				T6 (3 cm) Biases		
	Run	Azimuth (Mils)	Elevation (Mils)	Range (Yds)	Azimuth (Mils)	Elevation (Mils)	Range (Yds)
Azimuth Increasing	3	+0.2	-0.9	-5	-0.0	-2.7	-17
	5	-0.1	-1.1	-7	+0.1	-3.1	-12
	7	+0.5	-1.1	-11	-0.1	-3.2	-14
	9	+0.5	-1.0	-14	-0.1	-3.1	-10
Azimuth Decreasing	4	+0.4	-0.8	-21	+0.1	-2.8	-18
	6	+0.5	-1.1	-22	-0.2	-3.0	-15
	8	+0.5	-1.1	-19	-0.2	-3.1	-12
	10	+0.6	-1.0	-24	-0.3	-3.0	+12 (std)
Probable Errors with Bias Removed	All	0.67	0.75	4.5	0.37	0.22	3.5

An additional reference^② was located which highlights the bias errors of a supposedly calibrated radar in proving ground tests. After data was taken on some 47 target paths, with thousands of data points, it was found that "for every course there was an average positive bias of about 1.5 to 4.5 mils in elevation and about 50 to 100 yards in slant range." Averaged over all of the data, the average biases were "2.4 mils in elevation, 70 yards in slant range, and 1.6 mils in azimuth."

It is suggested that a moderate effort to collect proving ground test data on modern fire control radars from existing files will provide estimates of expected radar calibration biases under optimum conditions. A survey of operational radars in field use (not proving ground instrumentation radars) should show somewhat larger calibration errors. Special field tests may have to be arranged to obtain valid estimates of calibration errors likely to arise under combat conditions.

APPENDIX B

TERMINAL CORRECTION OF BIAS ERRORS IN PREDICTION-CORRECTED PROJECTILE SYSTEM

In Section 5.0 a concept of a predicted-corrected projectile system was outlined, in which it was suggested that the problem of boresighting the projectile predicted beam and the target tracking beam might be mitigated by applying a terminal correction when the tracking beam was able to observe the target and the projectile simultaneously. In this Appendix we present some estimates of the conditions under which this may be possible.

The geometry of the situation is shown in Figure B-1. The target tracking beam is assumed to have a half-beam width in angular measure θ . This is not the beam width between half power points, which would be 2θ .

We consider an idealized situation for initial estimates. The projectile is flying a predicted beam and would hit the target, except that the predicted beam has been misoriented by a small bias error e_b , with $e_b \ll \theta$. It is assumed that the projectile can be detected when it is within an angle θ of the axis of the tracking beam.

Hence the tracking beam will illuminate the projectile when the target is at an angle θ from the predicted intercept point. The angular velocity of tracking is

$$d\Omega/dt = V_t \sin \Omega / D \quad (\text{B.1})$$

where V_t = target velocity, and D - slant range.

Hence the "time to go" to intercept is

$$t_g = \theta / \dot{\Omega} = \theta D / (V_t \sin \Omega) \quad (\text{B.2})$$

and in this time interval the projectile must be acquired, its position measured, a corrective command issued, and a lateral acceleration developed. We assign a time delay Δ seconds to this process, and it is assumed that after Δ the projectile has developed a constant maximum lateral acceleration

$$A_L = n_a g \quad (\text{B.3})$$

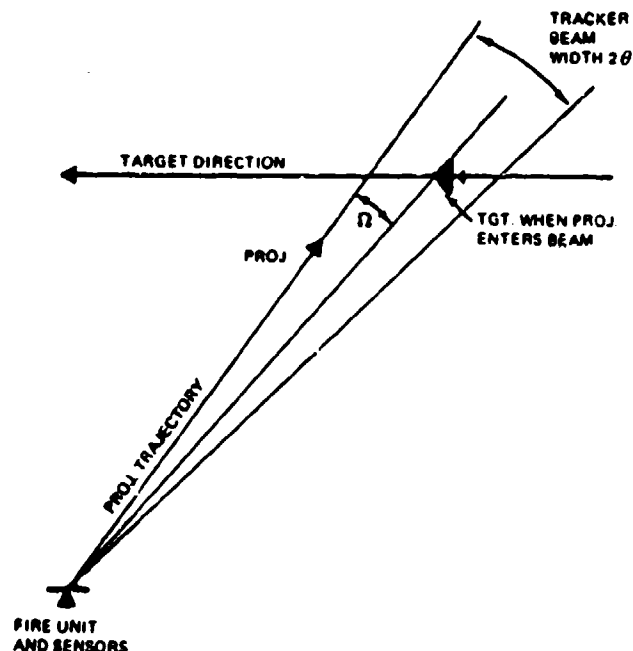


Figure B-1. Geometry

40001 500

The linear error to be corrected as a result of the bias is $e_b D$, hence for the correction to be achieved,

$$e_b D = (1/2) A_L (t_g - \Delta)^2 \quad (B.4)$$

The most difficult point on a fly-by pass to achieve the desired correction is at midpoint, where the angular velocity of the tracking beam is highest. Assuming a 300 m/s target and a maximum lateral acceleration of 5g for the projectile, Figure B-2 shows the required tracking beam width to fully correct for a 5 mil bias, vs. slant range at midpoint and zero and 0.20 seconds lag.

Figures B-3 and B-4 show the regions in the slant plane defined by the target velocity vector and the fire unit, outside of which a full 5 mil bias correction can be achieved for 5.0 and 2.5° half beam widths, and for zero lag and 0.20 seconds lag. Within these regions only corrections less than 5 mils can be achieved.

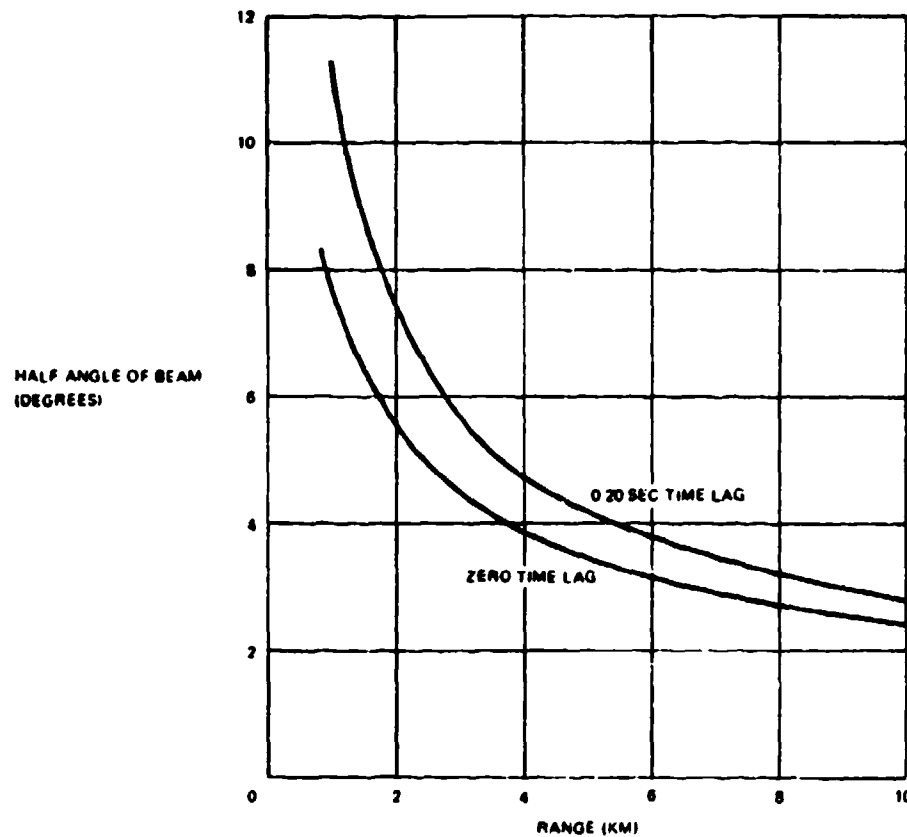
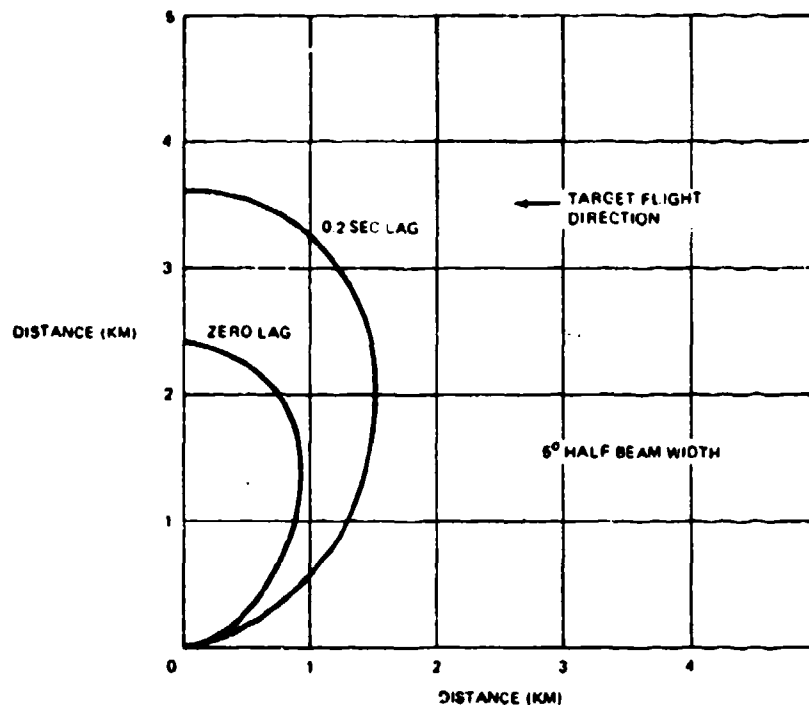


Figure B-2. Required Tracking Beam Half Width for Terminal Correction at Midpoint of 5 Mil Bias vs. Time Lag and Range

Figure B-4 shows how the maximum correction that can be achieved at midpoint varies with slant range at midpoint and beam width, and 0.20 seconds lag. If boresight error is only one mil, a 2.5° half beam angle can make this correction at midpoint for any target beyond 4 km, and the correction zone contour would be close to that of Figure B-3 for 5° and 5 mils.



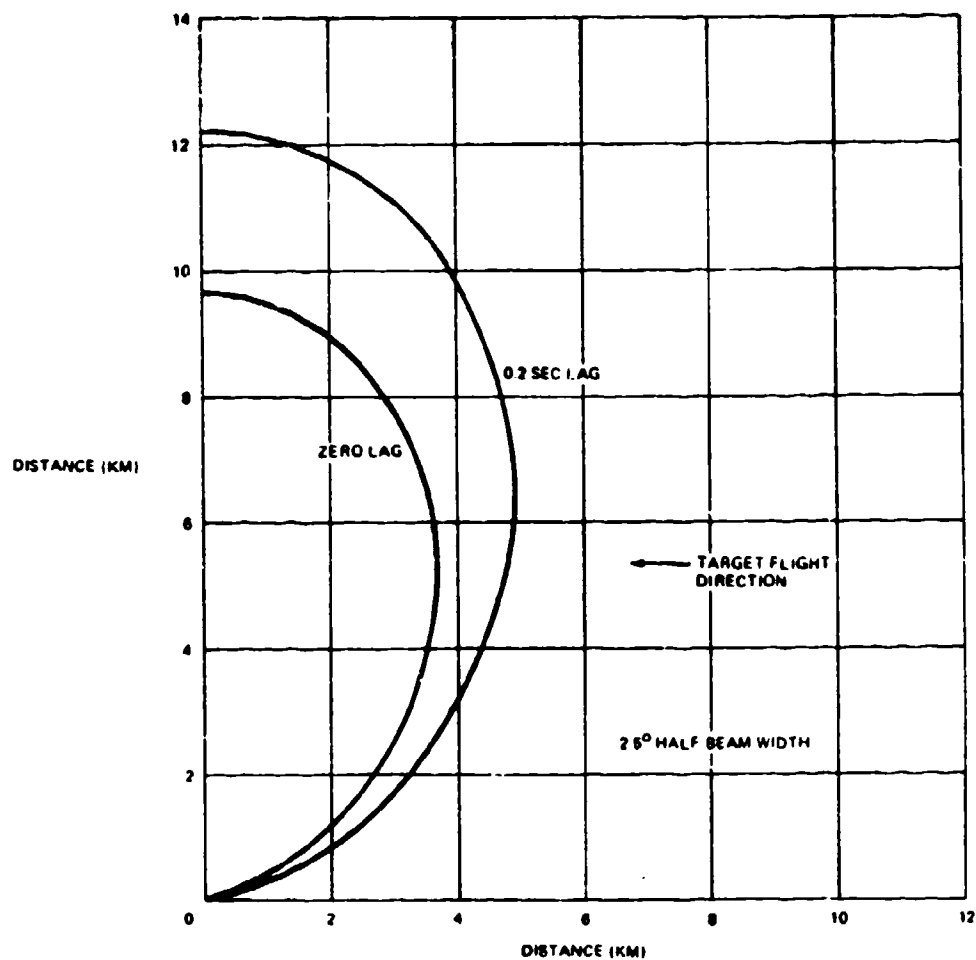
40001 502

Figure B-3. Region Outside of Which a 5 Mil Bias Error Can be Corrected vs. Lag Time For 5° Half Beam Width

Since the concept envisions using the terminal measure as a "closed loop" correction device in addition to terminal command generation for each projectile, in those regions where a full correction is not achieved on the first projectile fired, subsequent projectiles will have the advantage of bias reduction based on the first measurement.

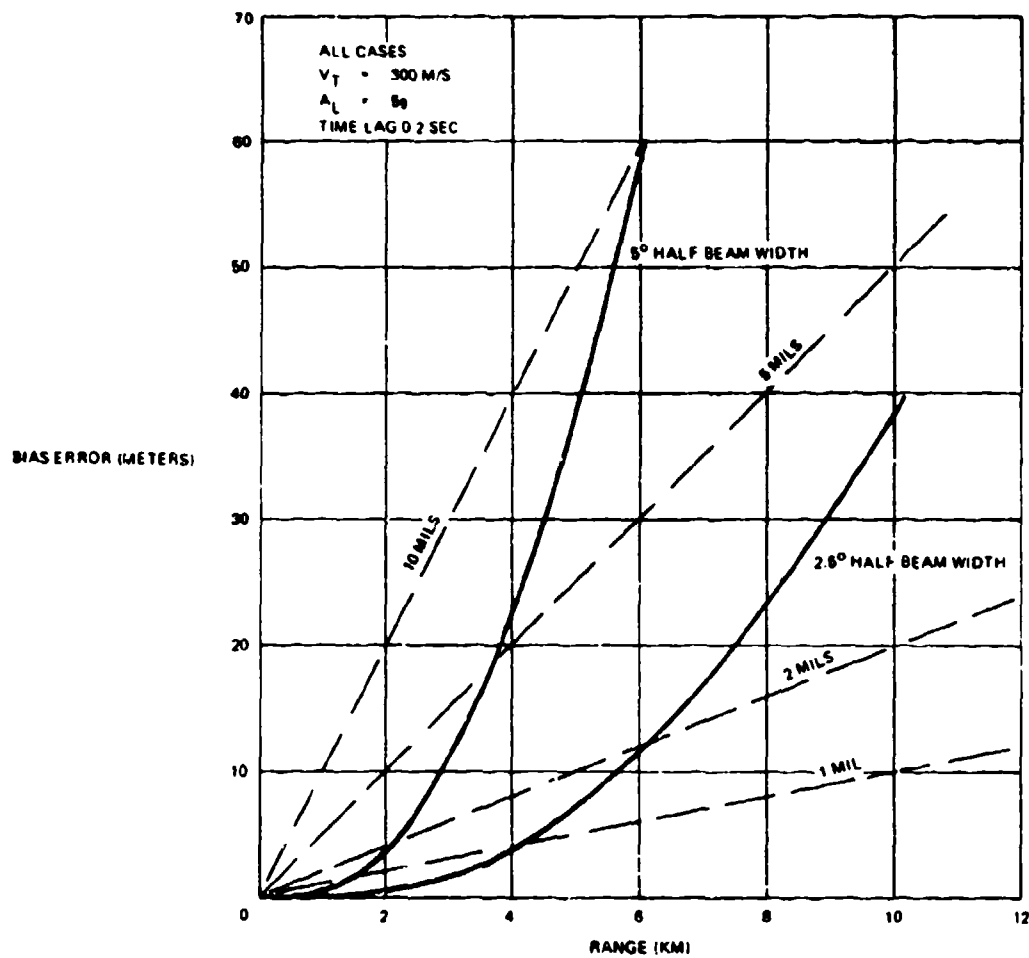
In all of the cases shown, full corrections can always be achieved for target positions with small approach angles so that observation of initial rounds fired at these angles will reduce the biases associated with later projectiles fired near midpoint, if the target has not been destroyed by that time.

These preliminary estimates tend to confirm the potential feasibility of the concept.



40001 803

Figure B-4. Region Outside Which a 5 Mil Bias Error Can be Corrected vs. Lag Time for 2.5° Half Beam Width



40001 504

Figure B-5. Correctable Bias Error at Midpoint Versus Range and Beam Width

APPENDIX C

CLOSED LOOP PERFORMANCE WITH SPECIFIED INITIAL BIAS

The closed loop algorithms based on Kalman methodology attempt to minimize the variance of the system biases. But a bias is a component of the miss vector that is constant for a very long time. Hence the "variance of the bias" refers to the way in which the bias varies across a large number of target engagements, with enough intervening time and environmental change to make the initial bias at each new engagement independent of that at the prior engagement.

This definition is helpful to the mathematical analysis, but one really wants to know what the closed loop system does to a particular bias vector in a particular engagement. To show this in detail, the most convenient method is probably to use a computer simulation. However we take a compromise approach here that is illuminating. We use the simplest case of a closed loop system: a one coordinate system, no geometric variation, and a low rate of fire, so that time of flight lag can be ignored. The system has an initial specified bias, and a constant random round to round dispersion, assumed to be large compared with the corresponding component of miss measurement.

Define

$f(x_j)$ = probability density function of the impact point of the j 'th round.

$f(x_{j+1} | x_j)$ = probability density function of the impact point of the $j+1$ 'th round, given an observation of x_j and subsequent correction of point of aim.

\underline{x}_j = residual bias associated with the j 'th round.

x_j = impact point of the j 'th round.

σ_j^2 = variance of the dispersion of the j 'th round.

k_j = fraction of the observation x_j applied as a bias correction before firing round $j+1$.

σ^2 = dispersion variance of all rounds if no correction for bias were made.

σ_b^2 = a priori estimate of the bias variance over many "Independent" samples.

From Kalman filter theory

$$k_j = \frac{1}{\mu + j} ; \mu = (\sigma/\sigma_b)^2 \quad (C-1)$$

Note that

$$\sigma_j^2 > \sigma^2 \quad (C-2)$$

because the correction process carries some of the random component of the j'th observation into the j+1 firing.

We have then

$$f(x_j) = \left[\frac{1}{(2\pi)^{1/2} \sigma_j} \right] e^{-(x_j - \bar{x}_j)^2 / 2\sigma_j^2} \quad (C-3)$$

and

$$f(x_{j+1} | x_j) = \left[\frac{1}{(2\pi)^{1/2} \sigma} \right] e^{-[x_{j+1} - (\bar{x}_j - k_j x_j)]^2 / 2\sigma^2} \quad (C-4)$$

Average over all x_j to obtain

$$f(x_{j+1}) = \int_{-\infty}^{\infty} f(x_{j+1} | x_j) f(x_j) dx_j \quad (C-5)$$

$$f(x_{j+1}) = \left[\frac{1}{(2\pi)^{-1/2} (\sigma^2 + k_j^2 \sigma_j^2)^{1/2}} \right] e^{-[x_{j+1} - \bar{x}_j (1 - k_j)]^2 / [2(\sigma^2 + k_j^2 \sigma_j^2)]} \quad (C-6)$$

Hence the residual bias evolves according to

$$\bar{x}_{j+1} = \bar{x}_j (1 - k_j) \quad (C-7)$$

whence

$$\underline{x}_n = \underline{x}_0 / (\mu + n) \quad (C-8)$$

where \underline{x}_0 = the initial bias magnitude.

The random component associated with the $j+1$ round is

$$\sigma_{j+1}^2 = \sigma^2 + k_j^2 \sigma_j^2 \quad (C-9)$$

Increasing k_j above the Kalman value would produce a more rapid reduction of bias, but at the expense of increased random dispersion. The Kalman method provides a compromise between residual bias averaged over many independent samples, and the random component of miss.

An alternate approach would be to generalize the above simple model for the evolution of the probability density function, leaving the k_j as parameters to be optimized, introduce the target survival probability as a function of the bias and dispersion at the j 'th round, given specified initial biases, then average the survival probability over the initial distribution of biases. The resulting expression would then be optimized by choice of k_j . This would provide the k_j set to maximize the probability of killing the target; it would be different from the Kalman values. However the mathematics turns out to be far more difficult than the variance minimization of the Kalman method.

REFERENCES/BIBLIOGRAPHY

FOREWORD

Final Report on a Parametric Study of the Advanced Forward Area Air Defense Weapon System (AFAADS), Data Systems Division, Litton Systems, Inc., 2 Oct. 1970,

- 1. Volume I - Systems Analysis, AD 881 170 L**
- 2. Volume II - Simulation Model, AD 881 171 L**

Final Report on Supplement to Parametric Study of Advanced Forward Area Air Defense Weapon System (AFAADS), Data Systems Division, Litton Systems, Inc., 15 Sept. 1972,

- 3. Volume I - Analysis, AD-903 969 L**
- 4. Volume II - Simulation Model, AD-903 970 L**
- 5. Volume III - Effectiveness, AD-903 971 L**

SECTION 3
REFERENCES/BIBLIOGRAPHY

1. Final Report on a Parametric Study of the Advanced Forward Area Air Defense Weapon System (AFAADS), Data Systems Division, Litton Systems, Inc. 2 October 1970, Volume I - Systems Analysis, AD 881 170L.
- 2,3. Final Report on Supplement to Parametric Study of Advanced Forward Area Air Defense Weapon System (AFAADS), Data Systems Division, Litton Systems, Inc., 15 September 1972, Volume I - Analysis, AD-903 969 L, Volume III - Effectiveness, AD-903 971 L.
4. C.E. French, Miss Distance Radar (MIDI) - A Development for Air Defense Weapons Testing, Army Air Defense Board, Fort Bliss, Texas, 1972, AD-750 323.
5. Harry Sohn, Bullet Position Measuring System Feasibility Investigation, AMSAA Technical Report No. 68, September 1972, AD 759-269.
6. Laser Focus, 1973 Buyer's Guide.
7. Barry Miller, FLIR Gaining Wider Service Acceptance, Aviation Week & Space Technology, 7 May 1973.
8. Barry Miller, Cost Reductions Key to Wider FLIR Use, Aviation Week & Space Technology, 21 May 1973.
9. R.S. Berkowitz, ed., Modern Radar, Chapter 5. Radar Cross Section Target Models, W.W. Weinstock, Wiley, 1965.
10. J.W. Crispin and K.M. Siegel, ed., Methods of Radar Cross Section Analysis, Academic Press, 1968.
11. M. Skolnik, Radar Handbook, McGraw Hill, 1970.
12. Proceedings of the IEEE, Special Issue on Radar Reflectivity, Vol. 53, No. 8, pp. 769-1168, August 1965.
13. F.E. Nathanson, Radar Design Principles, McGraw Hill, 1969.
14. W.L. Wolfe, ed., Handbook of Military Infrared Technology, ONR, Supt. of Documents, U.S. Govt. Print Office, 1965, Washington, DC.
15. R.C. Hudson, Jr., Infrared System Engineering, Wiley, 1969.
16. M. Ross, Laser Receivers, Wiley, 1966.
17. M. Skolnik, Radar Handbook, McGraw Hill, 1970, (Chapter 37, C.M. Johnson, Laser Radars)
18. L.M. Biberman, S. Nudelman, Photoelectric Imaging Device, Vols. I and II, Plenum Press, 1970.

19. M. A. Bramson, Infrared Radiation, Plenum Press, 1968.
20. Robertson, Sloan D., Targets for Radar Navigation, Bell System Technical Journal, Vol. 26, October 1947, pp. 852-869.
21. Picatinny Arsenal, Encyclopedia of Explosives and Related Items, 1962 obtainable from Dept. of Commerce Clearinghouse, Vols. I to IV. Sketches of projectile configurations are given in Vol. IV.
22. V. Richard, Millimeter Wave Radar Applications to Weapons Systems, BRL Interim Report, 61, October 1972.
23. So named after the "Callipygean Venus".
24. Paul Kruse, L.D. McGlauchlin and R.B. McQuistan, Elements of Infrared Technology, Wiley, 1963.
25. James L. Alward, Spatial Frequency Filtering, Willow Run Laboratories of the University of Michigan, NAVSO, P-2499, December 1965.
26. VISTA: Weiss's²⁷ Ingenious Synthetic Trajectory Algorithm.
27. 9W
28. A. E. Bryson and Y. C. Ho, Applied Optimal Control, Blaisdell, 1969.

SECTION 4

REFERENCES/BIBLIOGRAPHY

1. Herbert K. Weiss, "The Evasive Airplane" Report to President, Antiaircraft Artillery Board, Fort Bliss, Texas, 28 February 1945. A copy of this World War II paper has been recovered and made available to the author through the good offices of Dr. Charles Meyer of the Applied Physics Laboratory.

SECTION 5

REFERENCES/BIBLIOGRAPHY

1. Jane's Weapons Systems All years
2. International Defense Review All issues
3. Hayes, Elements of Ordnance
4. Principles of Naval Ordnance and Gunnery, NAVPERS 10733-A
5. Ley, Willy, Rockets, Missiles and Men in Space, Signetbooks, (paper) 1969, New York, Hardcover Original, Viking Press, New York, 1944. Missiles and Rockets, July 1957
6. W. Stutz, Schiesslehre, Birkhäuser Verlag, Basel 1959
7. Army Almanac 1950
8. T. Cliffe, Military Technology and the European Balance, Int Inst for Strat Studies, London, 1972, Adelphi Papers No. 89
9. C. H. Murphy et al, Gun-Launched Sounding Rockets and Projectiles, Annals of the New York Academy of Sciences, Vol. 187, pp 304-323; Jan. 25, 1972
10. M. M. Postan et al Design and Development of Weapons, Studies in Government and Industrial Organization, H. M. S. Stationary Office, London, 1964
11. Technical Side, Guns and Ammunition, February 1973, p. 83
12. Dr. W. M. Spalding "The 35mm Twin AA Field Gun, Oerlikon CONTRAVES" NATO's Five Nations publication, June-July 1972, pp. 105-109
13. I. G. Henry, Open Chamber Guns, Ordnance, Nov-Dec 1970, pp 3-7
14. Don Stoehr, HIVAP, 1972 Guns and Ammunition Annual
15. Caseless Ammunition, Military Review, Dec. 1969
16. Gun World Magazine 9 Aug 1973
17. David Dardick et al., Gun/Projectile Systems, Space/Aeronautics, March 1967, pp. 92-99
18. Dale M. Davis, Airborne Guns and Rockets, Ordnance, March-April 1973, pp. 388-391

19. B. Bollermann, et al., Design, Development and Flight Test of the Super Loki Dart Meteorological Rocket Systems, Space Data Corp. Final Report, 30 May 1972, AFCRL-72-0380, AD 750 796.
20. Design for Control of Projectile Flight Characteristics, AMC Pamphlet AMCP 706-242, Sept 1966
21. Trajectories, Differential Effects and Data for Projectiles, AMCP 706-140 August 1963
22. Interior Ballistics of Guns, AMCP 706-150, February 1965
23. F. Schreier, The Oerlikon-Contraves 35-mm AA Tank - Some Operational Considerations, International Defense Review, Vol 5, No. 4, Aug 1972, pp. 377-383
24. M. Shinbrot and G. C. Carpenter, An Analysis of the Optimization of a Beam Rider Missile System, NACA TN 4145, March 1958
25. E. C. Stewart, Application of Statistical Theory to Beam-Rider Guidance in the Presence of Noise. II-Modified Wiener Filter Theory, NACA TN 4278, June 1958
26. C. F. Price and R. S. Warren, Performance Evaluation of Homing Guidance Laws for Tactical Missiles, Analytic Sciences Corp., TR-170-4, 1 Jan 1973, AD 761 626
27. I. V. Hogg, German Secret Weapons of World War II, Arco Publishing Co., Inc. New York, 1970
28. Crotale: A Missile Defense System against Supersonic Low-level Attack, International Defense Review, Vol 3, No. 1, March 1970 pp 70,71
29. Roland: A Cost Effective Weapons System, Intl Def Review, Vol 4, No. 1, Feb 1971 pp 79-83
30. The ACRA Anti-Tank Weapon System, Int Def Review, Vol 13, No. 2, June 1970, pp 203-204
31. M. J. H. Taylor and J. W. R. Taylor, Missiles of the World, Scribner's Sons, N.Y. 1972
32. Proceedings of the IAS Symposium on Vehicle Systems Optimization, Nov. 28-29, 1961, Institute of Aerospace Sciences, New York.
33. G. Leitmann, Optimization Techniques, Academic Press, 1962, New York

34. E. C. Ludvigsen, Army Weapons and Equipment 1973: The Tyranny of Rising Costs Army Green Book, Oct. 1973 Assoc. of the U.S. Army
35. K. Macksey and J. H. Batchelor, Tank, A History of the Armored Fighting Vehicle, Ballantine Books, New York, 1971. This volume is one of the finest current references to armor and the methods that have been devised for fighting it.

SECTION 6

REFERENCES/BIBLIOGRAPHY

1. Industry Observer, Aviation Week, 8 October 1973, p. 9.
2. Stutz, Walter, Schiesslehre, Birhauser Verlag, Basel, 1959.
3. Hoffschmidt, E.J. et al, German Tank and Antitank in WW-II, and Tank Data, I, II, III, W.E. Inc., Old Greenwich, Connecticut.
4. Nishiwaki, Jien, Resistance to the Penetration of a Bullet Through an Aluminum Plate, Journal of the Physical Society of Japan, Volume 6, No. 5, September-October 1951, pp. 374-378.
5. Forman, R.G. et al, Vulnerability of Aircraft Structures Exposed to Small Arms Fire Projectile Impact Damage, Air Force Flight Dynamics Laboratory, AFSC, AFFDL-TR-67-157, February 1968, AD 829.
6. C. Rougeron, Das Bomenflugwesen, (L'Aviation de Bombardment) ins Deutsch ubertragen von E. Margis, Rowohlt Verlag, Berlin, 1938.
7. W.P. Dunn and Y.K. Huang, Ballistic Impact of Single and Spaced Plates, Watervliet Arsenal, December 1972, WVT 7267, AD 756 403.
8. E. Ulsamer, The A-10 Approach to Close Air Support, Air Force Magazine, May 1972. See also Air Force, January 1973, Interavia 8, 1972, and International Defense Review, Volume 5, No. 4, August 1972.
9. Encyclopedia of Explosives, Government Printing Office, p. B 335.
10. Janes Weapon Systems.
11. International Defense Review, all issues.
12. Ibid, Volume 5, No. 4, August 1972.
13. Elements of Ordnance, Hayes, Wiley, 1938.
14. K. Macksey and J.H. Batchelor, Tank, A History of the Armored Fighting Vehicle, Ballantine Books, New York, 1971. Contains excellent drawings of all types of projectiles for the defeat of armor.

SECTION 7

REFERENCES/BIBLIOGRAPHY

1. Aviation Week and Space Technology, 15 October 1973
2. Ibid, 22 October 1973
3. Ibid, 29 October 1973
4. Ibid, 5 November 1973
5. Ibid, 3 December 1973
6. Ibid, 10 December 1973
7. Ibid, 17 December 1973
8. Barry Miller, Four Part Electronic Warfare Special Report, Aviation Week and Space Technology Reprint, McGraw-Hill, 1969
9. Special Report, Electronic Countermeasures, Aviation Week and Space Technology Reprint, McGraw-Hill, 1972
10. The Growing Threat, New Soviet Weapons Technology, Aviation Week and Space Technology Reprint, McGraw-Hill, 1971
11. R.H. Kent, The Probability of Hitting an Airplane as Dependent upon Errors in the Height Finder and Director, Ballistic Research Laboratories Report, No. 127, December 1938, AD 701 865
12. H.K. Weiss, AFAADS Report, Vol. III, Effectiveness, 15 September 1972, loc cit supra, pp. 7-7, 7-8

SECTION 8

REFERENCES/BIBLIOGRAPHY

1. Trevor Cliffe, Military Technology and the European Balance, Adelphi Papers, No. 89, Int. Inst. for Strat. Studies, London, August 1972, Appendix J, Unit Costs of Weapons Systems.
2. LTC E. L. Alvey, Analysis of Operating Costs of Selected Missile Units USAREUR FY 1968, 3rd Annual Cost Symposium, DOD, AD 833 207.
3. FY 1974 Authorization for Mil. Proc., R&D Hearings, U.S. Senate, Committee on Armed Forces 10 April - 1 May 1973, p. 540.
4. Forward Air Defense Cut Worries Allies, Aviation Week and Space Technology, August 27, 1973.
5. Production AIM -7F Enters Test, Ibid.
6. "Official Price List" Aviations Studies Atlantic, London.
7. DMS Market Intelligence Reports.
8. G. W. Kalal, Cost Estimating Relationships for Machine Guns Theoretical First Unit Cost, AMSWE-CPE 73-2, February 1973, AD 761 095.
9. Cost Estimating Relationships for Gun Barrel Procurement Unit Cost, AMSWE-CPE 72-15, November 1972, AD 761 096.
10. Cost Estimating Relationships for Manufacturing Hardware; Cost of Gun/Howitzer Cannons, AMSWE-CPE 72-8, August 1972, AD 757163.
11. Cost Estimating Relationships for Manufacturing Hardware; Cost of Howitzer Carriages and Recoil Mechanisms, September 1972, AMSWE-CPE 72-10 AD 757 164.
12. M.J.H.Taylor & J.W.R.Taylor, Missiles of the World, Scribners, 1972.
13. Janes Weapon Systems, all years.
14. J. Jackson, The Cost of Performance in a Missile, or What Price Range? 4th Annual Cost Symposium, 17-18 March 1969, DOD, AD 854 663.
15. C. D. Billing, A Cost Model for Radar Guidance and Control Sections of Air Defense Missiles, Volume II of 5th Annual Cost Symposium, DOD, March 24-25 1970 Volume I AD 875 742, Volume II AD 875, 743.
16. Hearings on Military Posture and H R 12604, Committee on Armed Services, House of Reps., on FY 1973 Budget, January-April 1972.
17. International Defense Digest, all issues.

18. F. Leary, Tactical Air Defense, Space/Aeronautics, September 1966.
19. General "Billy" Mitchell, Winged Defense, 1925, reissued by Kennikat Press, Port Washington N Y 1971.
20. Military Pay - Figures that Scare Experts, L A Times, 4 January 1973
C. A. Robinson, Jr.
21. SAM-D Readied for Firing Tests, Av Week and Space Technology, June 11, 1973, pp 42-47.
22. J. W. Noah and R. W. Smith, Cost-Quantity Calculator, RAND Corp. RM-2786-PR, January 1962.
23. A Modular Look for Radar, Business Week, 8 September, 1973, pp 64M-64P.
24. Barry Miller, Cost Reductions Key to Wider FLIR Use, Aviation Week and Space Technology, 21 May 1973, pp 48-53.
25. E. C. Ludvigsen, Army Weapons and Equipment 1973: The Tyranny of Rising Costs 1973 Green Book, Army, October 1973.
26. J. D. McCullough, "Design to Cost" BUZZ-WORD or VIABLE CONCEPT?, IDA Paper P-968, July 1973 (contains Stinger Cost goals) AD 763, 624.
27. Barry Miller, Mideast War Spurs Interest in Standoff Weapons, Aviation Week and Space Technology, 10 December 1973.
28. Willy Ley, Rockets, Missiles and Man in Space, New American Library, New York 1969.
29. Rapier, Brochure by Norden Division of United Aircraft Corporation, and McDonnell Douglas Corporation, 1973.
30. Robert S. Allen, Arab-Israeli War, Some Military Lessons for the United States, Human Events, 5 January 1974, Allen estimates Sagger cost at \$1000, and less than TOW.
31. Armament Data Sheets, Aviation Studies Atlantic, London contains tables of warhead weights as well as vehicle dimensions and performance.
32. Cost Data, AWCP 37-2, HQ U S Army Weapons Command, 21 December 1973.
33. Flying Annual, 1973, Zuff Dan's Pub. Co.
34. I. V. Hogg, German Secret Weapons of World War 2, Arco. Pub. Co., Inc. 1970.

APPENDIX A
REFERENCES/BIBLIOGRAPHY

1. J. Leeder Comparative Tests of Radar Trackers T-5 and T-6 BRL Report 643,
8 Sept. 1947
2. F. Q. Barnett and J. J. Dunne, A Study of Prediction Errors, AAFC8 T-33D
BRL Report 932, 1955